

Copyright

by

David Barra Birrcher

2009

The Dissertation Committee for David Barra Birrcher certifies that this is the approved version of the following dissertation:

**DESIGN OF REINFORCED CONCRETE DEEP BEAMS FOR STRENGTH AND SERVICEABILITY**

Committee:

---

Oguzhan Bayrak, Supervisor

---

Sharon L. Wood

---

James O. Jirsa

---

John E. Breen

---

Ofodike A. Ezekoye

**DESIGN OF REINFORCED CONCRETE DEEP BEAMS FOR STRENGTH AND  
SERVICEABILITY**

by

**David Barra Birrcher, B.S., M.S.**

**Dissertation**

Presented to the Faculty of the Graduate School of

The University of Texas at Austin

in Partial Fulfillment

of the Requirements

for the Degree of

**Doctor of Philosophy**

The University of Texas at Austin

May 2009

## **Acknowledgements**

I am very grateful for the generous support of the Texas Department of Transportation. Specifically, I would like to thank Dean Van Landuyt (TxDOT Project Director) and John Vogel (TxDOT Project Advisor) for their guidance, suggestions, and expertise throughout the course of Project 5253.

To Dr. Bayrak, your passion for structural engineering has been an inspiration to me. I cannot thank you enough for the countless impromptu sit-downs, late-night phone conversations, and technical brainstorming sessions over the years. I am a better engineer having been exposed to your technical and practical structural engineering expertise. I would also like to thank the rest of my committee, Dr. Wood, Dr. Jirsa, Dr. Breen, and Dr. Ezekoye, for your advice and tutelage throughout my pursuit of a Ph.D.

I am extremely grateful to my fellow beam buster Robin Tuchscherer. Your efficiency and productive nature allowed us to achieve as much as we did in this project. Your personality and character made working with you a delight. I really appreciate your help and friendship. To Matt Huizinga, thank you your groundbreaking efforts in Project 5253. When I refer to you as our “fullback,” I do it with great appreciation and respect.

The completion of Project 5253 would not have been possible without the assistance of numerous individuals in the Ferguson Structural Engineering Laboratory. Many thanks go to Mike McCarthy, Gary Lehman, Thomas Stablon, Brian Schnittker, Erin O’Malley, Patrick Harkin, James Kleineck, James Plantes, Ryan Kalina, and David Wald. Also, I really appreciate the advice and friendship of InSung Kim, Dean Deschenes, and Mike Brown. Nothing in the lab would get done without the help of Blake Stassney, Dennis Fillip, Andrew Valentine, Eric Schell, Mike Wason, Jessica Hanten, and Barbara Howard. Thank you for your unsung contributions.

To my parents, thank you for your commitment to my education and for making me the person that I am today. I am forever indebted to you both. To Christine and Wesley, thank you for your unconditional support. And to Heather, Calvin, and Jane, your love and encouragement made this possible.



# **DESIGN OF REINFORCED CONCRETE DEEP BEAMS FOR STRENGTH AND SERVICEABILITY**

David Barra Birrcher, Ph.D.  
The University of Texas at Austin, 2009

Supervisor: Oguzhan Bayrak

Several reinforced concrete bent caps (deep beams) in Texas have developed significant diagonal cracks in service. The cracking in two bent caps was so extensive that costly retrofits were implemented to strengthen the structures. Strut-and-tie modeling is currently recommended in most U.S. design specifications for the design of reinforced concrete bent caps and deep beams. Designers have expressed concerns with the lack of clarity and serviceability-related considerations in strut-and-tie model design provisions.

Due to concerns with strut-and-tie modeling design provisions and field problems of in-service bent caps, TxDOT Project 5253 was funded. Several tasks conducted within Project 5253 are addressed in this dissertation. The effects of minimum web reinforcement and member depth on the strength and serviceability behavior of deep beams are presented. The transition between deep beam shear capacity and sectional shear capacity near a shear-span-to-depth ( $a/d$ ) ratio of 2 is addressed. A service-load shear check to limit diagonal cracking in service is outlined. Lastly, a simple chart that correlates the maximum width of diagonal cracks in a deep beam to its residual capacity is developed.

To accomplish the objectives of Project 5253, thirty-seven tests were conducted on reinforced concrete beams with the following cross-sectional dimensions: 21"x23", 21"x42", 21"x44", 21"x75", and 36"x48." The specimens were loaded with  $a/d$  ratios of

1.2, 1.85, and 2.5. The test specimens are among the largest reinforced concrete deep beams in the literature.

To supplement the findings of the experimental program, a database of deep beam test results was compiled. Entries in the database that lacked sufficient information and that did not meet established cross-sectional size or web reinforcement criteria were filtered from the database. The use of the database in conjunction with the experimental program enabled each objective to be addressed from both broad and specific viewpoints.

Several recommendations for improving the strength and serviceability design of deep beams are presented including a minimum web reinforcement requirement, provisions to ease the transition between calculated deep beam and sectional shear capacity, and a design check to limit diagonal cracking in service.

## TABLE OF CONTENTS

LIST OF TABLES.....	xiii
---------------------	------

LIST OF FIGURES.....	xiv
----------------------	-----

CHAPTER 1 Introduction.....	1
-----------------------------	---

1.1 Overview.....	1
1.2 Project Objectives and Scope .....	2
1.3 Organization .....	3

CHAPTER 2 Background Information.....	5
---------------------------------------	---

2.1 Overview.....	5
2.2 Field Problems .....	5
2.3 Strut-and-Tie Modeling for Deep Beams .....	10
2.3.1 What is a Deep Beam?.....	10
2.3.2 Overview of Strut-and-Tie Modeling .....	12
2.3.3 Elements of Strut-and-Tie Modeling .....	16
2.3.3.1 Nodes .....	16
2.3.3.2 Struts .....	25
2.3.3.3 Ties.....	26
2.3.4 Strut-and-Tie Model Design Provisions .....	27
2.3.4.1 AASHTO LRFD (2008) STM Provisions .....	27
2.3.4.2 ACI 318-08 Appendix A STM Provisions.....	29
2.3.4.3 Project 5253 STM Provisions .....	32
2.3.4.4 Evaluation of STM Design Provisions with Deep Beam Data .....	36
2.4 Deep Beam Database .....	40
2.4.1 Filtered Database .....	41
2.4.2 Evaluation Database .....	42

2.5	Summary.....	44
<b>CHAPTER 3 Experimental Program .....</b>		<b>46</b>
3.1	Overview.....	46
3.2	Testing Program.....	46
3.2.1	Overall Design of Test Specimens .....	49
3.2.2	Series I: Distribution of Stirrups across Beam Web.....	51
3.2.3	Series II: Triaxially Confined Nodal Regions .....	53
3.2.4	Series III: Minimum Web Reinforcement .....	56
3.2.5	Series IV: Depth Effect.....	59
3.2.6	Series M: Multiple Purpose .....	62
3.2.7	Summary of Test Specimen Details .....	63
3.3	Fabrication of Specimens .....	68
3.3.1	Steel Reinforcement.....	68
3.3.2	Concrete Mixture Design.....	68
3.3.3	Construction of Specimens .....	69
3.4	Testing Frame .....	74
3.5	Instrumentation .....	79
3.5.1	Strain Measurements using Reinforcing Bars .....	79
3.5.2	Load and Displacement Measurements .....	81
3.5.3	Crack Width Measurements .....	84
3.6	Test Procedure .....	84
3.7	Summary.....	89
<b>CHAPTER 4 Experimental Results .....</b>		<b>91</b>
4.1	Overview.....	91
4.2	Summary of Experimental Results .....	91
4.2.1	Evaluation of Strength Data.....	95

4.2.2	Evaluation of Serviceability Data.....	98
4.3	Minimum Web Reinforcement.....	103
4.3.1	Background.....	103
4.3.1.1	AASHTO LRFD 2008 and CHBDC 2006.....	104
4.3.1.2	CSA A23.3-04 and fib (CEB-FIP) 1999.....	105
4.3.1.3	ACI 318-08 .....	105
4.3.1.4	TxDOT 4371 Minimum Reinforcement Recommendations .....	107
4.3.1.5	Other minimum reinforcement provisions in AASHTO LRFD 2008 .....	108
4.3.1.6	Comparison of minimum reinforcement provisions .....	110
4.3.2	Strength Results.....	113
4.3.2.1	Strength Results from the Evaluation Database.....	113
4.3.2.2	Strength Results from the Experimental Program .....	117
4.3.2.3	Specimens tested at a/d ratio of 1.85.....	120
4.3.2.4	Specimens tested at other a/d ratios: 1.2 and 2.5 .....	128
4.3.3	Serviceability Results .....	131
4.3.3.1	Serviceability Results from the Evaluation Database .....	132
4.3.3.2	Serviceability Results from the Experimental Program.....	133
4.3.4	Design Recommendations .....	150
4.3.5	Summary.....	153
4.4	Member Depth.....	154
4.4.1	Background.....	155
4.4.2	Strength Results.....	156
4.4.2.1	Strength Results from the Literature.....	156
4.4.2.2	Strength Results from the Experimental Program .....	163
4.4.3	Serviceability Results .....	179
4.4.3.1	Serviceability Results from the Literature .....	179
4.4.3.2	Serviceability Results from the Experimental Program.....	183
4.4.4	Design Recommendations .....	191

4.4.5	Summary.....	191
4.5	Summary.....	192
<b>CHAPTER 5 Analysis of Results.....</b>		<b>193</b>
5.1	Overview.....	193
5.2	Discrepancy in Calculated Shear Strength at a/d Ratio of 2.0.....	193
5.2.1	Background.....	193
5.2.2	Effect of a/d ratio on Shear Behavior .....	196
5.2.2.1	Results from the Literature .....	197
5.2.2.2	Results from the Experimental Program.....	200
5.2.3	Reducing Discrepancy between Shear Models at a/d ratio of 2.0 .....	214
5.2.4	Design Implications .....	226
5.2.5	Summary and Conclusions .....	229
5.3	Diagonal Cracking under Service Loads .....	230
5.3.1	Background.....	230
5.3.2	Approach.....	232
5.3.3	Results.....	233
5.3.3.1	Variables that affect diagonal cracking loads of deep beams .....	234
5.3.3.2	Estimating Diagonal Cracking Loads .....	246
5.3.4	Design Implications .....	257
5.3.4.1	Summary and Conclusions.....	260
5.4	Correlation of Maximum Diagonal Crack Width to Capacity.....	261
5.4.1	Background.....	261
5.4.1.1	Variables affecting width of flexural cracks .....	261
5.4.1.2	Types of diagonal cracks.....	262
5.4.1.3	Effect of web reinforcement on diagonal crack widths of deep beams .....	263
5.4.1.4	Effect of a/d ratio on diagonal crack widths .....	266

5.4.1.5	Effect of longitudinal reinforcement on diagonal crack widths.....	268
5.4.1.6	Effect of concrete cover on diagonal crack widths .....	269
5.4.2	Approach.....	270
5.4.3	Results.....	274
5.4.3.1	Effect of web reinforcement on diagonal crack widths of deep beams .....	278
5.4.3.2	Effect of a/d ratio on diagonal crack widths of deep beams .....	279
5.4.3.3	Effect of longitudinal reinforcement on diagonal crack widths of deep beams .....	283
5.4.3.4	Correlation of Crack Width to Residual Capacity .....	285
5.4.4	Summary and Conclusions .....	292
5.5	Summary.....	293
<b>CHAPTER 6 Summary and Conclusions.....</b>		<b>294</b>
6.1	Summary.....	294
6.2	Examination of I-45 Bent Cap in Houston, Texas.....	296
6.3	Conclusions.....	298
6.3.1	Minimum Web Reinforcement.....	298
6.3.2	Effect of Member Depth.....	299
6.3.3	Discrepancy in Calculated Shear Strength at a/d Ratio of 2.....	300
6.3.4	Limiting Diagonal Cracking under Service Loads .....	301
6.3.5	Correlation of Maximum Diagonal Crack Width to Capacity.....	301
<b>APPENDIX A Example Problem.....</b>		<b>303</b>
A.1	Overview.....	303
A.2	Deep Beam Design .....	307
A.2.1	Determination of Preliminary Truss Model .....	308
A.2.2	Shear Region with an a/d Ratio Equal to 0.85 .....	309

A.2.2.1	Design of Region with $a/d = 0.85$ : Project 5253 Provisions .....	310
A.2.2.2	Design of Region with $a/d = 0.85$ : ACI 318-08 Appendix A .....	313
A.2.2.3	Design of Region with $a/d = 0.85$ : AASHTO LRFD.....	317
A.2.2.4	Comparison of Design Provisions for Shear Region with $a/d = 0.85$ .	319
A.2.2.5	Serviceability Behavior for Region with $a/d = 0.85$ .....	321
A.2.3	Shear Region with an $a/d$ Ratio Equal to 2.05 .....	322
A.2.3.1	Design of Region with $a/d$ Ratio Equal to 2.05: Project 5253 Method ....	324
A.2.3.2	Design of Region with $a/d$ Ratio Equal to 2.05: ACI 318-08 Appendix A .....	327
A.2.3.3	Design of Region with $a/d$ Ratio Equal to 2.05: AASHTO LRFD.....	330
A.2.3.4	Comparison of Design Provisions for Shear Region with $a/d = 2.05$ .	333
A.2.3.5	Serviceability Behavior for Region with $a/d = 2.05$ .....	335
A.3	Sectional Shear Design .....	336
A.3.1	Shear Region with $a/d$ Ratio Equal to 2.05 .....	337
A.3.1.1	ACI 318-08 §11.1, Shear Strength.....	337
A.3.1.2	AASHTO LRFD§5.8.3, Sectional Design Model (General Procedure) ...	338
A.3.2	Comparison of Deep Beam and Sectional Shear Provisions .....	340
A.4	Summary .....	341
<b>APPENDIX B Evaluation Database.....</b>		<b>344</b>
<b>APPENDIX C Project 5253 Crack Width Data.....</b>		<b>356</b>
<b>REFERENCES .....</b>		<b>363</b>
<b>VITA .....</b>		<b>370</b>



## LIST OF TABLES

Table 2.1: Summary of stress checks used to evaluate deep beams (Tuchscherer, 2008)	38
Table 2.2: Filtering of the deep beam ( $a/d \leq 2.5$ ) database.....	41
Table 3.1: Details of Series I specimens.....	53
Table 3.2: Details of Series II specimens.....	56
Table 3.3: Details of Series III specimens.....	59
Table 3.4: Details of Series IV specimens.....	61
Table 3.5: Details of Series M Specimens.....	63
Table 3.6: Summary of all beam details.....	66
Table 3.7: Concrete mixture design.....	69
Table 4.1: Summary of experimental results.....	93
Table 4.2: Tolerable widths of flexural cracks.....	101
Table 4.3: Assumptions made to plot minimum web reinforcement provisions.....	112
Table 4.4: Summary of strength results for specimens in minimum reinforcement task	119
Table 4.5: Amount of web reinforcement from several provisions used in current task	123
Table 4.6: Summary of diagonal cracking loads for specimens in minimum reinforcement task.....	134
Table 4.7: Strength results for depth effect specimens.....	167
Table 4.8: Diagonal cracking loads of depth effect specimens.....	184
Table 5.1: Comparison of calculated STM and sectional shear capacity for example problem in Appendix A.....	228
Table 5.2: Specimens used in correlating crack width-to-capacity (shaded tests not used) (1 of 2).....	276
Table 5.3: Summary of beam details for two specimens tested by Deschenes (2009)...	277
Table 5.4: Summary of test results for two specimens tested by Deschenes (2009).....	277
Table A.1. Shear Capacity of Original Cross-Section B ( $a/d = 2.05$ ).....	340
Table B.1: Evaluation Database.....	346
Table C.1: Measured crack width data for test specimens.....	357

## LIST OF FIGURES

Figure 2.1: Diagonal cracks in bent cap of bridge over Little Brazos River .....	6
Figure 2.2: Diagonal cracks in bent caps of an elevated roadway for DART .....	7
Figure 2.3: Diagonal cracks in I-345 straddle bent in Dallas, Texas .....	8
Figure 2.4: Post-tensioning retrofit of I-345 bent cap.....	8
Figure 2.5: Diagonal cracks in I-45 bent cap in Houston, Texas.....	9
Figure 2.6: Bearing wall retrofit of I-45 bent cap.....	10
Figure 2.7: Strain distribution in deep and slender portion of a beam.....	11
Figure 2.8: Examples of D-regions in several structures.....	13
Figure 2.9: One- and two-panel STM for deep beam .....	15
Figure 2.10: Most common node types in STM .....	16
Figure 2.11: Faces of sample CCT node.....	17
Figure 2.12: Hydrostatic and non-hydrostatic nodes (Thompson, 2002) .....	18
Figure 2.13: Examples of hydrostatic nodes.....	19
Figure 2.14: Non-hydrostatic proportions of CCC node .....	22
Figure 2.15: Non-hydrostatic proportions of CCT node.....	24
Figure 2.16: Non-hydrostatic proportions of CTT nodes .....	25
Figure 2.17: Longitudinal cracking and STM of bottle-shaped struts .....	26
Figure 2.18: Calculation of $\rho_{\perp}$ in ACI 318-08 Appendix A (ACI 318, 2008).....	31
Figure 2.19: Application of frustum to find $A_2$ from loaded area $A_1$ (ACI 318-08) .....	34
Figure 2.20: Stress condition at the back face of a CCT node due to: (a) bond stress; (b) bearing of an anchor plate; (c) interior node over a continuous support (Tuchscherer, 2008) .....	35
Figure 2.21: Single-panel STM and stress checks used to evaluate deep beams (Tuchscherer, 2008) .....	37
Figure 2.22: Evaluation of STM provisions with deep beam database (Tuchscherer, 2008) (N=179).....	39
Figure 2.23: Size and web reinforcement ratio of specimens in filtered database .....	43
Figure 3.1: Scaled comparison between actual bent caps and beams included in past research programs (Tuchscherer, 2008).....	48
Figure 3.2: Shear stress at failure for evaluation database used in specimen design.....	50
Figure 3.3: Difference between estimated shear and flexural capacity .....	50
Figure 3.4: Effective width of strut anchored by reinforcement at the CCT node .....	52
Figure 3.5: Series I beam details (Tuchscherer, 2008) .....	52
Figure 3.6: Series I: description of beam ID naming system (Tuchscherer, 2008) .....	53
Figure 3.7: Plate sizes investigated within Series II (Tuchscherer, 2008).....	54
Figure 3.8: Series II beam details (Tuchscherer, 2008).....	55
Figure 3.9: Series II: Description of beam ID naming system (Tuchscherer, 2008) .....	55
Figure 3.10: Definition for vertical and horizontal web reinforcement ratios.....	57
Figure 3.11: Series III beam details .....	58
Figure 3.12: Series III: Description of beam ID naming system .....	58

Figure 3.13: Series IV beam details.....	60
Figure 3.14: Series IV: Description of beam ID naming system.....	61
Figure 3.15: Series M beam details (Huizinga, 2007) .....	62
Figure 3.16: Series M - description of beam ID naming system .....	63
Figure 3.17: Comparison of beams sizes between current and past studies .....	64
Figure 3.18: Scaled comparison of actual bent caps and beams included in current and past research programs. (Tuchscherer, 2008) .....	64
Figure 3.19: Fabrication of a typical beam: (a) assembly of reinforcement cage (b) placement of cage in formwork (c) forms in place prior to concrete placement (d) placement of concrete (e) beam curing (f) test specimen after the removal of forms (Tuchscherer, 2008) .....	71
Figure 3.20: Fabrication of a 21"x75" beam: (a) movement of reinforcement cage into formwork (b) placement of concrete into steel formwork .....	72
Figure 3.21: Fabrication of a 36"x48" beam: (a) tied reinforcement cage with steel ducts (b) placement of concrete into wooden formwork (Huizinga, 2007) .....	73
Figure 3.22: Installation of strong floor: (a) steel platen (b) floor excavation (c) fabrication of platen support (d) lowering of platen into position, and (e) test setup (Tuchscherer, 2008).....	75
Figure 3.23: Elevation view of test setup (Huizinga, 2007) .....	76
Figure 3.24: Section view of test setup .....	77
Figure 3.25: 21"x23" specimen in test setup .....	78
Figure 3.26: Installation of strain gauge on mild reinforcement (Tuchscherer, 2008) .....	79
Figure 3.27: Typical internal strain gauge locations for Series III and IV .....	80
Figure 3.28: Load cells placed on each reaction rod .....	81
Figure 3.29: Location and picture of linear potentiometers.....	82
Figure 3.30: Diagram of beam displacements due to rigid body motion and flexural and shear deformations early in the test (Tuchscherer, 2008).....	83
Figure 3.31: Diagram of beam displacements due to rigid body motion and flexural and shear deformations after all reaction nuts are engaged.....	83
Figure 3.32: Example of crack width measurement technique.....	84
Figure 3.33: Each end of a beam is loaded to failure resulting in two tests: (a) shear failure in Test Region A (b) and shear failure in Test Region B with external post-tensioned clamps in Test Region A (Tuchscherer, 2008) .....	86
Figure 3.34: Hydraulic ram was not moved for 75-inch specimens: (a) shear failure in Test Region A (b) shear failure in Test Region B with external post- tensioned clamps in Test Region A .....	88
Figure 3.35: a). Location of test region pictures. b). Picture of failure of test region rotated to orient cracks like that of conventional simple beam test.....	89
Figure 4.1: Free-body and shear force diagram for typical test (Tuchscherer, 2008) .....	96
Figure 4.2: Visual and experimental determination of diagonal cracking load (Tuchscherer, 2008) .....	99
Figure 4.3: Sample crack width data for all series.....	100

Figure 4.4: Estimate of service load as a function of experimental capacity .....	102
Figure 4.5: Deep beam showing nomenclature for Equation 4.2 .....	106
Figure 4.6: Min. horizontal reinforcement for deep beams in several specifications .....	111
Figure 4.7: Minimum vertical reinforcement for deep beams in several specifications .....	111
Figure 4.8: Effect of horiz. reinforcement on strength of beams in evaluation database .....	114
Figure 4.9: Effect of vert. reinforcement on strength of beams in evaluation database .....	114
Figure 4.10: Effect of vertical web reinforcement on strength after first cracking .....	116
Figure 4.11: Effect of horizontal web reinforcement on strength after first cracking .....	117
Figure 4.12: Crack development in specimen without web reinforcement, III-1.85-0...	120
Figure 4.13: Crack development in specimen with 0.3% in each direction, III-1.85-03b .....	122
Figure 4.14: Strength results of Series III and IV specimens at a/d ratio of 1.85 .....	124
Figure 4.15: Strength results comparison of III-1.85-01 and III-1.85-03 .....	125
Figure 4.16: Strength results with web reinforcement as variable from Series M .....	127
Figure 4.17: Strength results with web reinforcement as variable from Series I .....	128
Figure 4.18: Strength results from specimens tested at a/d ratio of 1.2 .....	129
Figure 4.19: Crack development in III-2.5-0 .....	130
Figure 4.20: Strength results from specimens tested at an a/d ratio of 2.5 .....	131
Figure 4.21: Effect of vertical reinforcement on the diagonal cracking load .....	132
Figure 4.22: Effect of horizontal reinforcement on the diagonal cracking load .....	133
Figure 4.23: Diagonal cracking loads of specimens in current task .....	136
Figure 4.24: Maximum diagonal crack width for 6 - 21"x42" specimens tested at a/d of 1.85 .....	138
Figure 4.25: Crack patterns of four specimens at approximately 90% of capacity .....	140
Figure 4.26: Maximum diagonal crack width for 8 - 21"x42" specimens tested at a/d of 1.85 .....	141
Figure 4.27: Maximum diagonal crack widths of 8 - 21"x42" specimens versus applied shear .....	142
Figure 4.28: Max. crack widths for 21"x75" specimens with 0.2% and 0.3% reinf. ....	143
Figure 4.29: Max. crack widths for 36"x48" specimens with 0.2% and 0.3% reinf. ....	143
Figure 4.30: Max. crack widths for 21"x44" specimens with 0.2% or 0.3% 2-legged reinf. ....	144
Figure 4.31: Max. crack widths for 21"x44" specimens with 0.2% or 0.3% 4-legged reinf. ....	144
Figure 4.32: Maximum diagonal crack width data for all comparable specimens at a/d of 1.85 .....	145
Figure 4.33: Maximum diagonal crack widths of specimens tested at an a/d ratio of 1.2 .....	147
Figure 4.34: Maximum diagonal crack widths of specimens tested at an a/d ratio of 2.5 .....	147
Figure 4.35: Effect of stirrup spacing on crack width for specimens with 0.2% reinf. ..	149
Figure 4.36: Effect of stirrup spacing on crack width for specimens with 0.3% reinf. ..	149

Figure 4.37: Comparison of AASHTO LRFD (2008) and proposed minimum reinforcement .....	151
Figure 4.38: Proposed minimum web reinforcement requirements in AASHTO LRFD .....	153
Figure 4.39: Size effect strength results from Walraven and Lehwalter (1994).....	157
Figure 4.40: Size effect strength results from Tan and Lu (1999).....	158
Figure 4.41: Size effect strength results from Matsuo et al. (2001) .....	159
Figure 4.42: Size effect strength results from Zhang and Tan (2007) .....	160
Figure 4.43: FEM results in which bearing plate sizes increased with increasing member depth (Zhang and Tan, 2007).....	161
Figure 4.44: FEM results in which bearing plate sizes were constant with increasing member depth (Zhang and Tan, 2007).....	162
Figure 4.45: Bearing plate dimensions in several TxDOT bent caps (TxDOT, 2008)...	164
Figure 4.46: Relative size of nodal regions for depth effect specimens .....	165
Figure 4.47: Relative size of nodal regions in depth effect specimens (2) .....	166
Figure 4.48: Strength results of depth effect specimens at a/d of 1.85 .....	168
Figure 4.49: Failure photographs for depth effect specimens with a/d of 1.85 and 0.2% reinforcement .....	169
Figure 4.50: Strength results of all depth effect specimens .....	170
Figure 4.51: Failure photographs of depth effect specimens with a/d of 1.2.....	171
Figure 4.52: Failure photographs of depth effect specimens with a/d of 2.5.....	173
Figure 4.53: Experimental strength of depth effect specimens normalized by calculated strength.....	175
Figure 4.54: Strength results of size effect specimens with a/d of 2.5 .....	177
Figure 4.55: Level of conservatism in sectional shear provisions for specimens with a/d of 2.5 .....	178
Figure 4.56: Ultimate shear capacity (kips) of size effect specimens.....	179
Figure 4.57: Diagonal cracking loads of size effect specimens in literature .....	180
Figure 4.58: Diagonal cracking loads of size effect specimens in literature (function of ultimate) .....	182
Figure 4.59: Service loads (diagonal crack width = 0.012 in.) as function of ultimate for size effect specimens in literature .....	183
Figure 4.60: Normalized diagonal cracking loads for the depth effect specimens .....	185
Figure 4.61: Diagonal cracking loads normalized by ultimate strength for depth effect tests .....	187
Figure 4.62: Maximum diagonal crack widths for depth effect specimens with an a/d ratio of 1.2 .....	188
Figure 4.63: Maximum diagonal crack widths for depth effect specimens with an a/d ratio of 1.85 and 0.2% web reinforcement .....	188
Figure 4.64: Maximum diagonal crack widths for depth effect specimens with an a/d ratio of 1.85 and 0.3% web reinforcement .....	189
Figure 4.65: Maximum diagonal crack widths for depth effect specimens with an a/d ratio of 2.5 .....	189

Figure 5.1: Strain trajectories in an asymmetrically-loaded beam .....	195
Figure 5.2: Discontinuity in calculated shear capacity in AASHTO LRFD 2008 at a/d of 2.....	196
Figure 5.3: Proposed shear-strength envelope by Kani et al. (1979).....	198
Figure 5.4: Effect of a/d ratio on experimental strength of test specimens .....	201
Figure 5.5: Failure pictures of test specimens with 0.2% reinforcement and variable a/d .....	203
Figure 5.6: Failure pictures of test specimens with 0.3% reinforcement and variable a/d .....	205
Figure 5.7: Distribution of force in longitudinal tension steel along length of beam according to different shear models.....	207
Figure 5.8: Comparison of measured and calculated strain along the length of specimen with a/d of 1.85 .....	208
Figure 5.9: Comparison of measured and calculated strain along length of specimen with a/d of 1.2 and 2.5.....	210
Figure 5.10: Experimental strength divided by calculated strength for depth effect specimens.....	213
Figure 5.11: Difference in node geometry with increasing a/d ratio for single-panel STM .....	215
Figure 5.12: Level of conservatism in STM provisions with increasing a/d ratio.....	216
Figure 5.13: Free-body diagram used as basis for sectional shear model .....	218
Figure 5.14: Level of conservatism in sectional shear provisions with increasing a/d ratio .....	222
Figure 5.15: Level of conservatism in sectional shear provisions for a/d ratios between 2 and 2.5.....	223
Figure 5.16: Comparison of calculated capacity: Project 5253 STM vs. sectional shear.....	225
Figure 5.17: Reduction in discrepancy in shear capacity at a/d ratio of 2 with Project 5253 STM provisions.....	227
Figure 5.18: Types of cracks in reinforced concrete deep beams .....	231
Figure 5.19: First pictures taken after the formation of first diagonal crack in several tests .....	232
Figure 5.20: Stress trajectories in B-regions (Bernoulli) and in D-regions (discontinuity) .....	234
Figure 5.21: Effect of shear area on the diagonal cracking load of beams in evaluation database.....	236
Figure 5.22: Effect of tensile strength on diagonal cracking load of deep beams in database.....	238
Figure 5.23: Effect of a/d ratio on diagonal cracking load of deep beams in database ..	240
Figure 5.24: Effect of longitudinal reinforcement ratio on diagonal cracking load of beams in the database.....	241
Figure 5.25: Effect of longitudinal reinforcement ratio on diagonal cracking load of beams with the same a/d ratio .....	241

Figure 5.26: Effect of depth on the diagonal cracking load of beams in the evaluation database.....	243
Figure 5.27: Effect of depth on the diagonal cracking load of deep beams in testing program.....	243
Figure 5.28: Effect of web reinforcement on the diagonal cracking load of similarly sized deep beams.....	245
Figure 5.29: Comparison of measured and estimated diagonal cracking loads – ACI Eq. 11-5 .....	247
Figure 5.30: Comparison of measured and estimated diagonal cracking loads – Zsutty Equation .....	249
Figure 5.31: Comparison of measured and estimated cracking loads – Shin et al. Equation .....	251
Figure 5.32: Comparison of measured and estimated cracking loads – AASHTO $V_{ci}$ ..	254
Figure 5.33: Diagonal cracking loads for nominally-identical specimens .....	255
Figure 5.34: Development of proposed equation for a conservative estimate of diagonal cracking.....	256
Figure 5.35: Types of cracks in reinforced concrete deep beams.....	263
Figure 5.36: Effect of transverse reinforcement on width of diagonal cracks (Bracci et al., 2000) .....	266
Figure 5.37: Effect of a/d ratio on maximum width of diagonal cracks (Kong et al., 1970) .....	267
Figure 5.38: Effect of a/d ratio on maximum diagonal crack width (Smith and Vantsiotis, 1982) .....	268
Figure 5.39: Preliminary analytical model for estimating diagonal crack widths .....	271
Figure 5.40: Effect of web reinforcement on diagonal crack widths of test specimens .	278
Figure 5.41: Effect of a/d ratio on maximum diagonal cracking widths, 3 specimens, 0.3% reinf.....	280
Figure 5.42: Effect of a/d ratio on maximum diagonal crack widths, 9 specimens, 0.3% reinf. ....	281
Figure 5.43: Effect of a/d ratio on maximum diagonal crack widths, 2 specimens, 0.2% reinf. ....	282
Figure 5.44: Effect of a/d ratio on maximum diagonal crack widths, 11 specimens, 0.2% reinf. ....	282
Figure 5.45: Effect of longitudinal reinforcement on diagonal cracks in shear-critical members.....	284
Figure 5.46: All crack width data used in this task with trend lines.....	286
Figure 5.47: All crack width data used in this task with multiple straight line approximations.....	287
Figure 5.48: Proposed chart that links diagonal crack width to percent of capacity of deep beams .....	288
Figure 5.49: Comparison of crack width data from Bracci et al. (2000) and chart estimates.....	289

Figure 5.50: Comparison of data from specimens tested at $a/d$ of 1.2 and chart estimates .....	291
Figure 6.1: Diagonal cracks in I-45 bent cap in Houston, Texas.....	297
Figure A.1: I-45 over Greens Road Bent Cap.....	304
Figure A.2: Preliminary plan; elevation; and cross-sectional details at critical shear regions.....	305
Figure A.3: Strut-and-tie model with AASHTO LRFD (2008) factored loads. ....	308
Figure A.4: Critical strut in region with $a/d$ equal to 0.85 (AASHTO LRFD factored loads).....	309
Figure A.5: Determination of Triaxial Confinement Factor .....	310
Figure A-6. Strut proportions associated with an increase in overall depth of 18 in. and increase in back face of Node A of 2.5 in. (ACI 318-08 load factors) .....	316
Figure A.7: Comparison of required cross-section per the Project 5253 method, ACI 318-08, and AASHTO LRFD: $a/d$ ratio = 0.85.....	320
Figure A-8. Critical strut in region with $a/d = 2.05$ . ....	323
Figure A-9: Strut proportions and forces associated with a 6-inch increase in depth of bent.....	326
Figure A.10: Strut proportions and forces associated with a 25-inch increase in bent height and 6-inch increase in depth of Node E (ACI 318 factored loads). ....	329
Figure A.11: Strut proportions and forces associated with a 35-inch increase in bent depth and 10.5-inch increase in depth of Node E (AASHTO LRFD factored loads).....	332
Figure A.12: Comparison of required cross-section per the Project 5253 method, ACI 318-08, and AASHTO LRFD (2007): $a/d$ ratio = 2.05.....	334



# CHAPTER 1

## Introduction

### 1.1 OVERVIEW

A reinforced concrete member in which the total span or shear span is exceptionally small in relation to its depth is called a deep beam. Some examples of deep beams include bridge bent caps, transfer girders, and pile caps. In Texas, several reinforced concrete bent caps have developed significant diagonal cracks in service. The cracking was so extensive in two cases that costly retrofits were implemented to strengthen the structures (Section 2.2). The Texas Department of Transportation was interested in determining the cause of the cracking, in developing methods to quantify distress in reinforced concrete bent caps, and in refining strength and serviceability design provisions for reinforced concrete bent caps and other deep beams.

Historically, reinforced concrete deep beams were designed with empirical methods or simple approximations. Within the last decade, strut-and-tie modeling has become the preferred method for designing deep beams in U.S. design specifications, such as the Bridge Design Specifications of the American Association of State and Highway Transportation Officials (AASHTO LRFD, 2008) and the Building Code Requirements for Structural Concrete of the American Concrete Institute (ACI 318-08). Designers have expressed concern with the freedom associated with the strut-and-tie method, with overly conservative estimates of strength calculated using strut-and-tie models (STMs), with the lack of serviceability-related considerations in the strut-and-tie method, and with overall inconsistencies between STM provisions in different codes.

The field problems of bridge bent caps and the concerns associated with using strut-and-tie model provisions for bent cap design were the primary reasons that TxDOT funded Project 5253. Eight objectives related to these concerns were addressed within this project (Section 1.2).

To accomplish the eight objectives of this study, an extensive experimental program was conducted. Thirty-seven (37) tests on reinforced concrete beams were performed in the Phil M. Ferguson Structural Engineering Laboratory at the University of Texas at Austin. To meet the objectives of this study and to best improve the design and performance of actual bent caps, it was necessary to test specimens that were of comparable size to typical bent caps in Texas. The specimens tested within TxDOT Project 5253 are among the largest deep beams ever reported in the literature.

To supplement the experimental program, a database of deep beam test results was compiled from the available literature. The database was an expansion of a database originally compiled by Brown et al. (2006). The total number of deep beam test results (shear-span-to-depth ratio ( $a/d \leq 2.5$ ) in the database is 905 (including 37 tests from the Project 5253 experimental program). Entries in the database that lacked sufficient information to perform a strut-and-tie analysis and that did not meet established cross-sectional size or web reinforcement criteria were filtered from the database (Section 2.4). The use of the database in conjunction with the Project 5253 experimental program enabled each objective to be addressed from both broad and specific viewpoints.

## **1.2 PROJECT OBJECTIVES AND SCOPE**

The eight tasks addressed in TxDOT Project 5253 are:

- (1). Determine the influence of the distribution of stirrups across the width of a beam web on the strength and serviceability behavior of a deep beam.
- (2). Determine the influence of singular nodes triaxially confined by concrete on the strength and serviceability behavior of a deep beam.
- (3). Determine an appropriate amount of minimum web reinforcement (stirrups and longitudinal side face reinforcement) considering the strength and serviceability demand of a deep beam.
- (4). Determine the influence of member depth on the strength and serviceability behavior of a deep beam.

- (5). Develop a simple STM design methodology, including node proportioning techniques, allowable stresses, and applicable design checks, for the design of deep beams.
- (6). Develop a means to reduce the discrepancy between shear strength calculated using STM and sectional shear provisions at an  $a/d$  ratio of 2.
- (7). Develop a means to mitigate the formation of diagonal cracks under service loads.
- (8). Develop a means to relate the maximum diagonal crack width of a deep beam to its residual capacity for field assessment of diagonally-cracked bent caps.

In this dissertation, the results of five of the eight tasks are presented in detail. Minimum web reinforcement requirements and the influence of member depth on deep beams are evaluated (Tasks 3 and 4). In addition, the tasks of reducing the discrepancy between shear strength calculated using STM and sectional shear provisions near an  $a/d$  ratio of 2, of limiting diagonal cracking under service loads, and of correlating maximum diagonal crack width to the residual capacity of a deep beam are addressed as well (Tasks 6, 7, and 8). The results of the other tasks (1, 2, and 5) are presented by Tuchscherer (2008). Since the proposed STM design provisions (Task 5) are used to calculate deep beam capacity throughout this dissertation, they are presented and compared to those in AASHTO LRFD (2008) and ACI 318-08 Appendix A in Section 2.3.4.

### **1.3 ORGANIZATION**

Three topics are addressed in Chapter 2. Details of several bent caps that developed diagonal cracks in service and of the filtering of the deep beam database is presented. In addition, background information on strut-and-tie modeling including a comparison of the STM design provisions of AASHTO LRFD (2008), ACI 318-08, and Project 5253 is provided. In Chapter 3, the experimental program including the design, fabrication, and testing of the specimens is described. Experimental test results detailing the effect of minimum web reinforcement and of member depth on the strength and

serviceability of deep beams are discussed with appropriate design recommendations in Chapter 4. In Chapter 5, the results of the remaining three tasks are provided. Design provisions that reduce the difference in shear capacity calculated with STM and sectional shear provisions at the transition between deep beam and slender beam behavior ( $a/d = 2$ ) are presented in Section 5.2. A service load design check is outlined to limit the formation of diagonal cracks in service in Section 5.3. Lastly, a simple means of relating the maximum diagonal crack width in a deep beam to its capacity is detailed in Section 5.4. The conclusions for each task addressed within this dissertation are summarized in Chapter 6. An example problem prepared by Tuchscherer (2008) is included in Appendix A to illustrate several of the deep beam design recommendations proposed within Project 5253. In Appendix B, the beam details of the specimens in the evaluation database are listed. In Appendix C, diagonal crack width data from all of the specimens tested within Project 5253 are presented.

## **CHAPTER 2**

### **Background Information**

#### **2.1 OVERVIEW**

In this chapter, three topics are addressed. First, several cases of diagonally-cracked bent caps in service are presented. The costly retrofits of two structures with extensive diagonal cracking were one of the major incentives to fund the current project. Next, background information on deep beam behavior and strut-and-tie modeling is provided. The purpose of this section is to introduce strut-and-tie modeling concepts and design provisions that are used throughout this dissertation. Lastly, a description of a database of deep beam test results is discussed. This database was used in conjunction with the data obtained in the experimental program to address the objectives of TxDOT Project 5253.

#### **2.2 FIELD PROBLEMS**

Diagonal cracks have been observed in several reinforced concrete bent caps in service throughout the state of Texas. While flexural cracking is expected in reinforced concrete members, diagonal cracking is less desirable. It is necessary to limit crack widths for aesthetic and durability considerations. More importantly, extensive diagonal cracking may indicate that the member is structurally inadequate. Providing insight into the cause of the cracking, considering both strength and serviceability deficiencies, was one of the overall goals of this study.

The diagonally-cracked bent caps of two structures are presented in Figure 2.1 and Figure 2.2. A bent cap supporting a two-lane elevated roadway bridge over the Little Brazos River near Hearne, Texas on FM 485 is illustrated in Figure 2.1. Several of the numerous bent caps in this structure had diagonal cracks extending from the exterior girder supports to the exterior columns of the bent cap. In general, the maximum width

of the diagonal cracks was small ( $\leq 0.016$  in.). In Figure 2.2, a bent cap supporting an elevated portion of the Dallas Area Rapid Transit (DART) rail line is shown. Several hammerhead bent caps in this structure exhibited parallel, diagonal cracks extending from the girder supports towards the bent cap column. The maximum width of the cracks in this structure was also small in general ( $\leq 0.016$  in.). To the knowledge of the author, no retrofits were required for either structure.

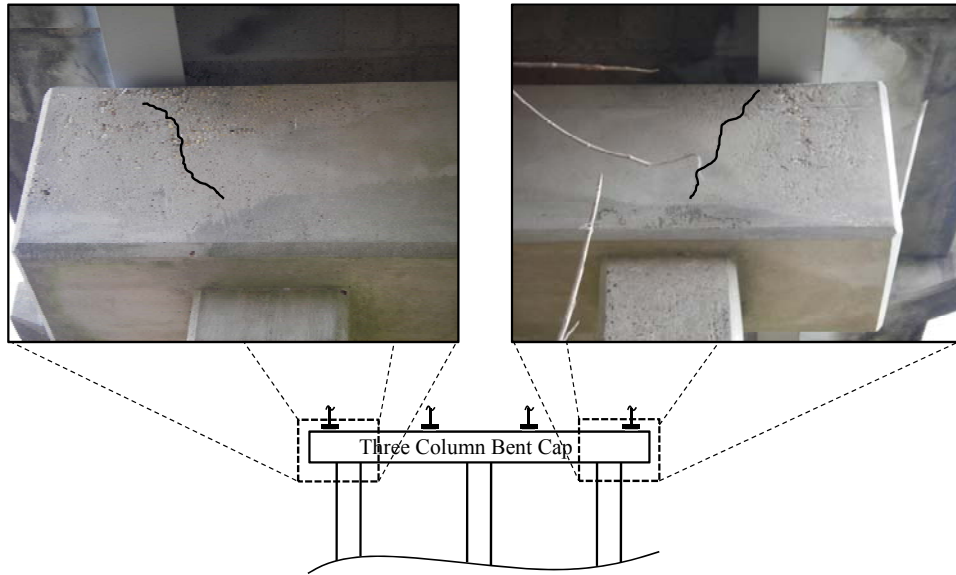


***Figure 2.1: Diagonal cracks in bent cap of bridge over Little Brazos River***

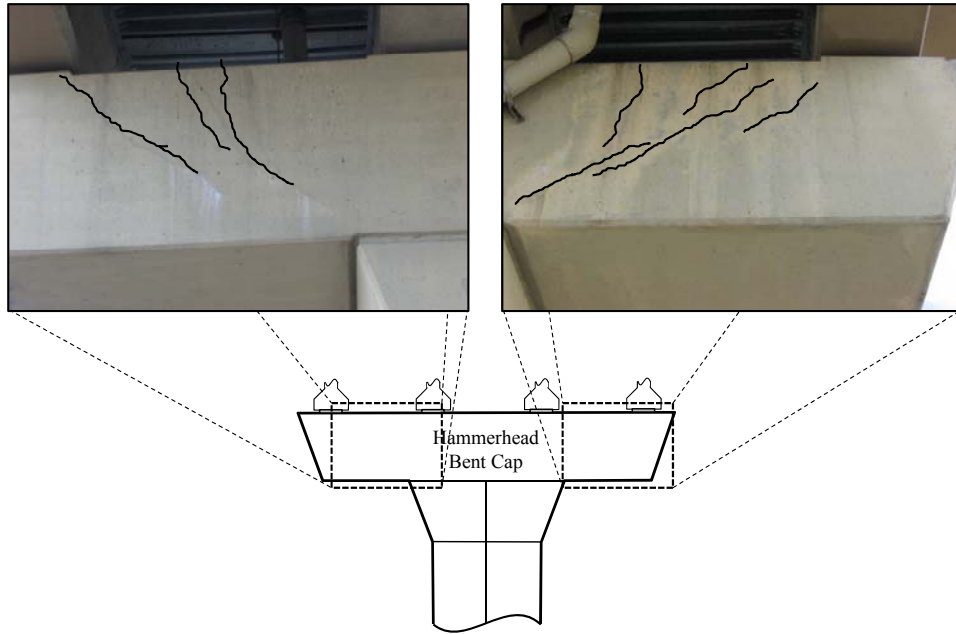


***Figure 2.2: Diagonal cracks in bent caps of an elevated roadway for DART***

In two other cases, costly retrofits were implemented to increase the strength of bent caps with extensive diagonal cracking. A large, straddle bent cap supporting I-345 (extension of US 75) in downtown Dallas, Texas had parallel, diagonal cracks extending from the column to the pot bearing of a haunched, steel plate girder (Figure 2.3). The maximum width of the cracks in the 10 ft. deep member was approximately 0.035 in. Due to the width of the cracks, the beam was strengthened with external post-tensioning as shown in Figure 2.4. The post-tensioning introduced compression into the member and provided an uplift force at the bottom of the member beneath the bearing for the plate girder. The total cost of the retrofit was approximately \$200,000.

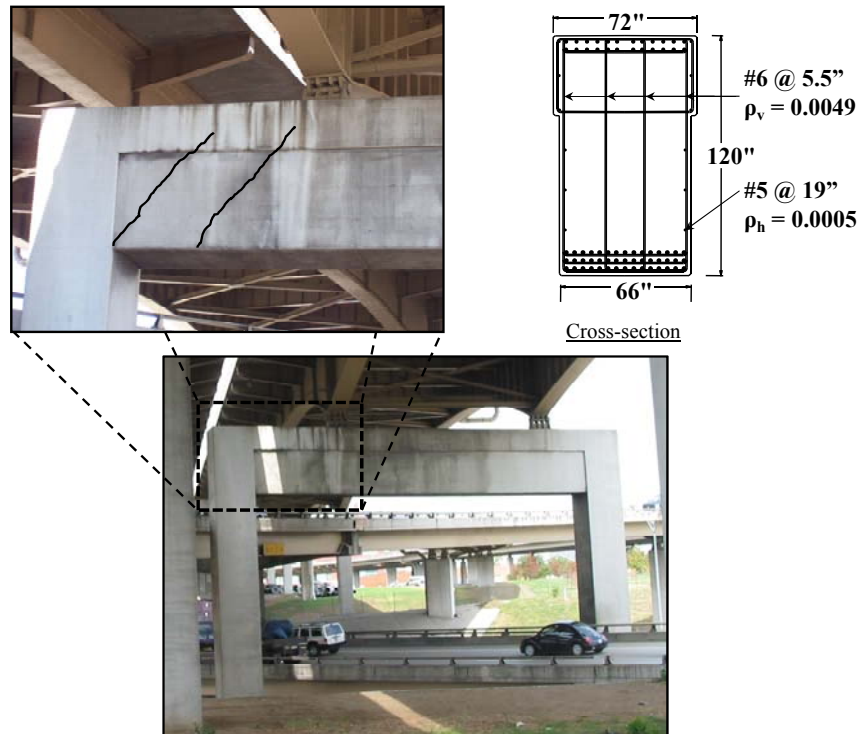


**Figure 2.3: Diagonal cracks in I-345 straddle bent in Dallas, Texas**



**Figure 2.4: Post-tensioning retrofit of I-345 bent cap**



All of the bent caps in a wide overpass of I-45 across Greens Road in Houston, Texas experienced extensive diagonal cracking in service. The overpass contained two- and three-column haunched, bent caps supporting steel, trapezoidal box girders. The widespread cracking in one of the three-column bent caps is illustrated in Figure 2.5. Due to the large width (approximately 0.035 in.) and extensive nature of the cracking, all of the bent caps in the overpass were strengthened. Reinforced concrete walls were cast beneath the bent caps to distribute the loads from the overpass directly to drilled shafts beneath the columns without beam action (Figure 2.6). Care was taken to ensure a positive connection between the underside of the bent cap and the newly-cast wall. The diagonal cracks were also injected with epoxy. The cost of retrofitting all of the bent caps in this overpass was approximately \$300,000.

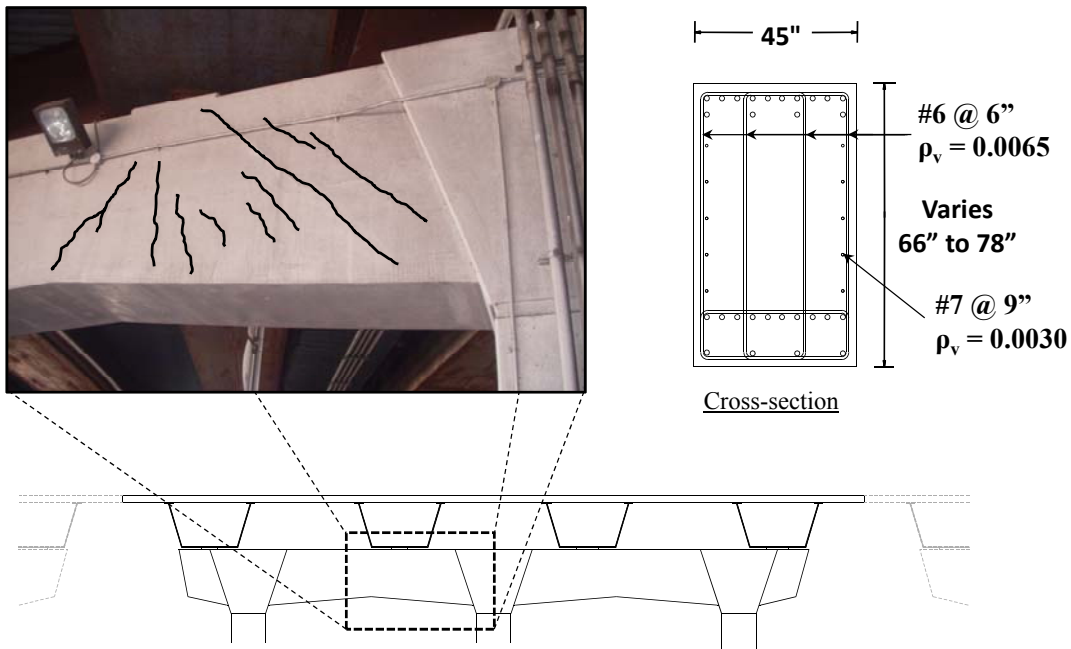


**Figure 2.5: Diagonal cracks in I-45 bent cap in Houston, Texas**



**Figure 2.6: Bearing wall retrofit of I-45 bent cap**

The aforementioned cases of diagonally-cracked bent caps in service were one of the reasons for the funding of this project (TxDOT Project 5253). Insight into the cause of cracking – whether it was the result of strength or serviceability deficiencies, or a combination of both – was desired by TxDOT engineers. Furthermore, improved design provisions for reinforced concrete bent caps to prevent this problem from reoccurring in the future were sought after.

## **2.3 STRUT-AND-TIE MODELING FOR DEEP BEAMS**

### **2.3.1 What is a Deep Beam?**

Deep beams are defined by MacGregor (1997) as follows:

*...a beam in which a significant amount of load is carried to the supports by a compression thrust joining the load and the reaction. This occurs if a concentrated load acts closer than about  $2d$  to the support, or for uniformly loaded beams with a span-to-depth ratio,  $l_n/d$ , less than about 4 to 5.*

where,

$d$  is the depth of the member

$l_n$  is the total span of the member

$a$  is the distance between a concentrated load and the reaction

Thus, a deep beam is characterized by the ratio of the loading arm (centerline distance between the load and the reaction ( $a$ )) or total span ( $l_n$ ) to the depth of the member ( $d$ ). The basis for this definition is that within a distance of ‘ $d$ ’ from a disturbance such as a concentrated load or support, the strain distribution in the member is nonlinear (St. Venant’s principle, Schlaich et al., 1987). Plane sections do not remain plane. Regions of nonlinear strain distribution along the height of the cross-section are called D-regions where ‘D’ stands for discontinuity or disturbed. Regions of linear strain distribution are called B-regions where ‘B’ stands for Bernoulli or beam. The B- and D-regions of an asymmetrically-loaded beam are shown in Figure 2.7 with the principle strain trajectories.

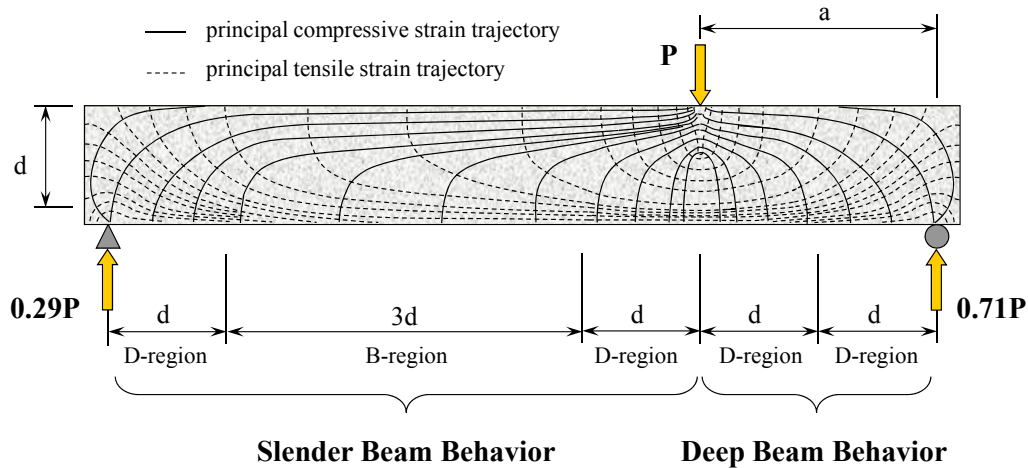


**Figure 2.7: Strain distribution in deep and slender portion of a beam**

In Figure 2.7, the portion of the beam to the right of the concentrated load is comprised entirely of D-regions and meets the deep beam definition given by MacGregor (1997). Since section-based approaches are not valid where plane sections do not remain plane, this region would be designed with empirical models, past experience, nonlinear

analyses, or most recently, by using strut-and-tie models. The portion of the beam to the left of the concentrated load would be categorized by slender beam behavior and would be designed with section-based models. The D-regions to the left of the applied load and at the left support could be designed with strut-and-tie models. However, this portion of the member is generally controlled by flexure with low levels of shear. As a result, only stresses at the bearing locations would be checked in conjunction with sectional design.

As in the definition by MacGregor (1997), a deep beam is often categorized by the ratio of the shear span or loading arm for a concentrated load ('a' in Figure 2.7) to the effective member depth 'd.' In AASHTO LRFD 2008 and ACI 318-08, beams or components are considered deep when the shear-span-to-depth ratio (a/d ratio) is less than or equal to 2. Some researchers suggest that deep beam behavior can exist to an a/d ratio of 2.5 (Kani et al., 1979). Throughout this dissertation reinforced concrete deep beam behavior will be defined by the a/d ratio. The effect of a/d ratio on the behavior of deep beams is addressed specifically in Section 5.2.2.

Examples of deep beams in practice include bent caps, pile caps, transfer girders, and some walls, among others.

### **2.3.2 Overview of Strut-and-Tie Modeling**

Strut-and-tie modeling is a design procedure for structural concrete that replaces complex states of stress with simple, uniaxial stress paths (Schlaich et al., 1987). The flow of forces through a structure is modeled with a collection of compression elements (struts) and tension elements (ties). The intersection of struts and ties are called nodes. The collection of struts, ties, and nodes is considered to be a strut-and-tie model (STM).

Strut-and-tie modeling is based on the lower bound theory of plasticity. The theory states that if equilibrium and yield conditions are satisfied, a lower bound estimate of capacity is obtained (Nielson, 1998). External equilibrium and equilibrium at each node in a STM is satisfied with statics and an acceptable arrangement of struts and ties, respectively. The yield condition of each strut, tie, and face of a node are satisfied with the comparison of allowable and applied stresses. Allowable stresses for each element of

a STM (struts, ties, and each face of a node) are obtained from empirical relationships presented in design specifications. The applied stresses on each element are calculated from the internal forces in the STM and assumed dimensions of the elements that are proportioned using accepted guidelines. Compatibility constraints are not directly considered in strut-and-tie modeling since they are not required in the lower bound theory of plasticity and since complicated nonlinear strain distributions generally exist.

One of the primary advantages of strut-and-tie modeling is its widespread applicability. In theory, any structural concrete member can be represented by a truss model of compression and tension elements and designed with strut-and-tie modeling principles. However, in cases where flexural theory and section-based design approaches are valid, the use of strut-and-tie modeling is generally too complicated. It is most useful for applications where complicated states of stress exist such as deep beams, corbels, dapped-ends, post-tensioned anchorage zones, or other structural components with loading or geometric discontinuities. Some examples of structures with D-regions are provided in Figure 2.8.

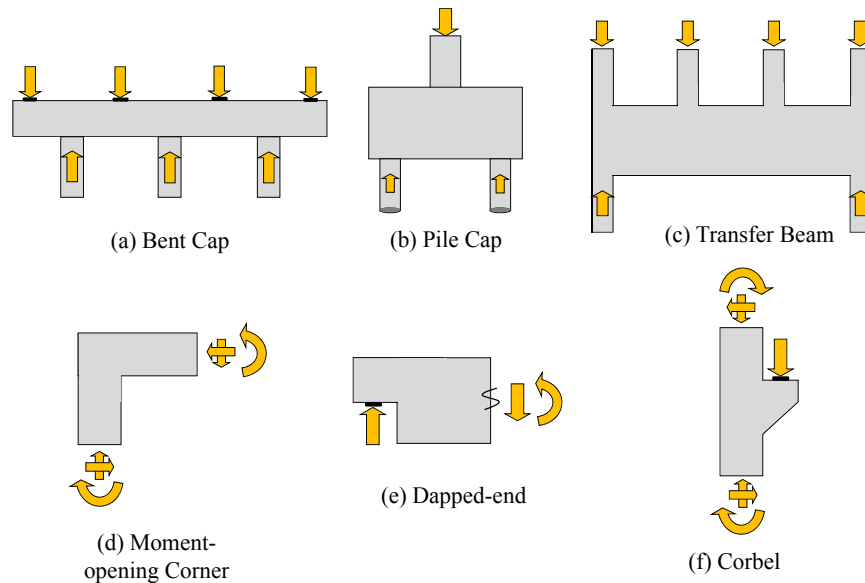


**Figure 2.8: Examples of D-regions in several structures**

Another advantage of strut-and-tie modeling is its inherent conservatism. In theory, conservatism is guaranteed through the fulfillment of equilibrium and yield constraints according to the lower bound theory of plasticity. However, there are a few additional requirements. It is assumed that there is enough deformation (or plastic-redistribution) capacity such that the forces in the actual structure can be distributed according to the assumed model. Wide cracks may develop as a result of the plastic redistribution of forces since compatibility constraints are not considered within the design procedure. Potential compatibility problems are avoided with empirical guidelines such as limits on angles between struts and ties and minimum reinforcement requirements. In addition, the elements of the STM can be aligned according to the elastic stress distribution as recommended by Schlaich et al. (1987). Detailing requirements must also be met for a conservative solution. Sufficient anchorage for tie reinforcement and adequate transverse tensile capacity of compressive struts are required to develop the full design strength of these elements.

Two STMs for the beam depicted in Figure 2.7 are provided in Figure 2.9. In both examples, the portions of the model to the left of the applied load are identical. As noted previously, this portion of the beam would be designed with section-based methods. However, for illustrative purposes, it is interesting to note that the elements of the STM in the slender portion of the beam match well with the known stress distribution. That is, a compression chord exists along the top of the member and a tension chord exists on the bottom. Vertical ties or stirrups resist the shear in the span. Two different models are shown to the right of the applied load. The first model is called a single- or one-panel model; the second is called a multiple- or two-panel model. Either model (or a combination of the two) is acceptable provided that equilibrium and yield conditions are met. The choice of the model is left to the designer. To avoid compatibility problems and for efficiency, it is good practice for the STM to agree well with the dominant mechanism of force transfer in the structure. For structural components in which the dominant transfer mechanism is unknown, it may be beneficial to perform a linear finite element analysis, to research experimental test results, or to provide redundancy by

overlapping several STMs. Using overlapping strut-and-tie models is a technique to provide redundancy to the structure by enabling multiple force paths for the applied loads. However, it is necessary to check stresses in defined nodal regions from the total applied load. The choice between single- and two-panel models for deep beams is addressed specifically in Section 5.2.2 of this dissertation.

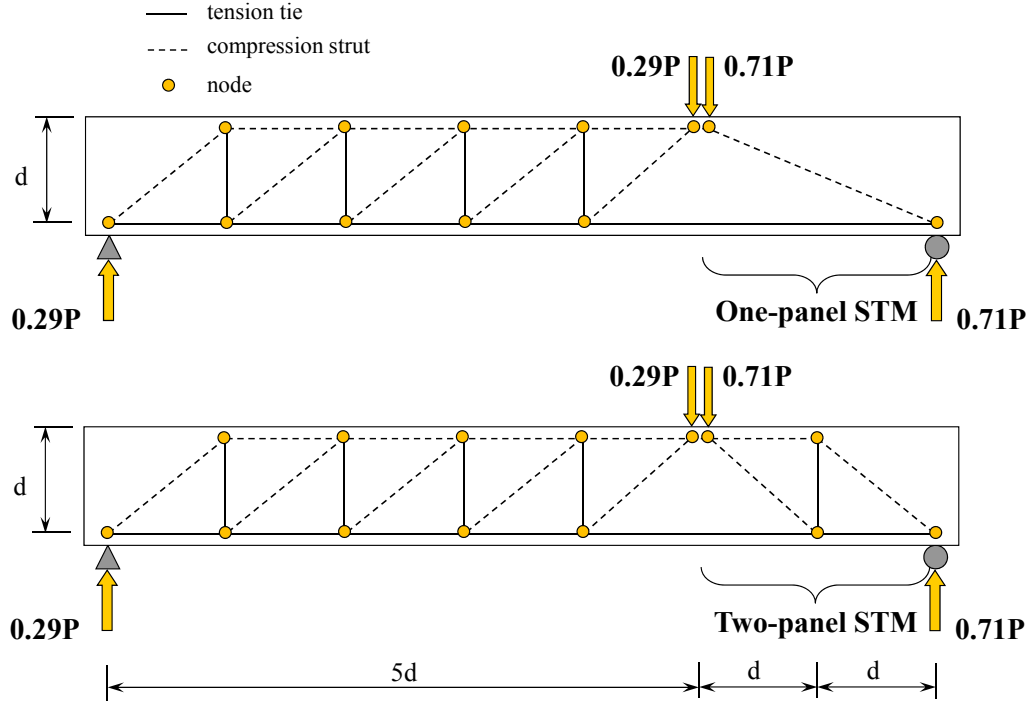


**Figure 2.9: One- and two-panel STM for deep beam**

It is important to note that the diagonal struts in the deep beam STMs in Figure 2.9 were not modeled as bottle-shaped struts for simplicity. Bottle-shaped struts are defined and discussed in Section 2.3.3.2 of this chapter.

Additional background information on strut-and-tie modeling can be found in several references (Schlaich et al., 1987, Bergmeister et al., 1993, Collins and Mitchell, 1997, and *fib*, 1999).

### 2.3.3 Elements of Strut-and-Tie Modeling

#### 2.3.3.1 Nodes

A node is labeled by the number of struts and ties framing into it. For instance, if three compression struts frame into one node, that node is labeled a CCC node ('C' for compression). If two compression struts and one tension tie frame into a node, that node is labeled a CCT node ('T' for tension). The same is true for CTT and TTT nodes. If more than three elements frame into a node at different angles, similar elements can be combined into one, acting at the resultant angle. Examples of CCC, CCT, and CTT nodes are provided in Figure 2.10. A node generally has three in-plane faces that have individual capacities: the bearing face, the vertical back face, and the node-to-strut interface. A CCT node is enlarged in Figure 2.11.

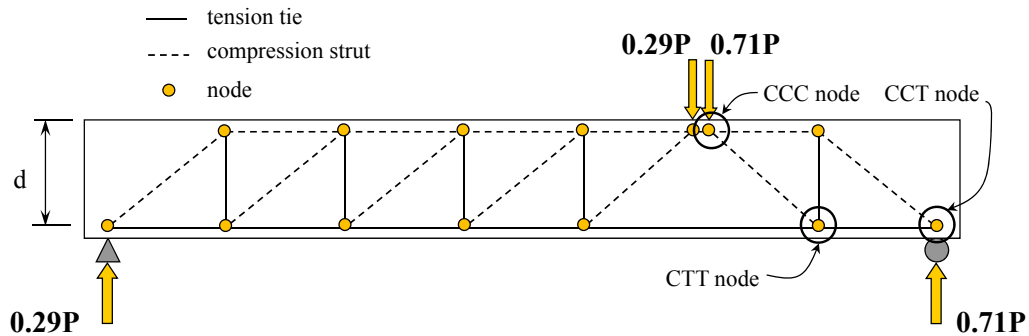


**Figure 2.10: Most common node types in STM**



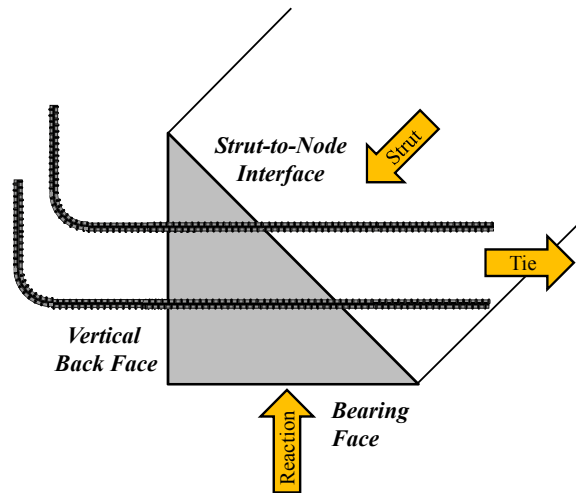


**Figure 2.11: Faces of sample CCT node**

Proportioning the dimensions of nodes is an important step in strut-and-tie modeling. Defining the geometry of the nodal regions is required to calculate stresses on each nodal face that are later compared to allowable design stresses. Also, nodal geometry must be consistent with the placement of tie reinforcement and is used to determine the width of the struts that frame into the node. There are two techniques for proportioning nodes that have been established by previous researchers and code committees. The use of each technique results in hydrostatic or non-hydrostatic nodes. In both cases, nodal geometry is an approximation of regions in the strut-and-tie model where struts and ties are equilibrated.

If a node is proportioned such that equal stresses exist on all in-plane faces of the node, then it is considered a hydrostatic node. The area of each face is directly proportional to the magnitude of the applied force on that face. Shear is not present in the node if the principal stresses ( $\sigma_1$  and  $\sigma_2$  in Figure 2.12) are equal. If a node is proportioned such that the principal stresses are not equal, then it is considered a non-hydrostatic node. Shear is present in non-hydrostatic nodes due to the difference in principal stresses. The difference in stress conditions between a hydrostatic and non-hydrostatic node is shown in Figure 2.12.

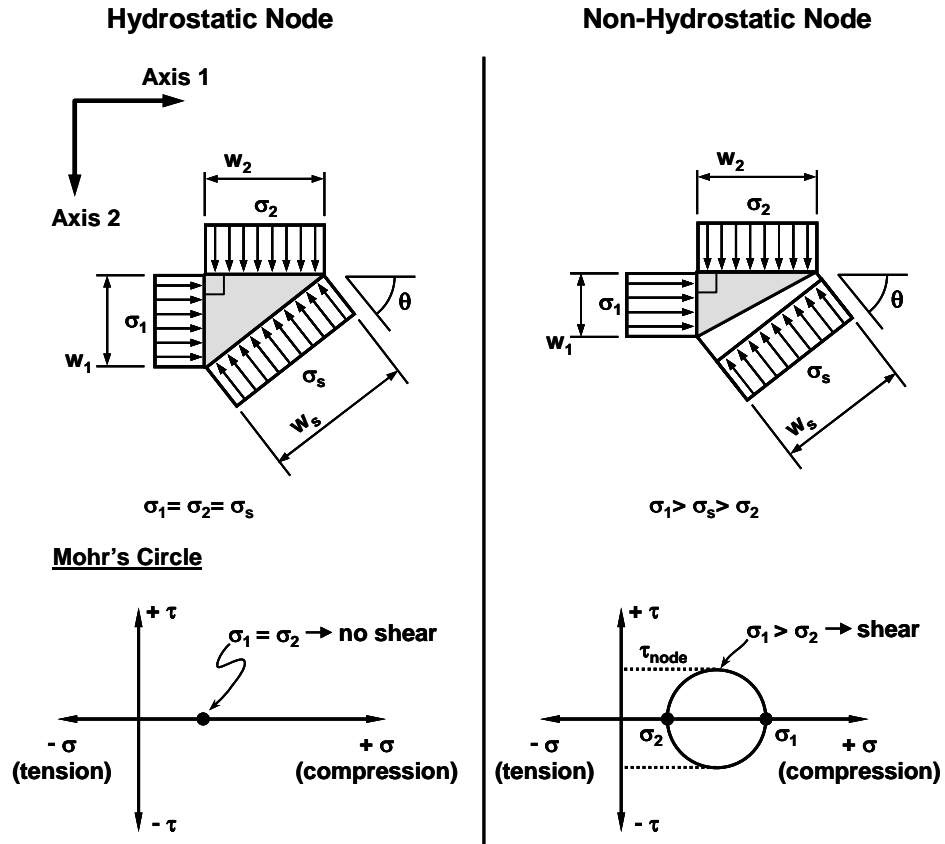


*Figure 2.12: Hydrostatic and non-hydrostatic nodes (Thompson, 2002)*

A hydrostatic node is proportioned based on the bearing or vertical back face dimension of the node ( $w_1$  or  $w_2$  in Figure 2.12). With this dimension, the out-of-plane width of the node, and the applied force on that face, the stress on the face can be calculated. The other dimensions of the node are proportioned so that the same stress exists with their respective applied forces. It is left to the designer to choose which face of the node, bearing or back face, to base the other dimensions on. Typically, the bearing dimension is pre-determined by a standard plate size or fixed column dimension. As such, the bearing dimension is often used to proportion the other nodal dimensions. In hydrostatic nodes, the line connecting the edge of the bearing face to the back face is perpendicular to the axis of the compression strut.

The absence of shear in the node is the primary advantage of using hydrostatic nodes. The primary disadvantage is the difficulty of satisfying hydrostatic nodal principles as the strut angle increases. The sizes of hydrostatic nodes for a single-panel STM with three different  $a/h$  ratios and with two different bearing plate sizes are provided in Figure 2.13 (' $h$ ' is the height of the member). As the angle of a strut with respect to a tie decreases (or the  $a/h$  ratio increases), the horizontal component of the strut becomes much larger than the vertical component. As such, the vertical back face dimension must increase with respect to the bearing face dimension. For the nodes to be hydrostatic, equal stresses must exist on all three faces of the node and the axis of the strut must be perpendicular to a line connecting the bearing and back face. This requirement causes hydrostatic nodes to enlarge to impractical sizes with increasing  $a/h$  ratio. The corresponding placement of longitudinal reinforcement becomes impractical as well. As the  $a/h$  ratio approaches 2, it may be impossible to satisfy hydrostatic nodal requirements with a pre-determined bearing plate size as seen in Figure 2.13. The effect of increasing the bearing plate length is seen in Figure 2.13 by moving left to right.

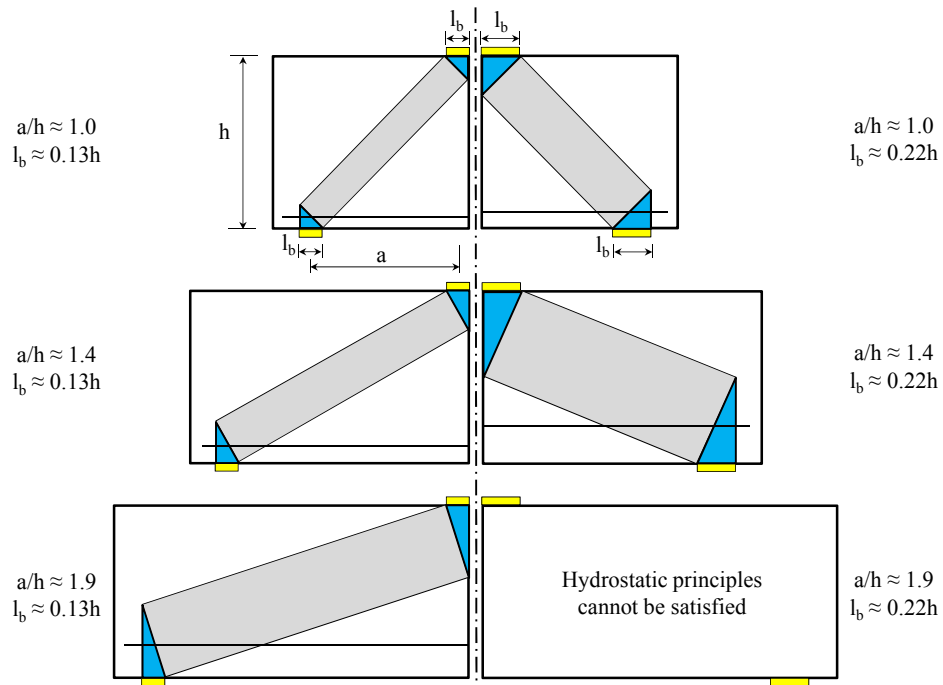


**Figure 2.13: Examples of hydrostatic nodes**

A non-hydrostatic node is proportioned differently. The dimensions of the vertical back face and bearing face are determined independently of each other. The size of the bearing face is often pre-determined by plate size or fixed column size as in the case of hydrostatic nodes. The back face of non-hydrostatic nodes, however, is proportioned by considering the origin of the applied stress. In the case of CCC nodes, the back face dimension can be taken as the effective depth of the compression block ( $\beta_1 c$ ) as determined by a flexural analysis. If a flexural analysis is not applicable, another reasonable assumption that approximates the stress condition on the back face of the node should be made. In the case of CCT or CTT nodes, the back face dimension can be taken as twice the distance from the centroid of the longitudinal reinforcement to the extreme tension fiber of the beam. The purpose of these proportioning techniques is for the assumed nodal geometry to more closely match the actual stress concentrations on these nodal faces. There is no requirement for equal stresses on all faces of the node. Schlaich et al. (1987) recommends limiting the ratio of the largest dimension to the smallest dimension of the node to 2 to limit shear stresses. While a limit such as this may be necessary, it is hard to justify a number considering the dimensions of nodal faces are idealizations of highly stressed regions in the member. Regardless, entirely preventing shear stresses in concrete nodal regions as with hydrostatic nodes seems unnecessary due to the ability of concrete to resist shear stresses.

The STMs in Figure 2.13 can be reproduced using non-hydrostatic nodes, but assumptions are required to proportion the nodal regions. Since the back face dimensions of the nodes are based on the specific stress conditions in the member, an array of possibilities exist for these general cases. However, it is possible to imagine that the sizes of non-hydrostatic nodes will not increase with increasing  $a/h$  ratio to such an extent as with hydrostatic nodes unless the stress conditions in the member justify it. Based on the direct correlation between nodal geometry and stress conditions in the member, non-hydrostatic nodes are preferred in design.

Very little guidance is given in AASHTO LRFD (2008) regarding the proportioning of the nodal regions. In the commentary of Section 5.6.3.2, it states the following:

*Establishing the geometry of the truss involves trial and error in which member sizes are assumed, the truss geometry is established, member forces are determined, and the assumed member sizes are verified (AASHTO LRFD (2008)).*

This statement seems to encourage the use of hydrostatic nodes because the sizes of the members (and nodes) are checked with the member forces. However, it is not very clear. A few drawings are included in AASHTO LRFD (2008) with nodal geometry that appears to be dimensioned hydrostatically, yet there is no mention of hydrostatic nodes. As such, proportioning the nodal regions using the STM provisions of AASHTO LRFD (2008) is largely left to the discretion of the designer. In ACI 318-08 Appendix A, more information on nodal regions is provided. Hydrostatic nodes are defined and illustrated well. Their use is encouraged throughout the STM provisions. However, non-hydrostatic nodes are also detailed in several figures of CCT nodes and are referenced indirectly. It appears that the use of hydrostatic nodes is preferred, yet the use of non-hydrostatic nodes is permitted. There are no guidelines for proportioning CCC nodes and little emphasis is placed on proportioning nodal regions to match stress conditions in the member. Since allowable stresses are applied to the dimensions of nodal faces to calculate the capacity of a given face, having consistent proportioning techniques is necessary. In this dissertation, non-hydrostatic nodes are used with the proportioning techniques described in Figure 2.14 through Figure 2.16.

An example of calculated nodal geometry for the CCC node from the single-panel STM in Figure 2.9 is provided in Figure 2.14. The vertical back face dimension was calculated using Equation 2.1 as the depth of the effective compression block in flexure. The limiting strain in the concrete was set at 0.003, and the strain in the compression steel was consistent with the strain profile. While flexural assumptions are not valid for structural components in D-regions, this assumption is conservative and should be

reasonably accurate for a deep beam with an  $a/d$  ratio approaching 2. The width of the strut-to-node interface ( $w_s$ ) is calculated according to Equation 2.2. It is based on the bearing face dimension, the vertical back face dimension, and the strut angle,  $\theta$ . In this example, only 71% of the applied load is flowing to the near support, so only 71% of the bearing plate is used to determine the dimensions of the CCC node.

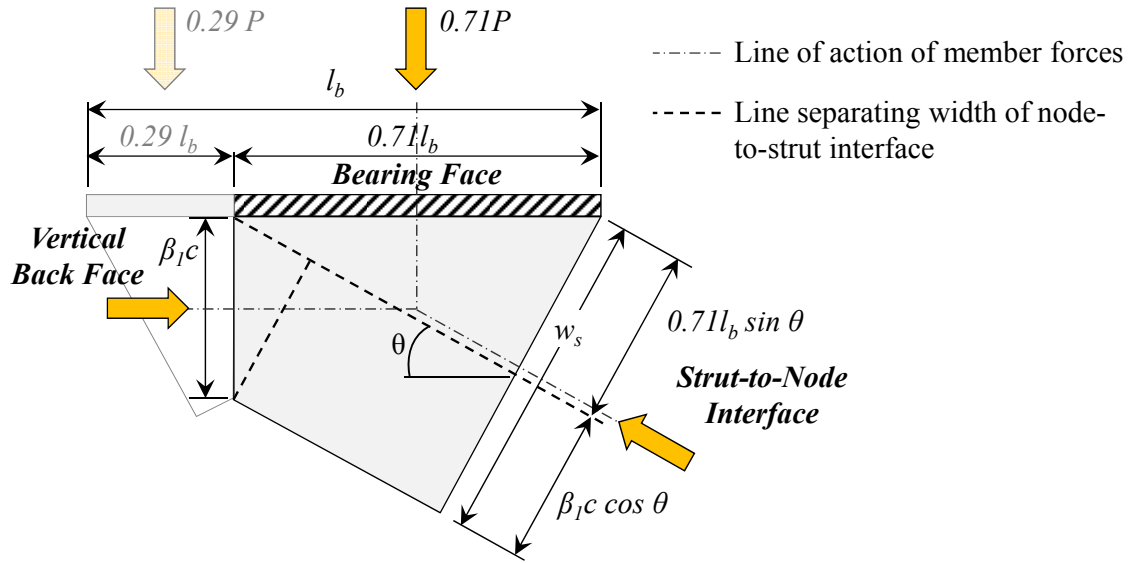


**Figure 2.14: Non-hydrostatic proportions of CCC node**

$$\beta_1 c = \frac{(A_s \cdot f_s - A_s' \cdot f_s')}{0.85 f_c' \cdot b_w} \quad (2.1)$$

where,

- $A_s$  = area of tension reinforcement, in<sup>2</sup>
- $f_s$  = stress in tension reinforcement, psi
- $A_s'$  = area of compression reinforcement, in<sup>2</sup>
- $f_s'$  = stress in compression reinforcement, psi
- $f_c'$  = concrete compressive strength, psi
- $b_w$  = width of beam web, in.

$$w_s = 0.71l_b \cdot \sin \theta + \beta_{1c} \cdot \cos \theta \quad (2.2)$$

where,

- $l_b$  = length of bearing plate, in.
- $\theta$  = angle of strut with respect to horizontal axis, deg.
- $\beta_{1c}$  = height of vertical back face, effective depth of compression block, in.

The calculated nodal geometry for the CCT node from the single-panel STM in Figure 2.9 is provided in Figure 2.15. The full length of the bearing plate,  $l_b$ , is used for this node. Equation 2.3 is used to calculate the width of the strut-to-node interface. It is identical to Equation 2.2 with the exception of the 0.71 factor and the dimension of the vertical back face,  $w_t$ . The dimension of the vertical back face is taken as twice the distance from the centroid of the longitudinal reinforcement to the extreme tension fiber.

$$w_s = l_b \cdot \sin \theta + w_t \cdot \cos \theta \quad (2.3)$$

where,

- $l_b$  = length of bearing plate, in.
- $\theta$  = angle of strut with respect to horizontal axis, deg.
- $w_t$  = height of vertical back face, twice the distance from centroid of reinforcement to extreme tension fiber, in.

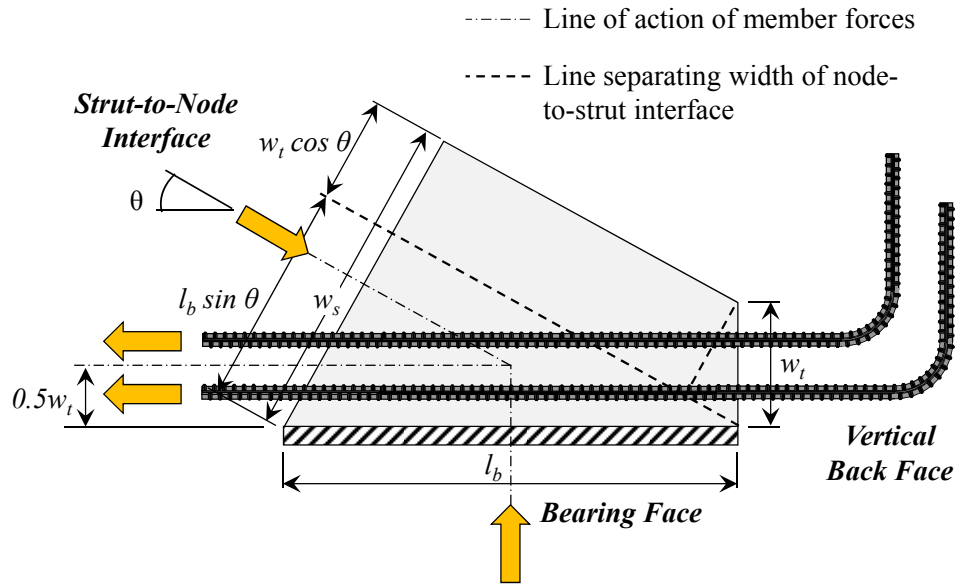


**Figure 2.15: Non-hydrostatic proportions of CCT node**

The calculated nodal geometry for the CTT node from the multiple-panel STM in Figure 2.9 is provided in Figure 2.16. It is difficult to determine the length of a CTT node ( $l_a$ ) because there is not a discrete boundary created by a bearing plate. It is proposed by Wight and Parra-Montesinos (2003) that the length of the CTT node be determined by the number of stirrups that are within 25 deg. with respect to the vertical of adjacent struts. Schlaich et al. (1987) refers to these types of nodes as *smeared* in that the forces in the node are “smeared (or spread) over some length.” Due to the unclear boundaries of smeared nodes, Schlaich et al. (1987) states that “a check of concrete stresses in smeared nodes is unnecessary.” Exceptions to this statement may exist for CTT nodes near reentrant corners or voids since the available concrete in the node is limited (*fib*, 1999). In all cases, the capacity and anchorage of the tie should be checked.



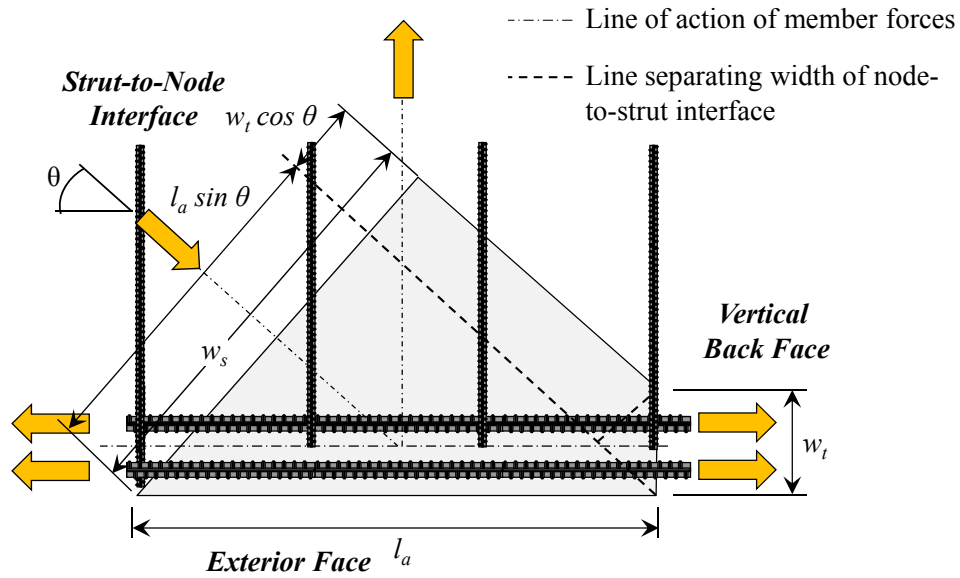


**Figure 2.16: Non-hydrostatic proportions of CTT nodes**

### 2.3.3.2 Struts

Struts are generally categorized as prismatic or bottle-shaped. Prismatic struts have a constant width along their entire length. Typical examples of prismatic struts are a compression chord for a beam in bending in which strut spreading is restricted by the neutral axis and a prismatic column uniformly loaded across the entire cross-section. Bottle-shaped struts are wider at midlength than at their ends. They form where there is additional concrete along the length of the strut for compressive stresses to spread laterally. Bottle-shaped struts are much more common than prismatic struts since defined nodal areas are often smaller than the available space near the midheight of a strut.

Transverse tensile stresses are created due to the spreading of compressive stresses in a bottle-shaped strut (Figure 2.17). To offset the transverse tension, tensile strength of concrete or tensile reinforcement is required. In general, it is not acceptable to rely on tensile strength of concrete. As such, it is important to provide enough reinforcement in the strut to resist transverse tensile stresses so that the strut can reach its design strength and avoid premature strut splitting. Several STM specifications require web or strut reinforcement for this purpose. These requirements are reviewed in Section

4.3.1 on minimum web reinforcement. Alternatively, bottle-shaped struts can be modeled to account for transverse tension as shown in Figure 2.17 and proportioned with reinforcement accordingly.

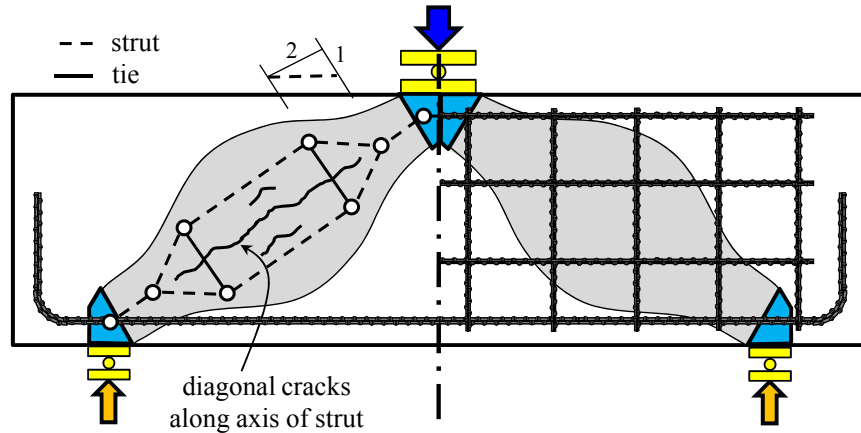


**Figure 2.17: Longitudinal cracking and STM of bottle-shaped struts**

Struts are proportioned based on the dimensions of the nodal regions at the end of the strut. In the case of a bottle-shaped strut, the compressive stress in the strut is greatest at one of the node-to-strut interfaces because the width is smallest there. In the case of a prismatic strut, the stress is uniform along its length. Thus, the stress conditions in a strut are most critical at the node-to-strut interface (provided that enough transverse reinforcement exists to avoid strut splitting).

### 2.3.3.3 Ties

Ties are reinforcement that resist tensile forces in a strut-and-tie model. They are proportioned and placed based on the required amount and location of tensile forces in the STM, respectively. Proper bar spacing and cover requirements must be satisfied when placing tie reinforcement coincident with the centroid of a tie. Also, ties must be properly anchored through development, heads, anchor plates, or other acceptable forms of anchorage.

### 2.3.4 Strut-and-Tie Model Design Provisions

In this section, the strut-and-tie model design provisions from two U.S. specifications – AASHTO LRFD (2008) and ACI 318-08 – are compared with the Project 5253 proposed provisions. As noted in Section 1.2, one of the main objectives of TxDOT Project 5253 was to develop new STM provisions for deep beams (Task 5). The development of the Project 5253 provisions is discussed in detail by Tuchscherer (2008) and Birrcher et al. (2009). The provisions were largely based on the STM recommendations of the *fédération internationale du béton (fib, 1999; i.e. international concrete federation)*. Since the Project 5253 STM provisions and those in AASHTO LRFD (2008) and ACI 318-08 Appendix A are used in some of the tasks addressed in this dissertation, they are presented and compared in this section.

Strut-and-tie modeling was adopted as the preferred method of deep beam design by the AASHTO LRFD Bridge Design Specifications and ACI Building Code (ACI 318) Appendix A in 1994 and 2002, respectively. The STM provisions in each specification have not changed much from inception to the current editions: AASHTO LRFD (2008) and ACI 318-08 Appendix A. However, the STM provisions differ greatly between the two and in both cases, are considered by many to be unclear.

#### 2.3.4.1 AASHTO LRFD (2008) STM Provisions

The strut-and-tie model design specifications in AASHTO LRFD (2008) provide allowable stresses for the three elements in STMs: struts, nodes, and ties. The reduced nominal capacity of each element must be compared to the factored forces on that element as in Equation 2.4.

$$\phi P_n \geq P_u \quad (2.4)$$

where,

$\phi$  = strength reduction factor, 0.70 for compression and 1.0 for tension

$P_n$  = nominal resistance of strut, node face, or tie, kips

$P_u$  = factored force in strut, node face, or tie, kips

The nominal strength of a strut is calculated as follows (excluding reinforcement parallel to the strut):

$$P_n = f_{cu} A_{cs} \quad (2.5)$$

with,

$$f_{cu} = \frac{f'_c}{0.8 + 170\varepsilon_1} \quad (2.6)$$

$$\varepsilon_1 = \varepsilon_s + (\varepsilon_s + 0.002) \cot^2 \alpha_s \quad (2.7)$$

where,

- $A_{cs}$  = effective cross-sectional area of a strut, in.<sup>2</sup>
- $f'_c$  = specified compressive strength of concrete, ksi.
- $\varepsilon_s$  = the tensile strain in the concrete in the direction of the tension tie, in./in.
- $\alpha_s$  = the smallest angle between the compressive strut and adjoining ties, deg.

In Equation 2.6, the limiting compressive stress in a strut,  $f_{cu}$ , is a function of the amount of principle tensile strain in cracked concrete,  $\varepsilon_1$ .  $\varepsilon_1$  is calculated with Equation 2.7 which is a function of the tensile strain in the concrete in the direction of the tension tie due to factored loads,  $\varepsilon_s$ . As the angle between the strut and the tie decreases, the concrete strain at the tension tie ( $\varepsilon_s$ ) increases and the limiting compressive stress in the strut,  $f_{cu}$ , decreases. Thus, the strength of a strut in AASHTO LRFD (2008) decreases as the angle between the strut and the tie decreases or as the a/d ratio increases for a single-panel strut-and-tie model.

In determining the effective cross-sectional area of a strut ( $A_{cs}$ ), CTT nodes must be considered in addition to CCC and CCT nodes. Details are given to proportion the width of a strut framing into a CTT node. Thus, the AASHTO LRFD (2008) STM provisions require checking of concrete stresses in smeared nodes (CTT).

The nominal concrete compressive stress in the node regions of the strut shall not exceed the values listed below. The strength of node regions may be increased by the effects of confinement reinforcement if supported by tests and analyses.

Node regions bounded by compressive struts and bearing areas (CCC node):  $0.85 f'_c$

Node regions anchoring a one-direction tension tie (CCT node):  $0.75 f'_c$

Node regions anchoring tension ties in more than one direction (CTT node):  $0.65 f'_c$

Reinforcement must be proportioned to resist the tie forces in the strut-and-tie model, must be placed to coincide with the location of the ties, and must be appropriately anchored. The nominal resistance of a tension tie shall be taken as:

$$P_n = f_y A_{st} + A_{ps} (f_{pe} + f_y) \quad (2.8)$$

where,

$f_y$  = yield strength of mild steel longitudinal reinforcement, ksi.

$A_{st}$  = total area of longitudinal mild steel reinforcement in the tie, in.<sup>2</sup>

$A_{ps}$  = area of prestressing steel, in.<sup>2</sup>

$f_{pe}$  = stress in prestressing steel due to prestress after losses, ksi.

Lastly, the STM provisions in AASHTO LRFD (2008) specify that crack control reinforcement must be provided in both orthogonal directions near each face. The ratio of reinforcement area to gross concrete area shall not be less than 0.003, and the reinforcement spacing shall not exceed 12 in.

#### **2.3.4.2 ACI 318-08 Appendix A STM Provisions**

The strut-and-tie model provisions in Appendix A of the ACI 318-08 Building Code also provide allowable stresses for struts, nodal zones, and ties in a STM. As in AASHTO LRFD, the reduced nominal capacity must be greater than or equal to the factored load on each element as in Equation 2.9:

$$\phi F_n \geq F_u \quad (2.9)$$

where,

- $\phi$  = strength reduction factor, 0.75
- $F_n$  = nominal resistance of strut, node face, or tie, lbs.
- $F_u$  = factored force in strut, node face, or tie, lbs.

The nominal strength of a strut is calculated as follows (excluding reinforcement parallel to the strut):

$$F_{ns} = f_{ce} A_{cs} \quad (2.10)$$

where,

- $f_{ce}$  = smaller of (a) the effective compressive strength of the concrete in the strut and (b) the effective compressive strength of the concrete in the nodal zone, psi
- $A_{cs}$  = cross-sectional area of end of strut, perpendicular to axis of strut, in.<sup>2</sup>

The effective compressive strength of the concrete in the strut,  $f_{ce}$ , shall be taken as:

$$f_{ce} = 0.85 \beta_s f'_c \quad (2.11)$$

where,

- $\beta_s$  = strut efficiency factor
  - = 1.0 for prismatic struts,
  - = 0.75 for adequately-reinforced struts (Equation 2.12),
  - = 0.60 for inadequately-reinforced struts.
- $f'_c$  = specified compressive strength of concrete, psi.

The efficiency factor for bottle-shaped struts depends on the amount of strut reinforcement. If Equation 2.12 is satisfied, an efficiency factor of 0.75 is used. If not, an efficiency factor of 0.60 is used. The purpose of strut reinforcement is to resist transverse tensile stresses in bottle-shaped struts. Equation 2.12 encourages the

placement of reinforcement perpendicular to the axis of the strut to more efficiently resist transverse tension. The calculation of  $\rho_{\perp}$  is explained in Figure 2.18. Through the use of a smaller efficiency factor (0.60), the provisions in ACI 318-08 Appendix A permit the use of unreinforced struts. In these cases, the tensile capacity of the concrete is required to resist the transverse tension.

$$\rho_{\perp} = \sum \frac{A_{si}}{b_s s_i} \sin \alpha_i \geq 0.003 \quad (2.12)$$

where,

- $A_{si}$  = total area of surface reinforcement at spacing  $s_i$  in the  $i$ -th layer crossing a strut, with reinforcement at an angle  $\alpha_i$  to the axis of the strut, in.<sup>2</sup> strut
- $b_s$  = width of strut, in.
- $s_i$  = spacing of reinforcement in  $i$ -th layer, in.
- $\alpha_i$  = angle between  $i$ -th layer of reinforcement and axis of strut, deg.

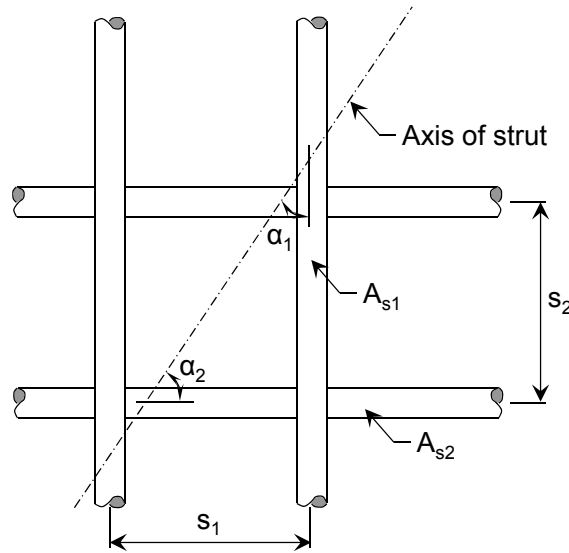


**Figure 2.18: Calculation of  $\rho_{\perp}$  in ACI 318-08 Appendix A (ACI 318, 2008)**

The nominal compressive strength of a nodal zone,  $F_{nn}$ , is calculated with Equation 2.13. The effective compressive stress,  $f_{ce}$ , on a face of a nodal zone may be increased due to effects of confining reinforcement as supported by tests and analyses.

$$F_{nn} = f_{ce} A_{nz} \quad (2.13)$$

with,

$$f_{ce} = 0.85 \beta_n f'_c \quad (2.14)$$

where,

$A_{nz}$  = the smaller of (a) the area of the nodal face perpendicular to  $F_u$  and (b) the area of a section through a nodal zone perpendicular to the resultant force on the section, in.<sup>2</sup>

$\beta_n$  = node efficiency factor  
= 1.0 for CCC nodes,  
= 0.80 for CCT nodes,  
= 0.60 for CTT and TTT nodes.

$f'_c$  = specified compressive strength of concrete, psi.

Reinforcement must be proportioned to resist the tie forces in the strut-and-tie model, be placed such that the axis of the reinforcement coincides with the axis of the tie, and be appropriately anchored. The nominal strength of a tension tie shall be taken as:

$$F_{nt} = A_{ts} f_y + A_{tp} (f_{se} + \Delta f_p) \quad (2.15)$$

where,

$A_{ts}$  = area of nonprestressed reinforcement in a tie, in.<sup>2</sup>

$f_y$  = specified yield strength of reinforcement, psi.

$A_{tp}$  = area of prestressing steel in a tie, in.<sup>2</sup>

$f_{se}$  = effective stress in prestressing steel, psi.

$\Delta f_p$  = increase in stress in prestressing steel due to factored loads, psi.

#### **2.3.4.3 Project 5253 STM Provisions**

The development of the TxDOT Project 5253 STM provisions is discussed in detail by Tuchscherer (2008). The provisions were based on the analysis of an



experimental database of 179 deep beam tests and on STM provisions of the *fédération internationale du béton (fib, 1999)*; i.e. international concrete federation).

As with other provisions, the reduced nominal capacity must exceed the factored force on each element as in Equation 2.9. The  $\phi$  factor would be consistent with the adopting specification.

The nominal strength of a nodal zone,  $F_n$ , shall be calculated as follows:

$$F_n = f_{ce} A_{nz} \quad (2.16)$$

where,

$$\begin{aligned} f_{ce} &= \text{effective compressive strength of concrete in nodal zone, psi} \\ A_{nz} &= \text{cross-sectional area of the face of the nodal zone, in.}^2 \end{aligned}$$

The effective compressive strength,  $f_{ce}$ , on the face of a nodal zone shall be calculated as follows:

$$f_{ce} = m \nu f'_c \quad (2.17)$$

where,

$$\begin{aligned} m &= \text{triaxial confinement modification factor, } \sqrt{A_2/A_1} \leq 2 \text{ with } A_2 \text{ and } A_1 \\ &\quad \text{defined in Figure 2.19.} \\ \nu &= \text{node efficiency factor} \\ &= 0.85 \text{ for bearing and back face of CCC nodes} \\ &= 0.70 \text{ for bearing and back face of CCT nodes} \\ &= 0.45 \leq \left( 0.85 - f'_c / 20 \text{ksi} \right) \leq 0.65 \text{ for CCC and CCT node-to-strut interfaces} \\ &\quad \text{with crack control reinforcement} \\ &= 0.45 \text{ for CCC and CCT node-to-strut interfaces without crack control} \\ &\quad \text{reinforcement.} \\ f'_c &= \text{specified compressive strength of concrete, psi.} \end{aligned}$$

While the beneficial effects of triaxial confinement by surrounding concrete is recognized in bearing calculations in AASHTO LRFD (2008) and ACI 318-08, it is not recognized in their respective STM provisions. The triaxial confinement factor,  $m$ , in the Project 5253 provisions accounts for confinement of concrete. It was substantiated with experimental tests (Tuchscherer, 2008) and is consistent with the bearing stress check in ACI 318-08. The areas  $A_2$  and  $A_1$  are illustrated in Figure 2.19.

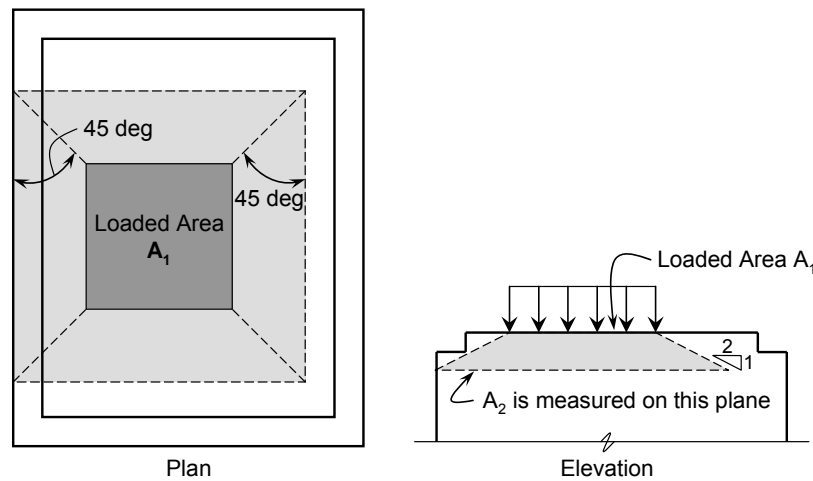


**Figure 2.19: Application of frustum to find  $A_2$  from loaded area  $A_1$  (ACI 318-08)**

The nodal efficiency factor,  $\nu$ , is similar to that in AASHTO LRFD (2008) and ACI 318-08 for the bearing face at CCC and CCT nodes and for the back face of CCC nodes. However, for the back face of CCT nodes, bond stresses from an adequately developed tension tie should not be applied to the back face of the node. Only concentrated stresses such as those due to bearing of a plate anchoring an unbonded bar or due to an external indeterminacy (Figure 2.20) should be applied to the back face of CCT nodes and checked with the 0.70 efficiency factor. It was determined through experimental testing and with an analysis of a database of test results that applying bond stresses to the back face of CCT nodes is unnecessary (Tuchscherer, 2008). It is necessary, though, for the tie to be properly anchored.

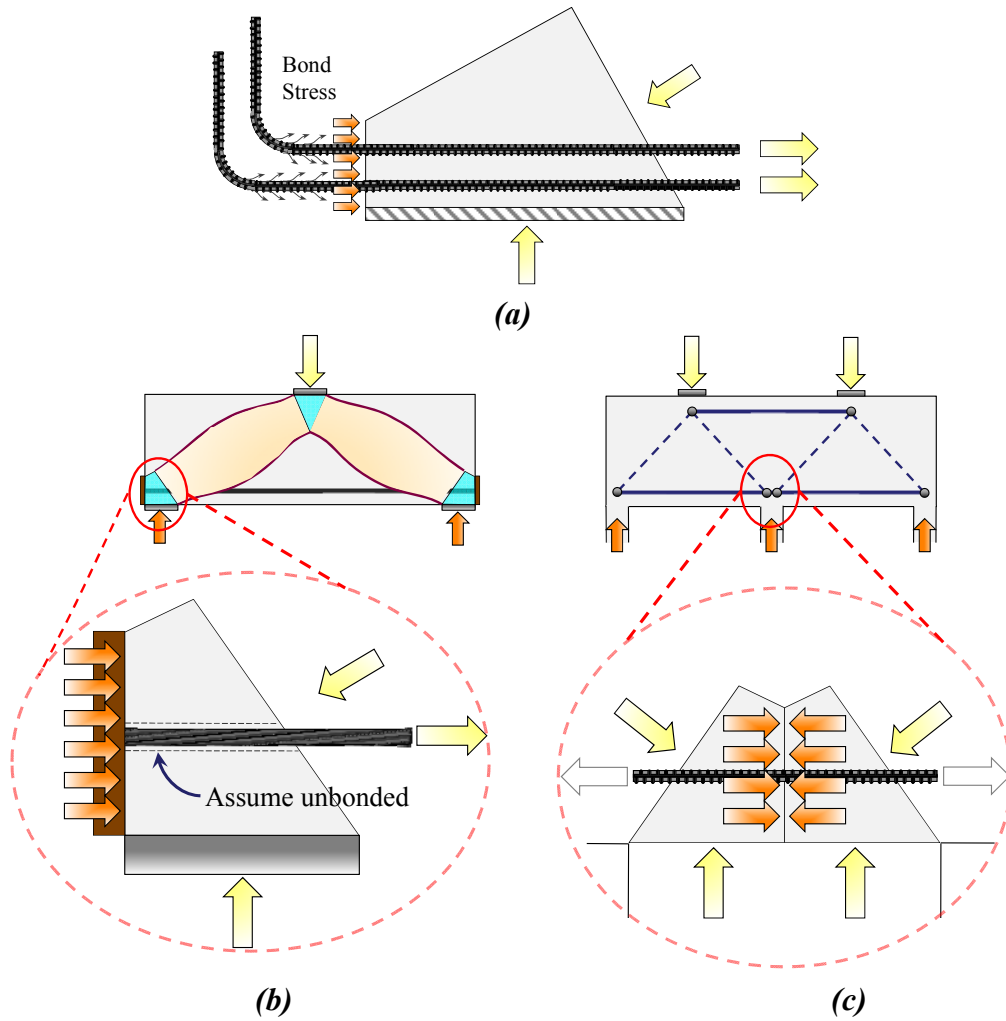


**Figure 2.20. Stress condition at the back face of a CCT node due to: (a) bond stress; (b) bearing of an anchor plate; (c) interior node over a continuous support (Tuchscherer, 2008)**

In the Project 5253 STM provisions, there is not a separate check of the compressive stress in a strut. The stress in the strut is checked at the node-to-strut interface since the stress is highest at this location. The efficiency factor at the node-to-strut interface varies with the compressive strength of concrete and has a minimum and maximum limit of 0.45 and 0.65, respectively. Premature strut splitting is avoided by providing orthogonal grids of web reinforcement or by limiting the efficiency factor at

the node-to-strut interface to 0.45. The required amount of minimum orthogonal web reinforcement is a topic of this dissertation. It is discussed in detail in Section 4.3.

No concrete stress checks are required in the Project 5253 provisions in CTT or other smeared nodes. As noted by Schlaich et al. (1987), the geometry of smeared nodes is not discrete, and therefore, checking stress limits is unnecessary. Tension reinforcement in CTT nodes near reentrant corners or voids should be as well-distributed as possible to reduce high stress concentrations in regions where available concrete is limited (fib, 1999). Ties in CTT nodes must be checked and adequately developed or anchored.

No changes were recommended to the nominal strength equations for tension ties in AASHTO LRFD (2008) or ACI 318-08 Appendix A. Tie reinforcement must be proportioned to resist the tie forces in the strut-and-tie model, be placed such that the axis of the reinforcement coincides with the axis of the tie, and be appropriately developed or anchored.

#### ***2.3.4.4 Evaluation of STM Design Provisions with Deep Beam Data***

In the previous three sections, the strut-and-tie model design provisions of AASHTO LRFD (2008), ACI 318-08 Appendix A, and TxDOT Research Project 5253 were listed. In this section, the implications of using each set of provisions to estimate the capacity of a deep beam ( $a/d < 2$ ) are discussed. For the discussion, results obtained by Tuchscherer (2008) are presented in which the experimental strength of 179 deep beam tests was compared to the calculated strength using a single-panel STM with each set of design provisions. A  $\phi$  factor of 1.0 was used in all calculations since the tests were conducted under laboratory conditions.

The strut-and-tie model shown in Figure 2.21 was used to estimate the capacity of 179 deep beams compiled into a database within Project 5253. Details of the database are provided in Section 2.4 and Appendix B. The same STM was used for all of the deep beams even though the  $a/d$  ratio reached 2.5. A single-panel model is justified to an  $a/d$  ratio of 2, whereas, a sectional model is typically required in design specifications at  $a/d$

ratios exceeding 2. However, some researchers have concluded that deep beam behavior extends to an  $a/d$  ratio of 2.5. The implications of using a single-panel STM for  $a/d$  ratios reaching 2.5 are discussed in Section 4.4.2.2 and 5.2.2.2.

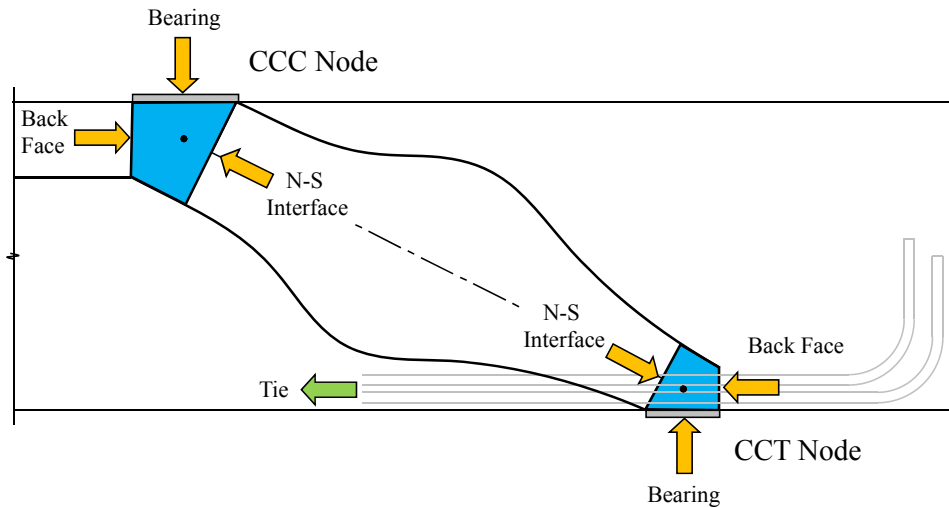


**Figure 2.21: Single-panel STM and stress checks used to evaluate deep beams**  
(Tuchscherer, 2008)

Non-hydrostatic nodes were used in the STM in Figure 2.21. The specific proportioning techniques were defined previously in Figure 2.14 and Figure 2.15. The specifications in AASHTO LRFD (2008) and ACI 318-08 support the use of non-hydrostatic nodes, but are generally vague in how nodes should be proportioned. The seven design checks displayed in Figure 2.21 were performed on each specimen in the database. Premature strut splitting was addressed by only including specimens in the database with sufficient web reinforcement to reinforce the bottle-shaped strut. For reference, the efficiency factor used according to each set of STM provisions for each design check is listed in Table 2.1. The governing design check determined the calculated capacity of the specimen. The calculated capacity was compared to the experimental strength to evaluate each set of design provisions.

**Table 2.1: Summary of stress checks used to evaluate deep beams (Tuchscherer, 2008)**

Element	Design Check	Design Provisions	Allowable Stress
CCC Node	Bearing	AASHTO LRFD	$0.85 f_c'$
		ACI 318	$0.85 f_c'$
		Project 5253	$0.85 f_c'$
	Back Face	AASHTO LRFD	$0.85 f_c'$
		ACI 318	$0.85 f_c'$
		Project 5253	$0.85 f_c'$
	N-S Interface	AASHTO LRFD	$0.85 f_c'$
		ACI 318	$0.85 (0.75) f_c' = 0.64 f_c'$
		Project 5253	$[0.45 \leq (0.85 - f_c'/20\text{ksi}) \leq 0.65] f_c'$
CCT Node	Bearing	AASHTO LRFD	$0.75 f_c'$
		ACI 318	$0.85 (0.80) f_c' = 0.68 f_c'$
		Project 5253	$0.70 f_c'$
	Back Face	AASHTO LRFD	$0.75 f_c'$
		ACI 318	$0.85 (0.80) f_c' = 0.68 f_c'$
		Project 5253	N/A
	N-S Interface	AASHTO LRFD	$f_c' / (0.8 + 170\epsilon_1) \leq 0.85 f_c'$
		ACI 318	$0.85 (0.75) f_c' = 0.64 f_c'$
		Project 5253	$[0.45 \leq (0.85 - f_c'/20\text{ksi}) \leq 0.65] f_c'$
Tie	Tie	ALL	$f_y$

The results obtained by Tuchscherer (2008) are presented in Figure 2.22. The experimental strength was divided by the calculated capacity and plotted in a histogram. A value less than 1.0 implies that the experimental strength was unconservatively estimated. A value greater than 1.0 implies a conservative estimate. The mean and coefficient of variation (COV) of the results using each set of STM provisions are presented as well.

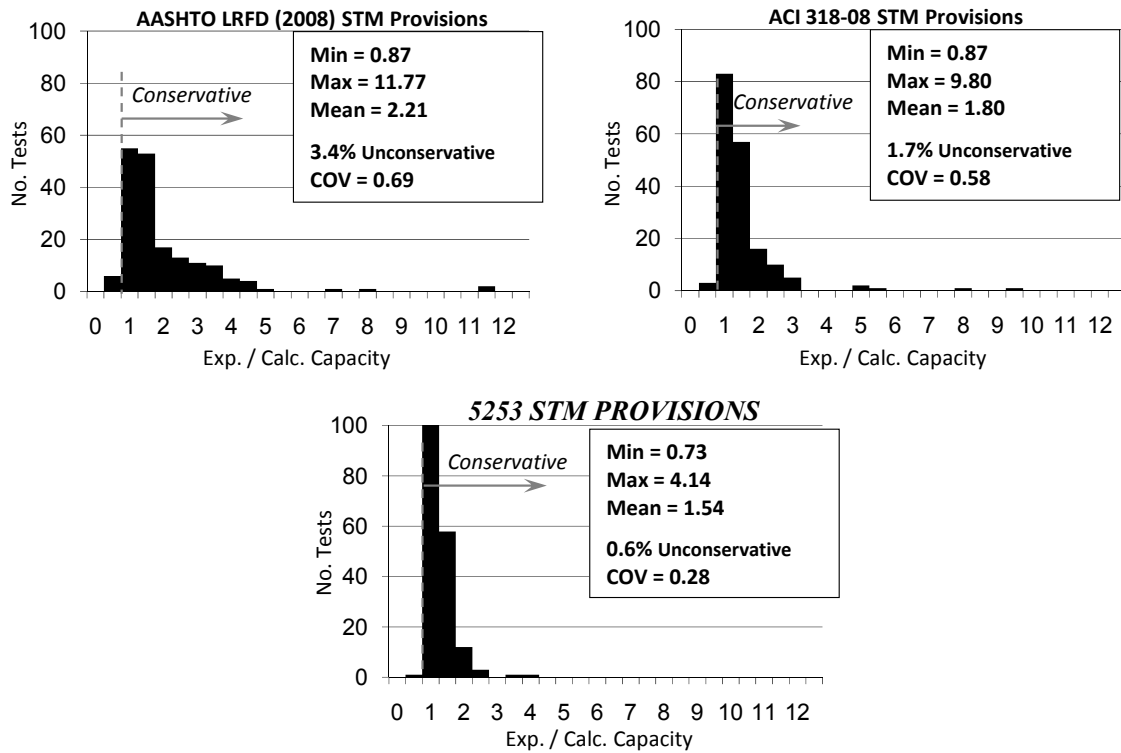


**Figure 2.22: Evaluation of STM provisions with deep beam database (Tuchscherer, 2008) (N=179)**

The results indicate that all of the STM design provisions provided conservative estimates of strength. However, there was a considerable difference in accuracy. The mean Exp. / Calc. value using the AASHTO LRFD (2008) provisions was 2.21. The COV was 0.69. These high values were largely the result of an efficiency factor at the CCT node-to-strut interface that decreases considerably with decreasing strut angle (increasing  $a/d$  ratio). It is likely that this AASHTO LRFD efficiency factor was originally derived with hydrostatic nodes that increase in size with decreasing strut angle (Figure 2.13), thereby offsetting the decreasing efficiency factor. However, as noted previously, the use of non-hydrostatic nodes is preferred in design and is more practical. The use of the ACI 318-08 Appendix A STM provisions provided better results. The mean Exp. / Calc. value was 1.80, and the COV was 0.58. Two main deficiencies in the ACI 318-08 provisions are the checking of bond stresses at the back face of CCT nodes

and the lack of accounting for triaxial confinement of surrounding concrete. The deficiencies in the STM provisions in AASHTO LRFD (2008) and ACI 318-08 Appendix A are remedied in the Project 5253 STM design recommendations. The mean Exp. / Calc. value was 1.54 and the COV was 0.28. The improved accuracy was the result of addressing the aforementioned deficiencies in AASHTO LRFD (2008) and ACI 318-08 and also reducing the efficiency of high-strength concrete at the node-to-strut interface. It is important to note that the Project 5253 provisions were largely based on those in *fib* (1999).

In this section, it was shown that the Project 5253 STM provisions are more accurate, have less design checks, and yet are as conservative as those in AASHTO LRFD (2008) and ACI 318-08 Appendix A. The Project 5253 STM design recommendations are incorporated into the AASHTO LRFD Design Specifications and Appendix A of ACI 318 elsewhere (Tuchscherer, 2008). Deep beam capacity is calculated using the Project 5253 STM provisions throughout this dissertation.

## **2.4 DEEP BEAM DATABASE**

The third topic addressed in this chapter is the compilation of a deep beam database. In Project 5253, a database of deep beam shear tests ( $a/d \leq 2.5$ ) was compiled to supplement the findings of the experimental program. The Project 5253 database is an expansion of a database originally compiled by Brown et al. (2006). All of the specimens from the Brown et al. (2006) database with an  $a/d$  ratio greater than 2.5 were removed. The remaining entries were double-checked, and additional deep beam data were added. The total number of deep beam shear tests is 905 (including 37 tests conducted within Project 5253). This database is called the *collection database*. The references for the data from other research projects in the collection database are given elsewhere (Birrer et al., 2009).

The collection database was filtered in two stages (Table 2.2). In the first stage, test results were removed, for the most part, due to a lack of sufficient details to perform a strut-and-tie analysis. The resulting database is called the *filtered database*. In the



second stage of filtering, additional specimens were removed that were considered especially unrepresentative of field members. The resulting database is called the *evaluation database*. An overview of the number of specimens that were removed from the database in each stage is provided in Table 2.2. Explanations for the removal of these test results are provided in the next two sections.

**Table 2.2: Filtering of the deep beam ( $a/d \leq 2.5$ ) database**

<b><i>Collection Database</i></b>		<b><i>905 tests</i></b>
Stage 1 filtering	- incomplete plate size information	- 284 tests
	- subjected to uniform loads	- 7 tests
	- stub column failure	- 3 tests
	- $f'_c < 2,000$ psi	- 4 tests
<b><i>Filtered Database</i></b>		<b><i>607 tests</i></b>
Stage 2 filtering	- $b_w < 4.5$ in.	- 222 tests
	- $b_w d < 100$ in. <sup>2</sup>	- 73 tests
	- $d < 12$ in.	- 13 tests
	- $\sum \rho_{\perp} < 0.001^*$	- 120 tests
<b><i>Evaluation Database</i></b>		<b><i>179 tests</i></b>

\*  $\rho_{\perp}$  is defined in Equation 2.12

#### 2.4.1 Filtered Database

A large number of specimens in the collection database (284) did not contain verifiable bearing plate dimensions. This information was required to perform a strut-and-tie analysis on the specimens. In some of the 284 cases, bearing plates were sketched in figures of the test setup, but were not dimensioned. It was determined that only the specimens with clearly defined bearing plates would be analyzed. As such, the results from these 284 tests were removed.

Of the remaining tests, specimens that were subjected to uniform loads, that did not fail in the anticipated test region, and that contained concrete with a compressive strength less than 2,000 psi were filtered from the database. Only beams loaded with one

or two concentrated loads were retained in the database for ease in defining the  $a/d$  ratio and in defining nodal regions. Three specimens tested by Foster and Gilbert (1998) experienced crushing in the stub columns that were used to load the beams. At the onset of crushing, the tests were abandoned by the researchers. These data were removed from the database as a result. Lastly, four specimens were fabricated with concrete that had a compressive strength at the time of testing of less than 2,000 psi. In general, concrete is not considered structural if the compressive strength is less than 2,000 psi.

The filtered database contains data from 607 tests. The specimens in the filtered database have adequate details necessary to perform strut-and-tie analyses with reliability and relative ease.

#### **2.4.2 Evaluation Database**

A second stage of filtering was performed to remove specimens that were considered especially unrepresentative of field members. A large percentage of the specimens in the filtered database had small ( $< 100 \text{ in.}^2$ ) shear areas ( $b_w d$ ) as seen in Figure 2.23. Also, many of the specimens did not contain any web reinforcement. Typical bent caps in Texas have shear areas of  $1200 \text{ in.}^2$  and contain significant amounts of web reinforcement. With these considerations, additional filtering criteria were established.

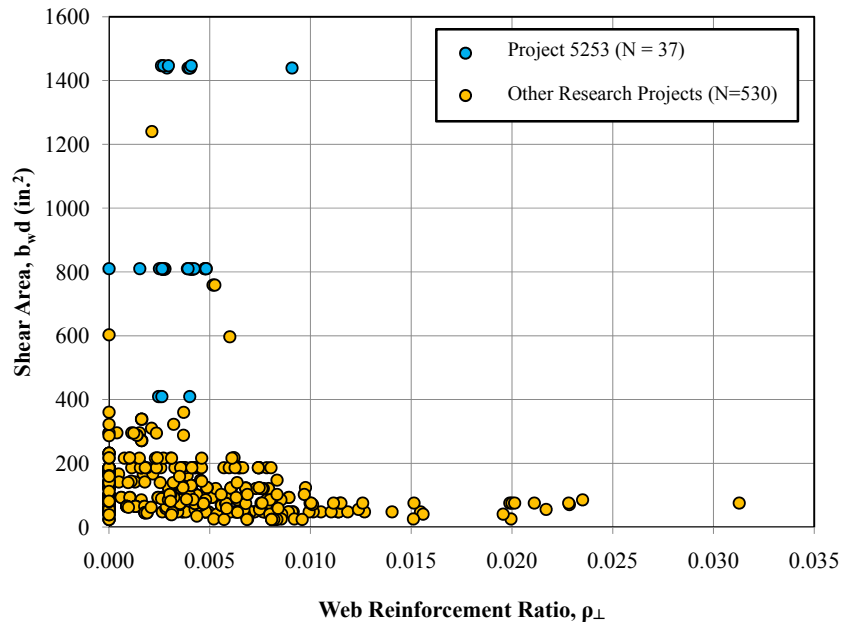


***Figure 2.23: Size and web reinforcement ratio of specimens in filtered database***

It was determined that the specimens in the database should have a beam width of at least 4.5 in. This dimension was approximated as the minimum width required to fit a 2-legged #3 stirrup with  $\frac{3}{4}$ -in. cover and a couple of longitudinal bars (#5's with 1-in. clear spacing). 222 of the 607 specimens in the filtered database were removed due to this limitation.

A minimum shear area of 100 in.<sup>2</sup> and a minimum effective depth of 12 in. was also used to filter the database to remove specimens of less representative size. These criteria filtered out 73 and 13 tests, respectively.

Lastly, it was determined that deep beams without transverse reinforcement are not representative of those in the field. However, it was preferred to have some beams in the database that were lightly reinforced so that the affects of additional transverse reinforcement could be evaluated. A  $\rho_{\perp}$  of 0.001 was established as the minimum amount of web reinforcement. 120 additional specimens were removed due to this requirement.

The remaining dataset contains 179 specimens and is called the *evaluation database*. Of the 179 specimens, 35 were tested within Project 5253 (two specimens tested during TxDOT Project 5253 were filtered out due to insufficient web reinforcement). 14 of the 179 specimens were isolated-strut panels tested by Brown et al. (2006). The panels were loaded in uniaxial compression ( $a/d = 0$ ) with the quantity of web reinforcement and the size of the bearing plates as the primary variables. While these specimens are not deep beams, their test results were retained in the database to provide additional data for specimens with low  $a/d$  ratios. For simplicity, all of the entries in the evaluation database will be referred to as deep beams in this dissertation. The evaluation database was used in conjunction with the results of the experimental program to address the objectives of Project 5253. Details of the beams in the evaluation database are provided in Appendix B. It is believed that the test results in the evaluation database are much more representative of field members than those that were removed.

It is important to note that specimens that failed in shear and in flexure, as reported by the researcher, were both included in the evaluation database. Since strut-and-tie modeling is a general procedure that accounts for both shear and flexure through the numerous design checks of each nodal face and tension tie, it is appropriate to evaluate both failure modes.

## **2.5 SUMMARY**

Three different topics were reviewed in this chapter. First, several cases of diagonally-cracked bent caps in service were presented. In two cases, costly retrofits were required to strengthen the bent caps due to extensive diagonal cracking in service. Second, background information on deep beam behavior and strut-and-tie modeling was provided. It was shown that deep beam behavior is categorized by nonlinear strain distribution that exists in members with small shear-span-to-depth ( $a/d$ ) ratios or clear-span-to-depth ( $l_n/d$ ) ratios. Strut-and-tie modeling is a design tool that replaces the complex states of stress in members like deep beams with a collection of uniaxial struts and ties interconnected by nodes. Three sets of strut-and-tie modeling design provisions

were presented and compared. It was shown that the Project 5253 STM provisions were more accurate and yet just as conservative as those in AASHTO LRFD (2008) and ACI 318-08 Appendix A. In addition, the Project 5253 STM provisions have less design checks with additional and much-needed clarification. Lastly, a database of 179 deep beam ( $a/d < 2.5$ ) tests that was compiled within Project 5253 was discussed. The database is used throughout the dissertation to supplement the findings of the experimental program.

## **CHAPTER 3**

### **Experimental Program**

#### **3.1 OVERVIEW**

In this chapter, details of the experimental program are provided. The design, fabrication, and testing of the specimens at the Phil M. Ferguson Structural Engineering Laboratory at the University of Texas at Austin are discussed in detail. Overall, thirty-seven (37), simply-supported tests were conducted on 19 beams within Project 5253.

#### **3.2 TESTING PROGRAM**

In Project 5253, eight objectives were addressed (Section 1.2). The first four objectives consisted of evaluating the effect of the following parameters on the strength and serviceability performance of reinforced concrete deep beams:

1. the distribution of stirrups across the width of a beam web (2-legged stirrups versus 4-legged stirrups)
2. the triaxial confinement of singular nodal regions by surrounding concrete
3. the amount of minimum web reinforcement (stirrups and longitudinal side-face reinforcement)
4. the member depth

The remaining four objectives included:

5. Developing a simple STM design methodology for the design of deep beams
6. Reducing the discrepancy between shear strength calculated using STM and sectional shear provisions at an  $a/d$  ratio of 2
7. Limiting diagonal cracking under service loads
8. Developing a means to relate the maximum diagonal crack width of a deep beam to its residual capacity

To accomplish the objectives of Project 5253, it was necessary to develop an extensive testing program. Data in the literature were generally insufficient to address the tasks of the project for two reasons. First, very little serviceability information, primarily diagonal crack width data, exists in the literature. With the exception of task 6, all of the project objectives required the evaluation of the serviceability performance of deep beams. Second, the cross-sectional dimensions of deep beams, particularly the beam width, tested in the past are drastically smaller than those of members in service. Two of the aforementioned tasks required data from specimens with widths of realistic size (tasks 1 and 2). Task 8 was aimed at the specific performance of in-service bent caps and thus, benefitted from data from beams of comparable size. As a whole, it was determined that testing specimens of comparable size to that of members in service provided the best means to improve their design and performance.

The cross-sectional dimensions of several bent caps in Texas are compared to those of test specimens in the literature in Figure 3.1. The cross-sections of two bent caps that experienced significant diagonal cracking problems in service are shown at the far left. The cracking problem and required retrofit of the I-345 and I-45 bent caps were discussed in Section 2.2. The cross sections of two standard bent caps used by TxDOT to support Type IV and Type C prestressed girders are also shown in Figure 3.1. The cross-sections used in several testing programs that provided the basis for much of the current deep beam design provisions are illustrated at the far right of Figure 3.1. It is clear that the sizes of bent caps in service are significantly larger than that of the deep-beam specimens tested previously.

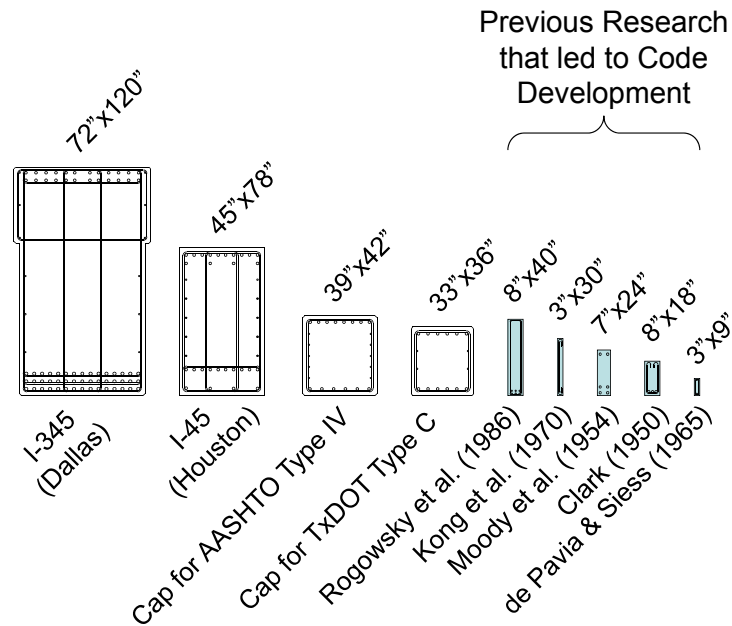


**Figure 3.1: Scaled comparison between actual bent caps and beams included in past research programs (Tuchscherer, 2008)**

The testing program was divided into five series to isolate the primary objectives of the research project. The purpose of Series I through IV was to address tasks 1 through 4 of the current project. Series M consisted of five tests in which multiple objectives were evaluated. The specimens in Series III and IV were tested at three different  $a/d$  ratios to specifically address task 6. All of the specimens in the experimental program were used to address tasks 5, 7, and 8. Many of the beam details were kept constant across each test series to permit the use of test data for multiple project objectives. For this reason, details of all of the specimens fabricated and tested in Project 5253 are presented in this dissertation. The titles of each series are as follows:

- Series I: Distribution of Stirrups across the Beam Web (2 legs vs. 4 legs)
- Series II: Triaxially Confined Nodal Regions
- Series III: Minimum Web Reinforcement (transverse and longitudinal)
- Series IV: Depth Effect
- Series M: Multiple Purpose



### 3.2.1 Overall Design of Test Specimens

The test specimens were designed to fail in shear since the objectives of the current study were associated with shear-dominated behavior. At a given  $a/d$  ratio, a reasonable upperbound estimate of the normalized shear stress at failure was obtained from the evaluation database (Figure 3.2). With this strength estimate, the longitudinal reinforcement was selected such that the moment capacity exceeded the upperbound shear capacity. For the specimens in Series I through IV, a longitudinal tension reinforcement ratio of 2.3% was sufficient for the beam to fail in shear. Compression reinforcement ( $\sim 1.1\%$ ) was added to these specimens to increase the moment capacity and to make the section tension-controlled in flexure. The difference between the estimated shear capacity and the estimated moment capacity of the Series I through IV specimens loaded with an  $a/d$  ratio of 1.85 is shown in Figure 3.3. It is clear in Figure 3.3 that for a given section depth, the specimens are expected to fail in shear prior to failing in flexure. For the Series M specimens, the longitudinal tension reinforcement ratio was 2.9% and the compression reinforcement ratio ranged from 0.2% to 0.4%. Additional information regarding the design of the Series M specimens can be found elsewhere (Huizinga, 2007).

In Series I through IV, the sections with the following cross-sectional dimensions were designed: 21"x23", 21"x42", 21"x44", and 21"x75". The overall length of the Series I through IV specimens was 332 in. In Series M, specimens with a 36"x48" cross-section were designed with an overall length of 284 in.

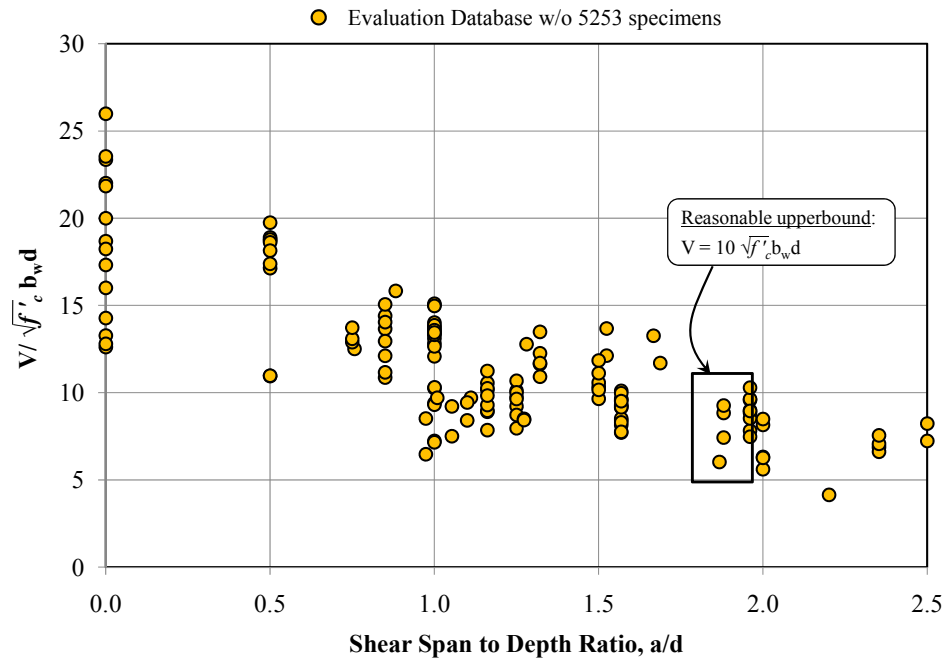


**Figure 3.2: Shear stress at failure for evaluation database used in specimen design**

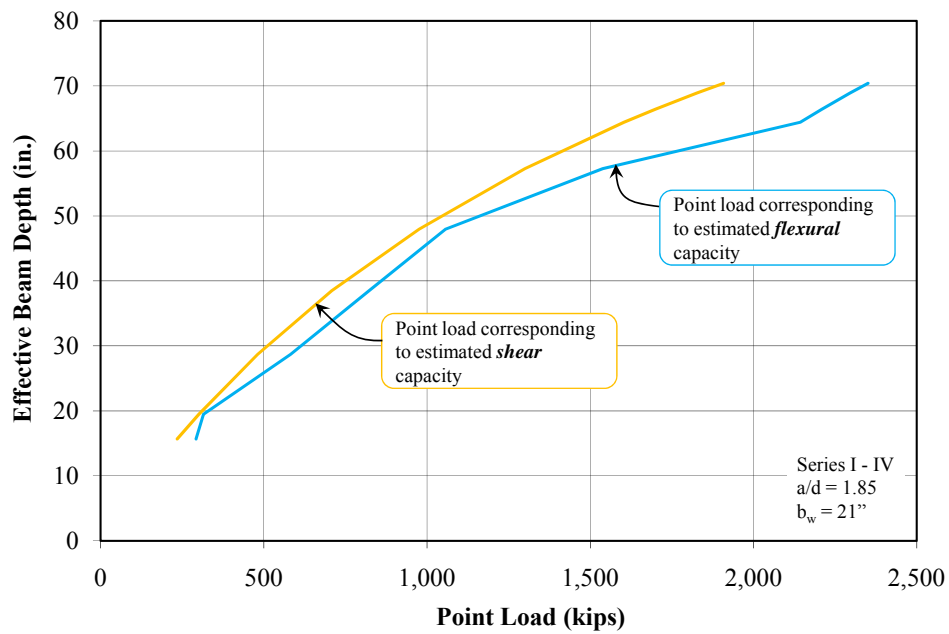


**Figure 3.3: Difference between estimated shear and flexural capacity**

Requirements in ACI 318-08 and AASHTO LRFD (2008) were satisfied in the design of the test specimens. Spacing requirements between adjacent bars and between layers of bars were met. Sufficient anchorage of the longitudinal reinforcement was provided with 90-degree hooks. Cover requirements consistent with precast conditions were satisfied since the specimens were fabricated in the laboratory with steel formwork and formwork-attached vibrators.

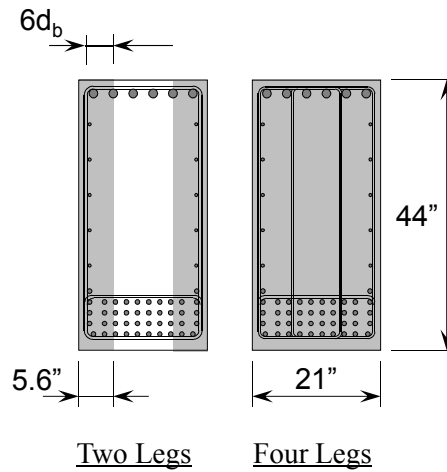
A brief description of each testing series is provided in Section 3.2.2 to 3.2.6. The pertinent beam details for all of the test specimens are provided in Section 3.2.7.

### **3.2.2 Series I: Distribution of Stirrups across Beam Web**

In ACI 318-08 and AASHTO LRFD (2008), provisions exist that recommend the distribution of stirrup legs across the width of the beam web. It is stated in ACI 318-08 that the reduction of “the transverse spacing of stirrup legs across the section” improves shear behavior (ACI 318 § R11.4.7, 2008). In AASHTO LRFD (2008), the width of a strut framing into a CTT node is limited to the distance equal to six longitudinal bar diameters from the center of the stirrup (AASHTO Figure 5.6.3.3.2-1 (a)). To use the full section width for the strut width, multiple stirrups legs may be needed, especially for reasonably wide members.

Four tests were conducted on specimens with a 21”x44” cross-section to investigate the effect of distributing stirrups across the web of a beam. All of the specimens were loaded at an  $a/d$  ratio of 1.85. The reinforcement for the Series I specimens was designed to evaluate the provision in AASHTO LRFD (2008). Companion tests were conducted such that the only primary variable between two tests was the number of stirrup legs: two or four. Based on the provision in AASHTO LRFD (2008), the design width of the internal strut in the two-legged specimen was 11.3 in.; while the design width of the strut in the four-legged specimen was 21 in., the full section width. The cross-sections of two test specimens are provided in Figure 3.4.

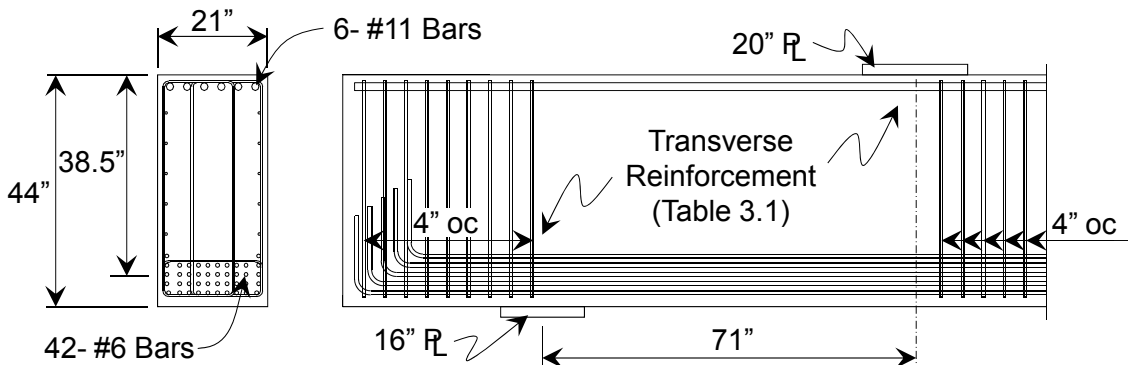
Shaded areas denote available strut width  
according to AASHTO LRFD (2008)



**Series I Test Specimens**

**Figure 3.4: Effective width of strut anchored by reinforcement at the CCT node**

Other geometric, reinforcement, and loading details for the Series I specimens are presented in Figure 3.5. The spacing of the #6 longitudinal reinforcement bars was controlled with steel chairs. The transverse reinforcement ratio was identical for companion tests but varied between each pair. One pair of tests had 0.2% web reinforcement in each direction; the other pair had 0.3% web reinforcement in each direction. The effect of distributing stirrups across the web of a beam is discussed by Tuchscherer (2008).



Clear Cover =  $\frac{3}{4}$ " (side); 1" (top and bottom)

**Figure 3.5: Series I beam details (Tuchscherer, 2008)**

The naming system presented in Figure 3.6 was used for the Series I specimens. The first numeral denotes the series number. The remaining numerals represent the variables within the testing series. In the case of Series I, the web reinforcement ratio and the number of stirrup legs varied. All other beam details were reasonably constant within Series I and are listed in Table 3.1.

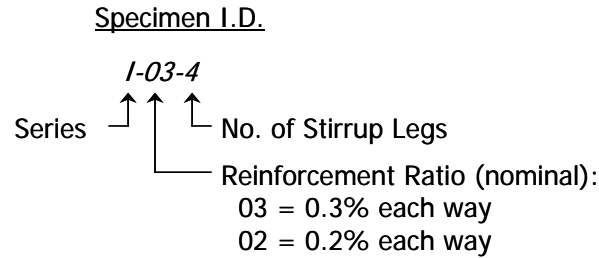


**Figure 3.6: Series I: description of beam ID naming system (Tuchscherer, 2008)**

**Table 3.1: Details of Series I specimens**

Beam I.D.	d in.	$\rho_v$	Size and Spacing ( $s_v$ )	$\rho_h$	Size and Spacing ( $s_h$ )	Support Plate in.	Load Plate in.
I-03-2	38.5	0.0029	#4 @ 6.5"	0.0033	#4 @ 5.75"	16x21	20x21
I-03-4	38.5	0.0030	#3 @ 7.0"	0.0033	#4 @ 5.75"	16x21	20x21
I-02-2	38.5	0.0020	#4 @ 9.5"	0.0020	#4 @ 9.5"	16x21	20x21
I-02-4	38.5	0.0021	#3 @ 10.0"	0.0020	#4 @ 9.5"	16x21	20x21

### 3.2.3 Series II: Triaxially Confined Nodal Regions

In the strut-and-tie model design provisions in AASHTO LRFD (2008) and ACI 318-08 Appendix A, there are no allowances for the benefit of triaxial confinement from surrounding concrete. Several researchers have illustrated the increase in the compressive strength of concrete due to confinement from surrounding concrete (Hawkins, 1968; Adebar and Zhou, 1993; and MacGregor and Wight, 2005). Based on this research, confinement from concrete is accounted for in the calculation of bearing capacity. However, the research has not extended to strut-and-tie model applications

where the size of bearing plates has a pronounced effect on design capacity. It should be noted that benefits of *confining reinforcement* is permitted in the STM provisions of ACI 318-08 Appendix A and AASHTO LRFD (2008) if the design values are supported by tests or analyses.

Based on this deficiency, eight tests were conducted on 21"x42" specimens in Project 5253. All of the specimens were loaded at an a/d ratio of 1.85. The size of the bearing plates at the load (CCC node) and at the support (CCT node) were systematically varied between each test. The width of the triaxially-confined bearing plates was three times smaller than the full width of the specimen (7 in. vs. 21 in.). The different sizes of bearing plates used in the Series II testing series are illustrated in Figure 3.7.

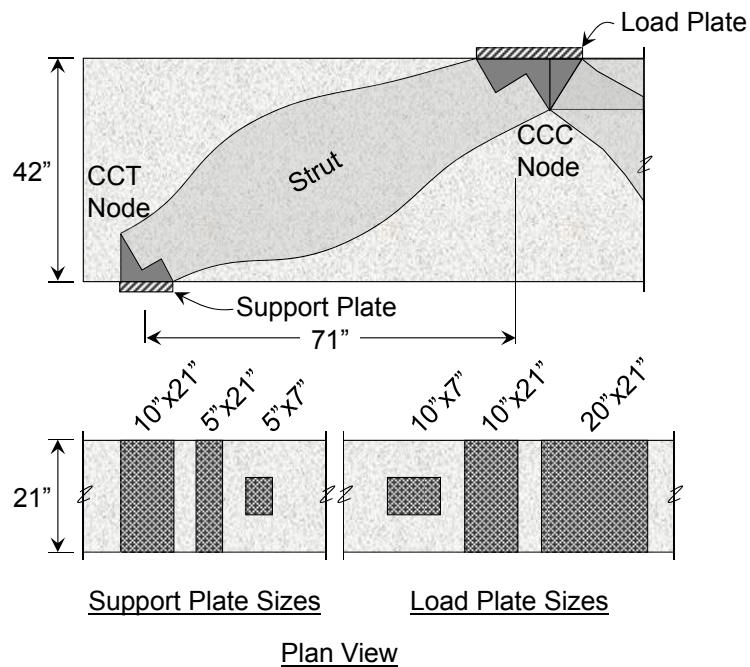


**Figure 3.7: Plate sizes investigated within Series II (Tuchscherer, 2008)**

Other geometric, reinforcement, and loading details for the Series II specimens are presented in Figure 3.8. The web reinforcement also varied in Series II for tests with identical bearing plates to evaluate whether the beneficial effects of confinement were influenced by the amount of web reinforcement. The effect of confining nodal regions with surrounding concrete is discussed by Tuchscherer (2008).

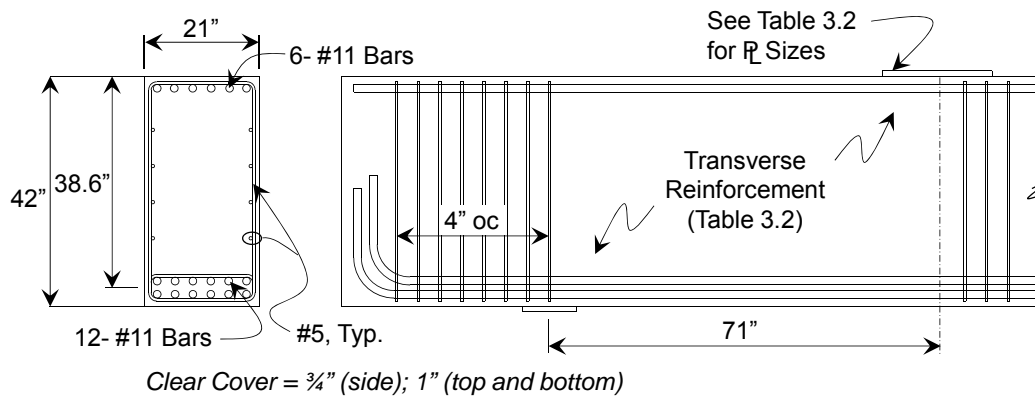


**Figure 3.8: Series II beam details (Tuchscherer, 2008)**

The naming system presented in Figure 3.9 was used for the Series II specimens. As previously noted, the amount of web reinforcement and the size of the bearing plate at the load and support were the variables in this series. The nodal region (i.e. CCC or CCT) that was investigated within each test was identified in the last numeral of the specimen ID as well. All other beam details were constant within Series II and are listed in Table 3.2.

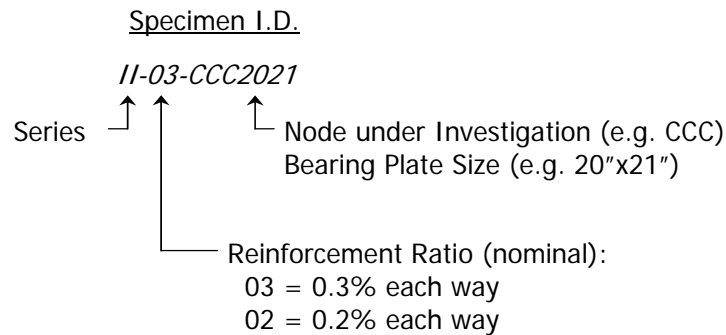


**Figure 3.9: Series II: Description of beam ID naming system (Tuchscherer, 2008)**

**Table 3.2: Details of Series II specimens**

Beam I.D.	d in.	$\rho_v$	Size and Spacing ( $s_v$ )	$\rho_h$	Size and Spacing ( $s_h$ )	Support Plate in.	Load Plate in.
II-03-CCC2021	38.6	0.0031	#5 @ 9.5"	0.0045	#5 @ 6.6"	10x21	20x21
II-03-CCC1007	38.6	0.0031	#5 @ 9.5"	0.0045	#5 @ 6.6"	10x21	10x7
II-03-CCT1021	38.6	0.0031	#5 @ 9.5"	0.0045	#5 @ 6.6"	10x21	36x21
II-03-CCT0507	38.6	0.0031	#5 @ 9.5"	0.0045	#5 @ 6.6"	5x7	36x21
II-02-CCT0507	38.6	0.0020	#5 @ 15.0"	0.0019	#4 @ 10"	5x7	36x21
II-02-CCC1007	38.6	0.0020	#5 @ 15.0"	0.0019	#4 @ 10.1"	10x21	10x7
II-02-CCC1021	38.6	0.0020	#5 @ 15.0"	0.0019	#4 @ 10.1"	10x21	10x21
II-02-CCT0521	38.6	0.0020	#5 @ 15.0"	0.0019	#4 @ 10.1"	5x21	20x21

### 3.2.4 Series III: Minimum Web Reinforcement

In the strut-and-tie model provisions in several design specifications (AASHTO LRFD (2008), ACI 318-08 Appendix A, CHBDC 2006, CSA A23.3-04, and *fib* 1999), different recommendations exist for minimum web reinforcement. There is little consensus regarding whether minimum reinforcement should address both strength and serviceability considerations. The purpose of the Series III testing series is to determine the appropriate amount of minimum reinforcement considering both the strength and serviceability performance of deep beams. The test results of the Series III specimens are provided in Section 4.3.

Twelve tests were conducted in Series III on 21"x42" specimens. The specimens were tested at three different a/d ratios: 1.2, 1.85, and 2.5. At an a/d ratio of 1.85, several specimens were tested in which the only variable was the quantity of vertical and horizontal web reinforcement. At a/d ratios of 1.2 and 2.5, reinforcement corresponding to 0.2% and 0.3% in each orthogonal direction was placed in companion specimens.

The amount of web reinforcement in the test specimens was categorized by the reinforcement ratio definitions given in Figure 3.10. The vertical and horizontal reinforcement was placed evenly throughout the shear span and the strut area,



respectively. The height of the strut was estimated by subtracting twice the distance from the extreme tension fiber to the centroid of the tension reinforcement and twice the distance from the extreme compression fiber to the centroid of the compression reinforcement from the total height of the section (Van Landuyt, 2006). This definition differed from the minimum reinforcement provisions in the STM section of AASHTO LRFD (2008) which bases the total amount of horizontal reinforcement on the gross concrete section ( $b_w h$ ). Since this reinforcement is intended primarily to reinforce bottle-shaped struts, it is appropriate to base the amount of reinforcement on the area of the bottle-shaped strut.

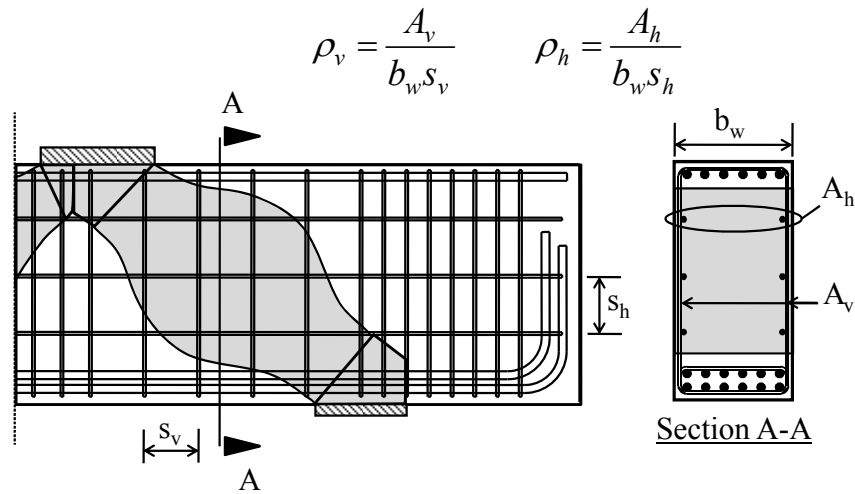


**Figure 3.10: Definition for vertical and horizontal web reinforcement ratios**

Other geometric, reinforcement, and loading details for the Series III specimens are presented in Figure 3.11. The primary variables for this testing series were the  $a/d$  ratio and the amount of web reinforcement. The effects of different spacing of the web reinforcement were not directly studied, but some comparisons were made possible through the extensive testing program. The size of the bearing plates was constant in Series III.

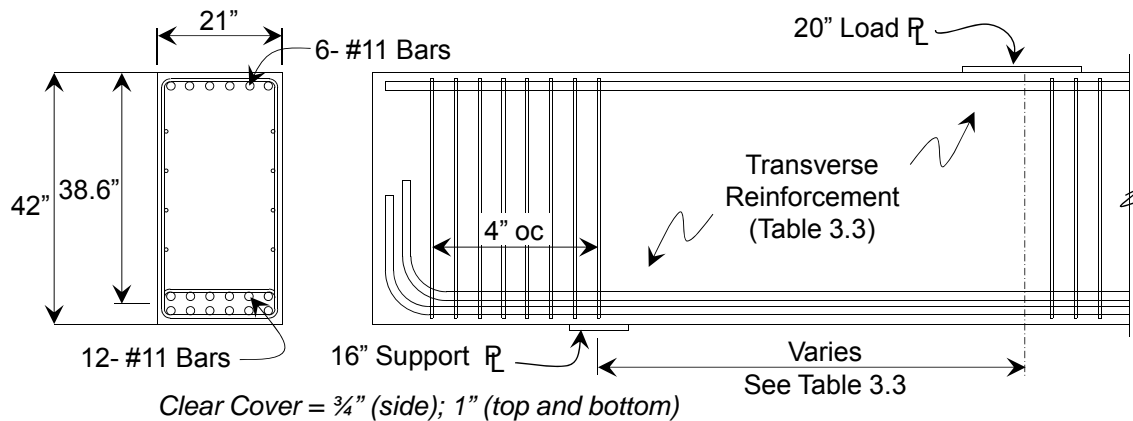


**Figure 3.11: Series III beam details**

The naming system presented in Figure 3.12 was used for the Series III specimens. As previously noted, the  $a/d$  ratio and the amount of web reinforcement were the variables in this series. All other pertinent beam details were constant within Series II and are listed in Table 3.3.

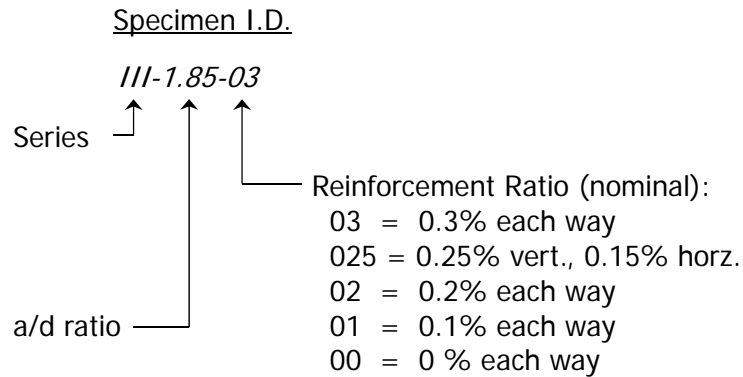


**Figure 3.12: Series III: Description of beam ID naming system**

**Table 3.3: Details of Series III specimens**

<b>Beam I.D.</b>	<b>d in.</b>	<b><math>\rho_v</math></b>	<b>Size and Spacing (<math>s_v</math>)</b>	<b><math>\rho_h</math></b>	<b>Size and Spacing (<math>s_h</math>)</b>	<b>Support Plate in.</b>	<b>Load Plate in.</b>
III-1.85-00	38.6	0	-	0	-	16x21	20x21
III-2.5-00	38.6	0	-	0	-	16x21	20x21
III-1.85-02	38.6	0.0020	#5 @ 14.5"	0.0019	#4 @ 10.1"	16x21	20x21
III-1.85-025	38.6	0.0024	#5 @ 12.0"	0.0014	#3 @ 7.6"	16x21	20x21
III-1.85-03	38.6	0.0029	#5 @ 10.0"	0.0029	#5 @ 10.1	16x21	20x21
III-1.85-01	38.6	0.0010	#4 @ 18.0"	0.0014	#3 @ 7.6"	16x21	20x21
III-1.85-03b	38.6	0.0031	#4 @ 6.0"	0.0029	#5 @ 10.1"	16x21	20x21
III-1.85-02b	38.6	0.0020	#4 @ 9.5"	0.0019	#4 @ 10.1"	16x21	20x21
III-1.2-02	38.6	0.0020	#4 @ 9.5"	0.0019	#4 @ 10.1"	16x21	20x21
III-1.2-03	38.6	0.0031	#5 @ 9.5"	0.0029	#5 @ 10.1"	16x21	20x21
III-2.5-02	38.6	0.002	#4 @ 9.5"	0.0019	#4 @ 10.1"	16x21	20x21
III-2.5-03	38.6	0.0029	#5 @ 9.5"	0.0029	#5 @ 10.1"	16x21	20x21

### **3.2.5 Series IV: Depth Effect**

Most of the bent caps in service in Texas are considerably larger (in width and in depth) than those in the literature (Figure 3.1). It is necessary to understand the effect that member depth may have on the performance of deep beams to improve the design of actual structures. The purpose of the Series IV specimens was to investigate the effect of member depth on the strength and serviceability performance of reinforced concrete deep beams. Other researchers have concluded that the width of deep beams does not affect their performance provided that the beam is laterally stable and can be properly detailed (Kani et al., 1979).

In Series IV, four tests were conducted on beams with a 21"x75" cross-section. Four tests were conducted on beams with a 21"x23" cross-section. At an a/d ratio of 1.85, a specimen was tested at each depth with 0.2% and 0.3% web reinforcement in each direction. At a/d ratios of 1.2 and 2.5, specimens were tested at each depth with 0.2%

web reinforcement. The specimens were designed such that they could be directly compared with the 21"x42" specimens tested in Series III. The geometric, reinforcement, and loading details for the Series IV specimens loaded at an a/d ratio of 1.85 are presented in Figure 3.13.

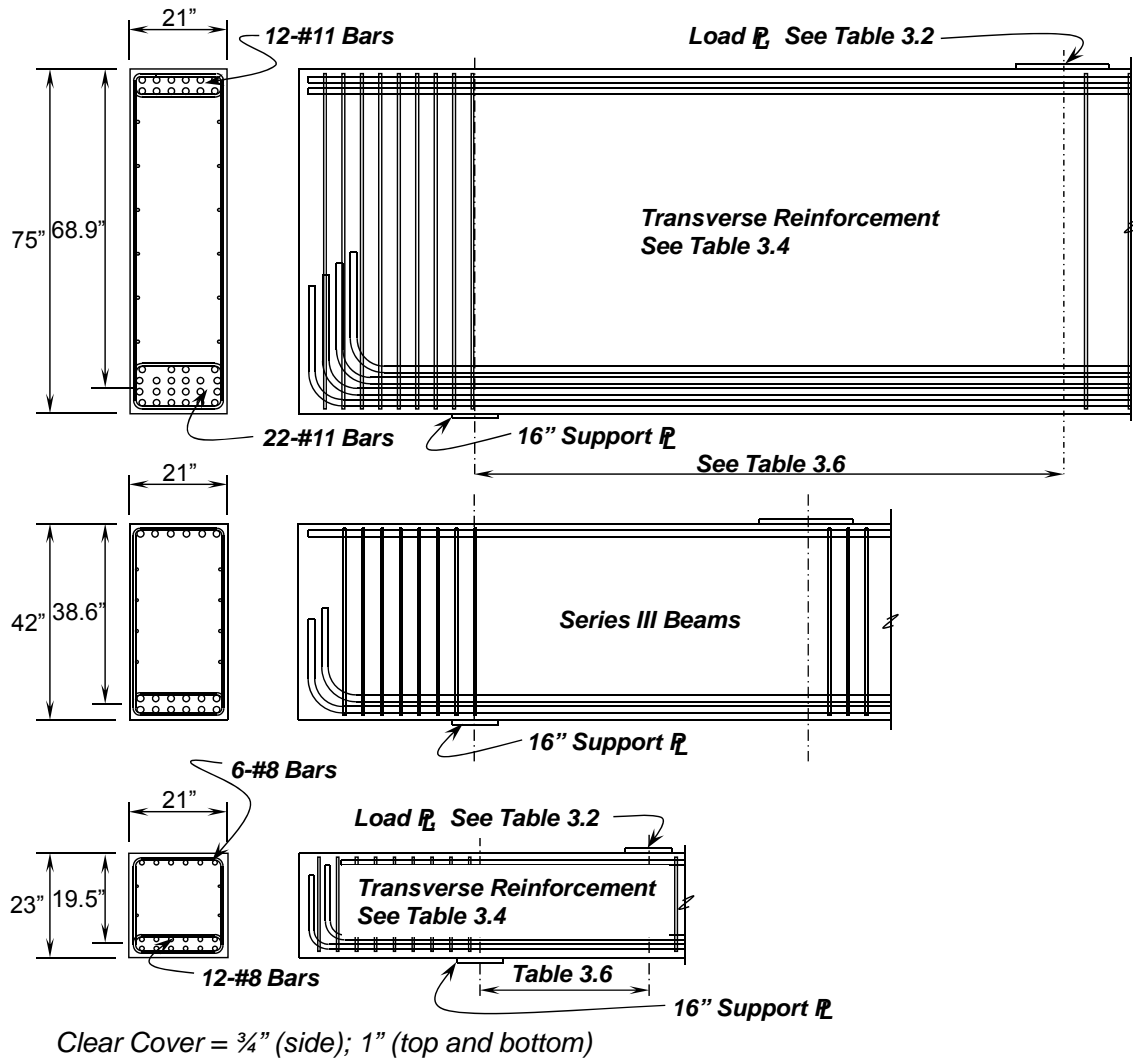


**Figure 3.13: Series IV beam details**

The size of the nodal regions (CCC and CCT) was kept relatively constant for the specimens with different depths that were tested at the same a/d ratio. This decision was made to evaluate the effect of changing the depth of the member without proportionately

changing the size of the nodal regions. In this way, the depth of the member was the only variable between each test. Additional discussion regarding the Series IV specimens and their test results is provided in Section 4.4.

The naming system presented in Figure 3.14 was used for the Series IV specimens. In Series IV, the primary variables were the member depth, the a/d ratio, and the quantity of web reinforcement. All other pertinent beam details were constant within Series IV and are listed in Table 3.4.

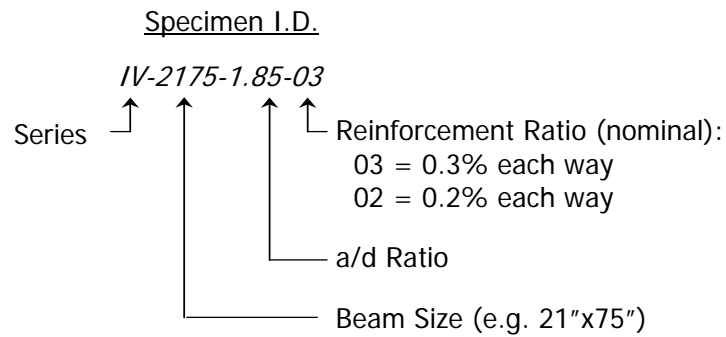


**Figure 3.14: Series IV: Description of beam ID naming system**

**Table 3.4: Details of Series IV specimens**

Beam I.D.	d in.	$\rho_v$	Size and Spacing ( $s_v$ )	$\rho_h$	Size and Spacing ( $s_h$ )	Support Plate in.	Load Plate in.
IV-2175-1.85-02	68.9	0.0021	#4 @ 9.5"	0.0019	#4 @ 10.1"	16x21	29x21
IV-2175-1.85-03	68.9	0.0031	#5 @ 9.5"	0.0029	#5 @ 10.1"	16x21	29x21
IV-2175-2.5-02	68.9	0.0021	#5 @ 14.25"	0.0021	#5 @ 14.25"	16x21	24x21
IV-2175-1.2-02	68.9	0.0021	#5 @ 14.25"	0.0021	#5 @ 14.25"	16x21	24x21
IV-2123-1.85-03	19.5	0.0030	#4 @ 6.25"	0.0030	#4 @ 6.25"	16x21	16.5x21
IV-2123-1.85-02	19.5	0.0020	#3 @ 5.25"	0.0017	#3 @ 6.25"	16x21	16.5x21
IV-2123-2.5-02	19.5	0.0020	#3 @ 5.25"	0.0017	#3 @ 6.25"	16x21	15.5x21
IV-2123-1.2-02	19.5	0.0020	#3 @ 5.25"	0.0017	#3 @ 6.25"	16x21	18x21

### 3.2.6 Series M: Multiple Purpose

The Series M specimens were the first specimens fabricated and tested in Project 5253. All of the Series M specimens had a 36" x 48" cross-section. The primary variables in Series M were the amount of web reinforcement, the distribution of stirrups across the web, and the size of the load plate. Five tests were conducted. The results of these tests were used to design the rest of the experimental program (Series I through IV) and are included with the results of the other Series that addressed a similar objective. The results from the Series M specimens were exceptionally valuable due to the size of the cross-section. Geometric, reinforcement, and loading details for the Series M specimens are provided in Figure 3.15.

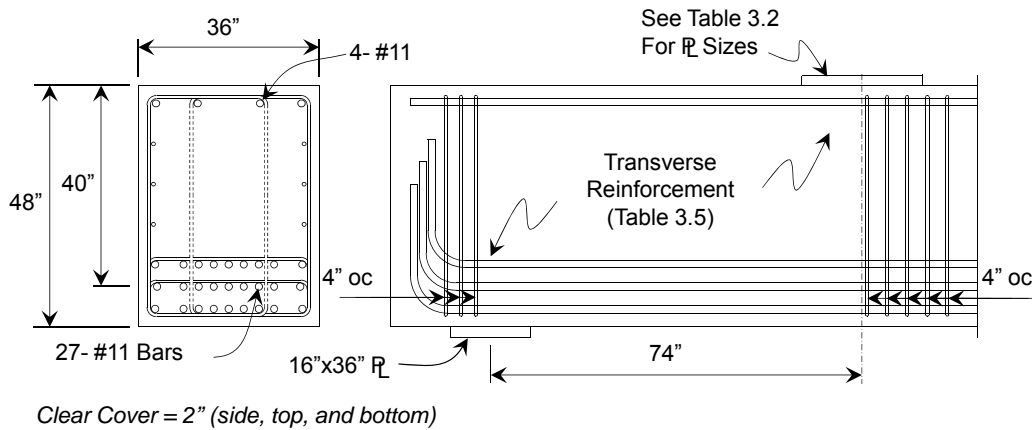


**Figure 3.15: Series M beam details (Huizinga, 2007)**

There were some differences between the Series M specimens and those in the other series such as the beam width, the ratio of the longitudinal compression reinforcement to the effective area (0.44%), the ratio of the longitudinal tension reinforcement to the effective area (2.9%), and the concrete cover. A larger cover (2" all sides) was used in the Series M specimens as compared to those in Series I through IV since these members were cast with wood formwork and without the benefit of form vibrators (Section 3.3.3). Additional information regarding the design, fabrication, and testing of the Series M specimens is discussed by Huizinga (2007).

The naming system presented in Figure 3.16 was used for the Series M specimens. In Series M, the primary variables were the quantity of web reinforcement,

the number of stirrup legs, and the size of the bearing plate at the load point. All other beam details were constant within Series M and are listed in Table 3.5.

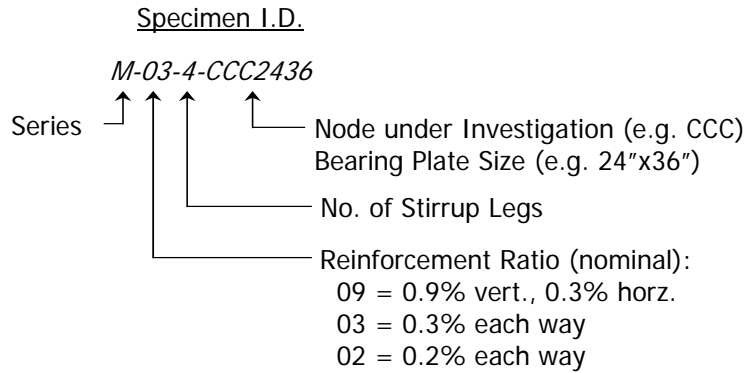


**Figure 3.16: Series M - description of beam ID naming system**

**Table 3.5: Details of Series M Specimens**

Beam I.D.	d in.	$\rho_v$	Size and Spacing ( $s_v$ )	$\rho_h$	Size and Spacing ( $s_h$ )	Support Plate in.	Load Plate in.
M-03-4-CCC2436	40	0.0031	#5 @ 11"	0.0027	#5 @ 6.5"	16x36	24x26
M-03-4-CCC0812	40	0.0031	#5 @ 11"	0.0027	#5 @ 6.5"	16x36	8x12
M-09-4-CCC2436	40	0.0086	#5 @ 4"	0.0027	#5 @ 6.5"	16x36	24x36
M-02-4-CCC2436	40	0.0022	#4 @ 10"	0.0022	#5 @ 8"	16x36	24x36
M-03-2-CCC2436	40	0.0031	#7 @ 11"	0.0027	#5 @ 6.5"	16x36	24x36

### 3.2.7 Summary of Test Specimen Details

Thirty-seven tests were conducted in the current experimental program. The deep beams tested represent some of the largest deep beam shear tests available in the literature as seen in Figure 3.17. The specimens from the current study populate the upper bound of the deep beam data in the literature as measured by the shear area of the beam ( $b_w d$ ). A comparison between bent caps used in the State of Texas, the beams in the current study, and beams from previous research projects is provided in Figure 3.18.

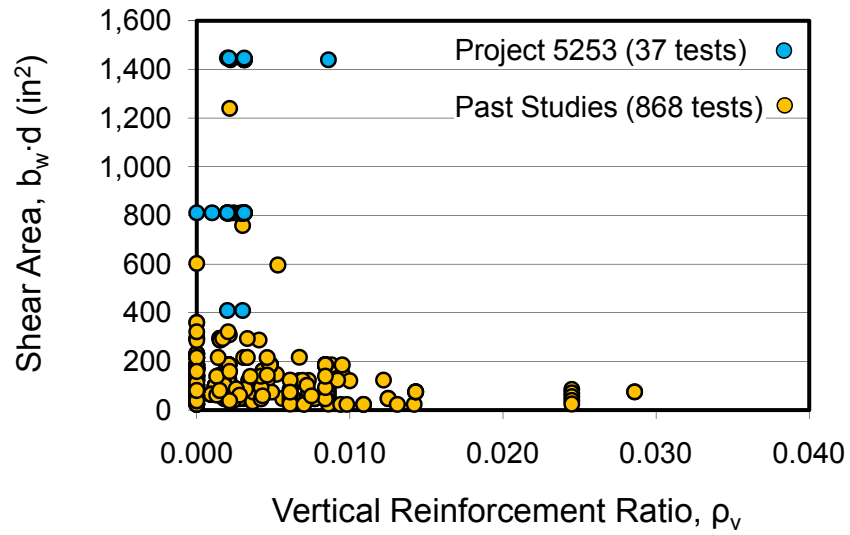


**Figure 3.17: Comparison of beams sizes between current and past studies**

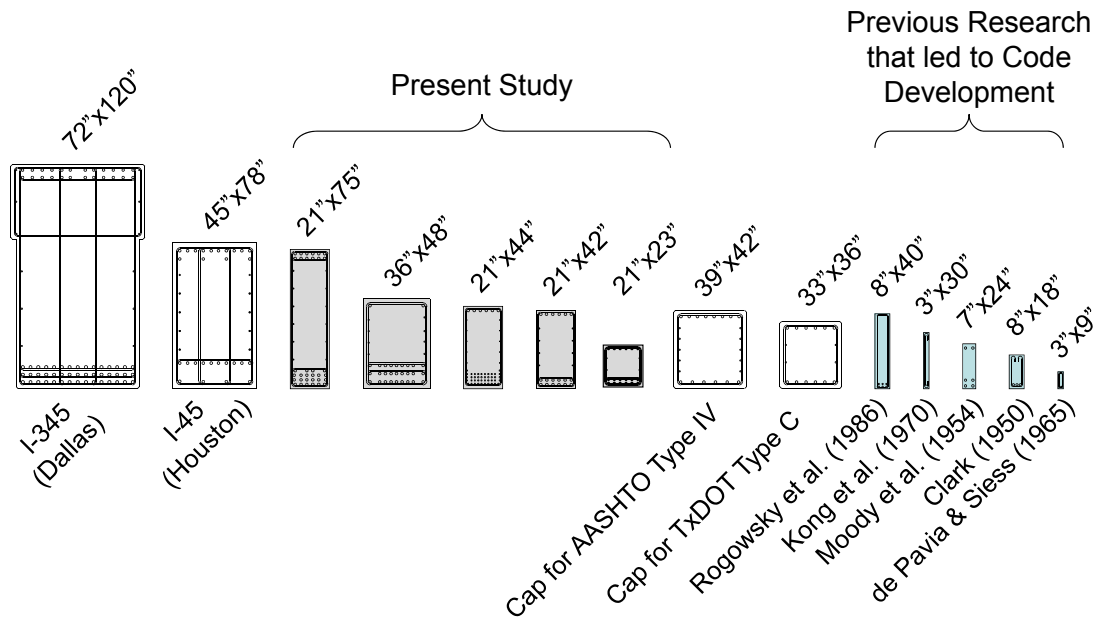


**Figure 3.18: Scaled comparison of actual bent caps and beams included in current and past research programs. (Tuchscherer, 2008)**

A summary of details for the 37 tests in the experimental program is presented in Table 3.6. A summary of experimental results for all of the test specimens is provided in Section 4.2. The variables used in Table 3.6 are defined as follows:



- $b_w$  = beam width, in.
- $h$  = beam height, in.
- $d$  = distance from extreme compression fiber to centroid of tensile reinforcement, in.
- $\rho_l$  = ratio of longitudinal tensile reinforcement to effective area ( $A_s / b_w d$ )
- $\rho_l'$  = ratio of longitudinal compression reinforcement to effective area ( $A_s' / b_w d$ )
- $\rho_v$  = ratio of vertical web reinforcement to effective area ( $A_v / b_w s_v$ )
- $s_v$  = spacing of vertical web reinforcement, in.
- $\rho_h$  = ratio of horizontal web reinforcement to effective area ( $A_h / b_w s_h$ )
- $s_h$  = spacing of horizontal web reinforcement, in.
- $a$  = centerline distance between load and support plates
- Load Plate** = dimensions of the load bearing plate measured in the longitudinal and transverse direction of the beam ( $l \times w$ ), in.
- Support Plate** = dimensions of the support bearing plate measured in the longitudinal and transverse direction of the beam ( $l \times w$ ), in.
- a/d ratio** = shear span-to-depth ratio

**Table 3.6: Summary of all beam details**

<b>Beam I.D.</b>	<b>b<sub>w</sub> in.</b>	<b>h in.</b>	<b>d in.</b>	<b><math>\rho_l</math></b>	<b><math>\rho_l'</math></b>	<b><math>\rho_v</math></b>	<b>Size and Spacing (s<sub>v</sub>)</b>	<b><math>\rho_h</math></b>	<b>Size and Spacing (s<sub>h</sub>)</b>	<b>Support Plate in.</b>	<b>Load Plate in.</b>	<b>a/d ratio</b>
I-03-2	21	44	38.5	0.0229	0.0116	0.0029	#4 @ 6.5"	0.0033	#4 @ 5.75"	16x21	20x21	1.84
I-03-4	21	44	38.5	0.0229	0.0116	0.0030	#3 @ 7.0"	0.0033	#4 @ 5.75"	16x21	20x21	1.84
I-02-2	21	44	38.5	0.0229	0.0116	0.0020	#4 @ 9.5"	0.0020	#4 @ 9.5"	16x21	20x21	1.84
I-02-4	21	44	38.5	0.0229	0.0116	0.0021	#3 @ 10.0"	0.0020	#4 @ 9.5"	16x21	20x21	1.84
II-03-CCC2021	21	42	38.6	0.0231	0.0115	0.0031	#5 @ 9.5"	0.0045	#5 @ 6.6"	10x21	20x21	1.84
II-03-CCC1007	21	42	38.6	0.0231	0.0115	0.0031	#5 @ 9.5"	0.0045	#5 @ 6.6"	10x21	10x7	1.84
II-03-CCT1021	21	42	38.6	0.0231	0.0115	0.0031	#5 @ 9.5"	0.0045	#5 @ 6.6"	10x21	36x21	1.84
II-03-CCT0507	21	42	38.6	0.0231	0.0115	0.0031	#5 @ 9.5"	0.0045	#5 @ 6.6"	5x7	36x21	1.84
II-02-CCT0507	21	42	38.6	0.0231	0.0115	0.0020	#5 @ 15.0"	0.0019	#4 @ 10"	5x7	36x21	1.84
II-02-CCC1007	21	42	38.6	0.0231	0.0115	0.0020	#5 @ 15.0"	0.0019	#4 @ 10.1"	10x21	10x7	1.84
II-02-CCC1021	21	42	38.6	0.0231	0.0115	0.0020	#5 @ 15.0"	0.0019	#4 @ 10.1"	10x21	10x21	1.84
II-02-CCT0521	21	42	38.6	0.0231	0.0115	0.0020	#5 @ 15.0"	0.0019	#4 @ 10.1"	5x21	20x21	1.84
III-1.85-00	21	42	38.6	0.0231	0.0115	0.000	-	0	-	16x21	20x21	1.84
III-2.5-00	21	42	38.6	0.0231	0.0115	0.000	-	0	-	16x21	20x21	2.47
III-1.85-02	21	42	38.6	0.0231	0.0115	0.0020	#5 @ 14.5"	0.0019	#4 @ 10.1"	16x21	20x21	1.84
III-1.85-025	21	42	38.6	0.0231	0.0115	0.0024	#5 @ 12.0"	0.0014	#3 @ 7.6"	16x21	20x21	1.84
III-1.85-03	21	42	38.6	0.0231	0.0115	0.0029	#5 @ 10.0"	0.0029	#5 @ 10.1	16x21	20x21	1.84
III-1.85-01	21	42	38.6	0.0231	0.0115	0.0010	#4 @ 18.0"	0.0014	#3 @ 7.6"	16x21	20x21	1.84

**Table 3.6 (cont.'d): Summary of all beam details**

<b>Beam I.D.</b>	<b>b<sub>w</sub> in.</b>	<b>h in.</b>	<b>d in.</b>	<b>ρ<sub>l</sub></b>	<b>ρ<sub>l</sub>'</b>	<b>ρ<sub>v</sub></b>	<b>Size and Spacing (s<sub>v</sub>)</b>	<b>ρ<sub>h</sub></b>	<b>Size and Spacing (s<sub>h</sub>)</b>	<b>Support Plate in.</b>	<b>Load Plate in.</b>	<b>a/d ratio</b>
III-1.85-03b	21	42	38.6	0.0231	0.0115	0.0031	#4 @ 6.0"	0.0029	#5 @ 10.1"	16x21	20x21	1.84
III-1.85-02b	21	42	38.6	0.0231	0.0115	0.002	#4 @ 9.5"	0.0019	#4 @ 10.1"	16x21	20x21	1.84
III-1.2-02	21	42	38.6	0.0231	0.0115	0.002	#4 @ 9.5"	0.0019	#4 @ 10.1"	16x21	20x21	1.20
III-1.2-03	21	42	38.6	0.0231	0.0115	0.0031	#5 @ 9.5"	0.0029	#5 @ 10.1"	16x21	20x21	1.20
III-2.5-02	21	42	38.6	0.0231	0.0115	0.002	#4 @ 9.5"	0.0019	#4 @ 10.1"	16x21	20x21	2.49
III-2.5-03	21	42	38.6	0.0231	0.0115	0.0031	#5 @ 9.5"	0.0029	#5 @ 10.1"	16x21	20x21	2.49
IV-2175-1.85-02	21	75	68.9	0.0237	0.0129	0.0021	#4 @ 9.5"	0.0019	#4 @ 10.1"	16x21	29x21	1.85
IV-2175-1.85-03	21	75	68.9	0.0237	0.0129	0.0031	#5 @ 9.5"	0.0029	#5 @ 10.1"	16x21	29x21	1.85
IV-2175-2.5-02	21	75	68.9	0.0237	0.0129	0.0021	#5 @ 14.25"	0.0021	#5 @ 14.25"	16x21	24x21	2.50
IV-2175-1.2-02	21	75	68.9	0.0237	0.0129	0.0021	#5 @ 14.25"	0.0021	#5 @ 14.25"	16x21	24x21	1.20
IV-2123-1.85-03	21	23	19.5	0.0232	0.0116	0.0030	#4 @ 6.25"	0.0030	#4 @ 6.25"	16x21	16.5x21	1.85
IV-2123-1.85-02	21	23	19.5	0.0232	0.0116	0.0020	#3 @ 5.25"	0.0017	#3 @ 6.25"	16x21	16.5x21	1.85
IV-2123-2.5-02	21	23	19.5	0.0232	0.0116	0.0020	#3 @ 5.25"	0.0017	#3 @ 6.25"	16x21	15.5x21	2.50
IV-2123-1.2-02	21	23	19.5	0.0232	0.0116	0.0020	#3 @ 5.25"	0.0017	#3 @ 6.25"	16x21	18x21	1.20
M-03-4-CCC2436	36	48	40	0.0293	0.0043	0.0031	#5 @ 11"	0.0027	#5 @ 6.5"	16x36	24x36	1.85
M-03-4-CCC0812	36	48	40	0.0293	0.0043	0.0031	#5 @ 11"	0.0027	#5 @ 6.5"	16x36	8x12	1.85
M-09-4-CCC2436	36	48	40	0.0293	0.0043	0.0086	#5 @ 4"	0.0027	#5 @ 6.5"	16x36	24x36	1.85
M-02-4-CCC2436	36	48	40	0.0293	0.0043	0.0022	#4 @ 10"	0.0022	#5 @ 8"	16x36	24x36	1.85
M-03-2-CCC2436	36	48	40	0.0293	0.0022	0.0031	#7 @ 11"	0.0027	#5 @ 6.5"	16x36	24x36	1.85

### **3.3 FABRICATION OF SPECIMENS**

All of the test specimens were fabricated in the Ferguson Structural Engineering Laboratory at the University of Texas at Austin. Each beam took approximately two weeks to fabricate.

#### **3.3.1 Steel Reinforcement**

Grade 60, deformed reinforcement satisfying the requirements of ASTM A615 was used in the test specimens. Three or four tensile coupons were ordered for each bar size in every batch of rebar shipped from the manufacturer. The tensile strength of the coupons was measured in accordance with ASTM A370 with a universal testing machine. The tensile strength of the longitudinal and web reinforcement for all test specimens, as measured from the coupon tests, is provided in Section 4.2.

#### **3.3.2 Concrete Mixture Design**

Ready-mix concrete designed for 4,000 psi strength at 28 days was used in the test specimens. The mixture design included Type I cement and  $\frac{3}{4}$ -inch river rock coarse aggregate. The concrete mixture design is presented in Table 3.7. The compressive strength of concrete was measured in accordance with ASTM C39 for standard 4"x8" cylinders. The measured compressive strength of concrete for each specimen is provided with the summary of experimental results in Section 4.2.

**Table 3.7: Concrete mixture design**

<b>Material</b>	<b>Quantity</b>
<b><i>Type I Portland Cement</i></b>	300 to 317 lb/cy
<b><i>Fly Ash</i></b>	79 to 83 lb/cy
<b><i>CA: ¾" River Rock</i></b>	1800 to 1850 lb/cy
<b><i>FA: Sand</i></b>	1370 to 1515 lb/cy
<b><i>Water</i></b>	29 to 31 gallons/cy
<b><i>HRWR* Admixture</i></b>	15 to 20 oz/cy
<b><i>Set Retardant Admixture</i></b>	6 oz/cy
<b><i>Water/Cement Ratio</i></b>	0.62 to 0.68
<b><i>Slump</i></b>	4 to 8 inches

*\*HRWR: High Range Water Reducing (i.e. Superplasticizer)*

### **3.3.3 Construction of Specimens**

The reinforcing steel was delivered in the specified lengths and with the appropriate bends from a local supplier. The reinforcement cages were assembled in the laboratory and upon completion, were moved to the casting area. The specimens were cast in the same orientation that they were tested. Since the specimens were loaded with a point load at the bottom of the beam, the primary longitudinal (tension) reinforcement was placed at the top of the section. Likewise, compression reinforcement was placed at the bottom of the section.

The concrete used to fabricate the test specimens was provided by a local ready-mix supplier. A slump test was performed according to ASTM C143 upon the arrival of the mixing truck to the laboratory. The targeted slump was between 4 in. and 8 in. In some cases, water was added to meet the targeted slump range. However, the additional water did not exceed the recommended limit on the batch ticket.

A minimum of twelve 4"x8" cylinders were made with each beam. The cylinders were cast at the same time as the test specimen in accordance with ASTM C31 and were cured under the same ambient conditions. A plastic tarp was placed on top of the cylinders to limit the loss of water due to shrinkage.

The Series I through IV specimens were cast with steel formwork. The concrete was placed in the formwork via a 1-yard overhead hopper in approximately 3 lifts. Upon placement of each hopper of concrete, external vibrators attached to a sliding track on the steel formwork helped consolidate the concrete. Internal rod vibrators, or stingers, were used to help consolidate the concrete near the top of the section. The specimens cured under the ambient temperature in the laboratory with a plastic tarp positioned across the top of the beam.

An illustration of the fabrication procedure for a 21"x42" specimen is presented in Figure 3.19.



(a)



(b)



(c)



(d)



(e)



(f)

**Figure 3.19: Fabrication of a typical beam: (a) assembly of reinforcement cage (b) placement of cage in formwork (c) forms in place prior to concrete placement (d) placement of concrete (e) beam curing (f) test specimen after the removal of forms (Tuchscherer, 2008)**

The fabrication of the 21"x23" and the 21"x75" specimens was carried out in a similar fashion to that of the 21"x42" specimens. For the 23-inch deep specimens, smaller 24-inch tall steel side forms were used to cast the beams. For the 75-inch specimens, the 24-inch side forms were bolted to the top of the original 52-inch tall side forms with 33 – 5/8-inch diameter bolts. A couple of pictures illustrating the fabrication of a 21"x75" specimen are provided in Figure 3.20.



***Figure 3.20: Fabrication of a 21"x75" beam: (a) movement of reinforcement cage into formwork (b) placement of concrete into steel formwork***

The Series M specimens (36"x48") were cast with wooden formwork. Numerous crossties and wooden kickers were used to provide lateral stability to the formwork. Internal rod vibrators were used to aid in the consolidation of the concrete. Since steel formwork and formwork-attached vibrators were not used, a clear cover of 2 in. was provided for these specimens. Also, two steel ducts were placed at the ends of each beam to allow 3-inch diameter rods to pass through the member during testing. The fabrication of a 36"x48" specimen is illustrated in Figure 3.21.





(a)



(b)

***Figure 3.21: Fabrication of a 36"x48" beam: (a) tied reinforcement cage with steel ducts (b) placement of concrete into wooden formwork (Huizinga, 2007)***

For the 21"x75" and the 36"x48" specimens, two ready-mix trucks were required to supply enough concrete to cast each individual specimen. Both trucks were filled with the same mixture design from the same batch plant. In every case, the second truck arrived approximately 30 minutes after the first truck. This schedule kept the idling time for the second truck at a minimum and eliminated the presence of a cold joint. Standard 4"x8" cylinders were prepared from the concrete in each truck. The measured concrete strength from one truck was generally within 20% of the strength of the other. The compressive strength values reported for these large specimens were the weighted average of the results of three cylinders from each truck on the day of the test.

After casting, all of the specimens were moved into the test setup with an overhead crane. Two- or three-inch diameter steel bars were inserted into PVC sleeves that were cast in the specimen. The PVC sleeves were placed directly below the primary tension reinforcement outside of the test region, where possible. Large steel cables were looped around the steel bars immediately adjacent to the side of the specimen to limit bending of the bars. The specimen was then lifted and placed in the test setup with an overhead, 25-ton capacity crane.

### **3.4 TESTING FRAME**

To load the specimens to failure, a test setup was designed in the Phil M. Ferguson Structural Engineering Laboratory (FSEL). The setup was designed around a 96,000-pound steel platen that was used as a strong floor. Previously, the steel platen was the lower reaction floor of a six-million pound capacity testing frame that was decommissioned by the U.S. Navy and donated to FSEL. The construction of the test setup is illustrated in Figure 3.22. Details of the test setup with a 21"x42" specimen in position are depicted in Figure 3.23 and Figure 3.24. For additional information regarding the construction of the test frame refer to Huizinga (2007).



(a)



(b)



(c)



(d)



(e)

**Figure 3.22: Installation of strong floor: (a) steel platen (b) floor excavation (c) fabrication of platen support (d) lowering of platen into position, and (e) test setup (Tuchscherer, 2008)**

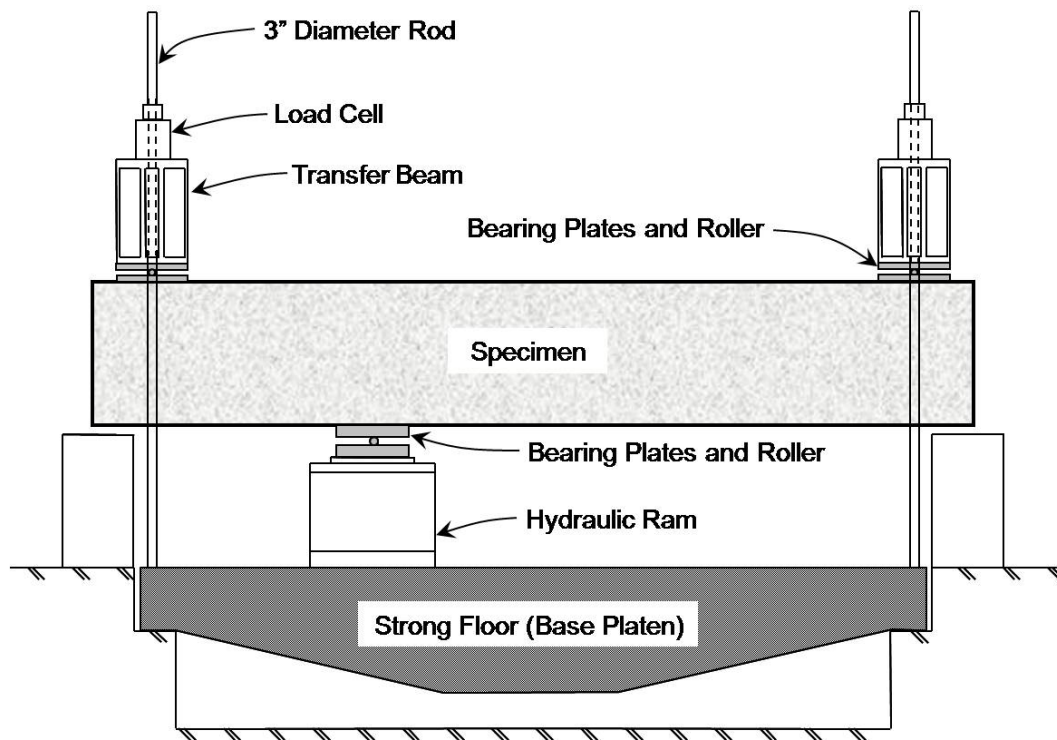


*Figure 3.23: Elevation view of test setup (Huizinga, 2007)*

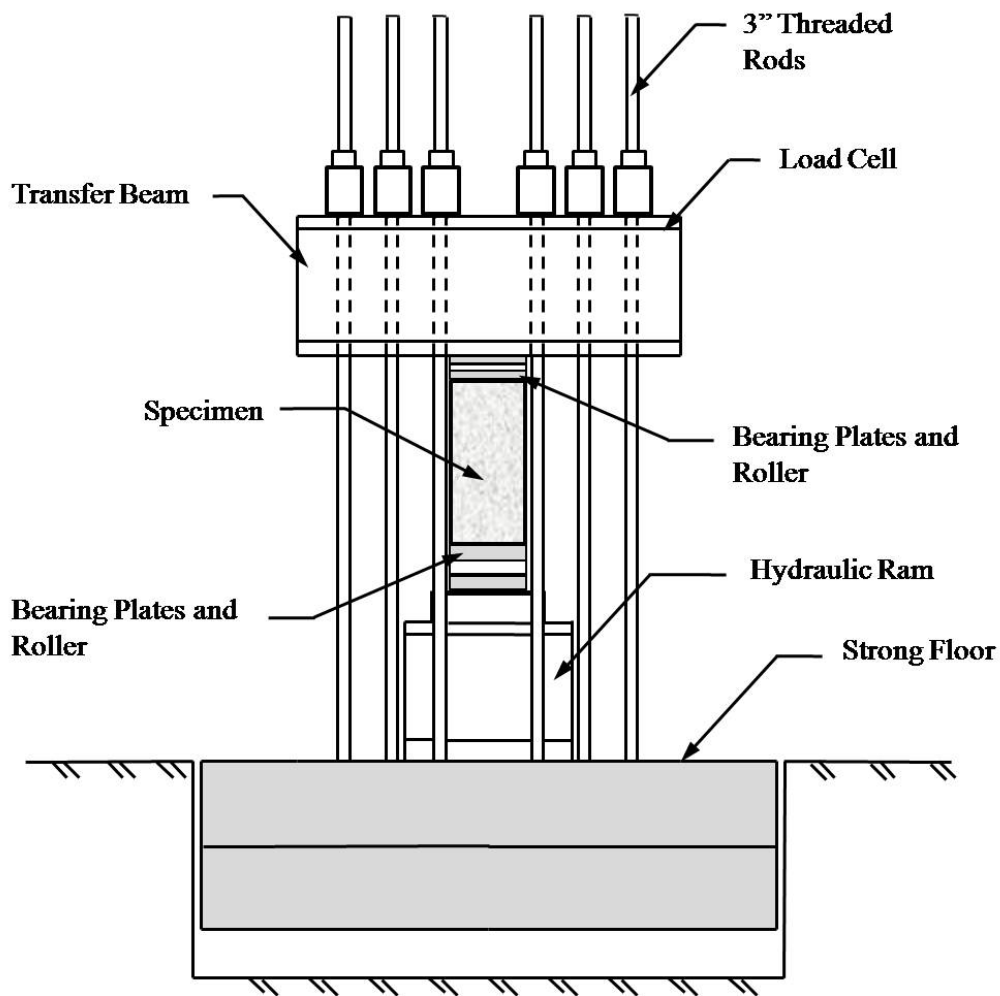


*Figure 3.24: Section view of test setup*

The test setup was designed for an upside-down simply-supported beam test. The load was applied via a 6 million pound capacity, double-acting hydraulic ram. At each support, 6 – 3-inch diameter, threaded rods resisted the applied load. The setup is self-equilibrating in that the applied loads are resisted within the test frame, not by the surrounding concrete floor. In the current configuration, the test setup can resist a shear force of approximately 1.5 million pounds or an applied load at midspan of approximately 3 million pounds.

At each support, pin connections were created with two 2-inch steel plates sandwiching a two-inch diameter steel bar. The bar was welded to the bottom plate to



simulate a pinned connection. Horizontal movement was permitted by the flexibility of the 6 threaded rods at each support. A thin layer of hydrostone was applied to the top surface of the test specimens at the location of the support plates to provide a planar reaction surface. At the applied load, rotation was permitted with a 3-inch diameter steel bar. The bar was allowed to roll freely between two four-inch thick steel plates. A smaller ½-inch thick steel plate was placed on top of the upper 4-inch plate to obtain the desired size of the load plate. Hydrostone was also placed between this plate and the bottom surface of the test specimen to obtain a planar bearing surface.

The two internal reaction rods of the setup are positioned to accommodate a 21"-wide specimen between them. This was the reason for the selection of the 21" dimension in the majority of the test specimens. For the 36"x48" specimens, the two internal reaction rods passed through the ends of the beam via the steel ducts that were placed in the specimen prior to casting.

Also, it is important to note that the test setup was slightly adjusted to accommodate the smaller sized 21"x23" specimens. A 2 million pound capacity ram was used to load the specimens, a 12-inch thick steel plate was used as a spacer beneath the ram, and back-to-back channel assemblies were used as spacers between the roller supports and the transfer beam. A picture of a 21"x23" specimen in the test setup is provided in Figure 3.25.



***Figure 3.25: 21"x23" specimen in test setup***

### 3.5 INSTRUMENTATION

Several different instruments were used to obtain data during the tests in the experimental program. The instruments included electrical strain gauges, linear potentiometers, load cells, and crack comparator cards. Details regarding each of these devices are provided in this section.

#### 3.5.1 Strain Measurements using Reinforcing Bars

Strain gauges were affixed to the transverse and longitudinal reinforcement in order to measure the change in strain. The gauge type was *FLA-3-11-5LT* manufactured by Tokyo Sokki Kenkyujo Co. These gauges are intended for general purpose mild steel applications. The width and length of the gauges were 1.5- and 3-mm, respectively, with a resistance of 120 ohms ( $\pm 0.5$ ) (Figure 3.26). The surface of the reinforcement was lightly sanded and polished to provide a relatively smooth surface for the application of the strain gauges. Care was taken not to significantly reduce the cross section of the reinforcement. The gauges were glued to the reinforcement, sealed with acrylic, protected with a neoprene pad, and taped to further isolate them from the water in the concrete.



**Figure 3.26: Installation of strain gauge on mild reinforcement (Tuchscherer, 2008)**

Typical locations of internal strain gauges for the Series III and IV specimens are illustrated in Figure 3.27. The location of internal gauges in the specimens in other series can be found elsewhere (Birrer et al., 2009). They were not included herein because the strain gauge data for these specimens was not used in the tasks discussed in this dissertation.

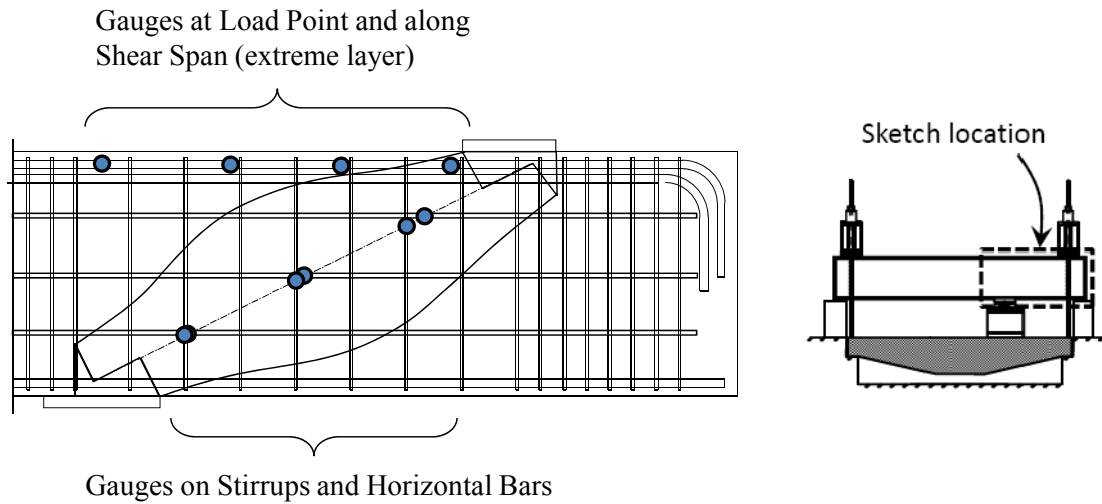


**Figure 3.27: Typical internal strain gauge locations for Series III and IV**

Strain gauges were attached to both legs of stirrups along the assumed centerline of the inclined strut. They were also attached to the horizontal bars on each face at the intersection with the assumed diagonal strut. The purpose of locating a gauge along the strut centerline was to measure steel strains at or close to the primary diagonal splitting crack.

The strain in the primary tension reinforcement was also monitored in each specimen. At the location of the applied load, the longitudinal strain was measured in at least three of the bars in the outermost layer of reinforcement (Figure 3.27). The purpose of providing gauges at this location was to monitor the maximum strain in the reinforcement as the beam was loaded to failure. Additional strain gauges were attached to the longitudinal reinforcement along the test region (Figure 3.27). The purpose of these gauges was to monitor the strain in the primary tension tie throughout the shear span. Other researchers have monitored strain in a similar fashion to compare the behavior of the test specimen to an assumed strut-and-tie model (Moody et al., 1954; Watstein and Mathey, 1958; Rogowsky et al., 1986; Quintero-Febres et al., 2006; and Tan et al., 2007). In a single-panel strut-and-tie model, the force in the primary tension tie is constant throughout the shear span. Therefore, the strain gauge data from the



longitudinal reinforcement were used to assess the applicability of a single-panel STM for several  $a/d$  ratios and specimen sizes.

### 3.5.2 Load and Displacement Measurements

The reaction at each support was measured by 500-kip capacity load cells. They were placed between the transfer beam and the nuts on each of the 12 threaded rods, 6 at each support. The load cells at one support are illustrated in Figure 3.28. The load cells were individually calibrated in a universal testing machine. Also, readings from the load cells at the supports were confirmed with the use of a pressure transducer in the feed line of the hydraulic ram.

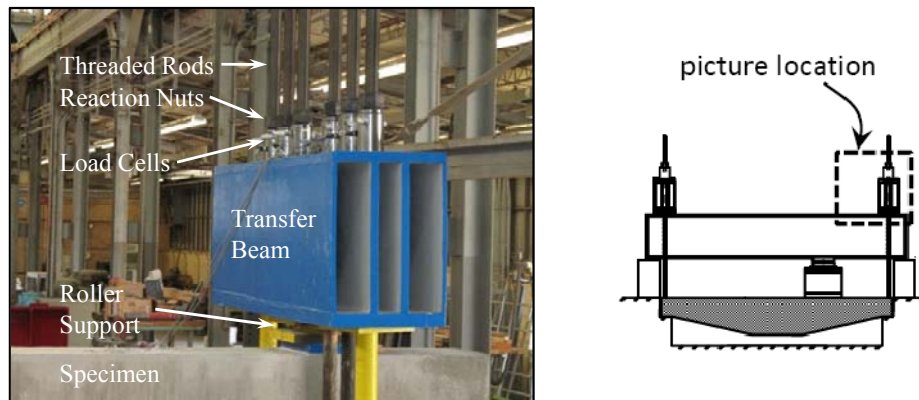


**Figure 3.28: Load cells placed on each reaction rod**

The displacement of the beam during testing was measured with 6-inch linear potentiometers located at the supports, the applied load, and the midspan of the beam. The position of the linear potentiometers is depicted in Figure 3.29.

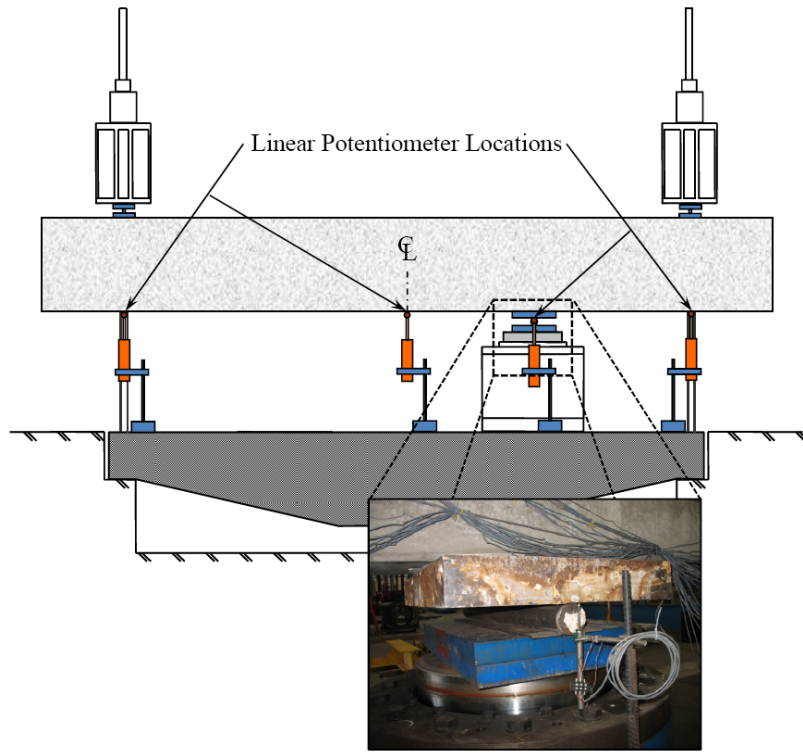


**Figure 3.29: Location and picture of linear potentiometers**

At the beginning of a test, rigid body motion due to the beam being lifted off of the supports by the asymmetrically-applied load was recorded. During the test, additional rigid body motion due to the small elongation of the threaded rods and deformation of the beam due to the effects of the applied load were measured. An illustration of the rigid body motion and beam deformation early in the test is presented in Figure 3.30. An illustration of the rigid body motion (sans differential elongation of the threaded rods) and beam deformation after both transfer girders engaged the reaction nuts is presented in Figure 3.31. It is important to note that the shear in the test region was accurately measured throughout this loading history due to the location of the load cells on each support rod. The beam displacement at the location of the load throughout the test,  $\Delta_{BEAM}$ , was determined according to Equation 3-1.

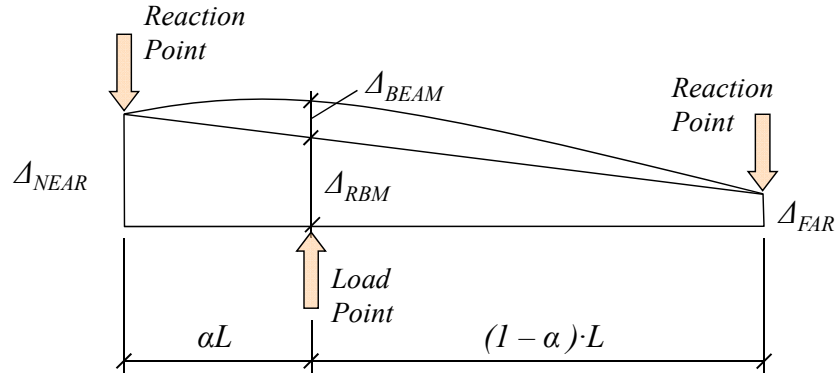


**Figure 3.30: Diagram of beam displacements due to rigid body motion and flexural and shear deformations early in the test (Tuchscherer, 2008)**

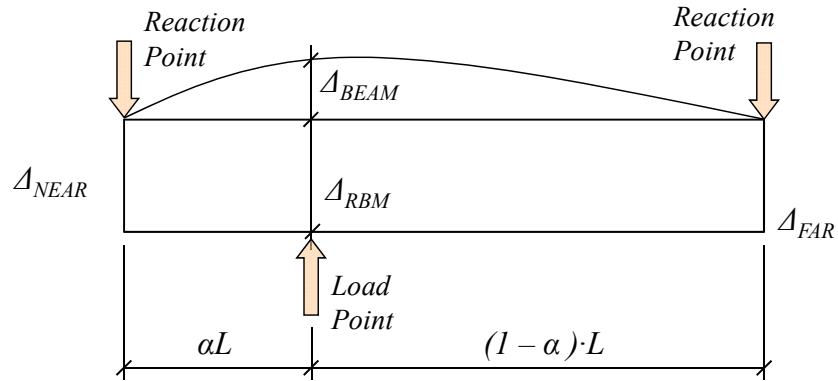


**Figure 3.31: Diagram of beam displacements due to rigid body motion and flexural and shear deformations after all reaction nuts are engaged**

$$\begin{aligned}\Delta_{RBM} &= \Delta_{FAR} + (1 - \alpha) \cdot (\Delta_{NEAR} - \Delta_{FAR}) \\ \Delta_{BEAM} &= \Delta_{LOAD} - \Delta_{RBM}\end{aligned}\tag{3.1}$$

where  $\Delta_{RBM}$  = Displacement due to rigid body motion  
 $\Delta_{NEAR}$  = Recorded displacement at near reaction point  
 $\Delta_{FAR}$  = Recorded displacement at far reaction point  
 $\Delta_{LOAD}$  = Recorded displacement at load point  
 $\Delta_{BEAM}$  = Displacement due to flexural and shear deformations

### 3.5.3 Crack Width Measurements

Diagonal crack width measurements were collected for the test specimens as part of the experimental program. At each load increment, the maximum width of any diagonal crack was recorded on each face of the shear span under investigation. The measurements were obtained by graduate students with the use of a crack comparator card (Figure 3.32). The measurements from the two students were averaged producing diagonal crack width data at each load increment for each face of the test specimen. No distinction was made between flexure-shear cracks or web-shear cracks. As long as the crack formed a significant angle with respect to the vertical, it was considered a diagonal crack. A picture illustrating the crack width measurement for a 21"x75" test specimen is shown in Figure 3.32. Due to the size of these specimens, scaffolding was needed to access it.

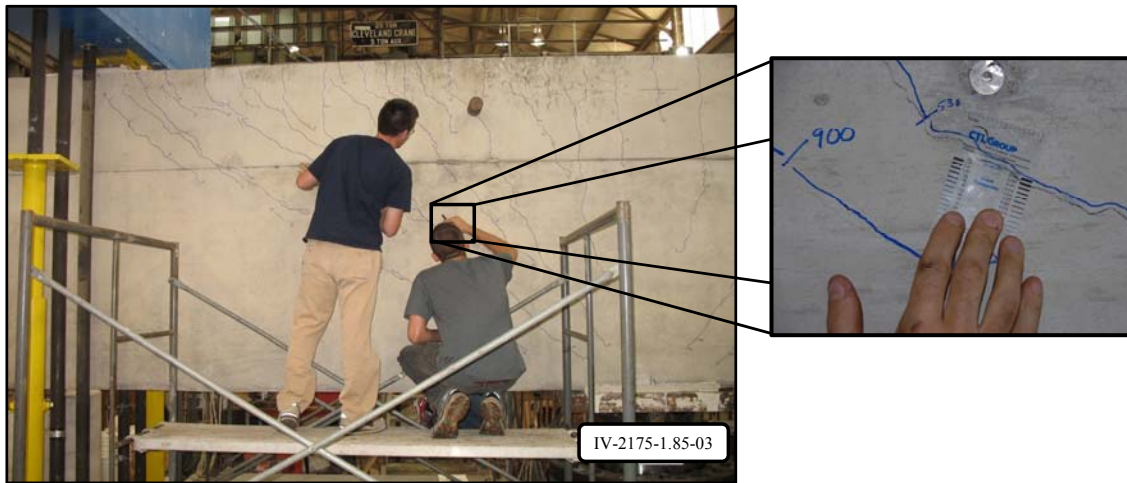


*Figure 3.32: Example of crack width measurement technique*

## 3.6 TEST PROCEDURE

Beams were loaded monotonically in 50- to 150-kip increments depending on the conditions of the test. Generally, the amount of load in each increment was taken as 10% of the expected capacity. Cracks were marked and the width of the widest diagonal shear crack on each face of the specimen was recorded at each load break. In addition,

photographs were taken from a tripod at each load break to illustrate the crack growth throughout the test. The behavior of the specimen throughout the test and at failure was recorded with a video camera.

Two tests were conducted on each beam. First, the beam was loaded near one support corresponding to the appropriate  $a/d$  ratio. The behavior of the specimen was monitored until failure was reached in the test region. Then, external post-tensioned clamps were installed to strengthen the previously sheared portion of the beam. The hydraulic ram was moved to the opposite end of the beam and positioned based on the appropriate  $a/d$  ratio. The beam was loaded again, and the behavior of the second test region was monitored. Overall, thirty-seven tests were conducted on 19 beams fabricated in Project 5253. Pictures illustrating the appearance of a 42-inch beam prior to the first and second test conducted on it are presented in Figure 3.33.

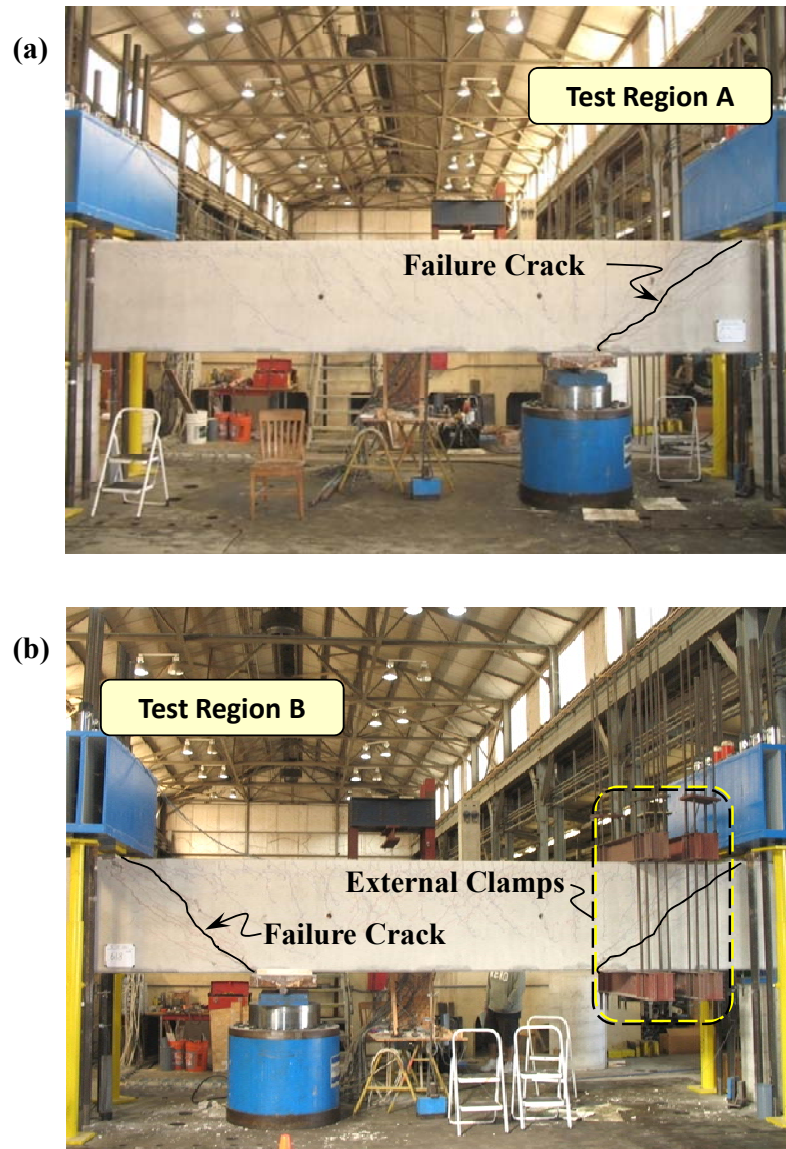


**Figure 3.33: Each end of a beam is loaded to failure resulting in two tests: (a) shear failure in Test Region A (b) and shear failure in Test Region B with external post-tensioned clamps in Test Region A (Tuchscherer, 2008)**

During the first test of each 42- or 48-inch specimen, the low-shear span was subjected to shear up to 40% of its capacity. Under this amount of load and corresponding moment, the specimen generally cracked. Therefore, the second test of each 42- or 48-inch beam was conducted on a *pre-cracked* shear span. As a result, the load at first diagonal cracking was only obtained for the first test of each 42- or 48-inch

specimen. For the 23-inch specimens, the region for the second test remained uncracked during the first test due to the low level of shear and moment in the region of the second test. For the two 75-inch specimens, the size of the specimen was chosen such that the resulting  $a/d$  ratios on each side of the beam matched the appropriate  $a/d$  ratios of the experimental program. Therefore, two tests were conducted simultaneously for these two beams. Both sides of the beam were monitored during the start of the test. After one side of the beam failed, the applied load was removed and external post-tensioned clamps were attached to the failed shear span as before. Then, the load was reapplied at the same location until the other side of the beam failed. In both cases, the external clamps provided enough additional shear strength to obtain a shear failure in the opposite span. Pictures illustrating the two tests IV-2175-2.5-02 and IV-2175-1.2-02 are provided in Figure 3.34.



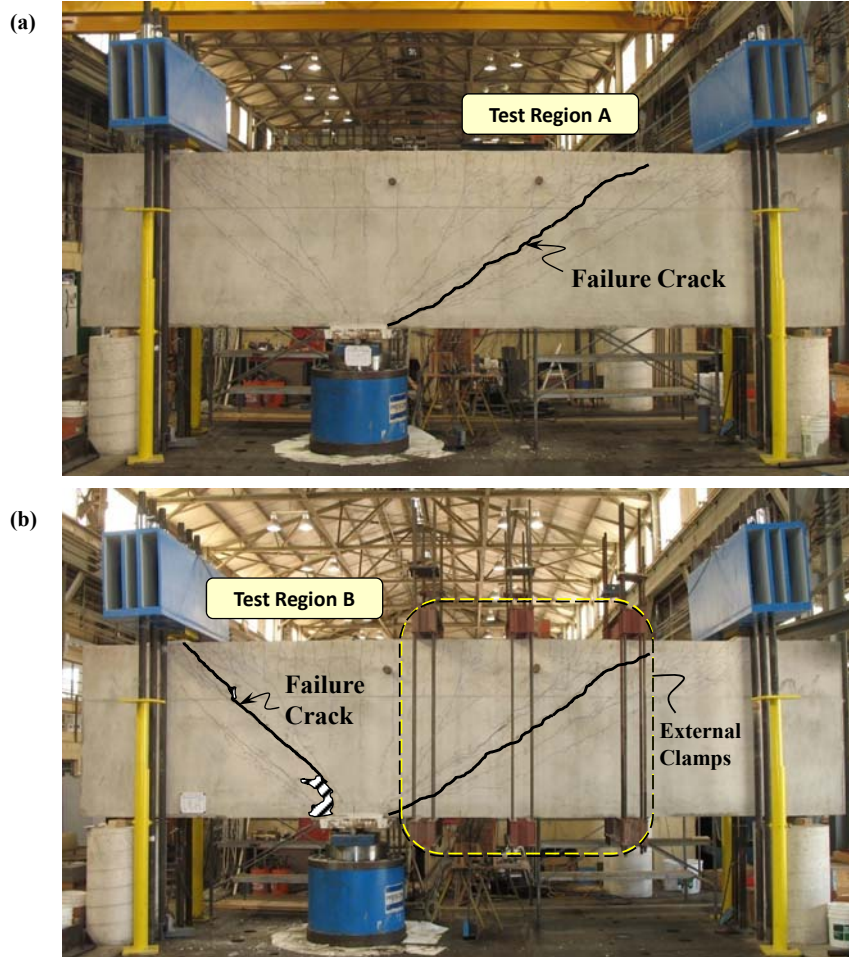


**Figure 3.34: Hydraulic ram was not moved for 75-inch specimens: (a) shear failure in Test Region A (b) shear failure in Test Region B with external post-tensioned clamps in Test Region A**

Nineteen beams were tested in the aforementioned manners, i.e. two tests on each beam. One test on a 36"x48" specimen was a pilot test in which the size of the load plate was changed twice prior to reaching failure in the specimen. The results of this test are not included in this report since the bearing plate dimensions were not constant in the test. As such, 37 valid tests were conducted in the experimental program.

The photographs of the test regions in this dissertation are generally rotated so that the shear region is viewed like a typical simply-supported beam test, i.e. with the load applied from the top. A picture of a 42-inch beam loaded at an  $a/d$  ratio of 1.2 in the



test setup is presented in Figure 3.35 (a). A rotated picture of the test region consistent with the failure photographs presented throughout this dissertation is provided in Figure 3.35 (b).

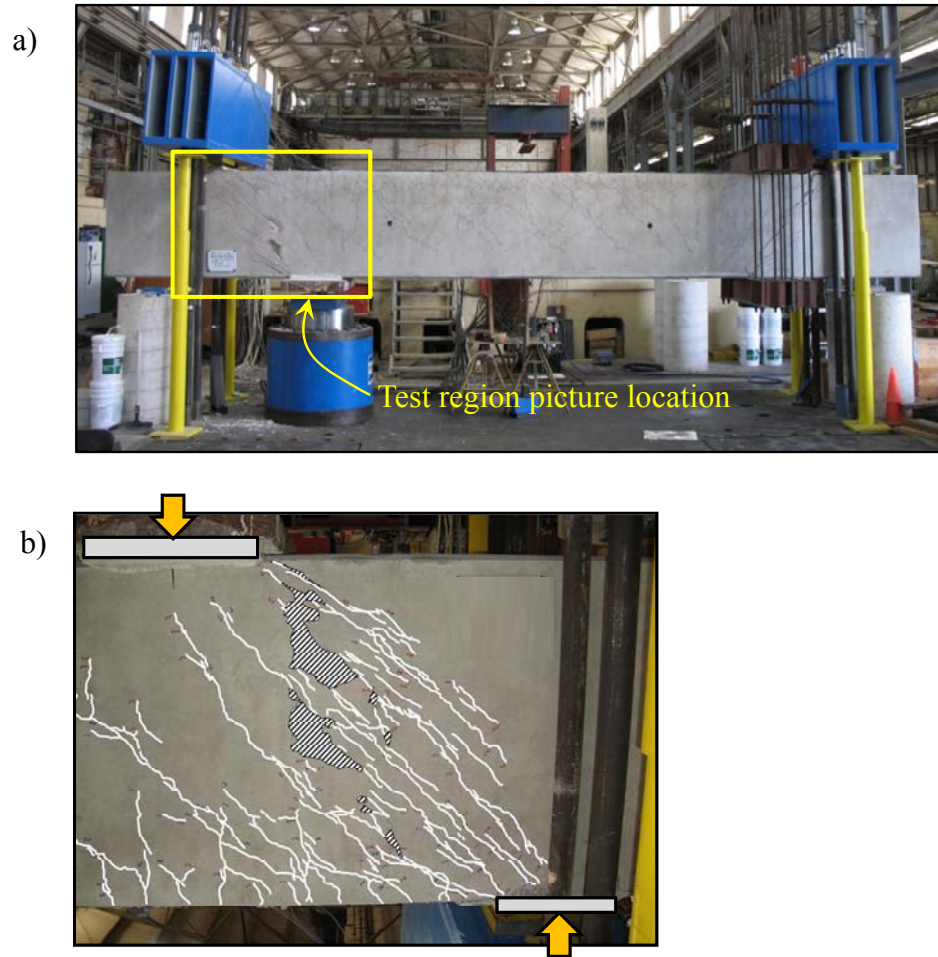


**Figure 3.35: a). Location of test region pictures. b). Picture of failure of test region rotated to orient cracks like that of conventional simple beam test**

### 3.7 SUMMARY

In this chapter, details of the experimental program were provided. Test specimens of comparable size to field members were designed and tested to address the project objectives. Overall, thirty-seven tests were conducted on 19 beams with the following cross-sections: 21"x23", 21"x42", 21"x44", 21"x75", and 36"x48". The sizes

of the test specimens were shown to be among the largest deep beams available in the literature.

Two static tests were conducted on each beam, with the exception of one beam in which only one test was conducted. During each test, several instruments were monitored. They included 500-kip capacity load cells on each support rod, electrical strain gauges on the rebar, and linear potentiometers measuring the deflection of the beam. Also, the maximum width of diagonal cracks was recorded during each load increment on both sides of the test region.

## CHAPTER 4

### Experimental Results

#### 4.1 OVERVIEW

In this chapter, the experimental results of the testing program are presented. A summary of the results of the 37 tests conducted in TxDOT Project 5253 and basic information regarding the evaluation of the test results are presented in Section 4.2. The effect of the amount of minimum web reinforcement and of the member depth on the strength and serviceability of reinforced concrete deep beams is discussed in detail in Sections 4.3 and 4.4, respectively.

#### 4.2 SUMMARY OF EXPERIMENTAL RESULTS

The experimental results for the 37 tests conducted in the experimental program are presented in Table 4.1. Other important details of the test specimens were provided previously in Table 3.6. The variables used in Table 4.1 are defined as follows:

- $b_w$  = beam width, in.
- $d$  = distance from extreme compression fiber to centroid of tensile reinforcement, in.
- $f'_c$  = compressive strength of concrete at the time of testing measured in accordance with ASTM C39, psi.
- $f_{yl}$  = yield strength of longitudinal reinforcement measured in accordance with ASTM A370, ksi.
- $f_{yv}$  = yield strength of vertical web reinforcement measured in accordance with ASTM A370, ksi.
- $f_{yh}$  = yield strength of horizontal web reinforcement measured in accordance with ASTM A370, ksi.

**a/d ratio** = shear span-to-depth ratio

**V<sub>crack</sub>** = shear carried in the test region when the first diagonal crack formed, kips

*Specific details regarding the determination of the diagonal cracking load are presented in Section 4.2.2*

**V<sub>test</sub>** = maximum shear carried in test region, including the estimated self weight of the specimen and transfer girders, kips

*Specific details regarding the determination of the applied shear force are presented in Section 4.2.1*

**Table 4.1: Summary of experimental results.**

Beam I.D.	b <sub>w</sub> in.	d in.	f' <sub>c</sub> psi	f <sub>yl</sub> ksi	f <sub>yv</sub> ksi	f <sub>yh</sub> ksi	a/d ratio	V <sub>crack</sub> kip	$\frac{V_{crack}}{\sqrt{f'_c} \cdot b_w d}$	V <sub>crack</sub> / V <sub>test</sub>	V <sub>test</sub> kip	$\frac{V_{test}}{f'_c \cdot b_w d}$	$\frac{V_{test}}{\sqrt{f'_c} \cdot b_w d}$
I-03-2	21	38.5	5240	73	67	67	1.84	144	2.5	0.25	569	0.13	9.7
I-03-4	21	38.5	5330	73	73	67	1.84	-	-	-	657	0.15	11.1
I-02-2	21	38.5	3950	73	67	67	1.84	121	2.4	0.27	454	0.14	8.9
I-02-4	21	38.5	4160	73	73	67	1.84	-	-	-	528	0.16	10.1
II-03-CCC2021	21	38.6	3290	64	65	65	1.84	139	3.0	0.28	500	0.19	10.7
II-03-CCC1007	21	38.6	3480	64	65	65	1.84	-	-	-	477	0.17	10.0
II-03-CCT1021	21	38.6	4210	66	71	71	1.84	-	-	-	635	0.19	12.1
II-03-CCT0507	21	38.6	4410	66	71	71	1.84	146	2.7	0.24	597	0.17	11.1
II-02-CCT0507	21	38.6	3120	69	64	63	1.84	94	2.1	0.23	401	0.16	8.9
II-02-CCC1007	21	38.6	3140	69	64	63	1.84	-	-	-	335	0.13	7.4
II-02-CCC1021	21	38.6	4620	69	67	62	1.84	132	2.4	0.40	329	0.09	6.0
II-02-CCT0521	21	38.6	4740	69	67	62	1.84	-	-	-	567	0.15	10.2
III-1.85-00	21	38.6	3170	66	-	-	1.84	98	2.1	0.27	365	0.14	8.0
III-2.5-00	21	38.6	3200	66	-	-	2.47	-	-	-	82	0.03	1.8
III-1.85-02	21	38.6	4100	69	64	62	1.84	112	2.2	0.23	488	0.15	9.4
III-1.85-025	21	38.6	4100	69	64	73	1.84	-	-	-	516	0.16	9.9
III-1.85-03	21	38.6	4990	69	64	63	1.84	137	2.4	0.33	412	0.10	7.2
III-1.85-01	21	38.6	5010	69	63	73	1.84	-	-	-	273	0.07	4.8

**Table 4.1 (cont.'d): Summary of experimental results.**

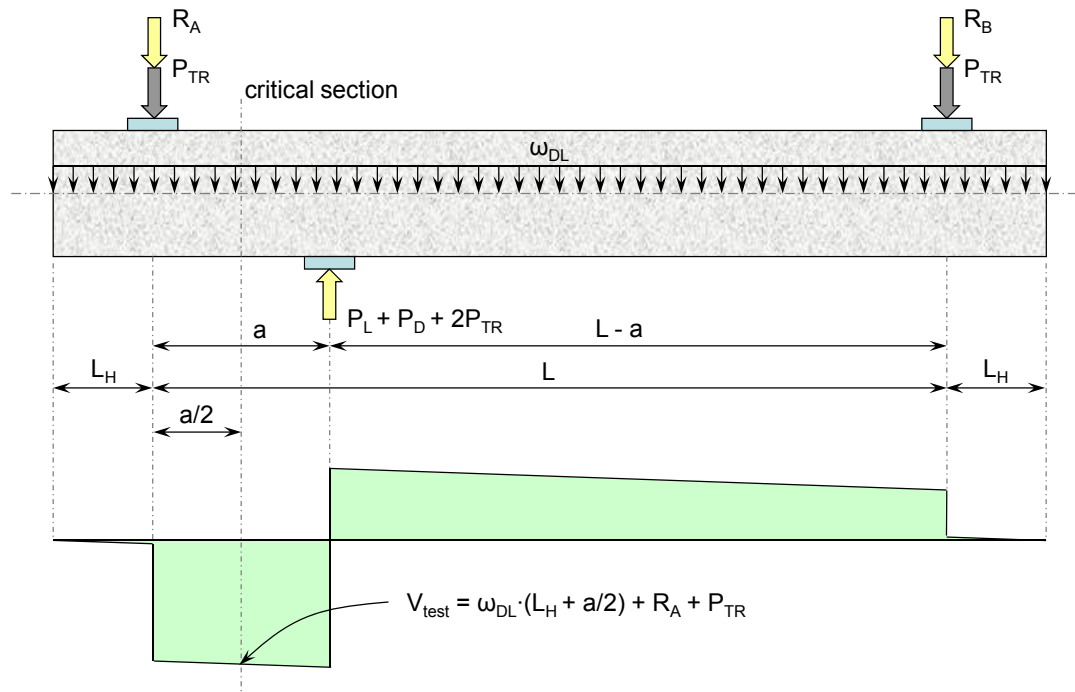
Beam I.D.	$b_w$ in.	$d$ in.	$f'_c$ psi	$f_{yl}$ ksi	$f_{yv}$ ksi	$f_{yh}$ ksi	$a/d$ ratio	$V_{crack}$ kip	$\frac{V_{crack}}{\sqrt{f'_c} \cdot b_w d}$	$V_{crack} / V_{test}$	$V_{test}$ kip	$\frac{V_{test}}{f'_c \cdot b_w d}$	$\frac{V_{test}}{\sqrt{f'_c} \cdot b_w d}$
III-1.85-03b	21	38.6	3300	69	62	67	1.84	114	2.4	0.24	471	0.18	10.1
III-1.85-02b	21	38.6	3300	69	62	62	1.84	-	-	-	468	0.17	10.1
III-1.2-02	21	38.6	4100	66	60	60	1.20	165	3.2	0.20	846	0.25	16.3
III-1.2-03	21	38.6	4220	66	68	68	1.20	-	-	-	829	0.24	15.7
III-2.5-02	21	38.6	4630	66	62	62	2.49	105	1.9	0.35	298	0.08	5.4
III-2.5-03	21	38.6	5030	66	65	65	2.49	-	-	-	516	0.13	9.0
IV-2175-1.85-02	21	68.9	4930	68	66	66	1.85	216	2.1	0.28	763	0.11	7.5
IV-2175-1.85-03	21	68.9	4930	68	66	66	1.85	218	2.1	0.26	842	0.12	8.3
IV-2175-2.5-02	21	68.9	5010	68	64	64	2.50	144	1.4	0.28	510	0.07	5.0
IV-2175-1.2-02	21	68.9	5010	68	64	64	1.20	262	2.6	0.21	1223	0.17	11.9
IV-2123-1.85-03	21	19.5	4160	66	66	66	1.85	60	2.3	0.18	329	0.19	12.5
IV-2123-1.85-02	21	19.5	4220	66	81	81	1.85	65	2.4	0.19	347	0.20	13.0
IV-2123-2.5-02	21	19.5	4570	65	58	64	2.50	51	1.8	0.32	161	0.09	5.8
IV-2123-1.2-02	21	19.5	4630	65	58	64	1.20	124	4.5	0.21	592(f)	0.31	21.2
M-03-4-CCC2436	36	40	4100	67	61	61	1.85	354	3.8	0.31	1128	0.19	12.2
M-03-4-CCC0812	36	40	3000	65	63	63	1.85	-	-	-	930	0.22	11.8
M-09-4-CCC2436	36	40	4100	67	61	61	1.85	-	-	-	1415(f)	0.24	15.3
M-02-4-CCC2436	36	40	2800	65	63	63	1.85	256	3.4	0.23	1102	0.27	14.5
M-03-2-CCC2436	36	40	4900	68	62	62	1.85	-	-	-	1096(i)	0.16	10.9

(f) Maximum shear carried at flexural failure – yielding of tensile reinforcement and concrete crushing at the compression face

(i) Maximum shear carried upon initiation of yielding of tensile reinforcement and crushing of concrete at compression face

#### 4.2.1 Evaluation of Strength Data

The shear strength of the test specimens,  $V_{\text{test}}$  in Table 4.1, was the shear at the critical section at the maximum applied load. The critical section was defined as the point halfway between the support and the applied load in the test region. At this location, a portion of the beam weight and the weight of one transfer girder was added to the load cell readings from the near support to obtain the appropriate shear. The equation for calculating  $V_{\text{test}}$  is provided in Figure 4.1. In Figure 4.1,  $R_A$  and  $R_B$  denote the reactions measured by the load cells.  $P_{\text{TR}}$  represents the weight of each blue transfer girder (7.8 kips), and  $P_D$  represents the weight of the test specimen. For the 23-in. specimens, a spacer was provided between the transfer girder and the roller support that effectively increased  $P_{\text{TR}}$  from 7.8 kips to 8 kips.



WHERE,	$P_L = R_A + R_B$	$L = 255.25"$	$\omega_{21 \times 23} = 0.49 \text{ kip/ft}$	$\omega_{21 \times 75} = 1.63 \text{ kip/ft}$
	$P_D = \omega_{DL} \cdot (2L_H + L)$	$L_H = 38.375"$	$\omega_{21 \times 42} = 0.92 \text{ kip/ft}$	$\omega_{36 \times 48} = 1.80 \text{ kip/ft}$
		$P_{TR} = 7.8 \text{ kip}$	$\omega_{21 \times 44} = 0.96 \text{ kip/ft}$	

**Figure 4.1: Free-body and shear force diagram for typical test (Tuchscherer, 2008)**

It should be noted that three specimens in the experimental program failed in flexure. These specimens are denoted with an (f) or an (i) in Table 4.1. The values of  $V_{test}$  in Table 4.1 for these specimens are the shear in the test region at flexural failure. The test results were considered valid since a strut-and-tie analysis inherently considers both shear and flexural failures. Furthermore, beams are often designed such that flexure governs. As a result, it was determined that the results of these specimens should be included in all of the analyses. Where appropriate, a flexural failure note was attached to the data from these specimens. In general, the rest of the specimens in the experimental program failed in shear. For the beams loaded with an  $a/d$  ratio  $< 2$ , the failure was consistent with a direct-strut transfer mechanism. That is, failure ensued after crushing along a direct strut between the load and the support or at the nodal regions. For the



beams loaded with an  $a/d$  ratio  $> 2$ , the failure was consistent with a sectional shear failure. The specific failure modes of many of the specimens are discussed individually in Chapters 4 and 5.

Traditionally, the shear capacity of test specimens is normalized by the cross-sectional dimensions and the strength of concrete to account for variations in section size and concrete strength. For experimental loads that are associated with the tensile strength of concrete, such as the diagonal cracking load or the sectional shear (diagonal tension) strength of a member, it is appropriate to normalize the value by  $\sqrt{f_c'}$ . For experimental loads that are associated with the compressive strength of concrete, such as the capacity of a deep beam, it is appropriate to normalize the value by  $f_c'$ . In Table 4.1, the diagonal cracking loads of the test specimens are normalized by  $\sqrt{f_c'} b_w d$ , and the capacity of the test specimens are normalized by both  $f_c' b_w d$  and  $\sqrt{f_c'} b_w d$ . Regarding the capacity, both normalization techniques were utilized since different modes of failures were observed in the test specimens. At low  $a/d$  ratios ( $< 2.0$ ), the mode of failure was generally consistent with the crushing of a direct strut between the load and the support. Normalizing the capacity by  $f_c' b_w d$  was appropriate for these specimens. At higher  $a/d$  ratios ( $> 2.0$ ), the mode of failure was often consistent with a sectional shear (or diagonal tension) failure. Normalizing the capacity by  $\sqrt{f_c'} b_w d$  was appropriate for these specimens. It should be noted that the only difference between the normalization techniques is the manner with which the strength of concrete is taken into account.

One exception to the aforementioned normalization techniques is for deep beams of significantly different depths. Normalizing the shear capacity of a deep beam by  $f_c' b_w d$  suggests that the capacity of the member is a function of the section size. A strut-and-tie model analysis would suggest that the strength of a deep beam is a function of the nodes, struts, and ties, not the depth explicitly. As such, when comparing the strength of deep beams with significantly different depths, normalizing the capacity by  $f_c' b_w d$  can impose unwanted errors. This issue is addressed specifically in Section 4.4. When comparing

the strength of deep beams with similar depths however, normalizing the capacity by  $f_c' b_w d$  is appropriate and is therefore used throughout this report.

#### **4.2.2 Evaluation of Serviceability Data**

In the experimental program, the diagonal cracking loads and the maximum width of all diagonal cracks at each load increment were obtained to measure serviceability performance.

The first diagonal cracking load was determined by a sudden increase in strain measured by gauges affixed to the web reinforcement and was confirmed by visual observation. The magnitude of shear at which the stirrup strains increased abruptly was considered to be the first diagonal cracking load (Figure 4.2). This load was confirmed with the diagonal cracking load obtained by visual inspection during each test. In general, the first diagonal crack formed at a 45-degree angle with respect to the load plate. It usually extended from a pre-existing flexural crack or formed simultaneously with a flexural crack. In all cases, the first diagonal crack extended beyond the mid-depth of the member and formed a considerable angle with respect to the vertical. An example of the determination of the first cracking load is presented in Figure 4.2. The 'E' and 'W' symbols in the figure represent the east and west side of the beam, respectively.

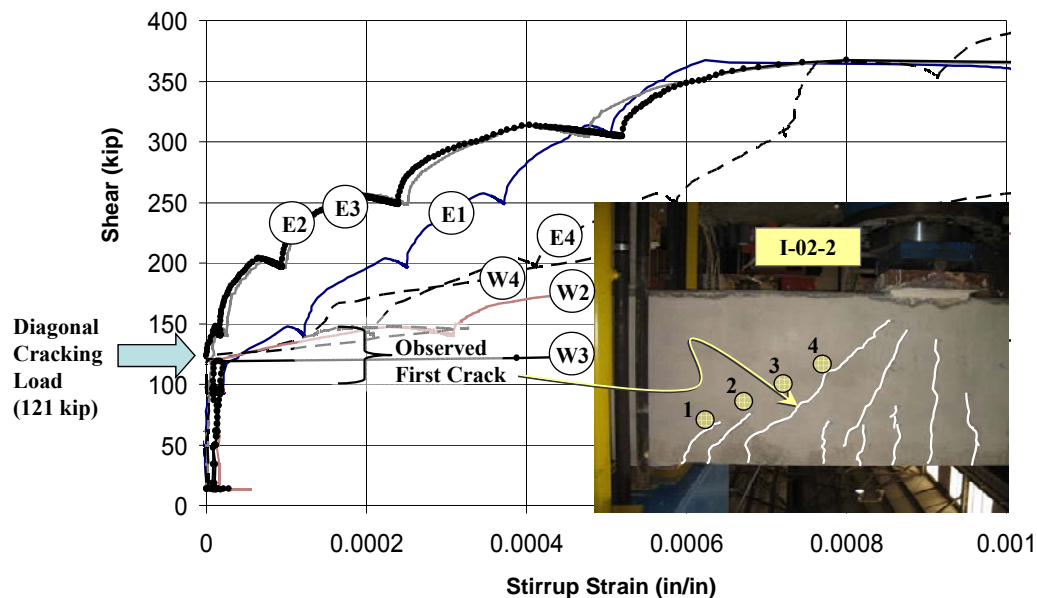


**Figure 4.2: Visual and experimental determination of diagonal cracking load**  
(Tuchscherer, 2008)

As noted in Section 3.6, the diagonal cracking loads were only obtained for the first test of each 42-, 44-, and 48-in. specimen. The region for the second test of each 42-, 44-, and 48-in. specimen was cracked during the first test. Diagonal cracking loads were obtained for both tests on the 23- and 75-in. specimens.

The maximum width of the diagonal cracks in each specimen was also monitored throughout the test to evaluate the serviceability performance of deep beams. In general, the maximum width of a diagonal crack was near the midheight of the member. As noted in Section 3.5.3, these measurements were recorded using crack comparator cards. Measurements were obtained on each face of the test region by two students. The measurements between the students were averaged such that, at a given load level, two crack width values were recorded that represent the maximum crack width on each face of the test specimen as an average of two independent measurements. If two data points do not exist at a given load level, then the width of the diagonal cracks were identical on both sides of the test region. An example of the presentation of crack width data is given in Figure 4.3. An approximate service load level and a benchmark crack width are

presented with the crack width data. Explanations for these values are given later in this section.

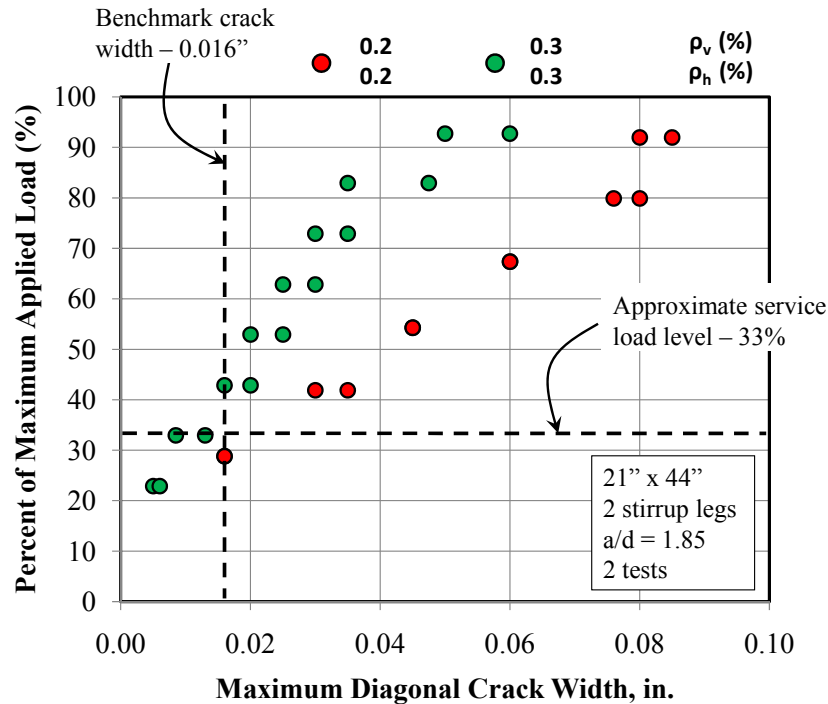


**Figure 4.3: Sample crack width data for all series**

In this dissertation, the crack width data are plotted versus the percent of the maximum applied load. This method was chosen to be consistent with the *correlation of crack width to capacity* objective of the research project (Section 5.4). Also, it was evident from the trends in the data that the width of diagonal cracks was proportional to the percent of maximum applied load.

To evaluate the serviceability data obtained in the experimental program, criteria were needed. In ACI 318-95, spacing of flexural reinforcement was based on limiting flexural crack widths for structures with interior exposure to 0.016 in. and with exterior exposure to 0.013 in. (ACI-318-95). In subsequent versions of ACI-318, the specific reference to these crack width limits were removed, primarily due to “the inherent variability in cracking” (ACI 318 Committee Closure, 1999). It was determined that

specifying distinct limits for crack widths was impractical. Similar limits were found in ACI 224R-01: Control of Cracking in Concrete Structures. A tolerable crack width of 0.012 in. was suggested for moist conditions; a tolerable crack width of 0.016 in. was suggested for dry conditions. In the concrete design recommendations developed by the *fédération internationale du béton (fib)*; i.e. international concrete federation), the same tolerable crack widths that existed in ACI 224R-01 were provided. Again, they were a function of the exposure condition of the member. Even though these limits were intended for flexural crack widths, they provide the only available guidance for tolerable crack widths in reinforced concrete structures. The tolerable crack widths are shown in Table 4.2.

***Table 4.2: Tolerable widths of flexural cracks***

<b>Exposure Condition</b>	<b>ACI 224R-01 (in.)</b>	<b><i>fib</i> (1999) (in.)</b>
Dry air, protective membrane, indoors	0.016	0.016
Humidity, moist air, soil, cyclic wet and dry	0.012	0.012

It is likely that the tolerable crack width limits in Table 4.2 are intended to represent average crack widths to be used with design. The following quote is present in ACI 224R-01 in reference to these limits:

*It should be expected that a portion of the cracks in the structure will exceed these values...These are general guidelines for design to be used in conjunction with sound engineering judgment.*

*(ACI 224R-01, 2001)*

In view of the above quote (similar statements exist in *fib* (1999)), it may not be appropriate to directly compare the crack width limits in Table 4.2 to the *maximum* diagonal crack width data obtained in this study.

In an internal discussion amongst the members of the project team, it was determined that a crack width of 0.016 in. is the typical crack width at which attention is triggered in TxDOT (Vogel, 2008). Based on this discussion, a maximum crack width of 0.016 in. was used as a benchmark of performance in the current study. It is important to note that 0.016 in. is not endorsed as a tolerable crack width. The value of 0.016 in. can

be viewed as a liberal limit with which to gauge performance. A stricter limit is more appropriate for aggressive climates.

In conjunction with a crack width benchmark, an approximate service load as a function of the capacity of the test specimen was used to evaluate the crack width data. In a study by Tan and Lu (1999), the serviceability load was taken as the load at which the width of a diagonal crack reached a tolerable crack width limit. However, in the current project, it was determined that a service load independent of crack widths should be used. In a study by Grob and Thürlimann (1976), the service load was assumed to be equal to the theoretical capacity of the specimen divided by a global safety factor of 1.8. A similar approach to estimate the service load was used in the current study as detailed in Figure 4.4.

$\phi \text{ Nominal Capacity} \approx \eta \text{ Service Load}$	
$\frac{\phi}{\eta} \approx \frac{\text{Service Load}}{\text{Nominal Capacity}}$	
<u>Assumptions:</u>	<div style="display: flex; align-items: center;"> <div style="flex: 1;"> <p>1). Load Case: 1.25DL + 1.75LL</p> <p>2). DL = 75% of Service Load LL = 25% of Service Load</p> <p>3). Nominal = 2/3 Experimental</p> </div> <div style="font-size: 3em; margin: 0 10px;">}</div> <div style="vertical-align: middle;"> <math>\eta = 1.4</math> </div> </div>
$2/3 \frac{0.70}{1.4} = \textcolor{red}{0.33} \approx \frac{\text{Service Loads}}{\text{Experimental Capacity}}$	
<p><math>\phi</math> = strength reduction factor, 0.70  <math>\eta</math> = load factor  DL = dead load  LL = live load</p>	

**Figure 4.4: Estimate of service load as a function of experimental capacity**

As shown in Figure 4.4, the LRFD strength equation can be re-written such that the ratio of the strength reduction factor ( $\phi$ ) to the load factor ( $\eta$ ) is approximately equal to the ratio of the service load to the nominal capacity. The  $\phi$  factor for compression

elements in a strut-and-tie model is 0.70 in AASHTO LRFD (2008). The  $\eta$  factor is a function of the load case and the distribution of the loads for that particular case. If the following two assumptions are made, then  $\eta$  equals approximately 1.4:

- Strength I in AASHTO LRFD governs design,  $1.25DL + 1.75LL$ .
- 75% of the service load is DL; 25% of the service load is LL.

Lastly, the experimental capacity is taken as  $1\frac{1}{2}$  times the nominal capacity based on the strut-and-tie analysis of the evaluation database using the Project 5253 STM provisions discussed in Section 2.3.4.4. On average, inherent conservatism in the strut-and-tie modeling procedure resulted in experimental capacity being  $1\frac{1}{2}$  times the calculated capacity. Since this calculation of the service load is used to evaluate the serviceability performance of the member, the use of an average ratio of experimental to calculated capacity is appropriate. With the aforementioned methodology, the service load is calculated as  $1/3$  of the experimental capacity. It is clear that several assumptions are needed to estimate the service load as a function of the capacity of deep beams. Error in any of these assumptions can shift the estimated service load up or down accordingly. As such, it is important to treat this value (0.33) as a general representation of the service load on a deep beam.

In the following two sections, the experimental strength and serviceability results related to minimum web reinforcement and member depth are discussed in detail.

### **4.3 MINIMUM WEB REINFORCEMENT**

In this task, the effect of web reinforcement on the strength and serviceability behavior of reinforced concrete deep beams was evaluated. The purpose of the task was to recommend minimum horizontal and vertical reinforcement that ensures adequate strength and serviceability performance of deep beams.

#### **4.3.1 Background**

Minimum reinforcement provisions that pertain to deep beam design or strut-and-tie model design are compared for several different design specifications. For reference,

two other provisions in AASHTO LRFD that specify web reinforcement are discussed as well.

#### **4.3.1.1 AASHTO LRFD 2008 and CHBDC 2006**

There are two different minimum horizontal and vertical reinforcement requirements for deep beam design in AASHTO LRFD 2008. The first requirement is in the strut-and-tie model section (5.6.3.6) of the specification. An orthogonal grid of reinforcement is required at each face such that the ratio of the total reinforcement to the gross concrete area is equal to 0.003 (0.3%). The spacing of the reinforcement is limited to 12 in. In the commentary, the following excerpt is found:

*This reinforcement is intended to control the width of cracks and to ensure a minimum ductility for the member so that, if required, significant redistribution of internal stresses is possible.*

*(AASHTO C5.6.3.6, 2008)*

From this note in the commentary, it is evident that strength and serviceability were considered in this provision. The same minimum reinforcement is required in the Canadian Highway Bridge Design Code (CHBDC, 2006).

In Section 5.13.2.3 of AASHTO LRFD (2008), another minimum reinforcement provision for deep beams exists. Equation 5.13.2.3-2 in AASHTO LRFD is rewritten as Equation 4.1 in this dissertation in terms of the reinforcement ratio.

$$\frac{A_s}{b_v s} \geq \frac{0.12}{\phi f_y} \quad (4.1)$$

with  $A_s$  = area of steel within a distance  $s$  (in.<sup>2</sup>)

$b_v$  = width of web (in.)

$s$  = spacing of reinforcement (in.)

$\phi$  = resistance factor, 1.0 for tension members in STM

$f_y$  = yield strength of reinforcing steel (ksi.)



When  $f_y$  is equal to 60 ksi and  $\phi$  is equal to 1.0 (Section 5.5.4.2), a minimum reinforcement ratio of 0.002 is required. Both vertical and horizontal reinforcement must meet Equation 4.1 and must be well distributed. Maximum spacing for the vertical reinforcement is  $d/4$  or 12 in.; maximum spacing for horizontal reinforcement is  $d/3$  or 12 in., where  $d$  is the effective depth of the section. There is no indication in AASHTO LRFD (2008) as to whether this provision was based on strength or serviceability requirements.

#### **4.3.1.2 CSA A23.3-04 and fib (CEB-FIP) 1999**

The same minimum reinforcement requirements for deep beams are listed in the Canadian Building code and the *fib* recommendations. An orthogonal grid of reinforcement is required at each face such that the ratio of the total reinforcement to the gross concrete area is equal to 0.002 (0.2%) (CSA A23.3-04 11.4.5, 2004 and *fib* 7.3.2, 1999). There is no indication in either document as to the specific purpose of the reinforcement, i.e. for strength or serviceability, or both. Maximum spacing is restricted to 12 in.

#### **4.3.1.3 ACI 318-08**

There are two minimum reinforcement provisions that pertain to deep beam design in ACI 318-08. If the deep beam design provisions in section 11.8 are used, then reinforcement ratios of 0.0025 and 0.0015 are required in the vertical and the horizontal directions, respectively. Maximum spacing of the reinforcement in both cases shall not exceed  $d/5$  or 12 in. It is interesting to note that 0.25% reinforcement was required in the horizontal direction and 0.15% reinforcement was required in the vertical direction for this provision in ACI 318-71 through ACI 318-95. Data obtained from research conducted by Rogowsky et al. (1986) indicated that vertical reinforcement was more effective than horizontal reinforcement in terms of the shear strength of deep beams. As such, the provision was changed. No indication of serviceability performance was reported in the paper by Rogowsky et al. (1986). In the commentary, however, it is stated that the maximum spacing was reduced to 12 in. from 18 in. because “the steel is

provided to restrain the width of the cracks” (ACI 318-08 R11.8.4, 2008). Therefore, while this provision may not be based on serviceability considerations, ACI 318 acknowledges that the minimum reinforcement requirement should address serviceability.

If the strut-and-tie requirements of Appendix A are used in deep beam design, then the minimum reinforcement provisions for concrete struts apply. If a concrete strut efficiency factor,  $\beta_s$ , of 0.75 is used, then reinforcement satisfying Equation 4.2 must be provided. This reinforcement is “*related to the tension force in the concrete due to the spreading of the strut*” and is depicted in Figure 4.5 (ACI 318-08 RA.3.3). Due to the  $(\sin \alpha_i)$  term, this requirement favors the placement of reinforcement perpendicular to the axis of the strut, or the assumed inclination of the diagonal cracks. However, there is no requirement for a minimum amount of reinforcement in either the horizontal or vertical directions. If the same amount of reinforcement is desired in both directions, then Equation 4.2 requires a reinforcement ratio of approximately 0.0022 in each direction for the range of applicable values of theta, i.e. between 25 and 65 degrees. If a more efficient placement of reinforcement is desired with a minimum of 0.0015 in each direction, the required reinforcement ratio in the horizontal and vertical directions are those depicted in Figure 4.6 and Figure 4.7, respectively.

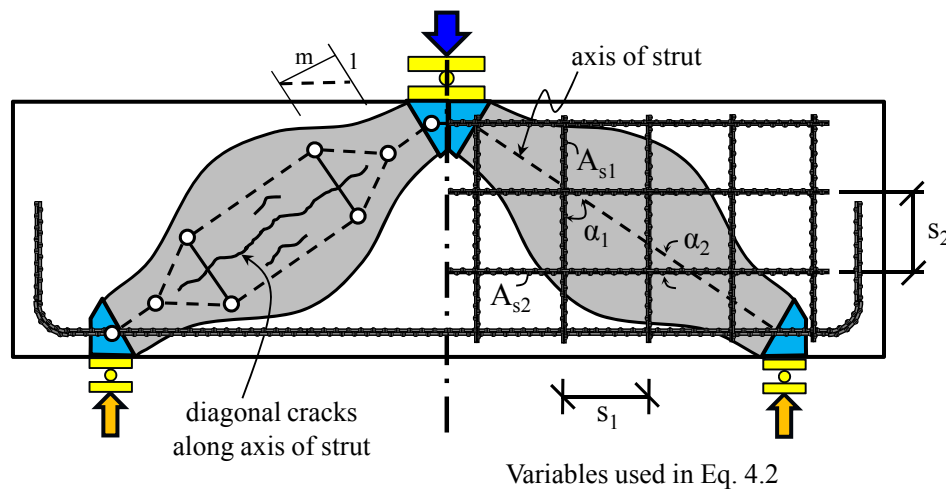


**Figure 4.5: Deep beam showing nomenclature for Equation 4.2**

$$\rho_{\perp} = \sum \frac{A_{si}}{b_s s_i} \sin \alpha_i \geq 0.003 \quad (4.2)$$

with  $A_s$  = area of reinforcement in the i-th later crossing strut (in.<sup>2</sup>)

$b_s$  = width of strut perpendicular to the plane of reinforcement (in.)

$s_i$  = spacing of reinforcement in i-th layer adjacent to member surface (in.)

$\alpha_i$  = angle between axis of strut and i-th layer of reinforcement

If a lower concrete strut efficiency factor,  $\beta_s$ , of 0.60 is used with the strut-and-tie method of ACI Appendix A, no minimum reinforcement is required. It is assumed that the tensile strength of the concrete can resist the transverse tension in the bottle-shaped struts depicted in Figure 4.5. Relying on the tensile strength of concrete is not recommended due to its inconsistency. The author believes this provision should be removed from ACI 318-08.

#### **4.3.1.4 TxDOT 4371 Minimum Reinforcement Recommendations**

In TxDOT Project 4371, an equation for minimum reinforcement was developed based on strength. The reinforcement required to resist the transverse tension forces associated with spreading compressive stresses in a bottle-shaped strut is calculated with Equation 4.3 (Figure 4.5). The equation is a function of the force in the strut and the slope of the angle of dispersion of the compressive stresses in the strut,  $m$ . It was recommended that this slope be calculated with a variable angle of dispersion model developed by Schlaich and Weischede (1982). When applied to the database, an equivalent reinforcement ratio perpendicular to the strut axis ( $\rho_{\perp}$ ) of 0.0015 (0.15%) is required by Equation 4.3 on average. Therefore, in general, half as much reinforcement is required according to Equation 4.3 compared to Equation 4.2. This difference is primarily attributed to the variable angle of dispersion used in the 4371 approach as opposed to ACI which assumes that the slope of the angle of dispersion,  $m$ , is 2. In the project 4371 report, it was stated that the amount of reinforcement according to Equation 4.3 was intended for strength only; additional research was recommended to determine

the serviceability demand. More detailed information of the 4371 minimum reinforcement recommendation and the variable angle of dispersion model can be found elsewhere (Brown et al., 2006).

$$\rho_{\perp \min} = \frac{\nu_R f'_c A_c \sin \theta}{f_y b d m} \quad (4.3)$$

with  $\nu_R$  = efficiency factor for reinforced struts developed in Project 4371

$f'_c$  = compressive strength of the concrete (psi)

$A_c$  = minimum cross-sectional area of the strut (in.<sup>2</sup>)

$\theta$  = angle of strut with respect to the horizontal

$f_y$  = yield strength of web reinforcement (psi)

$b$  = width of strut (in.)

$d$  = effective depth of the strut (in.)

$m$  = slope of the angle of dispersion

#### **4.3.1.5 Other minimum reinforcement provisions in AASHTO LRFD 2008**

In addition to the aforementioned provisions for deep beams, there are other minimum web reinforcement requirements for reinforced concrete members. Two relevant provisions include minimum transverse reinforcement required for members analyzed with a sectional shear model (i.e.  $V_c + V_s$ ) and minimum skin reinforcement required for the webs of members with large depths. For simplicity, only the AASHTO versions of these provisions are presented.

In the sectional shear design provisions of AASHTO LRFD 2008, Equation 4.4 is listed. With this equation, it is ensured that enough steel is present in the member to resist half of the concrete contribution to shear strength when performing a sectional analysis. When the compressive strength of the concrete is 4 ksi and the yield strength of the steel is 60 ksi, a reinforcement ratio of 0.001 (0.1%) is specified with Equation 4.4. This provision is solely based on strength considerations.

$$A_v \geq 0.0316 \sqrt{f'_c} \frac{b_v s}{f_y} \quad (4.4)$$

with  $A_v$  = area of transverse reinforcement within a distance  $s$  (in.<sup>2</sup>)

$f'_c$  = compressive strength of the concrete (ksi)

$b_v$  = width of web (in.)

$s$  = spacing of transverse reinforcement (in.)

$f_y$  = yield strength of the reinforcement (ksi)

In Section 5.7.3.4 of AASHTO LRFD, another requirement for web reinforcement exists (2008). This equation is reproduced as Equation 4.5. This provision applies to members with depths greater than 36 in. The reinforcement must be distributed within the distance  $d_e/2$  from the tension face of the member at a spacing of  $d_e/6$  or 12 in., where  $d_e$  is the effective member depth. The purpose of this provision is to restrain flexural cracks throughout the tension region of members of large depth. As such, it is based on serviceability considerations. It is important to note that the area of reinforcement calculated in Equation 4.5 is the amount per face and per foot of section height.

$$A_{sk} \geq 0.012(d_e - 30) \leq \frac{A_s + A_{ps}}{4} \quad (4.5)$$

with  $A_{sk}$  = area of skin reinforcement on each side face in in.<sup>2</sup> / ft. of height

$d_e$  = effective member depth (in.)

$A_s$  = area of tension reinforcement (in.<sup>2</sup>)

$A_{ps}$  = area of prestressed reinforcement (in.<sup>2</sup>)

Equation 4.5 can be rewritten in terms of the reinforcement ratio based off the full width of the section and the tension region of the member ( $d_e/2$ ). In this way, it can be directly compared to the aforementioned minimum reinforcement requirements. The rewritten equation is presented as Equation 4.6. Values computed with Equation 4.6 are

plotted with assumed values of  $b_w$  with respect to the effective depth of the member in Figure 4.6.

$$\rho_{g\_sk} \geq \frac{0.002(d_e - 30)}{b_w} \quad (4.6)$$

with  $\rho_{g\_sk}$  = reinforcement ratio calculated from total web reinforcement according to Equation 4.5 and distributed within half the member depth  
 $b_w$  = width of web (in.)

#### ***4.3.1.6 Comparison of minimum reinforcement provisions***

The aforementioned provisions for minimum reinforcement in the horizontal and vertical directions are compared in Figure 4.6 and Figure 4.7, respectively. The minimum reinforcement requirement of Project 4371 was omitted from the following plots due to the large number of variables that are required to plot it. For some of the other provisions, minor assumptions were necessary to plot the equations in each graph. These assumptions are listed in Table 4.3.

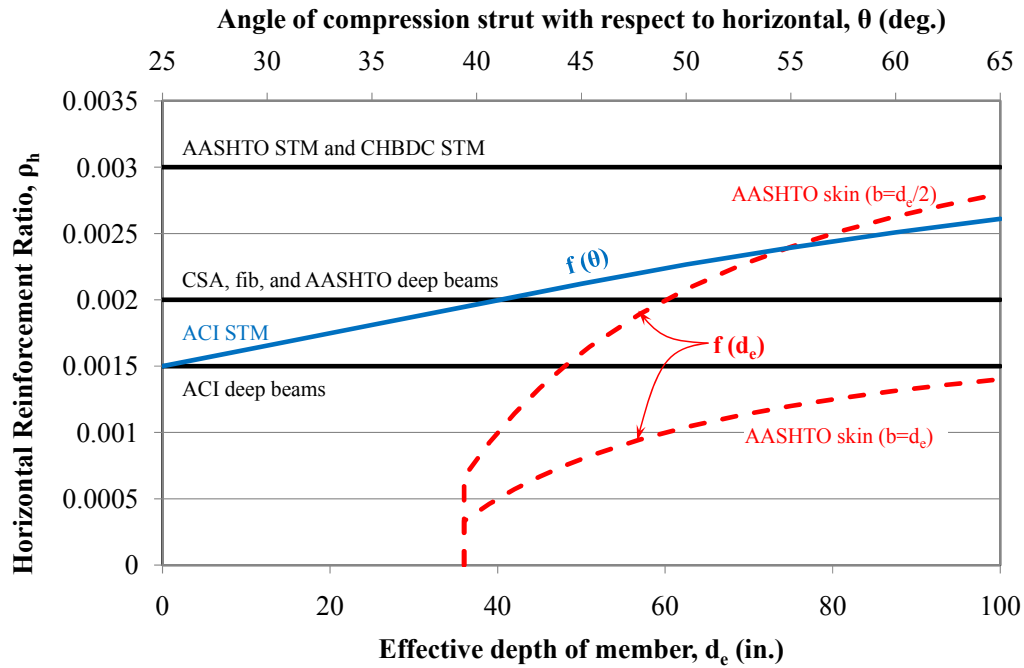


Figure 4.6: Min. horizontal reinforcement for deep beams in several specifications

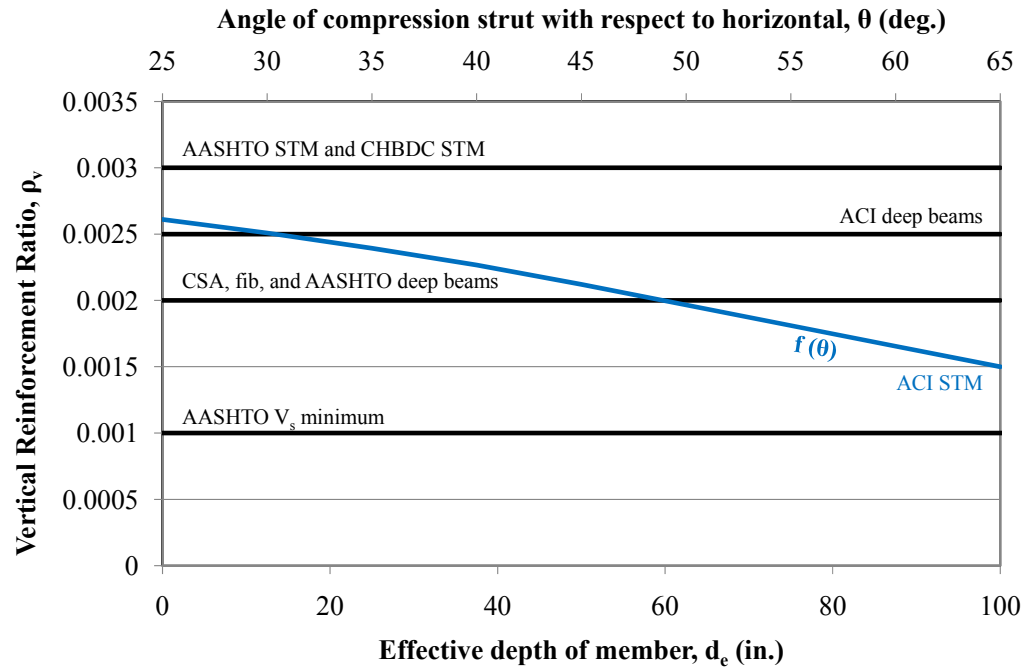


Figure 4.7: Minimum vertical reinforcement for deep beams in several specifications

**Table 4.3: Assumptions made to plot minimum web reinforcement provisions**

Use	Provision	$\rho_h$ (%)	$\rho_v$ (%)	Assumption for plotting
Deep Beams	AASHTO & CHBDC STM	0.3	0.3	N/A
	AASHTO Deep Beam	0.2	0.2	$f_y = 60$ ksi
	CSA / <i>fib</i>	0.2	0.2	N/A
	ACI Deep Beams	0.15	0.25	N/A
	ACI STM	function of $\theta$		Minimum $\rho_h$ & $\rho_v = 0.0015$
Other	AASHTO sectional	N/A	0.1	$f'_c = 4$ ksi & $f_y = 60$ ksi
	AASHTO skin	function of $d_e$	N/A	$b_w = d_e$ & $b_w = d_e/2$

In Figure 4.6 and Figure 4.7, it is evident that the minimum reinforcement provisions in several building and bridge design specifications differ for deep beams. The required minimum reinforcement in AASHTO LRFD 2008 and CHBDC 2006 corresponding to 0.003 in each direction is the most stringent requirement. In the commentary of AASHTO LRFD, it is stated that 0.003 in both directions is for both strength and serviceability considerations. The other minimum reinforcement requirements for deep beams plotted in Figures 4.2 and 4.3 range from 17% to 50% lower. The minimum reinforcement provision in the ACI STM specification (Equation 4.2 and blue line in above figures) is a function of the axis of the diagonal strut, or the  $a/d$  ratio for single-panel models. When the angle of the strut with respect to the horizontal approaches the lower limit ( $a/d \approx 2$ ), the ACI STM reinforcement is very similar to those in the ACI deep beam section ( $\rho_v = 0.0025$ ,  $\rho_h = 0.0015$ ). At  $a/d$  ratios close to 1 ( $\theta = 45$ -degrees), the ACI STM reinforcement approaches the minimum reinforcement provisions in the Canadian Building Code and *fib* (0.2% in each direction). Thus, these minimum reinforcement requirements do not differ greatly; they are similar to 0.2% in each



direction. It is not clear in the commentary of these specifications if 0.2% is intended to address strength and serviceability requirements.

In Figure 4.6 and Figure 4.7, two other minimum reinforcement provisions that do not explicitly address deep beam behavior are plotted for reference. The AASHTO sectional shear requirement for minimum reinforcement (Equation 4.4) is considerably lower than those for deep beams (Figure 4.7). The reason for this discrepancy is that deep beams are strongly influenced by shear behavior whereas Bernoulli beams are often governed by flexure. The AASHTO skin reinforcement provision (Equation 4.6) is also compared to minimum reinforcement requirements for deep beams (Figure 4.6). It is clear that the quantity of required skin reinforcement increases with increasing depth of the member. For most applications, the reinforcement according to this provision will be less than or equal to a  $\rho_h$  of 0.002. It is important to note that this provision is intended to restrain the width of flexural cracks which are oriented perpendicular to the reinforcement.

In the current task, the strength and serviceability performance of deep beams with reinforcement corresponding to 0.2% in each direction, 0.3% in each direction, and several other distributions were compared.

### **4.3.2 Strength Results**

The effect of web reinforcement on the strength of deep reinforced concrete members was determined with the evaluation database and through the current experimental program.

#### ***4.3.2.1 Strength Results from the Evaluation Database***

The experimental strength of the 179 beams in the evaluation database was plotted versus the horizontal and vertical reinforcement ratio of the member in Figures 4.4 and 4.5, respectively. The data were sorted into 5 groups by  $a/d$  ratio. All of the beams in the evaluation database have at least a vector summation of web reinforcement equal to or greater than 0.1%. This amount of reinforcement was considered to be the minimum required to satisfy equilibrium in the bottle-shaped strut. As such, the

following plots were used to assess the effect of additional web reinforcement on the strength of deep beams.

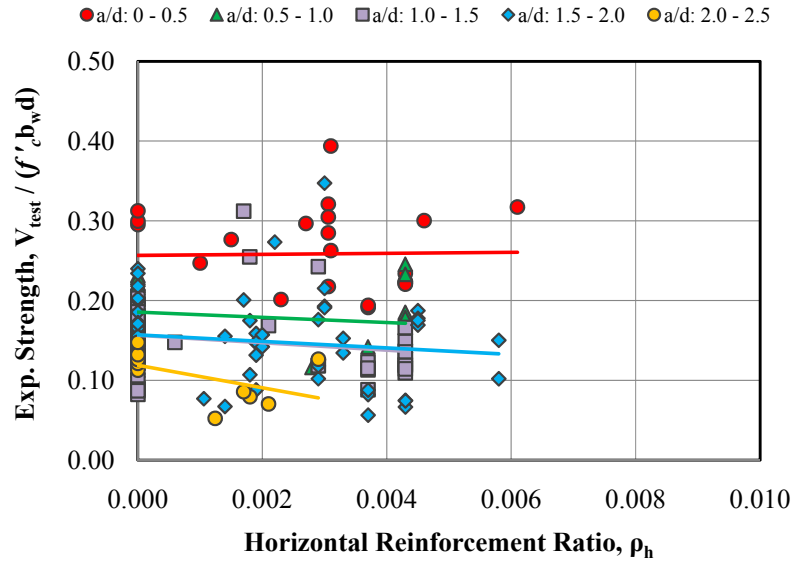


*Figure 4.8: Effect of horiz. reinforcement on strength of beams in evaluation database*

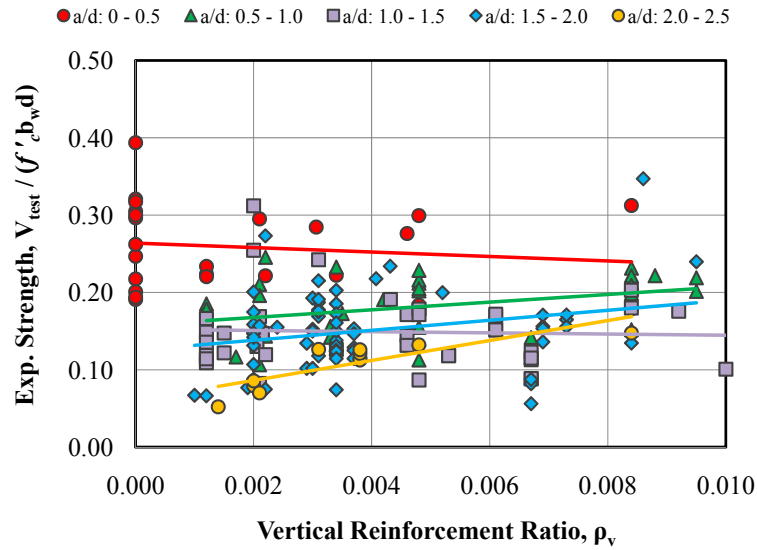


*Figure 4.9: Effect of vert. reinforcement on strength of beams in evaluation database*

In Figure 4.8, it is clear that horizontal reinforcement has little effect on the shear strength of deep beams. A similar conclusion was reached by many previous researchers. Smith and Vantsiotis (1982), Rogowsky et al. (1986), Oh and Shin (2001), Tan et al. (1997), and Brown et al. (2006) concluded that horizontal reinforcement did not have an appreciable effect on the shear strength of deep beams, especially for  $a/d$  ratios exceeding 1.0. Kong et al. noted that horizontal reinforcement was only effective at low  $a/d$  ratios (0.35) and if it was spaced near the tension reinforcement (1970). With this arrangement, the horizontal reinforcement improves the distribution of the stresses in the primary tension tie, but does not reinforce the bottle-shaped strut.

In Figure 4.9, the effect of vertical reinforcement on the shear strength of deep beams is illustrated. For  $a/d$  ratios less than or equal to 1.5, no increase in shear strength is seen for increasing amounts of vertical reinforcement. The same observation was made by De Paiva and Siess (1965), Rogowsky et al. (1986), and Brown et al. (2006). For  $a/d$  ratios approaching and exceeding 2.0, a slight increase in shear strength is seen for increasing amounts of vertical reinforcement (Figure 4.9). This conclusion was reached by several researchers as well (Kong et al., 1970, Smith and Vantsiotis, 1982, Oh and Shin, 2001, and Tan et al., 1997). In short, the effect of vertical web reinforcement on the shear strength of deep beams can be classified as minimal and is most evident at higher  $a/d$  ratios ( $a/d > 1.5$ ).

It is clear that web reinforcement does not play the same role in deep beam behavior as it does in slender beam behavior. The purpose of web reinforcement, in terms of a single-panel strut-and-tie analysis, is to resist the transverse tensile forces developed in a bottle-shaped strut. Increasing the amount of web reinforcement above the amount required to resist these transverse stresses does not significantly improve the shear strength of the member. As the  $a/d$  ratio increases and the behavior of the beam transitions from a deep beam to a slender (Bernoulli) beam, the effectiveness of vertical reinforcement increases.

The effect of web reinforcement on the diagonal cracking load as a percentage of the ultimate strength was also assessed with the evaluation database. Normalizing the

diagonal cracking load with the ultimate strength of the member quantifies the strength after first diagonal cracking. The results are plotted in Figure 4.10 and Figure 4.11 versus the quantity of web reinforcement in each orthogonal direction. In Figure 4.10, a slight trend with  $\rho_v$  exists on average. While there is minimal data at high values of  $\rho_v$ , the diagonal cracking load as a function of the ultimate strength decreases with increasing  $\rho_v$  on average. This slight trend indicates that vertical reinforcement in addition to that required for equilibrium may affect the strength of deep beams by providing reserve strength after first cracking. Additional vertical reinforcement improves the distribution of stress in the deep beam leading to a more robust member. In Figure 4.11, a trend with the amount of horizontal reinforcement is not apparent for the data as a whole. However, the trend of the data from the current project suggests a similar, but reduced benefit with respect to  $\rho_h$  as to  $\rho_v$ . In both cases, it appears that additional reinforcement provides additional redistribution capacity in the member. For a handful of specimens with less than 0.2% crack control reinforcement in each orthogonal direction, the reserve strength after first cracking was exceptionally small.

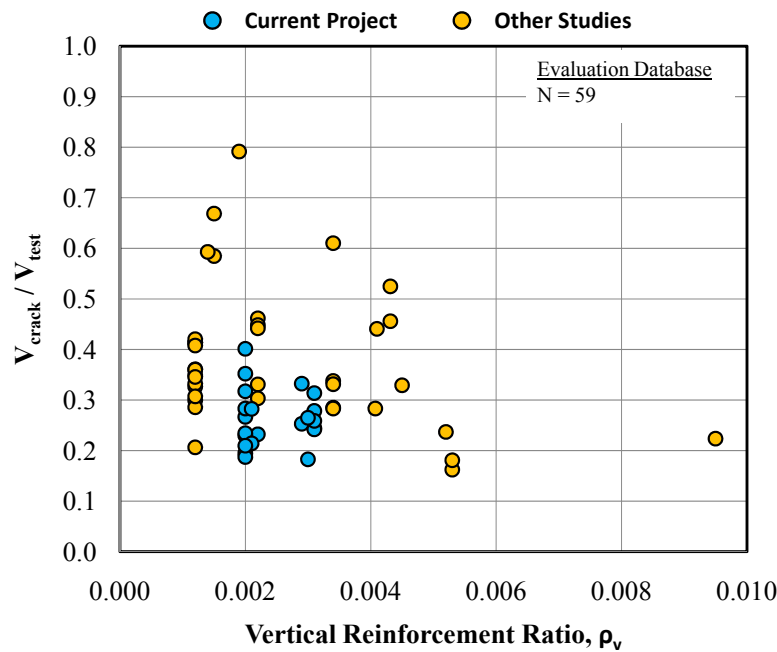


**Figure 4.10: Effect of vertical web reinforcement on strength after first cracking**

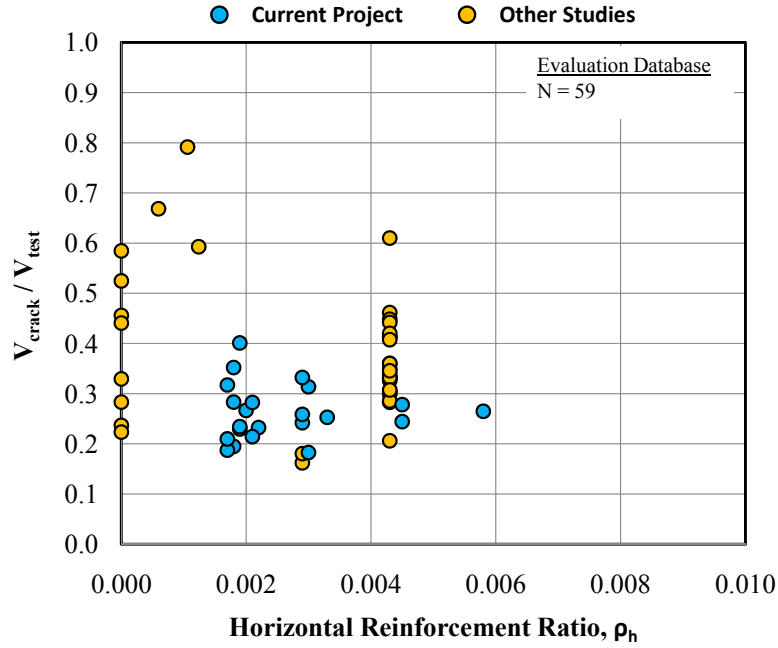


**Figure 4.11: Effect of horizontal web reinforcement on strength after first cracking**

#### **4.3.2.2 Strength Results from the Experimental Program**

In the current experimental program, numerous tests were conducted in which the amount of web reinforcement was the primary variable. Most of these tests were performed at a shear-span-to-depth ( $a/d$ ) ratio of 1.85. Two specimens were tested at an  $a/d$  ratio of 1.2; three specimens were tested at an  $a/d$  ratio of 2.5. The majority of the testing for this task was performed within Series III in which different quantities of web reinforcement were provided in each test region. Tests conducted within other series in which the quantity of web reinforcement was the only variable were also used in the current task. All of the tests in the experimental program that were relevant to the minimum web reinforcement task are listed in Table 4.4. The experimental shear strength and the amount of web reinforcement for each specimen are provided. It should be noted that the reinforcement ratios were calculated using the equations provided in Section 3.2.4. The vertical reinforcement was spaced evenly throughout the test region. The horizontal reinforcement was placed evenly throughout the effective strut area. The

horizontal and vertical spacing of the reinforcement was not a primary variable in the testing program.

**Table 4.4: Summary of strength results for specimens in minimum reinforcement task**

Beam I.D.	b <sub>w</sub> in.	d in.	ρ <sub>v</sub>	Bar size	s <sub>v</sub> in.	ρ <sub>h</sub>	Bar size	s <sub>h</sub> in.	a/d ratio	V <sub>test</sub> kip	$\frac{V_{test}}{f_c' \cdot b_w d}$	$\frac{V_{test}}{\sqrt{f_c'} \cdot b_w d}$
I-03-2	21	38.5	0.0029	#4	6.5	0.0033	#4	5.75	1.84	569	0.13	9.7
I-03-4	21	38.5	0.0030	#3	7.0	0.0033	#4	5.75	1.84	657	0.15	11.1
I-02-2	21	38.5	0.0020	#4	9.5	0.0020	#4	9.5	1.84	454	0.14	8.9
I-02-4	21	38.5	0.0021	#3	10	0.0020	#4	9.5	1.84	528	0.16	10.1
II-03-CCC2021	21	38.6	0.0031	#5	9.5	0.0045	#5	6.6	1.84	500	0.19	10.7
III-1.85-00	21	38.6	0	-	-	0	-	-	1.84	365	0.14	8.0
III-2.5-00	21	38.6	0	-	-	0	-	-	2.47	82	0.03	1.8
III-1.85-02	21	38.6	0.0020	#5	14.5	0.0019	#4	10.1	1.84	488	0.15	9.4
III-1.85-025	21	38.6	0.0024	#5	12	0.0014	#3	7.6	1.84	516	0.16	9.9
III-1.85-03	21	38.6	0.0029	#5	10	0.0029	#5	10.1	1.84	412	0.10	7.2
III-1.85-01	21	38.6	0.0011	#4	18	0.0014	#3	7.6	1.84	273	0.07	4.8
III-1.85-03b	21	38.6	0.0032	#4	6	0.0029	#5	10.1	1.84	471	0.18	10.1
III-1.85-02b	21	38.6	0.0020	#4	9.5	0.0019	#4	10.1	1.84	468	0.17	10.1
III-1.2-02	21	38.6	0.0020	#4	9.5	0.0019	#4	10.1	1.20	846	0.25	16.3
III-1.2-03	21	38.6	0.0031	#5	9.5	0.0029	#5	10.1	1.20	829	0.24	15.7
III-2.5-02	21	38.6	0.0020	#4	9.5	0.0019	#4	10.1	2.49	298	0.08	5.4
III-2.5-03	21	38.6	0.0031	#5	9.5	0.0029	#5	10.1	2.49	516	0.13	9.0
IV-2175-1.85-02	21	68.9	0.0020	#4	9.5	0.0019	#4	10.1	1.85	763	0.11	7.5
IV-2175-1.85-03	21	68.9	0.0031	#5	9.5	0.0029	#5	10.1	1.85	842	0.12	8.3
IV-2175-2.5-02	21	68.8	0.0021	#5	14.25	0.0021	#5	14.25	2.5	510	0.07	5.0
IV-2175-1.2-02	21	68.9	0.0021	#5	14.25	0.0021	#5	14.25	1.2	1223	0.17	11.9
IV-2123-1.85-03	21	19.5	0.0030	#4	6.25	0.0030	#4	6.25	1.85	329	0.19	12.5
IV-2123-1.85-02	21	19.5	0.0020	#3	5.25	0.0017	#3	6.25	1.85	347	0.20	13.0
M-03-4-CCC2436	36	40	0.0031	#5	11	0.0027	#5	6.5	1.85	1128	0.19	12.2
M-09-4-CCC2436	36	40	0.0086	#5	4	0.0027	#5	6.5	1.85	1415(f)	0.24	15.3
M-02-4-CCC2436	36	40	0.0022	#4	10	0.0022	#5	8	1.85	1102	0.27	14.5

#### 4.3.2.3 Specimens tested at $a/d$ ratio of 1.85

To evaluate the behavior and strength of a beam without web reinforcement, test III-1.85-0 was conducted. Pictures from the test are shown in Figure 4.12. For the duration of the test, a single, diagonal (flexure-shear) crack that extended from the load to the support dominated the behavior of the specimen. The crack increased in length and width with increasing applied load. At the maximum applied load, a parallel shear crack formed accompanied with a loud popping sound (Figure 4.12 (d)). The formation of this crack represented the splitting of the compression strut due to transverse tensile stresses. Since there was not any web reinforcement to transfer stresses across this crack, the beam could not resist any additional load after the parallel crack formed. Failure occurred at an applied shear of 365 kips or  $0.14f'_c b_w d$ .

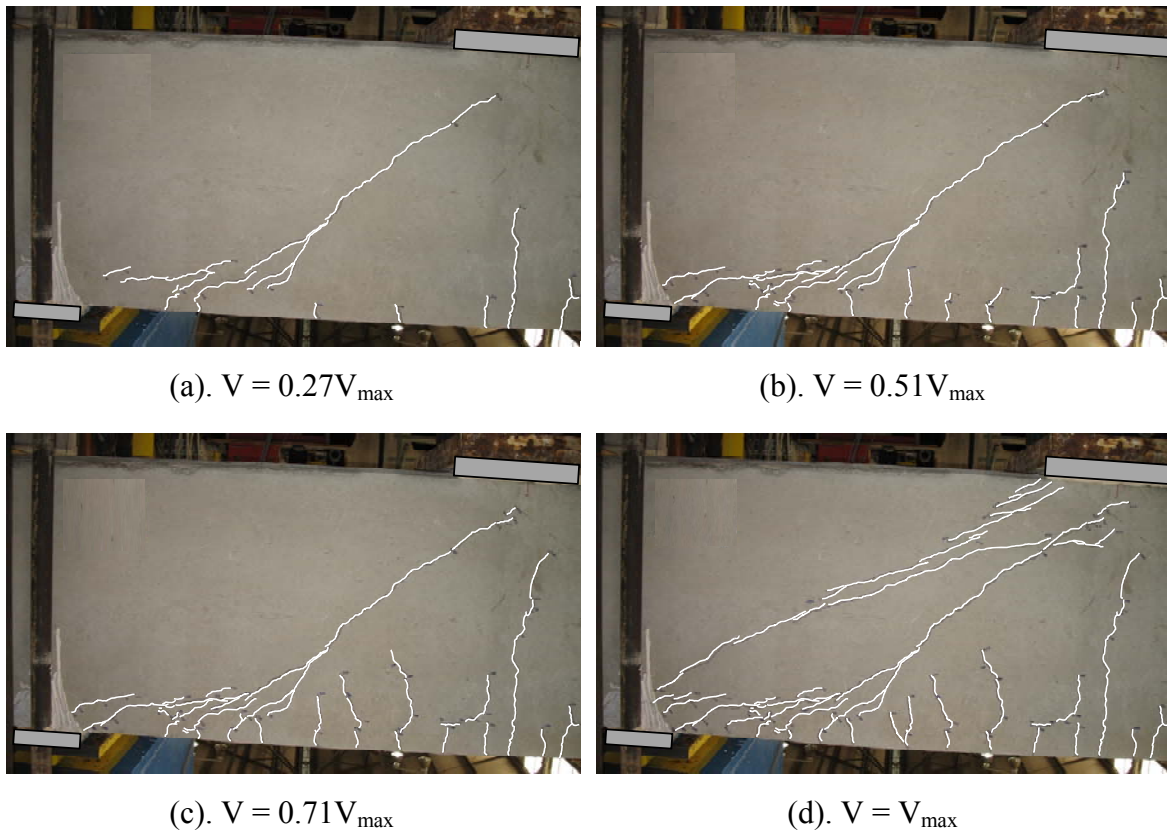


**Figure 4.12: Crack development in specimen without web reinforcement, III-1.85-0**



The behavior observed in test III-1.85-0 was consistent with a single-panel strut-and-tie model. The failure of the specimen was a result of the diagonal splitting of the compression strut. As such, the results of this test illustrated the primary role of web reinforcement in deep beams in regards to strength: to resist the transverse tensile stresses created in bottle-shaped struts. The shear strength of III-1.85-0 is compared to the shear strength of the other Series III beams in Figure 4.14.

In Figure 4.13, pictures of specimen III-1.85-03b are shown to illustrate the crack propagation in a typical test for a specimen with web reinforcement. At approximately 25% of the maximum applied load, the first diagonal shear crack formed in the test region. It extended from the tip of a flexural crack. With additional applied load, parallel shear cracks developed and grew in length and width. The presence of web reinforcement in the member ( $\rho_v = \rho_h = 0.003$ ) allowed for these parallel cracks to form. At the maximum applied load, extensive diagonal cracking was present in the deep beam region of the member. Crushing of the concrete occurred in several places along the strut and in the nodal regions. The effect of web reinforcement on the crack distribution and overall appearance of the member throughout its loading history is evident with the comparison of Figure 4.12 and Figure 4.13. Crack width information is discussed in detail in Section 4.5.3.

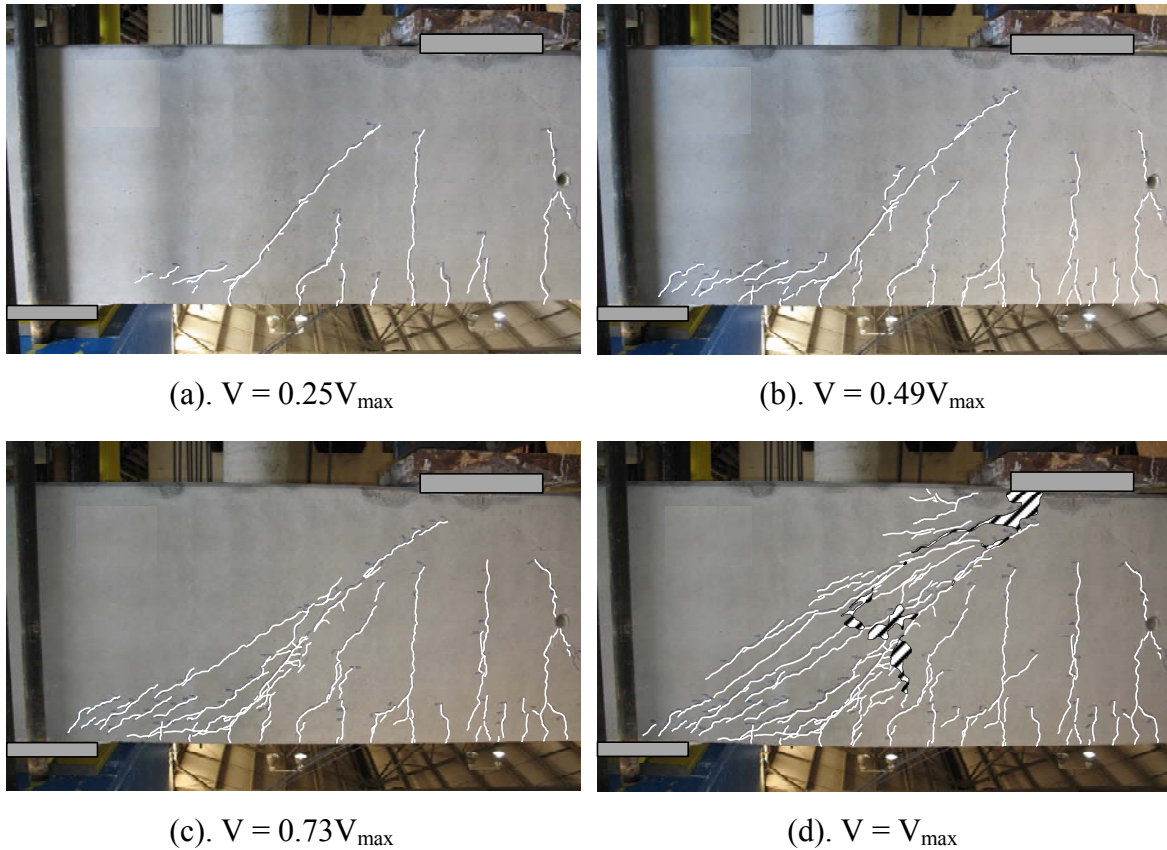


**Figure 4.13: Crack development in specimen with 0.3% in each direction, III-1.85-03b**

Several reinforcement arrangements were evaluated in the minimum web reinforcement task. Simplified versions of the minimum reinforcement provisions discussed in Section 4.3.1 were used specifically in the test specimens (Table 4.5). Note the two different horizontal reinforcement ratios according to the STM provisions of AASHTO LRFD (2008) and CHBDC (2006). These two ratios were the result of the literal interpretation of each provision and the revised interpretation discussed in Section 3.2.4. The literal interpretation consisted of a total amount of horizontal reinforcement equal to 0.003 times the gross concrete section. Distributing this amount of reinforcement within the effective strut area of the specimen produced a reinforcement ratio of 0.0045. The revised interpretation consisted of a total amount of horizontal reinforcement equal to 0.003 times the effective strut area. As such, both of these

arrangements were evaluated in the current task. As noted in Table 4.4, a few other reinforcement distributions in addition to those listed in Table 4.5 were evaluated in this task as well.

**Table 4.5: Amount of web reinforcement from several provisions used in current task**

<b>Minimum Reinforcement Provisions</b>	<b><math>\rho_v</math></b>	<b><math>\rho_h</math></b>
TxDOT 4371	0.001	0.001
CSA, <i>fib</i> , AASHTO Deep Beam	0.002	0.002
ACI Deep Beam	0.0025	0.0015
AASHTO, CHBDC STM (Section 3.2.3)	0.003	0.003
AASHTO, CHBDC STM	0.003	0.0045

The measured strength of several specimens with varying amounts of web reinforcement are provided in Figure 4.14. These tests were conducted in Series III and IV at an a/d ratio of 1.85. Specimens of the same size with different amounts of reinforcement failed at similar normalized shear stresses. Specifically, companion specimens of three different sizes (21"x23", 21"x42", and 21"x75") with reinforcement ratios corresponding to 0.2% or 0.3% in each direction failed at nearly identical levels of applied stress. In addition, the 21"x42" specimen with 0.25% reinforcement in the vertical direction and 0.15% reinforcement in the horizontal direction failed at a comparable shear stress as its companion specimen with 0.2% reinforcement in each direction. Since the mode of failure was generally the crushing of the direct strut between the load and the support, increasing the quantity of web reinforcement did not play an appreciable role in the capacity of the members. In general, the test results depicted in Figure 4.14 (at an a/d ratio of 1.85) agree favorably with those obtained from the database.

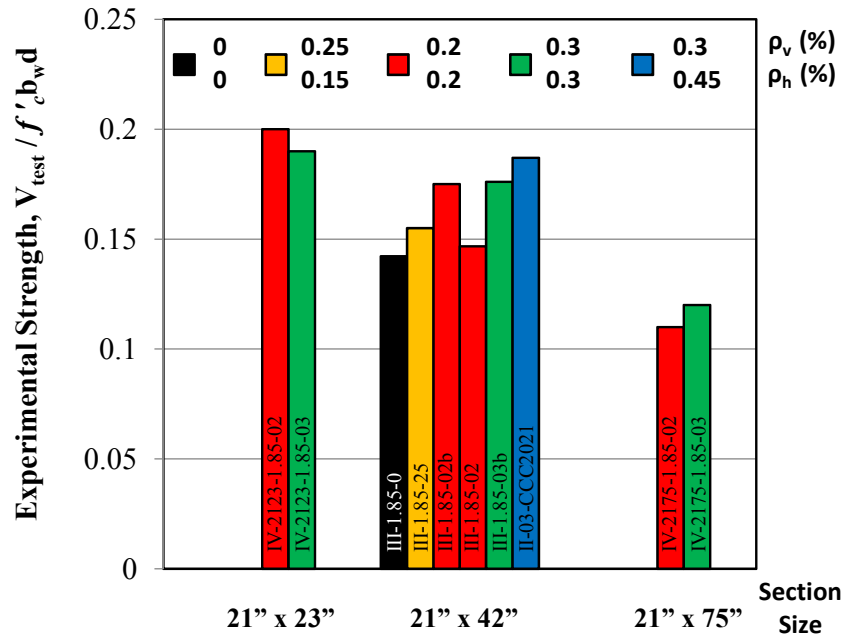


**Figure 4.14: Strength results of Series III and IV specimens at  $a/d$  ratio of 1.85**

The unreinforced specimen (III-1.85-0) failed at only a slightly smaller normalized shear stress than the reinforced beams. For this specimen, the tensile strength of the concrete was sufficient to resist the transverse tensile stresses in the bottle-shaped strut until an applied load comparable with that of the reinforced beams was placed on the member. However, relying on the tensile strength of concrete to consistently resist these tensile stresses is not advised.

The strength results from one beam consisting of tests III-1.85-01 and III-1.85-03 are provided in Figure 4.15. These results are discussed separately from those displayed in Figure 4.14 due to the unusually low experimental strength values for each test, particularly those of III-1.85-03. III-1.85-03 failed at a shear of  $0.10f'_c b_w d$ , while a nominally identical specimen, III-1.85-03b, failed at a shear of  $0.18f'_c b_w d$ . The reason for this discrepancy is unclear since a similar mixture design, grade of steel, fabrication technique, and testing procedure was used in all tests. At the same time, there is no reason to discount the validity of this test. At a minimum, the range of potential scatter in shear strength is illustrated by test III-1.85-03.

Comparing the measured strength to the calculated strength of test III-1.85-03 shows that the strength was conservatively calculated using the Project 5253 STM provisions discussed in Section 2.3.4.4 (Figure 4.15). This was not true for test III-1.85-01. Since the calculated strength of each specimen was identical, the difference in conservatism between the two was the result of the low experimental strength of test III-1.85-01. The lower amount of web reinforcement was the primary reason for the reduction in shear strength. Unlike the previously-discussed tests, the amount of web reinforcement in III-1.85-01 ( $\rho_v = \rho_h \approx 0.001$ ) significantly affected the experimental strength. The appearance of the beam at ultimate further supports this claim. As shown in the test pictures in Figure 4.15, the failure mode of III-1.85-03 was consistent with the crushing of a direct strut between the load and the support; whereas, the failure mode of III-1.85-01 had a sectional-shear appearance to it. There was not enough reinforcement to distribute the diagonal cracks within the test region. In general, a strut-crushing failure will occur at a higher applied stress than the stress corresponding to a sectional-shear failure.

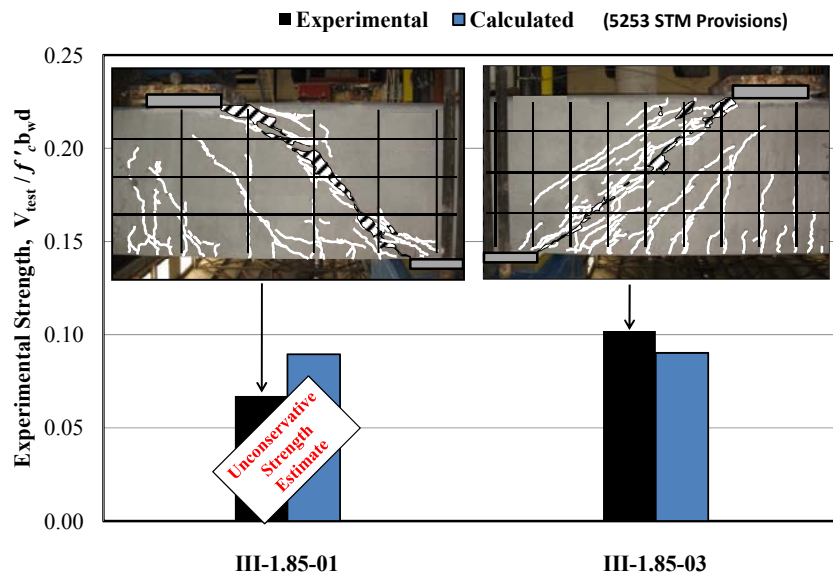


**Figure 4.15: Strength results comparison of III-1.85-01 and III-1.85-03**

In short, the results of tests III-1.85-01 and III-1.85-03 demonstrated two important points. First, significant scatter (50%) can exist for the experimental shear strength of deep beams. Second, while the amount of reinforcement does not generally affect the shear strength of deep beams, there may be cases where it can. If the quantity of web reinforcement is low ( $\rho_v \approx \rho_h \approx 0.001$ ) and the transverse spacing is relatively high ( $s_v = 18 \text{ in.} \approx d/2$ ), then the concrete strut may not be able to develop its full design strength. In the case of III-1.85-01, the strength was unconservatively estimated.

In Series M, three 36"x48" specimens were tested with different quantities of web reinforcement (Table 4.4). The results of these tests (Figure 4.16) were similar to those from Series III and IV plotted in Figure 4.14. The amount of web reinforcement did not play an appreciable role in the strength of the specimens. In fact, the specimen with 0.2% in each direction (M-02-4-CCC2436) failed at a higher normalized shear stress than the specimen with 0.3% in each direction (M-03-4-CCC2436). However, it should be noted that these tests were conducted on different beams where the compressive strength of the concrete,  $f'_c$ , was 2,800 psi and 4,100 psi, respectively. The shear force at ultimate was similar for the two tests: 1,102 kips for the beam with 0.2% steel, and 1,128 kips for the beam with 0.3% steel. Therefore, no discernible difference in strength was observed for the beams in Series M with either 0.2% or 0.3% web reinforcement in each direction.

M-03-4-CCC2436 and M-09-4-CCC2436 were companion tests conducted on the same beam. The only difference between the two tests was  $\rho_v$  equaled 0.003 and 0.009, in M-03-4-CCC2436 and M-09-4-CCC2436, respectively. Increasing the amount of web reinforcement by 300% altered the failure mode from shear to flexure, but only increased the capacity of the member by approximately 25%.

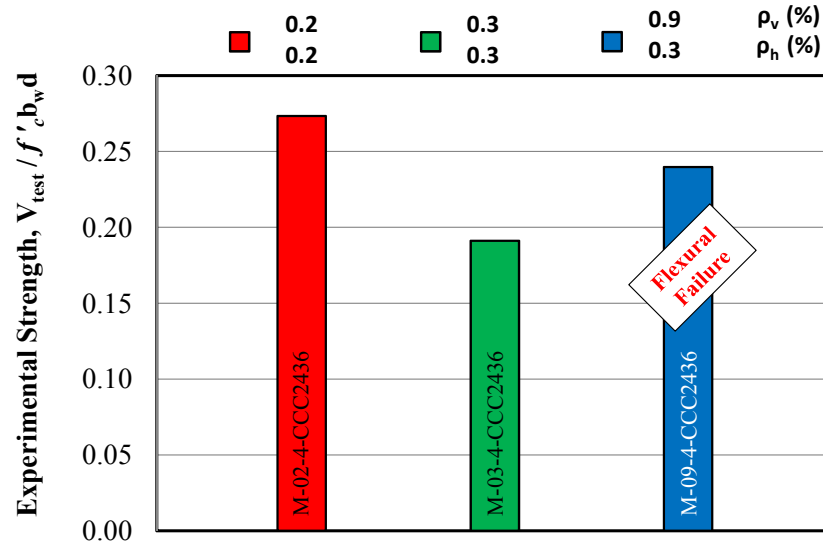


**Figure 4.16: Strength results with web reinforcement as variable from Series M**

The quantity of web reinforcement was varied in Series I as well. The results from this series further supported the aforementioned findings in regards to the effect of web reinforcement on the strength of deep beams. The experimental strength results of the four beams in Series I are plotted in Figure 4.17. A small decline in the normalized shear stress at failure was observed with *increasing* amount of web reinforcement in both cases. However, this reduction is well within the expected scatter in deep beam shear strength data.

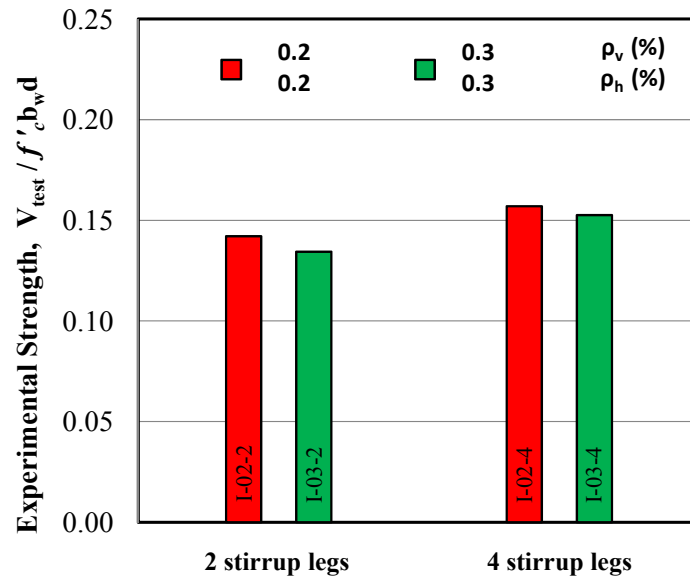


**Figure 4.17: Strength results with web reinforcement as variable from Series I**

#### **4.3.2.4 Specimens tested at other a/d ratios: 1.2 and 2.5**

In addition to an a/d ratio of 1.85, the effect of web reinforcement on the strength of deep beams was also evaluated at other a/d ratios. In Series III, two spans were tested at an a/d ratio of 1.2; three spans were tested at an a/d ratio of 2.5.

The two beams tested at an a/d ratio of 1.2 provided very consistent results with those tested at an a/d ratio of 1.85. As seen in Figure 4.18, the failure mode of each beam was the crushing of the direct strut between the load and support. There was no difference in strength between the beams with 0.2% or 0.3% in each orthogonal direction.



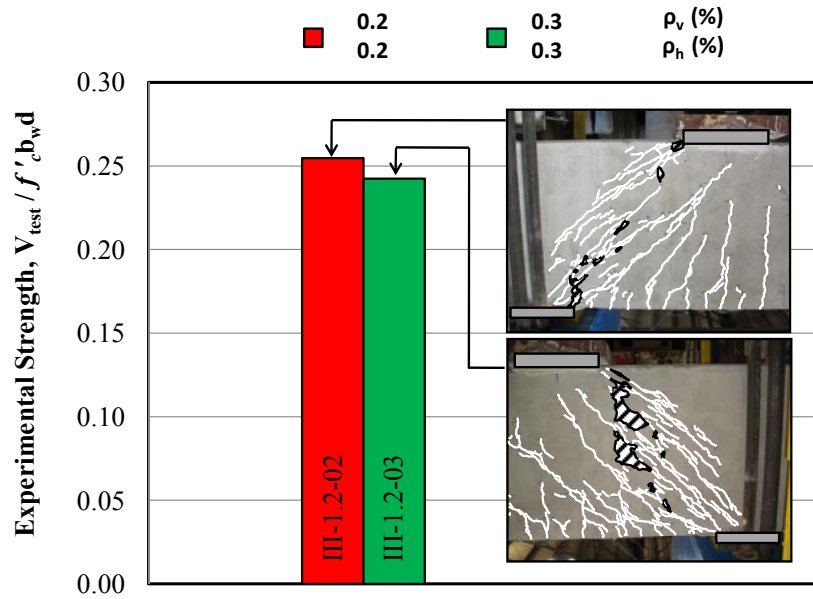


**Figure 4.18: Strength results from specimens tested at a/d ratio of 1.2**

Of the three specimens tested with an a/d ratio of 2.5, one did not have any web reinforcement (III-2.5-0). This test was the companion test of III-1.85-0. During the test of III-1.85-0, post-tensioned clamps were attached to the low-shear span (future region of test III-2.5-0) to prevent a premature failure. The condition of the test region for III-2.5-0 after the III-1.85-0 test is shown in Figure 4.19 (a). The condition of the test region at the maximum applied shear is provided in Figure 4.19 (b). It is evident from the failure picture that this beam failed due to sectional shear, i.e. diagonal tension. No evidence of crushing in the test region existed. The failure shear for this specimen was considerably low. In fact, it failed at  $1.8\sqrt{f'_c}b_wd$ , approximately 10% less than the ACI sectional shear equation for  $V_c$  ( $2\sqrt{f'_c}b_wd$ ) (ACI, 2008). It is possible that the precracked condition of the shear span contributed to the unconservative failure load. Nevertheless, the results of III-2.5-0 supports two conclusions. First, excluding transverse reinforcement from a concrete beam can result in dangerously low levels of shear strength. Second, at an a/d ratio of 2.5, a single-panel STM may not be appropriate. The behavior of III-2.5-0 was consistent with a sectional shear model, not a single-panel strut-and-tie model. This conclusion was not unexpected since both AASHTO LRFD (2008)

and ACI 318-08 limit the treatment of deep beams to an  $a/d$  ratio  $\leq 2.0$ . It should be noted that deep beam behavior has been reported in experiments up to an  $a/d$  ratio of 2.5 (Section 5.2).

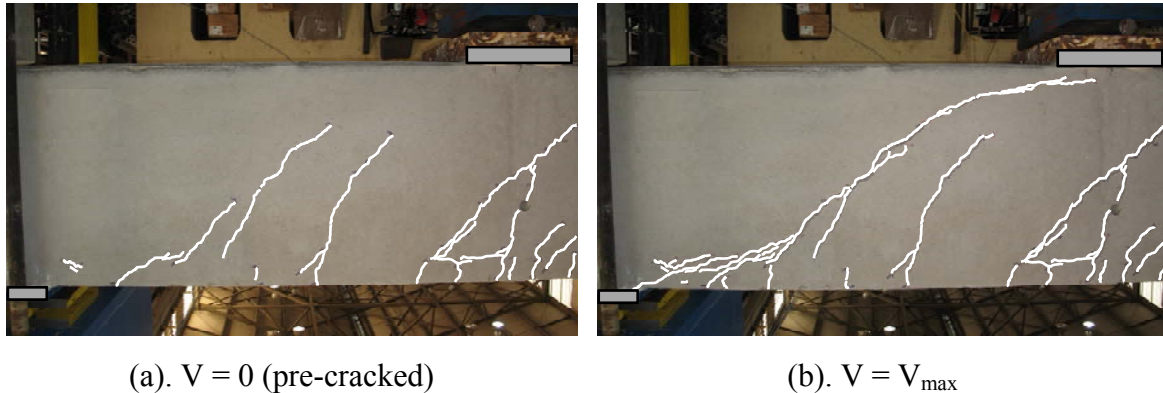


**Figure 4.19: Crack development in III-2.5-0**

The other two specimens tested at an  $a/d$  ratio of 2.5 had 0.2% (III-2.5-02) and 0.3% (III-2.5-03) crack control reinforcement in each orthogonal direction. The strength results and failure pictures for these two tests are presented in Figure 4.20. From this figure, it is evident that an increase in strength and a change in behavior existed as the amount of web reinforcement increased from 0.2% to 0.3% in each direction. The cracking pattern and failure picture for III-2.5-02 was very consistent with the sectional shear, or diagonal tension, failure seen in III-2.5-0. A single diagonal shear crack dominated the test region up until failure. Very little parallel diagonal cracking was observed. On the contrary, III-2.5-03 behaved more like a deep beam. Extensive redistribution of diagonal cracks occurred with increasing applied load, presumably due to the additional amount of web reinforcement. Near ultimate, a parallel shear crack formed along the axis of the assumed compression strut between the load and the support as observed in tests at smaller  $a/d$  ratios. An increase in load-carrying capacity of approximately 60% accompanied the change in failure mode.

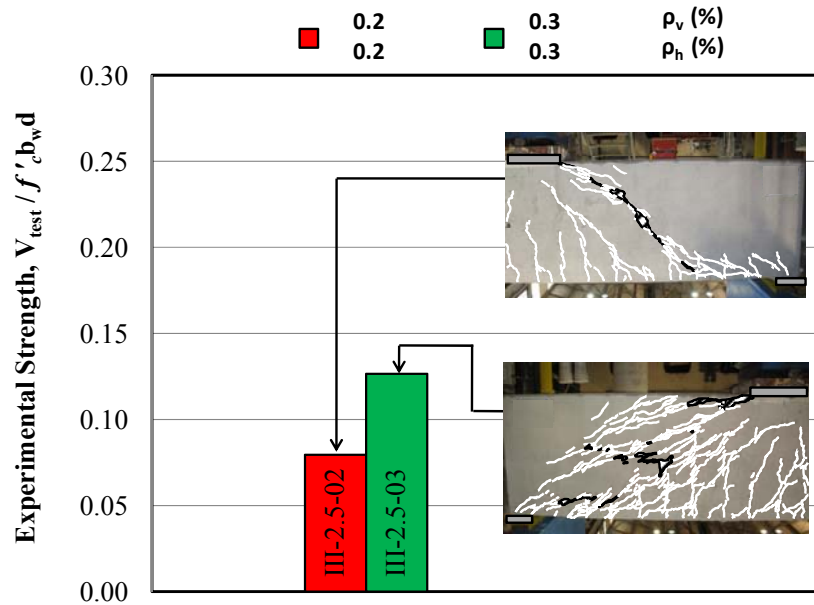


**Figure 4.20: Strength results from specimens tested at an  $a/d$  ratio of 2.5**

The comparison of III-2.5-02 to III-2.5-03 revealed that the quantity of web reinforcement becomes relevant at higher  $a/d$  ratios ( $a/d > 2$ ). The behavior of the test region is transitioning from strut-and-tie action to sectional shear behavior. Vertical reinforcement improves the sectional shear strength of reinforced concrete beams. In test III-2.5-03, the vertical reinforcement enabled significant redistribution to occur increasing the load-carrying capacity of the member. The final failure mode of this specimen was consistent with a combination of sectional shear and strut-and-tie behavior. It should be noted that the beneficial effect of web reinforcement on the strength of beams tested at  $a/d$  ratios in excess of 2 was also observed through the analysis of the database as shown in Figure 4.9. Additional information regarding the transition of deep beam behavior to sectional shear behavior is provided in Section 5.2.

### 4.3.3 Serviceability Results

The effect of web reinforcement on the serviceability of deep reinforced concrete beams was also investigated within this task. As previously discussed, the diagonal cracking loads and the width of diagonal cracks were used to assess the serviceability performance of deep beams.

#### 4.3.3.1 Serviceability Results from the Evaluation Database

Very little crack width data were available in the literature. However, the load at first diagonal cracking was recorded for 59 specimens in the evaluation database. The diagonal cracking loads were normalized by  $\sqrt{f'_c} b_w d$  and were plotted versus the reinforcement ratio in each direction in Figure 4.21 and Figure 4.22. The results in these figures did not reveal any effect of the quantity of reinforcement on the normalized diagonal cracking loads. This finding was plausible since reinforced concrete members behave elastically prior to cracking. The strain in the concrete at first cracking is very small preventing any effect of the reinforcement to be observed until cracks develop.

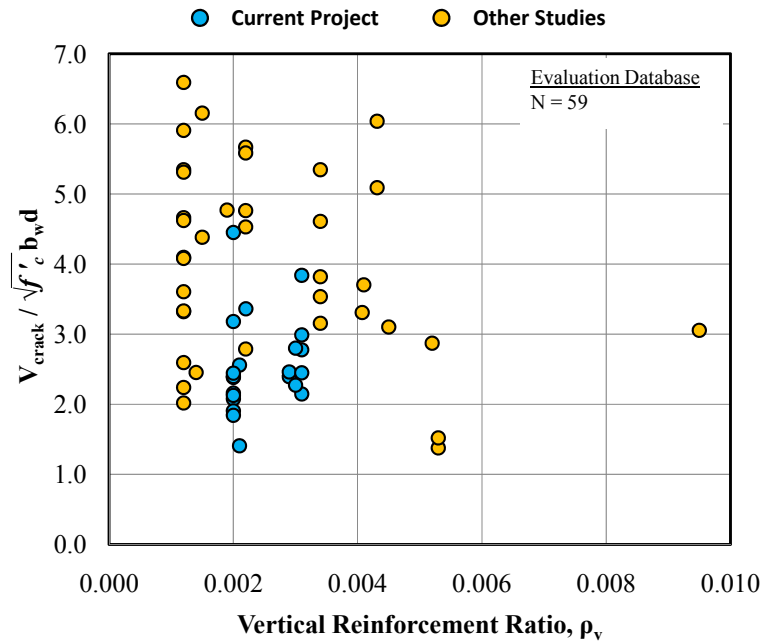


**Figure 4.21: Effect of vertical reinforcement on the diagonal cracking load**

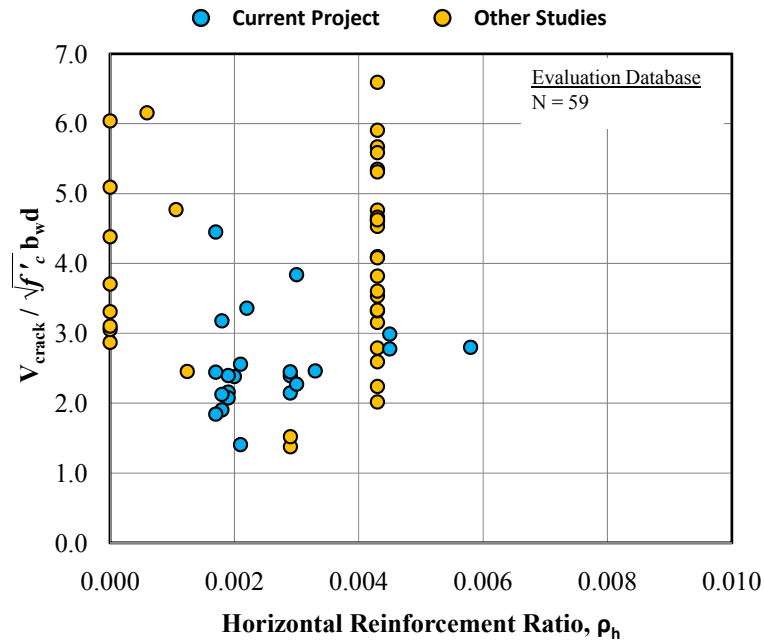


**Figure 4.22: Effect of horizontal reinforcement on the diagonal cracking load**

#### **4.3.3.2 Serviceability Results from the Experimental Program**

The diagonal cracking loads for each specimen relevant to the current task are provided in Table 4.6. The strength data for the same specimens in Table 4.6 were provided in Table 4.4. As noted in Section 3.6, it was only possible to obtain the cracking load for the first test on each 42-, 44-, and 48-in. specimen. The first cracking loads for both tests conducted on the 75- and 23-in. specimens were measured.

**Table 4.6: Summary of diagonal cracking loads for specimens in minimum reinforcement task**

<b>Beam I.D.</b>	<b>b<sub>w</sub> in.</b>	<b>d in.</b>	<b>ρ<sub>v</sub></b>	<b>Bar size</b>	<b>s<sub>v</sub> in.</b>	<b>ρ<sub>h</sub></b>	<b>Bar size</b>	<b>s<sub>h</sub> in.</b>	<b>a/d ratio</b>	<b>V<sub>crack</sub> kip</b>	$\frac{V_{crack}}{\sqrt{f'_c} \cdot b_w d}$
I-03-2	21	38.5	0.0029	#4	6.5	0.0033	#4	5.75	1.84	144	2.5
I-03-4	21	38.5	0.0030	#3	7.0	0.0033	#4	5.75	1.84	-	-
I-02-2	21	38.5	0.0020	#4	9.5	0.0020	#4	9.5	1.84	121	2.4
I-02-4	21	38.5	0.0021	#3	10	0.0020	#4	9.5	1.84	-	-
II-03-CCC2021	21	38.6	0.0031	#5	9.5	0.0045	#5	6.6	1.84	139	3.0
III-1.85-00	21	38.6	0	-	-	0	-	-	1.84	98	2.1
III-2.5-00	21	38.6	0	-	-	0	-	-	2.47	-	-
III-1.85-02	21	38.6	0.0020	#5	14.5	0.0019	#4	10.1	1.84	112	2.2
III-1.85-025	21	38.6	0.0024	#5	12	0.0014	#3	7.6	1.84	-	-
III-1.85-03	21	38.6	0.0029	#5	10	0.0029	#5	10.1	1.84	137	2.4
III-1.85-01	21	38.6	0.0011	#4	18	0.0014	#3	7.6	1.84	-	-
III-1.85-03b	21	38.6	0.0032	#4	6	0.0029	#5	10.1	1.84	114	2.4
III-1.85-02b	21	38.6	0.0020	#4	9.5	0.0019	#4	10.1	1.84	-	-
III-1.2-02	21	38.6	0.0020	#4	9.5	0.0019	#4	10.1	1.20	165	3.2
III-1.2-03	21	38.6	0.0031	#5	9.5	0.0029	#5	10.1	1.20	-	-
III-2.5-02	21	38.6	0.0020	#4	9.5	0.0019	#4	10.1	2.49	105	1.9
III-2.5-03	21	38.6	0.0031	#5	9.5	0.0029	#5	10.1	2.49	-	-
IV-2175-1.85-02	21	68.9	0.0020	#4	9.5	0.0019	#4	10.1	1.85	216	2.1
IV-2175-1.85-03	21	68.9	0.0031	#5	9.5	0.0029	#5	10.1	1.85	218	2.1
IV-2175-2.5-02	21	68.9	0.0021	#5	14.25	0.0021	#5	14.25	2.5	144	1.4
IV-2175-1.2-02	21	68.9	0.0021	#5	14.25	0.0021	#5	14.25	1.2	262	2.6
IV-2123-1.85-03	21	19.5	0.0030	#4	6.25	0.0030	#4	6.25	1.85	60	2.3
IV-2123-1.85-02	21	19.5	0.0020	#3	5.25	0.0017	#3	6.25	1.85	65	2.4
M-03-4-CCC2436	36	40	0.0031	#5	11	0.0027	#5	6.5	1.85	354	3.8
M-09-4-CCC2436	36	40	0.0086	#5	4	0.0027	#5	6.5	1.85	-	-
M-02-4-CCC2436	36	40	0.0022	#4	10	0.0022	#5	8	1.85	256	3.4

As shown in Table 4.6, the diagonal cracking loads of several specimens with different amounts of web reinforcement were measured. Information regarding the measurement of the diagonal cracking loads was provided in Section 4.2.2. The load at first diagonal cracking normalized by the  $\sqrt{f'_c} b_w d$  for each of these specimens is plotted in Figure 4.23. The results indicate that the quantity of web reinforcement has no effect on the diagonal cracking load. This finding is in agreement with the results from the evaluation database. As previously mentioned, the amount of reinforcement does not affect the behavior of reinforcement concrete members until after the beam has cracked. It is interesting to note that the normalized diagonal cracking loads of the 36"x48" specimens were considerably greater than those of the 21"x23", 21"x42", 21"x44", and 21"x75" specimens. It is likely that the higher longitudinal reinforcement ratio in the 36"x48" specimens (2.9% vs. 2.3%) contributed to the higher normalized diagonal cracking loads. Additional longitudinal reinforcement increases the transformed moment of inertia which would increase the cracking load. Also, since the first diagonal crack was generally a flexure-shear crack, the amount of reinforcement at the tip of the flexural crack affects the diagonal cracking load. Additional information regarding the factors affecting the load at first diagonal cracking is provided in Section 5.3.

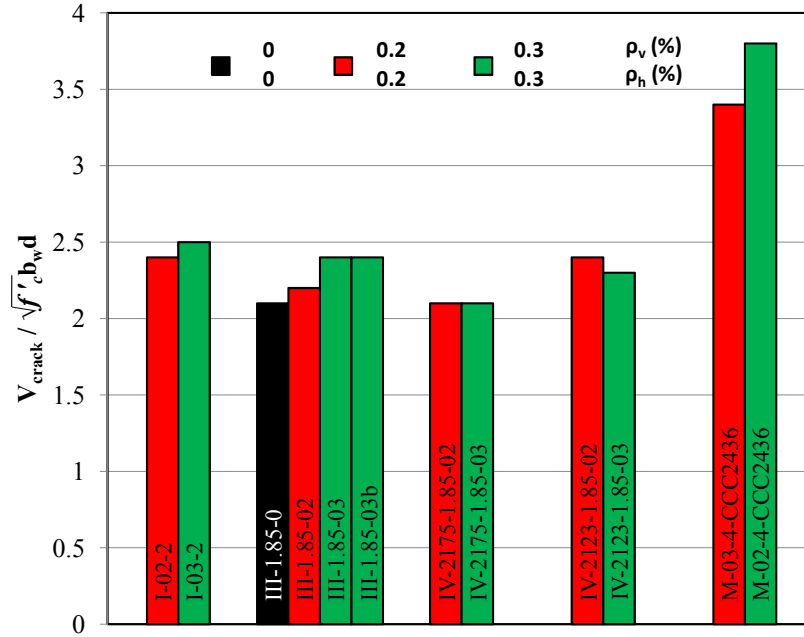


**Figure 4.23: Diagonal cracking loads of specimens in current task**

The serviceability performance of the test specimens was also evaluated with the maximum width of the diagonal cracks. The maximum diagonal crack widths were recorded for each side of the test specimen and were plotted versus the percent of the maximum applied load. Plotting the data in this manner was appropriate to permit specimens of different sizes and with different concrete strengths to be placed on the same plot. Also, this approach was consistent with another objective of the current research study: to correlate the maximum diagonal crack width with the residual capacity of the member (Section 5.4). The diagonal crack width data from the test specimens are tabulated in Appendix C.

Maximum diagonal crack widths for six 21”x42” specimens tested at an a/d ratio of 1.85 are presented in Figure 4.24. Several important observations can be made regarding this figure. First, it is clear that the quantity of web reinforcement directly influences the width of diagonal cracks. As the amount of reinforcement crossing the diagonal crack increases, the width of the diagonal crack decreases for a given percent of applied load. Therefore, the specimen with 0.3% reinforcement in the vertical direction



and 0.45% reinforcement in the horizontal direction (II-03-CCC2021) had the narrowest diagonal cracks throughout its loading history. The effectiveness of horizontal reinforcement was evaluated with this test as well. Comparing the crack widths of specimens II-03-CCC2021 and III-1.85-03b demonstrated that additional horizontal reinforcement effectively restrained diagonal crack widths at high  $a/d$  ratios ( $a/d = 1.85$ ). While it was emphasized in the literature and through the use of the database (Figure 4.8) that additional horizontal reinforcement had a negligible impact on the strength of deep beams, these crack width data suggested that horizontal reinforcement may be important for serviceability. Comparing the crack widths of specimens III-1.85-02 and III-1.85-025 did not reveal significant differences. This observation was not unexpected due to minimal differences in the spacing of the reinforcement required to target the reinforcement ratio in each specimen. The spacing of the #5 stirrups for these two specimens only differed by 2.5 in. As a result of these findings and of the format of several existing minimum reinforcement provisions, equal reinforcement in each orthogonal direction was targeted as the most effective and most practical solution for minimum web reinforcement in deep beams.

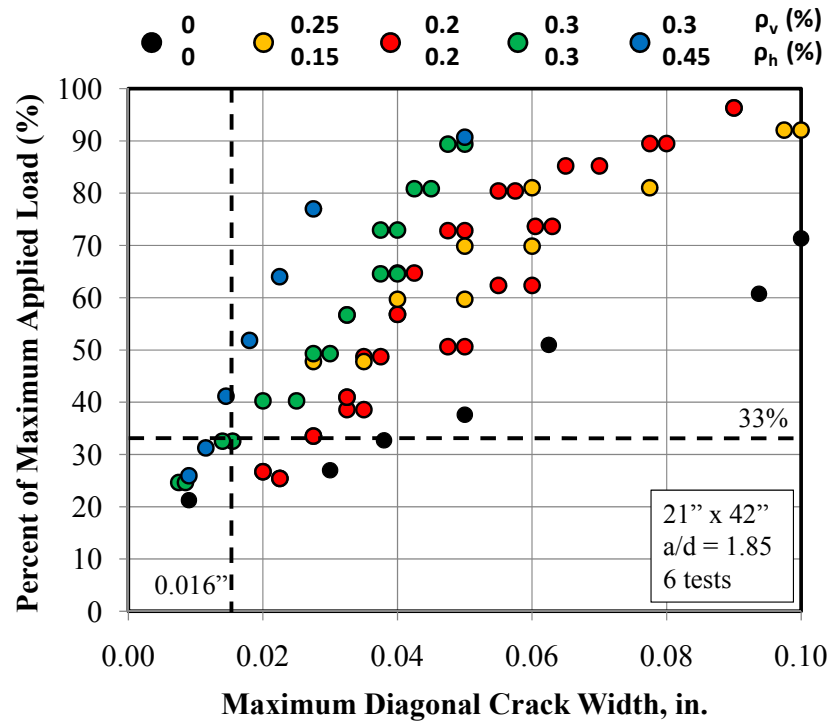
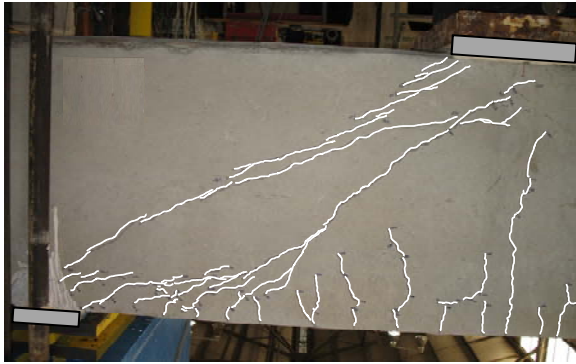


**Figure 4.24: Maximum diagonal crack width for 6 - 21"x42" specimens tested at a/d of 1.85**

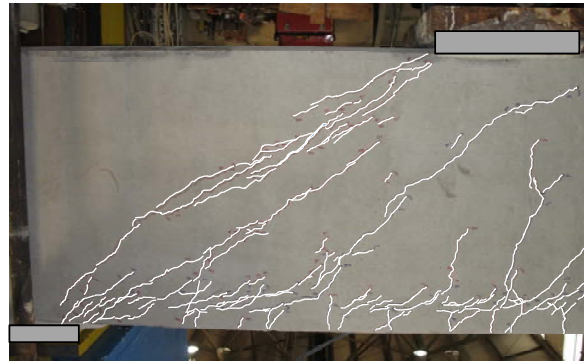
The crack width data in Figure 4.24 can be compared to the liberal benchmark crack width of 0.016 in. (Section 4.2.2). At first diagonal cracking, the maximum crack width for III-1.85-02 and III-1.85-02b exceeded 0.016 in. On the contrary, at the first cracking of specimens II-03-CCC2021 ( $\rho_v = 0.003$ ,  $\rho_h = 0.0045$ ) and III-1.85-03b ( $\rho_v = 0.003$ ,  $\rho_h = 0.003$ ), the maximum crack width was only approximately 0.009 in. The diagonal crack width did not reach 0.016 in. in these specimens until 30% to 40% of the maximum applied load was reached. For the unreinforced specimen (III-1.85-0), the maximum diagonal crack width was also less than 0.016 in. at first diagonal cracking. However, it is clear from Figure 4.24 that the crack width increased rapidly with a minimal increase in applied load. The data in Figure 4.24 can also be evaluated with respect to the estimated service load on the structure of 33% of the maximum applied load (Section 4.2.2). At this level, the specimens with 0.3% web reinforcement or greater in each direction had diagonal crack widths at or less than 0.016 in. The specimens

without any reinforcement or with 0.2% reinforcement had maximum crack widths of 0.038 in. and 0.028 in. respectively. It should be noted that the crack width limit of 0.016 in. and the estimated service load (33% of ultimate) should be not be treated as definite limits. They should be used as general benchmarks. Nevertheless, the data in Figure 4.24 clearly indicated that the specimens with at least 0.3% in each direction performed much better than those with less reinforcement.

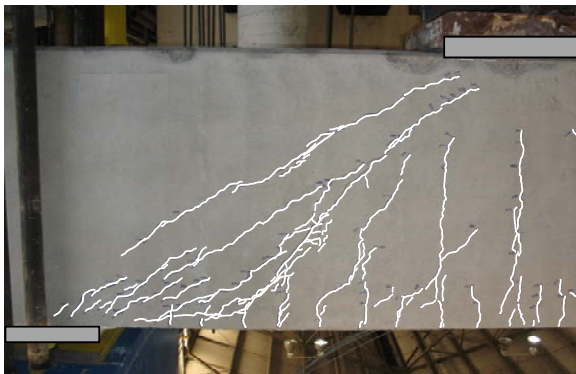
The crack patterns at approximately 90% of the maximum applied load for four of the aforementioned tests are provided in Figure 4.25. In a general sense, the crack patterns of each test specimen agree favorably with the maximum diagonal crack width data presented in Figure 4.24. At a given load stage, as the distribution of diagonal cracking, i.e. the number of parallel diagonal cracks, increased, the maximum diagonal crack width decreased. Comparing the crack patterns of test III-1.85-03b and II-03-CCC2021 further illustrated the benefit of horizontal reinforcement. While horizontal reinforcement was shown in the literature and through the use of the database (Figure 4.8) to be less effective than vertical reinforcement in terms of strength, the data from these tests suggested that it is important for limiting diagonal crack widths. This finding supported keeping the quantity of minimum web reinforcement the same in each orthogonal direction.



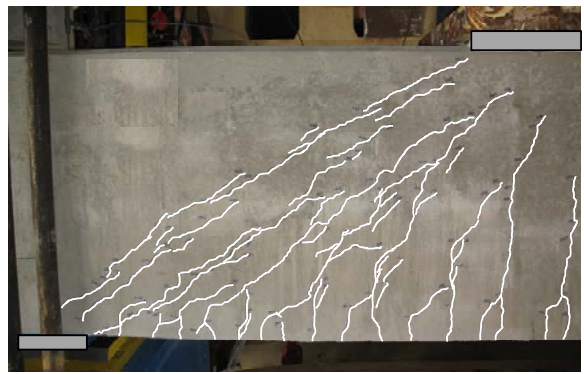
(a). III-1.85-0



(b). III-1.85-02b



(c). III-1.85-03b



(d). II-03-CCC2021

***Figure 4.25: Crack patterns of four specimens at approximately 90% of capacity***

The crack width data from tests III-1.85-01 and III-1.85-03 are presented in Figure 4.26 with the data from Figure 4.24. The maximum diagonal crack width data from III-1.85-03 agreed favorably with the data from the other specimen with the same web reinforcement (III-1.85-03b) even though they failed at considerably different normalized shear stresses. On the other hand, the crack width data from III-1.85-01 did not match the trend with reinforcement quantity that was otherwise represented in Figure 4.26. The reason for this discrepancy was the difference in failure modes between III-1.85-01 and the rest of the tests. As shown previously (Figure 4.15), the failure mode of III-1.85-01 more closely resembled a sectional shear failure than a deep beam failure, primarily due to insufficient web reinforcement.

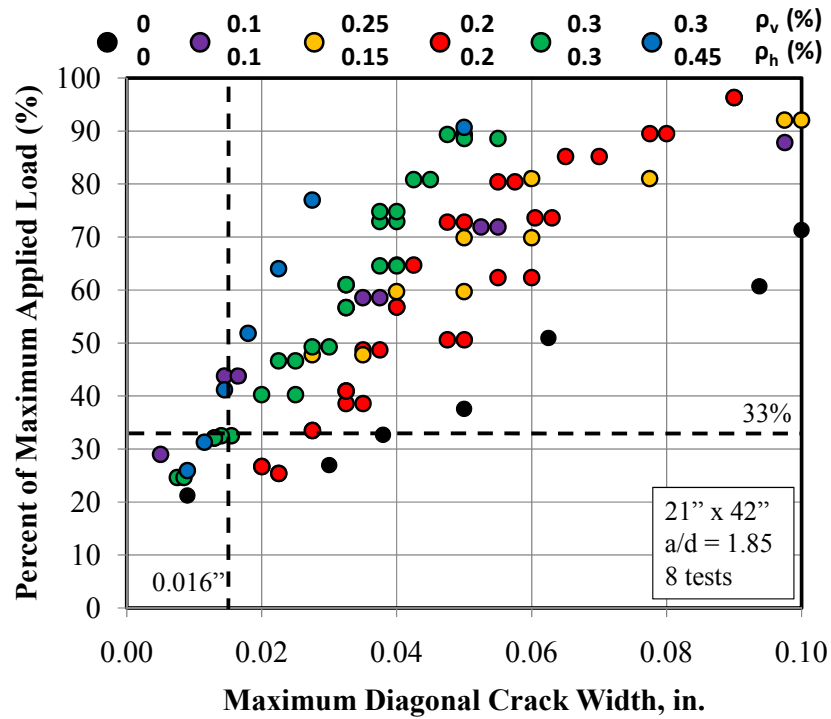


**Figure 4.26: Maximum diagonal crack width for 8 – 21"x42" specimens tested at  $a/d$  of 1.85**

Consistent load transfer mechanisms were required to compare diagonal crack width data when normalizing the applied load by the maximum applied load. If the crack width data in Figure 4.26 were plotted versus the applied shear, the trend in Figure 4.27 is obtained. This trend illustrates that regardless of the load transfer mechanism, maximum diagonal crack widths are a function of the applied shear and the quantity of web reinforcement. However, as previously discussed, plotting crack width data versus the percent of maximum applied load was more useful for the current project.

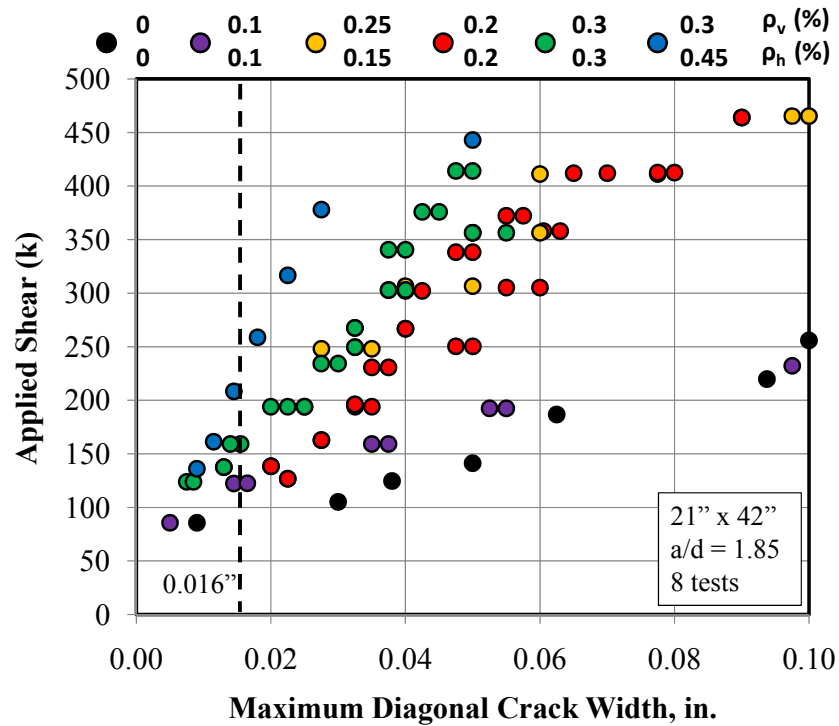


**Figure 4.27: Maximum diagonal crack widths of 8 – 21''x42'' specimens versus applied shear**

Several other tests were conducted at an a/d ratio of 1.85 within the experimental program to evaluate the difference between 0.2% and 0.3% web reinforcement in each orthogonal direction. The crack width data for these tests are provided in Figure 4.28 through Figure 4.31. The data in these figures can be used to compare the maximum diagonal crack widths for the 21''x75'' specimens, the 36''x48'' specimens, and the four 21''x44'' specimens with either 2 or 4 legged stirrups. In all cases, the same general conclusions regarding the effect of web reinforcement on maximum diagonal crack widths can be reached. Providing 0.3% reinforcement in each orthogonal direction better restrained the diagonal crack widths throughout the loading history of the member and at first cracking, in general. At the estimated service load (33% of ultimate), the maximum diagonal crack widths for the specimens with 0.3% reinforcement in each direction were generally at or below the crack width benchmark of 0.016 in. The crack widths for the

specimens with 0.2% reinforcement were generally greater than 0.016 in. at the estimated service load.

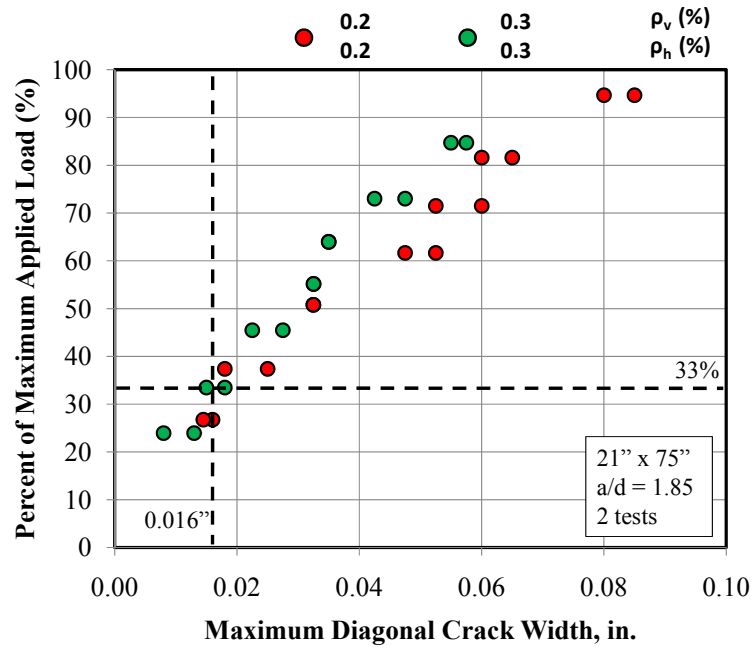


Figure 4.28: Max. crack widths for 21"x75" specimens with 0.2% and 0.3% reinf.

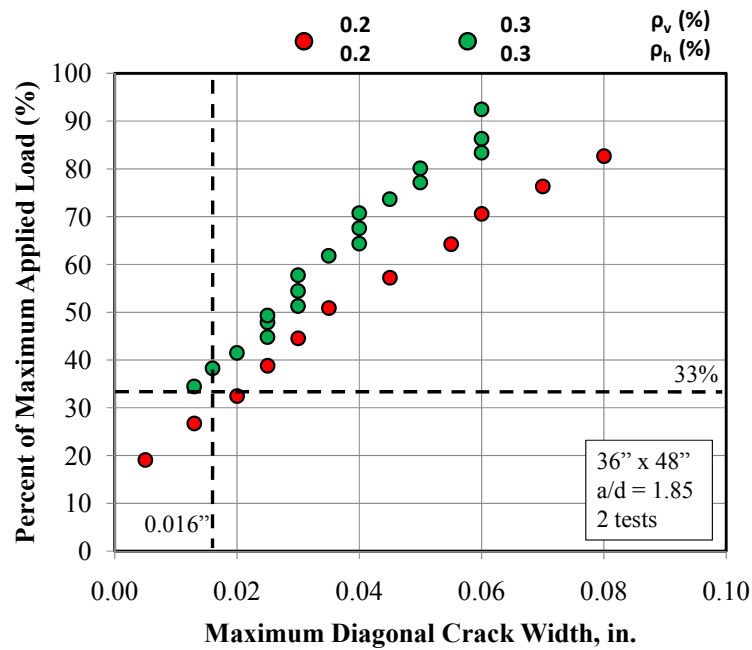
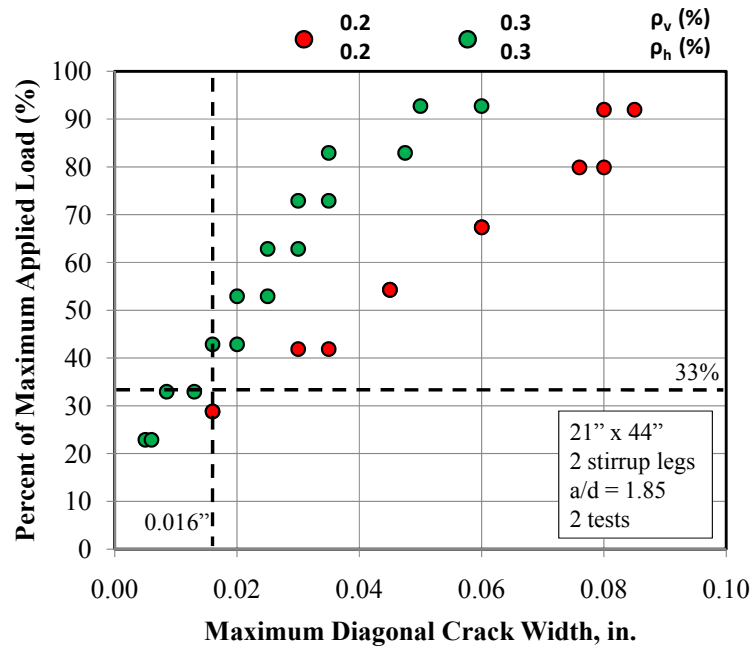
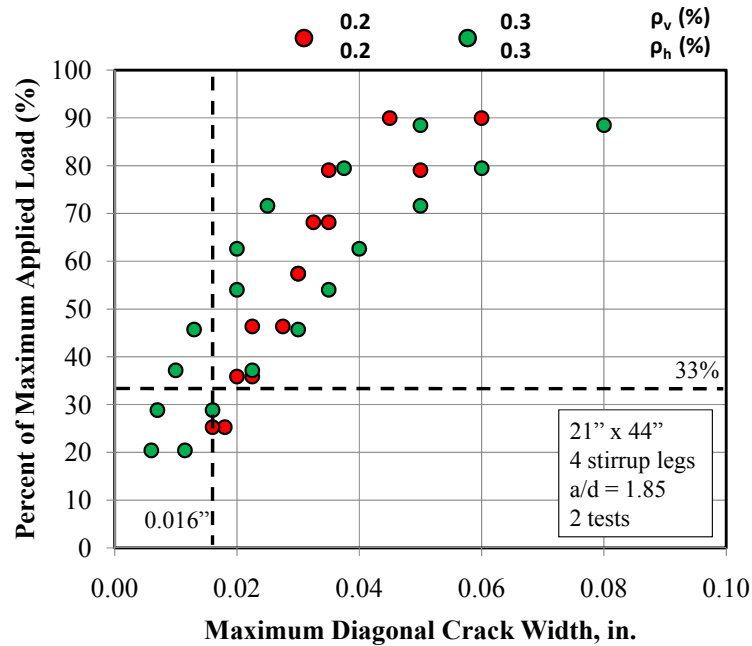


Figure 4.29: Max. crack widths for 36"x48" specimens with 0.2% and 0.3% reinf.



**Figure 4.30: Max. crack widths for 21"x44" specimens with 0.2% or 0.3% 2-legged reinf.**



**Figure 4.31: Max. crack widths for 21"x44" specimens with 0.2% or 0.3% 4-legged reinf.**



Due to the variable nature of crack width data, it is important to base overall conclusions on as much data as possible. The maximum crack width data for the specimens in the current task (Table 4.6) that were tested at an  $a/d$  ratio of 1.85 was plotted in Figure 4.32 with the exception of III-1.85-01. The data from this test were excluded because the load transfer mechanism was not consistent with a deep beam as noted previously. In short, the data from 16 tests were included in Figure 4.32. Among the tests were beams of several different sizes, with 2- and 4-legged stirrups, and with several different distributions of web reinforcement.

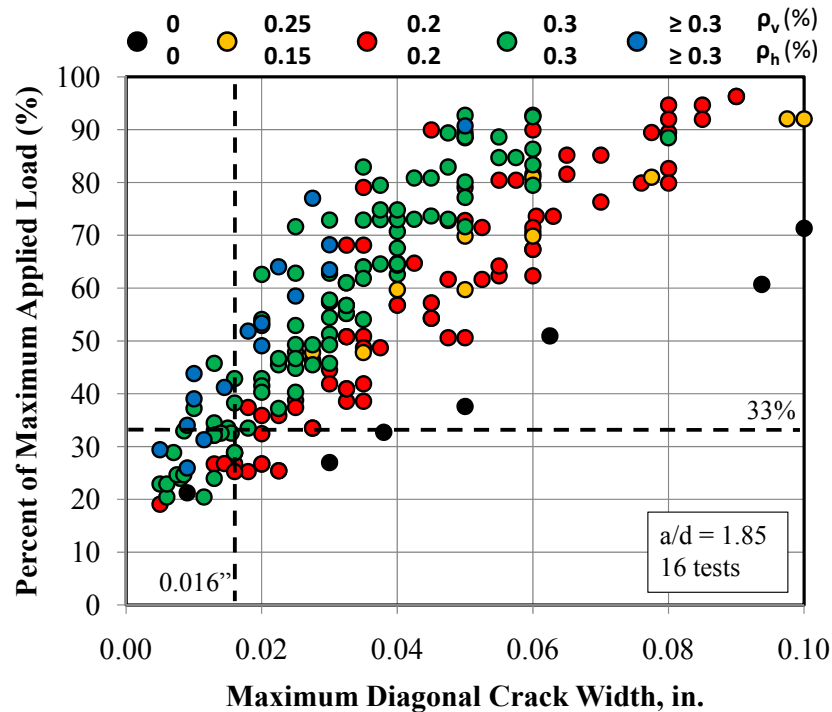


**Figure 4.32: Maximum diagonal crack width data for all comparable specimens at  $a/d$  of 1.85**

In Figure 4.32, it is evident that scatter existed with the diagonal crack width data. However, in general, the trend between maximum diagonal crack width and the web reinforcement ratio is clear. At first diagonal cracking, most of the specimens with 0.2% web reinforcement in each orthogonal direction reached or exceeded the crack width

benchmark of 0.016 in. 0.2% reinforcement was often not sufficient to restrict the width of diagonal cracks to this liberal limit even at first cracking. At the estimated service load level, the maximum crack widths of all of the specimens with 0.2% reinforcement far exceeded 0.016 in. Based on these data, it was determined that 0.2% web reinforcement was insufficient to ensure adequate serviceability performance of deep beams. The specimens with 0.3% in each orthogonal direction, on the other hand, had crack widths narrower than 0.016 in. at first diagonal cracking. In almost all cases, the maximum crack width was less than or equal to 0.016 in. at the estimated service load of 33% of ultimate. The performance of the specimens with 0.3% web reinforcement was considered acceptable, especially if this amount of reinforcement is treated as the minimum required for deep beams. In cases where the structure is exposed to aggressive climates or where crack widths need to be restricted further, it may be necessary to provide additional reinforcement (i.e. 0.016 in. is not endorsed as a tolerable crack width herein). The data in Figure 4.32 show that providing web reinforcement in excess of 0.3% in each direction did a better job than 0.3% at restraining diagonal crack widths, but the benefit may be greater at higher levels of applied load. Near first cracking and at the expected service load, there was only a moderate reduction in the maximum diagonal crack widths. The two specimens representing the blue data points in Figure 4.32 had the following amount of web reinforcement:

- II-03-CCC2021:  $\rho_v = 0.31\%$   $\rho_h = 0.45\%$
- M-09-4-CCC2436:  $\rho_v = 0.86\%$   $\rho_h = 0.27\%$

Even with a large increase in the amount of vertical reinforcement in test M-09-4-CCC2436, the maximum diagonal crack widths were only slightly narrower than those in specimens with 0.3% reinforcement. This observation suggested that near service loads, there are diminishing returns regarding the effect of web reinforcement on maximum diagonal crack widths.

In addition to an  $a/d$  ratio of 1.85, a few tests were conducted at  $a/d$  ratios of 1.2 and 2.5. Crack width data for the three specimens tested at an  $a/d$  ratio of 1.2 and the

three specimens tested at an  $a/d$  ratio of 2.5 are presented in Figure 4.33 and Figure 4.34, respectively.

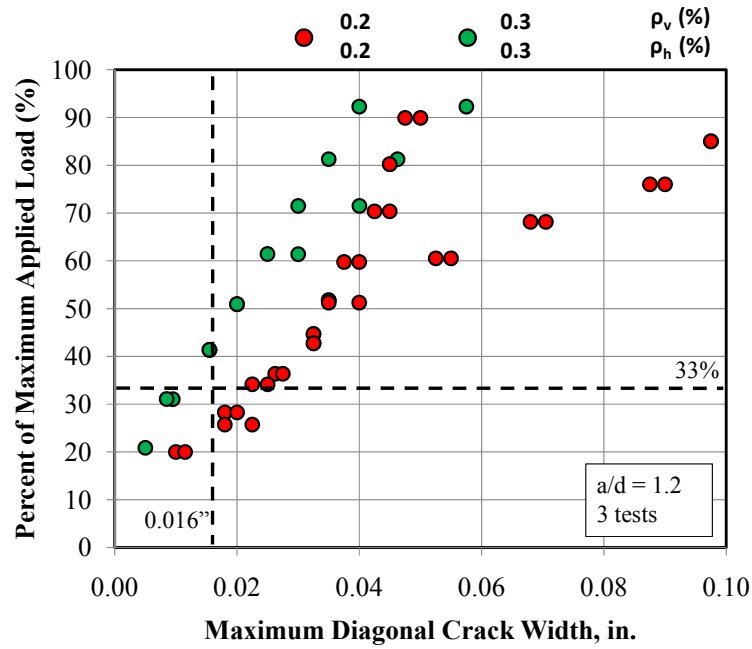


**Figure 4.33: Maximum diagonal crack widths of specimens tested at an  $a/d$  ratio of 1.2**

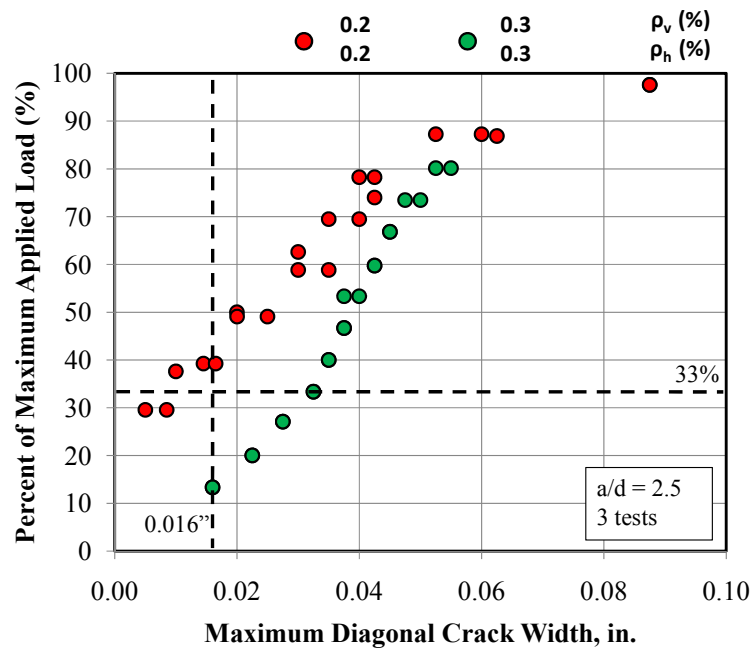


**Figure 4.34: Maximum diagonal crack widths of specimens tested at an  $a/d$  ratio of 2.5**

The results presented in Figure 4.33 ( $a/d = 1.2$ ) are consistent with the crack widths of beams tested at an  $a/d$  ratio of 1.85 (Figure 4.32). Web reinforcement in both directions corresponding to 0.3% better restrained the width of diagonal cracks than 0.2% in each direction. At the expected service load, the maximum width of the diagonal cracks in the specimen with 0.3% reinforcement is well below the benchmark of 0.016 in. On the other hand, the maximum crack width of the specimens with 0.2% reinforcement is approximately 0.02 in., exceeding the benchmark crack width slightly.

The results presented in Figure 4.34 are not in agreement with the data from the tests conducted at an  $a/d$  ratio less than 2. The reason for this discrepancy was that for the beams in Figure 4.34 with 0.2% reinforcement, the failure mode was consistent with a sectional shear or diagonal tension failure. The specimen with 0.3% reinforcement in each direction (III-2.5-03) failed in a manner consistent with a combination of deep beam and sectional shear behavior. The extra web reinforcement in specimen III-2.5-03 provided additional redistribution capacity that increased the strength of the beam. Specimen III-2.5-03 failed at a load approximately 60% higher than specimen II-2.5-02. While additional stirrups increased the sectional shear strength ( $a/d = 2.5$ ), the results in Figure 4.34 indicate a negative effect of supplementing sectional shear strength with additional stirrups ( $V_s$ ) on diagonal crack widths. At a given percentage of maximum applied load, diagonal crack widths will increase as the contribution of the stirrups to sectional shear strength increases ( $V_s/V_c$  ratio increases). It may be necessary to limit the ratio of  $V_s$  to  $V_c$  in sectional shear for the purpose of limiting diagonal crack widths.

The required spacing of minimum web reinforcement was not explicitly evaluated in the experimental program. However, a couple of valid comparisons were possible. Two pairs of tests were conducted at an  $a/d$  ratio of 1.85. In both cases, the difference between each test in the pair was the spacing of the stirrups ( $s_v$ ). The spacing of the horizontal reinforcement was the same in all four tests (10 in.). The crack width data for the two specimens with 0.2% reinforcement (III-1.85-02 and III-1.85-02b) are plotted in Figure 4.35. The crack width data for the two specimens with 0.3% reinforcement (III-1.85-03 and III-1.85-03b) are plotted in Figure 4.36.

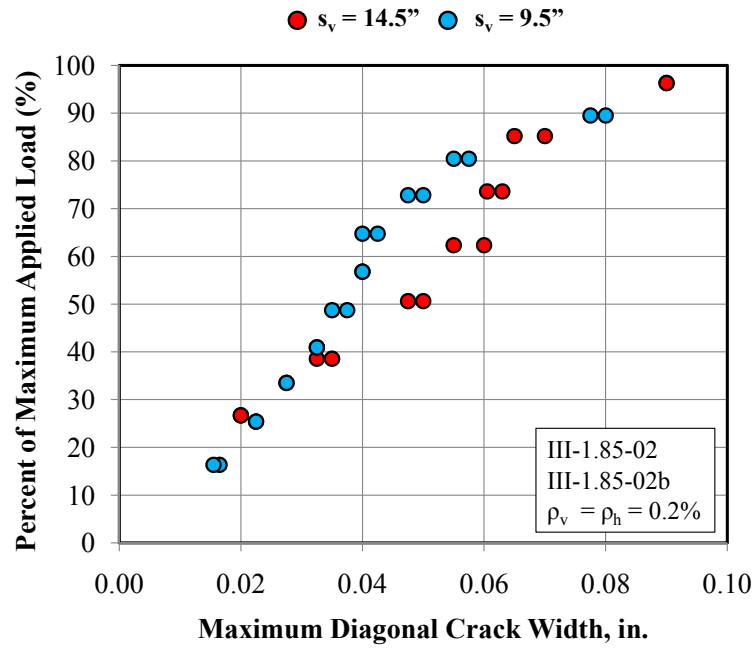


**Figure 4.35: Effect of stirrup spacing on crack width for specimens with 0.2% reinf.**

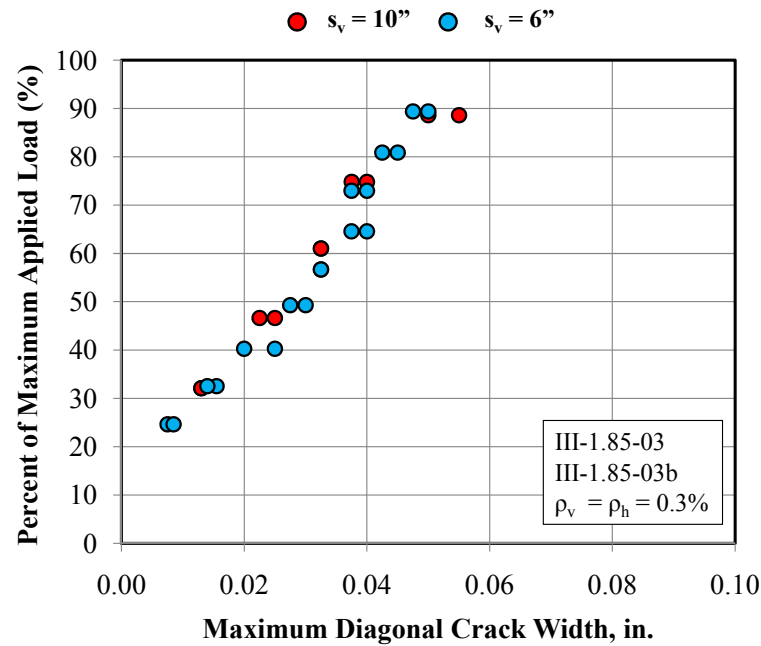


**Figure 4.36: Effect of stirrup spacing on crack width for specimens with 0.3% reinf.**

In Figure 4.35, the crack width data indicate that larger stirrup spacing may result in wider cracks. For specimen III-1.85-02, the stirrups were spaced at 14.5 in. or

approximately  $d/2.5$ . This spacing is larger than that required by many of the minimum reinforcement provisions reviewed in Section 4.3.1. In general, spacing of minimum reinforcement is limited to  $d/4$ ,  $d/5$ , or 12 in. While the effect shown in Figure 4.35 is minimal, it does show the benefits of restricting the spacing of crack control reinforcement. In Figure 4.36, the crack width data for the specimens with 0.3% reinforcement indicate that stirrup spacing smaller than 10 in. or approximately  $d/4$  did not further reduce maximum diagonal crack widths. Thus, there is no apparent benefit from recommending a spacing limit less than  $d/4$ . Based on the results in Figure 4.35 and Figure 4.36 and to be consistent with previous recommendations for the spacing of minimum web reinforcement, it is proposed that the spacing be limited to the smaller of  $d/4$  or 12 in. This limit is the same that is recommended in Article 5.13.2.3 of AASHTO LRFD (2008).

#### **4.3.4 Design Recommendations**

Based on the strength and serviceability results discussed in Section 4.3.1 through 4.3.3, minimum reinforcement of 0.3% in each orthogonal direction is recommended for use in deep beams. This amount of reinforcement ensured satisfactory strength performance. Also, 0.3% reinforcement adequately restrained the width of diagonal cracks at first cracking and up to an approximate service load level of 33% of ultimate. In aggressive climates or where the maximum width of diagonal cracks needs to be restricted further, additional web reinforcement or post-tensioning should be provided. Reinforcement of 0.2% ensured satisfactory strength performance but did not adequately restrain the width of diagonal cracks. In many specimens with 0.2% reinforcement, the maximum crack width exceeded the liberal benchmark of 0.016 in. at first diagonal cracking. It is possible that for applications in which the restraint of diagonal crack widths is not needed, then minimum web reinforcement of 0.2% in each direction would be satisfactory.

In regards to the minimum reinforcement provisions in current design specifications, 0.3% in each orthogonal direction is similar to that required in AASHTO LRFD (2008) and CHBDC (2006). The only difference is that in AASHTO LRFD and in

CHBDC the total horizontal reinforcement is based on the gross concrete section whereas the reinforcement recommended herein is based on the effective strut area. The difference in required horizontal reinforcement from these two definitions is shown in Figure 4.37. The effective strut area is calculated as the total depth minus twice the distance from the extreme fibers to the centroids of the compression and tension reinforcement. The proposed clarification reduces the total quantity of horizontal web reinforcement required by AASHTO LRFD (2008) by about 25% for this particular example  $((2.6-1.9)/2.6 \cdot 100 \approx 25\%)$ .

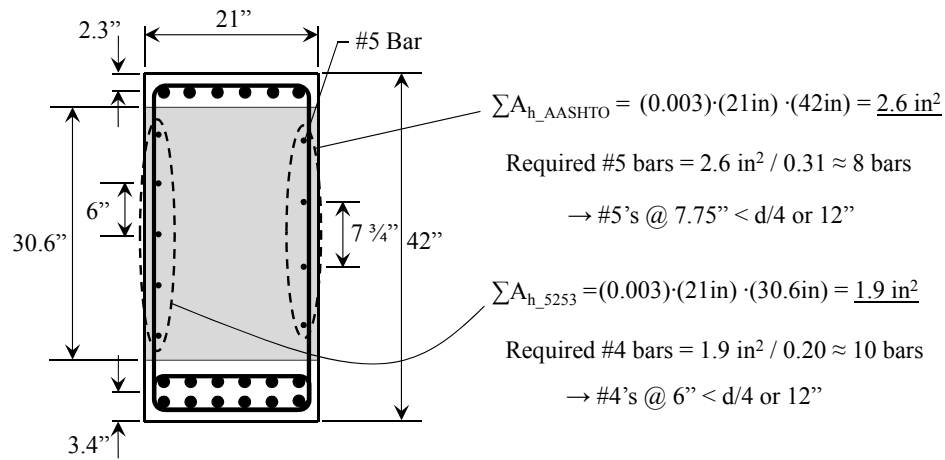


**Figure 4.37: Comparison of AASHTO LRFD (2008) and proposed minimum reinforcement**

It was observed that limiting the spacing of the web reinforcement was important for reaching the full design strength of the strut and for distributing the diagonal cracks. Currently, in AASHTO LRFD (2008), the spacing of crack control reinforcement is restricted to 12 in. It is proposed that this limit be supplemented with a restriction of d/4. Thus, the spacing of the web reinforcement in each direction shall not exceed d/4 or 12 in. This limit is consistent with the spacing limits of the other minimum reinforcement provisions reviewed in Section 4.3.1.

The proposed minimum reinforcement in the vertical and horizontal direction to be adopted by AASHTO LRFD in the STM provisions is as follows, including Figure 4.38 in the commentary:

$$\frac{A_v}{b_w s_v} \geq 0.003 \quad (4.7)$$

$$\frac{A_h}{b_w s_h} \geq 0.003 \quad (4.8)$$

where,

$A_v, A_h$  = total area of vertical and horizontal crack control reinforcement within spacing  $s_v$  and  $s_h$ , respectively (in.<sup>2</sup>)

$b_w$  = width of member web (in.)

$s_v, s_h$  = spacing of vertical and horizontal crack control reinforcement, respectively (in.), shall not exceed  $d/4$  or 12 in.

To calculate the required web reinforcement, it may be most convenient to select a bar size and calculate the required spacing according to Equations 4.7 and 4.8. That spacing should satisfy the  $d/4$  or 12 in. criteria. The required web reinforcement should be distributed evenly near the side faces of the effective strut area. Where necessary, interior layers of crack control reinforcement may be used.



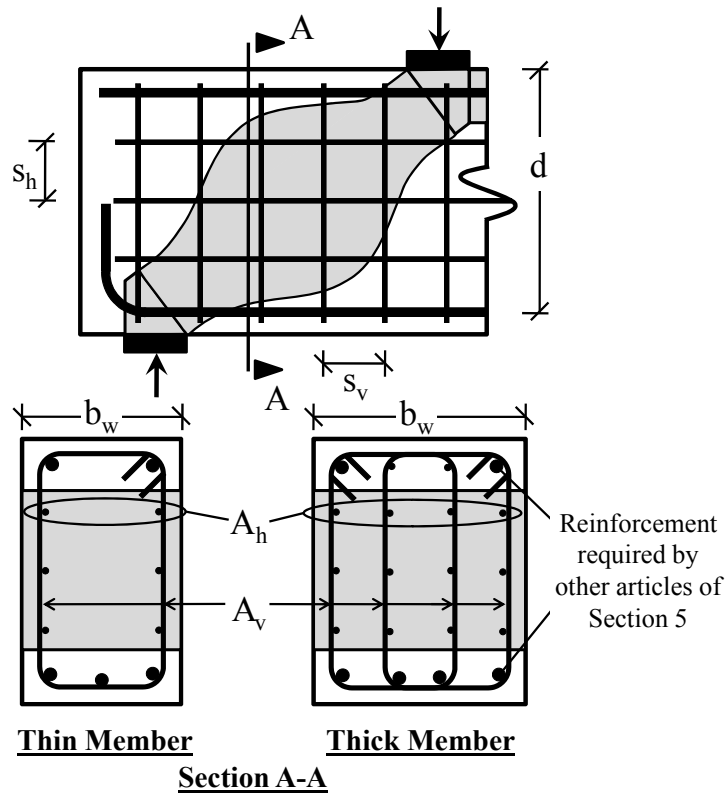


**Figure 4.38: Proposed minimum web reinforcement requirements in AASHTO LRFD**

For TxDOT reinforced concrete bent caps, the quantity of web reinforcement is seldom a pay item. The cost of the bent cap is often based on the total cubic yards of the member. If not, it is likely that the cost of web reinforcement is a very small percentage of the total cost of the bent cap. As such, from a cost perspective, providing additional web reinforcement may be advantageous to the owner.

#### 4.3.5 Summary

In Section 4.3, the effect of web reinforcement on the strength and serviceability performance of deep beams was addressed. The results indicated that minimum orthogonal reinforcement pertaining to 0.3% of the strut area should be provided in deep beams ( $a/d < 2$ ). This conclusion was based on the test results of beams of various size (21"x23", 21"x42", 21"x44", 36"x48", and 21"x75"), of beams tested at  $a/d$  ratios of 1.2 and 1.85, and of beams with either 2- or 4-legged stirrups.

In general, the failure mode and overall performance of the deep beam specimens was consistent with a single-panel strut-and-tie model in which the load was transferred through the member via a direct, diagonal strut. As such, the purpose of the reinforcement in terms of strength was to resist the transverse tensile stress in the bottle-shaped strut. For this reason, companion specimens with different amounts of reinforcement in each direction had similar shear strength provided that at least 0.2% reinforcement was provided. However, a difference in performance was observed in regards to the width of diagonal cracks. The results indicated that the width of the cracks were proportional to the amount of web reinforcement with diminishing returns near service load levels as the reinforcement greatly exceeded 0.3% in each direction. Specifically, the data suggested that 0.2% reinforcement in each orthogonal direction was insufficient to restrain the width of the cracks to a liberal limit of 0.016 in. at service loads and often at first cracking. Specimens with 0.3% reinforcement in each direction performed significantly better with crack widths less than 0.016 in. at first cracking and at service loads.

For the few members tested at an  $a/d$  ratio of 2.5, the amount of web reinforcement did affect the shear strength. The specimen with 0.3% reinforcement in each direction failed at a load 60% higher than the companion specimen with 0.2% in each direction. The failure mode of test III-2.5-02 was consistent with a sectional shear failure with minimal parallel diagonal cracking. The failure mode of test III-2.5-03 was consistent with the combination of a deep beam and sectional shear failure due to presence of the additional reinforcement. While additional stirrups increase shear strength, it may be necessary to limit the ratio of  $V_s$  to  $V_c$  in sectional shear for the purpose of limiting diagonal crack widths.

#### **4.4 MEMBER DEPTH**

The purpose of this task was to evaluate the effect of member depth on the strength and serviceability performance of reinforced concrete deep beams. A brief review of the literature associated with the effect of depth on deep beams is provided.

After that, the strength and serviceability results obtained through the experimental program are presented.

#### **4.4.1 Background**

Numerous research studies have been conducted on the effect of depth on the shear strength of reinforced concrete beams. Most of the work has focused on slender beams in which the  $a/d$  ratio is greater than 2. However, several studies conducted within the last fifteen years have addressed the effect of depth on the behavior of deep beams as well ( $a/d < 2$ ). In both cases, most of these investigations have concluded that a size effect exists. Here, size effect refers to a reduction in ultimate shear strength, typically measured by a normalized shear stress at failure ( $V / f_c b_w d$  or  $V / \sqrt{f_c'} b_w d$ ), as the depth of the member increases. There are numerous theories in the literature that attempt to explain size effect, but there is little consensus. Three of the most common size effect theories for shear are based upon material strength variations, diagonal crack widths, and fracture mechanics.

The oldest size effect theory, that of statistical strength variations, was based on the work of Weibull in 1939. Applied to reinforced concrete, the theory justifies the reduction in strength that exists with an increase in member size to the randomness of material strength. A reinforced concrete structure is compared to a series of chain links in which the failure of one link causes the entire chain to fail. As the depth of a beam gets larger, the number of links increases and the probability of a lower stress at failure increases due to the variability in the material strength of concrete.

Size effect has also been explained in terms of the width of diagonal cracks. According to modified compression field theory, as the depth of a beam increases, the spacing of diagonal cracks increase and thus, the width of diagonal cracks increase (Collins and Kuchma, 1999 and Macgregor and Wight, 2005). The increase in crack width reduces the ability to transmit shear across the diagonal crack by aggregate interlock. Thus, size effect is explained by the reduced effectiveness of the interface shear transfer mechanism.

Other researchers explain size effect for shear in reinforced concrete beams with fracture mechanics (Reinhardt, 1981 and Bazant and Kazemi, 1991). It is theorized that there are differences in the rate at which stored energy is released during crack propagation for beams of different sizes. Specifically, cracks propagate faster in larger beams than in smaller beams. Several research studies have shown that the cracking pattern of a larger beam is more extensive than an otherwise identical smaller beam at the same shear stress (Walraven and Lehwalter, 1994 and Tan and Lu, 1999).

In general, these theories were originally derived for slender beams ( $a/d > 2$ ). While they can be applied to the study of deep beams ( $a/d < 2$ ) to some degree, another approach may be more appropriate. After strength results from the literature and from the experimental program are presented, it will be apparent that the effect of depth on the strength of deep beams can be better understood in terms of a strut-and-tie model analysis.

#### **4.4.2 Strength Results**

##### ***4.4.2.1 Strength Results from the Literature***

Numerous experimental studies have been conducted on the size effect of deep beam shear. Four studies will be reviewed in this section in detail. In 1994, thirteen (13) reinforced concrete deep beams were tested at an  $a/d$  ratio of 1.0 by Walraven and Lehwalter. All of the beams were approximately 9.8-inches wide. The effective depth ranged from 6.3 in. to 36.6 in. The length ( $l_l$ ) of the load plate and support plate varied with the effective depth ( $d$ ) such that the ratio between the them ( $l_l / d$ ) equaled 0.25. Each beam was simply supported and was loaded with a single concentrated load at midspan. The test specimens were divided into three groups. The first group did not have any web reinforcement. The second and third groups had vertical reinforcement corresponding to a  $\rho_v$  of approximately 0.0015 and 0.003, respectively. The experimental shear strength normalized by the shear area and the compressive strength of concrete are plotted versus the effective depth in Figure 4.39. From the test results, a size effect is

apparent. As the depth of the member increases, the normalized shear stress at failure decreases. The loss in shear strength was attributed to the difference in the rate of crack propagation for the beams of different depths. Specifically, the ability to transmit tensile stress across diagonal cracks was reduced for the larger beams due to larger crack widths when compared to smaller beams at similar stress levels.

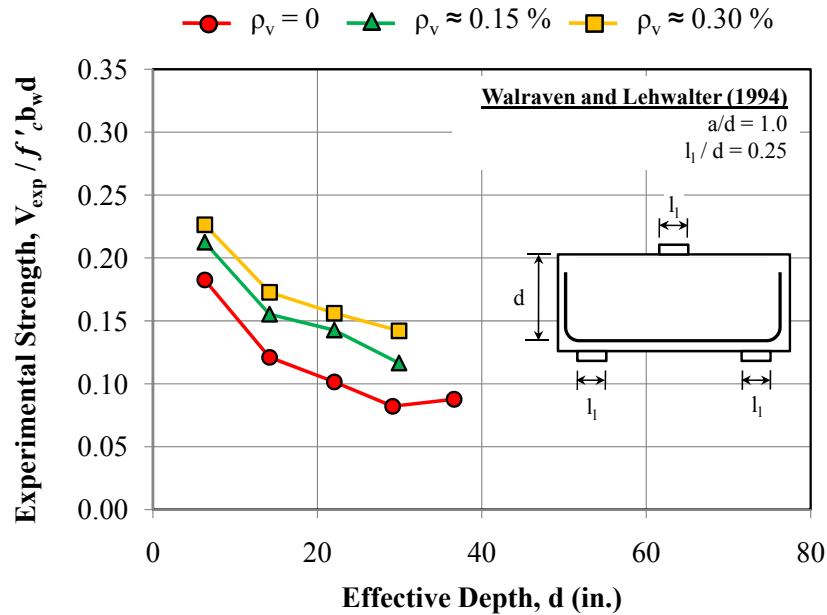


**Figure 4.39: Size effect strength results from Walraven and Lehwalter (1994)**

In 1999, twelve reinforced concrete deep beams were tested by Tan and Lu. Size effect in deep beam shear was studied at three different  $a/d$  ratios: 0.56, 0.84, and 1.13. All of the beams had a width of 5.8 in. The effective depths ranged from 17.5 in. to 61.4 in. The length of the bearing plates at the load and the support were kept constant at 9.8 in. for all of the specimens (Tan and Cheng, 2006). Each beam was simply supported and was loaded with two point loads at the third points. The test specimens were divided into three groups by the  $a/d$  ratio. The smallest beam in each group ( $d=17.5$  in.) did not have any web reinforcement. The other three beams in each group had equal reinforcement in the horizontal and vertical directions satisfying a reinforcement ratio of 0.0012. The test results are plotted in Figure 4.40. These test results agree well with

those in Figure 4.39. The normalized shear stress at failure decreases with the increasing depth of the member. The authors attributed the decline in strength to the difference in the rate of energy release due to crack propagation for the beams of different sizes. Specifically, they noted that the larger beams had more developed cracks than the smaller beams at a given shear stress. In addition, the authors noted that size effect was greatest when the effective depth increased from 17.5 in. to 34.8 in. At depths larger than 34.8 in., the reduction in shear stress at failure was not as high.

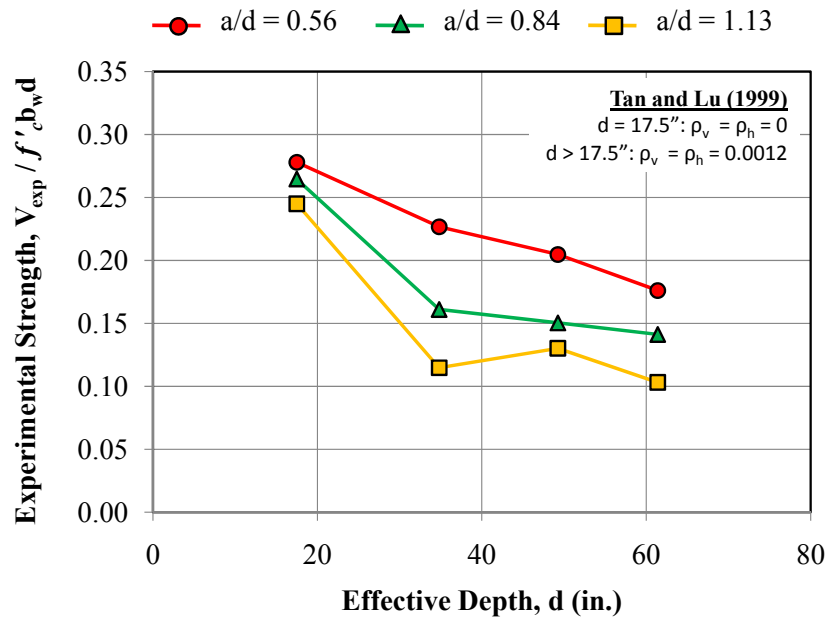


**Figure 4.40: Size effect strength results from Tan and Lu (1999)**

In 2001, nine reinforced concrete deep beams were tested at an a/d ratio of 1.0 by Matsuo et al. All of the beams were 5.9 in. in width. The effective depths ranged from 7.9 in. to 23.6 in. Similar to the study by Walraven and Lehwalter, the length of the load and support plates were varied with the effective depth of the beam such that the ratio between the two was 0.25 for all of the specimens. Also, the beams were simply-supported and were tested with a single concentrated load at midspan. Three beams did not have any web reinforcement; three beams had vertical reinforcement corresponding to a  $\rho_v$  of 0.0042; three beams had vertical reinforcement corresponding to a  $\rho_v$  of 0.0084.

No horizontal web reinforcement was present in the test specimens. The test results are plotted in Figure 4.41. All of the beams failed according to a shear-compression mode with a considerable amount of crushing around the loading point. For the specimens without web reinforcement, the normalized shear stress at failure decreased with increasing depth, indicating size effect. While the shear strength of the specimens with web reinforcement generally decreased with increasing depth as well, the reduction was not as consistent. It is possible that web reinforcement acted to alleviate size effect to some degree. According to the authors, the size effect was attributed to a reduction in “the ratio of the region of compression failure to total region of the specimen” (Matsuo et al., 2001).

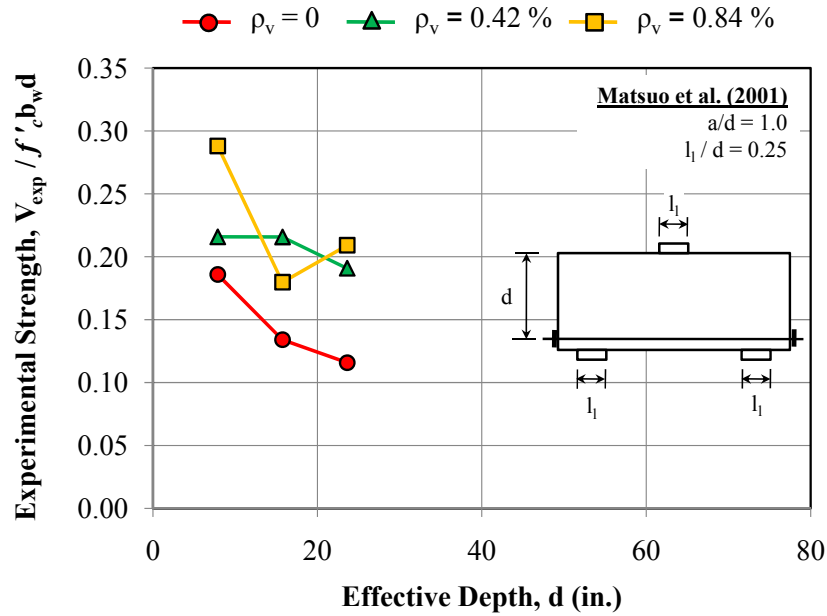


**Figure 4.41: Size effect strength results from Matsuo et al. (2001)**

In 2007, twelve reinforced concrete deep beams were tested at an  $a/d$  ratio of 1.1 by Zhang and Tan. The test specimens were divided into three groups of four. Within each group, the effective depth of the beam varied from 12.3 in. to 35.6 in. In the first group, the beam width was constant at 3.2 in., and there was no web reinforcement. In the second group, there was also no web reinforcement; but the beam width varied from 3.2 in. to 9.8 in. In the third group, the beam width varied as in group 2; and web

reinforcement corresponding to a  $\rho_v$  of approximately 0.004 was provided ( $\rho_h = 0$ ). For all of the specimens, the length ( $l_l$ ) of the load and support plates varied with the effective depth ( $d$ ) such that the ratio between them ( $l_l / d$ ) was approximately 0.17. The beams in this study were loaded with two concentrated loads at the third points. The test results are plotted in Figure 4.42. Unlike the data plotted in Figure 4.39 through Figure 4.41, no size effect is apparent for the tests conducted by Zhang and Tan. The authors attributed the lack of size effect to the appropriate proportioning of the length of the load and support plates to the depth of the beams. “Thus, [controlling] strut geometry plays a dominant role in mitigating the size effect in ultimate shear strength of deep beams” (Zhang and Tan, 2007). From a strut-and-tie model perspective, where the strength of a deep beam is often governed by dimensions of the struts and nodes, these results seem reasonable.

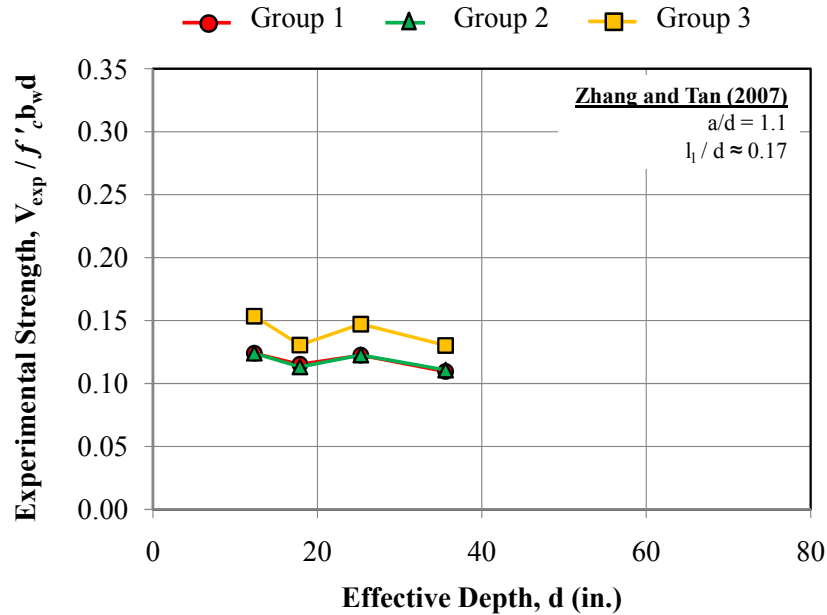


**Figure 4.42: Size effect strength results from Zhang and Tan (2007)**

The experimental results in Figure 4.42 were further explained with finite element models (FEM) by Zhang and Tan (2007). Two sets of analyses were conducted. In the first set, each of the twelve test specimens were analyzed with the same loading conditions as the actual tests. The FEM results agreed well with the test results. In the



second set, the lengths of the support and load plates were not varied with the depth of the specimens as they were in the actual tests. Instead, a constant length of 2.1 in. was used for the length of all bearing plates in all of the beams. This length equaled the length of the plates for the smallest test specimen ( $d = 12.3$  in.). The results of the analyses are illustrated in Figure 4.43 and Figure 4.44. When the bearing plates were varied with the depth of the member, no apparent size effect existed. Whereas, when the bearing plate sizes were kept constant as the depth of the member increased, size effect was present. These results indicate that the geometry of the strut where it intersects the node (node-to-strut interface) dominates the ultimate shear strength of deep beams, and controlling this geometry can effectively mitigate size effect.

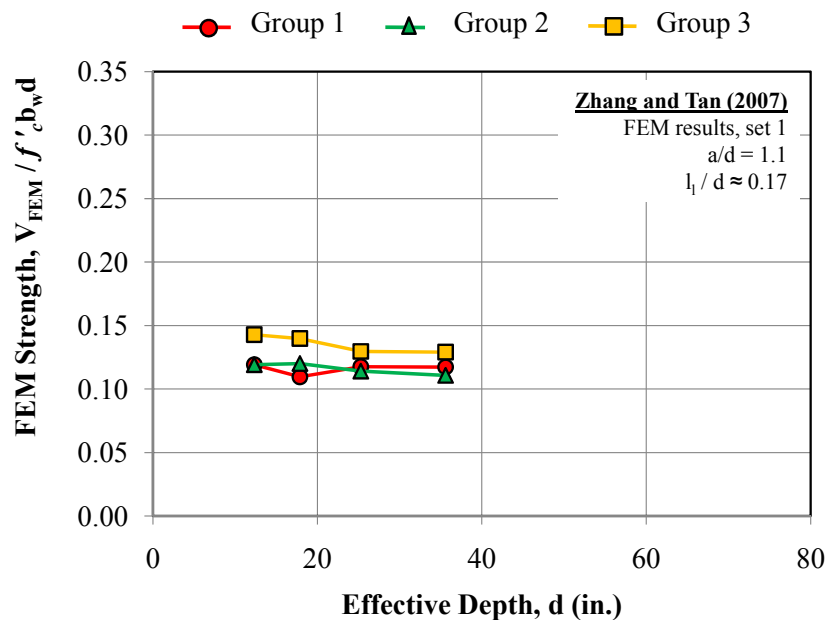


**Figure 4.43: FEM results in which bearing plate sizes increased with increasing member depth (Zhang and Tan, 2007)**

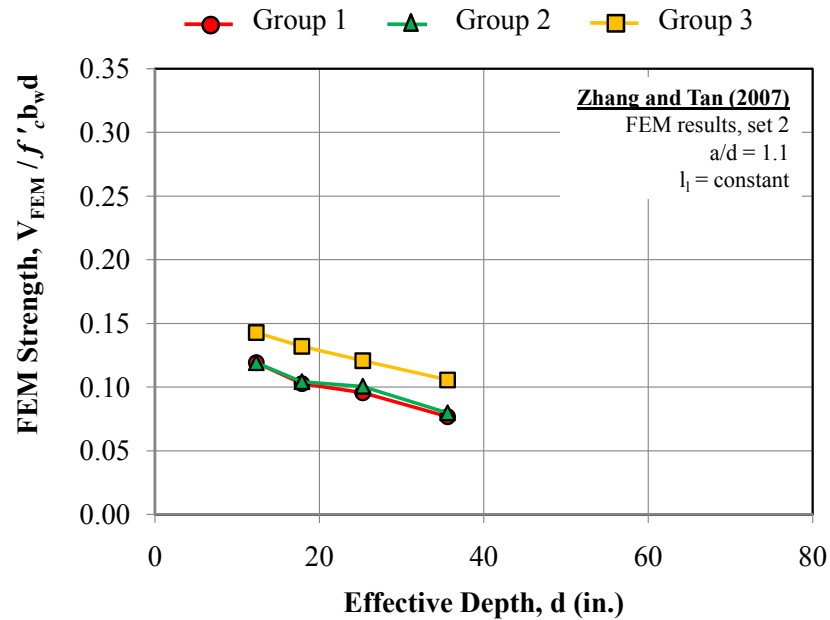


**Figure 4.44: FEM results in which bearing plate sizes were constant with increasing member depth (Zhang and Tan, 2007)**

There is some disagreement between the findings of Zhang and Tan (2007) and the test results of Walraven and Lehwalter (1994) and Matsuo et al. (2001). By proportioning the length of the load and support plates according to the depth of the beam, Zhang and Tan were able to mitigate size effect. However, when both Walraven and Lehwalter and Matsuo et al. proportioned their bearing plates in the same manner, size effect was not mitigated. Zhang and Tan attributed the discrepancy between their findings and those of Walraven and Lehwalter to the “*uneven distribution of shear reinforcement*” for the different beam sizes of the latter. The spacing of the transverse reinforcement in specimens of Walraven and Lehwalter was approximately  $d/4$  for each beam regardless of the size. However, the same numerical spacing of approximately 5.9 in. was used for all of the beams of Zhang and Tan. While the distribution of reinforcement for the larger beams may have contributed to the discrepancy between the results of these two studies, it was not solely responsible. In the study by Matsuo et al., the bearing plates were varied according to the depth of the beam and the distribution of

reinforcement was consistent between each of the beams. Size effect was still apparent in these tests, albeit not as pronounced.

It is plausible that the other contributing factor to the discrepancy between the aforementioned studies is the loading configuration. Walraven and Lehwalter and Matsuo et al. tested their specimens with a single concentrated load at midspan. They proportioned the length of the load and the support plates according to the depth of the beam. However, since a single load is applied at midspan, the bearing stresses at the load are twice as high as those at the supports. Conversely, Zhang and Tan tested their specimens with two concentrated loads applied at the third points. Due to this arrangement, the bearing stresses at the load and the support were equivalent. It seems likely that the uneven proportioning of the length of the load and support plates in the tests by Walraven and Lehwalter and Matsuo et al. contributed to the difference in results with those of Zhang and Tan.

From the aforementioned studies, it was shown that a reduction in the normalized shear stress at failure ( $V/f_c'b_wd$ ) existed when the load and support plates were not properly proportioned according to the depth of the beam. When the length of the bearing plates were increased with the depth of the member, no size effect was apparent, especially for members with web reinforcement. From a strut-and-tie model perspective, these results make sense. In STM, the strength of a deep beam is often controlled by the stress on the nodal faces. If the size of the nodes is increased proportionally to the depth of the member, then a similar normalized stress at failure should be expected. (Node size increases,  $V_{ult}$  increases,  $d$  increases, and  $V/f_c'b_wd$  remains constant). Similarly, if the node size remains constant as the depth of the member increases, then a reduction in the normalized shear stress at failure should be expected. (Node size is similar,  $V_{ult}$  is similar,  $d$  increases, and  $V/f_c'b_wd$  decreases). Therefore, evaluating the effect of depth on the strength of deep beams should be done from a strut-and-tie model perspective.

#### ***4.4.2.2 Strength Results from the Experimental Program***

Before the tests in Series IV could be conducted, the size of the load and support plates of the different-sized specimens needed to be determined. Based on previous

research studies, it was apparent that the length of the bearing plates affected the strength of deep beams as the effective depth increased. Also, the tests in Project 5253 on triaxially-confined nodal regions (Series II) revealed that the length of the bearing plates were far more important to the strength of deep beams than the width of the bearing plates at CCC nodes (Tuchscherer, 2008). Thus, the bearing plate dimensions used for the tests in Series IV were carefully chosen.

The dimensions for the bearing plates and the supporting columns of several TxDOT bent caps were studied (Figure 4.45). In general, the length of the bearing plates appeared to be based on the size of the girder supported by the bent cap, rather than the depth of the bent cap itself. The length of the bearing plates used in the Greens Road bent caps and in standard Type IV bent caps were identical even though the overall depth of these members differed by nearly a factor of 2. The length of the pot bearings used in the I-345 bent cap in Dallas, however, were large due to the size of the continuous steel plate girders resting on top of it. Therefore, notwithstanding the I-345 bent cap, the length of bearing plates were generally independent of the depth of the member.

Bent Cap	Bent Cap Size (b x h)	Girder Type	Bearing Plate Size (l x b)	Supporting Column Size
Standard Interior Bent Cap	33" x 36"	A*	12" x 7"	circular $\phi = 30"$
		B*	14" x 7"	
		C*	16" x 7"	
	39" x 42"	IV*	22" x 7"	circular $\phi = 36"$
	42" x 42"	Tx28 – Tx54*	21" x 8"	
Greens Road	45" x 78"	Steel Box	22" x 22"	rect. 57" x 56"
I-345	72" x 120"	Steel Plate	42" x 36"	rect. 72" x 72"

\* Two pads per girder line

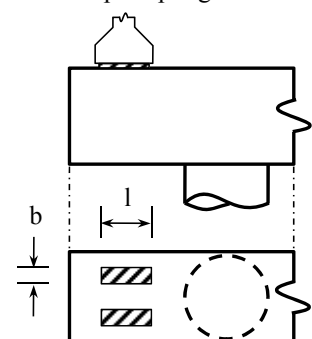


**Figure 4.45: Bearing plate dimensions in several TxDOT bent caps (TxDOT, 2008)**

For the Series IV specimens, the sizes of the bearing plates were not linked to the depth of the member. Instead, the bearing plate dimensions were selected to create similar size nodal regions (CCC and CCT) for each of the three sections tested within this task. The effect of increasing the member depth without increasing the size of the nodal

regions on the strength of deep beams was evaluated with this choice. More importantly, it appeared to be more consistent with typical TxDOT practice. The relative sizes of the nodal regions using a single-panel STM for the three sections tested within this task are depicted in Figure 4.46 and Figure 4.47.

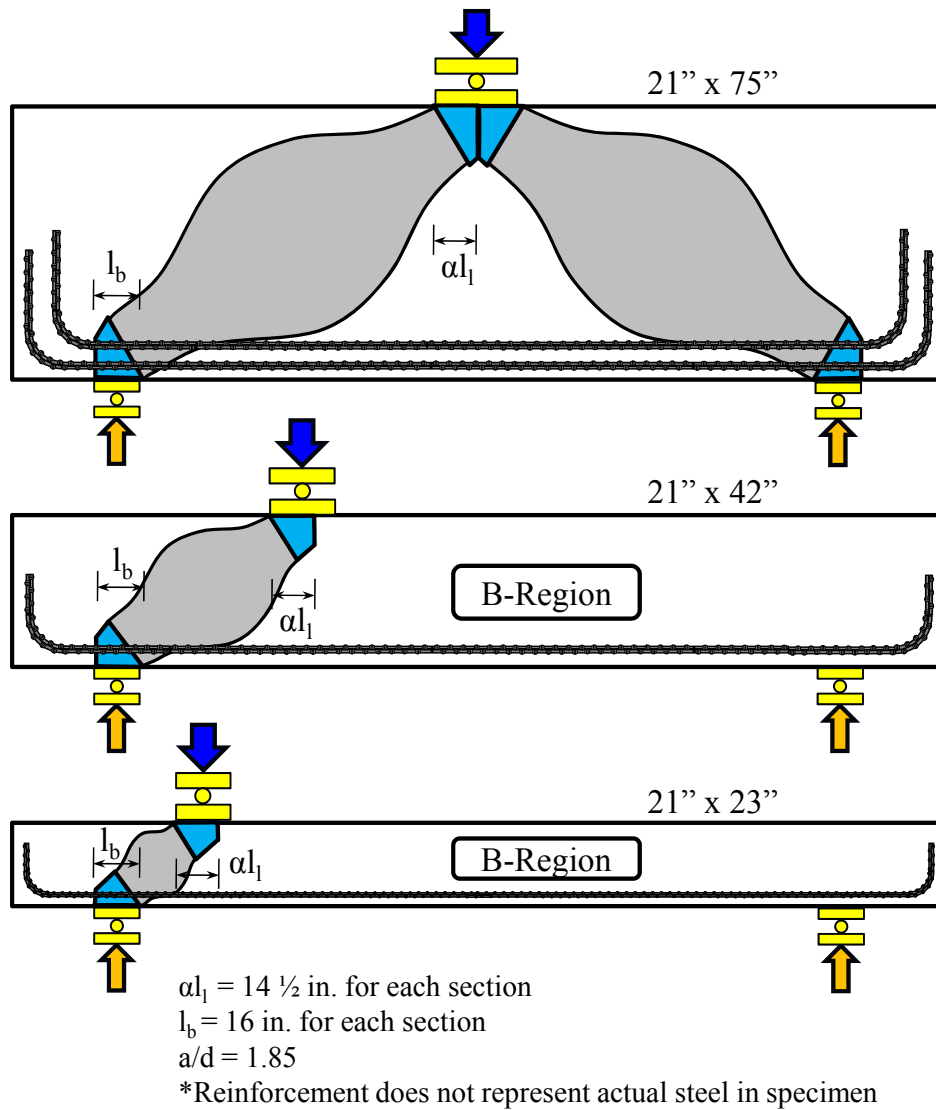


**Figure 4.46: Relative size of nodal regions for depth effect specimens**

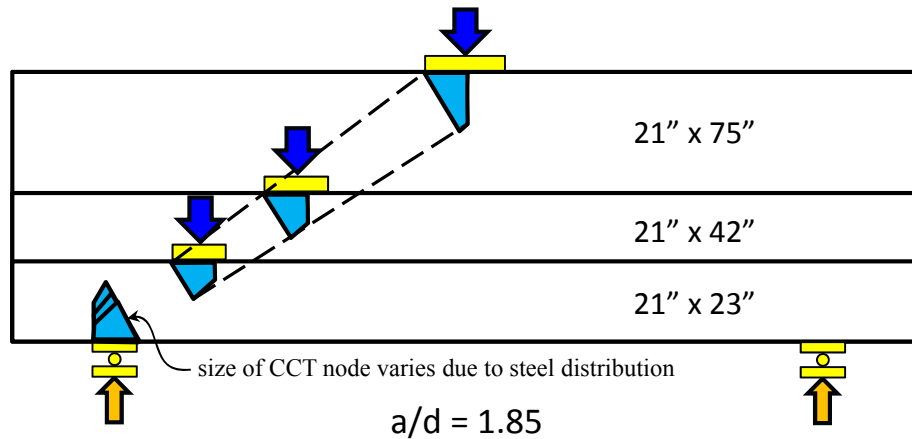


**Figure 4.47: Relative size of nodal regions in depth effect specimens (2)**

Since the test specimens were loaded with a single point load, the critical dimension at the load point was not the full length of the bearing plate, but rather the percentage of the bearing plate that was used in the strut-and-tie model for the test region. Therefore, this dimension,  $\alpha l_1$ , was kept constant for the three beam sizes (14.5 in.). For reference,  $\alpha$  equals 0.5 for the specimen loaded at midspan. The length of the support plates was constant for all of the beams (16 in.). As shown in Figure 4.47, the resulting sizes of the nodal regions were fairly equal even though the overall depth of the test specimen increased from 23 in. to 75 in. The size of the node-to-strut interface increased slightly as the depth increased due to the increase in the back face dimensions of both the CCC and CCT nodes. It was not possible to keep these dimensions constant for specimens of different sizes while maintaining the same longitudinal reinforcement ratio.

The test specimens from the experimental program used to evaluate the effect of depth on the strength of deep beams are listed in Table 4.7. The small (21"x23") and the large (21"x75") sections were tested in Series IV. The results of these tests were compared with similar tests conducted on the 21"x42" section in Series III. The experimental strength results and the relevant information about each specimen is listed in Table 4.7.

**Table 4.7: Strength results for depth effect specimens**

Beam I.D.	$b_w$ in.	$d$ in.	$f'_c$ psi	Nominal $\rho_v$ & $\rho_h$	Support Plate <sup>†</sup> in.	Load Plate <sup>†</sup> in.	$\alpha$	a/d ratio	$V_{test}$ kip	$\frac{V_{test}}{f'_c \cdot b_w d}$	$\frac{V_{test}}{\sqrt{f'_c} \cdot b_w d}$	$V_{crack} /$ $V_{test}$
III-1.85-02	21	38.6	4100	0.002	16x21	20x21	0.72	1.84	488	0.15	9.4	0.23
III-1.85-03b	21	38.6	3300	0.003	16x21	20x21	0.72	1.84	471	0.18	10.1	0.24
III-1.85-02b	21	38.6	3300	0.002	16x21	20x21	0.72	1.84	468	0.17	10.1	-
III-1.2-02	21	38.6	4100	0.002	16x21	20x21	0.82	1.20	846	0.25	16.3	0.20
III-1.2-03	21	38.6	4220	0.003	16x21	20x21	0.82	1.20	829	0.24	15.7	-
III-2.5-02	21	38.6	4630	0.002	16x21	20x21	0.62	2.49	298	0.08	5.4	0.35
III-2.5-03	21	38.6	5030	0.003	16x21	20x21	0.62	2.49	516	0.13	9.0	-
IV-2175-1.85-02	21	68.9	4930	0.002	16x21	29x21	0.50	1.85	763	0.11	7.5	0.28
IV-2175-1.85-03	21	68.9	4930	0.003	16x21	29x21	0.50	1.85	842	0.12	8.3	0.26
IV-2175-2.5-02	21	68.9	5010	0.002	16x21	24x21	0.33	2.50	510	0.07	5.0	0.28
IV-2175-1.2-02	21	68.9	5010	0.002	16x21	24x21	0.67	1.20	1223	0.17	11.9	0.21
IV-2123-1.85-03	21	19.5	4160	0.003	16x21	16.5x21	0.86	1.85	329	0.19	12.5	0.18
IV-2123-1.85-02	21	19.5	4220	0.002	16x21	16.5x21	0.86	1.85	347	0.20	13.0	0.19
IV-2123-2.5-02	21	19.5	4570	0.002	16x21	15.5x21	0.81	2.50	161	0.09	5.8	0.32
IV-2123-1.2-02	21	19.5	4630	0.002	16x21	18x21	0.91	1.20	592(f)	0.31	21.2	0.21

<sup>†</sup> Length along span ( $l$ )  $\times$  length along width ( $w$ )

(f) Maximum shear carried in specimen upon the occurrence of concrete crushing at the compression face.

The strength results for the specimens in Table 4.7 tested at an  $a/d$  ratio of 1.85 are plotted in Figure 4.48. The experimental shear strength was normalized by the shear area and the compressive strength of concrete. It is clear from the plot that with increasing depth, the normalized shear stress at failure decreases. These results are consistent with those of previous research studies (Walraven and Lewalter, 1994; Tan and Lu, 1999; and Matsuo et al., 2001). It is also clear from the plot that increasing the web reinforcement ratio in each direction from 0.2% to 0.3% did not affect the strength of the member. This finding confirms the results discussed in Section 4.3.2 regarding the effect of web reinforcement on the strength of deep beams.

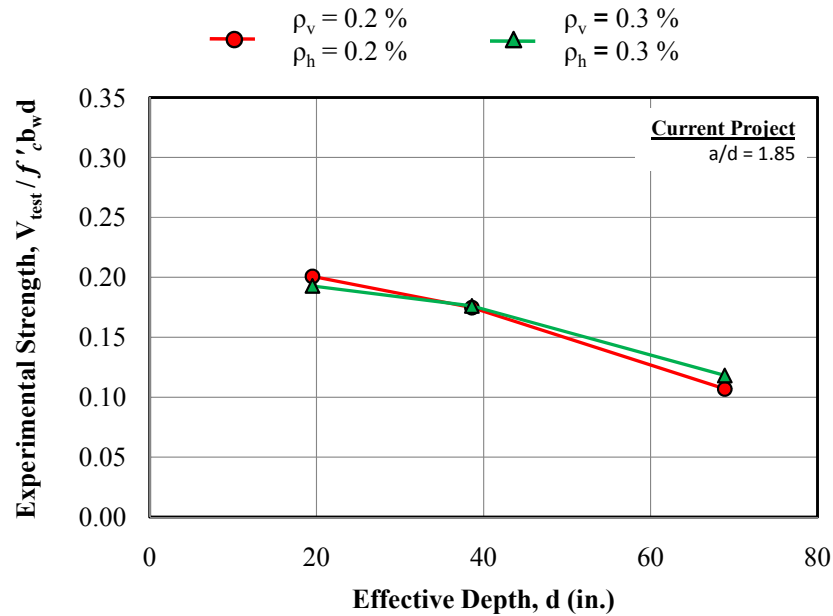


**Figure 4.48: Strength results of depth effect specimens at  $a/d$  of 1.85**

The test regions at failure for the three specimens representing the red line in Figure 4.48 ( $\rho_v = \rho_h = 0.002$ ) are illustrated in Figure 4.49. The mode of failure observed in these tests was generally the same. Numerous parallel cracks formed along the line between the applied load and the support indicating the presence of a direct strut transfer mechanism. At the ultimate applied load, local crushing near the load point and along the strut occurred. The black lines in Figure 4.49 represent the final failure crack of each



specimen, where the final failure crack is defined as the widest crack at failure. It is interesting to note that the final failure crack for the 75-in. specimen extended from the edge of the load plate at an angle of approximately 45 deg. instead of extending from the edge of both plates as in other tests. Similar cracking patterns at ultimate exist for the specimens with 0.3% reinforcement.

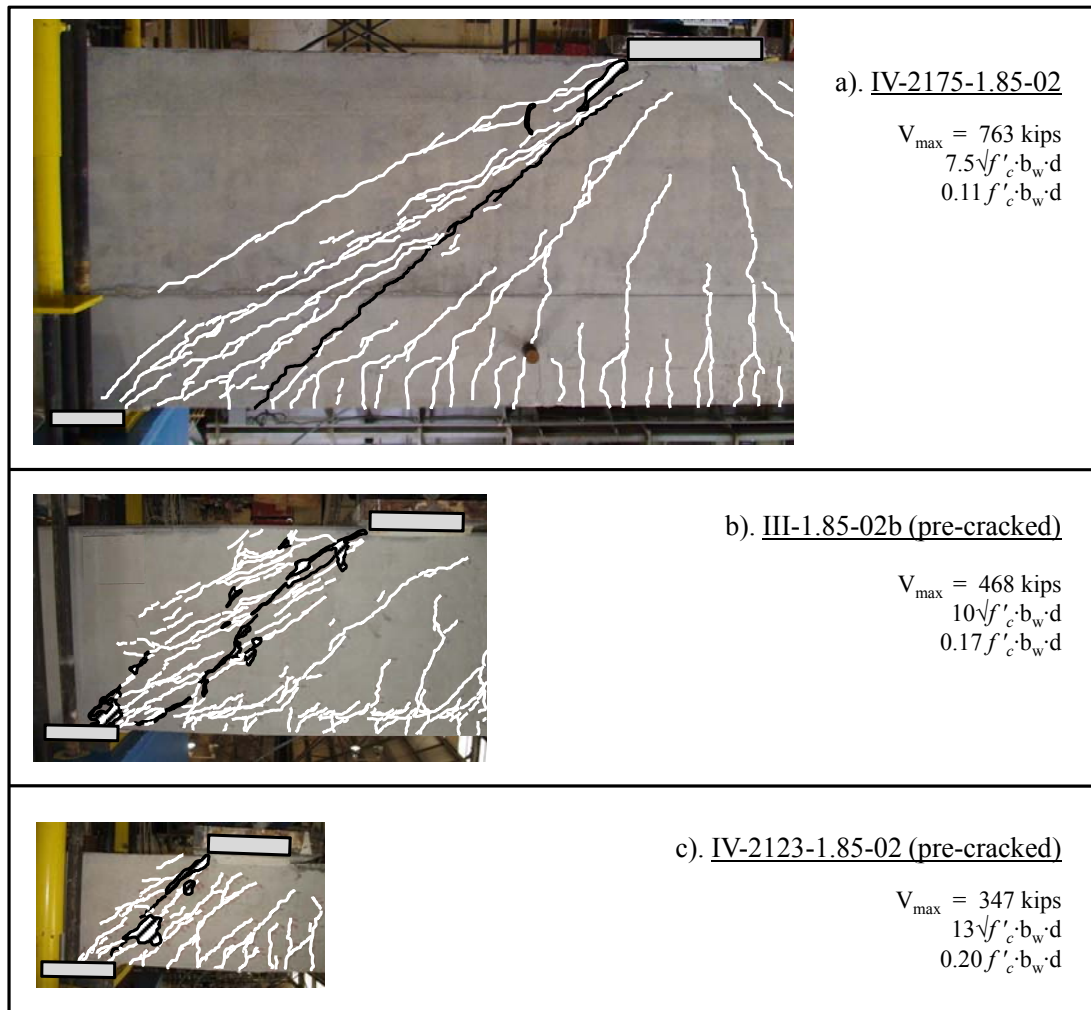


**Figure 4.49: Failure photographs for depth effect specimens with  $a/d$  of 1.85 and 0.2% reinforcement**

The strength results for the specimens tested at several  $a/d$  ratios (1.2, 1.85, and 2.5) and with 0.2% web reinforcement in each direction are plotted in Figure 4.50. The

normalized shear strength of the specimens decreased with increasing depth as before. It is important to note that the normalized shear strength of the 23-in. specimens at  $a/d$  ratios of 1.2 and 1.85 differ with that of the 75-in. specimens by a factor of 2. For the specimens tested at an  $a/d$  ratio of 2.5, the normalized shear strength only slightly decreased with increasing effective depth. The reduction in size effect as the  $a/d$  ratio increases was also reported by Tan et al. (2005). In their study, the strength results indicated that size effect was more dominant for beams tested at an  $a/d$  ratio of 1.69 and less as compared to similar beams tested at an  $a/d$  ratio of 3.38.

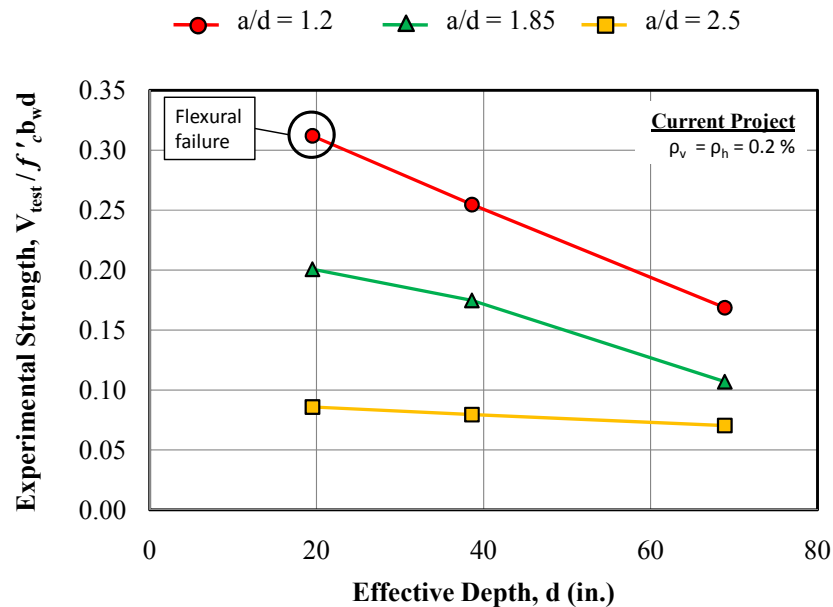


**Figure 4.50: Strength results of all depth effect specimens**

The test regions at failure for the three specimens representing the red line in Figure 4.50 ( $a/d = 1.2$ ) are illustrated in Figure 4.51. The mode of failure for the 42- and the 75-in. specimen was the crushing of the direct strut between the load and the support. The cracking patterns and the presence of local crushing along the strut and near the applied load were similar to those of the specimens tested at an  $a/d$  ratio of 1.85 (Figure 4.49). The 23-in. specimen, however, failed in flexure. The size of the nodal regions in relation to the shear span increased the shear capacity to the point where flexure was the

controlling failure mechanism. From an academic standpoint, it can be inferred that the actual shear strength of this specimen was greater than the shear that produces the flexural failure. It is important to note that the strut-and-tie procedure accounts for flexural failures with the check of tensions ties and the back face of CCC nodes.

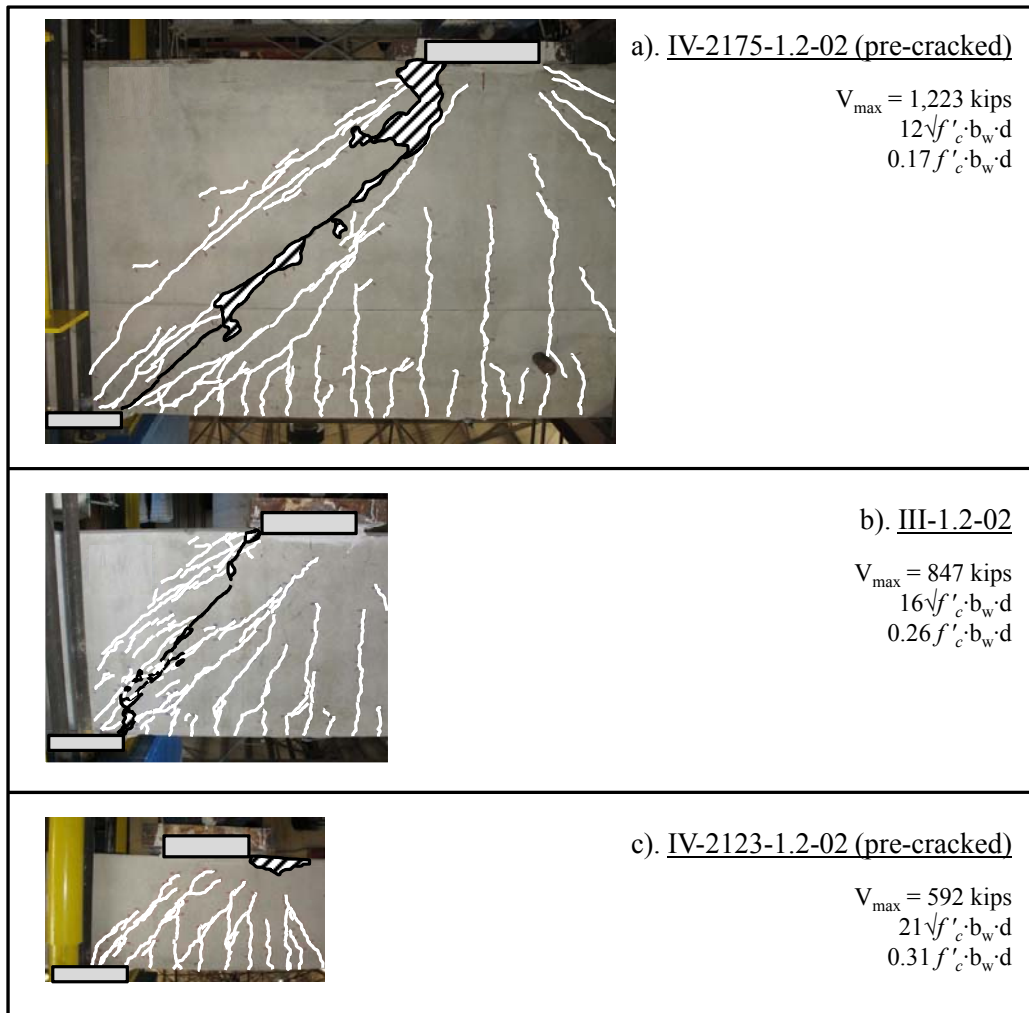


**Figure 4.51: Failure photographs of depth effect specimens with  $a/d$  of 1.2**

Lastly, the test regions at failure for the specimens loaded at an  $a/d$  ratio of 2.5 (orange line in Figure 4.50) are provided in Figure 4.52. For the 23- and 42-in. specimens, the mode of failure was drastically different than those at the other  $a/d$  ratios. As seen in Figure 4.52, the failure crack resembled a sectional shear, or diagonal tension,

crack. Very little crushing or parallel cracking was detected in the region of a direct strut. This difference in behavior was not surprising since it is well known that as the  $a/d$  ratio approaches 2, the dominant shear transfer mechanism starts to change. At low  $a/d$  ratios ( $a/d < 2$ ), an arching or direct strut mechanism is dominant. At higher  $a/d$  ratios ( $a/d > 2$ ), a sectional shear mechanism in which shear resistance is provided by the concrete ( $V_c$ ) and steel ( $V_s$ ) is dominant. For the 75-in. specimen, the final failure crack slightly resembled a sectional shear crack, but there was a considerable amount of parallel cracking in the region of the direct strut. The behavior of this test further illustrates that the transition between deep beam behavior and sectional behavior is gradual; it does not occur at a distinct  $a/d$  ratio. The transition between deep beam behavior and sectional behavior and variables that affect it are addressed explicitly in Section 5.2. From the test results of these three beams (orange line in Figure 4.50), it is clear that size effect depends upon the dominant transfer mechanism and thus, the  $a/d$  ratio.

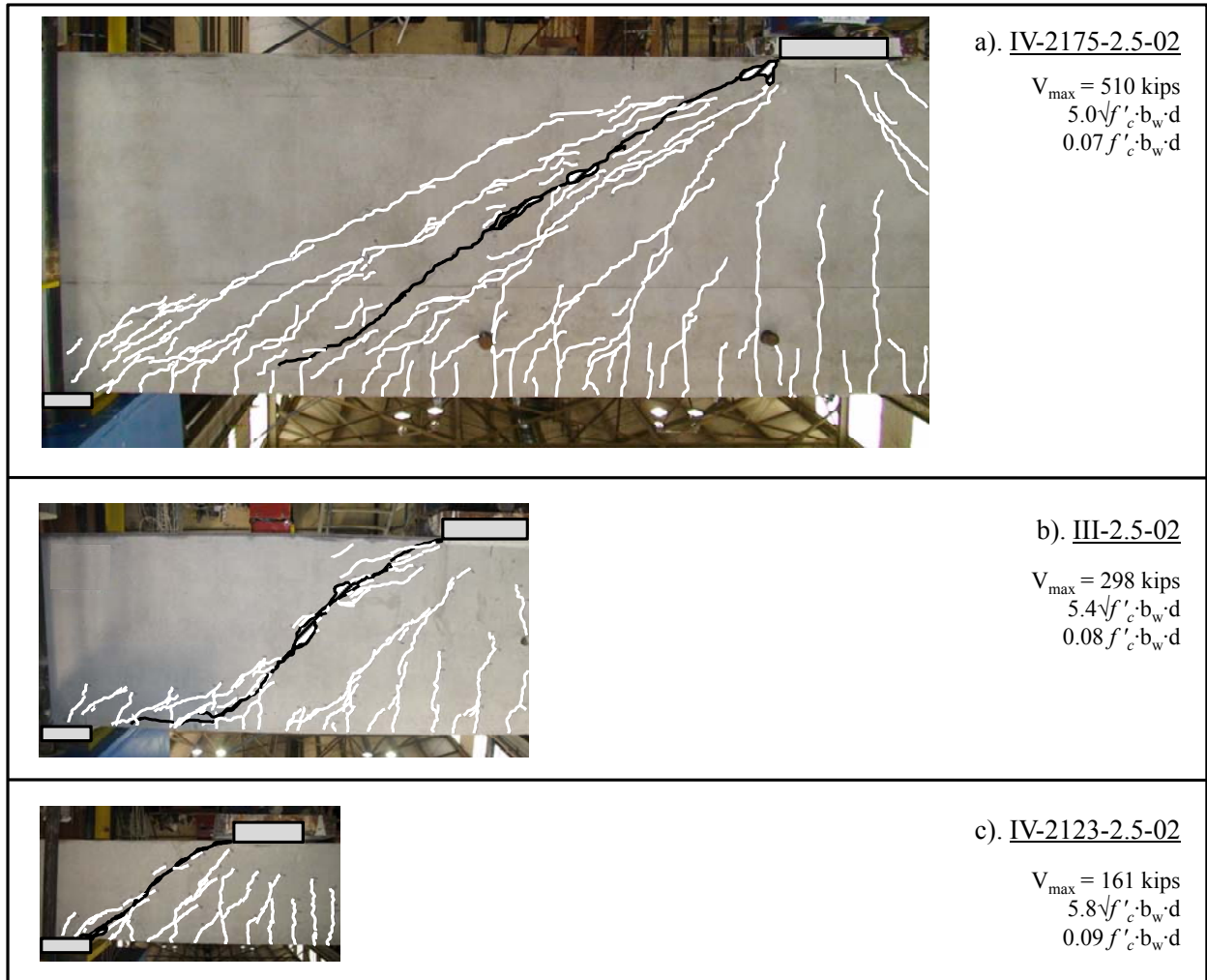


**Figure 4.52: Failure photographs of depth effect specimens with  $a/d$  of 2.5**

The reduction in the normalized shear strength with increasing depth (size effect) in Figure 4.48 and Figure 4.50 can be explained with a strut-and-tie model analysis. As discussed in Section 5.2, the primary load carrying mechanism for deep beams ( $a/d < 2$ ) is captured with a single-panel strut-and-tie model. According to the model, the capacity of deep beams is often governed by the size of the nodal regions. The depth of the member does not directly affect the strength. Therefore, it is inappropriate to normalize the experimental strength of deep beams by the member depth. Doing so assumes that the strength of deep beams is a function of the beam depth. A similar conclusion was reached by Zhang and Tan (2007). They, too, noted that the primary cause of size effect

was the inappropriate use of the “conventional definition of shear strength of  $V/(bd)$ ” for concrete deep beams (Zhang and Tan, 2007).

From a design perspective, the most appropriate way to normalize experimental strength is with design strength. The design procedure should account for every major variable that affects the strength of the member, and therefore, should provide a consistent means of comparison between beams with any combination of these variables. The experimental strength of the specimens tested in the current task was normalized with the design strength computed according to the 5253 strut-and-tie model provisions (Section 2.3.4.4). The results are plotted in Figure 4.53. For the deep beams ( $a/d < 2$ ), there was a fairly uniform level of conservatism as the depth of the member increased. The reserve capacity ( $V_{\text{test}} / V_{\text{calc.}}$ ) of the 75-in. deep beams ( $a/d < 2$ ) was approximately 15% less than that of the 23-in. deep beams. This reduction is a significant improvement to the difference of a factor of 2 in the normalized shear stresses at failure presented in Figure 4.50. Due to the numerous stress checks that can govern the capacity of a strut-and-tie model, some scatter in the values of  $V_{\text{test}} / V_{\text{calc.}}$  should be expected. In addition, there is little difference in the reserve capacity of the specimens tested at an  $a/d$  ratio of 1.2 and 1.85. These results indicate that the single-panel strut-and-tie model adequately captured the experimental behavior of the specimens tested at an  $a/d$  ratio less than 2, regardless of the size and  $a/d$  ratio. It should be noted that similar conclusions would be reached with respect to effective depth if the STM provisions in ACI 318-08 Appendix A or AASHTO LRFD (2008) were used to estimate capacity.

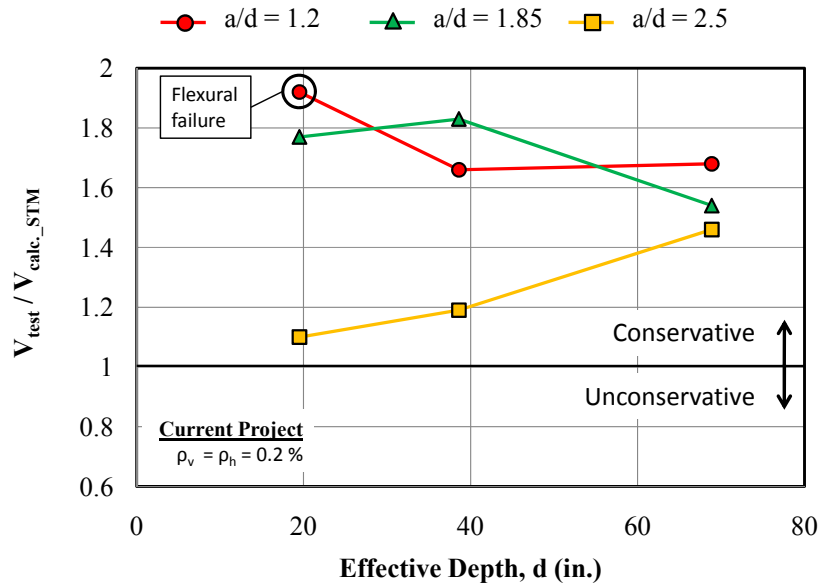


**Figure 4.53: Experimental strength of depth effect specimens normalized by calculated strength**

Based on the results and discussion of this task, it appears that size effect (reduction in efficiency as beam depth increases) is largely eliminated when a strut-and-tie analysis is used to design deep beams ( $a/d < 2$ ). The specimens tested in the current experimental program at an  $a/d$  ratio less than 2 failed in agreement with a single-panel strut-and-tie model. The calculated capacity of the deep beam specimens in Figure 4.53 was governed by the stresses at the CCT node-to-strut interface or the CCC back face in general. As such, their strength was a function of the size and stress conditions in the nodal regions, not a function of their effective depth. The size effect in deep beams reported in the literature is largely the result of assuming that their strength is a function of section size.

For the beams tested at an  $a/d$  ratio of 2.5, the same conclusions did not apply. As noted in Figure 4.52, the specimens tested at this  $a/d$  ratio did not fail in a consistent manner with a single-panel STM. Instead, their failure modes more closely resembled sectional shear, or diagonal tension, failures. For this reason, the reserve capacity ( $V_{\text{test.}} / V_{\text{calc.}}$ ) for these specimens was not consistent with the rest of the tests (Figure 4.53).

However, in all three cases, the strength was conservatively estimated due to the inherent conservatism in the strut-and-tie modeling procedure. These results illustrate a limitation of using a single-panel STM on beams loaded with an  $a/d$  ratio greater than 2. When the behavior of the member is not consistent with the design procedure, the chance of calculating an unconservative estimate of strength increases.

Therefore, in general, it may not be appropriate to apply a single panel STM analysis to design deep beams with  $a/d$  ratios of 2.5. The experimental behavior of these members does not match the behavior assumed in a single-panel STM. Similarly, size effect of beams loaded with an  $a/d$  ratio of 2.5 should not be evaluated by normalizing the experimental strength with calculated strength from a single panel STM. Instead, size effect of these members should be evaluated by normalizing the strength with  $\sqrt{f'_c} b_w d$  since these variables are known to be linked to members governed by sectional shear.

The strength results of the specimens tested at an  $a/d$  ratio of 2.5, normalized with  $\sqrt{f'_c} b_w d$ , are presented in Figure 4.54. In this plot, the data indicated that with increasing depth a small decrease in the normalized shear strength existed. The normalized strength dropped by approximately 10% between each increase in section size. This amount of strength loss is small considering the range of scatter that is consistent with experimental shear tests. It should be noted that there was some difference in the maximum diagonal crack widths between the 23-in. specimens and the larger specimens that may have contributed to this slight loss in strength. However, the maximum diagonal crack widths for the 42- and 75-in. specimens were similar. The crack width data will be presented in Section 4.4.3.



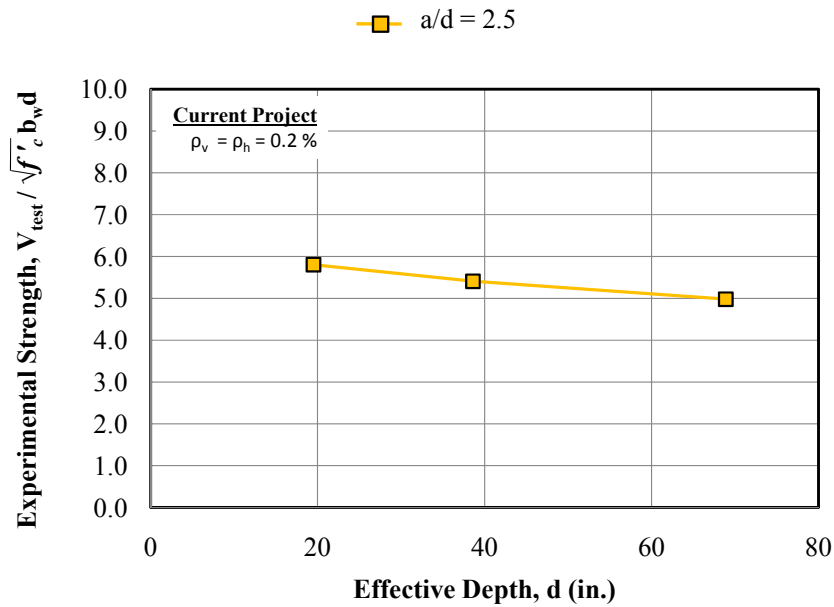


**Figure 4.54: Strength results of size effect specimens with  $a/d$  of 2.5**

The experimental strength of the specimens with an  $a/d$  of 2.5 is compared to the calculated strength using the sectional shear provisions ( $V_c + V_s$ ) in AASHTO LRFD (2008) and ACI 318-08 in Figure 4.55. The results indicate that even though there was a loss in strength with increasing depth, the strength was estimated conservatively with the provisions in both specifications. Since the calculated capacity according to each provision does not account for a size effect, there is a slightly decreasing level of conservatism ( $V_{test} / (V_c + V_s)$ ) with increasing depth. For the strength estimate according to the AASHTO LRFD 2008 provisions, the approximate procedure (Article 5.8.3.4.1) was used since each specimen contained sufficient transverse reinforcement. The sectional shear provisions in AASHTO LRFD (2008) and ACI 318-08 are provided in Section 5.2.3 for reference.

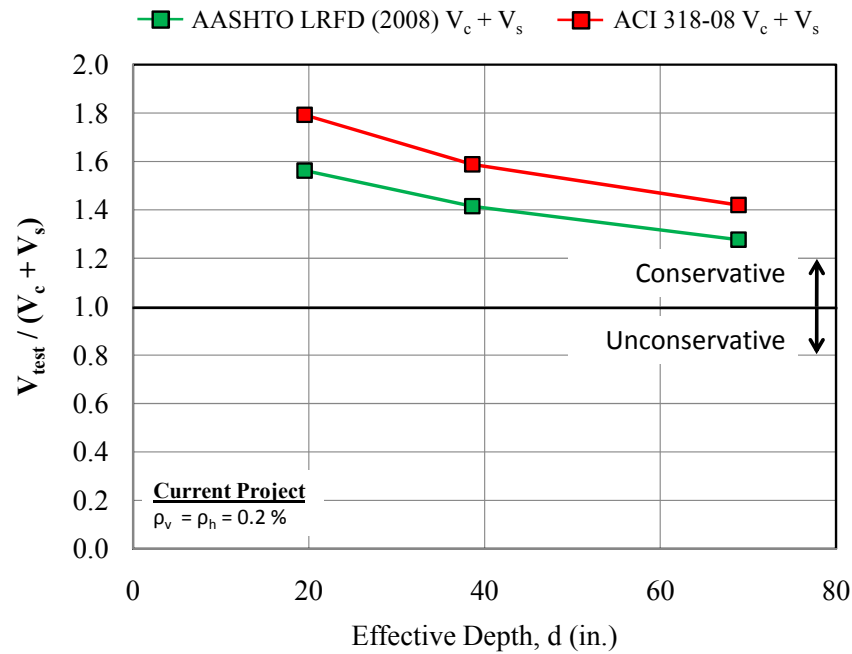


**Figure 4.55: Level of conservatism in sectional shear provisions for specimens with  $a/d$  of 2.5**

The experimental shear strength, measured in kips, of the beams tested for the depth effect task is plotted in Figure 4.56. The purpose of this plot is to illustrate that the actual load carrying capacity of all the specimens did in fact increase with increasing depth. However, the reason for the increase in strength was not the same for all of the specimens. For the specimens tested at an  $a/d$  ratio less than 2, the increase in strength with increasing depth was a result of a slight increase in the size of the back face of the CCC node and CCT nodes and the resulting increase in the length of the node-strut interface of each node (Figure 4.47). For these tests, the node-strut interface at the CCT node generally governed the design capacity computed according to the 5253 STM provisions. It is clear that the increase in load carrying capacity was not proportional to the increase in depth for the deep beams ( $a/d < 2$ ) (Figure 4.50). For the specimens tested at an  $a/d$  ratio of 2.5, the increase in strength was directly related to the increase in depth, with a minimal reduction due to size effect (Figure 4.54). Section-based design approaches are more applicable to beams with  $a/d$  ratios of 2.5.

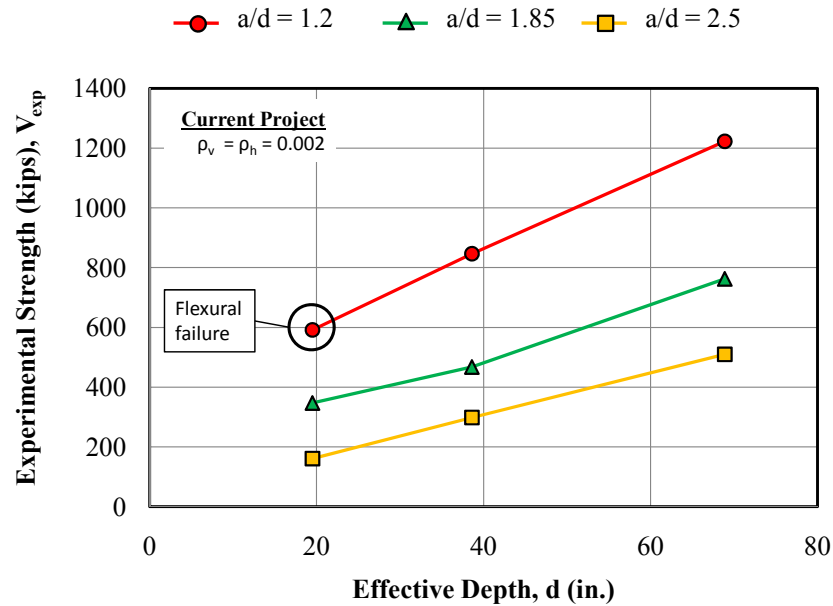


**Figure 4.56: Ultimate shear capacity (kips) of size effect specimens**

In the context of strut-and-tie modeling, size effect of deep beams is not applicable. Size effect needs to be evaluated in terms of the shear transfer mechanism that governs the behavior of the specimen. In previous studies, it was assumed that the strength of deep beams was a function of the shear area ( $b_w d$ ). While this assumption does not affect the comparisons of beams with similar depths, it is inappropriate for evaluating the performance of beams of varying depth. The strength of deep beams ( $a/d < 2$ ) is not a function of their shear area, but rather, a function of a single-panel strut-and-tie model.

#### 4.4.3 Serviceability Results

##### 4.4.3.1 Serviceability Results from the Literature

A few of the experimental studies that investigated the effect of depth on deep beam performance recorded serviceability information. Most of the researchers noted the diagonal cracking loads of their test specimens. Some studies emphasized the load at

which the maximum diagonal crack width reached a limiting value (such as 0.012 in. or 0.016 in.). The serviceability results of test specimens with web reinforcement from three previously-reviewed studies are presented in this section.

Minimal effect of depth on the shear stress at first diagonal cracking was detected. The experimental test results are plotted in Figure 4.57. The loads at first diagonal cracking were normalized by  $\sqrt{f'_c} b_w d$ . In the context of a single-panel STM, the mechanism of diagonal cracking in deep beams is a function of the spreading of compressive stress in the bottle-shaped strut. For the member to crack, the transverse tensile stress in the strut must exceed the tensile capacity of the concrete. Thus, normalizing the diagonal cracking loads by the approximate cross-sectional area of the strut,  $b_w d$ , and the tensile strength of concrete,  $\sqrt{f'_c}$ , is consistent with the mechanism of behavior.

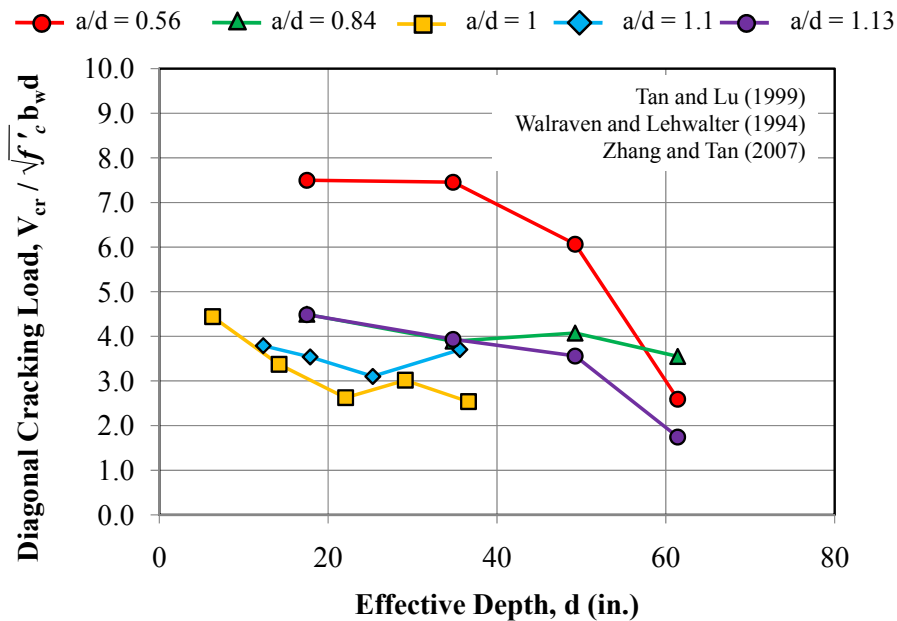


**Figure 4.57: Diagonal cracking loads of size effect specimens in literature**

The data in Figure 4.57 are not conclusive regarding the effect of depth on the normalized shear stress at first diagonal cracking. Consider the specimens tested at  $a/d$  ratios of 0.56 and 1.13 by Tan and Lu (1999). When the effective depth of the member increased from 49 in. to 61 in., a significant reduction in stress at first diagonal cracking was observed. Tan and Lu attributed the drop in stress with increasing depth to Weibull's statistical theory (Weibull, 1939). In this theory, the diagonal cracking strength of a beam is compared to a chain of links in which the strength of the chain is governed by the weakest link. As the depth of the beam increases, the number of links increases and a lower cracking strength is expected. The first diagonal cracking loads of the specimens tested at an  $a/d$  ratio of 1.0 by Walraven and Lehwalter (1994) showed a slight size effect with respect to the smallest 7.9-in. specimen. For the other data in Figure 4.57, the effect of depth on the first diagonal cracking stress was not apparent. Walraven and Lehwalter (1994) and Zhang and Tan (2007) made the following conclusions regarding the effect of depth on first diagonal cracking:

*“...the load at which inclined cracking occurs is hardly size-dependent.” (Walraven and Lehwalter, 1994)*

*“...the diagonal cracking strengths of deep beams are not size dependent.” (Zhang and Tan, 2007)*

The diagonal cracking loads from these research studies can also be normalized by the load carrying capacity. The results are illustrated in Figure 4.58. The diagonal cracking loads of the test specimens represented in Figure 4.58 ranged from approximately 20% to 60% of the ultimate load-carrying capacity. There is not a distinct trend with increasing depth.

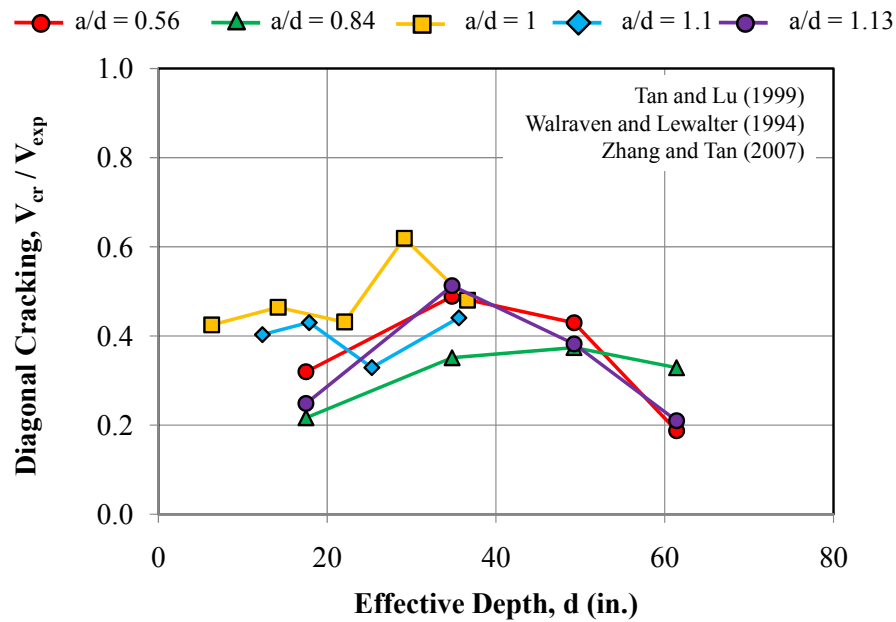


**Figure 4.58: Diagonal cracking loads of size effect specimens in literature (function of ultimate)**

The loads at which the width of the inclined cracks reached 0.012 in. (0.3 mm) were recorded in a couple of research studies as well. These loads were termed the serviceability loads since a crack width of 0.012 in. is generally accepted as a tolerable crack width for exterior exposure conditions (ACI 224R-01). The experimental test results are plotted in Figure 4.59. In this plot, the serviceability loads were also normalized by the ultimate load-carrying capacity. The serviceability loads as a percentage of the capacity generally decreased with increasing depth, albeit with some inconsistency. The diagonal crack widths reached the limiting width at lower percentages of their ultimate strength as the depth of the member increased. It seems plausible to extend the results in Figure 4.59 to suggest that with increasing depth, diagonal crack widths increase for a given percentage of capacity.

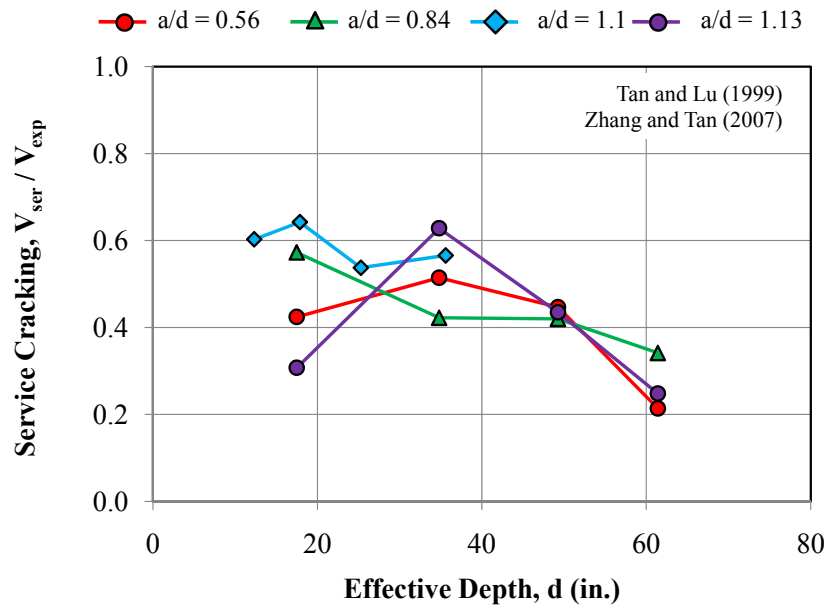


**Figure 4.59: Service loads (diagonal crack width = 0.012 in.) as function of ultimate for size effect specimens in literature**

#### 4.4.3.2 Serviceability Results from the Experimental Program

In the current task, the effect of depth on the serviceability performance of deep beams was also evaluated. The serviceability performance was measured with first diagonal cracking loads and with the maximum diagonal crack width at first cracking and at each load increment thereafter.

The load at which the first diagonal crack was detected was recorded for all of the tests in the current project. As noted in Section 4.2.2, for the test regions that were pre-cracked prior to testing, a load at first diagonal cracking was not available. This restriction did not apply for the beams in Series IV. For the 75-in. specimens, the diagonal cracking loads for each test region were obtained during the first test since the position of the ram did not change between the two tests. For the 21-in. specimens, the test region for the second test of each beam was uncracked due to the low level of load resisted by the long shear span. The diagonal cracking loads for the test specimens relevant to the current task are listed in Table 4.8.

**Table 4.8: Diagonal cracking loads of depth effect specimens**

Beam I.D.	$b_w$ in.	$d$ in.	$f'_c$ psi	Nominal $\rho_v$ & $\rho_h$	Support Plate <sup>†</sup> in.	Load Plate <sup>†</sup> in.	$\alpha$	a/d ratio	$V_{crack}$ kip	$\frac{V_{crack}}{\sqrt{f'_c} \cdot b_w d}$	$V_{crack} / V_{test}$
III-1.85-02	21	38.6	4100	0.002	16x21	20x21	0.72	1.84	112	2.2	0.23
III-1.85-03b	21	38.6	3300	0.003	16x21	20x21	0.72	1.84	114	2.4	0.24
III-1.85-02b	21	38.6	3300	0.002	16x21	20x21	0.72	1.84	-	-	
III-1.2-02	21	38.6	4100	0.002	16x21	20x21	0.82	1.20	165	3.2	0.20
III-1.2-03	21	38.6	4220	0.003	16x21	20x21	0.82	1.20	-	-	
III-2.5-02	21	38.6	4630	0.002	16x21	20x21	0.62	2.49	105	1.9	0.35
III-2.5-03	21	38.6	5030	0.003	16x21	20x21	0.62	2.49	-	-	
IV-2175-1.85-02	21	68.9	4930	0.002	16x21	29x21	0.5	1.85	216	2.1	0.28
IV-2175-1.85-03	21	68.9	4930	0.003	16x21	29x21	0.5	1.85	218	2.1	0.26
IV-2175-2.5-02	21	68.9	5010	0.002	16x21	24x21	0.33	2.50	144	1.4	0.28
IV-2175-1.2-02	21	68.9	5010	0.002	16x21	24x21	0.67	1.20	262	2.6	0.21
IV-2123-1.85-03	21	19.5	4160	0.003	16x21	16.5x21	0.86	1.85	60	2.3	0.18
IV-2123-1.85-02	21	19.5	4220	0.002	16x21	16.5x21	0.86	1.85	65	2.4	0.19
IV-2123-2.5-02	21	19.5	4570	0.002	16x21	15.5x21	0.81	2.50	51	1.8	0.32
IV-2123-1.2-02	21	19.5	4630	0.002	16x21	18x21	0.91	1.20	124	4.5	0.21

<sup>†</sup> Length along span ( $l$ ) x length along width ( $w$ )

(f) Maximum shear carried in specimen upon the occurrence of concrete crushing at the compression face.



The experimental load at first diagonal cracking for the beams in the current task were normalized, as before, by  $\sqrt{f'_c} b_w d$ . Information regarding the measurement of the diagonal cracking loads was provided in Section 4.2.2. The results for the beams in the current task are plotted in Figure 4.60.

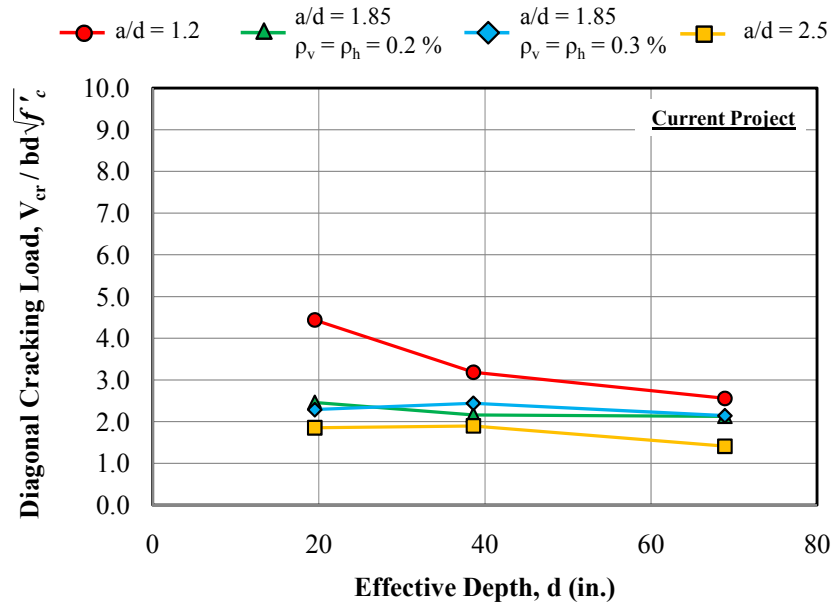


**Figure 4.60: Normalized diagonal cracking loads for the depth effect specimens**

The test results in Figure 4.60 do not show consistent trends with effective depth. For the specimens tested at  $a/d$  ratios of 1.85, a negligible difference in diagonal cracking strength existed as the depth of the member increased. It is interesting to note that for these members, the shear at first diagonal cracking was approximately  $2\sqrt{f'_c} b_w d$  which is the assumed diagonal cracking strength (and concrete contribution to shear strength) of members subjected to sectional shear. For the specimens tested at an  $a/d$  ratio of 1.2, however, the shear stress at first diagonal cracking decreased with increasing depth. The high stress at first diagonal cracking for specimen IV-2123-1.2-02 could have been due to the size of the bearing plates in relation to the shear span, effectively decreasing the  $a/d$  ratio (Figure 4.46). However, this explanation cannot be used to explain the differences

in shear stress at diagonal cracking between the 42- and 75-in. specimens. Similarly, the diagonal cracking load decreased between the 42- and 75-in. specimens tested at an a/d ratio of 2.5. It is possible that a Weibull-type statistical size effect or a variation in the tensile strength of concrete contributed to the reduction in stress at first diagonal cracking for these members. The lack of consistent trends in the diagonal cracking load of the test specimens and those in the literature with increasing depth suggest that the effect highly variable.

As with the data from the literature, the diagonal cracking shears can be normalized with the ultimate load carrying capacity. This normalization technique applied to the beams tested in the current task is provided in Figure 4.61. In this figure, the diagonal cracking strength of the specimens ranged from approximately 20% to 35% of the capacity. Also, as the depth of the specimen increased, the ratio of the cracking shear to the ultimate shear was fairly constant for the beams tested at each a/d ratio. This finding was particularly interesting for the set tested at an a/d ratio of 1.2. The results indicated that the diagonal cracking strength of deep beams may not be just a function of the shear area and the  $\sqrt{f'_c}$ . Perhaps, other variables that affect the capacity, namely the size of the bearing plates, may also affect the diagonal cracking strength. More research in this area is recommended.

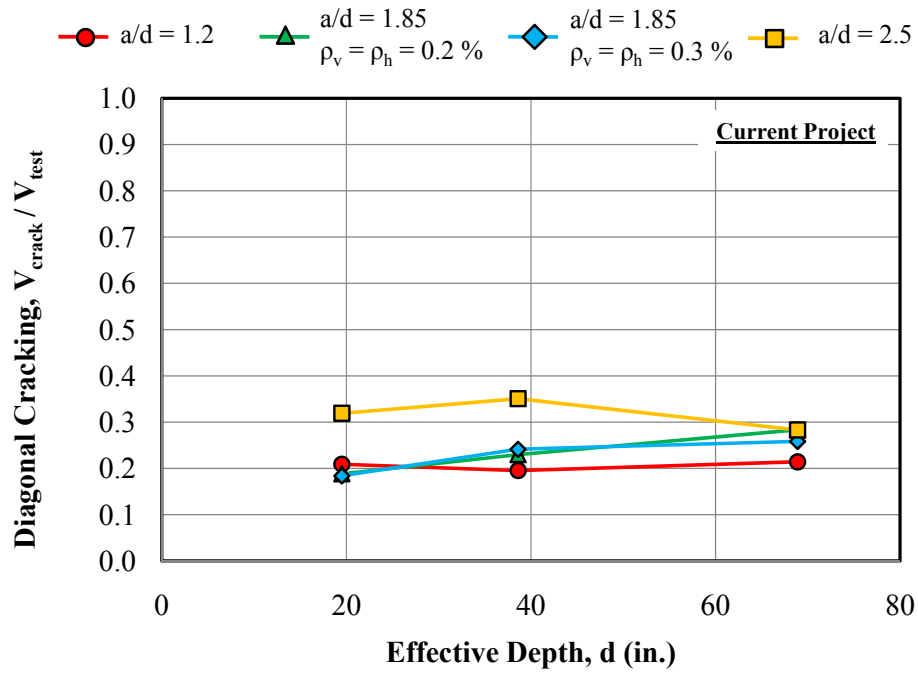


**Figure 4.61: Diagonal cracking loads normalized by ultimate strength for depth effect tests**

In addition to obtaining the diagonal cracking loads of the test specimens, the maximum width of the primary diagonal crack was recorded for the duration of each test. As noted in Section 3.5.3, the width of the diagonal cracks was measured using a crack comparator card. Measurements were taken on each side of the specimen and at each load increment. The crack width data for all of the specimens relevant to this task are provided in Figure 4.62 through Figure 4.65. Each plot contains the crack width data for a set of tests where the only difference among the specimens is their depth. As before, the maximum diagonal crack widths are plotted versus the percent of the maximum applied load for the reasons cited in Section 4.2.2.

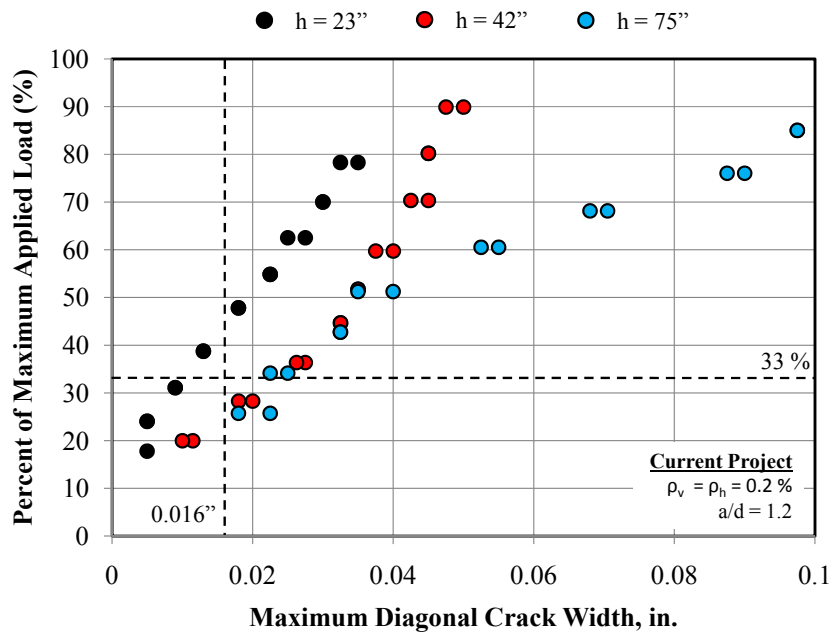


*Figure 4.62: Maximum diagonal crack widths for depth effect specimens with an  $a/d$  ratio of 1.2*

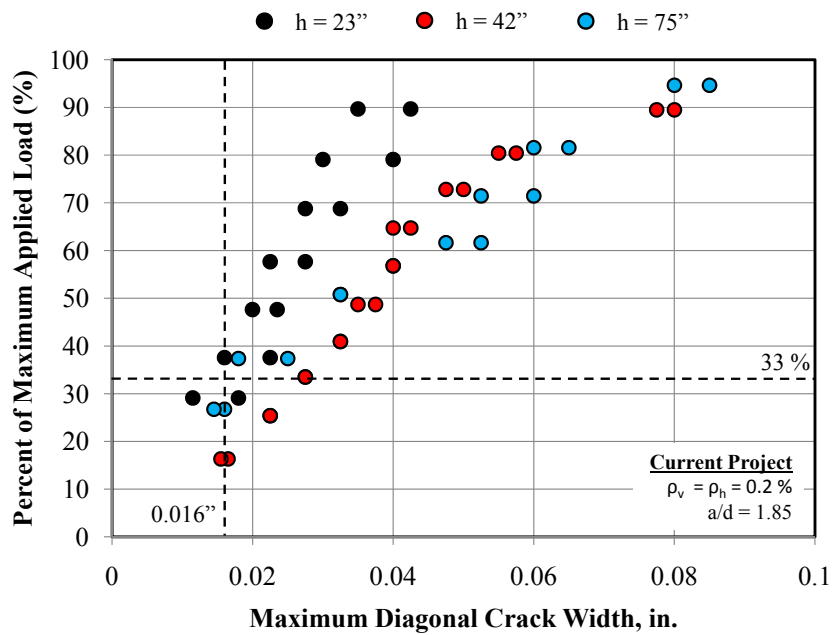


*Figure 4.63: Maximum diagonal crack widths for depth effect specimens with an  $a/d$  ratio of 1.85 and 0.2% web reinforcement*

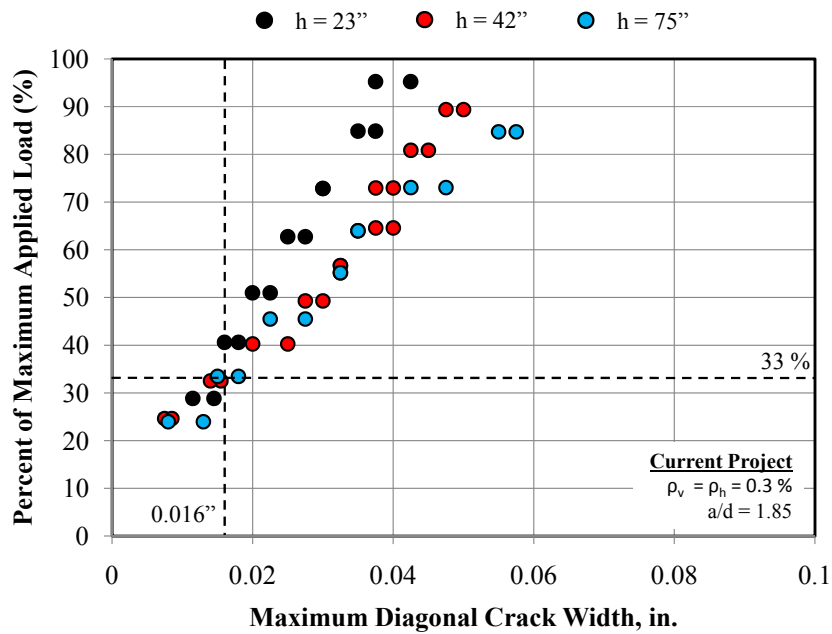


*Figure 4.64: Maximum diagonal crack widths for depth effect specimens with an  $a/d$  ratio of 1.85 and 0.3% web reinforcement*

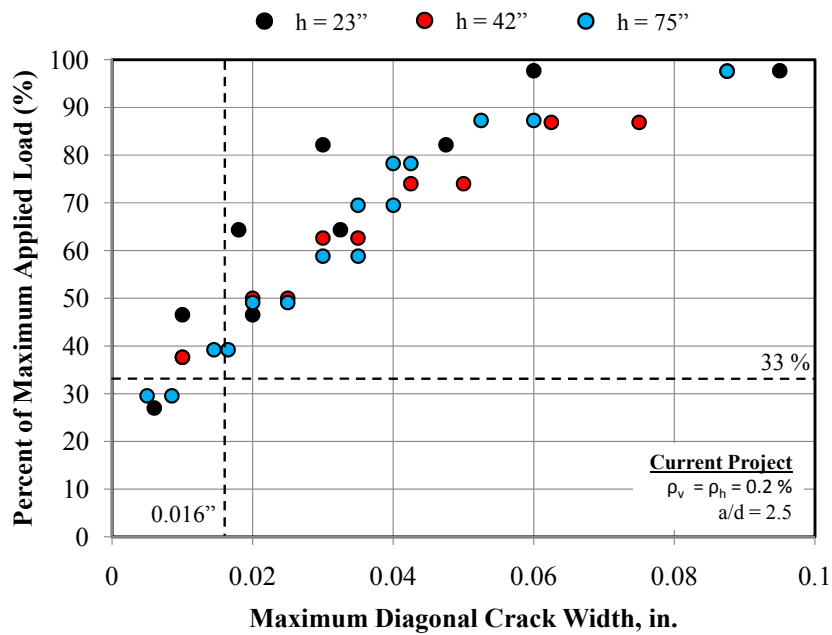


*Figure 4.65: Maximum diagonal crack widths for depth effect specimens with an  $a/d$  ratio of 2.5*

In Figure 4.62 through Figure 4.65, the diagonal crack width data for the depth effect series were provided. In general, the widths of the diagonal cracks in the 42- and 75-in. specimens were fairly consistent for all three  $a/d$  ratios. An increase in depth from 42 in. to 75 in. did not significantly affect the maximum diagonal crack width. The widths of the diagonal cracks in the 23-in. specimens, however, were consistently narrower than the larger specimens at a given percentage of capacity for all three  $a/d$  ratios. These data indicated that caution should be used in extrapolating crack width data from smaller members to large or full-scale members. Also, the data presented in Figure 4.62 through Figure 4.65 was fairly consistent with the results from the literature presented in Figure 4.59. Crack width data presented by Tan and Lu (1999) and Zhang and Tan (2007) indicated that the width of diagonal cracks for larger members reached the tolerable crack width limit (0.012 in.) at lower percentages of their capacity than for smaller members.

The trend of the data in Figure 4.62 through Figure 4.65 can be explained with aspects of modified compression field theory. According to this theory, as the depth of the member increases, the spacing of the diagonal cracks tends to increase (Collins and Kuchma, 1999). The diagonal crack width is a function of transverse tensile strain in the member and the spacing of the cracks. Therefore, as the depth of the member increases, the width of the diagonal cracks is expected to increase due to the increase in crack spacing. It should be noted that this theory was formulated for the use with slender beams and was based on flexural theory assumptions. However, the dependence of crack spacing on member depth and the influence of spacing on crack width seem applicable to deep beams as well. It is important to note that an appreciable difference in crack width was only observed as the overall depth increased from 23 in. to 42 in. There were negligible differences in crack widths as the overall depth increased from 42 in. to 75 in. Thus, it would appear that effect of size on diagonal crack width is mitigated once the overall depth reaches 42 in.

#### 4.4.4 Design Recommendations

Based on the results presented and discussed in Section 4.4, the design of reinforced concrete deep beams ( $a/d < 2$ ) should be performed with a strut-and-tie analysis. The behavior of deep beams is often governed by the size and stress conditions of the nodal regions which single-panel STMs explicitly address. In this way, size effect of deep beams should not be considered. Sectional design approaches are unacceptable for reinforced concrete deep beams. They inappropriately assume that the strength of deep beams increases proportionally to an increase in depth.

It is important to note that from a design perspective, increasing the depth of a member often decreases the  $a/d$  ratio since span lengths are generally pre-determined. In this sense, there is a benefit to increasing the depth of a deep beam.

#### 4.4.5 Summary

In Section 4.4, the effect of member depth on the strength and serviceability performance of reinforced concrete deep beams was investigated. Tests were conducted at an  $a/d$  ratio of 1.2, 1.85, and 2.5 on specimens with a 21"x23", 21"x42", and 21"x75" cross-section. With increasing depth, the normalized shear strength at failure ( $V_{\text{test}}/f_c'b_wd$ ) decreased. The apparent reduction in strength is due to the incorrect association of deep beam capacity to the cross-sectional area ( $b_wd$ ). Rather, the strength of deep beams is appropriately captured by a single-panel strut-and-tie analysis. Provided that the bottle-shape strut is adequately reinforced and the force in the tension tie does not control, the strength of deep beams is governed by the size and stress conditions in the nodal regions, not by the effective depth of the member. The findings in this section illustrate the importance of using a strut-and-tie model analysis to design reinforced concrete deep beams. Section-based approaches are inappropriate.

Diagonal cracking loads and maximum diagonal crack widths were recorded at load stages to evaluate the effect of depth on the serviceability performance of a deep beam. It was shown that for the beams tested at an  $a/d$  ratio of 1.85, the diagonal cracking load, normalized by  $\sqrt{f_c'}b_wd$ , was not appreciably affected by an increase in

depth. For the beams tested at an  $a/d$  ratio of 1.2 and for one specimen tested at an  $a/d$  ratio of 2.5, a reduction in the normalized diagonal cracking load was observed. In light of previous findings in the literature, it is likely that depth can influence the diagonal cracking load to some extent, but the effect is erratic and highly variable. With increasing overall depth from 23" to 42," an increase in the maximum diagonal crack width at a given percentage of the maximum applied load was recorded. An increase in maximum diagonal crack widths was not observed when the overall depth increased from 42" to 75" in general. As a result, the crack width data indicated that a size effect exists in terms of the crack widths of small specimens. Caution should be used in basing recommendations on full-scale structures off of crack width data of small specimens. The measured data suggested that the effect of depth on crack widths is mitigated at depths greater than 42 in.

#### **4.5 SUMMARY**

In Chapter 4, a summary of the experimental results of the specimens tested in Project 5253 was presented. General information regarding the evaluation of the strength and serviceability data obtained in the experimental program such as normalization techniques, the computation of test shear, and serviceability criteria were provided. Then, the results of two primary tasks of Project 5253 were presented in detail. The effect of minimum web reinforcement on the strength and serviceability performance of deep beams was discussed in Section 4.3. The effect of member depth was discussed in Section 4.4.



## **CHAPTER 5**

### **Analysis of Results**

#### **5.1 OVERVIEW**

In Chapter 5, the results of three objectives of Project 5253 are presented. In Section 5.2, the task of reducing the discrepancy between shear strength calculated with STM and sectional shear provisions is addressed. In Section 5.3, methods of limiting diagonal cracking under service loads are presented. Lastly, in Section 5.4, the task of correlating the maximum diagonal crack width in a reinforced concrete deep beam to its residual capacity to aid field assessment of diagonally-cracked bent caps is accomplished. All three of these tasks were achieved through the analysis of data from the experimental program, the literature, and the evaluation database.

#### **5.2 DISCREPANCY IN CALCULATED SHEAR STRENGTH AT $a/d$ RATIO OF 2.0**

TxDOT engineers have expressed concern over large discrepancies in shear strength calculated using the STM and sectional shear provisions in AASHTO LRFD (2008) at  $a/d$  ratios near 2. The objective of this task was to reduce this discrepancy. In this section, a review of the effect of the  $a/d$  ratio on the shear behavior of reinforced concrete members is provided. Information regarding the transition from deep beam behavior to sectional shear behavior is emphasized. Based on data from the experimental program and from the literature, the use of a single-panel strut-and-tie model for  $a/d$  ratios up to 2 is justified. Lastly, the reason for the discrepancy between shear strength calculated using the STM and the sectional shear provisions at an  $a/d$  ratio of 2 is explained. With the use of the Project 5253 STM provisions, the discrepancy is largely eliminated.

##### **5.2.1 Background**

In Article 5.8.1.1 of AASHTO LRFD 2008, a deep component is defined as:

*Components in which the distance from the point of zero shear to the face of the support is less than  $2d$  or components in which a load causing more than  $\frac{1}{2}$  ( $\frac{1}{3}$  in case of segmental box girders) of the shear at a support is closer than  $2d$  from the face of the support.*

In this requirement, the shear span is defined; and the limiting ratio of shear span to effective depth is set at 2. It should be noted that in this dissertation, the shear span is taken from the centerline of the support, not the face as in the above definition. It is required in Article 5.13.2.1 that beams or components meeting the definition of a “deep component” be designed according to the strut-and-tie provisions in AASHTO LRFD (Article 5.6.3) or another recognized theory. The basis for restrictions on “deep components” is due to the nonlinear strain distribution that exists in regions near concentrated loads, supports, or abrupt changes in geometry. Conventional flexural theory, i.e. plane-sections-remain plane, is not valid in these regions. According to St. Venant’s principle, the strain distribution is not affected by the disturbance at approximately a distance ‘d’ away from it (Schlaich et al., 1987). This principle is the basis for the limit of a/d ratio of 2. In regions where “it is reasonable to assume that plane sections remain plane after loading,” the sectional model can be used for shear design (Article 5.8.1.1, AASHTO LRFD (2008)). The strain trajectories of an asymmetrically-loaded beam are shown in Figure 5.1. According to AASHTO LRFD (2008), different design models should be used in the regions to either side of the concentrated load. Bearing stresses should be checked at the left support and beneath the applied load in conjunction with the sectional design.

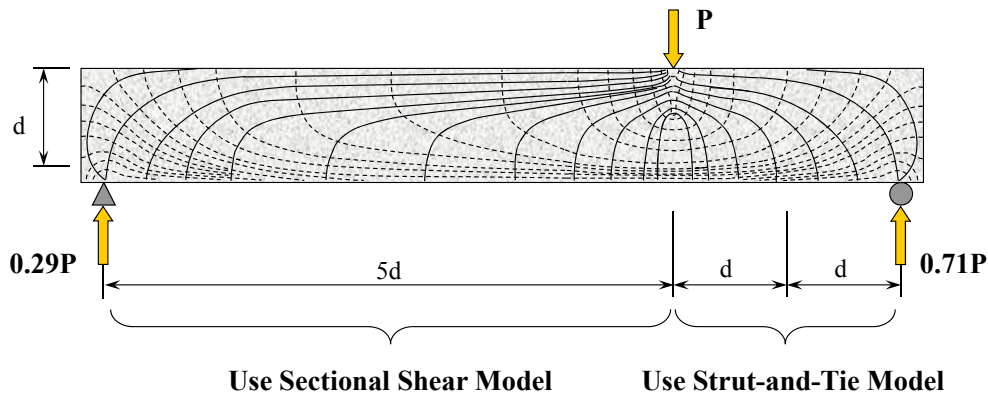


**Figure 5.1: Strain trajectories in an asymmetrically-loaded beam**

Therefore, at an  $a/d$  ratio of 2, there is a discontinuity in the required shear design model according to the specifications of AASHTO LRFD (2008). If a structure is loaded in such a way that an  $a/d$  ratio of 2.1 exists, then the sectional shear model applies for design. Conversely, if the structure is loaded such that an  $a/d$  ratio of 1.9 exists, then a strut-and-tie analysis is required. It is known that near an  $a/d$  ratio of 2, a gradual transition in the dominant shear transfer mechanism occurs consistent with each of the required models. The transition is not immediate and a large discrepancy in calculated capacity at an  $a/d$  ratio of 2 is not justified.

The main purpose of the current task is illustrated qualitatively in Figure 5.2. For members with an  $a/d$  ratio less than 2, shear capacity is computed according to the strut-and-tie provisions in AASHTO LRFD. Due to the efficiency factor at the CCT node-to-strut interface and the geometry of non-hydrostatic nodes, the calculated capacity decreases rapidly as the  $a/d$  ratio approaches 2. For members with an  $a/d$  ratio greater than 2, shear capacity is calculated with a sectional model consisting of  $V_c + V_s$  in AASHTO LRFD (2008). The capacity computed according to the sectional model is often greater than that according to the STM at an  $a/d$  of 2, especially if there is a considerable amount of transverse reinforcement in the member ( $V_s$ ). The purpose of the current task is to reduce the discrepancy between the calculated shear capacities from each model at an  $a/d$  ratio of 2, thereby providing a uniform level of conservatism across

the transition from deep beam to sectional shear behavior. Additional details explaining the computations associated with each model are provided in Section 5.2.3.

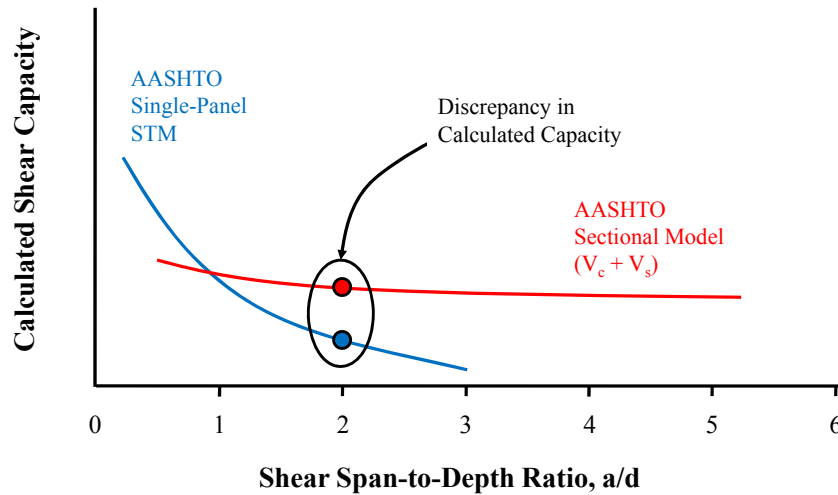


**Figure 5.2: Discontinuity in calculated shear capacity in AASHTO LRFD 2008 at  $a/d$  of 2**

### 5.2.2 Effect of $a/d$ ratio on Shear Behavior

Shear span-to-depth ratio ( $a/d$ ) has been recognized as an important parameter affecting the shear strength of reinforced concrete beams since the 1950s (ACI-ASCE Committee 326, 1962). For single or double concentrated loads acting on a beam, the shear span is clearly defined. For other types of loading, namely distributed loads, it is convenient to present the shear span-to-depth ratio as the ratio of  $M / Vd$  to aid in its application. A clear definition of the shear span-to-depth ratio is required for its proper use in empirical equations. For strut-and-tie models, the  $a/d$  ratio (and also the clear span-to-depth ratio in ACI 318-08) is used to determine if a strut-and-tie analysis is required. In calculating the strength of a member with a STM, the path of the applied loads is traced through the structure directly, without the direct use of the  $a/d$  ratio.

### ***5.2.2.1 Results from the Literature***

Numerous researchers have shown the effect of the  $a/d$  ratio on the shear strength and overall behavior of reinforced concrete beams. Several studies are reviewed in this section with an emphasis on the effect of the  $a/d$  ratio on the dominant transfer mechanism of the member.

In 1954, forty-two (42) reinforced concrete beams were loaded to failure by Moody et al. to evaluate their shear strength. The size and loading conditions of the test specimens were divided into three groups corresponding to three  $a/d$  ratios: approximately 1.5, 3, and 3.5. Primarily, the behavior of beams without transverse reinforcement was studied. Two specimens were tested with web reinforcement. The test results indicated that the beams with higher  $a/d$  ratios (3 and 3.5) failed soon after the load causing first diagonal cracking was reached. For the beams that were loaded with smaller  $a/d$  ratios (1.5), the beam had additional capacity after first diagonal cracking. A redistribution of internal stresses took place after the formation of diagonal cracks in which compression and shear stresses concentrated in the compression zone at the top of the inclined crack. It was observed that the stress distribution in the tension reinforcement along the shear span did not follow the distribution of external moments. The failure of the specimens loaded with an  $a/d$  ratio of 1.5 was classified as shear-compression (Moody et al., 1954).

In 1957, thirty-eight concrete beams without transverse reinforcement were tested by Morrow and Viest. The  $a/d$  ratio ranged from approximately 1 to 7.8 for the test specimens. It was observed that the  $a/d$  ratio greatly contributed to the failure mode and overall performance of the beams. At an  $a/d$  ratio less than about 3.4, the test specimens failed in shear-compression. The beams failed due to crushing of the compression zone above the diagonal crack at a higher load than the load at first diagonal cracking. With increasing  $a/d$  ratio, the ratio between the ultimate load and the first diagonal cracking load decreased. The beams loaded with an  $a/d$  ratio between 3.4 and 6.1 failed in diagonal tension in which the load at first cracking was synonymous with the ultimate load. Beams with an  $a/d$  ratio greater than 6.1 failed in flexure. The authors warned that

the aforementioned limits on  $a/d$  ratio were a function of the properties of the beams that were tested and should only be used qualitatively (Morrow and Viest, 1957). It is interesting to note that the transition between shear compression and diagonal tension failure was found to be 3.4 in this study. In other studies reviewed in this section, the  $a/d$  ratio at this transition is typically around 2 or 2.5. It is possible that the difference is due to the strict definition of a diagonal-tension failure as a case in which the first diagonal cracking load and the capacity are equivalent.

Hundreds of tests on reinforced concrete beams were conducted by Kani for the purpose of understanding the mechanism of diagonal failure, also called shear failure (Kani et al., 1979). Based on the observed behavior of the test specimens, two mechanics-based models were derived to form a shear-strength envelope. The applicability of each model was a function of the  $a/d$  ratio. The shear-strength envelope is illustrated in Figure 5.3.

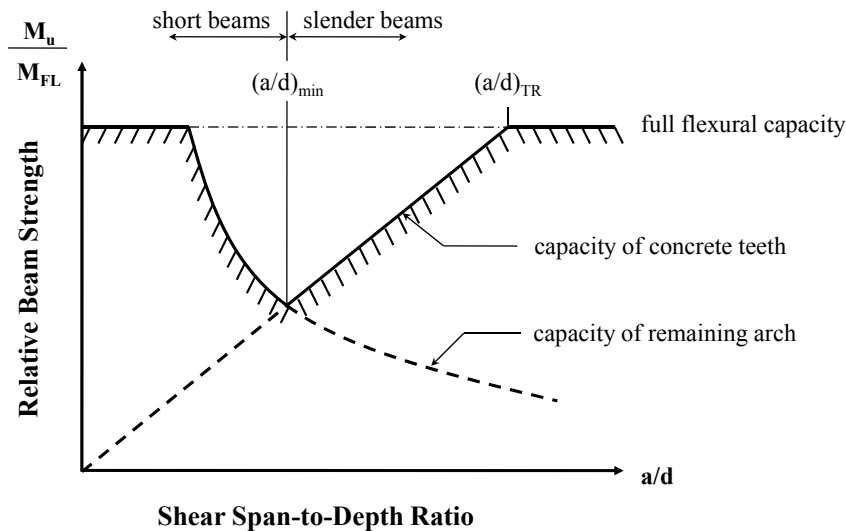


**Figure 5.3: Proposed shear-strength envelope by Kani et al. (1979)**

In Figure 5.3, the strength of the member is quantified as a percentage of the moment capacity. The moment capacity is not reached in a “valley of diagonal failure” bounded by two critical  $a/d$  ratios:  $(a/d)_{\min}$  and  $(a/d)_{TR}$ .  $(a/d)_{\min}$  is the intersection between the two models that govern diagonal failure.  $(a/d)_{TR}$  is the  $a/d$  ratio at which

flexural failure governs the capacity instead of diagonal, or shear, failure. At mid-range  $a/d$  ratios ( $(a/d)_{\min} < a/d < (a/d)_{\text{TR}}$ ), the shear strength of a beam is governed by the “capacity of concrete teeth.” This model consists of treating a cracked, reinforced concrete beam as a “comb-like structure” with a series of “concrete teeth” cantilevered from its base (Kani et al., 1979). The diagonal failure of the beam is a result of overstressing the tooth at its base. An equation for the capacity of a tooth was developed that was a function of the  $a/d$  ratio, the flexural strength of concrete, the flexural moment arm, the cross-sectional dimensions, and the width and length of the cracks. The width and length of the cracks outlined the dimension of the tooth and were determined empirically. At low  $a/d$  ratios ( $a/d < (a/d)_{\min}$ ), the shear strength of a beam was defined as a function of the “capacity of the arch.” This model treated the reinforced concrete beam as a tied arch in which the load transferred directly to the support. The equation that was developed for this model was simplified such that it was only a function of the flexural capacity of the beam and the  $a/d$  ratio. Good agreement existed between test data and the proposed models.

In his study of diagonal failure, Kani recognized the transition of the dominant mechanism of behavior as a function of the  $a/d$  ratio. At low  $a/d$  ratios ( $a/d < (a/d)_{\min}$ ), the shear strength of the beam was governed by a tied-arch failure. At higher  $a/d$  ratios ( $(a/d)_{\min} < a/d < (a/d)_{\text{TR}}$ ), the shear strength of the beam was governed by a bending failure of a “concrete tooth.” The transition between these different mechanisms was labeled  $(a/d)_{\min}$  because it coincided with the smallest shear strength of the member. The value of  $(a/d)_{\min}$  was a function of the longitudinal reinforcement ratio, the yield strength of the reinforcement, the flexural strength of the concrete, and the width and length of the cracks. Even though  $(a/d)_{\min}$  changed based on the properties of the beam, it was usually close to 2.5. This value was supported by experiments.

The effect of transverse reinforcement on the diagonal failure of reinforced concrete beams was also investigated by Kani. The function of the reinforcement was to create internal supports for the series of concrete arches that are formed by the concrete teeth. In a sense, the  $a/d$  ratio is essentially shortened by the internal supports created by

the transverse reinforcement. In terms of the shear-strength envelope, the region governed by the “capacity of the arch” is extended due to the effective shortening of the  $a/d$  ratio.

An experimental study was conducted by Ahmad and Lue (1987) on specimens with high-strength concrete ( $f'_c > 8,800$  psi). A model similar to the one proposed by Kani was developed that was applicable to beams with both normal- and high-strength concrete. Through the experimental study, it was determined that the capacity and the failure mode of the test specimens were largely a function of the  $a/d$  ratio. Four different failure modes were evident. At an  $a/d > 6$ , the beams generally failed in flexure. At an  $a/d$  ratio between 2.5 and 6, the failure of the beams was due to a diagonal tension crack that originally propagated from a flexural crack (flexure-shear crack). At an  $a/d$  ratio between 1.5 and 2.5, the beams failed by shear compression of the web. At  $a/d < 1.5$ , the failure was by crushing of the arch rib of the beams. Thus, a similar breakdown of failure modes to that observed by Kani was also observed by Ahmad and Lue (1987). At an  $a/d$  ratio of approximately 2.5, the shear behavior of the beam transitioned from a shear-compression type failure to a diagonal-tension type failure.

The experimental shear strength of high-strength concrete beams with an  $a/d$  ratio ranging from 1.5 to 2.5 was investigated by Shin et al. (1999). It was also observed in this study that the failure mode of the test specimens was dependent on the  $a/d$  ratio. However, in this study the transition in failure mode from shear-compression to shear-tension occurred at an  $a/d$  ratio of approximately 2.

#### ***5.2.2.2 Results from the Experimental Program***

In the experimental program of the current study, the effect of  $a/d$  ratio was also investigated. Tests were conducted on beams with shear-span-to-depth ( $a/d$ ) ratios of 1.2, 1.85, and 2.5. The normalized shear strength of six 21”x42” specimens in which the  $a/d$  ratio varied from 1.2 to 2.5 is depicted in Figure 5.4. With increasing  $a/d$  ratio, the normalized shear strength at failure decreased; and the failure mode of the test specimens changed.



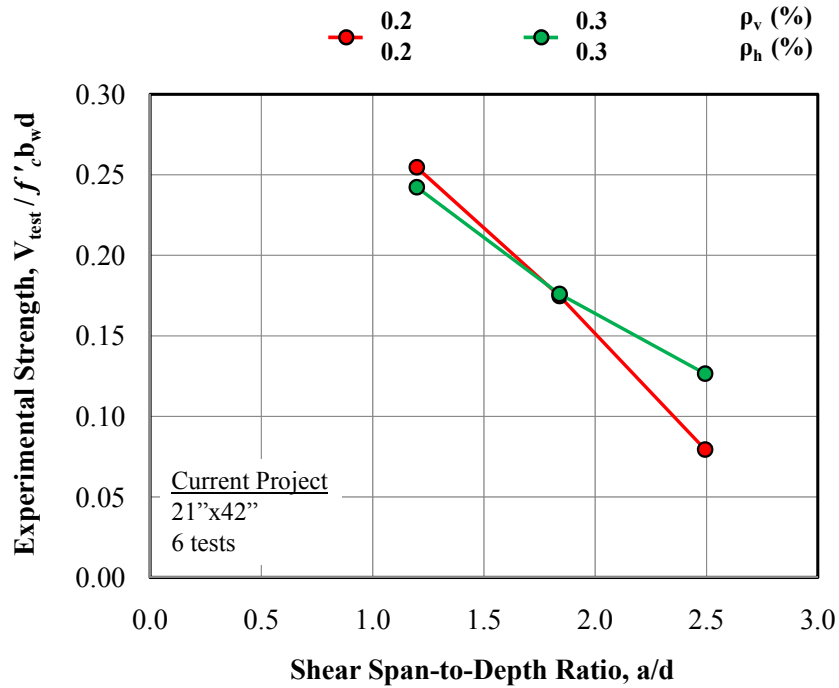


**Figure 5.4: Effect of  $a/d$  ratio on experimental strength of test specimens**

The pictures of the test regions at failure for the specimens represented by the red line in Figure 5.4 are displayed in Figure 5.5. It is important to emphasize that each of these specimens had identical reinforcement details (0.2% web reinforcement in each direction); the only difference among them was the  $a/d$  ratio. With increasing  $a/d$  ratio, a change in failure mode was evident. At an  $a/d$  ratio of 1.2, the failure of the specimen was the result of crushing along the diagonal strut and near the CCT nodal region. The orientation and number of the diagonal cracks was consistent with a single-panel strut-and-tie model in which the load is transferred to the support via an inclined strut. At an  $a/d$  ratio of 1.85, a similar appearance at failure existed. At failure, crushing was visible along the strut and near both the CCC and CCT nodal regions. Parallel, inclined cracks formed along the axis of a direct strut from the load to the support. The final failure crack slightly resembled the shape of an “S” which is customary to sectional shear failures. This detail may suggest that a portion of the shear is transferred by a sectional-shear mechanism at an  $a/d$  ratio of 1.85. However, it is evident from the amount of parallel cracking and local crushing in Figure 5.5 that a direct-strut mechanism still

governs at this  $a/d$  ratio. At an  $a/d$  ratio of 2.5, a completely different appearance at failure was present. Virtually no parallel, diagonal cracking existed in the shear span. The behavior of the specimen was dominated by a single, diagonal tension crack that formed an S-shape between the load and the support. Some local crushing was visible along the diagonal crack, but it was not due to crushing of the concrete, but rather the shearing of the interfaces between each side of the diagonal tension crack. It is clear from the behavior of this specimen (III-2.5-02) that at an  $a/d$  ratio of 2.5, the dominant mechanism of shear transfer is consistent with a sectional-shear model.

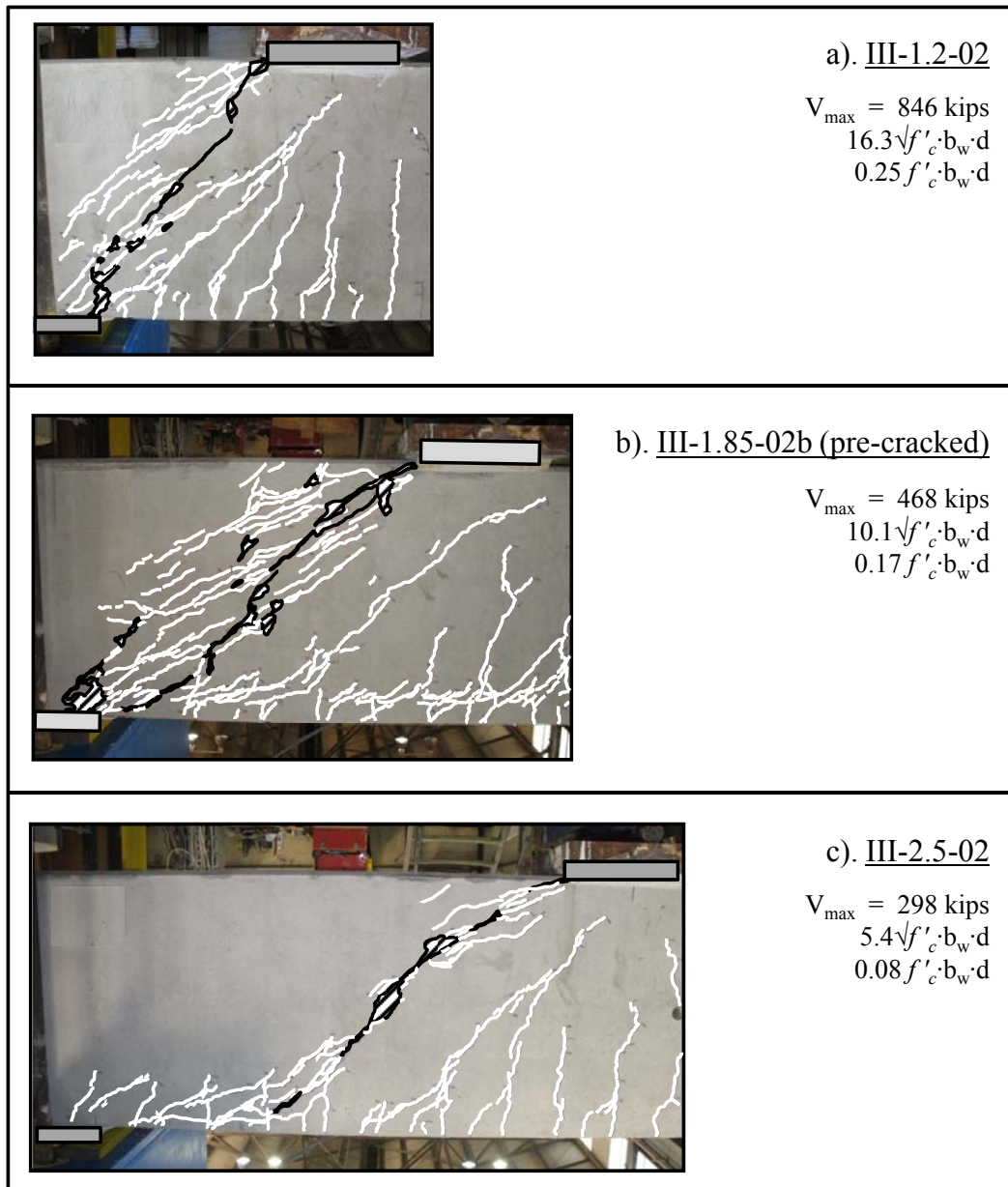


**Figure 5.5: Failure pictures of test specimens with 0.2% reinforcement and variable  $a/d$**

The pictures of the test regions at failure for the specimens representing the green line in Figure 5.4 are displayed in Figure 5.6. As before, the primary difference between the specimens was the  $a/d$  ratio. Each specimen contained 0.3% web reinforcement in each direction. At an  $a/d$  ratio of 1.2, a similar appearance at failure to the specimen with

0.2% reinforcement was observed. The only difference was that the parallel cracking was better distributed, thereby reducing the width of the diagonal cracks (Section 4.3.3) and enabling more crushing to occur. At an  $a/d$  ratio of 1.85, the failure mode was consistent with the companion specimen with 0.2% reinforcement. Several parallel cracks extended from the load to the support. At the ultimate load, concrete in the CCC nodal region and within the strut crushed. The behavior of both specimens at an  $a/d$  ratio  $< 2$  was consistent with a single-panel, direct strut transfer mechanism. At an  $a/d$  ratio of 2.5, a remarkable difference in performance with respect to the specimen with 0.2% web reinforcement was observed. The only difference between these two specimens (III-2.5-02 and III-2.5-03) was the size of the web reinforcement (#4 versus #5 bars). The spacing of the stirrups ( $s_v$ ) was identical at 9.5 in. The additional reinforcement in III-2.5-03 helped distribute the diagonal cracks such that the failure of the specimen was due to crushing along the diagonal strut and near the load plate. This switch in failure mode was accompanied by an increase in the shear strength by approximately 60%. This performance suggests that at an  $a/d$  ratio of 2.5, a significant portion of the applied load is transferred to the support by a sectional-shear mechanism since additional reinforcement increased the capacity.

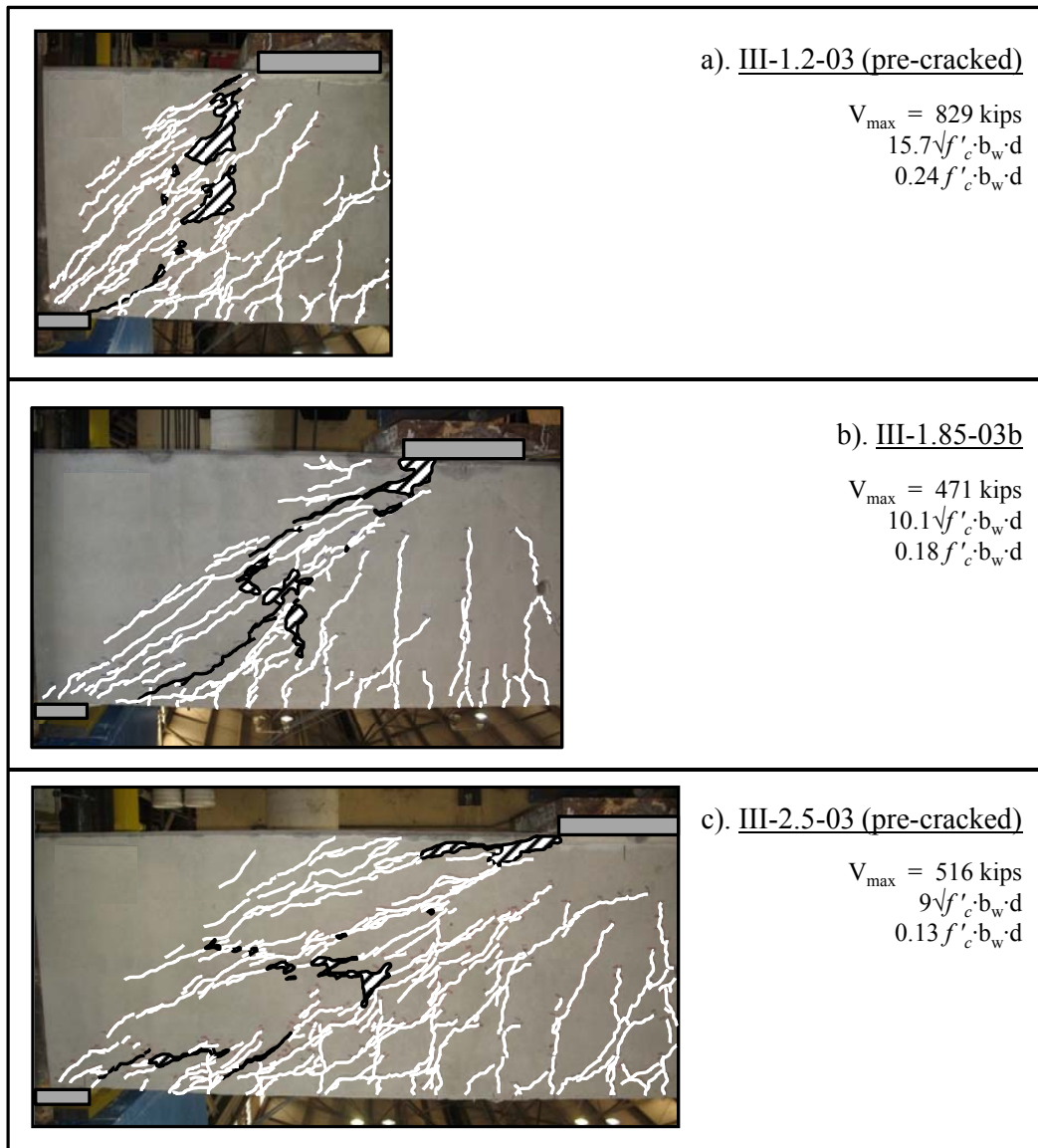


**Figure 5.6: Failure pictures of test specimens with 0.3% reinforcement and variable  $a/d$**

The results of the six tests displayed in Figure 5.5 and Figure 5.6 show that the transition from deep-beam to sectional-shear behavior does not occur at a distinct  $a/d$  ratio. Rather, it is a gradual process in which the effectiveness of one mechanism reduces with respect to the other. The results of these six tests support the idea that the quantity of web reinforcement affects the behavior and strength as the  $a/d$  ratio exceeds 2. This finding is in agreement with results from the database presented in Section 4.3.2 that

showed at  $a/d$  ratios greater than 2, the quantity of web reinforcement increases the strength of the member. Also, the results of these six tests show that at an  $a/d$  ratio less than 2, the quantity of web reinforcement does not affect the shear strength of the member provided that there is enough reinforcement to maintain equilibrium in the diagonal, bottle-shaped strut (Section 4.3.2).

The results of the 21"x75" tests provided additional data to understand the effect of  $a/d$  ratio on the shear behavior of reinforced concrete beams. In both of these members, the extreme layer of the longitudinal reinforcement was instrumented with strain gauges along the entire length of the beam (Section 3.5.1). The purpose of the instrumentation was to monitor the strain in the reinforcement at different locations along the shear span. These strain data were used to correlate the behavior of the specimen with the most appropriate type of shear model. For example, in a single-panel strut-and-tie model (STM) in which a direct strut carries the applied load to the support, the force in the tension tie is constant along the length of the shear span. Conversely, in a multiple-panel STM, the force in the tie reduces as a step function due to the intermittent compression diagonals along the shear span. In the case of a Bernoulli beam, in which a sectional shear model is used for shear design, the force in the tie varies approximately according to the moment diagram. These distributions of tensile force are illustrated in Figure 5.7. It is clear that the change in tie-force of a multiple-panel model is an approximation of the gradual decline of the tension force consistent with a Bernoulli beam. For a slender beam with well-distributed stirrups, the change in tie force according to a Bernoulli beam analysis and a multiple-panel STM analysis should be equivalent. Therefore, the data from the strain gauges along the longitudinal reinforcement in the test specimens were used to evaluate the governing shear transfer mechanism as the  $a/d$  ratio changed from 1.2 to 1.85 to 2.5. It is important to note that several researchers have measured strain in this fashion for similar purposes (Moody et al., 1954, Watstein and Mathey, 1958, Rogowsky et al., 1986, Quintero Febres et al., 2006, and Tan et al., 2007).

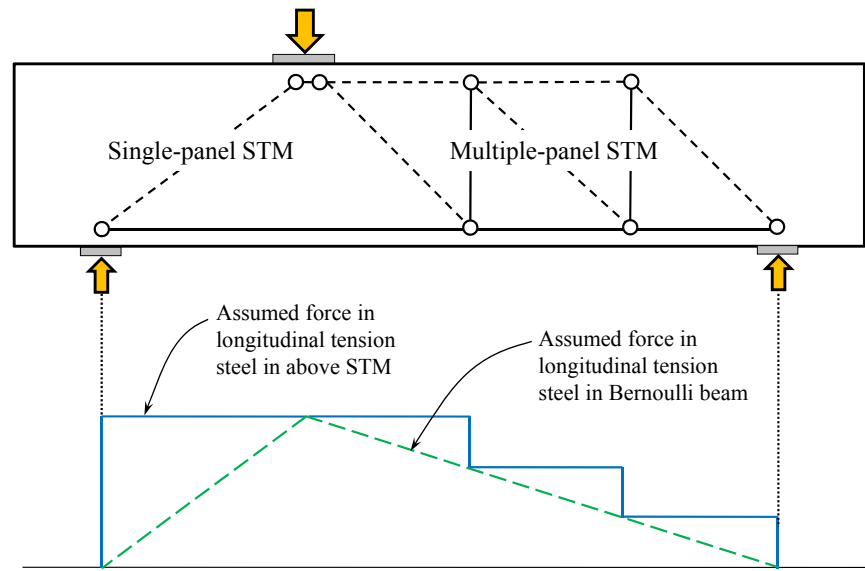


**Figure 5.7: Distribution of force in longitudinal tension steel along length of beam according to different shear models**

The strain measurements in the longitudinal steel for IV-2175-1.85-02 and IV-2175-1.85-03 are displayed in Figure 5.8. Recall from Section 3.6 that for the 21"x75" beams, two tests were conducted simultaneously. After one shear span failed, external, post-tensioned clamps strengthened the failed span; and the beam was re-loaded in the same arrangement. For the beam in Figure 5.8, the load was applied at midspan such that two tests were conducted at an  $a/d$  ratio of 1.85. The difference in the two tests was the quantity of web reinforcement. Strain gauges were applied on the extreme layer of tension reinforcement at midspan (beneath the load point) and at three locations along each shear span. The gauges closest to the support were located far enough away from the edge of the bearing plate to avoid any detection of local effects at the support, but close enough to represent the last probable location of a vertical tie in a multiple-panel STM. The gauges were placed near stirrups since it was observed in previous tests that cracks tended to form at the location of stirrups, and strain gauge data were generally more reliable near cracks. Two of the six longitudinal bars were instrumented in this fashion. One set of results is depicted in Figure 5.8, although the data were consistent for both sets. The strain measurements are plotted along the length of the specimen at three

different levels of applied load for the first test on this beam. At each load level, calculated strain values along the length of the beam are also provided. The calculated strain in the tension tie of a single-panel, strut-and-tie model is constant over the entire member. It is depicted for each load level as a dashed line in Figure 5.8 and will subsequently be referred to as  $\epsilon_{I\_STM}$ . The calculated strain in the reinforcement for a Bernoulli beam was also plotted in Figure 5.8 for each load level. This strain is identical to the strain in the tension tie of a single-panel STM at the applied load but varies approximately with the moment diagram, reaching zero at the supports. This strain will subsequently be referred to as  $\epsilon_{BEAM}$ .

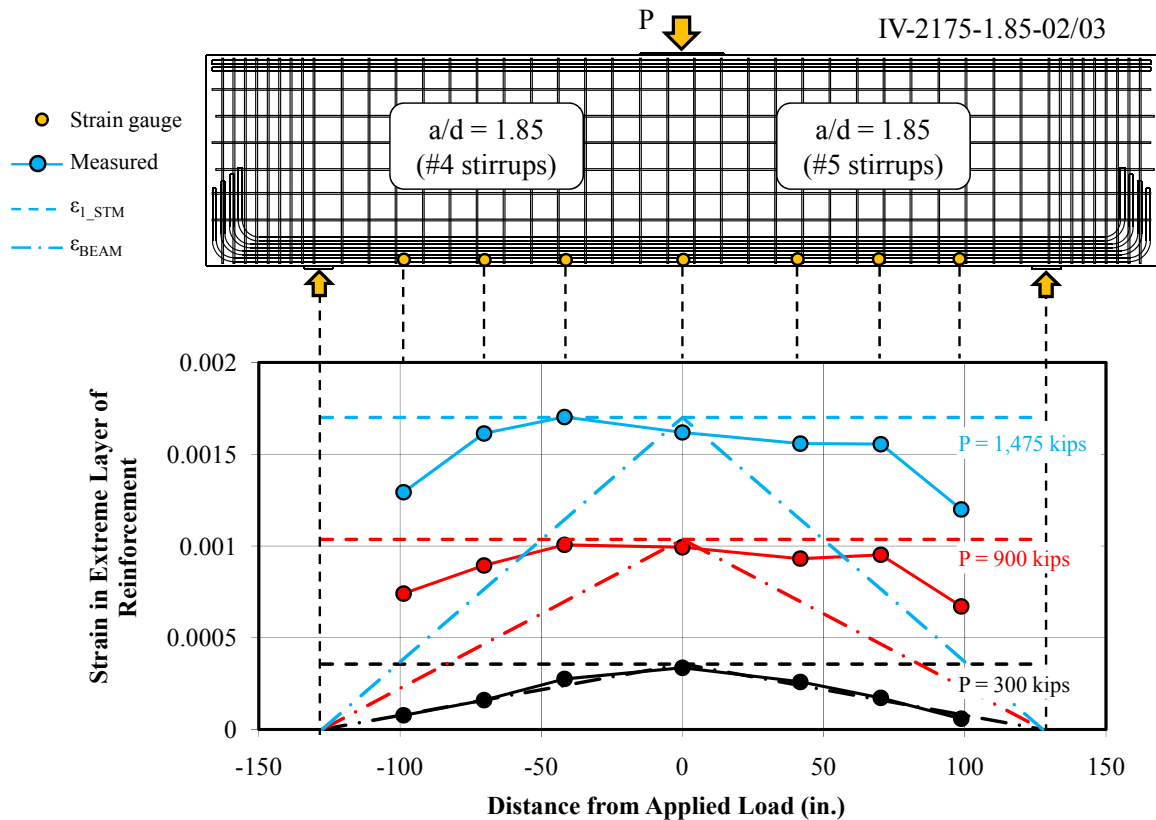


**Figure 5.8: Comparison of measured and calculated strain along the length of specimen with  $a/d$  of 1.85**

At an applied load of 300 kips (black lines in Figure 5.8), the beam had not developed diagonal cracks. The measured strain in the reinforcement matched the



assumed strain from a Bernoulli beam analysis. This finding matched a previous observation by Moody, Viest, Elstner, and Hognestad (1954):

*Until diagonal tension cracks form, the stresses in the tension steel and in the concrete are distributed along the length of the beam in the same way as the external moments so that these stresses at any section are approximately proportional to the moment at that particular section. The formation of diagonal tension cracks changes these relationships. Such changes are called the redistribution of internal stresses.*

At an applied load of 900 kips (well after diagonal cracking), the measured strains close to the load point were consistent with the calculated strain according to a single-panel, STM analysis. Further along each shear span, however, the measured strain gradually reduced. The reduction is an indication that a portion of the applied load is being transferred to the support via a multiple-panel or sectional shear model.

A similar distribution of measured strain exists along the member at an applied load of 1475 kips (ultimate for IV-2175-1.85-02 and at 90% of ultimate for IV-2175-1.85-03). The measured strain slightly reduces along the length of the shear span suggesting that a portion of the load was being transferred to the supports via a sectional shear model. It is clear that the measured strain in the two gauges adjacent to the supports is closer to  $\epsilon_{I\_STM}$  than  $\epsilon_{BEAM}$ . In fact, the difference between the measured strain and  $\epsilon_{I\_STM}$  is approximately 1/3 of the total difference between  $\epsilon_{I\_STM}$  and  $\epsilon_{BEAM}$ . This reduction implies that approximately 1/3 of the load is being transferred to the support with a sectional shear model. The results presented in Figure 5.8 suggest that at an a/d ratio of 1.85, the primary shear transfer mechanism is a single-panel, direct strut mechanism. However, a portion of the load (approximately 1/3) is being transferred via a sectional shear model signifying that the transition from deep beam behavior to sectional shear behavior has begun. If the measured strain along the length of the member was equal to the calculated Bernoulli beam strain, it would indicate that the full shear is transferred by a multiple-panel or sectional shear model.

The strain measurements in the longitudinal steel for IV-2175-1.2-02 and IV-2175-2.5-02 are displayed in Figure 5.9. As in the other 21"x75" beam, two tests were

conducted simultaneously. In this case, the difference between the two tests was the  $a/d$  ratio. The depth of the beam was calibrated with the length of the test setup to achieve this arrangement. Strain gauges were applied to the extreme layer of the tension reinforcement at the location of the load point and along each shear span. As before, gauges were placed reasonably close to the supports to capture any effect of sectional shear behavior without being influenced by local stress conditions at the support.

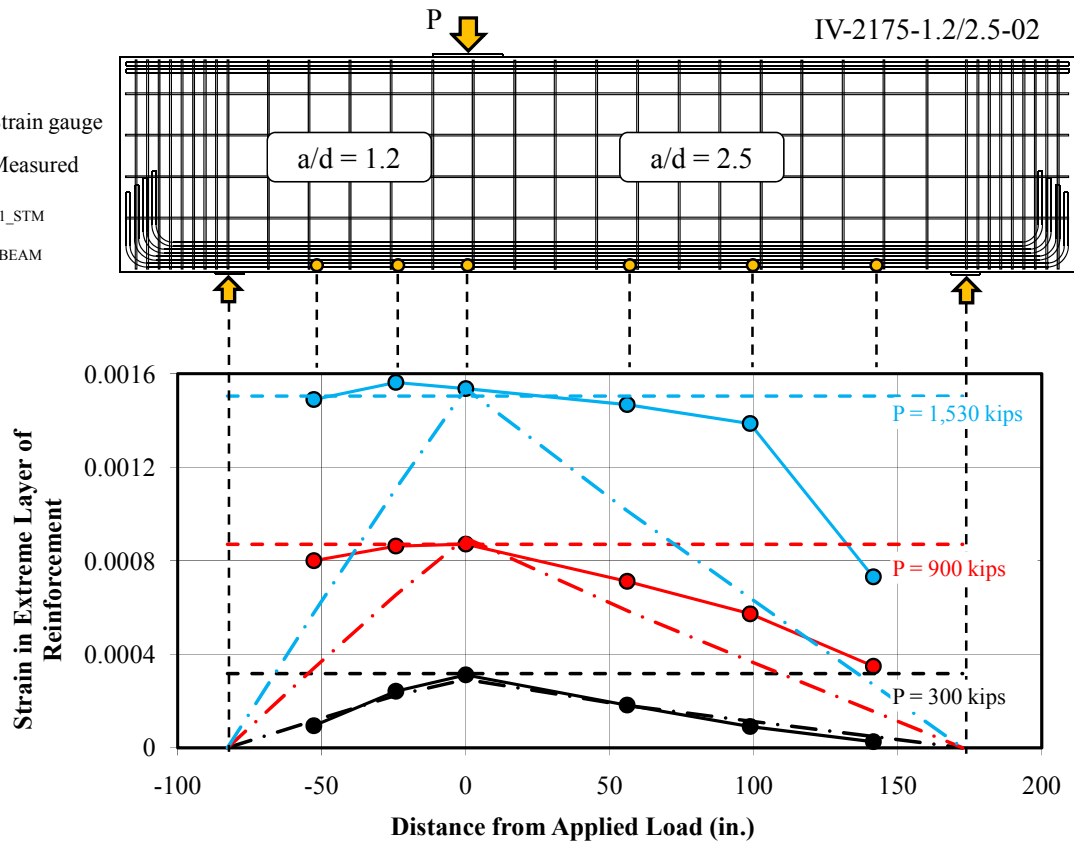


**Figure 5.9: Comparison of measured and calculated strain along length of specimen with  $a/d$  of 1.2 and 2.5**

At an applied load of 300 kips, the beam had not yet diagonally-cracked; and the measured strain in the longitudinal reinforcement matched  $\epsilon_{BEAM}$  along the entire length of the member. This observation was consistent with the results of the previous 21"x75" beam.

After the redistribution of internal stresses due to diagonal cracking, the measured strains depart from  $\epsilon_{\text{BEAM}}$  in both shear spans. At an applied load of 900 kips and 1,500 kips, a similar distribution of the strain in the reinforcement exists along the beam. At 1,500 kips, the shear span with an  $a/d$  ratio of 2.5 was at ultimate; whereas the shear span with an  $a/d$  ratio of 1.2 was at approximately 83% of ultimate. In the span with an  $a/d$  ratio of 1.2, the measured strains are very similar to  $\epsilon_{\text{I\_STM}}$ . This suggests that the shear in the short span was transferred to the support solely by a single-panel strut-and-tie model. On the contrary, in the span with an  $a/d$  ratio of 2.5, the measured strains are closer to  $\epsilon_{\text{BEAM}}$  than to  $\epsilon_{\text{I\_STM}}$ . By inspection, the difference between the measured strain and  $\epsilon_{\text{I\_STM}}$  is approximately 2/3 of the total difference between  $\epsilon_{\text{I\_STM}}$  and  $\epsilon_{\text{BEAM}}$ . These data suggest that approximately 2/3 of the shear in the long-shear span ( $a/d = 2.5$ ) was transferred to the support via a sectional-shear mechanism. Approximately 1/3 of the shear was transferred to the support by a mechanism consistent with a single-panel STM. Thus, from the data in Figure 5.9, it is evident that the dominant shear transfer mechanism has transitioned to a sectional shear mechanism at an  $a/d$  ratio of 2.5.

It is clear from the results in Figure 5.8 and Figure 5.9 that the transition between the dominant shear transfer mechanisms near an  $a/d$  ratio of 2 is a gradual process. This finding is consistent with the results presented in Figure 5.5 and Figure 5.6 for the 21"x42" specimens. It was shown that at an  $a/d$  ratio of 1.2, the shear was transferred to the support solely by a single-panel, direct-strut mechanism. At an  $a/d$  ratio of 1.85, evidence of the initiation of sectional shear behavior was observed; however, the dominant transfer mechanism was still consistent with a single-panel STM. At an  $a/d$  ratio of 2.5, the dominant shear transfer mechanism was consistent with a sectional shear model; however, a portion of the applied load was transferred by a single-panel STM.

From a design standpoint, the results in this section can be used to determine the most appropriate shear design model for a given  $a/d$  ratio. Clearly, for an  $a/d$  ratio of 1.2, a single-panel strut-and-tie model is the most suitable choice. For an  $a/d$  ratio of 1.85, a single-panel model is also the most appropriate choice, but to a slightly lesser extent. It can be argued that two overlapping models should be used. A single-panel STM could be

designed to carry 2/3 of the applied load, and a two-panel STM or a sectional shear model could be designed to carry 1/3 of the applied load. While this approach sounds attractive in theory, it is more difficult than using a single-panel STM for the total applied load; and it may be inappropriate. In the case of these two models, stresses are concentrated in the nodal regions. The capacity of the nodal regions cannot be double-counted or unchecked because different models are used. Since it is known that at an  $a/d$  ratio less than 2, the conditions in the nodal regions often govern the behavior, they should be emphasized in the design. Therefore, a single-panel strut-and-tie model should be used to design beams with an  $a/d$  ratio of 1.85. It is fairly simple; it appropriately accounts for the stress concentrations in the nodal regions due to the *total* applied load; and it is consistent with the dominant shear transfer mechanism.

For an  $a/d$  ratio of 2.5, it was shown that the dominant transfer mechanism is more consistent with a sectional shear model than a single-panel STM. The implications of using a single-panel model for a beam with an  $a/d$  ratio of 2.5 were discussed in Section 4.3.2. In that section, for the specimens tested as part of the depth effect series (Series IV), the experimental strength was compared to the calculated strength with a single-panel strut-and-tie model. For the beams with an  $a/d$  ratio of 1.2 and 1.85, there was a consistent level of reserve strength ( $V_{\text{test}} / V_{\text{calc.}}$ ) as the section size increased since the failure mode of these specimens reasonably matched the assumed behavior in the STM. For the beams with an  $a/d$  ratio of 2.5, however, there was not a uniform level of conservatism. The failure mode of these specimens was more consistent with a sectional shear model than a single-panel STM model. The results are replotted in Figure 5.10 for quick reference.

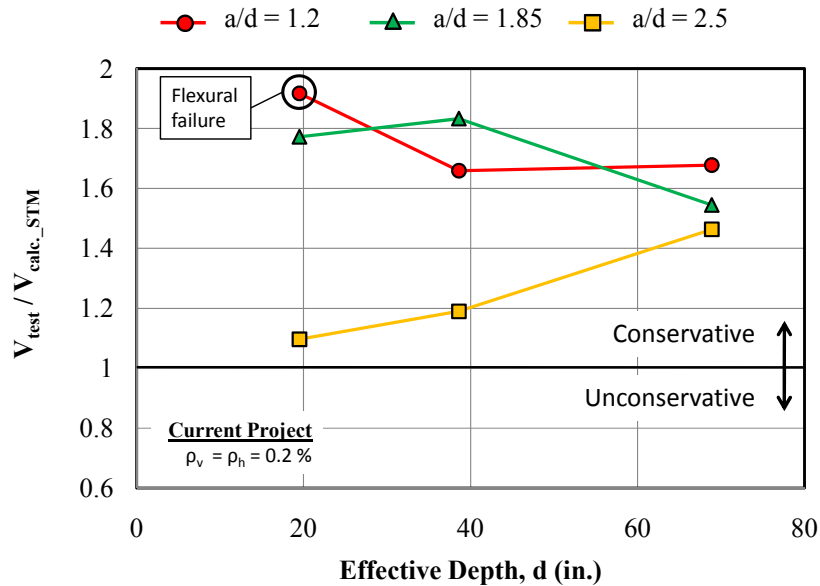


**Figure 5.10: Experimental strength divided by calculated strength for depth effect specimens**

As illustrated in Figure 5.10, the experimental strength of the specimens tested at an  $a/d$  ratio of 2.5 was conservatively estimated even though the failure mode of the specimens was more consistent with a sectional shear model. These results illustrate the inherent conservatism of the strut-and-tie modeling procedure. However, the difference in the level of conservatism between the beams tested at an  $a/d$  ratio of 2.5 and that of the deep beams ( $a/d < 2$ ) indicates that a single-panel STM should be used with caution when the  $a/d$  ratio exceeds 2. It is likely that the size of the bearing plates relative to the section size contributed to the decline in the level of conservatism as the effective depth decreased for the specimens with an  $a/d$  ratio of 2.5.

It was shown by Tuchscherer (2008) that the TxDOT Project 5253 efficiency factors were developed using the evaluation database which consisted of beams with  $a/d$  ratios up to 2.5 (Section 2.3.4.4). A single-panel strut-and-tie model was used to analyze all of the specimens. With the Project 5253 efficiency factors and the use of non-hydrostatic nodes, conservative and reasonably accurate estimates of strength were obtained. This finding further indicates that the inherent conservatism in strut-and-tie

modeling can account for some differences between the strut-and-tie model and the actual behavior of the member.

Therefore, it can be concluded that the transition from deep beam behavior to sectional shear behavior near an  $a/d$  ratio of 2 is a gradual process. The experimental results indicate that for an  $a/d$  ratio up to 1.85, the dominant shear transfer mechanism is consistent with a single panel strut-and-tie model. Due to the inherent conservatism in strut-and-tie modeling, it is appropriate to extend this finding up to an  $a/d$  ratio of 2. Thus, it is recommended that a single-panel strut-and-tie model be used to design deep beam regions with  $a/d$  ratios from 0 to 2. At  $a/d$  ratios above 2, the use of a single-panel strut-and-tie model gradually becomes less appropriate. Up to an  $a/d$  ratio of 2.5, a single-panel STM can estimate the experimental strength conservatively. However, the amount of conservatism in the strength estimate was greatly reduced with respect to that of the deep beam specimens ( $a/d < 2$ ). These findings are consistent with the current division of deep beam behavior ( $a/d \leq 2$ ) and sectional shear behavior ( $a/d \geq 2$ ) present in AASHTO LRFD (2008) and ACI 318-08.

### **5.2.3 Reducing Discrepancy between Shear Models at $a/d$ ratio of 2.0**

The discrepancy in the calculated strength of a member loaded near an  $a/d$  ratio of 2 using the STM and the sectional shear provisions in AASHTO LRFD (2008) is the result of a fundamental deficiency in the AASHTO LRFD STM provisions.

As discussed in the previous section (Section 5.2.2), it is known that the strength of deep beams decreases as the  $a/d$  ratio increases. This decline is due to the reduction in the effectiveness of a direct-strut mechanism as the  $a/d$  ratio increases. An appropriate model to design deep beams should account for this reduction. In the STM provisions in AASHTO LRFD (2008), the decline in strength with increasing  $a/d$  ratio is accounted for with a variable strut efficiency factor. As shown in Section 2.3.4.1, the efficiency factor of the strut at a CCT node is a function of the principle tensile strain in cracked concrete which, in turn, is related to the tensile strain in the direction of the tie at the CCT node. As the diagonal strut framing into a CCT node becomes shallower ( $a/d$  increases), the tensile strain in the tie increases and the efficiency factor decreases. The reduction in the

efficiency factor accounts for the decline in the strength with increasing  $a/d$  ratio (or decreasing strut angle).

If the AASHTO LRFD node-to-strut interface efficiency factor is used with hydrostatic nodes that increase with increasing  $a/d$  ratio (Figure 2.13 and Figure 5.11), the reduction in strength is mitigated to acceptable levels. When the efficiency factor is used with non-hydrostatic nodes, overly conservative estimates of strength are calculated. The reason is that the node-to-strut interface of a non-hydrostatic node, with a constant bearing plate dimension and back face dimension, decreases with increasing  $a/d$  ratio as shown in Figure 5.11. Thus, when using the STM provisions of AASHTO LRFD (2008) with non-hydrostatic nodes, the decline in strength with  $a/d$  ratio is counted for *twice*. Non-hydrostatic nodes are preferred in design since they are directly related to stress conditions in the member and do not have to satisfy stringent equal-stress requirements.

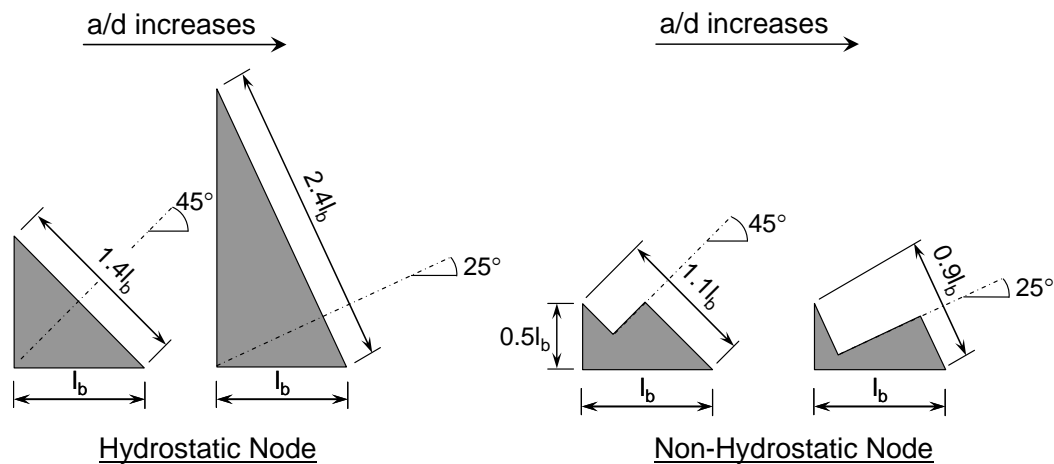


**Figure 5.11: Difference in node geometry with increasing  $a/d$  ratio for single-panel STM**

In the Project 5253 STM provisions presented in Section 2.3.4.3, the reduction in shear strength with increasing  $a/d$  ratio is accounted for solely with the reduction in the length of the node-strut interfaces. None of the Project 5253 efficiency factors vary with the  $a/d$  ratio. Thus, the reduction in strength with increasing  $a/d$  ratio is obtained in the

Project 5253 STM provisions by applying a constant efficiency factor (in terms of the  $a/d$  ratio) on a smaller length of the node-strut interface (Figure 5.11).

A comparison between the strength estimates for the beams in the evaluation database calculated using the AASHTO LRFD STM provisions and the Project 5253 STM provisions are depicted in Figure 5.12. For the 179 beams in the evaluation database, the experimental strength was divided by the calculated strength using a single-panel STM, non-hydrostatic nodes, and both the Project 5253 efficiency factors and those in AASHTO LRFD (2008). The results are plotted versus the  $a/d$  ratio to illustrate how increasing the  $a/d$  ratio affects the use of each set of provisions. It is important to note that the stress check at the CCT node-strut interface of AASHTO LRFD (2008) governs the capacity of the specimens in the database in nearly every case when the  $a/d \geq 1.5$ . A variety of design checks govern the capacity of the specimens calculated with the Project 5253 provisions.

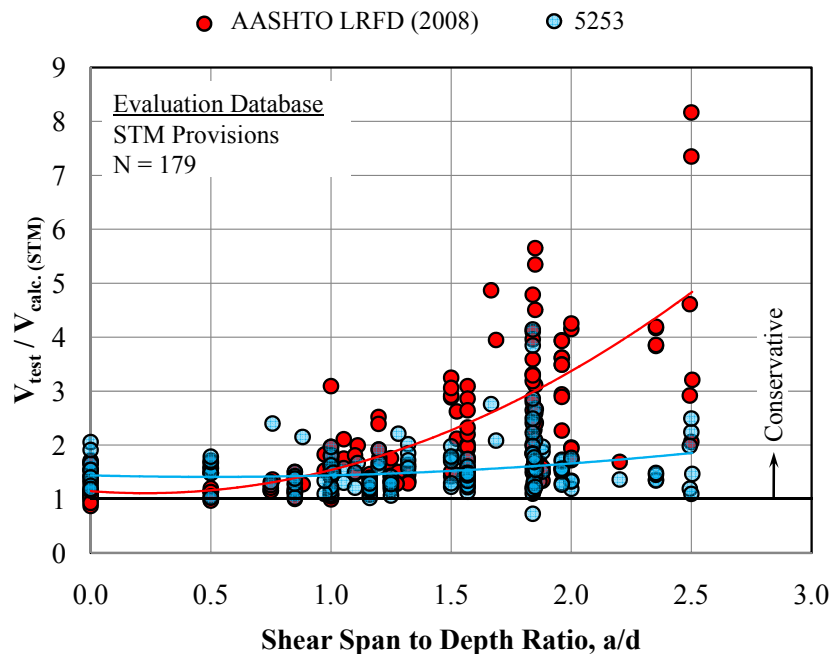


**Figure 5.12: Level of conservatism in STM provisions with increasing  $a/d$  ratio**

In Figure 5.12, at an  $a/d$  ratio  $\leq 1$ , the difference in the results from the Project 5253 STM provisions and those in AASHTO LRFD is negligible. In both procedures, a



fairly uniform level of conservatism exists. However, at  $a/d$  ratios approaching and exceeding 2, the difference in the results is substantial. Whereas a reasonably consistent amount of inherent conservatism ( $V_{\text{test}} / V_{\text{calc.}}$ ) exists with the use of the Project 5253 STM provisions, overly conservative estimates of capacity are calculated with the AASHTO STM provisions for  $a/d$  ratios ranging from 1 to 2.5. For instance, the capacity of a specimen at an  $a/d$  ratio of 2 is conservatively calculated with the AASHTO STM provisions by a factor of 4. The experimental capacity divided by the calculated capacity according to the Project 5253 STM provisions for the same beam is less than 2. Several examples such as these are illustrated in Figure 5.12. The consistent level of inherent conservatism provided by the Project 5253 STM provisions indicate that the primary variables that affect the strength of deep beams are appropriately accounted for. In general, the experimental strength was approximately 1.5 times the strength calculated using the Project 5253 STM provisions, which is appropriate for the scatter in deep beam shear strength. The unnecessary amount of conservatism that results with the use of the AASHTO LRFD (2008) STM provisions was the primary factor contributing to the large discrepancy in calculated shear capacity at the transition between deep beam and sectional shear behavior at an  $a/d$  ratio near 2.

To evaluate the difference in calculated shear strength between the Project 5253 STM provisions and the sectional shear provisions in AASHTO LRFD (2008), the sectional shear provisions need to be presented. When “it is reasonable to assume that plane sections remain plane” ( $a/d > 2$ ), the shear capacity of a member can be determined as the summation of a concrete component,  $V_c$ , and a stirrup component,  $V_s$  (AASHTO LRFD, 2008). This model is based on the free-body diagram presented as Figure 5.13. The shear at the diagonal tension crack is resisted by the stirrups crossing the diagonal crack and three different mechanisms of shear transfer that is lumped into the concrete contribution  $V_c$ . These mechanisms include the shear resistance of the concrete in the compression zone, aggregate interlock across the diagonal crack, and dowel action from the longitudinal reinforcement. It is important to note that this sectional shear model

differs from a multiple-panel STM in that no contribution from the concrete is recognized in the latter.

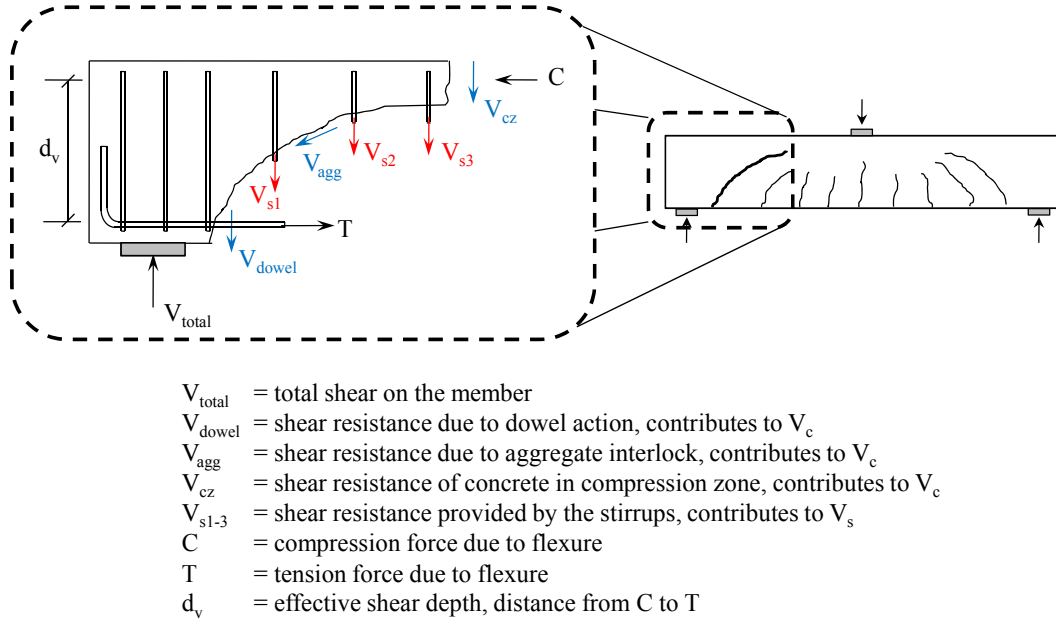


**Figure 5.13: Free-body diagram used as basis for sectional shear model**

The sectional shear provisions in AASHTO LRFD (2008) are presented as the following:

The nominal shear resistance,  $V_n$ , shall be determined as the lesser of:

$$V_n = V_c + V_s + V_p \quad (5.1)$$

$$V_n = 0.25 f'_c b_v d_v + V_p \quad (5.2)$$

in which:

$$V_c = 0.0316 \beta \sqrt{f'_c} b_v d_v \quad (5.3)$$

$$V_s = \frac{A_v f_y d_v \cot \theta}{s} \quad (5.4)$$

(oriented 90 deg. with longitudinal axis)

where  $f'_c$  = compressive strength of concrete (ksi)

$b_v$  = effective web width within  $d_v$  (in.)

- $d_v$  = effective shear depth, taken as the distance between the resultants of the tensile and compressive forces due to flexure (in.)
- $V_p$  = component of the prestressing force in direction of applied shear (kips)
- $\beta$  = factor indicating the ability of diagonally-cracked concrete to transmit tension and shear, assumed equal to 2 per article 5.8.3.4.1
- $A_v$  = area of shear reinforcement within distance  $s$  (in.<sup>2</sup>)
- $f_y$  = yield strength of shear reinforcement (ksi)
- $\theta$  = angle of inclination of diagonal compressive stresses, assumed equal to 45 degrees per article 5.8.3.4.1
- $s$  = spacing of stirrups (in.)

For comparison purposes, the equations for  $V_c$  and  $V_s$  in ACI 318-08 are presented as well:

The nominal shear resistance,  $V_n$ , shall be determined as the lesser of:

$$V_n = V_c + V_s \quad (5.5)$$

$$V_n = V_c + 8\sqrt{f'_c} b_w d \quad (5.6)$$

in which:

$$V_c = 2\lambda\sqrt{f'_c} b_w d \quad (5.7)$$

$$V_s = \frac{A_v f_{yt} d}{s} \quad (5.8)$$

where  $f'_c$  = compressive strength of concrete (psi)

$b_w$  = width of web (in.)

$d$  = effective depth, taken as the distance from extreme compression fiber to centroid of longitudinal tension reinforcement (in.)

$\lambda$  = modification factor for lightweight concrete

$A_v$  = area of shear reinforcement within distance  $s$  (in.<sup>2</sup>)

$f_{yt}$  = yield strength of shear reinforcement (ksi)

s = spacing of stirrups (in.)

The sectional shear provisions in AASHTO LRFD (2008) and ACI 318-08 are similar provided that the AASHTO LRFD simplified procedure for nonprestressed sections (Article 5.8.3.4.1) is used. It was determined that the simplified procedure was more appropriate for this analysis due to the difficulty in calculating  $V_c$  and  $V_s$  according to the general procedure. In the general procedure,  $\beta$  and  $\theta$  are not constant; they are a function of  $\epsilon_s$ , the strain in the longitudinal tension reinforcement.  $\epsilon_s$  is a function of  $M_u$  and  $V_u$ , the factored design forces on the section under consideration. Since design forces are not available for an experimental test, an assumption is required to calculate  $M_u$  and  $V_u$ . One assumption is to equate  $M_u$  and  $V_u$  to  $\phi M_n$  and  $\phi V_n$ . This assumption creates a circular reference which can be solved through iteration. The problem with this assumption is that it is equivalent to the worst-case scenario in which the reduced capacity exactly equals the factored forces. In addition, the general procedure is much more complicated than the simplified procedure. From a design perspective, it seems more likely that the requirements of the simplified procedure will be met for computational ease.

In the simplified procedure, a  $\beta$  of 2.0 and a  $\theta$  of 45 deg. are allowed if the member has a minimum amount of transverse reinforcement according to Equation 5.9. All of the beams in the evaluation database with a/d ratios between 2 and 2.5 satisfy the minimum reinforcement requirement.

$$A_v \geq 0.0316 \sqrt{f'_c} \frac{b_v s}{f_y} \quad (5.9)$$

where  $f'_c$  = compressive strength of concrete (ksi)

$b_v$  = effective web width within  $d_v$  (in.)

s = spacing of stirrups (in.)

$f_y$  = yield strength of shear reinforcement (ksi)

As in Figure 5.12, the experimental strength of the beams in the database can be compared to the calculated shear strength using the AASHTO LRFD (2008) and the ACI

318-08 sectional shear provisions. The experimental strength for each specimen is divided by the calculated strength and plotted versus the  $a/d$  ratio in Figure 5.14. It is clear from the results in Figure 5.14 and from the derivation of the sectional shear provisions that using  $V_c + V_s$  for beams with  $a/d$  ratios smaller than 2 is unacceptable. The model is completely inconsistent with the shear transfer mechanism. At  $a/d$  ratios between 2 and 2.5, however, there is a reasonable level of conservatism ( $V_{\text{test}} / (V_c + V_s)$ ) using both the AASHTO LRFD and the ACI 318 sectional shear provisions. It is interesting to note that the sectional shear provisions in ACI 318-08 estimate consistently higher shear capacity than those in AASHTO LRFD for the full-range of  $a/d$  ratios. Since the approximate procedure was used for the AASHTO LRFD provisions, the only difference between them and ACI 318 is the distance used for the effective depth of the section. In AASHTO LRFD, the depth is taken as the distance between the resultant of the compressive and tensile forces from a flexural analysis. In ACI 318-08, the depth is taken as the distance between the extreme compression fiber and the centroid of the longitudinal reinforcement. Thus, the depth used in the AASHTO LRFD equations is always less than that used in the ACI equations, which results in slightly more conservative estimates using AASHTO LRFD (2008).

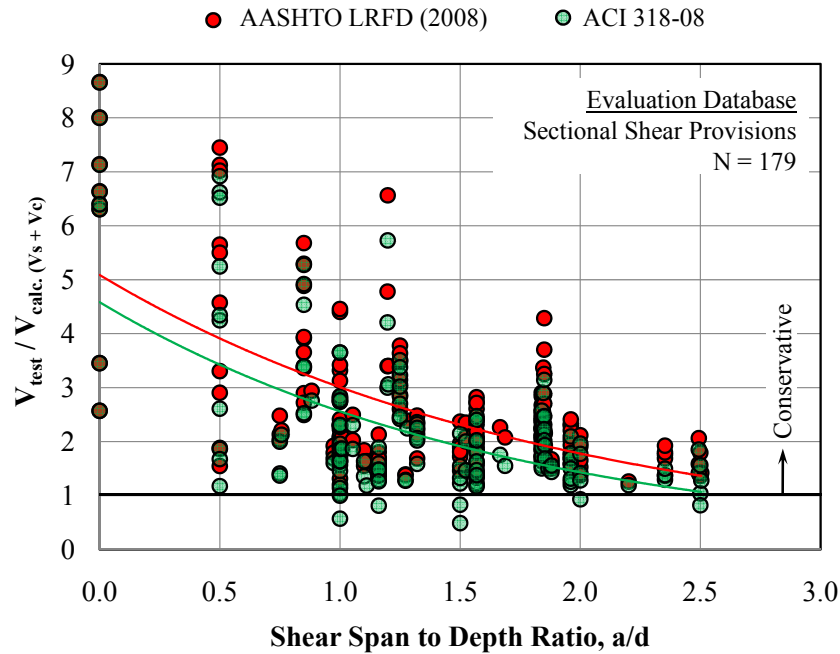


**Figure 5.14: Level of conservatism in sectional shear provisions with increasing  $a/d$  ratio**

From the results in Figure 5.14 and from the experimental program presented in Section 5.2.2.2, it is evident that only the beams with  $a/d$  ratios between 2 and 2.5 should be used to evaluate sectional shear provisions. There are 25 beams in the evaluation database that meet this criterion. Using the data from these specimens, the level of conservatism consistent with the sectional shear provisions in AASHTO LRFD (2008) and ACI 318-08 can be determined. This amount of conservatism can be compared to the amount of conservatism when using the Project 5253 STM provisions for beams with  $a/d$  ratios between 0 and 2. In this way, the discrepancy, if any, in the amount of inherent conservatism ( $V_{\text{test}} / V_{\text{calc.}}$ ) between the Project 5253 STM provisions and the sectional shear provisions in AASHTO LRFD and ACI 318 can be assessed. The experimental shear strength of the 25 beams in the evaluation database tested at  $a/d$  ratios between 2 and 2.5 are divided by the shear strength calculated with the sectional shear provisions in AASHTO LRFD and ACI 318 in Figure 5.15. The results are plotted versus the ratio of

$V_s/V_c$  to determine if this variable has any effect on the conservatism of the sectional shear provisions.

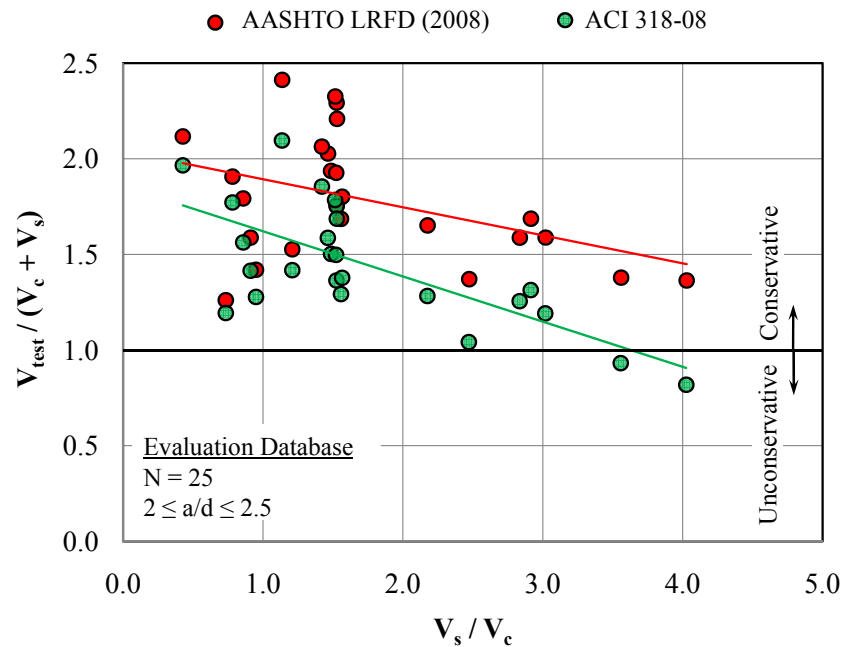


**Figure 5.15: Level of conservatism in sectional shear provisions for  $a/d$  ratios between 2 and 2.5**

The results in Figure 5.15 indicate that the sectional shear provisions in AASHTO LRFD conservatively estimate the strength of beams with an  $a/d$  ratio between 2 and 2.5 for a wide range of  $V_s/V_c$  ratios. While there is a downward trend in the red data in Figure 5.15, the lower bound indicates a fairly consistent level of inherent conservatism. The level of conservatism in Figure 5.15 for the AASHTO LRFD sectional shear provisions can be compared to the level of conservatism for the Project 5253 STM provisions at an  $a/d$  ratio near 2. From the data presented in Figure 5.12 at an  $a/d$  ratio of 2, the experimental shear strength was on average approximately 1.5 times the strength calculated with the Project 5253 STM provisions. This level of conservatism is reasonably consistent with the estimates from the AASHTO LRFD sectional shear provisions displayed in Figure 5.15, especially at  $V_s/V_c$  ratios between 2 and 4.

Therefore, at an  $a/d$  ratio near 2, the Project 5253 STM provisions and the AASHTO LRFD sectional shear provisions provide reasonably consistent levels of conservatism.

The results in Figure 5.15 in which the ACI sectional shear provisions were used to estimate shear strength (green data points) show a downward trend with the  $V_s/V_c$  ratio. When the  $V_s/V_c$  ratio is less than 2, a comparable level of conservatism exists between the ACI sectional shear provisions and the Project 5253 STM provisions ( $\sim 1.5$ ). At higher ratios of  $V_s/V_c$ , the level of conservatism when using the ACI sectional shear provisions decreases for beams with an  $a/d$  ratio between 2 and 2.5. These data suggest that at an  $a/d$  ratio near 2, the stirrup contribution to the total shear capacity of the member should be limited since the member is transitioning from deep beam behavior to sectional shear behavior. It may not be prudent to rely on a large amount of shear capacity from the stirrups at  $a/d$  ratios near 2.

It should be noted that the current study did not explicitly address the suitability of the sectional shear provisions in AASHTO LRFD (2008) or ACI 318-08. The sectional shear provisions in each specification were used to determine the appropriate level of conservatism that the Project 5253 STM provisions should target at an  $a/d$  ratio near 2. The results in Figure 5.15 indicate that the AASHTO sectional shear provisions, namely the use of an effective shear depth, may capture the behavior of beams at an  $a/d$  ratio between 2 and 2.5 better than the ACI sectional shear provisions. However, more research is needed in this area to reach a firm conclusion.

The results in Figure 5.12 and Figure 5.15 show that in terms of inherent conservatism ( $V_{\text{test}} / V_{\text{calc.}}$ ), there is a relatively smooth transition between the Project 5253 STM provisions and the AASHTO LRFD (2008) sectional shear provisions. The transition is not as smooth when the ACI 318-08 sectional shear provisions are used especially at high  $V_s/V_c$  ratios. The transition between design models can also be addressed strictly from a design perspective. That is, the design strength calculated with STM and sectional shear provisions can be compared for the beams in the database as shown in Figure 5.16.



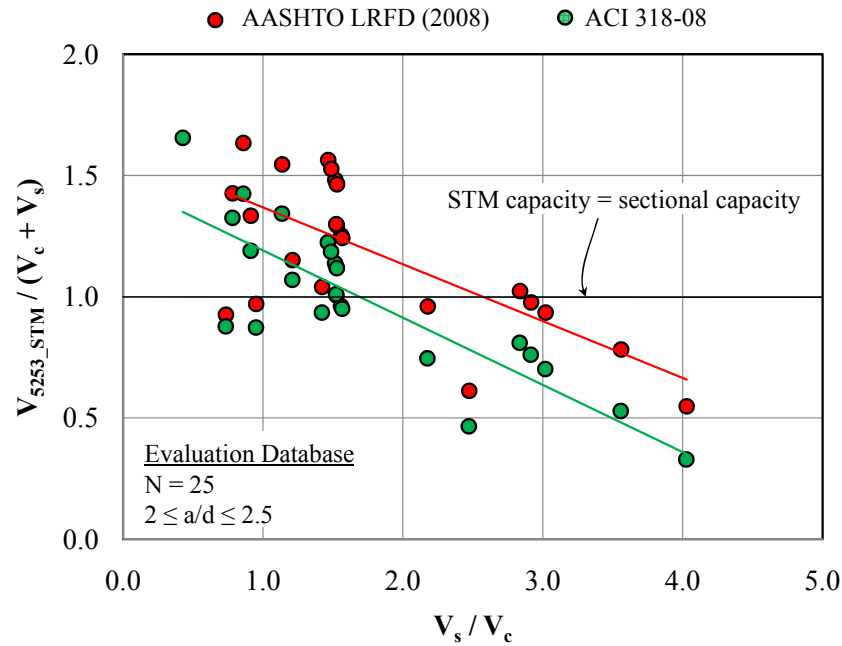


**Figure 5.16: Comparison of calculated capacity: Project 5253 STM vs. sectional shear**

In Figure 5.16, the Project 5253 STM calculated capacity is divided by the sectional shear capacity calculated according to AASHTO LRFD (2008) and ACI 318-08 for the 25 beams in the evaluation database with an  $a/d$  ratio between 2 and 2.5. The data are plotted versus the  $V_s/V_c$  ratio. The data indicate that with increasing  $V_s/V_c$  ratio, the calculated sectional shear capacity becomes larger than the calculated Project 5253 STM capacity. This finding is expected since the sectional shear provisions are a function of the stirrup contribution ( $V_s$ ) whereas the Project 5253 STM capacity is a function of a single-panel strut-and-tie model. In both cases, the Project 5253 STM capacity is closest to the sectional shear capacity at a  $V_s/V_c$  ratio near 2, albeit with a considerable amount of scatter. Thus, from a design perspective, limiting the ratio of  $V_s/V_c$  to 2 is recommended to reduce the discrepancy between shear strength calculated with STM and sectional shear provisions near for  $a/d$  ratios between 2 and 2.5. It is interesting to note that limiting the  $V_s/V_c$  ratio may also be beneficial for reducing diagonal crack widths in service as discussed in Section 4.3.3.1.

#### 5.2.4 Design Implications

The results in this section indicate that a single-panel STM should be used with the Project 5253 STM provisions for members with an  $a/d$  ratio less than 2. A single-panel model is consistent with the dominant shear transfer mechanism and is easy to apply. Multiple panel strut-and-tie models are not recommended for beams with  $a/d$  ratios less than 2. They are inconsistent with the dominant shear transfer mechanism and are often governed by the vertical tie force since this force is equal to the externally applied shear (Tuchscherer, 2008). Combinations of single- and two-panel models can be applied to deep beams ( $a/d < 2$ ), but the stress conditions in the nodal regions due to the total applied force must be accounted for. At  $a/d$  ratios greater than 2, multiple-panel STMs are consistent with the behavior of the member but do not account for the contribution of concrete to shear strength. In addition, the required tie reinforcement may be unnecessarily large if the diagonal struts are steeper than 45 deg. with respect to the horizontal. Therefore, it is recommended that a sectional shear model is used for members with  $a/d$  ratios greater than 2.

With the use of the Project 5253 STM provisions, a relatively smooth transition exists between deep beam and sectional shear capacity at an  $a/d$  ratio of 2. A similar level of inherent conservatism ( $V_{\text{test}} / V_{\text{calc.}}$ ) of approximately 1.5 exists on average when shear strength is calculated with the Project 5253 STM provisions and the sectional shear provisions in AASHTO LRFD (2008) and ACI 318-08. In addition, similar design capacities are calculated with these provisions when the  $V_s/V_c$  ratio in the sectional shear provisions is limited to 2. The improved transition between sectional shear capacity and deep beam shear capacity with the use of the Project 5253 STM provisions is illustrated qualitatively in Figure 5.17. Some discrepancy in the strength calculated between the Project 5253 STM provisions and the sectional shear provisions in AASHTO LRFD (2008) should be expected; however, the discrepancy is largely reduced relative to when the STM provisions in AASHTO LRFD (2008) are used to calculate deep beam shear strength. It is important to note that the Project 5253 STM provisions were not developed solely to reduce this discrepancy. The improved transition between deep beam and

sectional shear strength is the result of the careful calibration of the Project 5253 STM provisions with data from the evaluation database, from the experimental program, and from existing STM specifications (Tuchscherer, 2008).

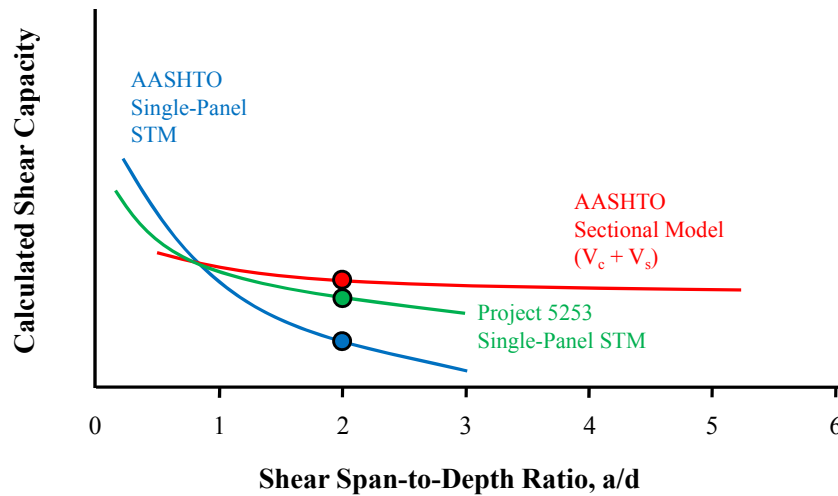


**Figure 5.17: Reduction in discrepancy in shear capacity at  $a/d$  ratio of 2 with Project 5253 STM provisions**

In Appendix A, an example problem largely developed by Tuchscherer (2008) is reproduced. In the example problem, the original cross-sections of the I-45 bent cap at Greens Road that experienced extensive diagonal cracking in service (Section 2.2) are evaluated with design provisions recommended in TxDOT Project 5253. One of the shear spans of the three column bent cap has an  $a/d$  ratio of 2.05. As such, it is an ideal case study to evaluate the discrepancy in calculated shear capacity as the member transitions from deep beam to slender beam behavior. The original cross-section with an  $a/d$  ratio of 2.05 was analyzed with the Project 5253 STM provisions. It was determined that the original section was overstressed by approximately 36% ( $\phi V_n / V_u = 0.74$ ) under the application of factored loads. This deficiency in strength was reasonable considering the amount of distress in the member in service (Section 2.2). When the same section was analyzed with the AASHTO LRFD (2008) STM specifications, it was determined that the section was overstressed by approximately 192% ( $\phi V_n / V_u = 0.34$ ). It is unlikely that the structure would be standing if it was under-designed by such a large amount.

Rather, it is probable that the STM provisions in AASHTO LRFD (2008) are overly conservative at  $a/d$  ratios approaching 2 (Figure 5.12). The original cross-section met the sectional shear requirements of the general procedure of AASHTO LRFD ( $\phi V_n / V_u = 2.33$ ) with a  $V_s/V_c$  ratio of 3.5 and those in ACI 318-08 ( $\phi V_n / V_u = 1.49$ ) with a  $V_s/V_c$  ratio of 3.0. If the simplified procedure is used in AASHTO LRFD (2008), the ratio of  $\phi V_n / V_u$  is 1.53 with a  $V_s/V_c$  ratio of 3.0.

The shear capacities calculated according to the aforementioned STM and sectional shear provisions can be compared for the original cross-section as in Table 5.1. In the far right column of Table 5.1, the calculated sectional shear capacity is divided by the calculated STM capacity to evaluate the discrepancy between the two. The calculated sectional shear capacity using the simplified AASHTO LRFD provisions is 2.07 times the Project 5253 STM capacity. While this amount of discrepancy is large, it is a significant improvement to the ratios of sectional shear capacity to STM capacity according to AASHTO LRFD (6.85) and ACI 318-08 (4.14). It is possible to further reduce the 2.07 factor by limiting the  $V_s/V_c$  ratio to 2 instead of the current value of 3. Also, additional STM capacity can be obtained without increasing the sectional shear strength by increasing the size of the nodal regions.

**Table 5.1: Comparison of calculated STM and sectional shear capacity for example problem in Appendix A**

Design Provisions	Capacity / Factored Load		$V_s/V_c$ Ratio	$\frac{\phi V_n - \text{Sectional}}{\phi V_n - \text{STM}}$
	STM $\phi V_n / V_u$	Sectional $\phi V_n / V_u$		
TxDOT Project 5253	0.74	1.53 <sup>†</sup>	3.0	2.07
ACI 318-08	0.36	1.49	3.0	4.14
AASHTO LRFD (2008)	0.34	2.33	3.5	6.85

<sup>†</sup>Simplified procedure in AASHTO LRFD (2008)

Completely removing the discrepancy between shear strength calculated with sectional shear and STM provisions near  $a/d$  ratios of 2 is unlikely. The design models are fundamentally different. However, through the use of the Project 5253 STM provisions and a limit of 2 for the  $V_s/V_c$  ratio, the discrepancy is largely reduced. For the design of members with  $a/d$  ratios near 2, it may be beneficial to compare the STM and sectional shear strength.

### **5.2.5 Summary and Conclusions**

The  $a/d$  ratio has a significant effect on the shear behavior of reinforced concrete beams. As the  $a/d$  ratio increases from 0, the shear strength of a member gradually declines due to the reduction in the effectiveness of a direct-strut mechanism. It was shown with results from the experimental program that the transition from deep beam behavior to sectional shear behavior was gradual. However, up to an  $a/d$  ratio of 1.85, the dominant shear transfer mechanism was consistent with a single-panel strut-and-tie model. Based on these results, it was concluded that a single-panel strut-and-tie model should be used to design regions of reinforced concrete members with  $a/d$  ratios less than 2. At  $a/d$  ratios greater than 2, the dominant shear transfer mechanism transitions to a sectional-shear mechanism. While it was shown that a single-panel strut-and-tie model can provide a conservative estimate of strength for beams with  $a/d$  ratios up to 2.5, the behavior of the member is generally not consistent with the assumed behavior in the STM. Therefore, for  $a/d$  ratios greater than 2, a sectional shear model should be used.

At  $a/d$  ratios approaching 2, overly conservative estimates of strength were calculated for the beams in the evaluation database using the AASHTO LRFD (2008) STM provisions. The excessive amount of conservatism was due to the inconsistency of the efficiency factor at the CCT node-strut interface with the geometry of non-hydrostatic nodes. Due to this excessive conservatism, a large discrepancy in calculated shear strength between the STM provisions and the sectional shear provisions in AASHTO LRFD (2008) exist at an  $a/d$  ratio of 2. With the use of the Project 5253 STM provisions (Section 2.3.4.3) and a limit on the  $V_s/V_c$  ratio of 2, the discrepancy in calculated shear strength is largely eliminated.

### **5.3 DIAGONAL CRACKING UNDER SERVICE LOADS**

The objective of this task was to develop a means of limiting diagonal cracking under service loads. It was determined that the most appropriate approach was to perform a separate design check comparing service level shear to an estimate for the diagonal cracking load. Data from the literature and the experimental program were used to develop an empirical equation that provides a reasonably conservative estimate for the diagonal cracking load of RC deep beams.

#### **5.3.1 Background**

It may not be possible to completely eliminate the presence of diagonal cracks in bent caps under service loads due to a variety of inconsistencies between design assumptions and field conditions such as overloads, restrained shrinkage, temperature changes, repeated loading, material properties of the concrete, etc. However, there are a few design considerations that can be made to restrict the width of diagonal cracks to an acceptable level or to mitigate the chance of the formation of diagonal cracks. In Section 4.3.3, the beneficial effect of web reinforcement on the width of diagonal cracks was discussed. It was shown that with minimum web reinforcement of 0.3% in each direction, the maximum width of diagonal cracks was limited to 0.016 in. at first cracking and up to an approximate service load (33% of ultimate). Providing additional reinforcement can further restrict the width of diagonal cracks to some degree. In this section, the task of reducing the risk of diagonal cracking under service loads is explicitly addressed.

Two types of diagonal cracks are recognized in reinforced concrete beams: flexure-shear cracks and web-shear cracks (MacGregor and Wight, 2005). Flexure-shear cracks form after or concurrently with flexural cracks. They extend from the tip of the flexural crack towards the origin of load. Web-shear cracks occur independently of flexural cracking. They form when the principal tension stress in the web of the member exceeds the tensile strength of concrete. In deep beams, web-shear cracks are also called bursting or splitting cracks. Specifically, they are caused by transverse tensile stresses

that exist due to the spreading of compressive stresses in bottle-shaped struts. It is apparent that the spreading of compressive stresses in deep beams contributes to the width of flexure-shear cracks as well. Both of these cracks are depicted in Figure 5.18.

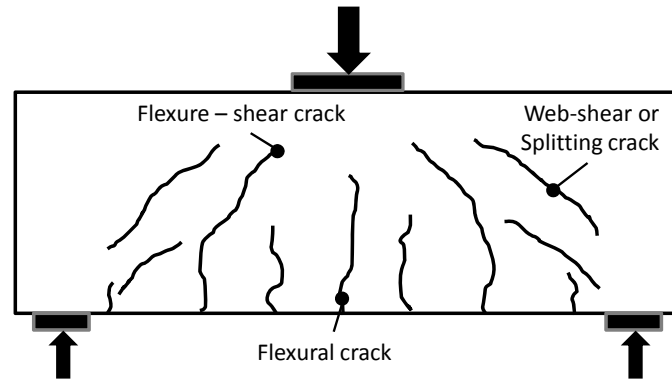


***Figure 5.18: Types of cracks in reinforced concrete deep beams***

With regard to this task, no distinction was made between flexure-shear or web shear cracks when evaluating the diagonal cracking load of the test specimens. Both were treated simply as inclined cracks. However, as noted in Section 4.2.2, the first diagonal crack to appear in the test specimens was generally a flexure-shear crack. The load at which it formed was determined through visual observation and with the help of strain gauges attached to the web reinforcement. For example, the appearances of the test regions of several specimens after first diagonal cracking are included in Figure 5.19. It is clear that the inclined cracks in these pictures are flexure-shear cracks. Also, note that the applied shear at the time the picture was taken is slightly greater than the cracking shear determined with the strain gauge data attached to the web reinforcement.

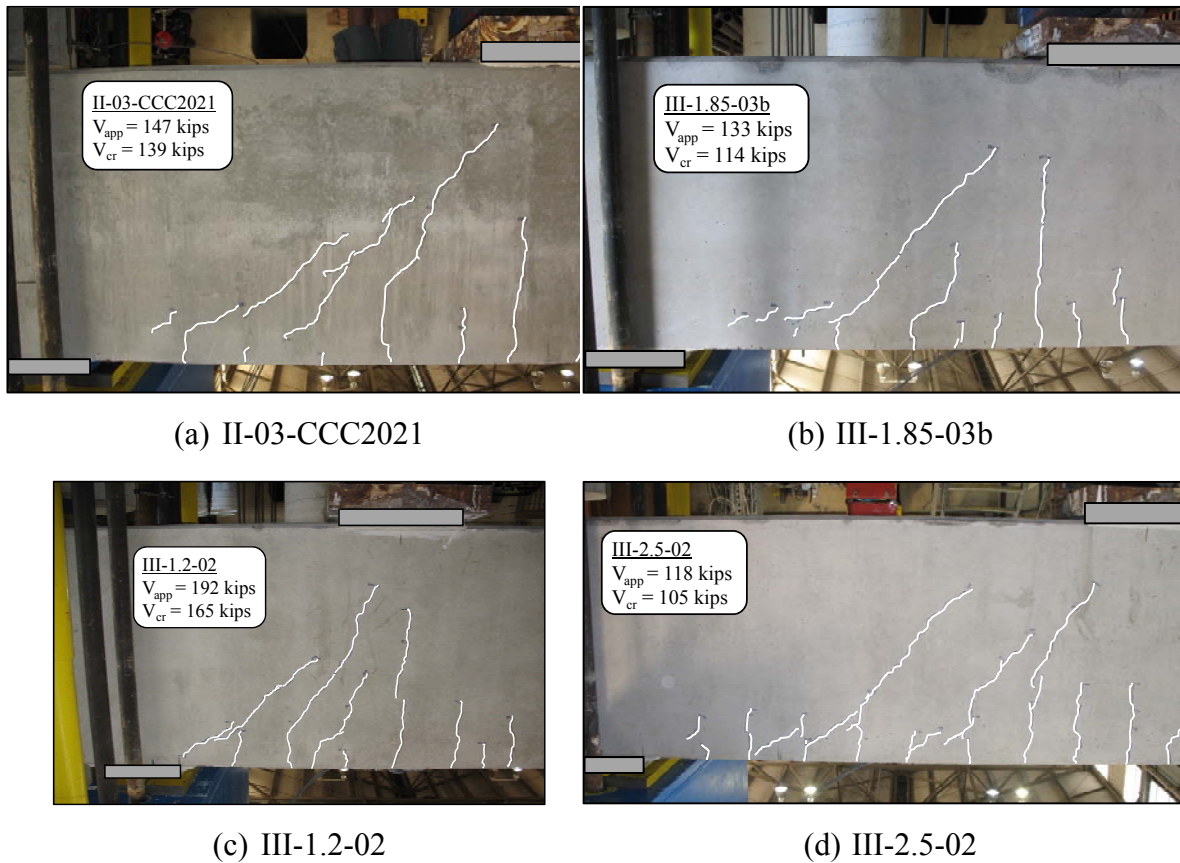


**Figure 5.19: First pictures taken after the formation of first diagonal crack in several tests**

### 5.3.2 Approach

Two approaches were considered to limit diagonal cracking under service loads. The first approach was associated with a single-panel strut-and-tie model. To limit diagonal cracking, the force generated in the bottle-shaped strut due to service loads would be limited to a specified percentage of the unfactored strut capacity. In effect, this strategy consisted of performing a separate service-load strut-and-tie analysis in which a reduced efficiency factor at the node-strut interface (consistent with the diagonal cracking strength of the strut) would be compared to the stress in the strut due to unfactored service loads. The advantage of this approach was that it could be integrated fairly easily with the ultimate-strength strut-and-tie analysis since the same model would be used.



The differences would be the applied loads and the efficiency factor at the node-strut interface.

However, it was determined that this approach was flawed. The basic theory behind strut-and-tie modeling is that it is a lower-bound plasticity-based approach. It is intended to be used in design to provide a safe estimate for ultimate strength. It is not intended to accurately estimate service level stresses or to limit diagonal cracking. In fact, cracking is expected to occur for the member to reach the capacity estimated by a strut-and-tie analysis. Therefore, it was inappropriate to use a STM-based approach to limit diagonal cracking under service loads.

The second approach considered for this task consisted of a separate, service load check. The service level shear would be compared to an estimate for the diagonal cracking load of the member. This check would be done separately from the ultimate strength analysis. It was more theoretically justified than the first approach and was still very simple. To use this approach, an estimate of the diagonal cracking load of deep beams was required. In this task, a recommendation is given to estimate the diagonal cracking load of deep beams based on data from the experimental program and the literature.

### **5.3.3 Results**

One approach to estimating the diagonal cracking load of a deep beam is to perform an elastic analysis. However, due to the proximity of the load to the support, there is a complicated state of stress in the member (Figure 5.20). Plane sections do not remain plane and general flexural theory assumptions do not apply. To address this difficulty, a finite element analysis (FEA) can be performed to determine the location and magnitude of the principal tension stress in the member. This procedure is plausible for cases in which the maximum principal stress is in the web of the member, indicating that the first crack should be a web-shear crack. However, in cases where the maximum principal stress is at the extreme tension fiber of the member, the beam is expected to develop flexural cracks first. After which, shear cracks will extend from the end of the flexural cracks (flexure-shear cracks). In this case, the elastic analysis needs to be

modified to account for the redistribution of stresses after flexural cracking (MacGregor and Wight, 2005). In the past, researchers have addressed the difficulty associated with an elastic analysis of a deep beam by estimating the diagonal cracking load with empirical models. This approach was taken in this project as well.

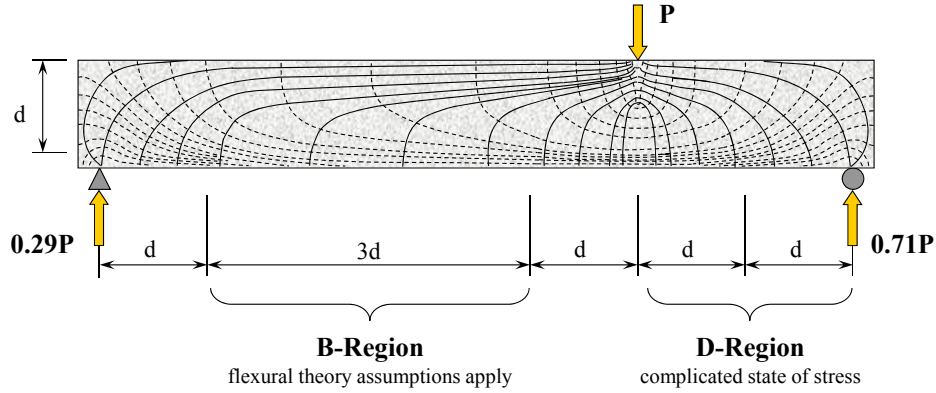


**Figure 5.20: Stress trajectories in B-regions (Bernoulli) and in D-regions (discontinuity)**

### 5.3.3.1 Variables that affect diagonal cracking loads of deep beams

In 1962, a landmark paper was published entitled “Shear and Diagonal Tension” by ACI-ASCE Committee 326. In this paper, the development of a semi-empirical equation for the diagonal tension cracking load of reinforced concrete beams was discussed. The equation was based off a principal stress analysis and was calibrated with test data from several research studies (ACI-ASCE Committee 326, 1962). The equation is presented as Equation 5.10.

$$V_{cr} = \left( 1.9\sqrt{f'_c} + 2500\rho_l \frac{V d}{M} \right) b_w d \quad (5.10)$$

with  $f'_c$  = compressive strength of concrete (psi)

$\rho_l$  = longitudinal reinforcement ratio ( $A_s / b_w d$ )

$V$  = shear at critical section (kips)

$M$  = moment at critical section (in-kips)

$b_w$  = web width of the member (in.)

$d$  = effective depth of the member (in.)

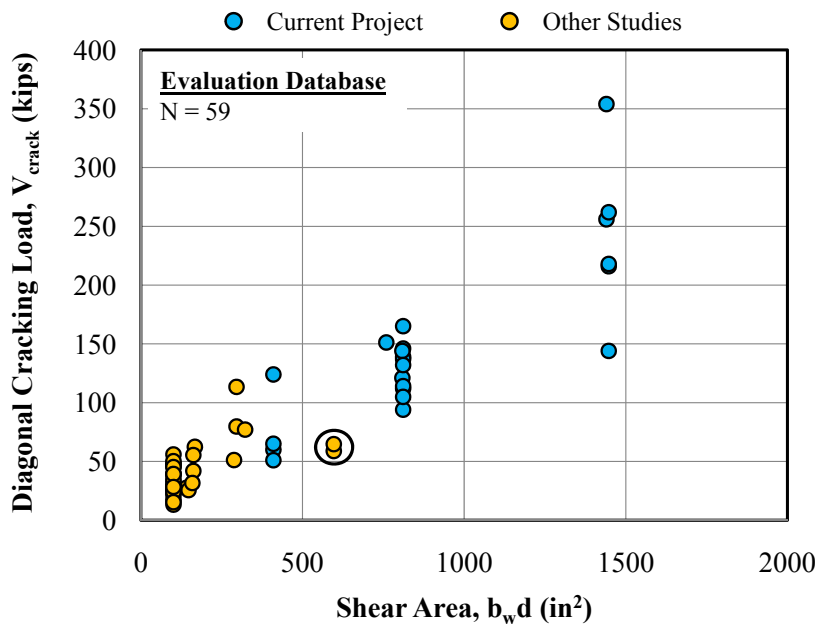
The equation incorporated all of the major variables that affected the diagonal cracking load of reinforced concrete beams known at the time, namely (1) the section size ( $b_w d$ ), (2) the tensile strength of concrete ( $\sqrt{f'_c}$ ), (3) the longitudinal reinforcement ratio ( $\rho_l$ ), and (4) the ratio of moment to shear at the critical section ( $M/V$ ). The equation could be applied to reinforced concrete beams with any  $a/d$  ratio as long as the critical section was appropriately defined. It was determined that for deep beams ( $a/d \leq 2$ ), the critical section is located at the middle of the shear span ( $a/2$ ). This critical section produces an  $M/V$  ratio for simple beams with single or double concentrated loads of  $a/2$ . For beams with an  $a/d > 2$ , the critical section is located at a distance ' $d$ ' from the maximum applied moment. In this case the  $M/V$  ratio is equal to ' $a$ ' minus ' $d$ .' Thus, the equation was intended to be used for beams with any  $a/d$  ratio and was calibrated as such.

In ACI 318-08, Equation 5.10 is listed as Equation 11-5. In the commentary (R11.2.2.1), it is stated that the variables accounted for in Equation 5.10 are still considered the primary variables that affect diagonal cracking loads. However, some research has shown that Equation 5.10 does not appropriately weigh each of the variables. In addition, it is suggested that the overall depth of the member may influence the diagonal cracking strength as well (ACI 318-08).

In the current task, the effects of the aforementioned variables ( $b_w d$ ,  $\sqrt{f'_c}$ ,  $a/d$ ,  $\rho_l$ ,  $d$ ) on the diagonal cracking load of deep beams were assessed with data from the experimental program and the literature through the use of the evaluation database. The purpose was to validate that these variables do affect the diagonal cracking loads of deep beams. Ultimately, this information was used to recommend an equation to estimate diagonal cracking loads for the purpose of limiting diagonal cracking in service.

The evaluation database consists of 179 specimens from the literature and the experimental program (Section 2.4.2). The diagonal cracking loads from more than half of the specimens from the literature were not reported. In addition, as noted in Section 3.6, only the cracking load of the first test of each 42 in-, 44 in-, and 48 in.-deep specimen was available due to the testing procedure. As a result, the diagonal cracking loads of 59 specimens existed in the evaluation database. The diagonal cracking loads for the Project 5253 specimens are listed in Table 4.1. The diagonal cracking loads for all of the specimens in the evaluation database are listed in Appendix B.

The effect of section size on the diagonal cracking load of the specimens in the evaluation database is shown in Figure 5.21. As expected, as the shear area ( $b_w d$ ) of the specimen increases, the diagonal cracking load increases. Prior to diagonal cracking, the member primarily behaves elastically. The entire section contributes to the diagonal cracking strength. It is important to note that this finding is not necessarily consistent with the ultimate strength of deep beams as shown in Section 4.4.2.



The diagonal cracking loads of two specimens from the literature were circled in Figure 5.21 because longitudinal bars were cut off within the shear span (Uribe and Alcocer, 2001). To ensure that the specimens would fail in shear, additional longitudinal reinforcement at midspan was provided; but the reinforcement was terminated at two locations within the shear span. It is likely that the stress concentrations that existed at the cutoff locations affected the first cracking load. These specimens were included in the evaluation database to illustrate the effect of bar cutoffs on the load at first diagonal cracking and because a similar situation could arise in practice.

It is clear from Figure 5.21 that within each group of data of the same section size there is a considerable amount of scatter. The scatter is a result of the other variables that contribute to the diagonal cracking load of deep beams. The effect of these variables ( $\sqrt{f_c'}$ ,  $a/d$ ,  $\rho_l$ ,  $d$ ) were assessed with the evaluation database as well. To isolate the effect of the tensile strength of concrete, the diagonal cracking load was normalized by the shear area and plotted versus  $\sqrt{f_c'}$  in Figure 5.22.

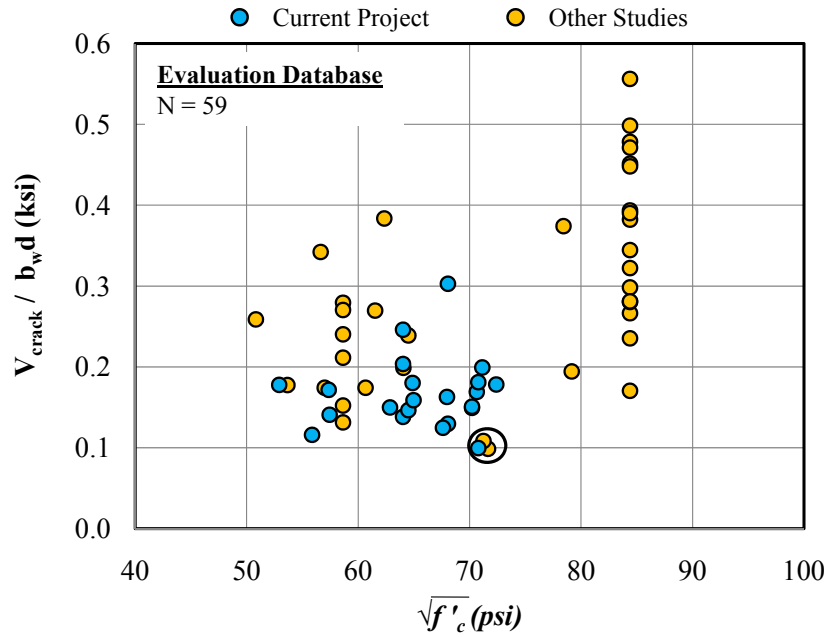


**Figure 5.22: Effect of tensile strength on diagonal cracking load of deep beams in database**

Since it is widely accepted that the tensile strength of concrete is a function of  $\sqrt{f'_c}$  (with considerable scatter), it is appropriate to evaluate the effect of the tensile strength of concrete on the diagonal cracking load by plotting it versus the square root of the compressive strength. The results in Figure 5.22 indicate that the diagonal cracking load is a function of the square root of the compressive strength of concrete, although the trend is relatively weak. It is expected that the diagonal cracking load would increase with increasing tensile strength since a crack forms when the principal tension stress exceeds the tensile strength of concrete. However, as before there is a substantial amount of scatter in Figure 5.22 for specimens with identical values of  $\sqrt{f'_c}$ . This scatter is the result of the contributions of other variables to the diagonal cracking load and of the inherent scatter associated with the tensile strength of concrete in general.

In the literature and throughout this report, diagonal cracking loads are normalized by the shear area and the square root of the compressive strength of concrete. It is accepted that both of these parameters are primary variables affecting the diagonal

cracking load. The results presented in Figure 5.21 and Figure 5.22 support this practice, albeit with significant amounts of scatter.

The effect of the shear-span-to-depth ( $a/d$ ) ratio on the load at first diagonal cracking is illustrated in Figure 5.23. With increasing  $a/d$  ratio, the normalized diagonal cracking load decreases for the most part. This trend is associated with the change in the principle tensile stress distribution that occurs as the  $a/d$  ratio changes. At low  $a/d$  ratios, a complicated state of stress exists due to the proximity of the applied load to the support. As the  $a/d$  ratio approaches and exceeds 2, the state of stress near midheight of the member is not affected by local support or loading conditions. The state of stress is consistent with flexural theory assumptions. As a result, as the  $a/d$  ratio approaches 2 in Figure 5.23, the diagonal cracking loads approach the diagonal cracking strength of slender beams,  $2\sqrt{f_c'}b_wd$ . For slender beams without transverse reinforcement, the diagonal cracking load of  $2\sqrt{f_c'}b_wd$  is equivalent to the ultimate strength. It is important to note that the trend of decreasing diagonal cracking loads with increasing  $a/d$  ratio was observed previously by numerous researchers for deep beams (Smith and Vantsiotis, 1982, Tan et al., 1995, Tan and Lu, 1999, Shin et al., 1999, and Oh and Shin, 2001).

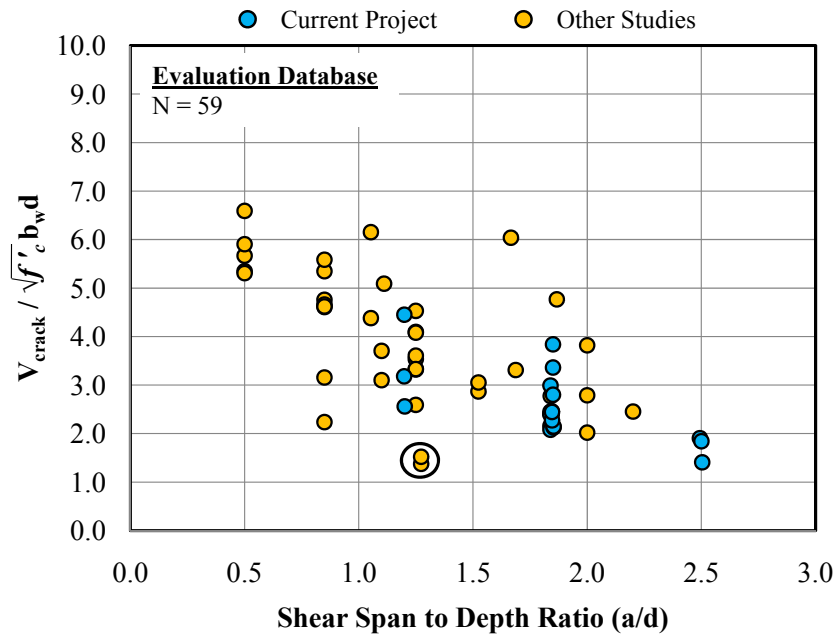


***Figure 5.23: Effect of  $a/d$  ratio on diagonal cracking load of deep beams in database***

The effect of the longitudinal reinforcement ratio,  $\rho_l$ , on the diagonal cracking load of the deep beams in the evaluation database is depicted in Figure 5.24. The results do not indicate a clear trend. It is likely that the lack of a significant number of specimens outside of the range of 1.5% to 2.5% reinforcement contributes to the lack of a trend. It is possible to isolate the effect of the longitudinal reinforcement ratio on the cracking load by only plotting data from similar specimens tested at similar  $a/d$  ratios. This approach was taken in Figure 5.25.



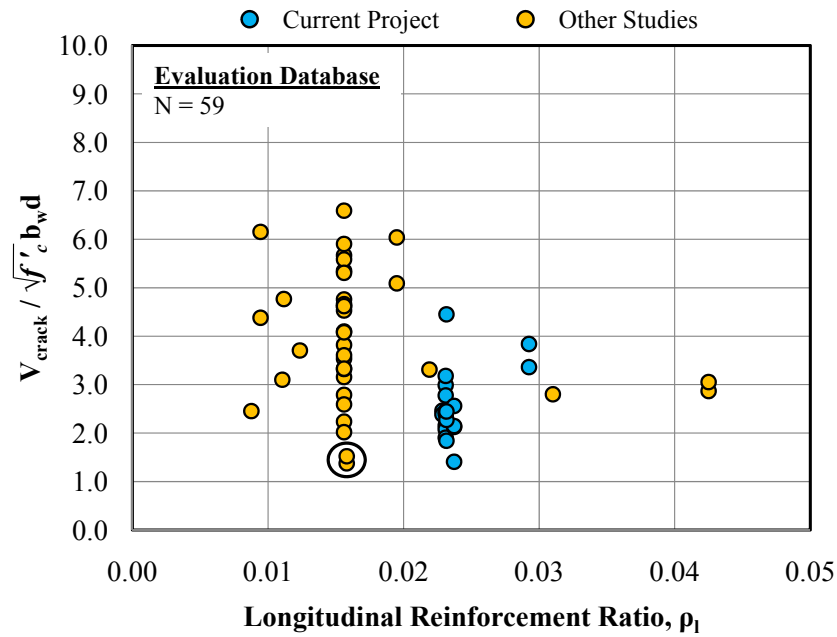


**Figure 5.24: Effect of longitudinal reinforcement ratio on diagonal cracking load of beams in the database**

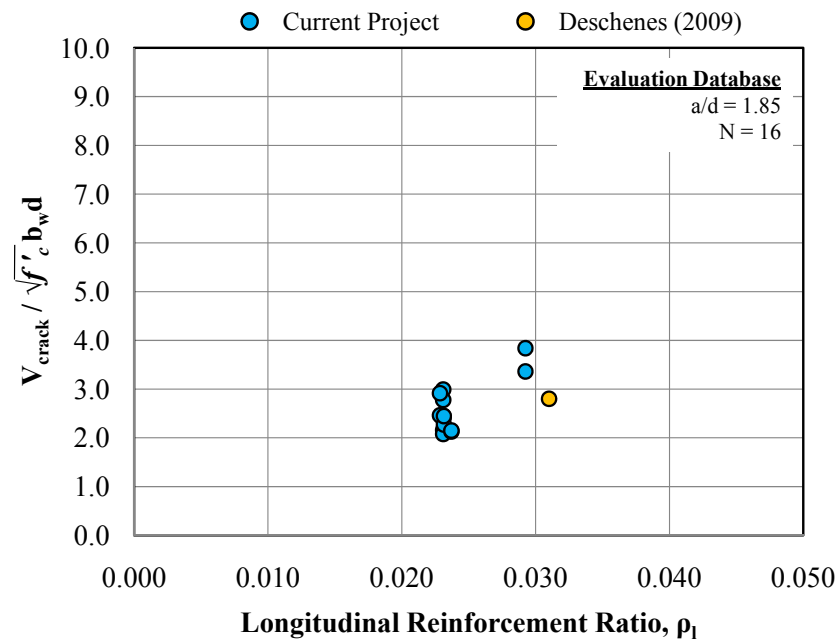


**Figure 5.25: Effect of longitudinal reinforcement ratio on diagonal cracking load of beams with the same  $a/d$  ratio**

The data in Figure 5.25 are from specimens tested in the experimental program and from one specimen tested by Deschenes (2009). All of the tests were conducted at an  $a/d$  ratio of 1.85. The 21-in. wide specimens in the experimental program had a longitudinal reinforcement ratio of 2.3%; the 36"x48" specimens had a longitudinal reinforcement ratio of 2.9%. The specimen tested by Deschenes had a 21"x42" cross-section and a longitudinal reinforcement ratio of 3.1%. Since all of the specimens in Figure 5.25 were tested at the same  $a/d$  ratio and were similar in size, the effect of the longitudinal reinforcement ratio on the diagonal cracking load can be isolated from other contributing variables. The results indicate that the normalized diagonal cracking load increases with increasing longitudinal reinforcement ratio to some degree. This finding is in agreement with the results of several research studies (Moody et al., 1954, Morrow and Viest, 1957, de Paiva and Siess, 1965), most of which were used in the development of Equation 5.10. The results in Figure 5.25 are justified since the first diagonal crack is generally a flexure-shear crack. At the tip of the flexural crack, the amount of longitudinal reinforcement reduces the principal tension stress thereby delaying the load at which the flexural crack turns into a diagonal crack.

The effect of depth on the diagonal cracking load of the beams in the evaluation database is shown in Figure 5.26. The results indicate that the diagonal cracking load of deep beams decreased with increasing depth, on average. However, it is possible that the scarcity of data for beams with effective depths greater than 40 in. contributed to this average reduction. From a lower bound perspective, the decrease in cracking load with increasing depth is small. As before, the effect of depth on the diagonal cracking load of deep beams can be isolated by plotting the data from specimens with different depths, but identical  $a/d$  ratios and beam parameters. The diagonal cracking loads of the beams tested in the experimental program are provided in Figure 5.27.

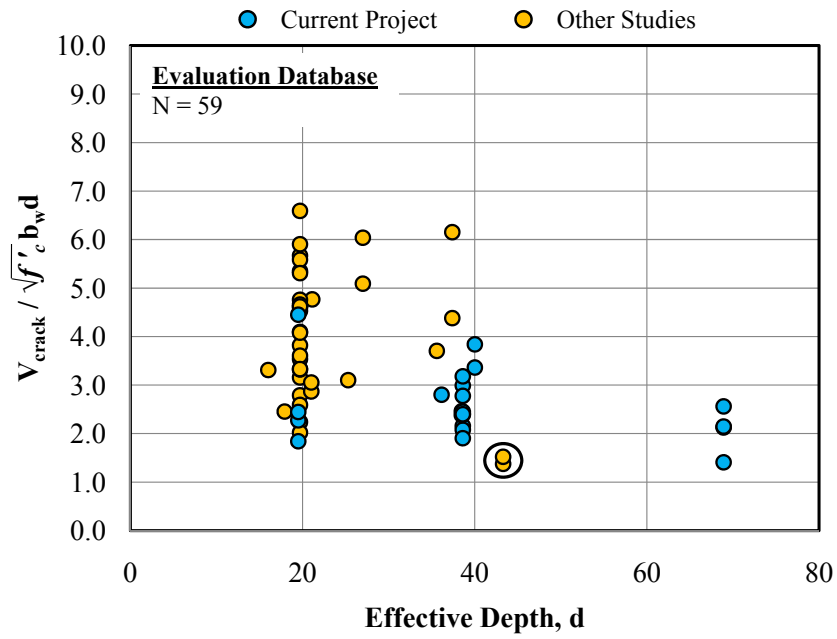


*Figure 5.26: Effect of depth on the diagonal cracking load of beams in the evaluation database*

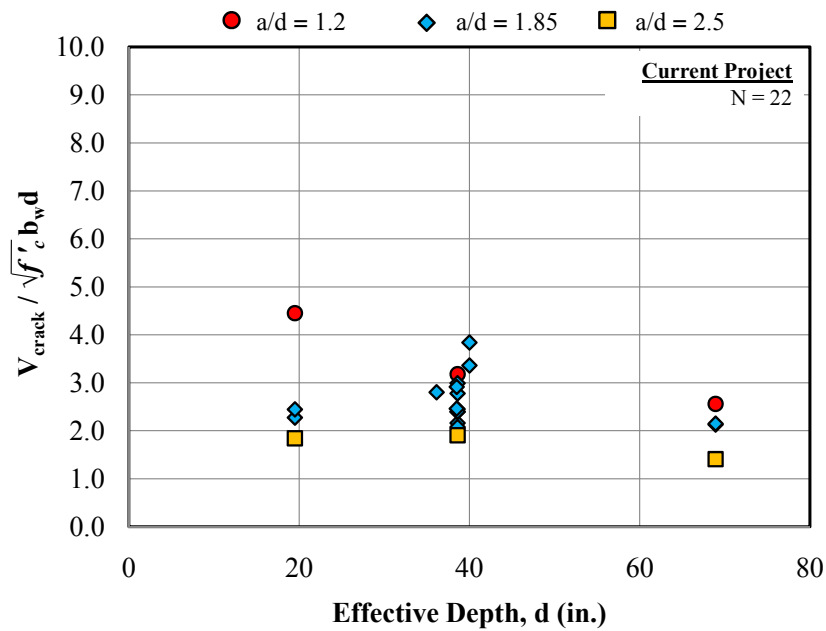


*Figure 5.27: Effect of depth on the diagonal cracking load of deep beams in testing program*

All of the data in Figure 5.27 are from the current experimental program. The normalized diagonal cracking loads of the specimens tested at an  $a/d$  ratio of 1.2 decreased with increasing depth. At an  $a/d$  ratio of 2.5, the normalized cracking load at first cracking decreased with an increase in effective depth of 38 to 69 in. At an  $a/d$  ratio of 1.85, little to no depth effect was apparent. As noted previously in Section 4.3.3, the reduction in diagonal cracking load for some of the specimens may be due to variations in tensile strength or to a Weibull statistical effect. Conflicting results on this issue exist in the literature. Similar results to that in Figure 5.27 were presented by Tan and Lu (1999) for specimens tested at  $a/d$  ratios of 0.56 and 1.13, but not for specimens tested at an  $a/d$  ratio 0.84. Conversely, in experimental studies by Walraven and Lehwalter (1994) and Zhang and Tan (2007), both researchers concluded that the diagonal cracking load of deep beams is not affected by size. The specimens in these studies were tested at an  $a/d$  ratio of approximately 1. As a result, it is possible that the effective depth of a deep beam contributes to the diagonal cracking load to some extent, but the lack of consistent trends suggests that the overall effect is small.

The effect of the quantity of web reinforcement on the diagonal cracking load of deep beams was also evaluated in the experimental program and with the evaluation database. In Section 4.3.3, it was shown that the diagonal cracking loads of deep beams were not appreciably affected by the quantity of web reinforcement, either in the horizontal or the vertical direction (Figure 4.21 and Figure 4.22). This finding is plausible since the web reinforcement should not affect the performance of the beam until diagonal cracks form. The results from the specimens in the experimental program in which web reinforcement was the primary variable are illustrated in Figure 5.28.

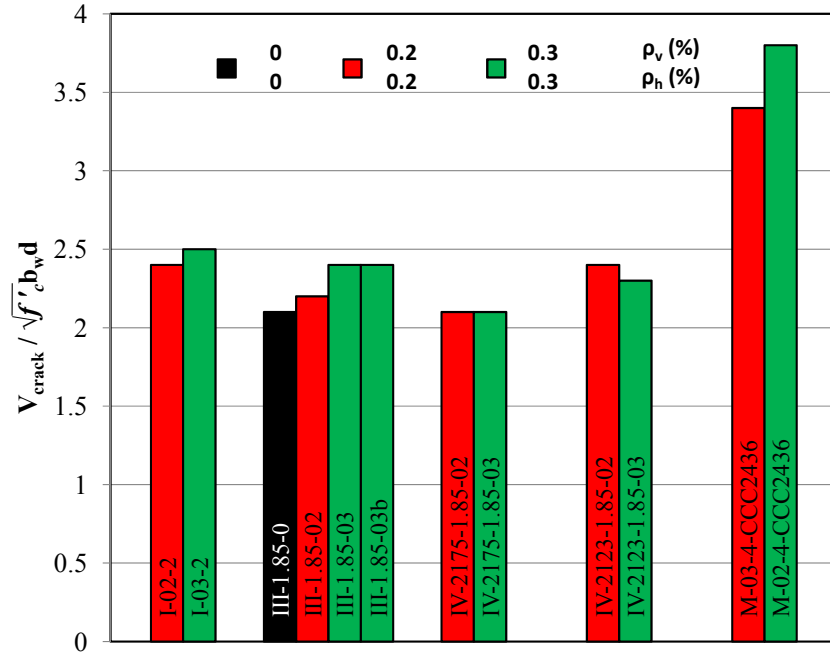


**Figure 5.28: Effect of web reinforcement on the diagonal cracking load of similarly sized deep beams**

In summary, based on the results presented in this section, it is apparent that a considerable amount of scatter exists in diagonal cracking loads of deep beams. One reason for the scatter is the number of variables that affect the load at first cracking. It was shown that the primary variables affecting the diagonal cracking load of deep beams are the section size ( $b_w d$ ), the tensile strength of the concrete ( $\sqrt{f'_c}$ ), and the  $a/d$  ratio. The longitudinal reinforcement ratio may contribute to the diagonal cracking load to some degree, although there was only a minimal amount of data available to evaluate this variable. Based on the results in Figure 5.26, Figure 5.27, and from the literature, it was shown that the effect of section depth on the diagonal cracking load is erratic and is likely small in general. Lastly, the load at first diagonal cracking was not noticeably affected by the quantity of web reinforcement.

It is important to note that the effect of repeated loading on the diagonal cracking strength of deep beams was not studied. It is possible that the cracking strength will reduce with numerous cycles of load. For this reason, it may be beneficial to take a

conservative approach in estimating the diagonal strength of reinforced concrete deep beams.

#### **5.3.3.2 *Estimating Diagonal Cracking Loads***

For this task, an estimate for the diagonal cracking load of deep beams was required. Previous researchers have proposed empirical equations aimed at estimating the diagonal cracking load of reinforced concrete beams. In general, the equations have accounted for the primary variables that affect diagonal cracking with the exception of the effective depth. In this section, a few equations from the literature and design specifications are evaluated with the data in the evaluation database.

The first equation to be evaluated is ACI-318-08 Equation 11-5, presented previously as Equation 5.10. This equation was developed in the early 1960s and accounts for the following variables:  $b_w d$ ,  $\sqrt{f'_c}$ ,  $a/d$ , and  $\rho_l$ . For each specimen in the database, the estimated cracking load according to Equation 5.10 was computed. For beams with an  $a/d \leq 2$ , the critical section was taken as the halfway point on the shear span producing an  $M/V$  ratio equal to  $a/2$ . For beams with an  $a/d > 2$ , the critical section was taken as  $d$  away from the location of maximum moment which slightly affected the  $M/V$  ratio for these specimens. The experimental diagonal cracking loads were divided by the estimated diagonal cracking loads. The results were plotted in Figure 5.29 versus the  $a/d$  ratio.

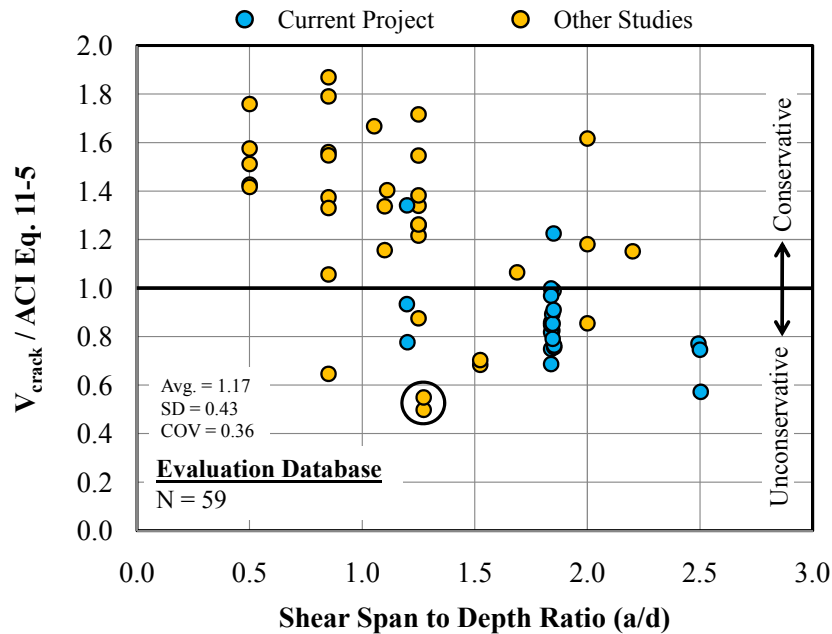


**Figure 5.29: Comparison of measured and estimated diagonal cracking loads – ACI Eq. 11-5**

In Figure 5.29, a value of 1.0 represents a cracking load estimate that is equal to the measured cracking load. Values below 1 represent unconservative estimates; values above 1 represent conservative estimates. A slight trend may exist with  $a/d$  ratio in Figure 5.29. As the  $a/d$  ratio increases, the estimated diagonal cracking load is less conservative on average. This slight trend implies that Equation 5.10 incorrectly accounts for the effect of the  $a/d$  ratio on the diagonal cracking load of deep beams. Another observation from Figure 5.29 is the large amount of scatter. On average, the diagonal cracking loads are computed conservatively (Avg. = 1.17), but with a very high standard deviation (SD = 0.43). The high standard deviation is a reflection of the inaccuracy of Equation 5.10 and the inherent scatter in the diagonal cracking loads themselves.

In 1968, an equation for the diagonal cracking load of reinforced concrete beams was developed by Zsutty. The equation was based on a linear regression analysis of data in the literature. Another equation was needed because Zsutty (1968) claimed that Equation 5.10 did not properly weigh the primary variables that affect the diagonal

cracking load. Zsutty's design equation is presented as Equation 5.11. In the derivation of the equation, the data were split by the a/d ratio. Beams with an a/d ratio  $> 2.5$  were considered slender. Beams with an a/d ratio  $< 2.5$  were considered short. The cutoff at an a/d ratio of 2.5 was made because Zsutty found that above this value, the diagonal cracking load data agreed well with his empirical equation. At an a/d ratio less than 2.5, there were significantly greater errors. Based on this abrupt change in performance, the cutoff between short beams and slender beams was taken at an a/d ratio of 2.5. The reason for the additional error in the short beam data was believed to be the result of the "arch action" in short beams (Zsutty, 1968). Improvements to the equation for short beams were attempted to no avail. In the words of the author: "several attempts to remove variables such as  $\rho$ , or add variables such as bond contact area ratio, did nothing to improve the prediction precision" (Zsutty, 1968). In a later publication, a modification to Equation 5.11 was made to estimate the ultimate strength of short beams (Zsutty, 1971). In estimating the ultimate strength of short beams, Zsutty commented that the equation "must contain an accurate representation of the top and bottom pressures due to load and support conditions" (Zsutty, 1968). No need was seen to alter the estimate for first diagonal cracking of short beams since these members carry additional load after first cracking. However, great attention was given to improving the estimated diagonal cracking load for slender beams since this value is often the ultimate strength of unreinforced specimens and is used as the concrete contribution in the sectional shear design model. The diagonal cracking loads in the evaluation database are compared to those estimated with Equation 5.11 in Figure 5.30.

$$V_{cr} = \left[ 59 \left( \frac{f'_c \rho_l d}{a} \right)^{\frac{1}{3}} \right] b_w d \quad (5.11)$$

- with  $f'_c$  = compressive strength of concrete (psi)  
 $\rho_l$  = longitudinal reinforcement ratio ( $A_s / b_w d$ )  
 $d$  = effective depth of the member (in.)  
 $a$  = shear span (in.)



$b_w$  = web width of the member (in.)

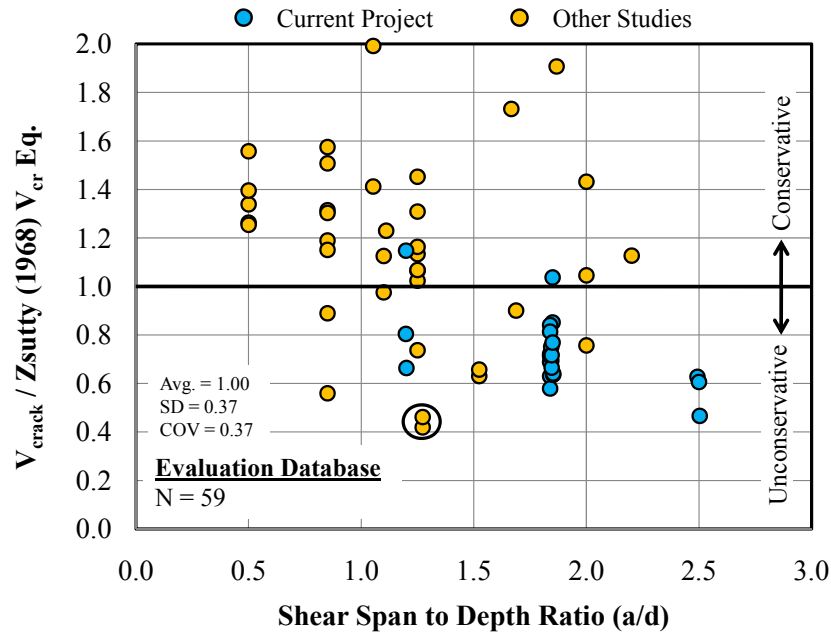


**Figure 5.30: Comparison of measured and estimated diagonal cracking loads – Zsutty Equation**

The results in Figure 5.30 do not show a significant improvement with respect to the results in Figure 5.29. There still appears to be a trend with increasing  $a/d$  ratio on average. Even though the average of the experimental diagonal cracking loads divided by the estimated diagonal cracking loads are 1.0 with Equation 5.11, the standard deviation ( $SD = 0.37$ ) and the coefficient of variation ( $COV = 0.37$ ) are high. The amount of error seen in Figure 5.30 is consistent with what Zsutty found. In his study, the error was attributed to “the wide dispersion of the arch action shear stress values,” not the inappropriate form of the equation (Zsutty, 1968). Even though it appears that the  $a/d$  ratio is not appropriately weighed in Equation 5.11 based on the results in Figure 5.30, it is likely that the scatter in diagonal cracking loads of nominally identical specimens greatly contributes to the inability to accurately predict them.

In 1999, an experimental study was conducted by Shin et al. in which thirty high-strength concrete beams were tested at  $a/d$  ratios ranging from 1.5 to 2.5. The cross-

section of the specimens was 4.9"x9.8" and the longitudinal reinforcement ratio was 3.8%. Two series of tests were conducted in which the concrete strength was either 7,600 psi or 10,600 psi. The diagonal cracking loads of the specimens were evaluated with Equations 5.10 and 5.11. The authors found that Equation 5.10 was overly conservative when used to estimate the cracking loads of their specimens. A fairly good correlation was found with the use of Equation 5.11. Based on a regression analysis of their test data, a different equation for the diagonal cracking load of deep beams was recommended. The equation is presented as Equation 5.12. The diagonal cracking loads in the evaluation database are compared to those estimated with Equation 5.12 in Figure 5.31.

$$V_{cr} = \left( 72(f'_c \rho_l)^{\frac{1}{3}} \left( \frac{d}{a} \right)^{\frac{1}{2}} \right) b_w d \quad (5.12)$$

- with  $f'_c$  = compressive strength of concrete (psi)  
 $\rho_l$  = longitudinal reinforcement ratio ( $A_s / b_w d$ )  
 $d$  = effective depth of the member (in.)  
 $a$  = shear span (in.)  
 $b_w$  = web width of the member (in.)

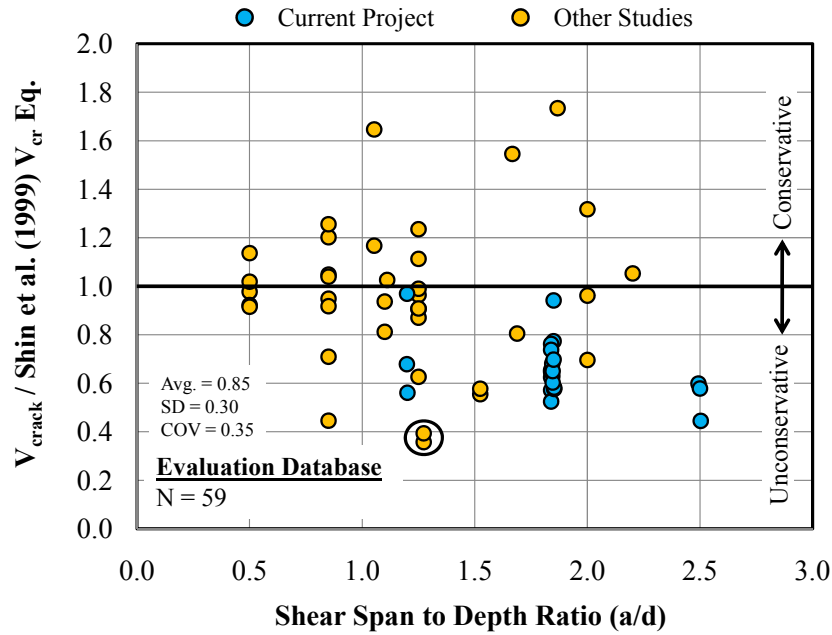


**Figure 5.31: Comparison of measured and estimated cracking loads – Shin et al. Equation**

At the conclusion of the study, it was warned by Shin et al. that “Strictly speaking, the equations are valid only within the ranges of variability of the parameters studied” (Shin et al., 1999). Since high-strength concrete and a reinforcement ratio of 3.8% were used in their test specimens, the beams in the evaluation database are not similar. Furthermore, only the beams loaded at  $a/d$  ratios ranging from 1.5 to 2.5 would be applicable. Nevertheless, for comparison purposes, the estimates obtained by using Equation 5.12 are compared to the cracking loads in the evaluation database as shown in Figure 5.31. It is clear from the figure that excluding the data at  $a/d$  ratios less than 1.5 would only further penalize the accuracy of Equation 5.12. With respect to the other equations, the use of Equation 5.12 did have slightly less scatter as measured by the standard deviation and coefficient of variation. However, the standard deviation ( $\text{SD} = 0.30$ ) and coefficient of variation ( $\text{COV} = 0.35$ ) are still fairly large; and the accuracy on average is unconservative ( $\text{Avg.} = 0.85$ ). The point of comparing the data in the evaluation database with Equation 5.12 is not to assess the accuracy of the equation since

it was obviously not calibrated with the range of parameters in the evaluation database. Instead, the point is to illustrate the wide range of scatter that can result when the quantities of the primary variables that affect the diagonal cracking load are altered. Whereas the data from the study by Shin et al. were predicted with their proposed equation with remarkable accuracy (Avg. = 1.0, SD = 0.06, COV = 0.06), the data in the evaluation database were not. This inconsistency suggests that while the parameters that affect diagonal cracking are correctly identified, it is difficult to weigh them appropriately for the wide range of values for each pertinent variable. In addition, there may be inconsistencies in the way with which each researcher is measuring the diagonal cracking load, although the description of first diagonal cracking in each study is similar.

In AASHTO LRFD (2008), there is an equation for  $V_{ci}$  that can be used to estimate first diagonal cracking.  $V_{ci}$  is defined as the “nominal resistance provided by concrete when inclined cracking results from combined shear and moment” (AASHTO LRFD, 2008). Specifically,  $V_{ci}$  refers to flexure-shear cracking which was the first type of diagonal crack observed in the specimens of the experimental program (Section 5.3.1). The equation for  $V_{ci}$  (5.13) was calibrated for both prestressed and reinforced concrete members as described in NCHRP Report 549 (Hawkins et al., 2005). The equation for the cracking moment needed to compute  $V_{ci}$  is provided in Equation 5.14. The diagonal cracking loads in the evaluation database are compared to those estimated with Equation 5.13 in Figure 5.32.

$$V_{ci} = 0.02\sqrt{f'_c}b_vd_v + V_d + \frac{V_iM_{cre}}{M_{max}} \geq 0.06\sqrt{f'_c}b_vd \quad (5.13)$$

- where  $f'_c$  = compressive strength of concrete (ksi)  
 $b_v$  = effective web width within  $d_v$  (in.)  
 $d_v$  = effective shear depth, taken as the distance between the resultants of the tensile and compressive forces due to flexure (in.)  
 $V_d$  = shear force at section due to unfactored dead load (kips)

$V_i$  = factored shear force at section due to externally applied loads occurring simultaneously with  $M_{\max}$  (kips)

$M_{cre}$  = moment causing flexural cracking at section due to externally applied loads (kip-in.)

$M_{\max}$  = maximum factored moment at section due to externally applied loads (kip-in.)

and

$$M_{cre} = S_c \left( f_r + f_{cpe} - \frac{M_{dnc}}{S_{nc}} \right) \quad (5.14)$$

where  $S_c$  = section modulus for extreme fiber of the composite section where tensile stress is caused by externally applied loads (in.<sup>3</sup>)

$f_r$  = modulus of rupture of concrete (ksi)

$f_{cpe}$  = compressive stress in concrete due to effective prestress forces only at extreme tensile fiber (ksi)

$M_{dnc}$  = total unfactored dead load moment on noncomposite section (kip-in.)

$S_{nc}$  = section modulus for extreme fiber of the noncomposite section where tensile stress is caused by externally applied loads (in.<sup>3</sup>)

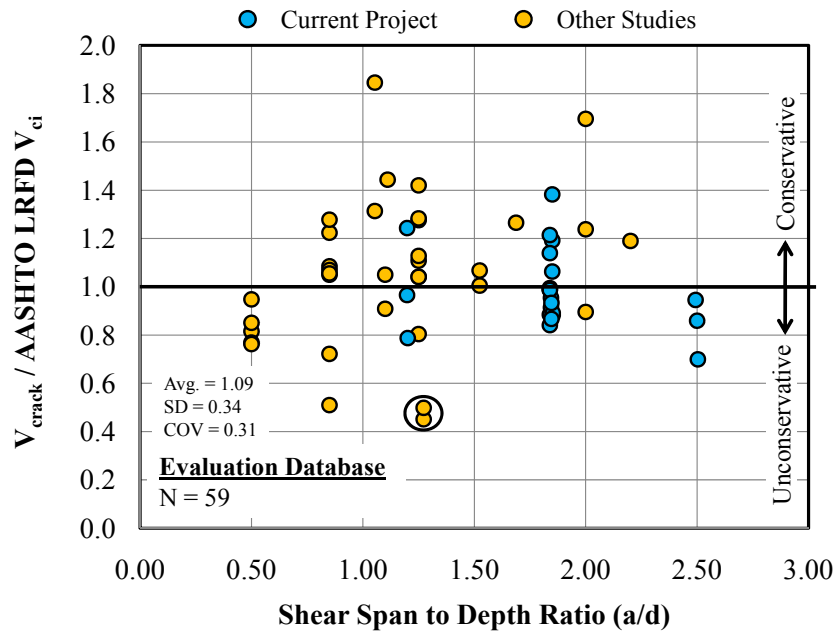


**Figure 5.32: Comparison of measured and estimated cracking loads – AASHTO  $V_{ci}$**

The results in Figure 5.32 with respect to those in Figure 5.29 through Figure 5.31 indicate that the AASHTO LRFD  $V_{ci}$  equation does a slightly better job estimating diagonal cracking loads than the other equations for the specimens in the database. The estimates are conservative on average (Avg. = 1.09) and are reasonably consistent for the full range of a/d ratios. However, a significant amount of scatter still exists as measured by the standard deviation (SD = 0.34) and coefficient of variation (COV = 0.31).

Based on the results presented in this section, it is clear that it is very difficult to estimate diagonal cracking loads of deep beams accurately. While the AASHTO LRFD (2008)  $V_{ci}$  equation appeared to do the best job of the equations that were evaluated, a considerable amount of error exists. This error is likely due to the interdependency of the wide range of variables that affect diagonal cracking loads and the variability in the diagonal cracking loads themselves as pointed out by Zsutty (1968). To illustrate the variability in diagonal cracking loads of nominally-identical specimens, the cracking loads of several beams from the evaluation database in which the only variable is the quantity of web reinforcement are plotted in Figure 5.33. Fifteen specimens with an identical cross-section and longitudinal reinforcement ratio from the research study

conducted by Oh and Shin (1999) are included. Eight specimens with the same longitudinal reinforcement ratio and cross-section from the experimental program are included as well.

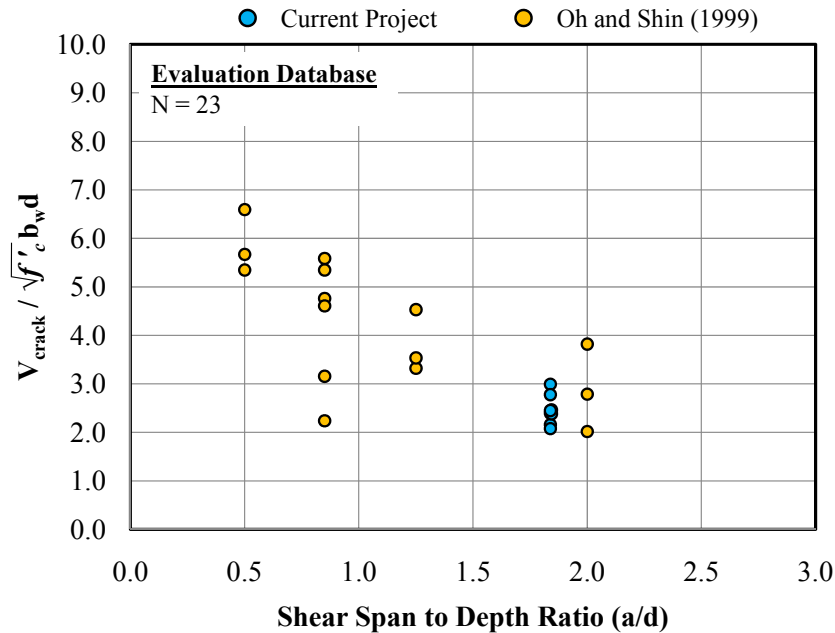


**Figure 5.33: Diagonal cracking loads for nominally-identical specimens**

As shown previously in Figure 5.28 and in Section 4.3.3, the quantity of web reinforcement did not have an appreciable effect on the diagonal cracking load. Therefore, the diagonal cracking loads in Figure 5.33 at each  $a/d$  ratio should be similar. Instead, a considerable amount of scatter exists. Often, the maximum diagonal cracking load in a group is 50% greater than the minimum. In a couple of cases, the maximum and minimum diagonal cracking load differ by a factor of 2. Thus, for nominally-identical specimens, the diagonal cracking loads are considerably different. The most likely reason for the scatter is the variability in the tensile strength of concrete. Improving the accuracy of diagonal cracking loads beyond the accuracy with which the tensile strength of concrete is estimated is not possible.

Due to the difficulties associated with estimating diagonal cracking loads, it is unlikely that an equation can be developed that will be significantly more accurate than

the AASHTO LRFD  $V_{ci}$  equation. However, since the purpose of the current task is to prevent diagonal cracking in service, a simple and conservative estimate may be more appropriate than an accurate one. With the data presented previously in Figure 5.23, a lower-bound estimate of the diagonal cracking load was determined. The proposed lower-bound equation is shown with the data in Figure 5.34. Since first diagonal cracking is a serviceability consideration, a more liberal lower-bound equation is warranted compared to a strength consideration.

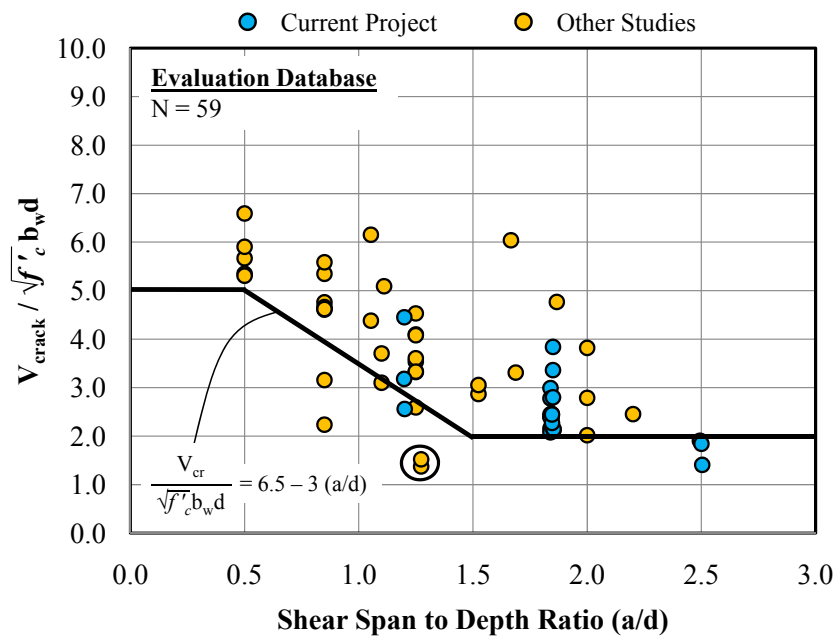


**Figure 5.34: Development of proposed equation for a conservative estimate of diagonal cracking**

The proposed diagonal cracking load equation is a reasonable lower-bound to the data from a serviceability perspective. The equation considers the primary variables that affect first cracking, namely the section size ( $b_w d$ ), the tensile strength of concrete ( $\sqrt{f'_c}$ ), and the  $a/d$  ratio of the member. For an  $a/d$  ratio less than 0.5, the estimated diagonal cracking load is  $5\sqrt{f'_c} b_w d$ . As the  $a/d$  ratio increases from 0.5 to 1.5, the estimated diagonal cracking load decreases from  $5\sqrt{f'_c} b_w d$  to  $2\sqrt{f'_c} b_w d$ . For an  $a/d$



ratio  $> 1.5$ , the diagonal cracking load is  $2\sqrt{f'_c} b_w d$ . Limiting the diagonal cracking load to  $2\sqrt{f'_c} b_w d$  at an  $a/d$  ratio of 2 is consistent with the diagonal cracking load of slender beams. Since the equation is a lower-bound estimate, it inherently accounts for other variables that may contribute to the scatter in Figure 5.34 (i.e. the longitudinal reinforcement ratio or the effective depth). Furthermore, it does not seem practical to recommend an equation that varies with the longitudinal reinforcement ratio since  $\rho_l$  in TxDOT structures does not vary as much as it does for beams in the literature. In typical bent caps, the longitudinal reinforcement ratio is generally less than 1% (TxDOT, 2008). It is important to emphasize that the proposed diagonal cracking load estimate is intended to be simple and reasonably conservative at the cost of being less accurate.

#### 5.3.4 Design Implications

To limit diagonal cracking under service loads, the following approach should be taken. After the completion of a strength analysis, a service load shear check should be performed. The shear in the member due to the unfactored service loads should be computed. This value should then be compared to the estimated diagonal cracking load given by the following equation:

$$V_{cr} = \left[ 6.5 - 3 \left( \frac{a}{d} \right) \right] \sqrt{f'_c} b_w d \quad (5.15)$$

but not greater than  $5\sqrt{f'_c} b_w d$  nor less than  $2\sqrt{f'_c} b_w d$

with  $a$  = shear span (in.)

$d$  = effective depth of the member (in.)

$f'_c$  = compressive strength of concrete (psi)

$b_w$  = web width of the member (in.)

If the service level shear is less than the estimated diagonal cracking load, then the member is not expected to crack in service. If the service level shear is greater than the estimated diagonal cracking load, several options exist for the designer. First, the

design of the member can be altered to increase the value of the diagonal cracking load. The section size ( $b_w d$ ) of the member can be increased. If the depth is increased, the  $a/d$  ratio of the member for the typical situation in which the span length is fixed will also be reduced. Alternatively, or in conjunction with an increase in section size, a higher compressive strength of concrete can be specified. Second, if these options are not practical, the designer can provide additional web reinforcement to help restrain the diagonal crack widths under service loads. However, as noted in Section 4.3.3, there are some diminishing returns in regards to the benefits of the quantity of web reinforcement for crack width control.

Alternatively, the AASHTO LRFD (2008)  $V_{ci}$  equation can be used to estimate the diagonal cracking load with the service load check outlined above. It is expected that this equation will provide a more accurate, yet potentially unconservative, estimate of the diagonal cracking load with additional calculation.

In the design example in Appendix A, a service load shear check is performed with the proposed lower-bound equation on two sections ( $a/d$  of 0.85 and 2.05) of the I-45 bent cap at Greens Road (Section 2.2). For the original cross-section with an  $a/d$  ratio of 2.05, the diagonal cracking load estimate ( $2\sqrt{f'_c} b_w d$ ) was equivalent to only 88% of the service dead load shear on the section. Thus, it is not surprising that extensive diagonal cracking was observed in this member in service. With the revised section that was designed according to the Project 5253 STM provisions (at  $a/d$  of 0.85 and 2), the diagonal cracking load estimate was equal to the full service dead load shear plus approximately 25% of the service live load shear. Thus, for these examples, diagonal cracking would still be expected under full service loads. To reduce the risk of diagonal cracking under full service loads, modifications to the cross-section will need to be made. This example indicates that it may be slightly impractical to design the cross-section to remain free of diagonal cracks under the application of the *full* service load. Instead, limiting diagonal cracking under the full dead load and a percentage of the live load may be more realistic. This adjustment can be made in the proposed service load shear check

by simply computing the shear due to the dead load plus a reasonable amount of live load.

The service load check outlined in this section provides an indication of the likelihood of diagonal cracks forming in service. If the service load shear exceeds the expected diagonal cracking load, the designer can determine at what percentage of the live load the member is expected to form a diagonal crack. In extreme cases (I-45 at Greens Road), this check will indicate if the member is expected to crack under service dead loads.

#### **5.3.4.1 Summary and Conclusions**

In this task, the variables that affect the diagonal cracking load of deep beams were determined with data from the experimental program and from the literature. It was verified that the cross section of the member ( $b_w d$ ), the tensile strength of concrete ( $\sqrt{f'_c}$ ), and the  $a/d$  ratio are primary variables. The diagonal cracking load appeared to be a function of the longitudinal reinforcement ratio to some degree, but there was not a wide enough range of data to evaluate this variable properly. It should be noted that the longitudinal reinforcement ratio does not vary much in TxDOT bent caps in general. It was shown that the effective depth of the member may have an effect on the normalized diagonal cracking load, but the effect was inconsistent and likely small overall. Using empirical equations presented in the literature and in design specifications, it was determined that accurately estimating the diagonal cracking load is difficult. The difficulty is due to the complexity of accounting for the wide range in the values of each variable that affect diagonal cracking and due to the inherent scatter of the diagonal cracking loads of nominally-identical specimens. The latter problem is likely due to the variability in the tensile strength of concrete. As a result, a simple empirical equation was recommended to estimate the diagonal cracking load of deep beams with a reasonable amount of conservatism. This estimate can be compared to service level shear to determine the likelihood of diagonal cracking in service.

Following the procedure outlined in this section will not guarantee that a reinforced concrete deep beam will remain uncracked in service, primarily due to the inconsistencies between many design assumptions and actual field conditions such as overloads, restrained shrinkage, temperature changes, repeated loadings, material properties of the concrete, etc. However, it is a simple and logical approach that can significantly reduce or limit diagonal cracking in service. Furthermore, it forces the designer to think about the serviceability performance of the structure in the design phase.

## **5.4 CORRELATION OF MAXIMUM DIAGONAL CRACK WIDTH TO CAPACITY**

On occasion, diagonal cracks are discovered in bent caps (deep beams) in service (Section 2.2). Upon inspection of the structures, field engineers are asked to assess the amount of distress in the cracked member. Currently, there is little information in the literature regarding a method to link the width of diagonal cracks to the amount of distress in the deep beam.

The objective of this task was to develop a means to aid field engineers in evaluating the residual capacity of a diagonally-cracked bent cap. Data from the literature and data from the experimental program were used to identify key variables that influence the width of diagonal cracks. Accounting for these variables, a simple chart was developed that correlates the maximum width of the primary diagonal crack in a deep beam to the corresponding percent of its capacity.

### **5.4.1 Background**

Contrary to that of diagonal cracks, the variables affecting the width of flexural cracks have been studied extensively over the last fifty years. Several empirical relationships based on experimental data exist for estimating the width of flexural cracks. A brief background on variables affecting the width of flexural cracks will be discussed in this section. Less information on the width of diagonal cracks is present in the literature, particularly for members governed by shear behavior. Of the many research projects conducted on deep beam shear, diagonal crack width information was only included in a few studies. These studies will provide some indication of the primary variables that affect diagonal crack width in shear-critical members.

#### ***5.4.1.1 Variables affecting width of flexural cracks***

Based on research conducted over the last fifty years, the three primary variables affecting flexural crack width are steel stress, concrete cover, and bar spacing. Test results indicate that steel stress is the most important of the three, especially at service load levels. In ACI 318-08, crack width is limited through the maximum bar spacing of the reinforcement (ACI, 2008). The equation for bar spacing accounts for the stress in

the reinforcement and concrete cover. In AASHTO LRFD 2008, crack width is also limited by restricting the spacing of mild reinforcement (AASHTO, 2008). However, the AASHTO equation for bar spacing addresses exposure condition and strain gradient in addition to concrete cover and steel stress. A distinction between exposure conditions is not made in ACI 318-08 due to “the inherent variability in cracking” and due to experimental evidence that does not support the width of cracks influencing corrosion at service-load levels (Committee Closure, 1999 and ACI 318-08, 2008). As noted in Section 4.2.2, exposure conditions were addressed in ACI-318 prior to the 1999 version of the code.

Tensile stress of the longitudinal reinforcement was confirmed as the primary variable affecting flexural crack widths in a research study conducted by Young et al. in 2002. Sixteen (16) full-scale reinforced concrete bent caps were tested at an  $a/d$  ratio of approximately 1.6 by Young et al. (2002). Limiting the longitudinal reinforcement stress at the face of the column to 30 ksi and 24 ksi under service load levels corresponded to maximum flexural crack widths of 0.016 in. and 0.013 in., respectively. It was found that the distribution of longitudinal reinforcement through transverse spacing had little effect on flexural crack widths.

#### ***5.4.1.2 Types of diagonal cracks***

As noted in Section 5.3.1, two different types of diagonal cracks exist in reinforced concrete deep beams: flexure-shear cracks and web-shear cracks. Flexure-shear cracks form after or concurrently with flexural cracks. They extend from the top of the flexural crack towards the origin of load. Web-shear cracks occur independently of flexural cracking. They form when the principal tension stress in the web of the member exceeds the tensile strength of concrete. In deep beams, web-shear cracks are also referred to as bursting or splitting cracks. Specifically, they are caused by transverse tensile stresses that exist due to the spreading of compressive stresses in bottle-shaped struts. It is apparent that the spreading of compressive stresses in deep beams contributes to the width of flexure-shear cracks as well. Both of these cracks are depicted in Figure 5.35.

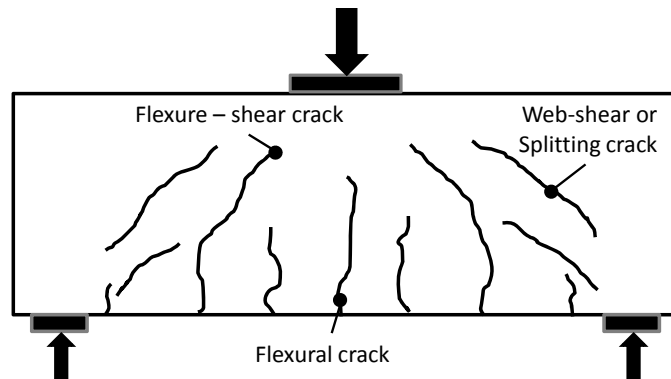


**Figure 5.35: Types of cracks in reinforced concrete deep beams**

The purpose of this task was to correlate maximum diagonal crack widths with the residual capacity of a deep beam bent cap. In the analysis of the crack width data from the experimental program and the literature, a distinction between web-shear cracks and flexure-shear cracks was not made. Both were treated simply as inclined cracks. The only relevant distinction between the two is related to the level of distress present in a shear-critical member. In general, the presence of web-shear cracks is a sign of impending failure (Section 4.3.2).

#### **5.4.1.3 Effect of web reinforcement on diagonal crack widths of deep beams**

In the literature, transverse reinforcement was found to be the most important variable in controlling diagonal crack widths. Unfortunately, very little diagonal crack width data were reported in the literature. A few studies in which diagonal crack widths were monitored during deep beam tests are discussed in this section. Crack width data from these studies are replotted where possible. In each case, the qualitative findings of the researchers are presented.

In a study by Smith and Vantsiotis (1982), fifty-two (52) deep reinforced concrete beams with a 4"x14" cross-section were tested to failure. The purpose of the study was to evaluate the effect of web reinforcement on the strength and overall performance of deep beams. Specimens were tested with simple supports at a/d ratios of 0.77, 1.01, 1.34, and 2.01. During the tests, maximum crack widths were recorded at

each load increment. In the paper, the maximum diagonal crack width at failure for each of the specimens was listed. However, only representative crack width data were provided from a beam at each  $a/d$ . Nevertheless, the authors indicated that “web reinforcement was effective in reducing crack widths at all corresponding load levels and particularly in beams with  $a/d > 1.0$ ” (Smith and Vantsiotis, 1982). Specifically, the researchers recommended minimum web reinforcement to restrain crack widths corresponding to 0.18% in the vertical direction and 0.23% in the horizontal direction ( $\rho_v = 0.0018$  and  $\rho_h = 0.0023$ ). It was apparent from the maximum crack width at failure data that reinforcement in addition to the minimum did little to further restrain the diagonal crack widths.

A research study conducted by Kong et al. (1970) focused on varying the amount of transverse reinforcement depending on the  $a/d$  ratio of the test specimen. Kong et al. tested thirty-five (35) reinforced concrete deep beams with  $a/d$  ratios ranging from 0.35 to 1.18. The crack width data indicated that at low  $a/d$  ratios (0.35), horizontal reinforcement placed near the tension steel was most effective at restraining crack widths. As the  $a/d$  ratio increased, the effectiveness of the vertical reinforcement at restraining diagonal cracks increased.

In an investigation by Tan et al. (1997), crack width data were recorded for eighteen (18) deep reinforced concrete beams. Six specimens each were tested at an  $a/d$  ratio of 0.85, 1.13, and 1.69. It was observed that for specimens with reinforcement in only one direction, vertical reinforcement was more effective than horizontal reinforcement at restraining crack widths. However, the most effective crack width restraint was provided by similar amounts of reinforcement in both orthogonal directions (Tan et al., 1997). These trends were evident at all three  $a/d$  ratios.

The effect of transverse reinforcement on the width of diagonal cracks was also evaluated in the full-scale study conducted by Bracci et al. (Bracci et al., 2000 and Young et al., 2002). Sixteen (16) 33”x36” bent caps were tested to failure at an  $a/d$  ratio of approximately 1.6. The longitudinal reinforcement ratio for the specimens ranged from 0.6% to 0.8%. Three different web reinforcement arrangements were included in the test



specimens. For the Group 1 and 2 specimens, the reinforcement in the horizontal direction ranged from 0.19% to 0.22%; the reinforcement in the vertical direction was 0.3%. The vertical reinforcement consisted of two-legged, #5 stirrups. In the Group 3 specimens, the horizontal reinforcement was 0.22% and the vertical reinforcement was 0.6%. The vertical reinforcement in the Group 3 specimens consisted of four-legged #5 stirrups. During the tests to failure, the maximum width of inclined cracks was recorded for each specimen. From the test results, it was observed that the additional vertical reinforcement in the Group 3 specimens promoted “a more desirable (ductile) flexural failure mechanism at ultimate loading” (Young et al., 2002). The diagonal crack width data from this study are replotted in Figure 5.36. From the data, it is evident that the additional vertical reinforcement did little to further restrain the diagonal crack widths at first cracking and in the service load range. Above 50% of the total applied load, however, the Group 3 specimens had narrower crack widths than the Group 1 or 2 specimens. These results agree well with the findings in Section 4.3.3 regarding minimum web reinforcement. Increasing the amount of vertical reinforcement from 0.3% to 0.6% did little to reduce the crack widths at first cracking or at typical service loads. These data indicate that there are diminishing returns in regards to the diagonal crack width restraint from increasing the amount of transverse reinforcement.

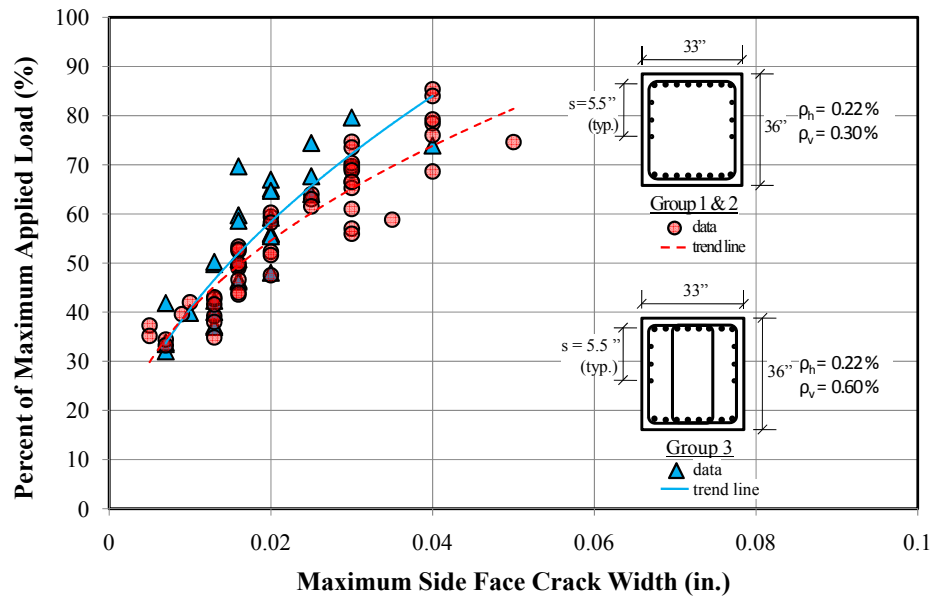


**Figure 5.36: Effect of transverse reinforcement on width of diagonal cracks (Bracci et al., 2000)**

#### 5.4.1.4 Effect of a/d ratio on diagonal crack widths

In the literature, there are mixed observations regarding the effect of a/d ratio on diagonal crack width. This effect was not comprehensively studied by any previous researcher. In a few research projects, some trends between diagonal cracks widths and a/d ratio were either noted or denied. When possible, only specimens with transverse reinforcement are evaluated in this section.

In the study by Kong et al. (1970), a trend with a/d ratio was detected. Thirty-five (35) deep beams were tested at a/d ratios of 0.35, 0.54, and 1.18. As the a/d ratio increased, average and maximum diagonal crack widths increased. The maximum crack width data from the Series 4 and 5 specimens are replotted in Figure 5.37. These series had the most practical reinforcement layouts of the beams tested. From the data, a considerable difference in the diagonal crack widths was seen at 50% of the maximum applied load and greater. The first cracking load for the specimens tested at an a/d ratio of 0.35 was approximately 40% of the maximum applied load. It is important to note that different a/d ratios were obtained by changing the depth of the section. It is possible that

the change in depth also influenced the crack widths based on the results that were presented in Section 4.4.3. In this case, the effect of depth would have mitigated the width of the diagonal cracks as the  $a/d$  ratio increased (and the depth of the member decreased).

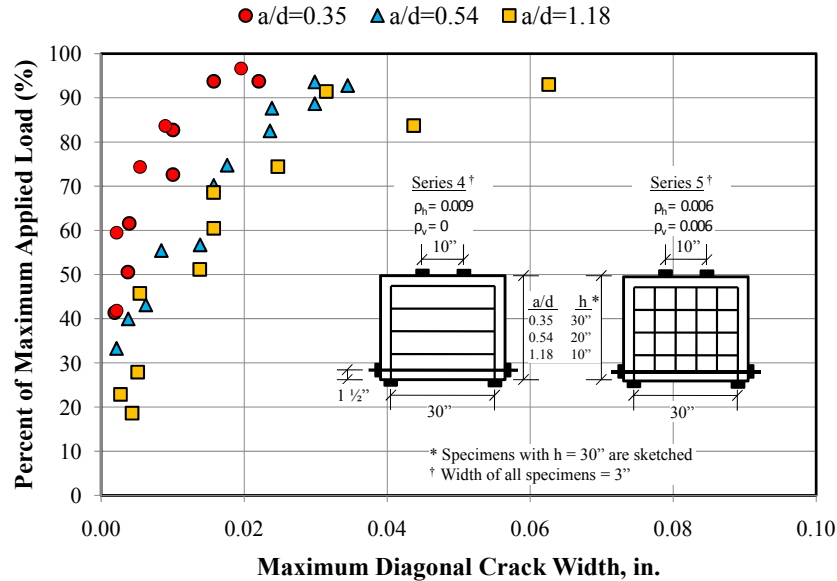


**Figure 5.37: Effect of  $a/d$  ratio on maximum width of diagonal cracks (Kong et al., 1970)**

In the study by Tan et al. (1997), a slight increase in diagonal crack widths with increasing  $a/d$  ratios was noticed. Diagonal crack width plots were provided for the beams tested at each  $a/d$  ratio: 0.85, 1.13, and 1.69. Unfortunately, only the general trends in the data were visible in the original reference; it was not possible to extract the data from the plots due to their size. Nevertheless, at similar percentages of the maximum applied load, it appeared that the diagonal crack widths were greater in the specimens with an  $a/d$  ratio of 1.69 when compared to those tested at an  $a/d$  ratio of 0.85 or 1.13. However, there was not a clear difference between the data from the specimens with an  $a/d$  ratio of 0.85 and 1.13. For the specimens tested at an  $a/d$  ratio of 1.69, it was noted that “the fastest development rate of the diagonal crack occurred” (Tan et al., 1997).

In the research study conducted by Smith and Vantsiotis (1982), however, no trend between diagonal crack widths and  $a/d$  ratio was detected. Fifty (50) reinforced concrete beams were tested at  $a/d$  ratios of 0.77, 1.01, and 1.34. Two (2) additional beams were tested at an  $a/d$  ratio of 2.0. Maximum crack width at failure was tabulated for all of the specimens. Negligible differences in maximum crack width at failure were evident as the  $a/d$  ratio changed for the test specimens. In addition, representative load versus crack width plots were provided at each  $a/d$  ratio. From these plots, an effect of  $a/d$  ratio on the width of diagonal cracks was not apparent. The data from the representative crack width plots are replotted in Figure 5.38.

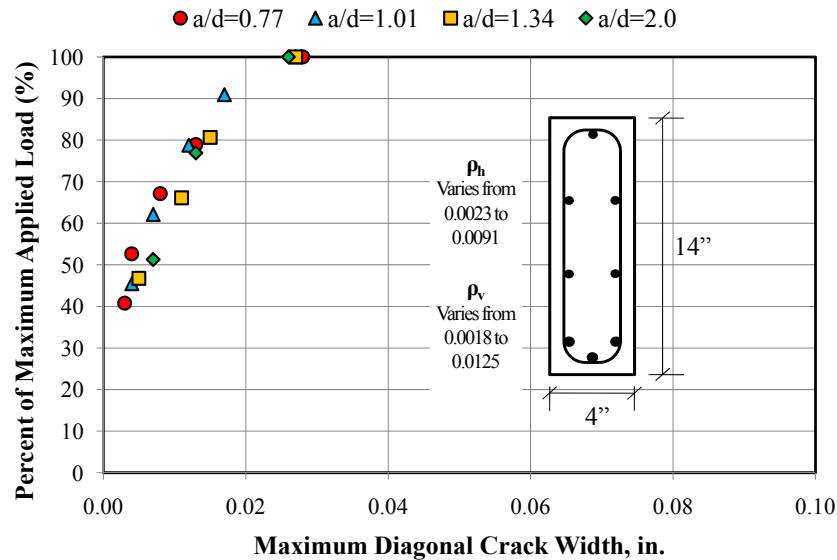


**Figure 5.38: Effect of  $a/d$  ratio on maximum diagonal crack width (Smith and Vantsiotis, 1982)**

#### 5.4.1.5 Effect of longitudinal reinforcement on diagonal crack widths

In 1971, Suter and Manuel tested twelve (12) deep beams (6" x 13") at an  $a/d$  ratio of 1.5 and 2.0. At each  $a/d$  ratio, the longitudinal reinforcement was either 0.96% or 2.44%. Four of the beams were unreinforced transversely; the remaining eight were reinforced with a single stirrup at the midspan of the beam. The experimental results suggested that the beams with greater longitudinal reinforcement (2.44%) were more

shear critical. Specifically, the width of diagonal cracks was more dominant than the flexural cracks at service loads and near ultimate. On the contrary, the width of the diagonal cracks of the beams with a lower amount of longitudinal reinforcement (0.96%) was not as critical as the flexural cracks at service loads ( $0.4M_{ultimate}$ ). At approximately 70% of the ultimate load, the width of the diagonal cracks exceeded that of the flexural cracks. All of the transversely reinforced beams with 0.96% longitudinal reinforcement failed in flexure; two of the four transversely reinforced beams with 2.44% longitudinal reinforcement failed in flexure; the other two in shear. This study illustrated that longitudinal reinforcement can affect the diagonal crack widths in a deep beam by affecting the governing mechanism of behavior.

#### ***5.4.1.6 Effect of concrete cover on diagonal crack widths***

It is known that the width of *flexural* cracks is affected by the thickness of the concrete cover to the extreme tension face (Gergely and Lutz, 1968 and Frosch, 1999). The reason is due to the strain gradient. The crack width measured at the extreme tension face will increase as the concrete cover increases because the restraint provided by the primary tension reinforcement is further away. The situation is different for diagonal crack widths and side face cover.

An experimental study was conducted by Rahal (2006) to investigate the effect of concrete cover on shear behavior. Attention was given to the effect on diagonal crack widths. Seven (7) tests were carried out at an a/d ratio of 3. The overall depth of the test specimens was 15.7 in. The width of the specimens ranged from 8.3 in. to 13.8 in. The side concrete cover to the stirrups increased proportionally with the width of the member. Four different covers were evaluated: 0.2 in., 1 in., 2 in., and 3 in. The diagonal crack widths were plotted versus the applied shear for the test specimens. A similar increase in the width of diagonal cracks with increasing applied load was observed for the specimens with 0.2 in., 1 in., and 2 in. of cover. When the cover was within this range, the diagonal crack widths were not affected. For the specimens with 3-in. side cover, however, “a sharp increase in crack width” occurred shortly after cracking, nearly 10-times larger than that of the specimens with smaller cover (Rahal, 2006). The same general trend was seen

for specimens with 3,600 psi and 6,000 psi concrete. Thus, the study by Rahal suggests that concrete cover should not affect the width of diagonal cracks provided that the cover is less than 2 in. For reference, the side face cover for most of the specimens in the Project 5253 experimental program was 0.75 in. which is smaller than that in the field (1.5 in. to 2 in.).

In summary, the primary variable that affects the width of diagonal cracks is the amount of web reinforcement. While there was not much crack width data in the literature showing this relationship, numerous researchers unanimously came to this conclusion. However, it was shown that there is a limit to the reduction in diagonal crack widths that can be obtained by providing additional web reinforcement. There was not as much consensus in the literature with regards to the effect of  $a/d$  ratio on the width of diagonal cracks. Based on the available data, it is likely that the  $a/d$  ratio affects the diagonal crack widths to some degree. Perhaps, the lack of consensus is an indication that the effect is relatively minor. Also, it was shown that the longitudinal reinforcement ratio can affect the width of diagonal cracks by altering the governing behavior of the member. In the current task, the performance of shear-critical members was addressed in response to the observed cracking patterns in field specimens (Section 2.2). With knowledge of the primary variables that affect diagonal crack widths, an approach to correlate them with the residual capacity of a deep beam can be determined.

#### **5.4.2 Approach**

In this task, a technique to link the maximum width of a diagonal crack with the residual capacity of an in-service bent cap was required. Two different approaches were considered that incorporated the primary variables that affect the width of diagonal cracks in deep beams.

First, an analytical approach was taken. The steps of the approach are illustrated in Figure 5.39. A simple strut-and-tie model was used to estimate the perpendicular tensile force in a bottle-shaped strut, assuming that the diagonal crack forms along the axis of the strut. The perpendicular tensile force was calculated as a function of the angle of spreading in the bottle-shaped strut, the angle of the strut with respect to the

horizontal, and the amount of shear on the section. The tensile force was converted to tensile strain assuming that all of the strain exists in the transverse steel, ignoring the strain in the concrete. Multiplying the perpendicular tensile strain by the perpendicular crack spacing provided an estimate for the average width of a diagonal crack. From the literature, a constant of 2.0 was used to convert the average width of the diagonal crack to the maximum diagonal crack width, or the 95-percentile crack width (Adebar, 2001). Several assumptions were required to estimate diagonal crack widths with this approach. They include the following:

- Strain in the concrete perpendicular to the diagonal crack was ignored
- Crack spacing perpendicular to the diagonal crack was calculated assuming that longitudinal crack spacing ( $s_l$ ) was equal to stirrup spacing
- The difference between average crack widths and maximum crack widths was taken as 2.0
- An angle of spreading ( $\alpha$ ) was assumed

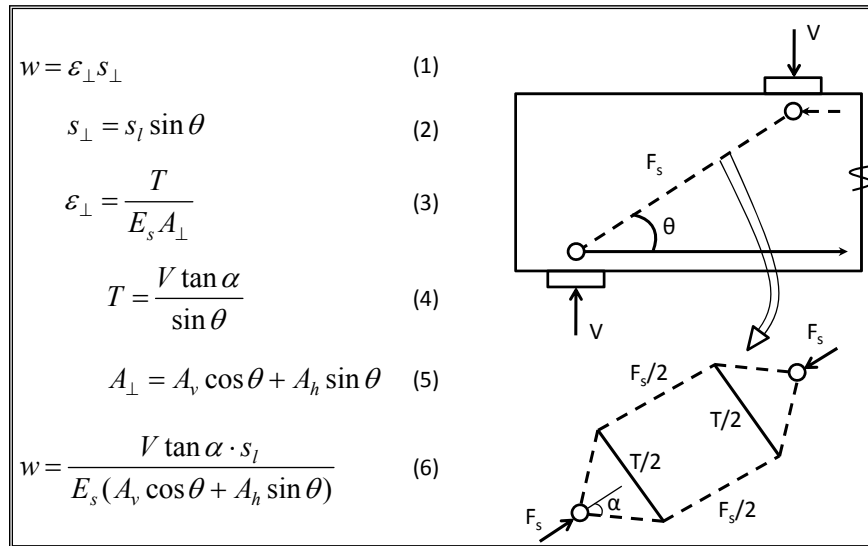


**Figure 5.39: Preliminary analytical model for estimating diagonal crack widths**

where  $w$  = diagonal crack width (in.)

$\epsilon_{\perp}$  = strain perpendicular to the diagonal strut

$s_{\perp}$  = crack spacing perpendicular to the diagonal strut (in.)

- $s_l$  = longitudinal crack spacing (in.)
- $T$  = total tie force in the bottle-shaped strut (kips)
- $E_s$  = modulus of elasticity of strut reinforcement (ksi)
- $A_v$  = area of vertical strut reinforcement (in.<sup>2</sup>)
- $A_h$  = area of horizontal strut reinforcement (in.<sup>2</sup>)
- $V$  = shear on the section (kips)
- $\theta$  = angle of diagonal strut with respect to horizontal (deg.)
- $\alpha$  = angle of spreading of diagonal strut (deg.)

A few of the aforementioned assumptions are troublesome. Neglecting the contribution of the concrete in resisting the transverse tensile stresses in a bottle-shaped strut is fairly reasonable. The tensile strain in the concrete between cracks is very small in relation to the strain in the reinforcement at the cracks. Assuming that the crack spacing equaled the stirrup spacing is also a fair assumption. The basis of this assumption was the crack patterns of similar specimens in the experimental program in which the main difference between them was a stirrup spacing of 6 in., 10 in., or 15 in. However, even though the crack spacing changed between these tests, the maximum diagonal crack width was not affected proportionally to the spacing. It is likely that the difference between average crack widths and maximum crack widths is not constant as the stirrup spacing changes. Lastly, and most important, it is difficult to justify an assumed angle of spreading. In ACI 318-08 Appendix A, the angle of spreading ( $\alpha$ ) is assumed to be approximately 26 deg., corresponding to a slope of 2:1 (ACI 318-08, 2008). In 1982, Schlaich and Weischede presented a model for estimating the spreading of compressive stresses in an elastic body based on the starting width of the bottle-shaped strut and an assumed width at midheight. In general, this approach yielded angles of spreading shallower than 26 deg. It is difficult to justify either assumption.

In addition to the problems with the assumptions of this analytical approach, there are significant problems with its applicability. Crack widths are calculated as a function of the shear in the member. Since this task is aimed at correlating crack widths to



residual capacity, an estimate for the load-carrying capacity of the member must be made as well. As such, a full strut-and-tie model analysis would be required. This level of calculation is inappropriate for a task conducted in the field. Lastly, conditions in the field can be very different from those in the laboratory. Some differences may include boundary conditions, axial restraint, long-term (time) effects, and the presence of repeated loads. The inherent variability of crack widths and the differences between field and laboratory conditions negate the level of accuracy that is implied with these detailed calculations.

It should be noted that a study was conducted by Zhu et al. (2003) aimed at crack width prediction using a “compatibility-aided strut-and-tie model.” This study focused specifically on the diagonal cracking of members with re-entrant corners. In this study, some of the aforementioned assumptions of the analytical approach were addressed. Strains in the concrete perpendicular to the diagonal crack were accounted for, but in conjunction with an assumed area of concrete contributing to the restraint. Instead of crack spacing, an estimate for gauge length was used that was calibrated with test data. Due to the dominance of a single crack at re-entrant corners, a difference between average and maximum crack widths was not made. Lastly, assumptions regarding the angle of spreading were not necessary due to the defined geometry of this application. While the approach by Zhu et al. (2003) is more sophisticated and more calibrated than the analytical approach discussed herein, it suffers from the same limitations in applicability in regards to the current task. The required amount of calculations is significant, an ultimate-strength estimate is required, and the level of accuracy is not justified due to inevitable differences between field and laboratory conditions.

The second approach used to address this task was empirically-based. Maximum crack width data were obtained for the specimens tested in the current study as discussed in Section 3.5.3. Each crack width measurement was plotted versus the corresponding percent of ultimate load. The data were grouped by the amount of web reinforcement in the test specimen. A strong relationship between the maximum diagonal crack width and the amount of web reinforcement crossing the crack was supported by the test data. A

chart was developed with the diagonal crack width data from the experimental program that links the maximum diagonal crack width to the amount of load in the member (quantified as a percent of the ultimate strength). Only the amount of web reinforcement in each direction is needed to use the chart.

The data used in the development of the chart are discussed in the next section. Following that, the chart is presented. Estimates from the chart are compared to crack width data from sixteen full-scale bent caps tested by Bracci et al. (2000) that were not used in the calibration of the chart.

### **5.4.3 Results**

All of the test specimens fabricated in the current project are listed in Table 5.2. Two specimens fabricated and tested by Deschenes are listed in the table as well (Deschenes, 2009). The beam details and test results for the specimens tested by Deschenes are provided in Table 5.3 and Table 5.4, respectively. The data from these specimens were included with the beams from the experimental program due to the scarcity of diagonal crack width data for full-scale, deep beams in the literature. In addition, the specimens contained different amounts of longitudinal and web reinforcement.

The shaded specimens in Table 5.2 were not used to address this task. The data from specimens with insufficient web reinforcement, overall beam height of 23 in., and abnormally large bearing plates were excluded because their details did not reflect typical TxDOT practice. Also, since the current project focused on deep beam behavior, specimens tested at an  $a/d$  ratio greater than 2 were not used. Lastly, the crack width data from two specimens, II-02-CCC1007 and M-03-2-CCC2436, were excluded because the data were unreliable.

Therefore, the results of 24 deep beam shear tests were used in the current task (two of which were tested by Deschenes (2009)). Twenty-one tests were conducted at an  $a/d$  ratio of 1.85; three tests were conducted at an  $a/d$  ratio of 1.2. The overall height of the specimens ranged from 42 in. to 75 in. The width ranged from 21 in. to 36 in. The minimum amount of web reinforcement in the specimens was either 0.2% in both

orthogonal directions or 0.25% in the vertical direction and 0.15% in the horizontal direction. The maximum amount of reinforcement in the vertical and horizontal direction was 0.86% and 0.58%, respectively. Several different bearing plate sizes were used as shown in Table 5.2. Lastly, the longitudinal reinforcement ratio ranged from 2.3% to 3.1%.

The measured diagonal crack width data from the tests in the experimental program were plotted versus the percent of maximum applied load. It was determined that plotting crack widths in this manner was an appropriate way to compare data from beams with a variety of different section parameters, such as size and compressive strength. Furthermore, it was consistent with the primary goal of this task: to correlate maximum diagonal crack widths to the load on the structure, quantified as a percent of the capacity. Provided that the depth of the member was greater than or equal to 42 in., the size of the member did not affect the diagonal crack width data when plotted in this fashion (Section 4.4.3). Also, the size of the bearing plates had no effect on the width of diagonal cracks as long as the size did not significantly alter the effective  $a/d$  ratio (Tuchscherer, 2008).

**Table 5.2: Specimens used in correlating crack width-to-capacity (shaded tests not used) (1 of 2)**

Testing Series	Beam I.D.	b in.	d in.	Support Plate†	Load Plate†	No. of Stirrup Legs	ρ <sub>v</sub>	ρ <sub>h</sub>	a/d ratio		
I	I-03-2	21	38.5	16"x21"	20"x21"	2	0.003	0.003	1.84		
	I-03-4					4					
	I-02-2					2	0.002	0.002			
	I-02-4					4					
II	II-03-CCC2021	21	38.6	10"x21"	20"x21"	2	0.003	0.0045	1.84		
	II-03-CCC1007			10"x21"	10"x7"						
	II-03-CCT1021			10"x21"	36"x21"						
	II-03-CCT0507			5"x7"	36"x21"						
	II-02-CCT0507			5"x7"	36"x21"		0.002	0.002			
	II-02-CCC1007			10"x21"	10"x7"						
	II-02-CCC1021			10"x21"	10"x21"						
	II-02-CCT0521			5"x21"	20"x21"						
III	III-1.85-0	21	38.6	16"x21"	20"x21"	-	0.000	0.000	1.84		
	III-2.5-0								2.47		
	III-1.85-02					2	0.002	0.002	1.84		
	III-1.85-025									0.0025	0.0015
	III-1.85-03									0.003	0.003
	III-1.85-01									0.001	0.001
	III-1.85-03b									0.003	0.003
	III-1.85-02b									0.002	0.002
	III-1.2-02								0.002	0.002	1.20
	III-1.2-03								0.003	0.003	
	III-2.5-02								0.002	0.002	2.49
	III-2.5-03								0.003	0.003	

<sup>†</sup> Load plate dimensions: [in direction of span] x [transverse to direction of span]

**Table 5.2 (cont.): Specimens used in correlating crack width-to-capacity (shaded tests not used) (2 of 2)**

Testing Series	Beam I.D.	b in.	d in.	Support Plate†	Load Plate†	No. of Stirrup Legs	ρ <sub>v</sub>	ρ <sub>h</sub>	a/d ratio
IV	IV-2175-1.85-02	21	68.9	16"x21"	29"x21"	2	0.002	0.002	1.85
	IV-2175-1.85-03				0.003		0.003		
	IV-2175-2.5-02				24"x21"		0.002	0.002	2.50
	IV-2175-1.2-02						0.002	0.002	1.20
	IV-2123-1.85-03	19.5	16.5"x21"				0.003	0.003	1.85
	IV-2123-1.85-02		0.002				0.002		
	IV-2123-2.5-02		15.5"x21		0.002		0.002	2.50	
	IV-2123-1.2-02		18"x21"		0.002		0.002	1.20	
M	M-03-4-CCC2436	36	40	16"x36"	24"x36"	4	0.003	0.003	1.85
	M-03-4-CCC0812				8"x12"		0.003	0.003	
	M-09-4-CCC2436				24"x36"		0.0086	0.003	
	M-02-4-CCC2436				24"x36"		0.002	0.002	
	M-03-2-CCC2436				24"x36"	2	0.003	0.003	
Deschenes (2009)	Validation	21	42	16"x21"	20"x21"	2	0.003	0.0058	1.85
	nR1						0.003	0.0058	

† Load plate dimensions: [in direction of span] x [transverse to direction of span]

**Table 5.3: Summary of beam details for two specimens tested by Deschenes (2009)**

Beam I.D.	b <sub>w</sub> (in.)	h (in.)	d (in.)	$\rho_l$	$\rho'_l$	$\rho_v$	$\rho_v$	Support Plate	Load Plate	a/d
Validation	21	42	36.1	0.031	0.01	0.003	0.0058	16"x21"	20"x21"	1.85
nR1	21	42	36.1	0.031	0.01	0.003	0.0058	16"x21"	20"x21"	1.8

**Table 5.4: Summary of test results for two specimens tested by Deschenes (2009)**

Beam I.D.	$f'_c$ (psi)	$f_{yl}$ (ksi)	$f_{yv}$ (ksi)	$V_{crack}$ (kips)	$V_{crack} /$ $V_{test}$	$V_{test}$ (kips)
Validation	5,060	66	65	151	0.26	571
nR1	7,250	66	65	-	-	561

#### 5.4.3.1 Effect of web reinforcement on diagonal crack widths of deep beams

The variables that affect the width of diagonal cracks of deep beams were explicitly evaluated with the tests in the experimental program. The most important variable noted in the literature was the amount of web reinforcement crossing the diagonal crack. The same conclusion was reached in this project. The effect of the quantity of web reinforcement on the diagonal crack widths of deep beams was previously discussed in Section 4.3.3. Diagonal crack width data from five 21"x42" specimens tested at an a/d ratio of 1.85 are shown in Figure 5.40. In general, the amount of transverse reinforcement directly affects the maximum width of the diagonal crack at first cracking and throughout the loading history. Providing web reinforcement of 0.25% in the vertical direction and 0.15% in the horizontal direction yielded similar results to providing 0.2% in each direction. For this reason, the data from these specimens were grouped together in the development of the crack-width-to-capacity chart later in this section.

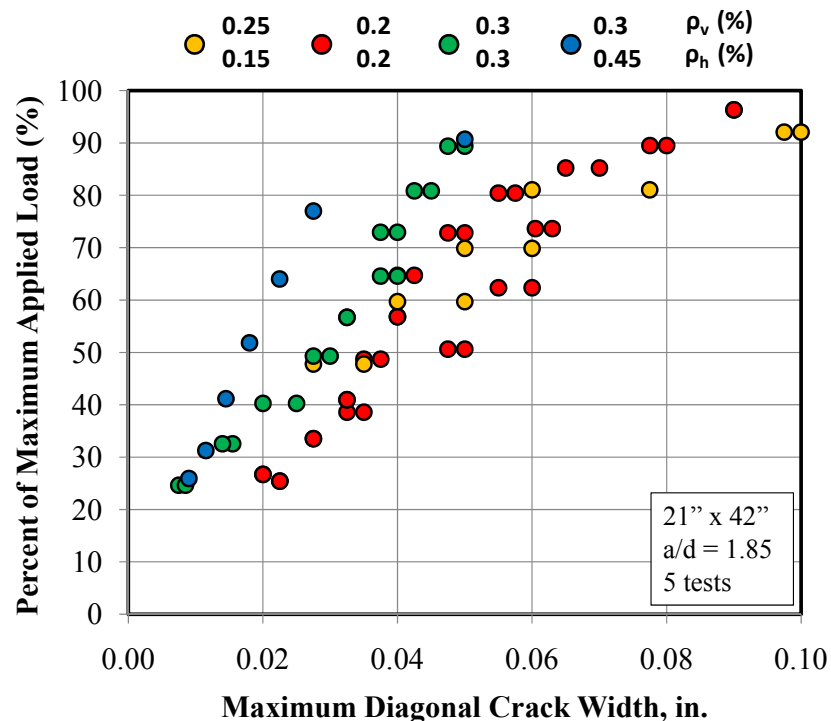
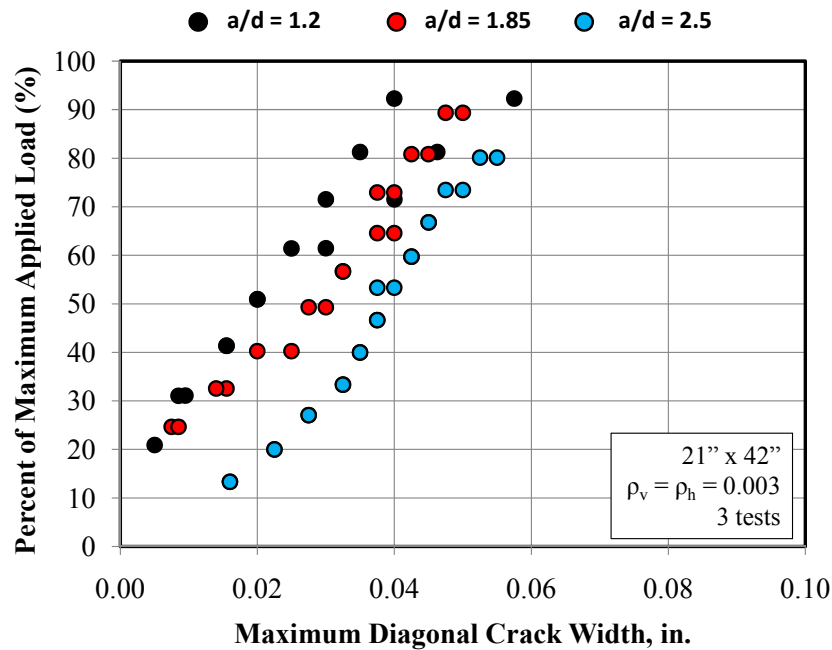


Figure 5.40: Effect of web reinforcement on diagonal crack widths of test specimens

The spacing of web reinforcement was not explicitly evaluated in the experimental program. However, a couple of valid comparisons were possible. As noted in Section 4.3.3, the spacing of the vertical reinforcement only slightly affected the width of diagonal cracks and only if the reinforcement was not adequately distributed. For one specimen, III-1.85-02, the spacing of the stirrups was 14.5 in. The diagonal crack widths for this specimen were compared to that of a nominally-identical specimen with a stirrup spacing of 9.5 in. The results indicated that the larger stirrup spacing in III-1.85-02 contributed to slightly wider cracks. However, the wider cracks were within the total scatter of crack widths recorded from specimens with similar section sizes and quantities of web reinforcement (Section 4.3.3). Thus, for the purposes of this task, the spacing of web reinforcement was not considered a primary variable that affects the width of diagonal cracks in deep beams.

#### ***5.4.3.2 Effect of $a/d$ ratio on diagonal crack widths of deep beams***

The effect of  $a/d$  ratio on the diagonal crack widths of deep beams was also evaluated through the tests in the experimental program. Little consensus exists in the literature regarding the effect of  $a/d$  ratio. In the experimental program, three full-scale tests were conducted at  $a/d$  ratios of 1.2 and 2.5. The test results of three specimens with identical beam details are presented in Figure 5.41. All three 21"x42" specimens had 0.3% web reinforcement in each direction. The only difference among the tests was the  $a/d$  ratio. Since the current task is limited to evaluating deep beams ( $a/d < 2$ ), the data from specimen III-2.5-03 were not specifically needed. It is included in Figure 5.41 for comparison purposes. It is appropriate to compare the data from this specimen with that of the other specimens because the final failure mode was consistent for all three (Section 4.3.2).



**Figure 5.41: Effect of  $a/d$  ratio on maximum diagonal cracking widths, 3 specimens, 0.3% reinf.**

In Figure 5.41, a trend between the  $a/d$  ratio and the maximum width of diagonal cracks is observed. For a given percentage of maximum applied load, the diagonal crack width increases as the  $a/d$  ratio increases. The data in Figure 5.41 plotted with the diagonal crack widths of the other applicable tests in the experimental program are shown in Figure 5.42. The data in Figure 5.42 indicate that while there may be an effect with  $a/d$  ratio, the effect is relatively small in light of the scatter that exists in diagonal crack width data. The change in the maximum width of diagonal cracks from an increase in  $a/d$  ratio from 1.2 to 1.85 was not greater than the scatter associated with the crack widths of similar specimens.



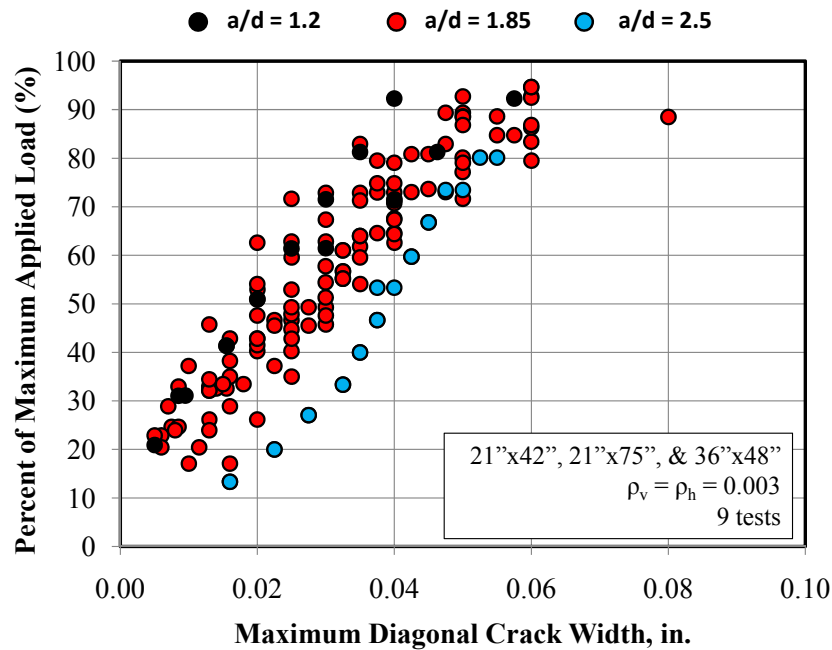


**Figure 5.42: Effect of  $a/d$  ratio on maximum diagonal crack widths, 9 specimens, 0.3% reinf.**

The diagonal crack width data for two similar specimens with 0.2% web reinforcement tested at an  $a/d$  ratio of 1.2 and 1.85 are presented in Figure 5.43. The specimens have a 21"x42" cross-section. A trend with  $a/d$  ratio is not evident in this plot. It should be noted that the crack width data from a similar specimen tested at an  $a/d$  ratio of 2.5 were excluded from Figure 5.43 because this specimen failed in sectional shear whereas the other two specimens failed by crushing of the direct strut. As noted previously (Section 4.3.3), the dominant shear transfer mechanism must be similar to compare crack width data from multiple tests. The crack width data from all of the specimens with 0.2% web reinforcement are plotted in Figure 5.44. The maximum diagonal crack widths from IV-2175-1.2-02 were included in this plot as well. In Figure 5.44, it is clear that no trend with  $a/d$  ratio is evident, especially considering the scatter that exists in diagonal crack width data.

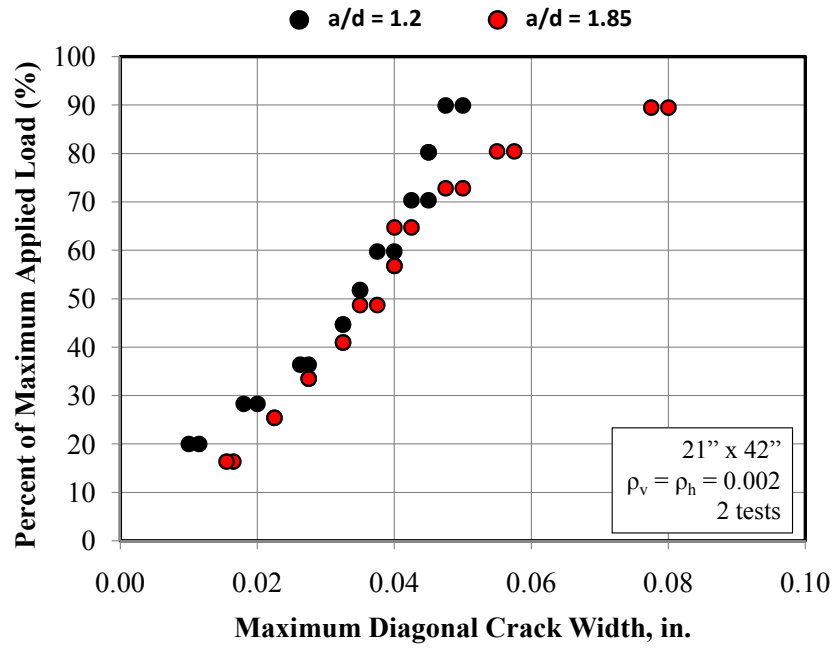


*Figure 5.43: Effect of  $a/d$  ratio on maximum diagonal crack widths, 2 specimens, 0.2% reinf.*

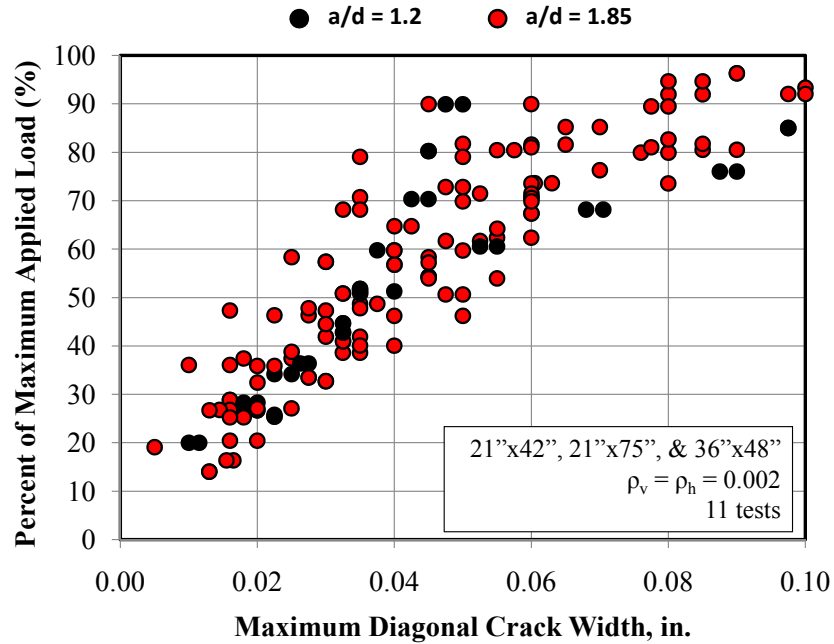


*Figure 5.44: Effect of  $a/d$  ratio on maximum diagonal crack widths, 11 specimens, 0.2% reinf.*

The results presented in Figure 5.41 indicate that a trend with  $a/d$  ratio exists to some extent. However, the results presented in Figure 5.42 through Figure 5.44 suggest that the trend is relatively weak considering the scatter in diagonal crack width data for deep beams. Based on these findings, it was determined that increasing the  $a/d$  ratio from 1.2 to 1.85 did not significantly affect diagonal crack widths. Thus, it was not considered a primary variable for the purpose of this task.

#### ***5.4.3.3 Effect of longitudinal reinforcement on diagonal crack widths of deep beams***

The effect of the longitudinal reinforcement ratio on the width of diagonal cracks was not explicitly studied in the experimental program. However, the crack width data from two tests with similar beam parameters but different longitudinal reinforcement can be compared to evaluate it to some degree. In Figure 5.45, the diagonal crack width data from two tests in the experimental program, II-03-CCC2021 and II-03-CCC1007, were compared to that of the two tests conducted by Deschenes (2009) that were described previously (Table 5.3 and Table 5.4). All four specimens had an identical cross-section and similar amounts of web reinforcement. The main difference between the specimens was the amount of longitudinal reinforcement. Specimens II-03-CCC2021 and II-03-CCC1007 had 2.3% longitudinal reinforcement; the beams tested by Deschenes (2009) had 3.1% reinforcement.

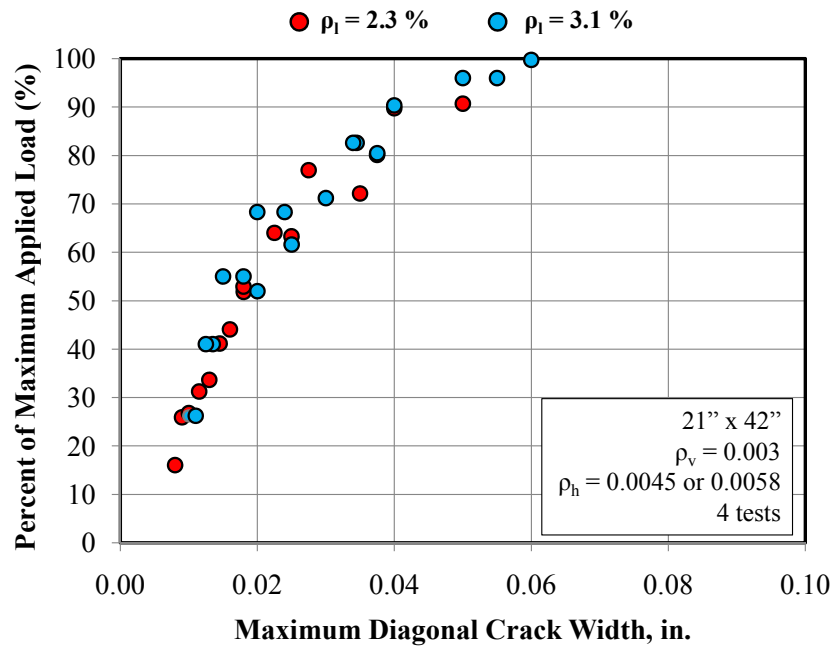


**Figure 5.45: Effect of longitudinal reinforcement on diagonal cracks in shear-critical members**

The results in Figure 5.45 indicate that the quantity of longitudinal reinforcement does not affect the width of diagonal cracks in deep beams in general. Since the maximum diagonal crack width was often measured near the mid-depth of the member, this finding makes sense. It should be noted, however, that the width of diagonal cracks can be affected by the longitudinal reinforcement by affecting the dominant mechanism of behavior as noted by Suter and Manuel (1971). More discussion related to the effect of longitudinal reinforcement on the width of diagonal cracks exists later in this section when the data from Bracci et al. (2000) are compared to the estimates from the proposed chart.

It was shown from the crack width data from the experimental program that the quantity of web reinforcement is the primary variable that affects the maximum width of diagonal cracks. To some extent, the  $a/d$  ratio contributed to the width of diagonal cracks. However, the effect was small in relation to the scatter associated with the crack widths of similar specimens. Also, it was shown with the data from the experimental

program that the longitudinal reinforcement ratio does not affect the width of diagonal cracks for shear-critical members. Lastly, based on the conclusions of Rahal (2006) regarding the influence of concrete side cover on diagonal crack widths, this variable is also unlikely to significantly affect the width of diagonal cracks (Section 5.4.1.6). As a result, a method for correlating the diagonal crack width to the residual capacity of the member was developed considering the quantity of web reinforcement as the primary variable.

#### ***5.4.3.4 Correlation of Crack Width to Residual Capacity***

The crack width data for the 21 specimens used in the current task are plotted in Figure 5.46. All of the beams represented in this plot were tested at an  $a/d$  ratio of 1.85. The data were separated into three groups by the quantity of web reinforcement: 0.2% reinforcement in each direction, 0.3% reinforcement in each direction, and greater than 0.3% reinforcement in each direction. The data from one specimen with 0.25% vertical reinforcement and 0.15% horizontal reinforcement were included in the 0.2% group (Figure 5.40). The data in the greater-than-0.3% group had a variety of different distributions in each direction. In general, the specimens in this group had reinforcement in one direction greater than 0.3% and reinforcement in the other direction of approximately 0.3%.

From the data in Figure 5.46, a consistent trend of the maximum diagonal crack width to the amount of web reinforcement is seen. It is clear that there is some scatter in the plot consistent with crack widths in general. A power function trend line was fitted through the data in each group. The square of the correlation coefficient ( $R^2$ ) is provided next to each trend line. This value quantifies the error between the trend line and the data points. An  $R^2$  value of 1.0 represents a perfect fit. In Figure 5.46, it is interesting to note that the  $R^2$  value increases as the quantity of web reinforcement increases in each group. This finding indicates that with less reinforcement (0.2% in each direction), there was generally more scatter in the diagonal crack width data. As the amount of web reinforcement approached and exceeded 0.3% in each direction, the maximum width of diagonal cracks at each load increment was more consistent.

In Figure 5.47, the power function trend line is replaced with several straight line segments. From these straight line segments, a table was created that correlated the maximum width of diagonal cracks to the corresponding percent of the capacity. At several values for the maximum diagonal crack width, the average percent of capacity was tabulated for each data group. With each average value, a range of the scatter in terms of the percent of capacity was placed in parentheses. The chart is included as Figure 5.48.

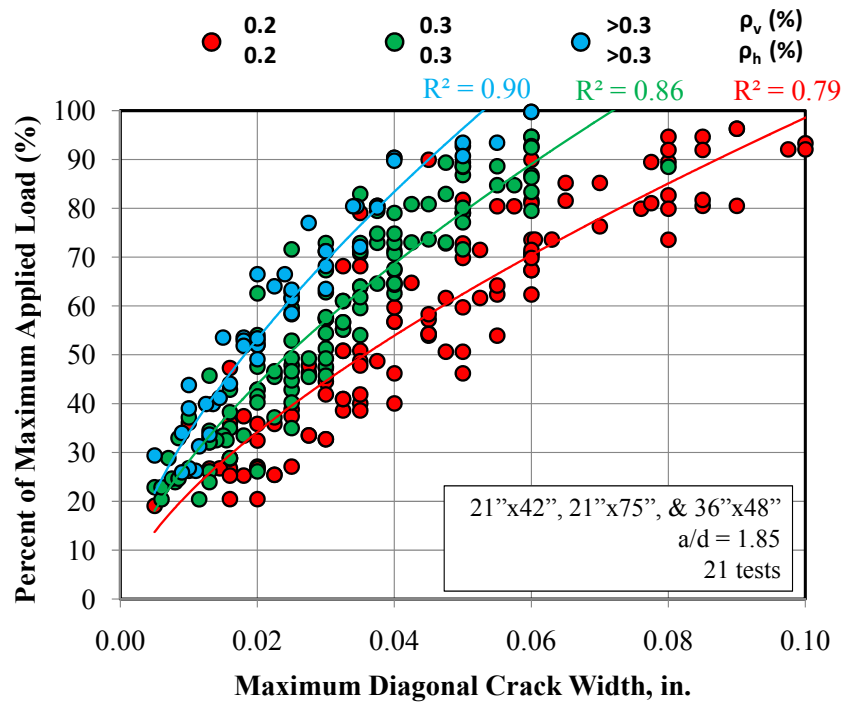


**Figure 5.46: All crack width data used in this task with trend lines**

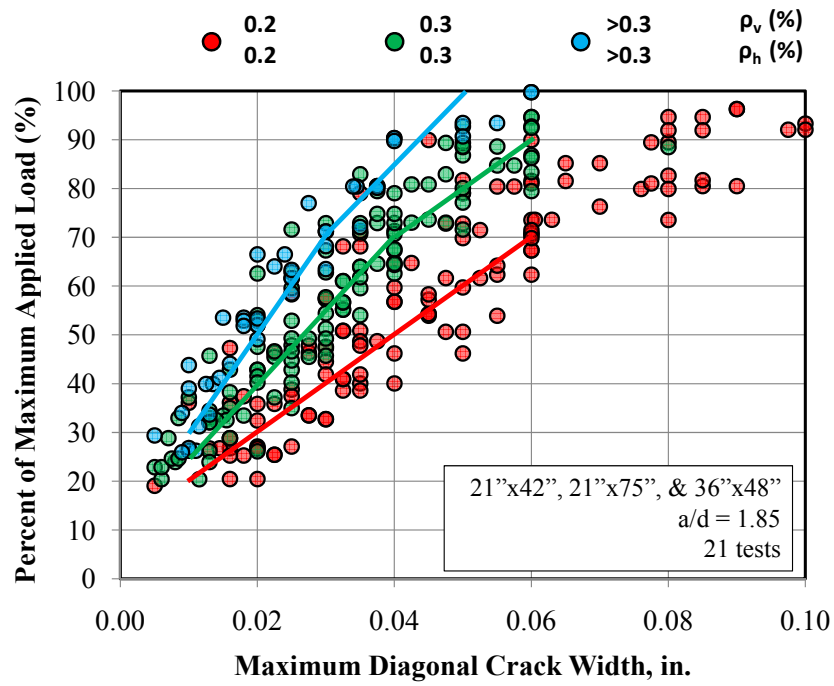


*Figure 5.47: All crack width data used in this task with multiple straight line approximations*

Load on the Member, Quantified as a Percent of Ultimate Capacity on Average ( $\pm$ scatter)							
Reinforcement $w_{\max}$ (in.)		0.01	0.02	0.03	0.04	0.05	0.06
$\rho_v = 0.002$	$\rho_h = 0.002$	20 ( $\pm 10$ )	30 ( $\pm 10$ )	40 ( $\pm 10$ )	50 ( $\pm 10$ )	60 ( $\pm 15$ )	70 ( $\pm 15$ )
$\rho_v = 0.003$	$\rho_h = 0.003$	25 ( $\pm 10$ )	40 ( $\pm 10$ )	55 ( $\pm 10$ )	70 ( $\pm 10$ )	80 ( $\pm 10$ )	90 ( $\pm 10$ )
$\rho_v > 0.003$	$\rho_h > 0.003$	30 ( $\pm 10$ )	50 ( $\pm 10$ )	70 ( $\pm 10$ )	85 ( $\pm 10$ )	~ Ultimate	~ Ultimate

**Notation:**

$w_{\max}$  = maximum measured diagonal crack width (in.)

$\rho_v$  = reinforcement ratio in vertical direction ( $\rho_v = A_v / bs_v$ )

$\rho_h$  = reinforcement ratio in horizontal direction ( $\rho_h = A_h / bs_h$ )

$A_v$  &  $A_h$  = total area of stirrups or horizontal bars in one spacing (in.<sup>2</sup>)

$s_v$  &  $s_h$  = spacing of stirrups or horizontal bars (in.)

$b$  = width of web (in.)

**Directions:**

- 1). Determine  $\rho_v$  and  $\rho_h$  for bent cap
- 2). Measure maximum diagonal crack width,  $w_{\max}$ , in inches
- 3). Use chart with  $w_{\max}$ ,  $\rho_v$ , and  $\rho_h$  to estimate % of capacity

**Important Notes:**

In this chart, the maximum width of the primary diagonal crack in a shear-critical member is linked to the load on the member, quantified as a percent of its ultimate capacity. The intent of this chart is to aide field engineers in evaluating residual capacity in diagonally-cracked, reinforced-concrete bent caps subjected to concentrated loads at a/d ratios between 1.0 and 2.0. This chart was developed from crack width data from 21 tests of simply-supported reinforced concrete beams with overall heights between 42" and 75". The testing was conducted at an a/d ratio of 1.85. Data has shown that diagonal crack widths may slightly decrease with decreasing a/d ratio. The same crack width at a smaller a/d ratio indicates that a higher percentage of capacity from the above chart has already been reached.

This chart should be used in conjunction with sound engineering judgement with consideration of the following limitations:

- variability in crack widths in general ( $\pm$  scatter)
- differences between field and laboratory conditions
- members loaded at a/d < 1.85 may be at slightly higher % of capacity
- implications of an unconservative estimate of capacity

This chart is not intended to be used for inverted-tee bent caps.

**Figure 5.48: Proposed chart that links diagonal crack width to percent of capacity of deep beams**



The crack width measurements obtained by Bracci et al. (2000) were compared to the estimates from the proposed chart. Two different distributions of web reinforcement were investigated by Bracci et al. Some judgment was required to group the data with the limits in the proposed chart. The specimens with 0.3% vertical reinforcement and 0.22% horizontal reinforcement were compared with the 0.3% group estimate. The specimens with 0.6% vertical reinforcement and 0.22% horizontal reinforcement were compared to the greater-than-0.3% group. The results of the comparisons are provided in Figure 5.49.

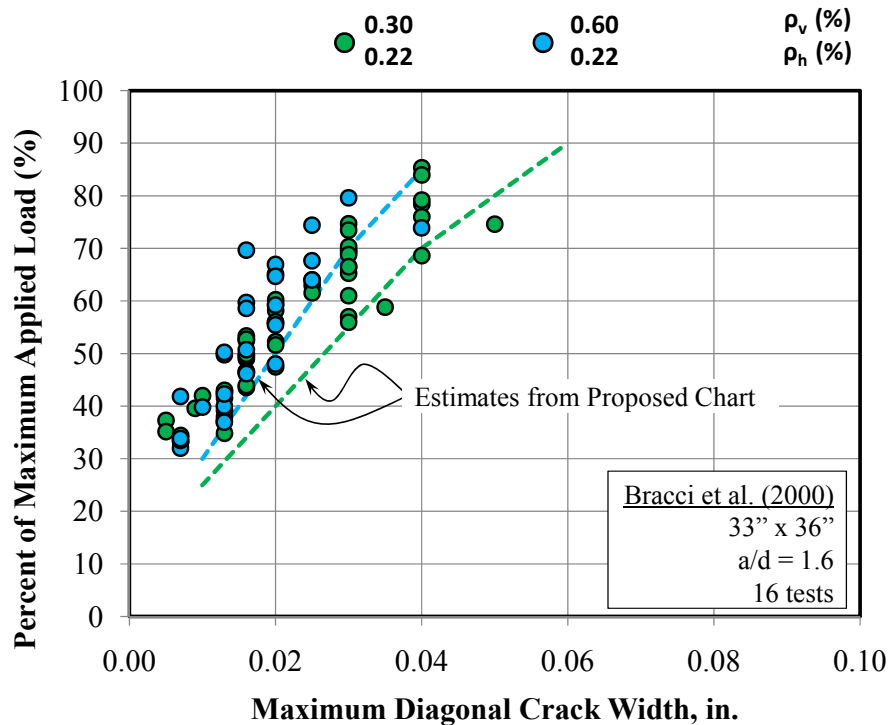


**Figure 5.49: Comparison of crack width data from Bracci et al. (2000) and chart estimates**

In Figure 5.49, the accuracy of the proposed chart was evaluated with independent crack width measurements of full-scale specimens. The specimens were tested at an a/d ratio of 1.6 and had longitudinal reinforcement ratios ranging from 0.6% to 0.8%. Considering the differences between the specimens tested by Bracci et al. (2000) and

those used to develop the chart, the level of accuracy is reasonable. In each group, at a given crack width, the chart estimated an amount of load on the member that was within 20 percentage points of the actual capacity. For example, at a crack width of 0.02 in., it was estimated with the chart that a member with 0.3% reinforcement in each direction was at approximately 40% ( $\pm 10\%$ ) of its capacity. The specimens with a similar amount of reinforcement at the same crack width were at anywhere from 48% to 60% of their capacity. It was estimated with the chart that specimens with web reinforcement exceeding 0.3% in each direction were at 50% ( $\pm 10\%$ ) of their capacity at a maximum diagonal crack width of 0.02 in. The specimens tested by Bracci et al. (2000) with similar amounts of reinforcement and with maximum crack widths of 0.02 in. were at 48% to 68% of their capacity.

It is clear from Figure 5.49 that the data from Bracci et al. (2000) is shifted to the left with respect to the estimates from the chart. One potential reason for the shift is the longitudinal reinforcement ratio. The smaller longitudinal reinforcement ratio in the specimens tested by Bracci et al. (2000) caused the specimens to be less shear-critical than those represented in the proposed chart. It is possible that the maximum width of the diagonal cracks reduced for this reason. Additional research is needed to improve the accuracy of the chart in relation to the effects of  $a/d$  ratio and the longitudinal reinforcement ratio.

The accuracy of the proposed chart was also compared to the specimens from the experimental program that were tested at an  $a/d$  ratio of 1.2. In this way, the implications of excluding an adjustment for the  $a/d$  ratio in the proposed chart could be evaluated. The results are presented in Figure 5.50. The results indicate that the chart does an adequate job of estimating the level of distress in each member until approximately 60% to 70% of the capacity is reached. Closer to ultimate, the crack widths for the specimens with 0.2% web reinforcement diverge from the estimated crack widths. As noted previously, changing the  $a/d$  ratio from 1.85 to 1.2 only slightly affected the maximum width of diagonal cracks.

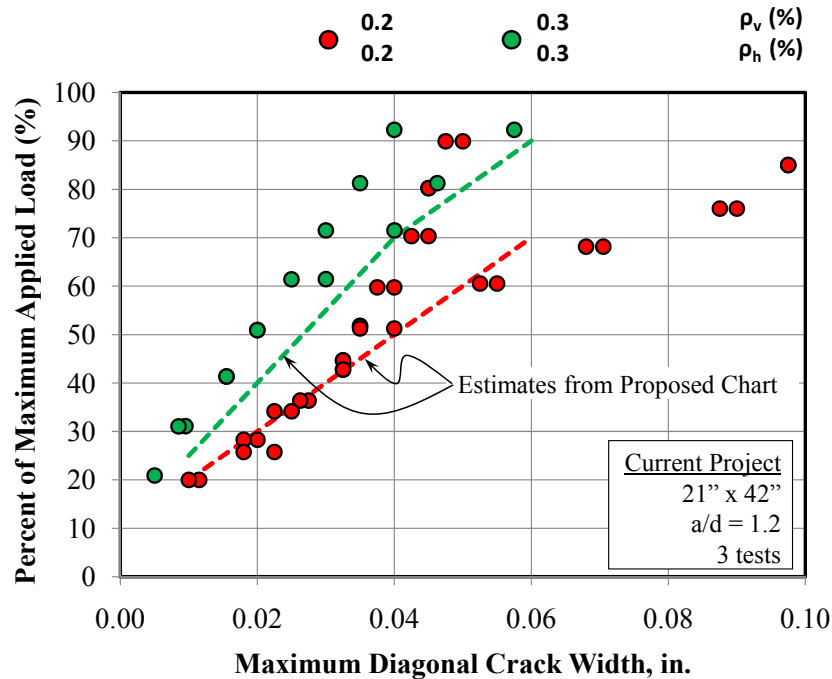


**Figure 5.50: Comparison of data from specimens tested at a/d of 1.2 and chart estimates**

Since the chart was developed with data from specimens tested at an a/d ratio of 1.85 and was evaluated with data from specimens at an a/d ratio of 1.2, it should not be used for cases well outside of this range. A range in a/d ratio from 1 to 2 seems appropriate due to the minor affect of a/d ratio on the width of diagonal cracks. It is not recommended to use the proposed chart for members with a/d ratios less than 1 since no data were obtained in this range. Maximum diagonal crack widths at a given percentage of capacity may slightly decrease with decreasing a/d ratio. As a result, a crack width of 0.03 in. may be more critical (higher percentage of capacity) for a member loaded with an a/d ratio < 1 than for a member loaded with an a/d ratio of 1.85.

The chart is not intended to be used for inverted-tee bent caps. No diagonal crack width data from inverted-tees were used in the calibration of the chart. It is possible that the presence of tension in the web of an inverted-tee member due to load applied to the flange could significantly alter the width of diagonal cracks. Future research is required to assess the applicability of this chart to inverted-tee bent caps.

It was shown in Section 2.2 that two bent caps in Texas were retrofitted due to extensive diagonal cracking in service. Web reinforcement corresponding to 0.05% and 0.49% in the horizontal and vertical directions, respectively, was placed in the I-345 bent cap in Dallas, Texas. The maximum diagonal crack width in this member was approximately 0.035 in. While the web reinforcement in this cap does not match the divisions in the proposed chart, the use of the chart with some judgment suggests that the I-345 bent cap was loaded to approximately 60% ( $\pm 10\%$ ) of its capacity. In the I-45 bent cap at Greens Road in Houston, Texas, 0.29% and 0.65% reinforcement in the horizontal and vertical directions, respectively, was provided. The maximum diagonal crack width in this member was approximately 0.035 in. as well. The use of the proposed chart suggests that this member was loaded to approximately 77% ( $\pm 10\%$ ) of its capacity. As such, the strengthening of both structures was largely justified.

The use of the proposed chart should be done in conjunction with sound engineering judgment. It is clear that conditions in the field can be drastically different than in the laboratory. The chart estimate can likely be off by as much as 20% of the capacity due to variability in crack width data, the limited variables accounted for in the chart, and the differences between field and laboratory conditions. Thus, the chart should be viewed as an important guide to making an informed decision regarding the level of distress in a diagonally-cracked bent cap, in the absence of more sophisticated means of distress evaluation.

#### **5.4.4 Summary and Conclusions**

For the current task, information from the literature and data from the experimental program were used to determine the primary variables that affect the maximum width of diagonal cracks in shear-critical deep beams. The results indicate that the amount of web reinforcement crossing the diagonal crack is the primary variable. The effect of changing the  $a/d$  ratio from 1.2 to 1.85 did not significantly affect the maximum width of the diagonal cracks considering the inherent amount of scatter in crack widths. From the crack width data obtained in the experimental program, a chart was prepared that correlates the maximum width of the primary diagonal crack to the

load acting on the member, quantified as a percent of the capacity. Experimental data from 21 full-scale tests on specimens that were 21"x42," 21"x44," 21"x75," and 36"x48" were used to develop the chart. The chart is applicable for a/d ratios between 1 and 2 and for a range of web reinforcement quantities. The chart should be used with sound engineering judgment considering the following limitations:

- Variability in crack widths in general
- Limited variables accounted for in the chart
- Differences between field and laboratory conditions
- Implications of an unconservative estimate of capacity

## **5.5 SUMMARY**

In Chapter 5, the results of three objectives of TxDOT Project 5253 were presented. In Section 5.2, it was shown that the discrepancy between calculated shear strength near an a/d ratio of 2 is largely eliminated with the use of the Project 5253 STM provisions. In Section 5.3, a service load check was developed that limits diagonal cracking under service loads. In Section 5.4, a simple chart that relates maximum diagonal crack widths to the residual capacity of a deep beam was presented to aid in the field assessment of diagonally-cracked bent caps. The results for these three tasks were obtained through the analysis of data from the experimental program, the literature, and the evaluation database.

## **CHAPTER 6**

### **Summary and Conclusions**

#### **6.1 SUMMARY**

Diagonal cracking has been observed in several reinforced concrete bent caps in service throughout the state of Texas. In two cases, costly retrofits were implemented to strengthen the cracked structures (Section 2.2). The Texas Department of Transportation (TxDOT) was interested in obtaining insight into the cause of the diagonal cracking, in developing a means to assess the residual capacity of diagonally-cracked bent caps, and in refining the strength and serviceability design provisions for bent caps and other deep beams.

In addition, with the advent of strut-and-tie modeling as the preferred method for deep beam design in U.S. design specifications within the last decade, TxDOT engineers have expressed concerns regarding the implementation of these provisions into their bent cap designs. Currently, the strut-and-tie model design provisions in AASHTO LRFD (2008) and ACI 318-08 Appendix A are often unclear and inconsistent. Also, serviceability-related provisions are not available to supplement the strut-and-tie modeling procedure.

Eight objectives related to the diagonal cracking of in-service bent caps and to the concerns associated with using strut-and-tie models to design deep beams were addressed within TxDOT Project 5253. The eight objectives are listed as follows:

- (1). Determine the influence of the distribution of stirrups across the width of a beam web on the strength and serviceability behavior of a deep beam.
- (2). Determine the influence of singular nodes triaxially confined by concrete on the strength and serviceability behavior of a deep beam.

- (3). Determine an appropriate amount of minimum web reinforcement (stirrups and longitudinal side face reinforcement) considering the strength and serviceability demand of a deep beam.
- (4). Determine the influence of member depth on the strength and serviceability behavior of a deep beam.
- (5). Develop a simple STM design methodology, including node proportioning techniques, allowable stresses, and applicable design checks, for the design of deep beams.
- (6). Develop a means to reduce the discrepancy between shear strength calculated using STMs and sectional shear provisions at an  $a/d$  ratio of 2.
- (7). Develop a means to mitigate the formation of diagonal cracks under service loads.
- (8). Develop a means to relate the maximum diagonal crack width of a deep beam to its residual capacity for field engineers.

The results of five of the eight objectives of Project 5253 were presented in this dissertation. In Chapter 4, the effect of minimum web reinforcement and of member depth on the strength and serviceability performance of deep beams was evaluated (objectives 3 and 4). Appropriate design recommendations were detailed for these tasks as well. In Chapter 5, objectives 6, 7, and 8 were addressed. Design provisions that reduced the discrepancy between the shear strength calculated with STMs and sectional shear provisions at an  $a/d$  ratio of 2 were provided in Section 5.2. A service load design check was outlined in Section 5.3 that limits the formation of diagonal cracks in service. Lastly, a simple chart that correlates the maximum diagonal crack width to the residual capacity of diagonally-cracked bent cap was developed in Section 5.4. The results of the other three objectives of Project 5253 (objectives 1, 2, and 5) were presented by Tuchscherer (2008).

To accomplish the aforementioned objectives, an extensive experimental program was conducted. Due to the specific nature of the objectives in this study and to best improve the design and performance of actual bent caps, it was necessary to test

specimens that were of comparable size to typical bent caps in Texas. Thirty-seven (37) tests were conducted on 19 reinforced concrete beams with the following cross-sectional dimensions: 21"x23", 21"x42", 21"x44", 21"x75", and 36"x48." The test specimens were among the largest reinforced concrete deep beams in the literature.

To supplement the experimental program, a database of deep beam test results was compiled from the literature. The database was an expansion of a database originally compiled by Brown et al. (2006). The total number of deep beam test results (shear-span-to-depth ratio  $(a/d) \leq 2.5$ ) in the database was 905 (including 37 from the 5253 experimental program). Entries in the database that lacked sufficient information to perform a strut-and-tie analysis and that did not meet established cross-sectional size or web reinforcement criteria were filtered from the database (Section 2.4). The final database was called the *evaluation database* and contained 179 deep beam test results (35 from the 5253 experimental program). The use of the evaluation database in conjunction with the 5253 experimental program enabled each objective to be addressed from broad and specific viewpoints.

## **6.2 EXAMINATION OF I-45 BENT CAP IN HOUSTON, TEXAS**

Insight into the cause of diagonal cracking in service of several I-45 bent caps in Houston, Texas (Figure 2.5) was obtained through the examination of the original design of one of the multiple-column bent caps in the interchange. In Appendix A, the original design was examined with strut-and-tie model and sectional shear design provisions from AASHTO LRFD (2008), ACI 318-08, and TxDOT Project 5253. It was found that the portion of the structure with an  $a/d$  ratio of 2.05 satisfied estimated design loads with sectional shear provisions but not with strut-and-tie model provisions. With the strut-and-tie model design procedure developed in TxDOT Project 5253 (Section 2.3.4.3), it was estimated that the node-to-strut interface at the bearing of the steel box girder was under-designed by approximately 36% (Section A.2.3.3). High ratios of the stirrup contribution to shear strength,  $V_s$ , to the concrete contribution to shear strength,  $V_c$ , were required to satisfy the design loads with sectional shear provisions. The  $V_s/V_c$  ratio was 3.5 and 3.0 according to the sectional shear design procedures in AASHTO LRFD (2008)



and ACI 318-08, respectively. In addition, the first diagonal cracking load of the original structure was estimated to be only 88% of the unfactored dead load according to the proposed equation in Section 5.3.4 of this dissertation. These findings largely explain the extensive amount of diagonal cracking present in the original structure (Figure 6.1).

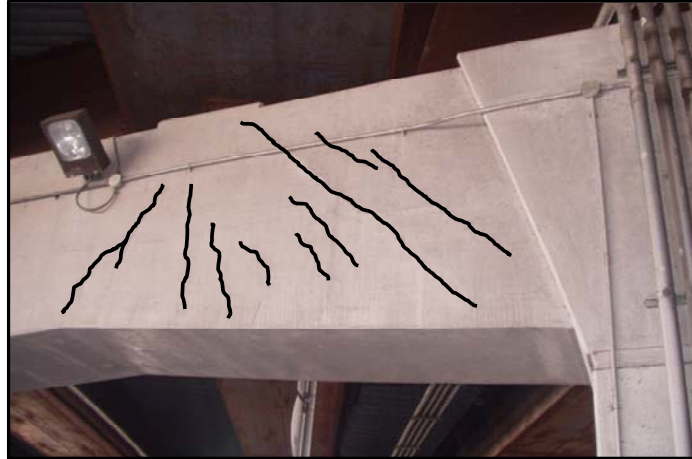


***Figure 6.1: Diagonal cracks in I-45 bent cap in Houston, Texas***

The results of examining the original design of the I-45 bent cap in Houston, Texas are consistent with several findings in this dissertation. The importance of accounting for high stresses in the nodal regions of deep beams with strut-and-tie models was illustrated in Section 4.4.2.2 with the analysis of the depth-effect specimens. Also, in Section 5.2.3 and 4.3.3.2, potential problems with using high ratios of  $V_s/V_c$  in sectional shear design was shown from a strength and serviceability perspective. In Section 5.2.3, it was shown that relying on large amounts of strength from stirrups (high  $V_s/V_c$  ratio) at  $a/d$  ratios near 2 may not be prudent. Similarly, diagonal crack width data presented in Section 4.3.3.2 illustrated that diagonal crack widths increase in service with increasing  $V_s/V_c$  ratios for specimens with an  $a/d$  ratio of 2.5. Lastly, applying the service load design check outlined in Section 5.3.4 suggested that the I-45 bent cap would diagonally-crack under dead loads. In light of several findings presented in this dissertation, it is not surprising that the original structure performed poorly in service.

### 6.3 CONCLUSIONS

The conclusions of the current study are presented in this section. The following conclusions are based on information from the literature, data from the experimental program, and the analysis of the evaluation database.

#### 6.3.1 Minimum Web Reinforcement

The purpose of this task was to recommend an appropriate amount of minimum web reinforcement to ensure adequate strength and serviceability performance in deep beams. Numerous tests in the experimental program were used to evaluate the effect of the quantity of web reinforcement on the performance of the member. At an a/d ratio of 1.85, tests were conducted on beams with a 21"x23", 21"x42", 21"x44", 21"x75", and 36"x48" cross-section. At a/d ratios of 1.2 and 2.5, two tests were conducted on beams with a 21"x42" cross-section. Several different distributions of web reinforcement were investigated. The majority of the test specimens had either 0.2% or 0.3% reinforcement in each direction. Stirrups with 2 and 4 legs were used. Two tests were conducted on specimens without web reinforcement.

- **For beams tested at an a/d ratio of 1.2 and 1.85, providing either 0.2% or 0.3% reinforcement did not affect the shear strength of the member. A specimen tested at an a/d ratio of 2.5 with 0.3% reinforcement in each direction failed at a substantially higher load than a companion specimen with 0.2% reinforcement.** The specimens tested at an a/d ratio less than 2 failed in a manner consistent with a single-panel, direct-strut mechanism. Thus, any reinforcement greater than that which is required to maintain equilibrium in the bottle-shaped strut is unnecessary for strength. The specimens tested at an a/d ratio of 2.5 generally failed in a manner that was consistent with a sectional-shear model, or a multiple-panel STM. At this a/d ratio, increasing the amount of vertical reinforcement increases the shear strength of the member.
- **To restrain maximum diagonal crack widths to 0.016 in. at first cracking and at estimated service loads, 0.3% reinforcement in each orthogonal direction should**

**be provided and spaced evenly near the side face of the effective strut area.** The maximum diagonal crack width of specimens with 0.2% reinforcement in each direction often exceeded 0.016 in. at first cracking and at estimated service loads (33% of ultimate), whereas those with 0.3% reinforcement satisfied this limit in general. 0.3% reinforcement is consistent with the current AASHTO LRFD provision (Article 5.6.3.6, 2008) except it is proposed that the amount of reinforcement need not be based on the gross concrete section. A revised definition is provided, for adoption into the AASHTO LRFD specifications, in Section 4.3.4.

### **6.3.2 Effect of Member Depth**

The purpose of this task was to evaluate the effect of member depth on the strength and serviceability performance of reinforced concrete deep beams. Tests were conducted at  $a/d$  ratios of 1.2, 1.85, and 2.5 on specimens with 21"x23", 21"x42", and 21"x75" cross-sections and with 0.2% web reinforcement in each direction. The size of the nodal regions was kept as constant as possible for the tests conducted at each  $a/d$  ratio. In this way, the effect of changing the depth of a deep beam without proportionally changing the size of the nodal regions was assessed.

- **Provided that the bottle-shaped strut is adequately reinforced and the force in the tension tie does not control, the strength of deep beams ( $a/d \leq 2$ ) is governed by the size and stress conditions in the nodal regions, not by the effective depth of the member.** The results in this task highlighted the importance of using a strut-and-tie analysis to design reinforced concrete deep beams in order to explicitly address the stress conditions in the nodal regions. Using section-based approaches to design deep beams is unacceptable and inappropriately suggests that a large size effect exists.
- **The maximum diagonal crack width at a given percentage of the maximum applied load tended to increase as the overall depth of the member increased from 23" to 42" but not from 42" to 75".** The results in this task suggested that diagonal crack width data from small specimens should be used with caution in

forming recommendations for full-scale structures. At a depth of 42 in. and greater, it appeared that the effect of depth on the width of diagonal cracks is mitigated.

### **6.3.3 Discrepancy in Calculated Shear Strength at a/d Ratio of 2**

The objective of this task was to reduce the discrepancy in shear strength calculated using the STM and the sectional shear provisions in AASHTO LRFD (2008) at an a/d ratio of 2. It is well known that as the a/d ratio approaches and exceeds 2, the dominant shear transfer mechanism transitions from a deep beam mechanism to a sectional shear mechanism. However, the transition in behavior is gradual, not immediate; and therefore, a large discrepancy between the shear strength calculated at an a/d ratio of 2 according to each design model is not justified. The level of conservatism consistent with the sectional shear provisions in AASHTO LRFD was compared to that of the AASHTO LRFD and 5253 STM provisions for specimens in the database with a/d ratios up to 2.5. Also, shear capacity calculated with the 5253 STM provisions was compared to capacity calculated with sectional shear provisions in AASHTO LRFD (2008) and ACI 318-08 for specimens in the database with a/d ratios between 2 and 2.5.

- **With the use of the 5253 STM provisions and a limit on the ratio of  $V_s/V_c$  in sectional shear provisions, a reasonably smooth transition exists as the shear design model changes at an a/d ratio of 2.** The 5253 STM provisions more appropriately account for the reduction in shear strength with increasing a/d ratio than the AASHTO LRFD STM provisions. As a result, excessive conservatism concurrent with the use of the AASHTO LRFD STM provisions near an a/d ratio of 2 has been largely eliminated. In terms of calculated design strength, limiting the ratio of  $V_s/V_c$  to 2 for sectional shear reduces the difference in capacity of the two design models near an a/d ratio of 2.
- **Data from the experimental program suggested that a single-panel strut-and-tie model is suitable for the design of deep beams with a/d ratios  $\leq 2$ .** The observed failure modes of the test specimens and measured strain data from specimens with a/d ratios of 1.2, 1.85, and 2.5 suggest that the dominant transfer mechanism for beams

with an  $a/d$  ratio  $\leq 2$  is consistent with a single-panel STM. The use of a multiple-panel model at an  $a/d$  ratio less than 2 is not recommended since it is not consistent with the dominant load transfer mechanism and thus, often results in an overly conservative estimate of strength.

#### **6.3.4 Limiting Diagonal Cracking under Service Loads**

The purpose of this task was to assess the feasibility of limiting diagonal cracking under service loads. In addition to providing minimum web reinforcement, it was determined that a service-load shear check was a simple way to limit diagonal cracking under service loads. Measured diagonal cracking loads from the experimental program and from the database were used to determine the primary variables that affect the diagonal cracking load of deep beams.

- **A simple and reasonably conservative equation to estimate the diagonal cracking load of deep beams was developed that was a function of the shear area, the square root of the compressive strength of concrete, and the  $a/d$  ratio.** With this equation, the service level shear in the member (full dead load + live load) can be checked with the estimated diagonal cracking load. If the service level shear exceeds the estimated diagonal cracking load, the design of the section can be modified. At the very least, this check encourages the designer to consider the likelihood of diagonal cracking in service.

#### **6.3.5 Correlation of Maximum Diagonal Crack Width to Capacity**

The purpose of this task was to develop a means to help field engineers in evaluating the residual capacity of a diagonally-cracked bent cap. On occasion, diagonal cracks are discovered in bent caps in service. Currently, there is little information in the literature regarding a method to link the width of diagonal cracks to the amount of distress in the member. Data from the literature and the current experimental program were used to identify primary variables that influence the width of diagonal cracks in deep beams. All of the crack width data was from specimens with a minimum overall depth of 42 in.

- **A simple chart was developed to correlate the maximum diagonal crack width in a deep beam to the load acting on the member, quantified as a percent of its capacity.** The chart applies to beams with an  $a/d$  ratio between 1 and 2 and is only a function of the amount of web reinforcement in the member. It was determined that the effect of  $a/d$  ratio within this range on diagonal crack widths was minimal relative to the amount of scatter inherent in diagonal crack width data. This chart is viewed as a simple means to make an informed decision regarding the amount of distress in a diagonally-cracked bent cap in the absence of a more sophisticated means of distress evaluation.

## **APPENDIX A**

### **Example Problem**

#### **A.1 OVERVIEW**

The following example problem was largely prepared by Tuchscherer (2008). Additional discussion regarding topics addressed within this dissertation, such as minimum web reinforcement, service load diagonal cracking, and the transition between deep beam and sectional shear, were added. In this example problem, one of several multiple-column bent caps that experienced diagonal cracking problems in service (Section 2.2 and Figure A.1) was examined. The cracking was so extensive that a costly retrofit project was undertaken in order to strengthen all of the bent caps in the interchange. Based on the load and support conditions, the bent cap contains several regions with different  $a/d$  ratios. The two regions that are analyzed within this example problem have an  $a/d$  ratio of 0.85 and 2.05. The original design of the member will be compared to designs consistent with the STM provisions in Project 5253, ACI 318-08 Appendix A, and AASHTO LRFD (2008). For the region with an  $a/d$  ratio of 2.05, sectional shear provisions will be used to check the capacity of the section as well. As a result, this example can be viewed as multiple examples within one structure in which the design of D-regions with relatively low and high  $a/d$  ratios can be evaluated. In addition, the capacity calculated with sectional shear provisions and STM provisions can be directly compared for the portion of the bent cap with an  $a/d$  ratio of 2.05. Where appropriate, serviceability design provisions will be implemented in addition to strength checks. It is interesting to note that the bent cap was originally designed according to sectional shear provisions. Strut-and-tie modeling was not used in the original structural design.



***Figure A.1: I-45 over Greens Road Bent Cap***

The multiple-column bent cap to be investigated is used to support an 86-foot wide portion of a 180-foot wide roadway, comprising nine 12-foot wide traffic lanes and one 25-foot wide *high occupancy vehicle* (HOV) lane. A layout of the bent cap is illustrated in Figure A.2. Cross-sectional details are presented for the two critical regions under investigation ( $a/d$  equal to 0.85 and 2.05).



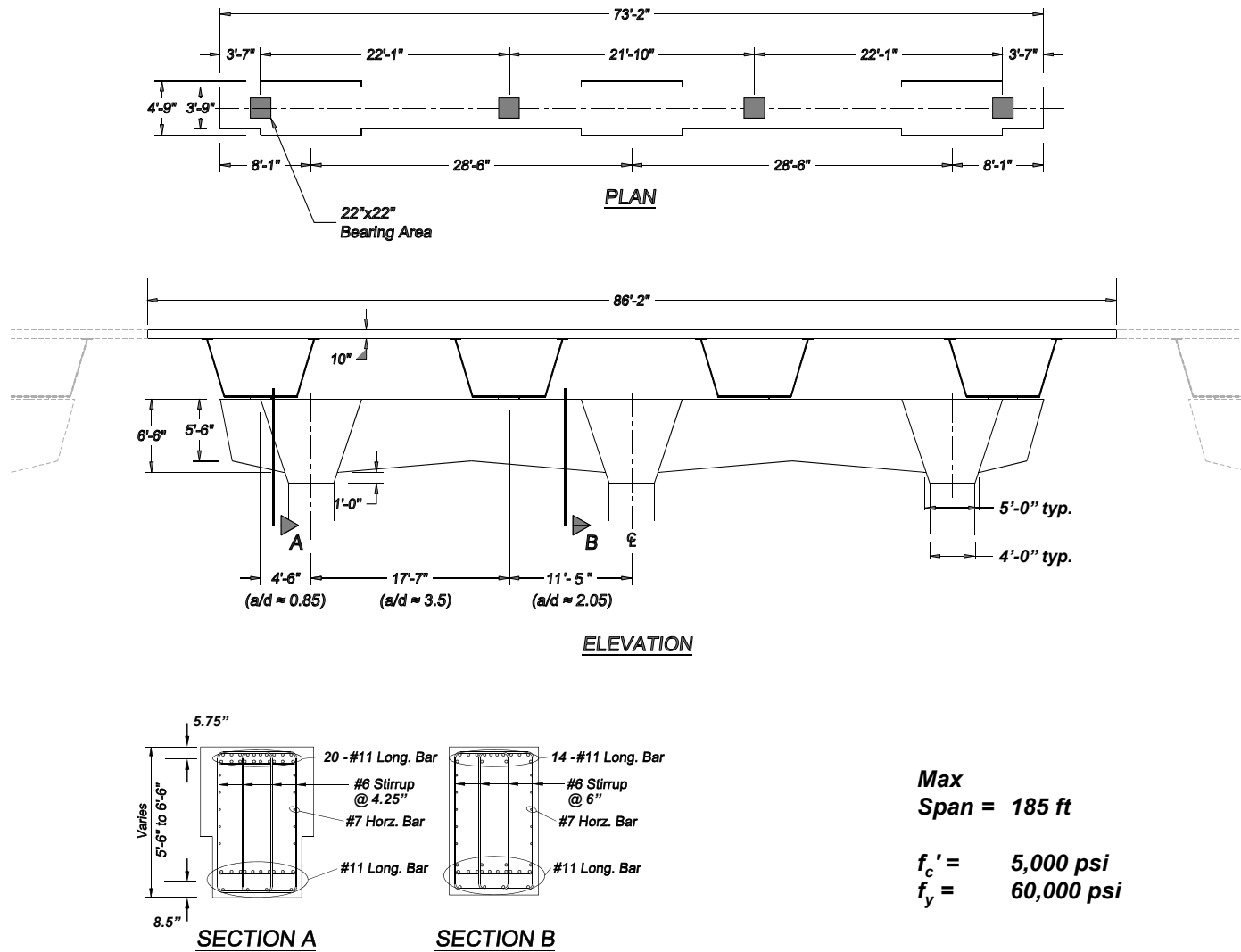


Figure A.2: Preliminary plan; elevation; and cross-sectional details at critical shear regions.

As mentioned, this cap exists in the field. The details of the original cross-section at the critical shear regions will be evaluated. Where necessary, the cross-section will be modified to meet the requirements of AASHTO LRFD (2008), ACI 318-08 Appendix A, and the Project 5253 provisions. Afterwards, the cross-sections proportioned to satisfy the three sets of STM provisions are compared for both shear regions.

The design dead and live loads applied to the bent cap from each steel box girder are presented as follows.

### **Dead Loads**

The dead load includes the weight of the steel box girder, the concrete deck, and the self-weight of the bent cap. For simplicity, the self weight of the bent is distributed to the four girder locations in order to easily apply it to a truss model.

$$P_{DL} = 792 \text{ kip}$$

### **Live Loads + Impact**

The live load includes lane load and truck load plus impact.

$$P_{LL} = 280 \text{ kip}$$

### **Service Load**

The load case that is used to examine the amount of service load applied to the structure is the SERVICE I load case specified in AASHTO LRFD (2008).

$$P_s = 792 \text{ kip (DL)} + 280 \text{ kip (LL + Impact)} \quad P_s = 1072 \text{ kip}$$

### **Factored Load**

Load factors specified by AASHTO LRFD (2008) and ACI 318-08 are slightly different. For the purpose of comparison, the Project 5253 methodology will use the same load factors as AASHTO LRFD (2008).

#### **AASHTO LRFD: STRENGTH I**

$$P_u = 1.25 \cdot (792 \text{ kip}) + 1.75 \cdot (280 \text{ kip}) \quad P_{u\_AASHTO} = 1480 \text{ kip}$$

#### **ACI 318-08**

$$P_u = 1.2 \cdot (792 \text{ kip}) + 1.6 \cdot (280 \text{ kip}) \quad P_{u\_ACI} = 1398 \text{ kip}$$

### Resistance Factors

Resistance factors specified by AASHTO LRFD (2007) and ACI 318-08 are slightly different. For the purpose of comparison, the Project 5253 methodology will use the same resistance factors as AASHTO LRFD.

#### AASHTO LRFD

Struts and Nodal Regions,  $\phi = 0.70$

Steel Tie,  $\phi = 0.90$

#### ACI 318-08

Struts and Nodal Regions,  $\phi = 0.75$

Steel Tie,  $\phi = 0.90$

## A.2 DEEP BEAM DESIGN

This bent example problem has three distinct shear regions. The first D-region has an  $a/d$  ratio of 0.85. This portion is re-designed using strut-and-tie provisions as presented in Section A.2.2. The next shear region has an  $a/d$  ratio greater than 3.5 and would be designed using typical sectional shear provisions. Finally, the third region has an  $a/d$  ratio of approximately 2.05 (the  $a/d$  ratio varies between 1.9 and 2.1 depending where the depth is measured). This portion of the beam is considered to be in the transition zone where the shear behavior of a beam converts from sectional to deep beam shear. Therefore, this portion of the structure could be designed using either a strut-and-tie model or typical sectional shear provisions. The STM design for this region is presented in Section A.2.3 and the sectional shear design for this region is presented in Section A.3.

When designing a D-region using a strut-and-tie model, the first step is to determine the configuration of the truss model and resulting forces in the truss elements. A preliminary truss model is determined as follows.

### A.2.1 Determination of Preliminary Truss Model

The structure illustrated in Figure A.2 is modeled as a truss with compressive struts and tensile ties as presented in Figure A.3. The AASHTO LRFD (2007) factored load,  $P_{u\_AASHTO}$ , is applied to the structure at each girder support. Only one half of the structure is presented; the bent is symmetric about its centerline, therefore, the loading and proportions of the other half are identical.

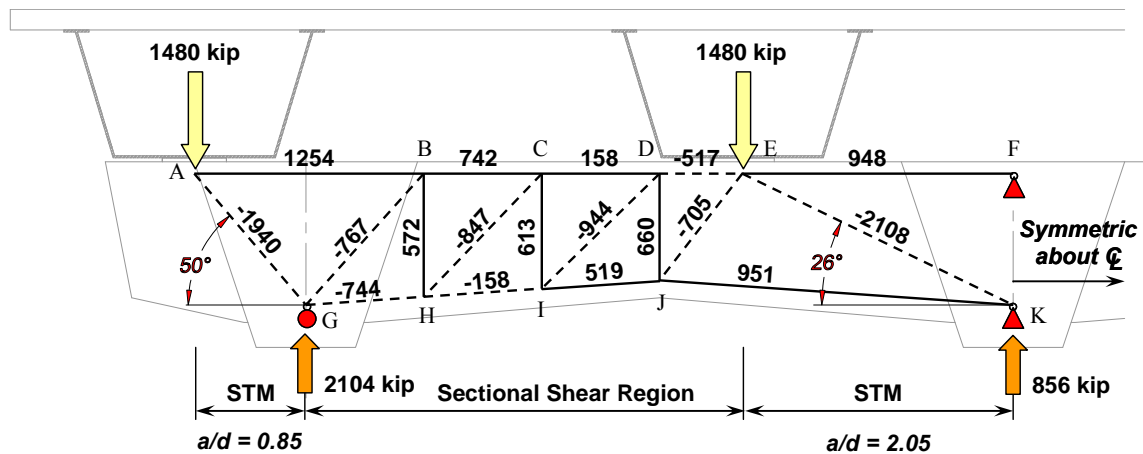


Figure A.3: Strut-and-tie model with AASHTO LRFD (2008) factored loads.

According to the Project 5253 STM provisions (Section 2.3.4.3), a deep beam region can be modeled with a single panel strut provided the  $a/d$  ratio is less than 2. Similarly, according to ACI 318-08, a single-panel strut may be used provided the angle of inclination is greater than 25-degrees; AASHTO LRFD (2008) does not limit a strut's angle of inclination. As a result, both D-regions are shown in Figure A.3 as single compression struts. While the  $a/d$  ratio of the interior D-region slightly exceeds 2, it is close enough to use either sectional shear or STM provisions. Also, it is necessary to model the sectional shear portion of the bent as part of the overall truss in order to adequately represent the entire structure. Even though this portion of the structure is designed using sectional shear provisions, it is necessary to model the entire bent so that the correct quantity of shear is transferred to Strut EK.

Typically, the top and bottom chords of a STM are positioned based on the location of the centroid of the longitudinal reinforcement or the depth of compression

zone depending on whether the chord resists tension or compression, respectively. In a continuous element, the top and bottom chord resist both tension and compression. For the sake of simplicity, both of their locations are based on the centroid of the longitudinal reinforcement. For this example problem, the centroid of the longitudinal reinforcement is, on average, taken to be 5.75 in below the top surface and 8.5 in above the bottom surface. These dimensions result in heights of the back face of the nodes of 11.5 in. and 17 in., respectively.

### A.2.2 Shear Region with an $a/d$ Ratio Equal to 0.85

A close-up of the critical Strut AG and respective nodal zones is presented to scale in Figure A.4. The dimensions of the node-to-strut interfaces (24.6 in. and 41.9 in. in Figure A.4) were calculated using the definition provided in Figures 2.14 and 2.15.

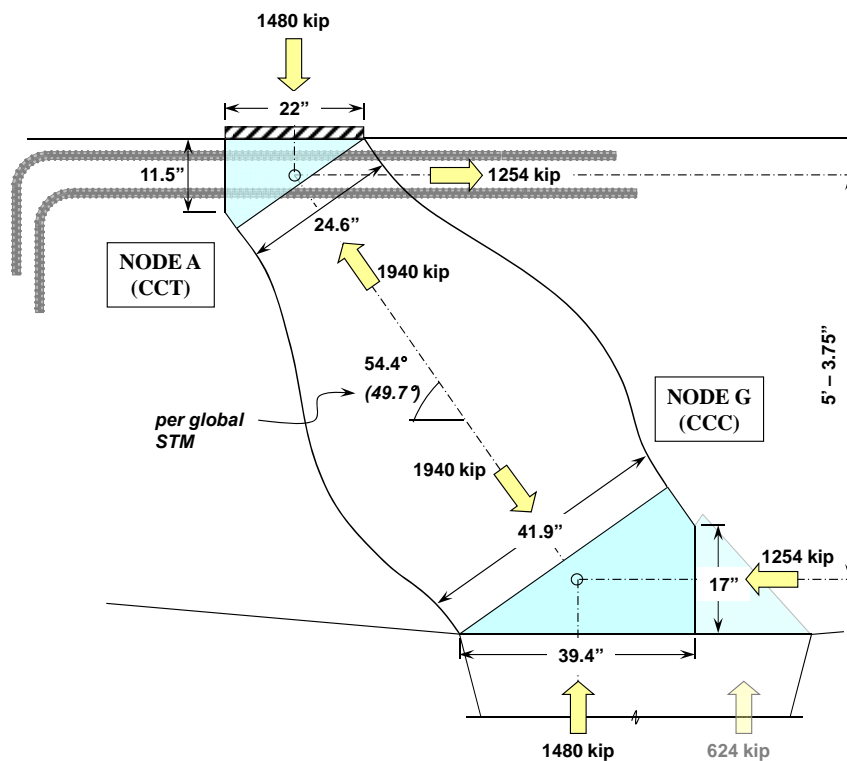


**Figure A.4: Critical strut in region with  $a/d$  equal to 0.85 (AASHTO LRFD factored loads).**

The length of Node G is proportioned based on the amount of force that is transferred to the near support. As a result, the angle of inclination of Strut AG shown in Figure A.4 is slightly different from the angle in the global model shown in Figure A.3 (54.4 deg. versus 49.7 deg., respectively). If the global truss model were to be updated with this new angle, then the forces in the elements would change slightly. However, it is common practice to ignore this slight discrepancy. Therefore, the truss elements shown in Figure A.4 are designed for the forces presented in Figure A.3.

In order to design Strut AG, the allowable capacity of each nodal face (i.e. bearing face, back face, and strut-to-node interface) must be greater than the force applied to the boundary. This procedure is presented for the Project 5253 method, ACI 318-08, and AASHTO LRFD (2008) provisions in the following sections.

#### ***A.2.2.1 Design of Region with $a/d = 0.85$ : Project 5253 Provisions***

##### **Node A (CCT Node)**

The back face of node A must resist the bond stresses developed by the anchorage of the tie. For this type of condition, stresses at the back face of a CCT node are not critical. The first step of the Project 5253 method is to determine the triaxial confinement factor,  $m$ , as illustrated in Figure A.5.

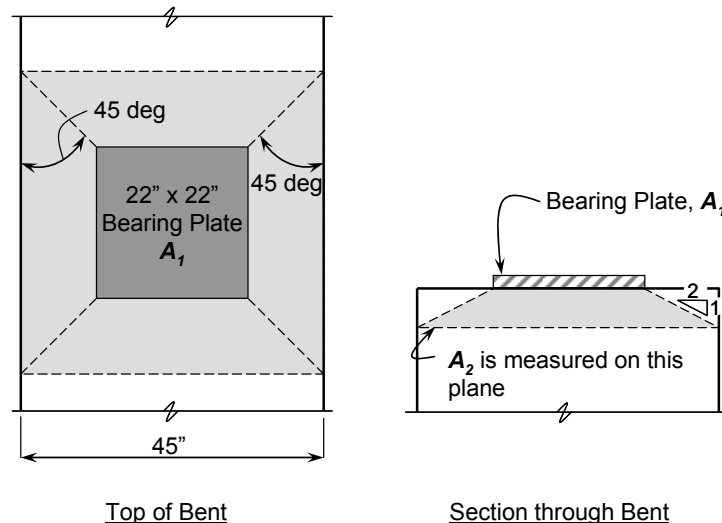


***Figure A.5: Determination of Triaxial Confinement Factor***

Triaxial Confinement Factor:  $m = \sqrt{\frac{(45\text{in})^2}{(22\text{in})^2}} = 2.04 \leq 2$

#### BEARING FACE

Factored Load:  $F_u = 1480 \text{ kip}$

Efficiency:  $v = 0.70$

Concrete Capacity:  $f_{cu} = m \cdot v \cdot f'_c = (2) \cdot (0.7) \cdot (5 \text{ ksi}) = 7.0 \text{ ksi}$   
 $\phi \cdot F_n = (0.7) \cdot (7.0 \text{ ksi}) \cdot (22 \text{ in.}) \cdot (22 \text{ in.})$   
 $= 2372 \text{ kip} > 1480 \text{ kip} \text{ **OK**}$

#### STRUT-TO-NODE INTERFACE

Factored Load:  $F_u = 1940 \text{ kip}$

Efficiency:  $0.65 \leq \left(0.85 - \frac{5 \text{ ksi}}{20 \text{ ksi}}\right) \leq 0.45 = 0.60$

Concrete Capacity:  $f_{cu} = m \cdot v \cdot f'_c = (2) \cdot (0.60) \cdot (5 \text{ ksi}) = 6.0 \text{ ksi}$   
 $\phi \cdot F_n = (0.7) \cdot (6.0 \text{ ksi}) \cdot (24.6 \text{ in.}) \cdot (22 \text{ in.})$   
 $= 2273 \text{ kip} > 1940 \text{ kip} \text{ **OK**}$

Thus, according to the Project 5253 procedure, the strength of Node A is sufficient to resist the applied forces. The capacity of Node G is determined as follows. Node G is not triaxially confined, so the confinement factor,  $m$ , is equal to one.

#### **Node G (CCC Node)**

Triaxial Confinement Factor:  $m = 1.0$

#### BEARING FACE

Factored Load:  $F_u = 1480 \text{ kip}$

Efficiency:  $v = 0.85$

Concrete Capacity:  $f_{cu} = m \cdot v \cdot f'_c = (1) \cdot (0.85) \cdot (5 \text{ ksi}) = 4.3 \text{ ksi}$   
 $\phi \cdot F_n = (0.7) \cdot (4.3 \text{ ksi}) \cdot (39.4 \text{ in.}) \cdot (45 \text{ in.})$   
 $= 5337 \text{ kip} > 1480 \text{ kip} \text{ **OK**}$

#### BACK FACE

Factored Load:  $F_u = 1254 \text{ kip}$

Efficiency:  $v = 0.85$

Concrete Capacity:  $f_{cu} = m \cdot v \cdot f_c' = (1) \cdot (0.85) \cdot (5 \text{ ksi}) = 4.3 \text{ ksi}$   
 $\phi \cdot F_n = (0.7) \cdot (4.3 \text{ ksi}) \cdot (17 \text{ in.}) \cdot (45 \text{ in.})$   
 $= 2303 \text{ kip} > 1254 \text{ kip} \text{ OK}$

#### STRUT-TO-NODE INTERFACE

Factored Load:  $F_u = 1940 \text{ kip}$   
Efficiency:  $0.65 \leq \left( 0.85 - \frac{5 \text{ ksi}}{20 \text{ ksi}} \right) \leq 0.45 = 0.60$   
Concrete Capacity:  $f_{cu} = m \cdot v \cdot f_c' = (1) \cdot (0.6) \cdot (5 \text{ ksi}) = 3.0 \text{ ksi}$   
 $\phi \cdot F_n = (0.7) \cdot (3.0 \text{ ksi}) \cdot (41.9 \text{ in.}) \cdot (45 \text{ in.})$   
 $= 3960 \text{ kip} > 1940 \text{ OK}$

Thus, according to the Project 5253 procedure, the strength of Node G is sufficient to resist the applied forces. The capacity of Tie AB must also be evaluated.

#### TIE AB

Factored Load:  $F_u = 1254 \text{ kip}$   
Efficiency:  $v = 1.0$   
Tie Capacity:  $(1.0) \cdot (60 \text{ ksi}) \cdot (20) \cdot (1.56 \text{ in}^2) = 1872 \text{ kip}$   
 $\phi \cdot F_n = (0.9) \cdot (1872 \text{ kip})$   
 $= 1685 \text{ kip} > 1254 \text{ kip} \text{ OK}$

Thus, the capacity of Tie AB is adequate. Verifying the tie capacity is essentially the same procedure for all three provisions. Therefore, this check is not repeated for other provisions.

#### Minimum Transverse Reinforcement

The original cross-section ( $a/d = 0.85$ ) had #6 4-legged stirrups at  $4\frac{1}{4}$ " and #7 horizontal bars at approximately 9" for web reinforcement. The corresponding reinforcement ratios in each direction are calculated as follows:

$$\rho_v = \frac{A_v}{b_w s_v} \rightarrow 4 \cdot (0.44 \text{ in}^2) / (45 \text{ in} \cdot 4\frac{1}{4} \text{ in}) = 0.0092$$

$$\rho_h = \frac{A_h}{b_w s_h} \rightarrow 2 \cdot (0.60 \text{ in}^2) / (45 \text{ in} \cdot 9 \text{ in}) = 0.0029$$



The original cross-section practically meets the minimum web reinforcement requirements of the Project 5253 provisions (Section 4.3.4). The amount of stirrups exceeds the minimum by a factor of 3. The quantity of horizontal reinforcement is slightly less than the required 0.3%. If only the minimum amount of web reinforcement was provided, the web reinforcement would be as follows:

$$A_v = 0.003 \cdot b_w \cdot s_1 \rightarrow 2 \cdot (0.44 \text{ in}^2) = 0.003 \cdot (45 \text{ in}) \cdot s_1$$

$$s_1 = 6.5 \text{ in}$$

$$A_{vh} = 0.003 \cdot b_w \cdot s_2 \rightarrow 2 \cdot (0.60 \text{ in}^2) = 0.003 \cdot (45 \text{ in}) \cdot s_2$$

$$s_2 = 8.9 \text{ in}$$

This reinforcement equates to #6 vertical stirrups (2 legs) at 6.5 in. and #7 horizontal bars at 8.5 in. on center. The minimum web reinforcement will be shown in the cross-section designed with the Project 5253 STM provisions for comparison with the cross-sections designed according to the other specifications. However, it is important to note that providing web reinforcement in excess of the minimum (as done in the original cross-section) is encouraged, albeit not required. Additional web reinforcement will reduce the width of diagonal cracks (with diminishing returns) and will provide additional redistribution capacity to the member.

A summary of the preceding design is presented in Figure A.7 along with the other provisions. Next, Strut AG and respective nodal regions are designed according to ACI 318-08.

#### ***A.2.2.2 Design of Region with $a/d = 0.85$ : ACI 318-08 Appendix A***

Check the ACI 318-08, §A.3.3.1 requirement for an adequately reinforced strut (discussed in Section 2.3.4.2, Equation 2.11).

$$\begin{aligned} \sum \frac{A_{si}}{b_s \cdot s_i} \sin \alpha_i &= \left( \frac{4 \cdot 0.44 \text{ in}^2}{45 \text{ in} \cdot 4.25 \text{ in}} \right) \sin 35.6^\circ + \left( \frac{2 \cdot 0.60 \text{ in}^2}{45 \text{ in} \cdot 8.6 \text{ in}} \right) \sin 54.4^\circ \\ &= 0.008 > 0.003 \text{ OK} \end{aligned}$$

Thus, according to ACI 318-08 §A3.2.2, the strut is adequately reinforced. As a result, a higher strut efficiency factor of 0.75 may be used.

Refer to Figure A.4 for preliminary strut proportions and applied loads. The ACI 318-08 load factors are lower than those applied to the STM presented in Figure A.3; as a result, the loads shown are multiplied by a factor of 0.945 (i.e.  $P_{u\_ACI}/P_{u\_AASHTO} = 1398/1480 = 0.945$ ).

### Node A (CCT Node)

#### BEARING FACE

$$\begin{aligned}
 \text{Factored Load:} \quad & F_u = 1398 \text{ kip} \\
 \text{Efficiency:} \quad & \beta = 0.80 \\
 \text{Concrete Capacity:} \quad & f_{cu} = 0.85 \cdot \beta \cdot f'_c = (0.85) \cdot (0.8) \cdot (5 \text{ ksi}) = 3.4 \text{ ksi} \\
 & \phi \cdot F_n = (0.75) \cdot (3.4 \text{ ksi}) \cdot (22 \text{ in.}) \cdot (22 \text{ in.}) \\
 & \quad \quad \quad = 1234 \text{ kip} < 1398 \text{ kip } \mathbf{NG!}
 \end{aligned}$$

#### BACK FACE

$$\begin{aligned}
 \text{Factored Load:} \quad & F_u = 1185 \text{ kip} \\
 \text{Efficiency:} \quad & \beta = 0.80 \\
 \text{Concrete Capacity:} \quad & f_{cu} = 0.85 \cdot \beta \cdot f'_c = (0.85) \cdot (0.8) \cdot (5 \text{ ksi}) = 3.4 \text{ ksi} \\
 & \phi \cdot F_n = (0.75) \cdot (3.4 \text{ ksi}) \cdot (11.5 \text{ in.}) \cdot (22 \text{ in.}) \\
 & \quad \quad \quad = 645 \text{ kip} < 1185 \text{ kip } \mathbf{NG!}
 \end{aligned}$$

#### STRUT-TO-NODE INTERFACE

$$\begin{aligned}
 \text{Factored Load:} \quad & F_u = 1833 \text{ kip} \\
 \text{Efficiency:} \quad & \beta = 0.75 \\
 \text{Concrete Capacity:} \quad & f_{cu} = 0.85 \cdot \beta \cdot f'_c = (0.85) \cdot (0.75) \cdot (5 \text{ ksi}) = 3.2 \text{ ksi} \\
 & \phi \cdot F_n = (0.75) \cdot (3.2 \text{ ksi}) \cdot (24.6 \text{ in.}) \cdot (22 \text{ in.}) \\
 & \quad \quad \quad = 1299 \text{ kip} < 1833 \text{ kip } \mathbf{NG!}
 \end{aligned}$$

Thus, the capacity of Node A does not meet the requirements of ACI 318-08. By inspection, Node A is more critical than Node G. The most critical location of Node A is its back face. Therefore, the bearing plates and bent must be resized in order to provide the back face of Node A with sufficient capacity.

Typically, if a designer wishes to increase the capacity of a truss element, the simplest way is to increase the size of the bearing plate. However, there are realistic limits to the maximum size of a plate that can be provided. For this example, a 30"x30" bearing plate is considered to be a reasonable maximum size. It follows that increasing the size of the bearing plate to 30"x30" does not sufficiently increase the capacity of Strut AG in order for it to meet the requirements of ACI 318-08.

Based on the ACI 318-08 STM provisions, additional shear capacity can be attained by increasing the depth of the bent (increasing strut angle, decreasing a/d ratio); increasing the compressive strength of concrete; providing supplementary longitudinal reinforcement in order to increase the assumed height of the back face of a CCT node; or by a combination of all three of these methods.

Increasing the compressive strength of concrete can be a very simple way to increase the capacity of a structure. However, TxDOT has expressed concern about maximum curing temperature in regard to concrete durability. Thus, it is believed to be impractical to exceed 5,000 psi compressive strength while complying with the maximum temperature limits of the TxDOT 2004 Specifications. Also, for the purpose of comparison among different design provisions, the compressive strength of concrete is constantly maintained to be 5,000 psi.

For the purpose of this example problem, additional capacity is acquired by increasing the depth of the bent and/or nodal region. Most likely, the solutions determined in this example would vary from those selected in a design office given the many external factors involved such as: site restrictions, construction costs, and personal preferences. Nonetheless, the conclusions formed from comparing the provisions to one another will remain valid regardless of differences in optimization preferences.

In order for Strut AG (Figure A.4) to meet the requirements of ACI 318-08, its overall depth must be increased by 18 in and the depth of the back face of Node A must be increased by 2.5 in. As a result, the depth of the global model shown in Figure A.3 is increased by 16.75 in. ( $18'' - \frac{2.5''}{2} = 16.75''$ ) and the forces in the truss members are recalculated accordingly. Specifically, the force in strut AG reduced due to the increase

in depth. The strut proportions and loads associated with these increases are illustrated in Figure A-6.

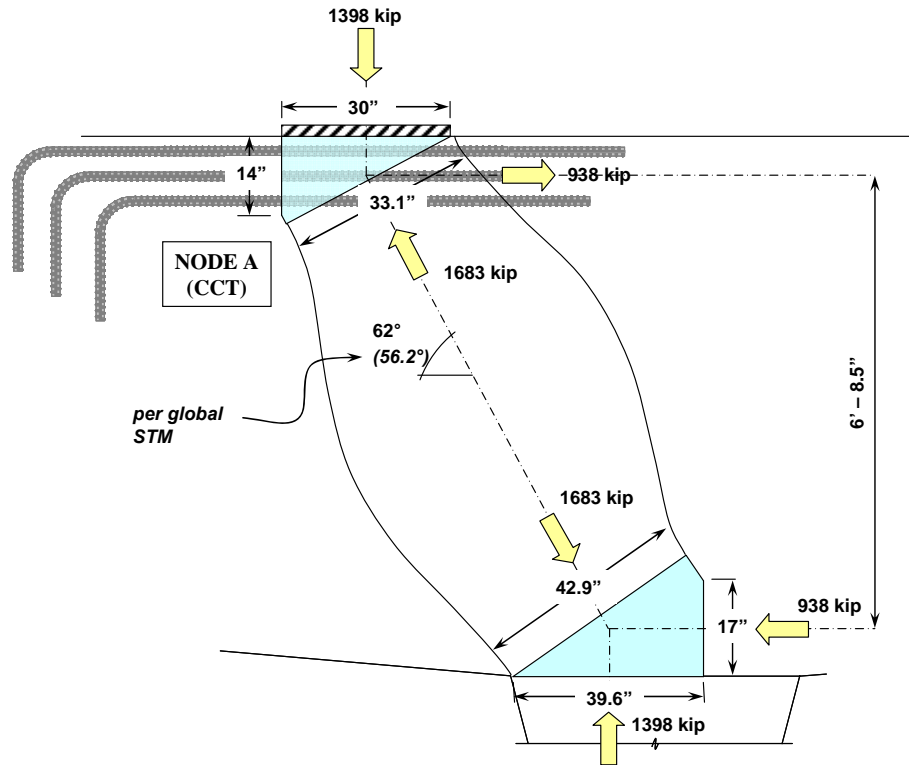


**Figure A-6. Strut proportions associated with an increase in overall depth of 18 in. and increase in back face of Node A of 2.5 in. (ACI 318-08 load factors)**

The capacity of the critical back face of Node A is calculated as follows according to ACI 318-08.

BACK FACE OF NODE A, PER FIGURE A-6

Factored Load:  $F_u = 938 \text{ kip}$

Efficiency:  $\beta = 0.80$

Concrete Capacity:  $f_{cu} = 0.85 \cdot \beta \cdot f'_c = (0.85) \cdot (0.8) \cdot (5 \text{ ksi}) = 3.4 \text{ ksi}$

$\phi \cdot F_n = (0.75) \cdot (3.4 \text{ ksi}) \cdot (14 \text{ in.}) \cdot (30 \text{ in.})$

$= 1071 \text{ kip} > 938 \text{ kip}$  **OK**

Thus, the capacity of the bent illustrated in Figure A-6 meets the requirements of ACI 318-08.

### Minimum Transverse Reinforcement

ACI 318-08 does not require a minimum amount of transverse reinforcement. However, in order to use the higher strut efficiency factor, the following minimum amount of reinforcement must be provided:

$$\sum \frac{A_{si}}{b_s \cdot s_i} \sin \alpha_i > 0.003$$

If it is assumed that the vertical and horizontal reinforcement ratios are identical,

$$\rho \cdot \sin 28^\circ + \rho \cdot \sin 62^\circ > 0.003$$

Thus,

$$\rho_v = \rho_{vh} > 0.0022$$

Provide #5 vertical stirrups at 6 in. and #6 horizontal bars at 8.5 in. on center.

A summary of the preceding ACI 318-08 design is presented in Figure A.7 along with the other provisions. Next, Strut AG and respective nodal regions are designed according to AASHTO LRFD (2008).

#### A.2.2.3 Design of Region with $a/d = 0.85$ : AASHTO LRFD

Refer to Figure A.4 for preliminary strut and nodal proportions, and respective applied loads.

#### Node A (CCT Node)

BEARING FACE

Factored Load:	$F_u = 1480 \text{ kip}$
Efficiency:	$v = 0.75$
Concrete Capacity:	$f_{cu} = v f_c' = (0.75) \cdot (5 \text{ ksi}) = 3.8 \text{ ksi}$
	$\phi \cdot F_n = (0.7) \cdot (3.8 \text{ ksi}) \cdot (22 \text{ in.}) \cdot (22 \text{ in.})$
	$= 1287 \text{ kip} < 1480 \text{ kip NG!}$

BACK FACE

Factored Load:	$F_u = 1254 \text{ kip}$
Efficiency:	$v = 0.75$

Concrete Capacity:  $f_{cu} = v \cdot f'_c = (0.75) \cdot (5 \text{ ksi}) = 3.8 \text{ ksi}$   
 $\phi \cdot F_n = (0.7) \cdot (3.8 \text{ ksi}) \cdot (11.5 \text{ in.}) \cdot (22 \text{ in.})$   
 $= 673 \text{ kip} < 1254 \text{ kip NG!}$

#### STRUT-TO-NODE INTERFACE

Factored Load:  $F_u = 1940 \text{ kip}$

Solve set of four equations simultaneously:

Concrete Efficiency:  $v = \frac{1}{0.8 + 170 \cdot \varepsilon_1} \leq 0.85 = 0.76$

Tensile Strain Term:  $\varepsilon_l = \varepsilon_s + (\varepsilon_s + 0.002) \cot^2 54.4^\circ = 0.0030$

Tie Tensile Strain:  $\varepsilon_s = \frac{F_n \cdot \cos 54.4^\circ}{(20 \cdot 1.56 \text{ in}^2) \cdot (29,000 \text{ ksi})} = 0.0013$

Strength of Nodal Face:  $F_n = v \cdot (5 \text{ ksi}) \cdot (24.6 \text{ in.}) \cdot (22 \text{ in.}) = 2058 \text{ kip}$   
 $\phi \cdot F_n = (0.7) \cdot (2058 \text{ kip})$   
 $= 1441 \text{ kip} < 1940 \text{ kip NG!}$

By inspection, Node A is more critical than Node G. The most critical location of Node A is its back face. Therefore, the bearing plates and beam are proportioned such that Node A meets the requirements of AASHTO LRFD (2008). For the purpose of comparison, the nominal capacity of Node A is determined for the same strut proportions required by ACI 318-08 (Figure A-6).

#### BACK FACE OF NODE A, PER FIGURE A-6

Factored Load:  $F_u = 993 \text{ kip}$

Efficiency:  $v = 0.75$

Concrete Capacity:  $f_{cu} = v \cdot f'_c = (0.75) \cdot (5 \text{ ksi}) = 3.8 \text{ ksi}$   
 $\phi \cdot F_n = (0.7) \cdot (3.8 \text{ ksi}) \cdot (14 \text{ in.}) \cdot (30 \text{ in.})$   
 $= 1117 \text{ kip} > 993 \text{ kip OK}$

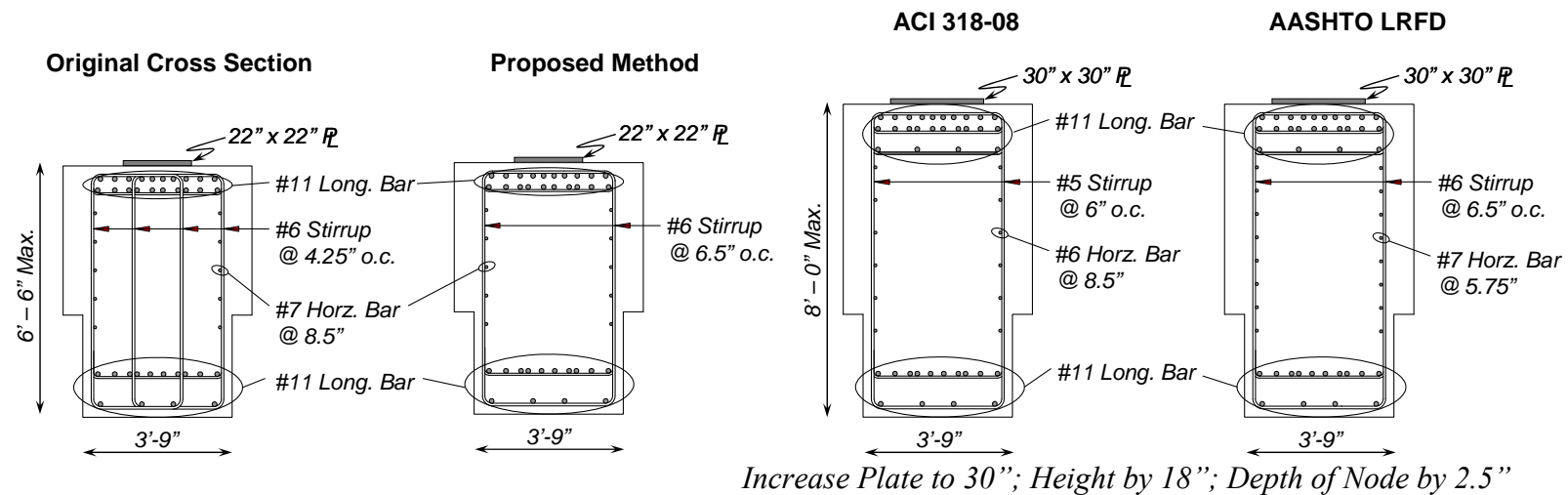
Thus, for an a/d ratio of 0.85, the requirements of AASHTO LRFD (2008) are similar to ACI 318-08.

### **Minimum Transverse Reinforcement**

AASHTO LRFD requires a vertical and horizontal reinforcement ratio of 0.3% of the gross area for the purpose of controlling crack widths. So, based on this requirement, provide #6 vertical stirrups at 6.5 in. and eighteen #7 horizontal bars distributed evenly across the height of the section (resulting spacing is 5.75 in.).

#### ***A.2.2.4 Comparison of Design Provisions for Shear Region with $a/d = 0.85$***

A comparison between the results obtained from the three design methodologies for the D-region with an  $a/d$  ratio equal to 0.85 (Figure A.2, Cross-Section A) is presented in Figure A.7.



Ratio of Capacity over Applied Load,  $\phi V_n / V_u$

Proposed = 1.17  
ACI 318 = 0.54  
AASHTO = 0.54

Proposed = 1.17  
ACI 318 = 0.54  
AASHTO = 0.54

ACI 318 = 1.14  
Proposed = 1.86  
AASHTO = 1.12

AASHTO = 1.12  
Proposed = 1.86  
ACI 318 = 1.14

Figure A.7: Comparison of required cross-section per the Project 5253 method, ACI 318-08, and AASHTO LRFD:  $a/d$  ratio = 0.85.



Based on a comparison of the three provisions, the following observations can be made:

The Project 5253 method results in a much higher nominal capacity than those obtained by using the ACI 318-08 and AASHTO LRFD (2008) provisions. As a result, the required cross-section is significantly smaller. This is primarily attributed to the fact that the Project 5253 provisions recognize that the back face check is overly conservative when the applied stress is attributed to bond of anchored reinforcement. The capacity of the structure as determined by the ACI 318-08 and AASHTO LRFD (2008) provisions is controlled by the capacity at the back face of the CCT node. According to the Project 5253 provisions, provided the tie is properly anchored behind the node, the stress check at this nodal face is not critical.

Also, the smaller bearing plate (22"x22") did not adversely affect the nominal capacity of the structure according to the Project 5253 provisions due to triaxial confinement. Alternatively, the ACI 318-08 and AASHTO LRFD (2008) provisions do not consider the increase provided by triaxial confinement, so the bearing plate dimensions had to be increased to the maximum possible size (i.e. 30"x30").

Finally, the minimum amount of transverse reinforcement required by the Project 5253 method, ACI 318-08 and the AASHTO LRFD (2008) specifications is significantly less than the amount contained in the existing bent. However, the fact that the structure contains an amount in excess of the minimum is not a deficiency. On the contrary, additional transverse reinforcement will provide for narrower crack widths and better distribution of cracks upon diagonal cracking with some diminishing returns.

Next, the service load diagonal cracking check is performed on the region of the bent cap with an  $a/d$  ratio of 0.85.

#### ***A.2.2.5 Serviceability Behavior for Region with $a/d = 0.85$***

By comparing the amount of shear due to service loads to the cracking strength of concrete, it is possible to estimate the likelihood that the structure will crack under service loads. The shear due to service loads for the portion of the bent with an  $a/d$  ratio of 0.85 is as follows:

$$V_{srv} = 1072 \text{ kip}$$

As presented in Section 5.3.4, for an a/d ratio of 0.85, the shear at which the first diagonal crack will form can be estimated as the following:

$$V_{cr} = (6.5 - 3a/d)\sqrt{f'_c} \cdot b_w \cdot d = 3.95\sqrt{5000}(45\text{in})(69.5\text{in}) = 874 \text{ kip}$$

As a result, with the original cross-section, it is likely that diagonal cracks will form under the application of the full service loads. Specifically, the first diagonal crack is expected to form under the full DL and 29-percent of the LL ( $792 + 0.29 \cdot 280 = 874$  kips). To reduce the likelihood of diagonal cracking under full service loads, the size of the cross-section can be increased (increasing 'd' will also reduce the a/d ratio) or a higher strength concrete can be specified. Minor diagonal cracking (single, narrow crack) was detected in this region of the actual structure.

### **A.2.3 Shear Region with an a/d Ratio Equal to 2.05**

In this section, the nominal capacity determined by the Project 5253 provisions is investigated for the portion of the bent with an a/d ratio equal to 2.05. Since the a/d ratio for this portion of the structure slightly exceeds 2, a sectional analysis would be recommended according to ACI 318-08 and AASTHO LRFD 2007. However, as shown in Section 5.2, the transition between deep beam and sectional beam behavior is gradual. Thus, a STM analysis at this a/d ratio should be performed and compared with a sectional analysis. A close-up of the critical strut proportions and respective nodal zones is presented to scale in Figure A-8. Note, the vertical reactions are slightly different from one another due to the inclined tie at Node K.

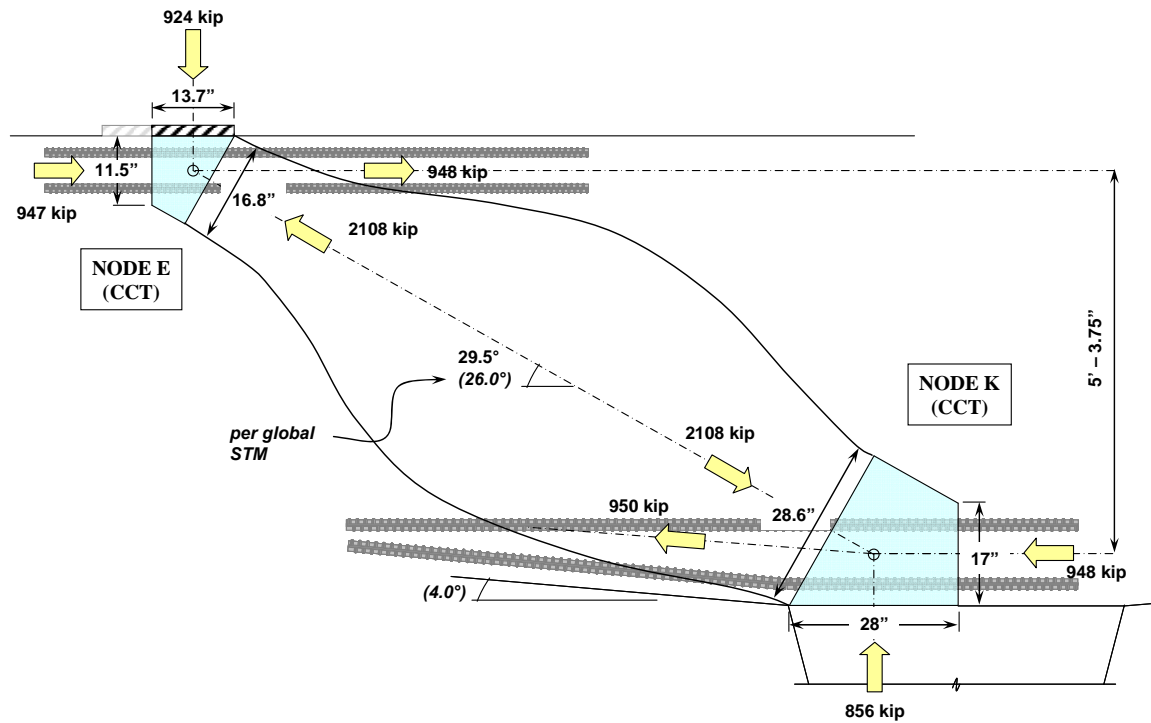


**Figure A-8. Critical strut in region with  $a/d = 2.05$ .**

The length of Nodes E and K are proportioned based on the amount of force that is transferred to the near support. As a result, the angle of inclination of the strut is slightly changed from the global model shown in Figure A.3. However, forces from the global model are not updated to account for the slight change in strut angle. This method is consistent with standard design practice.

Nodes E and K are classified as CCT nodes because of the presence of a horizontal tie to the right of Node E and to the left of Node K. Tensile stresses in the tie must be developed in the nodal region to some degree. However, the stress condition at the back face of Nodes E and K is more complicated because of the compressive force that is applied from an additional strut framing into each node. These compressive stresses are not attributed to the bond stress of an anchored tie. Therefore, they must be applied to the back face; and the nodes must be designed accordingly.

In order to design this portion of the structure, the allowable capacity of each nodal face (i.e. bearing face, back face, and strut-to-node interface) must be greater than

the applied force. This procedure is presented for the Project 5253 method, ACI 318-08 and the AASHTO LRFD (2008) provisions for Nodes E and K as follows.

#### ***A.2.3.1 Design of Region with a/d Ratio Equal to 2.05: Project 5253 Method***

##### **Node E (CCT Node)**

Triaxial Confinement Factor: 
$$m = \sqrt{\frac{(45\text{in})^2}{(22\text{in})^2}} = 2.04 \leq 2$$

##### BEARING FACE

Factored Load: 924 kip

Efficiency:  $v = 0.70$

Concrete Capacity: 
$$f_{cu} = m \cdot v \cdot f_c' = (2) \cdot (0.7) \cdot (5 \text{ ksi}) = 7.0 \text{ ksi}$$
$$\phi \cdot F_n = (0.7) \cdot (7.0 \text{ ksi}) \cdot (13.7 \text{ in.}) \cdot (22 \text{ in.})$$
$$= 1477 \text{ kip} > 924 \text{ kip } \mathbf{OK}$$

##### STRUT-TO-NODE INTERFACE

Factored Load: 2108 kip

Efficiency: 
$$0.65 \leq \left(0.85 - \frac{5\text{ksi}}{20\text{ksi}}\right) \leq 0.45 = 0.60$$

Concrete Capacity: 
$$f_{cu} = m \cdot v \cdot f_c' = (2) \cdot (0.60) \cdot (5 \text{ ksi}) = 6.0 \text{ ksi}$$
$$\phi \cdot F_n = (0.7) \cdot (6.0 \text{ ksi}) \cdot (16.8 \text{ in.}) \cdot (22 \text{ in.})$$
$$= 1552 \text{ kip} < 2108 \text{ kip } \mathbf{NG!}$$

##### BACK FACE

Factored Load: 947 kip

Efficiency:  $v = 0.70$

Concrete Capacity: 
$$f_{cu} = m v f_c' = (2)(0.70)(5 \text{ ksi}) = 7.0 \text{ ksi}$$
$$\phi F_n = (0.7)(7.0 \text{ ksi})(11.5 \text{ in.})(22 \text{ in.})$$
$$= 1240 \text{ kip} > 947 \text{ kip } \mathbf{OK}$$

##### **Node K (CCT Node)**

Triaxial Confinement Factor:  $m = 1.0$

##### BEARING FACE

Factored Load: 857 kip

$$\begin{aligned}
\text{Efficiency:} \quad & v = 0.70 \\
\text{Concrete Capacity:} \quad & f_{cu} = m \cdot v \cdot f_c' = (1) \cdot (0.70) \cdot (5 \text{ ksi}) = 3.5 \text{ ksi} \\
& \phi \cdot F_n = (0.7) \cdot (3.5 \text{ ksi}) \cdot (28 \text{ in.}) \cdot (45 \text{ in.}) \\
& = 3087 \text{ kip} > 857 \text{ kip } \mathbf{OK}
\end{aligned}$$

#### STRUT-TO-NODE INTERFACE

$$\begin{aligned}
\text{Factored Load:} \quad & 2108 \text{ kip} \\
\text{Efficiency:} \quad & 0.65 \leq \left( 0.85 - \frac{5 \text{ ksi}}{20 \text{ ksi}} \right) \leq 0.45 = 0.60 \\
\text{Concrete Capacity:} \quad & f_{cu} = m \cdot v \cdot f_c' = (1) \cdot (0.6) \cdot (5 \text{ ksi}) = 3.0 \text{ ksi} \\
& \phi \cdot F_n = (0.7) \cdot (3.0 \text{ ksi}) \cdot (28.6 \text{ in.}) \cdot (45 \text{ in.}) \\
& = 2703 \text{ kip} > 2108 \text{ kip } \mathbf{OK}
\end{aligned}$$

#### BACK FACE

$$\begin{aligned}
\text{Factored Load:} \quad & 948 \text{ kip} \\
\text{Efficiency:} \quad & v = 0.70 \\
\text{Concrete Capacity:} \quad & f_{cu} = m \cdot v \cdot f_c' = (1)(0.70)(5 \text{ ksi}) = 3.5 \text{ ksi} \\
& \phi F_n = (0.7)(3.5 \text{ ksi})(17 \text{ in.})(45 \text{ in.}) \\
& = 1874 \text{ kip} > 948 \text{ kip } \mathbf{OK}
\end{aligned}$$

#### Tie EF

$$\begin{aligned}
\text{Factored Load:} \quad & F_u = 948 \text{ kip} \\
\text{Efficiency:} \quad & v = 1.0 \\
\text{Tie Capacity:} \quad & (1.0) \cdot (60 \text{ ksi}) \cdot (14) \cdot (1.56 \text{ in}^2) = 1310 \text{ kip} \\
& \phi \cdot F_n = (0.9) \cdot (1310 \text{ kip}) \\
& = 1179 \text{ kip} > 948 \text{ kip } \mathbf{OK}
\end{aligned}$$

Thus, according to the Project 5253 procedure, the stress check at the strut-to-node interface at Node E is not satisfied. To increase the capacity, the beam width and the size of the bearing pad can be increased. Also, the depth of the member can be increased which will decrease the force in the inclined strut. All three of these options were used. The size of the bearing plate was increased to 30"x30." This was considered to be a reasonable maximum for the size of the bearing plate. Also, the beam width and beam depth were increased by 6 in. With these changes, the node-to-strut interface at

Node E has sufficient capacity. The updated strut proportions and forces are illustrated in Figure A-9.

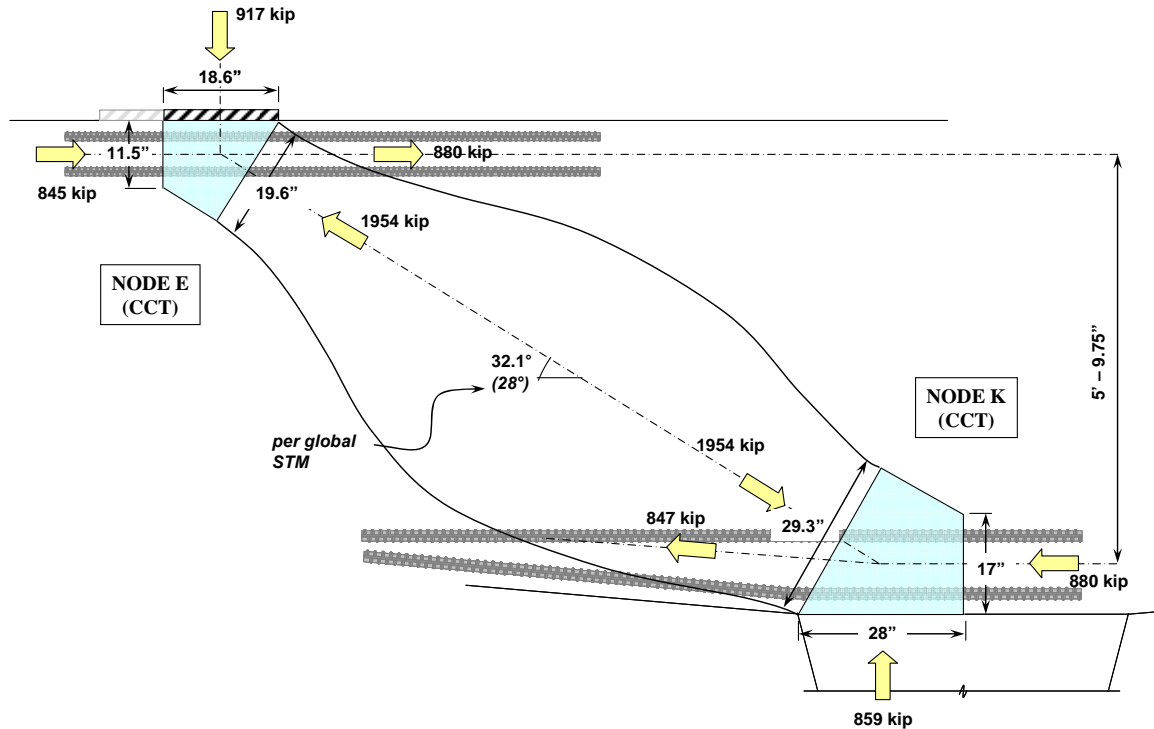


**Figure A-9: Strut proportions and forces associated with a 6-inch increase in depth of bent.**

NODE E STRUT-TO-NODE INTERFACE, PER FIGURE A-9

Factored Load: 1954 kip

Confinement Factor:  $m = \sqrt{\frac{(5 \text{ in})^2}{(30 \text{ in})^2}} = 1.7$

Efficiency:  $0.65 \leq \left(0.85 - \frac{5 \text{ ksi}}{20 \text{ ksi}}\right) \leq 0.45 = 0.60$

Concrete Capacity:  $f_{cu} = m \cdot v \cdot f_c' = (1.7) \cdot (0.60) \cdot (5 \text{ ksi}) = 5.1 \text{ ksi}$   
 $\phi \cdot F_n = (0.7) \cdot (5.1 \text{ ksi}) \cdot (19.6 \text{ in.}) \cdot (30 \text{ in.})$   
 $= 2099 \text{ kip} > 1954 \text{ kip OK}$

Thus, the capacity of strut illustrated in Figure A-9 meets the requirements of the Project 5253 method.

### Minimum Transverse Reinforcement

As shown in the previous section, the size of the original cross-section ( $a/d = 2.05$ ) was not sufficient according to the Project 5253 STM provisions. The minimum reinforcement required to ensure the satisfactory serviceability performance of the new section would be as follows:

$$A_v = 0.003 \cdot b_w \cdot s_1 \rightarrow 2 \cdot (0.44 \text{ in}^2) = 0.003 \cdot (51 \text{ in}) \cdot s_1$$

$$s_1 = 5.75 \text{ in}$$

$$A_{vh} = 0.003 \cdot b_w \cdot s_2 \rightarrow 2 \cdot (0.60 \text{ in}^2) = 0.003 \cdot (51 \text{ in}) \cdot s_2$$

$$s_2 = 7.8 \text{ in}$$

This reinforcement equates to #6 vertical stirrups at 5.5 in. and #7 horizontal bars at 7.5 in. on center. The reinforcement should be distributed as shown in Section 4.3.4.

A summary of the preceding design is presented in Figure A.12 along with the other provisions. Next, Strut EK and respective nodal regions are designed according to ACI 318-08.

#### A.2.3.2 Design of Region with $a/d$ Ratio Equal to 2.05: ACI 318-08 Appendix A

Refer to Figure A-8 for preliminary forces, strut, and nodal dimensions. By inspection, Node E is the most critical nodal zone. Therefore, the design of Strut EK is based on the design of Node E. Recall, that the ACI 318-08 load factors are less than those presented in Figure A-8. Therefore, all of the load values are multiplied by a factor of 0.945 (i.e.  $P_{u\_ACI}/P_{u\_AASHTO} = 1398/1480 = 0.945$ ).

#### Node E (CCT Node)

BEARING FACE

Factored Load:  $F_u = 873 \text{ kip}$

Efficiency:  $\beta = 0.80$

Concrete Capacity:  $f_{cu} = 0.85 \cdot \beta \cdot f'_c = (0.85) \cdot (0.8) \cdot (5 \text{ ksi}) = 3.4 \text{ ksi}$

$$\phi \cdot F_n = (0.75) \cdot (3.4 \text{ ksi}) \cdot (13.7 \text{ in.}) \cdot (22 \text{ in.})$$

$$= 769 \text{ kip} < 739 \text{ kip NG!}$$

#### BACK FACE

$$\begin{aligned}\text{Factored Load:} \quad & F_u = 895 \text{ kip} + 896 \text{ kip} = 1791 \text{ kip} \\ \text{Efficiency:} \quad & \beta = 0.80 \\ \text{Concrete Capacity:} \quad & f_{cu} = 0.85 \cdot \beta \cdot f'_c = (0.85) \cdot (0.8) \cdot (5 \text{ ksi}) = 3.4 \text{ ksi} \\ & \phi \cdot F_n = (0.75) \cdot (3.4 \text{ ksi}) \cdot (11.5 \text{ in.}) \cdot (22 \text{ in.}) \\ & = 645 \text{ kip} < 1791 \text{ kip} \text{ NG!}\end{aligned}$$

#### STRUT-TO-NODE INTERFACE

$$\begin{aligned}\text{Factored Load:} \quad & F_u = 1992 \text{ kip} \\ \text{Efficiency:} \quad & \beta = 0.75 \\ \text{Concrete Capacity:} \quad & f_{cu} = 0.85 \cdot \beta \cdot f'_c = (0.85) \cdot (0.75) \cdot (5 \text{ ksi}) = 3.2 \text{ ksi} \\ & \phi \cdot F_n = (0.75) \cdot (3.2 \text{ ksi}) \cdot (16.8 \text{ in.}) \cdot (22 \text{ in.}) \\ & = 887 \text{ kip} < 1992 \text{ kip} \text{ NG!}\end{aligned}$$

According to ACI 318-08, the back face of Node E is the most critical location. In order to properly design this region, the bent is proportioned such that the back face of Node E has adequate capacity. In addition to providing the maximum 30-inch bearing plate, the depth of the bent must be increased by 25 in. and the depth of the back face of Node E must be increased by 6 in. The width of the beam was not increased because triaxial confinement is not permitted in the ACI 318-08 specifications. Since the bearing plate is still less than the width of the member, an increase in beam width does not increase the width of the nodes. Strut proportions and forces associated with these changes are illustrated in Figure A.10.



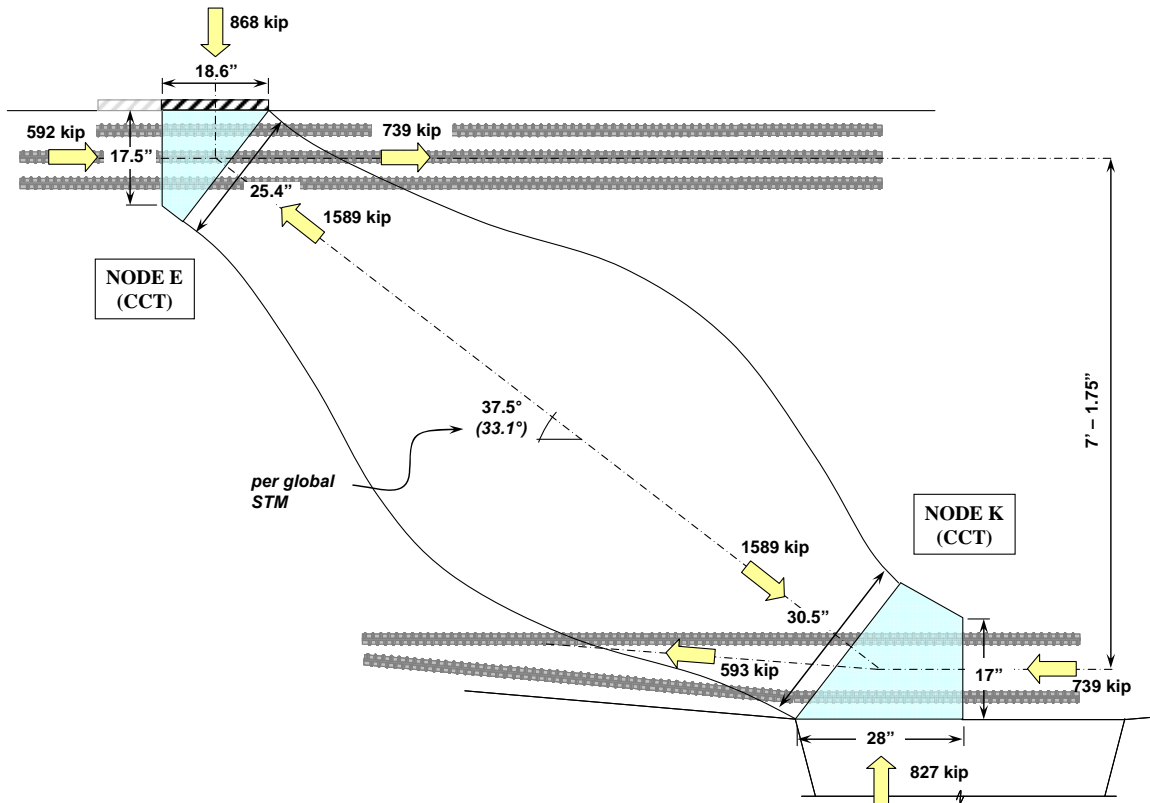


**Figure A.10: Strut proportions and forces associated with a 25-inch increase in bent height and 6-inch increase in depth of Node E (ACI 318 factored loads)**

BACK FACE OF NODE E: PER FIGURE A.10

Factored Load:  $F_u = 739 \text{ kip} + 592 \text{ kip} = 1331 \text{ kip}$

Efficiency:  $\beta = 0.80$

Concrete Capacity:  $f_{cu} = 0.85 \cdot \beta \cdot f'_c = (0.85) \cdot (0.8) \cdot (5 \text{ ksi}) = 3.4 \text{ ksi}$

$$\begin{aligned} \phi \cdot F_n &= (0.75) \cdot (3.4 \text{ ksi}) \cdot (17.5 \text{ in.}) \cdot (30 \text{ in.}) \\ &= 1339 \text{ kip} > 1331 \text{ kip} \text{ OK} \end{aligned}$$

Thus, the capacity of the bent illustrated in Figure A.10 meets the requirements of ACI 318-08.

### Minimum Transverse Reinforcement

ACI 318-08 does not stipulate a minimum amount of transverse reinforcement. However, in order to use the higher strut efficiency factor, the following minimum amount of reinforcement must be provided:

$$\sum \frac{A_{si}}{b_s \cdot s_i} \sin \alpha_i > 0.003$$

If it is assumed that the vertical and horizontal reinforcement ratios are identical,

$$\rho \cdot \sin 38^\circ + \rho \cdot \sin 52^\circ > 0.003$$

Thus,

$$\rho_v = \rho_{vh} > 0.0021$$

Provide #5 vertical stirrups at 6 in. and #6 horizontal bars at 8.5 in. on center.

A summary of the preceding ACI 318-08 results is presented in Figure A.12 along with the other provisions. Next, Strut EK and respective nodal regions are designed according to AASHTO LRFD.

#### ***A.2.3.3 Design of Region with a/d Ratio Equal to 2.05: AASHTO LRFD***

Refer to Figure A-8 for preliminary forces, strut and nodal proportions. By inspection, Node E is the most critical nodal zone. Therefore, design of Strut EK is based on the design of Node E.

##### **Node E (CCT Node)**

###### **BEARING FACE**

Factored Load:	$F_u = 924 \text{ kip}$
Efficiency:	$v = 0.75$
Concrete Capacity:	$f_{cu} = v \cdot f_c' = (0.75) \cdot (5 \text{ ksi}) = 3.8 \text{ ksi}$ $\phi \cdot F_n = (0.7) \cdot (3.8 \text{ ksi}) \cdot (13.7 \text{ in.}) \cdot (22 \text{ in.})$ $= 802 \text{ kip} < 924 \text{ kip NG!}$

###### **BACK FACE**

Factored Load:	$F_u = 947 \text{ kip} + 948 \text{ kip} = 1895 \text{ kip}$
Efficiency:	$v = 0.75$
Concrete Capacity:	$f_{cu} = v \cdot f_c' = (0.75) \cdot (5 \text{ ksi}) = 3.8 \text{ ksi}$ $\phi \cdot F_n = (0.7) \cdot (3.8 \text{ ksi}) \cdot (11.5 \text{ in.}) \cdot (22 \text{ in.})$ $= 673 \text{ kip} < 1895 \text{ kip NG!}$

###### **STRUT-TO-NODE INTERFACE**

Factored Load:  $F_u = 2108 \text{ kip}$

Solve set of four equations simultaneously:

Concrete Efficiency:  $\nu = \frac{I}{0.8 - 170 \cdot \varepsilon_l} \leq 0.85 = 0.39$

Tensile Strain Term:  $\varepsilon_l = \varepsilon_s + (\varepsilon_s + 0.002) \cot^2 29.5^\circ = 0.0103$

Tie Tensile Strain:  $\varepsilon_s = \frac{F_n \cdot \cos 29.5^\circ}{(21.8 \text{ in}^2) \cdot (29,000 \text{ ksi})} = 0.0010$

Strength of Nodal Face:  $F_n = \nu \cdot (5 \text{ ksi})(16.3 \text{ in.})(22 \text{ in.}) = 705 \text{ kip}$   
 $\phi \cdot F_n = (0.7)(705 \text{ kip})$   
 $= 722 \text{ kip} < 2108 \text{ kip NG!}$

The strut-to-node interface at Node E is the most critical location. Therefore, the size of the bent is increased in order to provide Node E with adequate capacity. As a preliminary check, evaluate whether or not the bent dimensions required per ACI 318-08 (Figure A.10) meet the requirements of AASHTO LRFD (2008). Recall, the loads illustrated in Figure A.10 are ACI 318-08 factored loads. AASHTO LRFD (2008) load factors are slightly higher, so the loads are multiplied by a factor of 1.059 (i.e.  $P_{u\_AASHTO}/P_{u\_ACI} = 1480/1398 = 1.059$ ).

NODE E STRUT-TO-NODE INTERFACE, PER FIGURE A.10

Factored Load:  $F_u = 1683 \text{ kip}$

Solve set of four equations simultaneously:

Concrete Efficiency:  $\nu = \frac{I}{0.8 - 170 \cdot \varepsilon_l} \leq 0.85 = 0.46$

Tensile Strain Term:  $\varepsilon_l = \varepsilon_s + (\varepsilon_s + 0.002) \cot^2 37.5^\circ = 0.0080$

Tie Tensile Strain:  $\varepsilon_s = \frac{F_n \cdot \cos 37.5^\circ}{(28.1 \text{ in}^2) \cdot (29,000 \text{ ksi})} = 0.0017$

Strength of Nodal Face:  $F_n = \nu \cdot (5 \text{ ksi})(25.4 \text{ in.})(30 \text{ in.}) = 1761 \text{ kip}$   
 $\phi \cdot F_n = (0.7)(1761 \text{ kip})$   
 $= 1233 \text{ kip} < 1683 \text{ kip NG!}$

In order for the bent to meet the requirements of AASHTO LRFD, the bent depth must be increased by 35 in. and the depth of Node E must be increased by 10.5 in. from the original cross-section. The width of the beam was not increased because triaxial confinement is not permitted in the AASHTO LRFD STM specifications. Since the bearing plate (30") is still less than the width of the member (45"), an increase in beam width does not increase the width of the nodes. Strut proportions associated with this increase and applied loads are illustrated in Figure A.11.

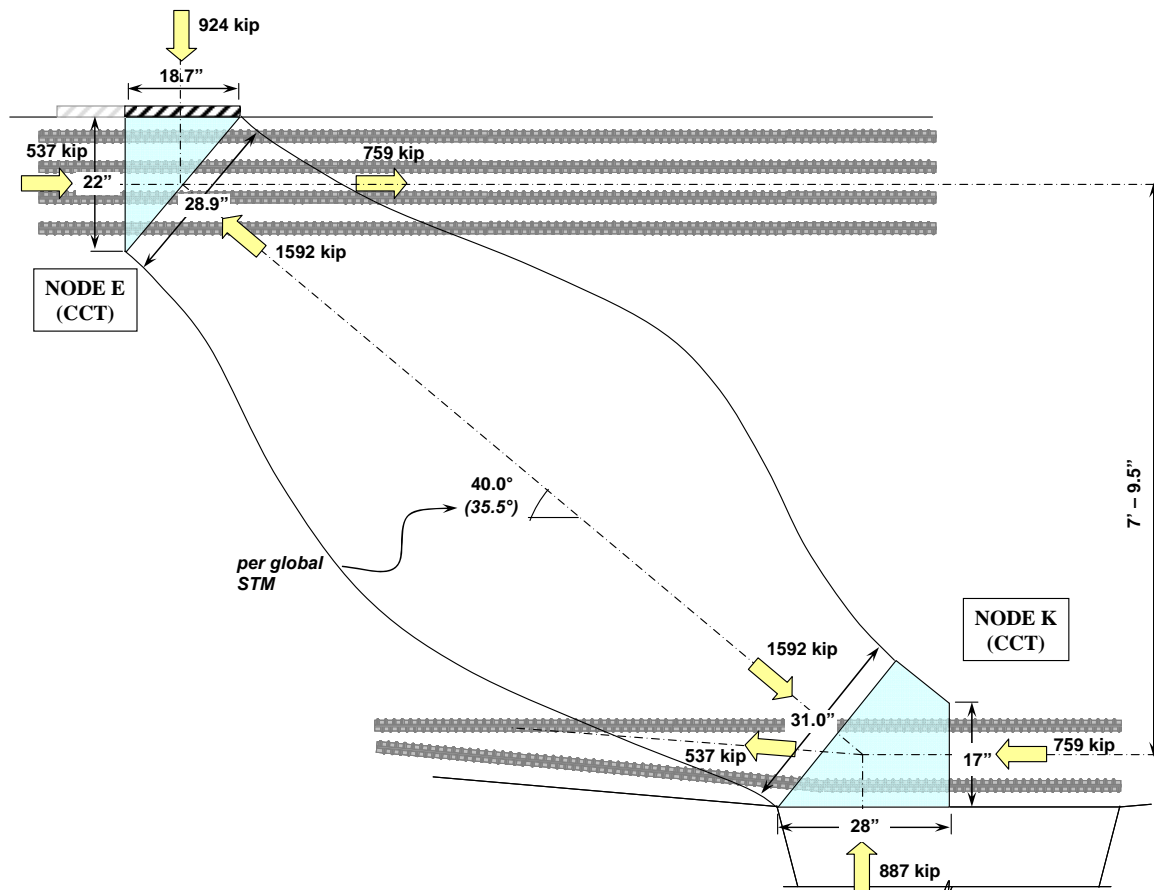


**Figure A.11: Strut proportions and forces associated with a 35-inch increase in bent depth and 10.5-inch increase in depth of Node E (AASHTO LRFD factored loads).**

NODE E STRUT-TO-NODE INTERFACE, PER FIGURE A.11

Factored Load: 1592 kip

Solve set of four equations simultaneously:

$$\begin{aligned}
\text{Concrete Efficiency:} \quad \nu &= \frac{I}{0.8 - 170 \cdot \varepsilon_I} \leq 0.85 = 0.53 \\
\text{Tensile Strain Term:} \quad \varepsilon_I &= \varepsilon_s + (\varepsilon_s + 0.002) \cot^2 40.0^\circ = 0.0064 \\
\text{Tie Tensile Strain:} \quad \varepsilon_s &= \frac{F_n \cdot \cos 40.0^\circ}{(40.6 \text{ in}^2) \cdot (29,000 \text{ ksi})} = 0.0015 \\
\text{Strength of Nodal Face:} \quad F_n &= \nu \cdot (5 \text{ ksi}) (28.9 \text{ in.}) (30 \text{ in.}) = 2287 \text{ kip} \\
\varphi \cdot F_n &= (0.7) (2287 \text{ kip}) \\
&= 1601 \text{ kip} > 1592 \text{ kip } \mathbf{OK}
\end{aligned}$$

Thus, the capacity of the bent illustrated in Figure A.11 meets the requirements of AASHTO LRFD (2007).

### **Minimum Transverse Reinforcement**

AASHTO LRFD requires a vertical and horizontal reinforcement ratio of 0.3% of the gross area for the purpose of controlling cracking. So, based on this requirement, provide #6 vertical stirrups at 6.5 in. and twenty #8 horizontal bars distributed evenly across the height of the section (resulting in a spacing of 7 in.).

A summary of the preceding AASHTO LRFD results is presented along with the other provisions in the following section.

#### ***A.2.3.4 Comparison of Design Provisions for Shear Region with $a/d = 2.05$***

A comparison between the results obtained from the three design methodologies (i.e. Project 5253 method, ACI 318-08, and AASHTO LRFD) for the portion of the bent with an  $a/d$  ratio equal to 2.05 (Figure A.2, Cross-Section B) is presented in Figure A.12.

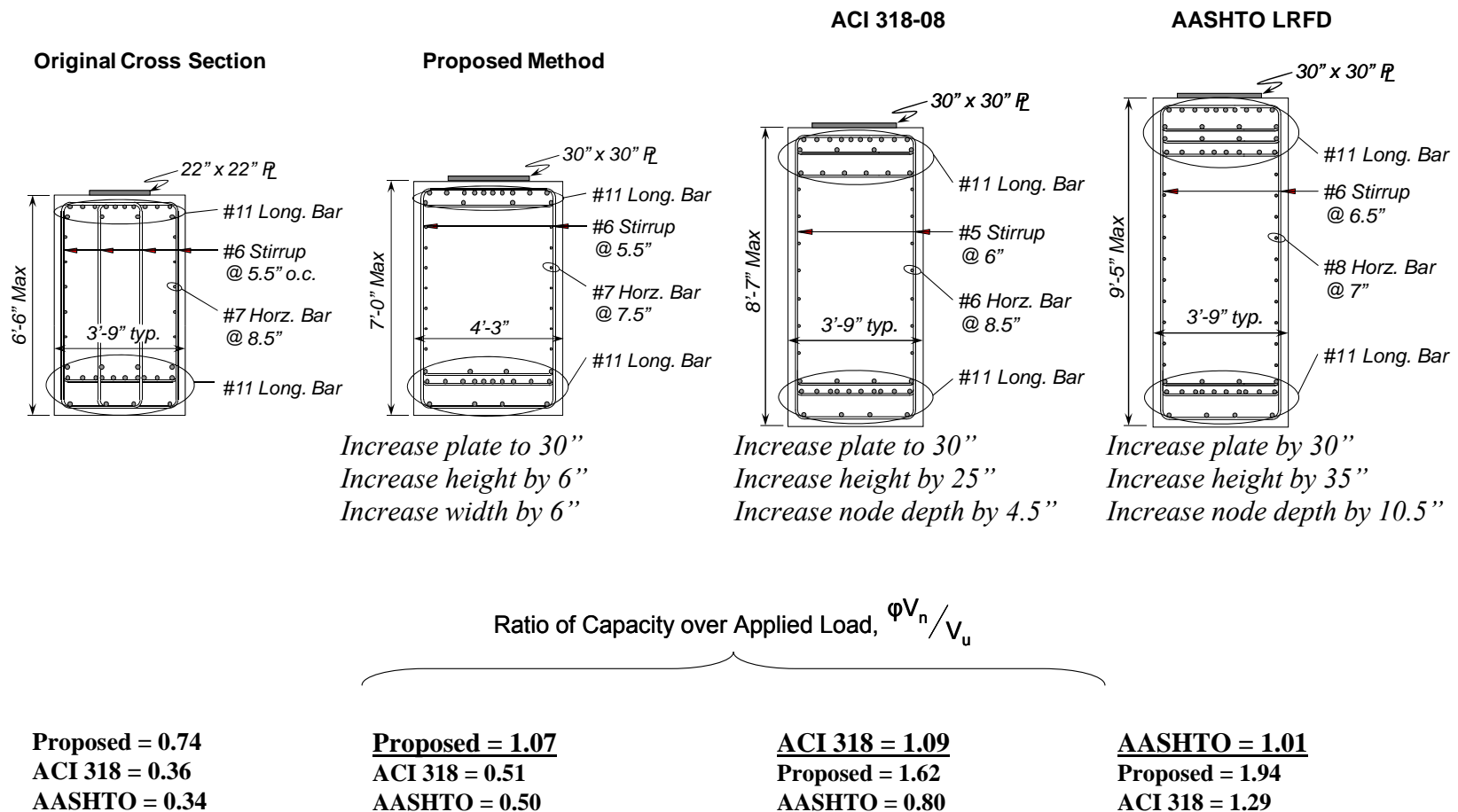


**Figure A.12: Comparison of required cross-section per the Project 5253 method, ACI 318-08, and AASHTO LRFD (2007):**  
*a/d ratio = 2.05.*

Based on a comparison of the three provisions, the following observations can be made:

The Project 5253 method results in a much higher capacity than the ACI 318-08 and AASHTO LRFD (2008) provisions. As a result, the cross-section required by the Project 5253 procedure is significantly smaller. One reason for the difference can be attributed to the fact that the Project 5253 procedure considers the increase in concrete compressive strength provided by triaxial confinement of the bearing plate. Neither the ACI 318-08 nor the AASHTO LRFD (2008) provisions consider the beneficial effects of triaxial confinement. In addition, according to the AASHTO LRFD (2008) provisions, the efficiency of the node-to-strut interface decreases as the shear span-to-depth ratio increases. It follows that excessively conservative results can be expected when using AASHTO LRFD (2008) for D-regions with an  $a/d$  ratio in the range of two. Despite the differences in the results of the three methods, they are similar in the fact that the results suggest that the dimensions of the original cross-section are inadequate to resist the application of the factored loads. This finding agrees with the extensive amount of diagonal cracking present in the actual structure in service.

Since this portion of the bent has an  $a/d$  ratio slightly greater than 2.0, the capacity of this region may be determined according to sectional shear provisions. The sectional shear strength of this region is determined according to ACI 318-08 and AASHTO LRFD (2008). A discussion on the implications of using a sectional analysis rather than a deep beam analysis is presented in Section A.3.

It is also of interest to examine the ratio of service load to diagonal cracking strength applied to this portion of the bent. The service load diagonal cracking check is performed on the region of the bent cap with an  $a/d$  ratio of 2.05 in the next section.

#### ***A.2.3.5 Serviceability Behavior for Region with $a/d = 2.05$***

By comparing the amount of service shear to the diagonal cracking strength of concrete, it is possible to estimate the likelihood that the structure will crack while in service. The shear force due to service loads for the portion of the bent with an  $a/d$  ratio of 2.05 is as follows:

$$V_{\text{srv}} = (856 \text{ kip}) \cdot (1072 \text{ kip} / 1480 \text{ kip}) = \mathbf{620 \text{ kip}}$$

According to Section 5.3.4, for an a/d ratio of 2.05, the shear at which the first diagonal crack will form with the original section dimensions can be estimated as the following:

$$V_{\text{cr}} = 2\sqrt{f'_c} \cdot b_w \cdot d = 2\sqrt{5000}(45 \text{ in})(63 \text{ in}) = \mathbf{401 \text{ kip}}$$

The cracking capacity of this portion of the structure is less than the full service level loading. As a result, it is expected that diagonal cracks will exist under full service loads. In fact, diagonal cracks are expected to form under the application of 65% of the service-level loading (i.e.  $401/620 = 0.65$ ) or 88% of the DL (i.e.  $(856/1480) \cdot 792 = 458$  kips DL;  $401/458 = 0.88$ ). In the actual structure, a number of parallel, diagonal cracks existed in this portion of the structure ( $a/d = 2.05$ ). The significant amount of cracking agrees with the above calculation regarding the expectancy of the member to crack under only 88% of the DL.

In order to prevent cracking from occurring under the application of service loads, bent dimensions or the compressive strength of concrete must be increased such that  $V_{\text{cr}} \geq V_{\text{srv}}$ . For the section satisfying the Project 5253 STM provisions, the diagonal cracking load can be estimated as:

$$V_{\text{cr}} = 2\sqrt{f'_c} \cdot b_w \cdot d = 2\sqrt{5000}(51 \text{ in})(69 \text{ in}) = \mathbf{498 \text{ kip}}$$

The cracking capacity of this portion of the structure is less than the full service level loading. However, diagonal cracks are not expected to form until the full dead load and approximately 25-percent of the live load is on the structure (i.e.  $498 - 458 = 40$  kips of LL;  $40 / (856 / 1480 \cdot 280) = 0.25$ ). To further reduce the likelihood of diagonal cracking under service, the design of the cross-section can be altered as before.

### A.3 SECTIONAL SHEAR DESIGN

The purpose of calculating the sectional shear capacity for the portion of the beam with an a/d ratio of 2.05 (Figure A.2, Section B) is to compare the results to those determined from a strut-and-tie model. The discrepancy in the shear capacity at an a/d



ratio near 2 determined by deep beam and sectional shear provisions is a topic of interest to the current project.

The ACI 318-08 and AASHTO LRFD (2008) provisions require that a designer use deep beam provisions for structures with a shear span-to-depth ratio less than or equal to two. For structures whose a/d ratio is near two, it is logical to expect that the capacity determined from a strut-and-tie model to be similar to that determined from a sectional model. In other words, the calculated capacity of a member should not significantly vary for an a/d ratio of 2.1 or 1.9. However, the difference in the allowable shear capacity according to sectional shear or a STM is often quite drastic (Section 5.2).

### **A.3.1 Shear Region with a/d Ratio Equal to 2.05**

Refer to Figure A.3 for the critical shear force in Section A. The AASHTO LRFD (2008) factored shear is 856-kip; the ACI 318-08 factored shear is 809-kip. The ACI 318-08 and AASHTO LRFD (2008) reduction factors for sectional shear are 0.75 and 0.9, respectively. The nominal shear capacity according to ACI 318-08 and AASHTO LRFD (2008) is presented as follows.

#### **A.3.1.1 ACI 318-08 §11.1, Shear Strength**

$$\text{Factored Load:} \quad V_u = 809 \text{ kip}$$

$$\text{Sectional Capacity:} \quad V_n = V_c + V_s$$

Where,

$$V_c = 2\sqrt{f'_c} \cdot b_w \cdot d = 2\sqrt{5000 \text{ psi}} \cdot (45 \text{ in}) \cdot (63 \text{ in}) = 401 \text{ kip}$$

$$V_s = A_v \cdot f_v \cdot d / s = 4 \cdot (0.44 \text{ in}^2) \cdot (60 \text{ ksi}) \cdot (63 \text{ in}) / 5.5 \text{ in} = 1210 \text{ kip}$$

$$\phi V_n = (0.75) \cdot (1611 \text{ kip}) = 1208 \text{ kip} > 809 \text{ kip} \textbf{ OK}$$

According to ACI 318-08, the strength of the bent is adequate. However, recall that according to the STM design previously presented, the depth of the bent had to be considerably increased in order to meet the requirements of ACI 318-08 Appendix A. The degree of discontinuity between sectional shear and STM provisions is discussed in

Section A.3.2. Next, the sectional shear capacity according to the AASHTO LRFD (2008) provisions is presented.

**A.3.1.2 AASHTO LRFD§5.8.3, Sectional Design Model (General Procedure)**

Factored Load:  $V_u = 856 \text{ kip}$

Sectional Capacity:  $V_n = V_c + V_s$

Where,

$$V_c = 0.0316 \beta \sqrt{f'_c} b_v d_v$$

$$V_s = \frac{A_v f_y d_v}{s \cdot \tan \theta}$$

and,

$\beta$  = factor indicating the ability of diagonally cracked concrete to transmit tension and shear.

According to AASHTO LRFD (2008), the factor,  $\beta$ , is determined based on the longitudinal strain, shear stress, spacing and inclination of cracking across the web. For non-prestressed beams, sufficiently reinforced, the factor,  $\beta$ , may be determined according to Equation A.1:

$$\beta_s = \frac{4.8}{(1 + 750 \varepsilon_s)} \quad (\text{A.1})$$

And the angle of inclination of the cracking,  $\theta$ , is determined according to Equation A.2:

$$\theta = 29 + 3500 \varepsilon_s \quad (\text{A.2})$$

Where the longitudinal strain,  $\varepsilon_s$ , in the web is determined according to Equation A.3.

$$\varepsilon_s = \frac{\left( \frac{|M_u|}{d_v} + 0.5 N_u + 0.5 |V_u| \cot \theta \right)}{2(E_s A_s)} \quad (\text{A.3})$$

Where,

$M_u$  = Factored moment at critical section, kip-in.

$$\begin{aligned}
V_u &= \text{Factored shear at critical section, kip} \\
N_u &= \text{Factor axial force at critical section, kip} \\
\theta &= \text{Angle of inclination of diagonal cracking, radian} \\
d_v &= \text{distance between longitudinal top and bottom reinforcement, in.} \\
E_s &= \text{Modulus of elasticity of steel reinforcement} \\
A_s &= \text{Area of flexural tension reinforcement, in}^2
\end{aligned}$$

Based on a linear analysis of the multiple-column bent, the factored moment at the critical section is 51,750-kip·inches and the factored shear force is 856-kip. The longitudinal strain and angle of inclination terms are simultaneously calculated as follows:

$$\begin{aligned}
\varepsilon_s &= \frac{\left( \frac{|51,750 \text{ kip} \cdot \text{in}|}{57 \text{ in}} + 0.5(0 \text{ kip}) + 0.5|856 \text{ kip}| \cot 32.4^\circ \right)}{2(29,000 \text{ ksi} \cdot 28.1 \text{ in}^2)} = 0.00097 \\
\theta &= 29 + 3500 \cdot (0.00097) = 32.4^\circ
\end{aligned}$$

Thus,

$$\beta_s = \frac{4.8}{(1 + 750 \cdot 0.00097)} = 2.78$$

Therefore, the nominal shear capacity can be calculated as follows:

$$\begin{aligned}
V_c &= 0.0316 \cdot 2.7 \sqrt{5 \text{ ksi}} \cdot (45 \text{ in.})(57 \text{ in.}) = 489 \text{ kip} \\
V_s &= 4(0.44 \text{ in}^2) \cdot (60 \text{ ksi}) \cdot (57 \text{ in.}) / (5.5 \text{ in.}) \tan 32.4^\circ = 1724 \text{ kip}
\end{aligned}$$

$$\phi V_n = (0.90) \cdot (2214 \text{ kip}) = 1992 \text{ kip} > 856 \text{ kip} \textbf{ OK}$$

According to AASHTO LRFD (2008), the strength of the bent is adequate. Yet, recall that the depth of the bent had to be considerably increased in order to meet the requirements of the strut-and-tie provisions of AASHTO LRFD (2008). The discontinuity between sectional shear and deep beam provisions is discussed in the following section.

### A.3.2 Comparison of Deep Beam and Sectional Shear Provisions

The capacity of the bent at Section B (Figure A.2) has been determined according to the Project 5253, ACI 318-08 Appendix A, and AASHTO LRFD (2008) STM provisions; and the ACI 318-08 and AASHTO LRFD (2008) section-based provisions. A comparison between the results of these analyses is presented in Table A.1.

**Table A.1. Shear Capacity of Original Cross-Section B ( $a/d = 2.05$ )**

Design Procedure	Capacity / Factored Load		$\frac{V_s}{V_c}$ Ratio	$\frac{\phi V_n \text{ Sectional}}{\phi V_n \text{ STM}}$
	STM, $\frac{\phi \cdot V_n}{V_u}$	Sectional, $\frac{\phi \cdot V_n}{V_u}$		
Project 5253	0.74	1.49 <sup>†</sup>	3.0	2.01
ACI 318	0.36	1.49	3.0	4.14
AASHTO LRFD	0.34	2.33	3.5	6.85

<sup>†</sup> ACI 318-08 sectional shear capacity

The information presented in Table A.1 illustrates the relative discontinuity in nominal capacity as determined by sectional shear and deep beam provisions. This phenomenon is especially apparent for a structure with an  $a/d$  ratio equal to 2.05. As an example, according to the AASHTO LRFD (2008) sectional shear provisions, the capacity of the structure under investigation is estimated to be 6.85 times greater than the capacity as determined per the deep beam provisions. The implication of such a discrepancy is that a bent over nine feet deep is required per AASHTO LRFD (2008) for an  $a/d$  ratio less than 2 (Figure A.12), yet a 6.5-foot deep bent is sufficient if the  $a/d$  ratio is slightly greater than 2.

The Project 5253 strut-and-tie modeling procedure addresses this discontinuity to a large extent. The ratio of the capacity according to a sectional shear model and that of the Project 5253 STM provisions is 2.01. That is, the sectional shear strength is 2.01 times the STM strength. While this amount of discrepancy is still large, it is a substantial improvement relative to the factors of 4.14 and 6.85 that result with the use of the STM provisions in ACI 318-08 and AASHTO LRFD (2008), respectively (Table A.1).

The discrepancy is increased by the large ratio of  $V_s/V_c$  as calculated in sectional shear. As noted in Section 5.2.3, the  $V_s/V_c$  ratio should be limited to a value of 2 to help reduce the discrepancy between sectional shear and deep beam shear capacity. For the AASHTO LRFD (2008) and the ACI 318-08 sectional shear provisions, the ratio of  $V_s/V_c$  was 3.5 and 3.0, respectively. It is not recommended to account for such a large percentage of shear capacity through stirrup contribution for members with an  $a/d$  ratio of 2. Also, additional STM capacity can be obtained without increasing the sectional shear strength by increasing the size of the nodal regions.

Completely eliminating the discrepancy between shear strength calculated with sectional shear and STM provisions is unlikely. The design models are completely different and a function of many variables. However, it was shown through this example and in Section 5.2 that with the use of the Project 5253 STM provisions, the discrepancy is largely reduced relative to the STM provisions in AASHTO LRFD (2008) and ACI 318-08. Also, limiting the  $V_s/V_c$  ratio to a value of 2 may help reduce the discrepancy in shear strength at an  $a/d$  ratio of 2.

#### **A.4 SUMMARY**

In this section, a multiple-column bent cap was evaluated. Several findings of Project 5253 were specifically implemented in the re-design or analysis of the structure. First and foremost, the Project 5253 STM provisions were used to check the capacity of the original cross-section. While the shear span with an  $a/d$  ratio of 0.85 was found to be satisfactory from a strength point of view, the shear span with an  $a/d$  ratio of 2.05 was not. Using the Project 5253 STM provisions, it was determined that one of the node-to-strut interfaces was overstressed by approximately 36% (2108/1552). It was determined that an increase in width of 6 in. and an increase in the bearing plate dimensions were necessary to increase the design strength. These parameters are directly related to node size and thus, directly affect deep beam strength (Tuchscherer, 2008). Also, the depth of the section was increased by 6 in. While it was shown that an increase in depth does not directly increase the strength of a deep beam (Section 4.4), it can in the case of fixed span

lengths by increasing the strut angle (decreasing the  $a/d$  ratio) and thus, reducing the force in the strut.

When the original bent cap was checked with the STM provisions in AASHTO LRFD (2008) and ACI 318-08 Appendix A, it was found to be too small. In fact, the use of the AASHTO LRFD (2008) and ACI 318-08 provisions recommended substantially larger cross-sections (Figure A.7 and Figure A.12). From a strength standpoint, it is unlikely that such a dramatic change is warranted. The reason for the amount of inefficiency in the designs according to AASHTO LRFD (2008) and ACI 318-08 was the treatment of bond stresses that require checking at the back face of CCT nodes and the lack of consideration of triaxial confinement.

To limit the width of diagonal cracks at service loads, minimum reinforcement can be provided. In addition, a simple serviceability check may be used to reduce the likelihood of diagonal cracking under service loads. In the example problem, it was shown that the recommended minimum reinforcement was actually less than that provided in the original cross-section. When practical, providing additional reinforcement in excess of the minimum is satisfactory and will reduce the width of diagonal cracks (with some diminishing returns) should they form. When service load shear checks were performed on the original cross-section, it was found that the member was expected to crack under service loads. For the span with an  $a/d$  ratio of 0.85, the load at first diagonal cracking was estimated to occur under full service load and approximately 29-percent of the live-load. For the span with an  $a/d$  ratio of 2.05, the load at first diagonal cracking was estimated to occur at only 88-percent of the dead load. From this check, it is clear that the original section was expected to crack in service. The amount of distress present in the bent cap in service (Figure A.1) seems to be fairly consistent with the level of distress implied by this serviceability check. After performing these checks on the sections proposed with the Project 5253 STM provisions, it was found that diagonal cracking was expected to occur under full dead loads and approximately 25-percent of the live load for both shear spans. Depending on the situation, this may not be satisfactory from a serviceability perspective. The designer has

the option to increase the size of the section and specify higher concrete strength to reduce the risk of diagonal cracking in service.

Since one portion of the structure was loaded at an  $a/d$  ratio of 2.05, it can be designed with a sectional shear model. In the example problem, it was illustrated that due to the unnecessary conservatism of the STM provisions in ACI 318-08 and AASHTO LRFD (2008) and the relatively high ratios of  $V_s/V_c$ , there was a large discrepancy between the sectional capacity and the STM capacity according to these provisions. When the capacity according to the Project 5253 STM provisions was compared to the sectional shear capacity, a more reasonable discrepancy was observed. This discrepancy can likely be further reduced by limiting the  $V_s/V_c$  ratio to a value of 2.

In short, the example problem presented in this section was a unique case study in which several of the findings of the Project 5253 could be applied directly. It is believed that the results of this example problem further support the recommendations of TxDOT Project 5253.

## APPENDIX B.

### Evaluation Database

#### B.1 OVERVIEW

The following details are presented in Table 0.1 for the 179 specimens in the *evaluation database*:

- b** = beam width, in.
- h** = beam height, in.
- d** = distance from extreme compression fiber to centroid of tensile reinforcement, in.

**$f_c'$**  = compressive strength of concrete at the time of testing, psi.

*Note: if the compressive strength was measured based on the test of a standard 100 or 150-mm cube, then it was converted to the equivalent 6-inch cylinder strength according to fib (1999).*

**$f_y$**  = yield strength of tensile reinforcement, ksi.

**$f_{yv}$**  = yield strength of vertical transverse reinforcement, ksi.

**$\rho_l$**  = ratio of longitudinal tensile reinforcement to effective area,  $A_s / b \cdot d$

**$\rho_l'$**  = ratio of long. compression reinforcement to effective area,  $A_s' / b \cdot d$

**$\rho_v$**  = ratio of vertical transverse reinforcement to effective area,  $A_v / b \cdot s_1$

**$\rho_h$**  = ratio of horizontal transverse reinforcement to effective area,  $A_{vh} / b \cdot s_2$

**s** = spacing of vertical stirrups, in.

**Load Plate** = dimensions of the load bearing plate measured in the longitudinal and transverse direction ( $l \times w$ ), in.

**Support Plate** = dimensions of the support bearing plate measured in the longitudinal and transverse direction ( $l \times w$ ), in.



<b>a/d ratio</b>	=	shear span-to-depth ratio
<b>V<sub>test</sub></b>	=	maximum shear carried in test region, including the estimated self weight of the specimen, kips
<b>V<sub>crack</sub></b>	=	shear in test region at first diagonal cracking, including the estimated self weight of the specimen, kips

**Table 0.1: Evaluation Database (1 of 10)**

<b>Beam I.D.</b>	<b>b</b> in.	<b>h</b> in.	<b>d</b> in.	<b><math>f'_c</math></b> psi	<b><math>f_y</math></b> ksi	<b><math>f_{yv}</math></b> ksi	<b><math>\rho_l'</math></b>	<b><math>\rho_l</math></b>	<b><math>\rho_v</math></b>	<b><math>\rho_h</math></b>	<b>s</b> in.	<b>Load Plate</b> l x w in.	<b>Support Plate</b> l x w in.	<b>a/d ratio</b>	<b>V<sub>test</sub></b> kips	<b>V<sub>crack</sub></b> kips
<b>Current Study (2008)</b>																
M-03-4-CCC2436	36	48	40	4100	67	61	0.0043	0.0293	0.0031	0.0030	11	24x36	16x36	1.85	1128.3	354.0
M-09-4-CCC2436	36	48	40	4100	67	61	0.0043	0.0293	0.0086	0.0030	4	24x36	16x36	1.85	1426.0	-
M-02-4-CCC2436	36	48	40	2800	65	63	0.0043	0.0293	0.0022	0.0022	10	24x36	16x36	1.85	1102.0	256.0
M-03-4-CCC0812	36	48	40	3000	65	63	0.0043	0.0293	0.0031	0.0030	11	8x12	16x36	1.85	930.0	-
M-03-2-CCC2436	36	48	40	4900	68	62	0.0022	0.0293	0.0031	0.0027	11	24x36	16x36	1.85	1096	-
I-03-2	21	44	38.5	5240	73	67	0.0116	0.0229	0.0029	0.0033	6.5	20x21	16x21	1.84	569.2	144.0
I-03-4	21	44	38.5	5330	73	73	0.0116	0.0229	0.0030	0.0033	7	20x21	16x21	1.84	657.4	-
I-02-2	21	44	38.5	3950	73	67	0.0116	0.0229	0.0020	0.0020	9.5	20x21	16x21	1.84	453.7	121.0
I-02-4	21	44	38.5	4160	73	73	0.0116	0.0229	0.0021	0.0020	10	20x21	16x21	1.84	528.1	-
II-03-CCC2021	21	42	38.6	3290	64	65	0.0115	0.0231	0.0031	0.0045	9.5	20x21	10x21	1.84	499.5	139.0
II-03-CCC1007	21	42	38.6	3480	64	65	0.0115	0.0231	0.0031	0.0045	9.5	10x7	10x21	1.84	477.4	-
II-03-CCT1021	21	42	38.6	4410	66	71	0.0115	0.0231	0.0031	0.0045	9.5	36x21	10x21	1.84	635.4	-
II-03-CCT0507	21	42	38.6	4210	66	71	0.0115	0.0231	0.0031	0.0045	9.5	36x21	5x7	1.84	597.4	146.0
II-02-CCT0507	21	42	38.6	3120	69	64	0.0115	0.0231	0.0020	0.0019	15	36x21	5x7	1.84	401.4	94.0
II-02-CCC1007	21	42	38.6	3140	69	64	0.0115	0.0231	0.0020	0.0019	15	10x7	10x21	1.84	334.8	-
II-02-CCC1021	21	42	38.6	4620	69	67	0.0115	0.0231	0.0020	0.0019	15	10x21	10x21	1.84	329.0	132.0
II-02-CCT0521	21	42	38.6	4740	69	67	0.0115	0.0231	0.0020	0.0019	15	20x21	5x21	1.84	567.4	-
III-1.85-02	21	42	38.6	4100	66	64	0.0115	0.0231	0.0020	0.0019	14.5	20x21	16x21	1.84	487.8	112.0
III-1.85-025	21	42	38.6	4100	66	64	0.0115	0.0231	0.0024	0.0014	12	20x21	16x21	1.84	515.6	-
III-1.85-03	21	42	38.6	4990	69	64	0.0115	0.0231	0.0029	0.0029	10	20x21	16x21	1.84	412.3	137.0
III-1.85-01	21	42	38.6	5010	69	63	0.0115	0.0231	0.0010	0.0014	18	20x21	16x21	1.84	272.6	-

**Table 0.1: Evaluation Database (2 of 10)**

Beam I.D.	b in.	h in.	d in.	$f'_c$ psi	$f_y$ ksi	$f_{yv}$ ksi	$\rho_l'$	$\rho_l$	$\rho_v$	$\rho_h$	s in.	Load Plate l x w in.	Support Plate l x w in.	a/d ratio	V <sub>test</sub> kips	V <sub>crack</sub> kips
<b>Current Study (2008), continued...</b>																
III-1.85-03b	21	42	38.6	3300	69	62	0.0115	0.0231	0.0031	0.0029	6	20x21	16x21	1.84	471.1	114.0
III-1.85-02b	21	42	38.6	3300	69	62	0.0115	0.0231	0.0020	0.0018	9.5	20x21	16x21	1.84	467.6	-
III-1.2-02	21	42	38.6	4100	66	60	0.0115	0.0231	0.0020	0.0018	9.5	20x21	16x21	1.84	846.5	165.0
III-1.2-03	21	42	38.6	4220	66	68	0.0115	0.0231	0.0031	0.0029	9.5	20x21	16x21	1.84	829.2	-
III-2.5-02	21	42	38.6	4630	66	62	0.0115	0.0231	0.0020	0.0018	9.5	20x21	16x21	1.84	298.3	105.0
III-2.5-03	21	42	38.6	5030	66	65	0.0115	0.0231	0.0031	0.0029	9.5	20x21	16x21	1.84	516.0	-
IV-2175-1.85-02	21	74.5	68.9	4930	68	66	0.0129	0.0237	0.0020	0.0018	9.5	29x21	16x21	1.85	762.7	216.0
IV-2175-1.85-03	21	74.5	68.9	4930	68	66	0.0129	0.0237	0.0031	0.0029	9.5	29x21	16x21	1.85	842.4	218.0
IV-2175-2.5-02	21	74.5	68.9	5010	68	64	0.0129	0.0237	0.0021	0.0021	14.3	24x21	16x21	2.50	509.9	144.0
IV-2175-1.2-02	21	74.5	68.9	5010	68	64	0.0129	0.0237	0.0021	0.0021	14.3	24x21	16x21	1.2	1222.8	262.0
IV-2123-1.85-03	21	22.5	19.5	4160	66	66	0.0232	0.0232	0.0030	0.0030	6.3	16.5x21	16x21	1.85	328.5	60.0
IV-2123-1.85-02	21	22.5	19.5	4220	66	81	0.0232	0.0232	0.0020	0.0017	5.3	16.5x21	16x21	1.85	347.0	65.0
IV-2123-2.5-02	21	22.5	19.5	4570	65	58	0.0232	0.0232	0.0020	0.0017	5.3	15.5x21	16x21	2.50	160.7	51.0
IV-2123-1.2-02	21	22.5	19.5	4630	65	58	0.0232	0.0232	0.0020	0.0017	5.3	18x21	16x21	1.20	591.6	124.0
<b>Rogowsky, MacGregor, and Ong (1986)</b>																
1/1.0N	7.9	39.4	37.4	3785	55	83	0.0000	0.0094	0.0015	0.0000	7.4	11.8x7.9	7.9x7.9	1.05	136.3	79.7
2/1.0N	7.9	39.4	37.4	3887	55	83	0.0003	0.0094	0.0015	0.0006	7.4	11.8x7.9	7.9x7.9	1.05	169.6	113.4
2/1.5N	7.9	23.6	21.1	6150	66	83	0.0005	0.0112	0.0019	0.0011	5.9	11.8x7.9	7.9x7.9	1.87	78.8	62.4
2/2.0N	7.9	19.7	17.9	6266	66	83	0.0006	0.0088	0.0014	0.0012	7.9	7.9x7.9	7.9x7.9	2.20	46.3	27.5

**Table 0.1: Evaluation Database (3 of 10)**

Beam I.D.	b in.	h in.	d in.	$f'_c$ psi	$f_y$ ksi	$f_{yw}$ ksi	$\rho_l'$	$\rho_l$	$\rho_v$	$\rho_h$	s in.	Load Plate l x w in.	Support Plate l x w in.	a/d ratio	V <sub>test</sub> kips	V <sub>crack</sub> kips
<b><i>Brown, Sankovich, Bayrak, Jirsa, Breen, and Wood (2006)</i></b>																
I-CL-8.5-0	6	30	27	2584	68	73	0.0195	0.0014	0.0043	0.0000	8.5	6x6	6x6	1.11	79.9	41.9
I-2C-8.5-0	6	30	27	3208	68	73	0.0195	0.0014	0.0043	0.0000	8.5	12x6	6x6	1.67	121.6	55.4
II-N-F-5.8-3	18	18	16	2880	68	73	0.0219	0.0008	0.0041	0.0000	3	10x18	6x18	1.69	180.8	51.2
<b><i>Moody, Viest, Elstner, and Hognestad (1954)</i></b>																
III-30	7	24	21	3680	44	47	0.0425	0.0213	0.0052	0.0000	6	8x7	8x7	1.52	108.1	25.6
III-31	7	24	21	3250	44	44	0.0425	0.0213	0.0095	0.0000	6	8x7	8x7	1.52	114.6	25.6
<b><i>Oh and Shin (2001)</i></b>																
N42A2	5.1	22.1	19.7	3440	60	60	0.0156	0.0022	0.0012	0.0043	16	7.1x5.1	5.1x5.1	0.85	64.1	13.2
N42B2	5.1	22.1	19.7	3440	60	60	0.0156	0.0022	0.0022	0.0043	8.7	7.1x5.1	5.1x5.1	0.85	84.9	28.1
N42C2	5.1	22.1	19.7	3440	60	60	0.0156	0.0022	0.0034	0.0043	5.7	7.1x5.1	5.1x5.1	0.85	80.6	27.2
H41A2(1)	5.1	22.1	19.7	7121	60	60	0.0156	0.0022	0.0012	0.0043	16	7.1x5.1	5.1x5.1	0.50	160.3	55.9
H41B2	5.1	22.1	19.7	7121	60	60	0.0156	0.0022	0.0022	0.0043	8.7	7.1x5.1	5.1x5.1	0.50	158.7	48.1
H41C2	5.1	22.1	19.7	7121	60	60	0.0156	0.0022	0.0034	0.0043	5.7	7.1x5.1	5.1x5.1	0.50	159.3	45.4
H42A2(1)	5.1	22.1	19.7	7121	60	60	0.0156	0.0022	0.0012	0.0043	16	7.1x5.1	5.1x5.1	0.85	109.9	45.4
H42B2(1)	5.1	22.1	19.7	7121	60	60	0.0156	0.0022	0.0022	0.0043	8.7	7.1x5.1	5.1x5.1	0.85	102.7	47.4
H42C2(1)	5.1	22.1	19.7	7121	60	60	0.0156	0.0022	0.0034	0.0043	5.7	7.1x5.1	5.1x5.1	0.85	94.7	26.8
H43A2(1)	5.1	22.1	19.7	7121	60	60	0.0156	0.0022	0.0012	0.0043	16	7.1x5.1	5.1x5.1	1.25	78.2	28.2
H43B2	5.1	22.1	19.7	7121	60	60	0.0156	0.0022	0.0022	0.0043	8.7	7.1x5.1	5.1x5.1	1.25	85.8	38.4
H43C2	5.1	22.1	19.7	7121	60	60	0.0156	0.0022	0.0034	0.0043	5.7	7.1x5.1	5.1x5.1	1.25	90.6	30.0
H45A2	5.1	22.1	19.7	7121	60	60	0.0156	0.0022	0.0012	0.0043	16	7.1x5.1	5.1x5.1	2.00	47.6	17.1
H45B2	5.1	22.1	19.7	7121	60	60	0.0156	0.0022	0.0022	0.0043	8.7	7.1x5.1	5.1x5.1	2.00	53.6	23.7

**Table 0.1: Evaluation Database (4 of 10)**

Beam I.D.	b in.	h in.	d in.	$f'_c$ psi	$f_y$ ksi	$f_{yv}$ ksi	$\rho_l'$	$\rho_l$	$\rho_v$	$\rho_h$	s in.	Load Plate l x w in.	Support Plate l x w in.	a/d ratio	V <sub>test</sub> kips	V <sub>crack</sub> kips
<i>Oh and Shin (2001), continued...</i>																
H45C2	5.1	22.1	19.7	7121	60	60	0.0156	0.0022	0.0034	0.0043	5.7	7.1x5.1	5.1x5.1	2.00	53.1	32.4
N33A2	5.1	22.1	19.7	3440	60	60	0.0156	0.0022	0.0012	0.0043	16	7.1x5.1	5.1x5.1	1.25	51.5	21.3
N43A2	5.1	22.1	19.7	3440	60	60	0.0156	0.0022	0.0012	0.0043	16	7.1x5.1	5.1x5.1	1.25	57.5	24.2
N53A2	5.1	22.1	19.7	3440	60	60	0.0156	0.0022	0.0012	0.0043	16	7.1x5.1	5.1x5.1	1.25	46.9	15.3
H31A2	5.1	22.1	19.7	7121	60	60	0.0156	0.0022	0.0012	0.0043	16	7.1x5.1	5.1x5.1	0.50	167.6	50.1
H32A2	5.1	22.1	19.7	7121	60	60	0.0156	0.0022	0.0012	0.0043	16	7.1x5.1	5.1x5.1	0.85	119.1	39.6
H33A2	5.1	22.1	19.7	7121	60	60	0.0156	0.0022	0.0012	0.0043	16	7.1x5.1	5.1x5.1	1.25	85.0	34.6
H51A2	5.1	22.1	19.7	7121	60	60	0.0156	0.0022	0.0012	0.0043	16	7.1x5.1	5.1x5.1	0.50	157.9	45.1
H52A2	5.1	22.1	19.7	7121	60	60	0.0156	0.0022	0.0012	0.0043	16	7.1x5.1	5.1x5.1	0.85	127.8	39.2
H53A2	5.1	22.1	19.7	7121	60	60	0.0156	0.0022	0.0012	0.0043	16	7.1x5.1	5.1x5.1	1.25	81.8	28.3
<i>Foster and Gilbert (1998)</i>																
B1.2-3	4.9	47.2	44.2	11603	58	62	0.0134	0.0017	0.0067	0.0028	3	9.8x4.9	9.8x4.9	0.76	292.9	-
B2.0-1	4.9	27.6	24.6	12038	58	62	0.0241	0.0030	0.0067	0.0037	3	9.8x4.9	9.8x4.9	1.32	179.0	-
B2.0-2	4.9	27.6	24.6	17404	58	62	0.0241	0.0030	0.0067	0.0037	3	9.8x4.9	9.8x4.9	1.32	185.8	-
B2.0-3	4.9	27.6	24.6	11313	58	62	0.0241	0.0030	0.0067	0.0037	3	9.8x4.9	9.8x4.9	1.32	157.7	-
B2.0A-4	4.9	27.6	24.6	12473	58	62	0.0241	0.0030	0.0067	0.0037	3	3.9x4.9	9.8x4.9	0.88	213.9	-
B2.0C-6	4.9	27.6	24.6	13489	58	62	0.0241	0.0030	0.0100	0.0000	2	9.8x4.9	9.8x4.9	1.32	164.4	-
B2.0D-7	4.9	27.6	24.6	15084	58	62	0.0241	0.0030	0.0067	0.0000	3	9.8x4.9	9.8x4.9	1.32	162.2	-
B3.0-1	4.9	27.6	24.6	11603	58	62	0.0241	0.0030	0.0067	0.0037	3	9.8x4.9	9.8x4.9	1.88	115.2	-
B3.0-2	4.9	27.6	24.6	17404	58	62	0.0241	0.0030	0.0067	0.0037	3	9.8x4.9	9.8x4.9	1.88	118.5	-

**Table 0.1: Evaluation Database (5 of 10)**

Beam I.D.	b in.	h in.	d in.	$f'_c$ psi	$f_y$ ksi	$f_{yv}$ ksi	$\rho_l'$	$\rho_l$	$\rho_v$	$\rho_h$	s in.	Load Plate l x w in.	Support Plate l x w in.	a/d ratio	V <sub>test</sub> kips	V <sub>crack</sub> kips
<i>Foster and Gilbert (1998), continued...</i>																
B3.0-3	4.9	27.6	24.6	11168	58	62	0.0241	0.0030	0.0067	0.0037	3	9.8x4.9	9.8x4.9	1.88	118.5	-
B3.0A-4	4.9	27.6	24.6	12763	58	62	0.0241	0.0030	0.0067	0.0037	3	3.9x4.9	9.8x4.9	1.28	174.7	-
<i>Clark (1951)</i>																
A1-1	8	18	15.3	3575	47	48	0.0310	0.0018	0.0038	0.0000	7.2	3.5x8	3.5x8	2.35	50.4	-
A1-2	8	18	15.3	3430	47	48	0.0310	0.0018	0.0038	0.0000	7.2	3.5x8	3.5x8	2.35	47.4	-
A1-3	8	18	15.3	3395	47	48	0.0310	0.0018	0.0038	0.0000	7.2	3.5x8	3.5x8	2.35	50.4	-
A1-4	8	18	15.3	3590	47	48	0.0310	0.0018	0.0038	0.0000	7.2	3.5x8	3.5x8	2.35	55.4	-
B1-1	8	18	15.3	3388	47	48	0.0310	0.0018	0.0037	0.0000	7.5	3.5x8	3.5x8	1.96	63.1	-
B1-2	8	18	15.3	3680	47	48	0.0310	0.0018	0.0037	0.0000	7.5	3.5x8	3.5x8	1.96	58.1	-
B1-3	8	18	15.3	3435	47	48	0.0310	0.0018	0.0037	0.0000	7.5	3.5x8	3.5x8	1.96	64.4	-
B1-4	8	18	15.3	3380	47	48	0.0310	0.0018	0.0037	0.0000	7.5	3.5x8	3.5x8	1.96	60.7	-
B1-5	8	18	15.3	3570	47	48	0.0310	0.0018	0.0037	0.0000	7.5	3.5x8	3.5x8	1.96	54.7	-
B2-1	8	18	15.3	3370	47	48	0.0310	0.0018	0.0073	0.0000	3.8	3.5x8	3.5x8	1.96	68.1	-
B2-2	8	18	15.3	3820	47	48	0.0310	0.0018	0.0073	0.0000	3.8	3.5x8	3.5x8	1.96	72.8	-
B2-3	8	18	15.3	3615	47	48	0.0310	0.0018	0.0073	0.0000	3.8	3.5x8	3.5x8	1.96	75.7	-
B6-1	8	18	15.3	6110	47	48	0.0310	0.0018	0.0037	0.0000	7.5	3.5x8	3.5x8	1.96	85.7	-

**Table 0.1: Evaluation Database (6 of 10)**

Beam I.D.	b in.	h in.	d in.	$f'_c$ psi	$f_y$ ksi	$f_{yv}$ ksi	$\rho_l'$	$\rho_l$	$\rho_v$	$\rho_h$	s in.	Load Plate l x w in.	Support Plate l x w in.	a/d ratio	$V_{test}$ kips	$V_{crack}$ kips
<i>Clark (1951) continued...</i>																
C1-1	8	18	15.3	3720	47	48	0.0207	0.0018	0.0034	0.0000	8	3.5x8	3.5x8	1.57	62.8	-
C1-2	8	18	15.3	3820	47	48	0.0207	0.0018	0.0034	0.0000	8	3.5x8	3.5x8	1.57	70.3	-
C1-3	8	18	15.3	3475	47	48	0.0207	0.0018	0.0034	0.0000	8	3.5x8	3.5x8	1.57	55.7	-
C1-4	8	18	15.3	4210	47	48	0.0207	0.0018	0.0034	0.0000	8	3.5x8	3.5x8	1.57	64.7	-
C2-1	8	18	15.3	3430	47	48	0.0207	0.0018	0.0069	0.0000	4	3.5x8	3.5x8	1.57	65.6	-
C2-2	8	18	15.3	3625	47	48	0.0207	0.0018	0.0069	0.0000	4	3.5x8	3.5x8	1.57	68.1	-
C2-3	8	18	15.3	3500	47	48	0.0207	0.0018	0.0069	0.0000	4	3.5x8	3.5x8	1.57	73.2	-
C2-4	8	18	15.3	3910	47	48	0.0207	0.0018	0.0069	0.0000	4	3.5x8	3.5x8	1.57	65.2	-
C3-1	8	18	15.3	2040	47	48	0.0207	0.0018	0.0034	0.0000	8	3.5x8	3.5x8	1.57	50.7	-
C3-2	8	18	15.3	2000	47	48	0.0207	0.0018	0.0034	0.0000	8	3.5x8	3.5x8	1.57	45.4	-
C3-3	8	18	15.3	2020	47	48	0.0207	0.0018	0.0034	0.0000	8	3.5x8	3.5x8	1.57	42.7	-
C4-1	8	18	15.3	3550	47	48	0.0310	0.0018	0.0034	0.0000	8	3.5x8	3.5x8	1.57	69.9	-
C6-2	8	18	15.3	6560	47	48	0.0310	0.0018	0.0034	0.0000	8	3.5x8	3.5x8	1.57	95.7	-
C6-3	8	18	15.3	6480	47	48	0.0310	0.0018	0.0034	0.0000	8	3.5x8	3.5x8	1.57	98.2	-
C6-4	8	18	15.3	6900	47	48	0.0310	0.0018	0.0034	0.0000	8	3.5x8	3.5x8	1.57	96.7	-
D1-1	8	18	15.5	3800	49	48	0.0163	0.0018	0.0046	0.0000	6	3.5x8	3.5x8	1.16	68.1	-
D1-2	8	18	15.5	3790	49	48	0.0163	0.0018	0.0046	0.0000	6	3.5x8	3.5x8	1.16	80.6	-
D1-3	8	18	15.5	3560	49	48	0.0163	0.0018	0.0046	0.0000	6	3.5x8	3.5x8	1.16	58.1	-
D2-1	8	18	15.5	3480	49	48	0.0163	0.0018	0.0061	0.0000	4.5	3.5x8	3.5x8	1.16	65.6	-
D2-2	8	18	15.5	3755	49	48	0.0163	0.0018	0.0061	0.0000	4.5	3.5x8	3.5x8	1.16	70.6	-

**Table 0.1: Evaluation Database (7 of 10)**

Beam I.D.	b in.	h in.	d in.	$f'_c$ psi	$f_y$ ksi	$f_{yv}$ ksi	$\rho_l'$	$\rho_l$	$\rho_v$	$\rho_h$	s in.	Load Plate l x w in.	Support Plate l x w in.	a/d ratio	V <sub>test</sub> kips	V <sub>crack</sub> kips
<i>Clark (1951) continued...</i>																
D2-3	8	18	15.5	3595	49	48	0.0163	0.0018	0.0061	0.0000	4.5	3.5x8	3.5x8	1.16	75.6	-
D2-4	8	18	15.5	3550	49	48	0.0163	0.0018	0.0061	0.0000	4.5	3.5x8	3.5x8	1.16	75.7	-
D3-1	8	18	15.5	4090	49	48	0.0244	0.0018	0.0092	0.0000	3	3.5x8	3.5x8	1.16	89.2	-
D4-1	8	18	15.5	3350	49	48	0.0163	0.0018	0.0122	0.0000	2.3	3.5x8	3.5x8	1.16	70.6	-
<i>Alcocer and Uribe (2008)</i>																
MR	13.8	47	43.3	5134	65	62	0.0158	0.0079	0.0053	0.0029	6	15.8x13.8	15.8x13.8	1.27	363.4	58.8
MT	13.8	47	43.3	5076	65	62	0.0158	0.0079	0.0053	0.029	6	15.8x13.8	15.8x13.8	1.27	358.3	64.6
<i>Tanimura and Sato (2005)</i>																
2A	11.8	17.7	15.8	3365	66	54	0.0214	0.0033	0.0021	0.0000	3.9	3.9x11.8	3.9x11.8	0.50	184.9	-
3A	11.8	17.7	15.8	3365	66	56	0.0214	0.0033	0.0048	0.0000	3.9	3.9x11.8	3.9x11.8	0.50	187.6	-
4A	11.8	17.7	15.8	3365	66	53	0.0214	0.0033	0.0084	0.0000	3.9	3.9x11.8	3.9x11.8	0.50	195.7	-
6A	11.8	17.7	15.8	4206	66	54	0.0214	0.0033	0.0021	0.0000	3.9	3.9x11.8	3.9x11.8	1.00	164.7	-
7A	11.8	17.7	15.8	4206	66	56	0.0214	0.0033	0.0048	0.0000	3.9	3.9x11.8	3.9x11.8	1.00	169.0	-
8A	11.8	17.7	15.8	4206	66	53	0.0214	0.0033	0.0084	0.0000	3.9	3.9x11.8	3.9x11.8	1.00	181.1	-
11A	11.8	17.7	15.8	3336	66	56	0.0214	0.0033	0.0048	0.0000	3.9	3.9x11.8	3.9x11.8	1.50	110.9	-
12A	11.8	17.7	15.8	3408	66	53	0.0214	0.0033	0.0084	0.0000	3.9	3.9x11.8	3.9x11.8	1.50	128.6	-
14B	11.8	17.7	15.8	4641	66	54	0.0214	0.0000	0.0021	0.0000	3.9	3.9x11.8	3.9x11.8	1.00	169.2	-
15B	11.8	17.7	15.8	4641	66	56	0.0214	0.0000	0.0048	0.0000	3.9	3.9x11.8	3.9x11.8	1.00	174.4	-
16B	11.8	17.7	15.8	4641	66	53	0.0214	0.0000	0.0084	0.0000	3.9	3.9x11.8	3.9x11.8	1.00	191.3	-
17C	11.8	17.7	15.8	4540	66	54	0.0214	0.0033	0.0021	0.0000	3.9	3.9x11.8	3.9x11.8	1.00	128.5	-
18C	11.8	17.7	15.8	4569	66	56	0.0214	0.0033	0.0048	0.0000	3.9	3.9x11.8	3.9x11.8	1.00	174.2	-



**Table 0.1: Evaluation Database (8 of 10)**

Beam I.D.	b in.	h in.	d in.	$f'_c$ psi	$f_y$ ksi	$f_{yw}$ ksi	$\rho_l'$	$\rho_l$	$\rho_v$	$\rho_h$	s in.	Load Plate l x w in.	Support Plate l x w in.	a/d ratio	V <sub>test</sub> kips	V <sub>crack</sub> kips
<i>Tanimura and Sato (2005), continued</i>																
19C	11.8	17.7	15.8	4612	66	53	0.0214	0.0033	0.0084	0.0000	3.9	3.9x11.8	3.9x11.8	1.00	170.4	-
20D	11.8	17.7	15.8	3524	102	138	0.0214	0.0033	0.0048	0.0000	3.9	3.9x11.8	3.9x11.8	1.00	149.9	-
21D	11.8	17.7	15.8	3902	102	152	0.0214	0.0033	0.0084	0.0000	3.9	3.9x11.8	3.9x11.8	1.00	149.0	-
22D	11.8	17.7	15.8	3800	102	138	0.0214	0.0033	0.0048	0.0000	3.9	3.9x11.8	3.9x11.8	1.50	121.2	-
23D	11.8	17.7	15.8	3814	102	152	0.0214	0.0033	0.0084	0.0000	3.9	3.9x11.8	3.9x11.8	1.50	127.7	-
28A	11.8	17.7	15.8	3698	66	56	0.0214	0.0033	0.0048	0.0000	3.9	3.9x11.8	3.9x11.8	0.75	145.8	-
29A	11.8	17.7	15.8	3800	66	53	0.0214	0.0033	0.0084	0.0000	3.9	3.9x11.8	3.9x11.8	0.75	150.0	-
30A	11.8	17.7	15.8	3829	66	56	0.0214	0.0033	0.0088	0.0000	5.9	3.9x11.8	3.9x11.8	0.75	157.9	-
31A	11.8	17.7	15.8	3858	102	56	0.0214	0.0033	0.0048	0.0000	3.9	3.9x11.8	3.9x11.8	2.00	94.1	-
32A	11.8	17.7	15.8	3974	102	53	0.0214	0.0033	0.0084	0.0000	3.9	3.9x11.8	3.9x11.8	2.00	99.5	-
33A	11.8	17.7	15.8	3582	66	56	0.0214	0.0033	0.0095	0.0000	2.0	3.9x11.8	3.9x11.8	1.00	145.9	-
34A	11.8	17.7	15.8	3597	66	54	0.0214	0.0033	0.0095	0.0000	7.9	3.9x11.8	3.9x11.8	1.00	134.8	-
36E	11.8	17.7	15.8	3553	193	56	0.0042	0.0033	0.0048	0.0000	3.9	3.9x11.8	3.9x11.8	0.50	121.5	-
37E	11.8	17.7	15.8	3742	193	53	0.0042	0.0033	0.0084	0.0000	3.9	3.9x11.8	3.9x11.8	0.50	124.8	-
39E	11.8	17.7	15.8	3684	193	56	0.0042	0.0033	0.0048	0.0000	3.9	3.9x11.8	3.9x11.8	1.00	106.1	-
40E	11.8	17.7	15.8	3756	193	53	0.0042	0.0033	0.0084	0.0000	3.9	3.9x11.8	3.9x11.8	1.00	106.1	-
41A	11.8	17.7	15.8	2988	109	56	0.0214	0.0033	0.0048	0.0000	3.9	3.9x11.8	3.9x11.8	2.50	73.5	-
42A	11.8	17.7	15.8	3104	109	53	0.0214	0.0033	0.0084	0.0000	3.9	3.9x11.8	3.9x11.8	2.50	85.2	-
46F	11.8	17.7	15.8	14141	109	139	0.0214	0.0033	0.0021	0.0000	3.9	3.9x11.8	3.9x11.8	1.00	279.8	-
47F	11.8	17.7	15.8	13967	109	138	0.0214	0.0033	0.0048	0.0000	3.9	3.9x11.8	3.9x11.8	1.00	292.7	-

**Table 0.1: Evaluation Database (9 of 10)**

Beam I.D.	b in.	h in.	d in.	$f'_c$ psi	$f_y$ ksi	$f_{yv}$ ksi	$\rho_l'$	$\rho_l$	$\rho_v$	$\rho_h$	s in.	Load Plate l x w in.	Support Plate l x w in.	a/d ratio	V <sub>test</sub> kips	V <sub>crack</sub> kips
<i>Tanimura and Sato (2005), continued...</i>																
48F	11.8	17.7	15.8	13706	109	139	0.0214	0.0033	0.0021	0.000	3.9	3.9x11.8	3.9x11.8	1.50	210.0	-
49F	11.8	17.7	15.8	13663	109	138	0.0214	0.0033	0.0048	0.000	3.9	3.9x11.8	3.9x11.8	1.50	220.8	-
L6	7.9	41.3	39.4	4525	147	56	0.002	0.004	0.0029	0.000	9.8	5.9x7.9	5.9x7.9	1.00	150.7	-
L7	15.8	80.7	78.7	4424	147	54	0.0005	0.004	0.0029	0.000	19.7	11.8x15.8	11.8x15.8	1.00	589.9	-
<i>Matsuo, Lertsrisakulrat, Yanagawa, and Niwa (2002)</i>																
D604	5.9	25.6	23.6	4960	146	48	0.0176	0.0006	0.0042	0.0000	3.9	5.9x5.9	5.9x5.9	1.00	132.1	-
D608	5.9	25.6	23.6	5120	146	48	0.0176	0.0006	0.0084	0.0000	2.0	5.9x5.9	5.9x5.9	1.00	149.5	-
<i>Brown, Sankovich, Bayrak, and Jirsa (2006)</i>																
G	6	36	36	4300	0	73	0.0005	0.0000	0.0031	0.0031	6	12x6	12x6	0.00	264.5	-
L	6	36	36	5290	0	73	0.0005	0.0000	0.0000	0.0031	0	12x6	12x6	0.00	366.8	-
M	6	36	36	4300	0	73	0.0005	0.0000	0.0000	0.0031	0	12x6	12x6	0.00	283.2	-
N	6	36	36	4300	0	73	0.0005	0.0000	0.0000	0.0031	0	6x6	6x6	0.00	202.1	-
O	6	36	36	5500	0	73	0.0002	0.0000	0.0000	0.0027	0	12x6	12x6	0.00	352.4	-
P	6	36	36	5500	0	73	0.0005	0.0000	0.0000	0.0061	0	12x6	12x6	0.00	377.0	-
Q	6	36	36	4200	0	73	0.0000	0.0000	0.0000	0.0010	0	12x6	12x6	0.00	224.0	-
T	6	36	36	5290	0	73	0.0000	0.0000	0.0000	0.0046	0	12x6	12x6	0.00	343.1	-
U	6	36	36	4350	0	73	0.0000	0.0000	0.0000	0.0023	0	6x6	6x6	0.00	189.0	-
V	6	36	36	4350	0	73	0.0000	0.0000	0.0046	0.0015	4	12x6	12x6	0.00	259.7	-
W	6	36	36	4350	0	73	0.0005	0.0000	0.0000	0.0031	0	16x6	16x6	0.00	370.1	-

**Table 0.1: Evaluation Database (10 of 10)**

Beam I.D.	b in.	h in.	d in.	$f'_c$ psi	$f_y$ ksi	$f_{yv}$ ksi	$\rho'_t$	$\rho_t$	$\rho_v$	$\rho_h$	s in.	Load Plate l x w in.	Support Plate l x w in.	a/d ratio	V <sub>test</sub> kips	V <sub>crack</sub> kips
<b><i>Brown, Sankovich, Bayrak, and Jirsa (2006), continued</i></b>																
X	6	36	36	4350	0	73	0.0005	0.0000	0.0000	0.0031	0	12x6	12x6	0.00	246.7	-
Y	10	36	36	4350	0	73	0.0010	0.0000	0.0000	0.0037	0	12x4	12x4	0.00	299.5	-
Z	10	36	36	4350	0	73	0.0010	0.0000	0.0000	0.0037	0	12x4	12x4	0.00	303.8	-
<b><i>Walraven and Lehwalter (1994)</i></b>																
V411/4	9.8	31.5	29.9	3083	60	60	0.0107	0.0000	0.0017	0.0000	7.5	7.5x9.8	7.5x9.8	0.97	105.7	-
V022/3	9.8	15.8	14.2	3554	60	60	0.0113	0.0000	0.0035	0.0000	3.9	3.5x9.8	3.5x9.8	1.00	85.6	-
V511/3	9.8	23.6	22.1	3861	60	60	0.0112	0.0000	0.0033	0.0000	5.9	5.5x9.8	5.5x9.8	1.01	130.8	-
V411/3	9.8	31.5	29.9	3590	60	60	0.0107	0.0000	0.0033	0.0000	7.5	7.5x9.8	7.5x9.8	0.97	150.2	-
<b><i>Zhang and Tan (2007)</i></b>																
1DB70bw	6.3	27.6	25.3	4104	76	54	0.0111	0.0010	0.0021	0.0000	5.9	4.1x6.3	4.1x6.3	1.10	96.2	31.7
1DB100bw	9.1	39.4	35.6	4162	75	66	0.0123	0.0007	0.0021	0.0000	5.9	5.9x9.1	5.9x9.1	1.10	174.9	77.1
<b><i>Deschenes (2009)</i></b>																
VALID	21	42	36.1	5061	66	65	0.0310	0.0100	0.0030	0.0058	9.5	20x21	16x21	1.85	576.6	151.2
NR1	21	42	36.1	7250	66	65	0.0310	0.0100	0.0030	0.0058	9.5	20x21	16x21	1.85	560.8	-

## APPENDIX C.

### Project 5253 Crack Width Data

#### C.1 OVERVIEW

For the tests in Project 5253, the maximum width of a diagonal crack was recorded on each side of the test region at first cracking and at each load increment thereafter. The data was obtained with crack comparator cards and is the average of two independent measurements. In some of the Series II and M specimens, only the maximum crack width for the entire test region, regardless of which side face it was measured on, was recorded. The crack width data is listed in Table C.1 for 34 tests conducted within Project 5253. No crack width data was obtained for test III-2.5-0 because it failed shortly after first cracking. The crack width data from tests II-02-CCC1007 and M-03-2-CCC2436 was unreliable. The variables presented in Table C.1 are defined as follows:

**a/d** = shear span-to-depth ratio

**$\rho_v$**  = ratio of vertical web reinforcement to effective area,  $A_v / b \cdot s_v$

**$\rho_h$**  = ratio of horizontal web reinforcement to effective area,  $A_h / b \cdot s_h$

**R** = percentage of maximum applied load, %

**$w_{max}$**  = maximum width of diagonal crack as average of two independent measurements

**SF** = side face of the member

**Table 0.1: Measured crack width data for test specimens (1 of 6)**

<b><u>Beam Details</u></b>	<b>R (%)</b>	<b>w<sub>max</sub> (in.)</b>	
		<b>SF 1</b>	<b>SF 2</b>
I-03-2 a/d = 1.85 $\rho_v = 0.0029$ $\rho_h = 0.0033$	23	0.005	0.006
	33	0.009	0.013
	43	0.016	0.020
	53	0.020	0.025
	63	0.030	0.025
	73	0.035	0.030
	83	0.048	0.035
	93	0.060	0.050

<b><u>Beam Details</u></b>	<b>R (%)</b>	<b>w<sub>max</sub> (in.)</b>	
		<b>SF 1</b>	<b>SF 2</b>
I-03-4 a/d = 1.85 $\rho_v = 0.0030$ $\rho_h = 0.0033$	20	0.012	0.006
	29	0.016	0.007
	37	0.023	0.010
	46	0.030	0.013
	54	0.035	0.020
	63	0.040	0.020
	72	0.050	0.025
	79	0.060	0.038
	88	0.080	0.050

<b><u>Beam Details</u></b>	<b>R (%)</b>	<b>w<sub>max</sub> (in.)</b>	
		<b>SF 1</b>	<b>SF 2</b>
I-02-2 a/d = 1.85 $\rho_v = 0.0020$ $\rho_h = 0.0020$	29	0.016	0.016
	42	0.030	0.035
	54	0.045	0.045
	67	0.060	0.060
	80	0.080	0.076
	92	0.080	0.085

<b><u>Beam Details</u></b>	<b>R (%)</b>	<b>w<sub>max</sub> (in.)</b>	
		<b>SF 1</b>	<b>SF 2</b>
I-02-4 a/d = 1.85 $\rho_v = 0.0021$ $\rho_h = 0.0020$	25	0.018	0.016
	36	0.023	0.020
	46	0.028	0.023
	57	0.030	0.030
	68	0.035	0.033
	79	0.050	0.035
	90	0.060	0.045

<b><u>Beam Details</u></b>	<b>R (%)</b>	<b>w<sub>max</sub> (in.)</b>	
		<b>SF 1</b>	<b>SF 2</b>
II-03-CCC2021 a/d = 1.85 $\rho_v = 0.0031$ $\rho_h = 0.0045$	26	0.009	-
	31	0.012	-
	41	0.015	-
	52	0.018	-
	64	0.023	-
	77	0.028	-
	91	0.050	-

<b><u>Beam Details</u></b>	<b>R (%)</b>	<b>w<sub>max</sub> (in.)</b>	
		<b>SF 1</b>	<b>SF 2</b>
II-03-CCC1007 a/d = 1.85 $\rho_v = 0.0031$ $\rho_h = 0.0045$	16	0.008	-
	27	0.010	-
	34	0.013	-
	44	0.016	-
	53	0.018	-
	63	0.025	-
	72	0.035	-
	80	0.038	-
	90	0.040	-

**Table 0.1 (cont.): Measured crack width data for test specimens (2 of 6)**

	R (%)	w <sub>max</sub> (in.)	
		SF 1	SF 2
<b><u>Beam Details</u></b>  II-03-CCT1021 a/d = 1.85 $\rho_v = 0.0031$ $\rho_h = 0.0045$	12	0.012	-
	20	0.016	-
	31	0.023	-
	38	0.030	-
	47	0.035	-
	55	0.040	-
	66	0.040	-
	73	0.040	-
	82	0.045	-
	91	0.050	-
	99	0.070	-

	R (%)	w <sub>max</sub> (in.)	
		SF 1	SF 2
<b><u>Beam Details</u></b>  II-03-CCT0507 a/d = 1.85 $\rho_v = 0.0031$ $\rho_h = 0.0045$	22	0.013	-
	31	0.019	-
	37	0.023	-
	45	0.028	-
	54	0.033	-
	61	0.040	-
	69	0.048	-
	76	0.060	-
	91	0.080	-

	R (%)	w <sub>max</sub> (in.)	
		SF 1	SF 2
<b><u>Beam Details</u></b>  II-02-CCT0507 a/d = 1.85 $\rho_v = 0.0020$ $\rho_h = 0.0019$	19	0.005	0.005
	29	0.020	0.016
	38	0.030	0.028
	48	0.038	0.038
	57	0.050	0.050
	66	0.060	0.060
	76	0.081	0.077
	85	0.090	0.090
	95	0.105	0.103

	R (%)	w <sub>max</sub> (in.)	
		SF 1	SF 2
<b><u>Beam Details</u></b>  II-02-CCT0521 a/d = 1.85 $\rho_v = 0.0020$ $\rho_h = 0.0019$	14	0.013	0.013
	20	0.016	0.020
	27	0.020	0.025
	33	0.030	0.030
	40	0.035	0.040
	46	0.040	0.050
	54	0.045	0.055
	74	0.060	0.080
	81	0.085	0.090
	93	0.100	0.110

	R (%)	w <sub>max</sub> (in.)	
		SF 1	SF 2
<b><u>Beam Details</u></b>  II-02-CCC1021 a/d = 1.85 $\rho_v = 0.0020$ $\rho_h = 0.0019$	36	0.010	0.016
	47	0.016	0.030
	58	0.025	0.045
	71	0.035	0.060
	82	0.050	0.085

	R (%)	w <sub>max</sub> (in.)	
		SF 1	SF 2
<b><u>Beam Details</u></b>  III-1.85-025 a/d = 1.85 $\rho_v = 0.0024$ $\rho_h = 0.0014$	48	0.035	0.028
	60	0.050	0.040
	70	0.060	0.050
	81	0.078	0.060
	92	0.100	0.098

**Table 0.1 (cont.): Measured crack width data for test specimens (3 of 6)**

<b>Beam Details</b>	<b>R (%)</b>	<b>w<sub>max</sub> (in.)</b>	
		<b>SF 1</b>	<b>SF 2</b>
III-1.85-02 a/d = 1.85 $\rho_v = 0.0020$ $\rho_h = 0.0019$	27	0.020	0.020
	39	0.033	0.035
	51	0.048	0.050
	62	0.055	0.060
	74	0.061	0.063
	85	0.065	0.070
	96	0.090	0.090

<b>Beam Details</b>	<b>R (%)</b>	<b>w<sub>max</sub> (in.)</b>	
		<b>SF 1</b>	<b>SF 2</b>
III-1.85-0 a/d = 1.85 $\rho_v = 0$ $\rho_h = 0$	21	0.009	-
	27	0.030	-
	33	0.038	-
	38	0.050	-
	51	0.063	-
	61	0.094	-
	71	0.100	-
	91	0.160	-

<b>Beam Details</b>	<b>R (%)</b>	<b>w<sub>max</sub> (in.)</b>	
		<b>SF 1</b>	<b>SF 2</b>
III-1.85-03 a/d = 1.85 $\rho_v = 0.0029$ $\rho_h = 0.0029$	32	0.013	0.013
	47	0.025	0.023
	61	0.033	0.033
	75	0.040	0.038
	89	0.055	0.050

<b>Beam Details</b>	<b>R (%)</b>	<b>w<sub>max</sub> (in.)</b>	
		<b>SF 1</b>	<b>SF 2</b>
III-1.85-01 a/d = 1.85 $\rho_v = 0.0010$ $\rho_h = 0.0014$	29	-	0.005
	44	0.015	0.017
	59	0.035	0.038
	72	0.053	0.055
	88	-	0.098

<b>Beam Details</b>	<b>R (%)</b>	<b>w<sub>max</sub> (in.)</b>	
		<b>SF 1</b>	<b>SF 2</b>
III-1.85-03b a/d = 1.85 $\rho_v = 0.0031$ $\rho_h = 0.0029$	25	0.008	0.009
	33	0.016	0.014
	40	0.025	0.020
	49	0.030	0.028
	57	0.033	0.033
	65	0.040	0.038
	73	0.040	0.038
	81	0.045	0.043
	89	0.048	0.050

<b>Beam Details</b>	<b>R (%)</b>	<b>w<sub>max</sub> (in.)</b>	
		<b>SF 1</b>	<b>SF 2</b>
III-1.85-02b a/d = 1.85 $\rho_v = 0.0020$ $\rho_h = 0.0018$	16	0.017	0.016
	25	0.023	0.023
	33	0.028	0.028
	41	0.033	0.033
	49	0.038	0.035
	57	0.040	0.040
	65	0.040	0.043
	73	0.048	0.050
	80	0.058	0.055
	89	0.078	0.080

**Table 0.1 (cont.): Measured crack width data for test specimens (4 of 6)**

<b><u>Beam Details</u></b>	<b>R (%)</b>	<b>w<sub>max</sub> (in.)</b>	
		<b>SF 1</b>	<b>SF 2</b>
III-1.2-02 a/d = 1.2 $\rho_v = 0.0020$ $\rho_h = 0.0018$	20	0.012	0.010
	28	0.020	0.018
	36	0.028	0.026
	45	0.033	0.033
	52	0.035	0.035
	60	0.040	0.038
	70	0.045	0.043
	80	0.045	0.045
	90	0.048	0.050

<b><u>Beam Details</u></b>	<b>R (%)</b>	<b>w<sub>max</sub> (in.)</b>	
		<b>SF 1</b>	<b>SF 2</b>
III-1.2-03 a/d = 1.2 $\rho_v = 0.0031$ $\rho_h = 0.0029$	21	0.005	-
	31	0.010	0.009
	41	0.016	0.016
	51	0.020	0.020
	61	0.030	0.025
	71	0.040	0.030
	81	0.046	0.035
	92	0.058	0.040

<b><u>Beam Details</u></b>	<b>R (%)</b>	<b>w<sub>max</sub> (in.)</b>	
		<b>SF 1</b>	<b>SF 2</b>
III-2.5-02 a/d = 2.5 $\rho_v = 0.0020$ $\rho_h = 0.0018$	38	0.010	0.010
	50	0.020	0.025
	63	0.030	0.035
	74	0.043	0.050
	87	0.063	0.075

<b><u>Beam Details</u></b>	<b>R (%)</b>	<b>w<sub>max</sub> (in.)</b>	
		<b>SF 1</b>	<b>SF 2</b>
III-2.5-03 a/d = 2.5 $\rho_v = 0.0031$ $\rho_h = 0.0029$	13	0.016	0.016
	20	0.023	0.023
	27	0.028	0.028
	33	0.033	0.033
	40	0.035	0.035
	53	0.038	0.040
	60	0.043	0.043
	67	0.045	0.045
	73	0.050	0.048
	80	0.053	0.055

<b><u>Beam Details</u></b>	<b>R (%)</b>	<b>w<sub>max</sub> (in.)</b>	
		<b>SF 1</b>	<b>SF 2</b>
IV-2175-1.85-02 a/d = 1.85 $\rho_v = 0.0020$ $\rho_h = 0.0018$	27	0.016	0.015
	37	0.018	0.025
	51	0.033	0.033
	62	0.048	0.053
	71	0.053	0.060
	82	0.060	0.065
	95	0.080	0.085

<b><u>Beam Details</u></b>	<b>R (%)</b>	<b>w<sub>max</sub> (in.)</b>	
		<b>SF 1</b>	<b>SF 2</b>
IV-2175-1.85-03 a/d = 1.85 $\rho_v = 0.0031$ $\rho_h = 0.0029$	24	0.013	0.008
	33	0.018	0.015
	45	0.028	0.023
	55	0.033	0.033
	64	0.035	0.035
	73	0.048	0.043
	85	0.058	0.055



**Table 0.1 (cont.): Measured crack width data for test specimens (5 of 6)**

<b>Beam Details</b>	<b>R (%)</b>	<b>w<sub>max</sub> (in.)</b>	
		<b>SF 1</b>	<b>SF 2</b>
IV-2175-2.5-02 a/d = 2.5 $\rho_v = 0.0021$ $\rho_h = 0.0021$	30	0.005	0.009
	39	0.015	0.017
	49	0.020	0.025
	59	0.030	0.035
	69	0.035	0.040
	78	0.040	0.043
	87	0.053	0.060
	98	0.088	0.088

<b>Beam Details</b>	<b>R (%)</b>	<b>w<sub>max</sub> (in.)</b>	
		<b>SF 1</b>	<b>SF 2</b>
IV-2175-1.2-02 a/d = 1.2 $\rho_v = 0.0021$ $\rho_h = 0.0021$	26	0.023	0.018
	34	0.025	0.023
	43	0.033	0.033
	51	0.040	0.035
	61	0.055	0.053
	68	0.071	0.068
	76	0.090	0.088
	85	0.098	0.098

<b>Beam Details</b>	<b>R (%)</b>	<b>w<sub>max</sub> (in.)</b>	
		<b>SF 1</b>	<b>SF 2</b>
IV-2123-1.85-03 a/d = 1.85 $\rho_v = 0.0030$ $\rho_h = 0.0030$	29	0.012	0.015
	41	0.016	0.018
	51	0.020	0.023
	63	0.025	0.028
	73	0.030	0.030
	85	0.038	0.035
	95	0.043	0.038

<b>Beam Details</b>	<b>R (%)</b>	<b>w<sub>max</sub> (in.)</b>	
		<b>SF 1</b>	<b>SF 2</b>
IV-2123-1.85-02 a/d = 1.85 $\rho_v = 0.0020$ $\rho_h = 0.0017$	29	0.012	0.018
	38	0.016	0.023
	48	0.020	0.024
	58	0.023	0.028
	69	0.028	0.033
	79	0.030	0.040
	90	0.035	0.043

<b>Beam Details</b>	<b>R (%)</b>	<b>w<sub>max</sub> (in.)</b>	
		<b>SF 1</b>	<b>SF 2</b>
IV-2123-2.5-02 a/d = 2.5 $\rho_v = 0.0020$ $\rho_h = 0.0017$	27	-	0.006
	47	0.010	0.020
	64	0.018	0.033
	82	0.030	0.048
	98	0.060	0.095

<b>Beam Details</b>	<b>R (%)</b>	<b>w<sub>max</sub> (in.)</b>	
		<b>SF 1</b>	<b>SF 2</b>
IV-2123-1.2-02 a/d = 1.2 $\rho_v = 0.0020$ $\rho_h = 0.0017$	18	-	0.005
	24	0.005	0.005
	31	0.009	0.009
	39	0.013	0.013
	48	0.018	0.018
	55	0.023	0.023
	63	0.028	0.025
	70	0.030	0.030
	78	0.033	0.035

**Table 0.1 (cont.): Measured crack width data for test specimens (6 of 6)**

	R (%)	w <sub>max</sub> (in.)	
		SF 1	SF 2
<b><u>Beam Details</u></b>  M-03-4- CCC2436 a/d = 1.85 $\rho_v = 0.0031$ $\rho_h = 0.0030$	34	0.013	-
	38	0.016	-
	41	0.020	-
	45	0.025	-
	48	0.025	-
	49	0.025	-
	51	0.030	-
	54	0.030	-
	58	0.030	-
	62	0.035	-
	64	0.040	-
	68	0.040	-
	71	0.040	-
	74	0.045	-
	77	0.050	-
	80	0.050	-
	83	0.060	-
	86	0.060	-
	92	0.060	-

	R (%)	w <sub>max</sub> (in.)	
		SF 1	SF 2
<b><u>Beam Details</u></b>  M-09-4- CCC2436 a/d = 1.85 $\rho_v = 0.0086$ $\rho_h = 0.0030$	24	0.005	-
	29	0.005	-
	34	0.009	-
	39	0.010	-
	44	0.010	-
	49	0.020	-
	53	0.020	-
	58	0.025	-
	63	0.030	-
	68	0.030	-

	R (%)	w <sub>max</sub> (in.)	
		SF 1	SF 2
<b><u>Beam Details</u></b>  M-02-4- CCC2436 a/d = 1.85 $\rho_v = 0.0022$ $\rho_h = 0.0022$	19	0.005	-
	27	0.013	-
	32	0.020	-
	39	0.025	-
	45	0.030	-
	51	0.035	-
	57	0.045	-
	64	0.055	-
	71	0.060	-
	76	0.070	-
	83	0.080	-

	R (%)	w <sub>max</sub> (in.)	
		SF 1	SF 2
<b><u>Beam Details</u></b>  M-03-4- CCC0812 a/d = 1.85 $\rho_v = 0.0031$ $\rho_h = 0.0030$	26	0.013	0.020
	35	0.016	0.025
	43	0.020	0.025
	48	0.020	0.030
	60	0.025	0.035
	67	0.030	0.040
	71	0.035	0.040
	79	0.040	0.050
	87	0.050	0.060
	95	0.060	0.060

## References

1. AASHTO LRFD, 2008 *Interim Revisions, Bridge Design Specifications, 4th Edition, 2007*, American Association of State Highway and Transportation Officials, Washington, D.C., 2008.
2. ACI Committee 224, “Control of Cracking in Concrete Structures” (ACI 224R-01), *ACI Manual of Concrete Practice*, American Concrete Institute, Farmington Hills, MI, 2002.
3. ACI Committee 318, “Closure to Public Comments on ACI 318-99,” *Concrete International*, May 1999, pp. 318-1 to 318-50.
4. ACI Committee 318-08, *Building Code Requirements for Reinforced Concrete (ACI 318-08)*, American Concrete Institute, Farmington Hills, MI, 2008.
5. ACI Committee 318-95, *Building Code Requirements for Reinforced Concrete (ACI 318-95)*, American Concrete Institute, Detroit, MI, 1995.
6. ACI-ASCE Committee 326, “Shear and Diagonal Tension,” American Concrete Institute, Farmington Hills, MI, 1962.
7. Adebar, P., “Diagonal Cracking and Diagonal Crack Control in Structural Concrete,” SP 204-4, American Concrete Institute, Farmington Hills, Michigan, 2001, pp. 85-116.
8. Adebar, P. and Zhou, Z., “Bearing Strength of Compressive Struts Confined by Plain Concrete,” *ACI Structural Journal*, Vol. 90, No. 5, September-October 1993, pp. 534-541.
9. Ahmad, S. A., and Lue, D. M., “Flexure-Shear Interaction of Reinforced High-Strength Concrete Beams,” *ACI Structural Journal*, V. 84, No. 4, 1987, pp. 330 – 341.
10. ASTM A 370 – 08a, *Standard Test Methods and Definitions for Mechanical Testing of Steel Products*, American Society for Testing and Materials, West Conshohocken, PA, May 2008.
11. ASTM A 615/A 615M – 08, *Standard Specification for Deformed and Plain Carbon-Steel Bars for Concrete Reinforcement*, American Society for Testing and Materials, West Conshohocken, PA, March 2008.

12. ASTM C 143/C 143M – 08, *Standard Test Method for the Slump of Hydraulic-Cement Concrete*, American Society for Testing and Materials, West Conshohocken, PA, March 2008.
13. ASTM C 31/C 31M – 08a, *Standard Practice for Making and Curing Concrete Test Specimens in the Field*, American Society for Testing and Materials, West Conshohocken, PA, April 2008.
14. ASTM C 39/C 39M – 05, *Standard Test Method for Compressive Strength of Cylindrical Concrete Specimens*, American Society for Testing and Materials, West Conshohocken, PA, November 2005.
15. Bažant, Z. P. and Kazemi, M. T., “Size Effect on Diagonal Shear Failure of Beams without Stirrups,” *ACI Structural Journal*, Vol. 88, No. 3, May-June 1991, pp. 268-276.
16. Bergmeister, K.; Breen, J. E.; Jirsa, J. O.; and Kreger, M. E., *Detailing for Structural Concrete*, Report No. 1127-3F, Center for Transportation Research, University of Texas at Austin, Austin, Texas, May 1993.
17. Birrcher, D., Tuchscherer, R., Huizinga, M., Bayrak, O., Wood, S., and Jirsa, J., *Strength and Serviceability Design of Reinforced Concrete Deep Beams*, Report No. 0-5253-1, Center for Transportation Research, University of Texas at Austin, Austin, Texas, March 2009.
18. Bracci, J. M., Keating, P. B., and Hueste, M. B. D., *Cracking in RC Bent Caps*, Research Report 1851-1, Texas Transportation Institute, The Texas A&M University System, College Station, Texas, Oct. 2000, 257 pp.
19. Brown, M. D.; Sankovich, C. L.; Bayrak, O.; Jirsa, J. O.; Breen, J. E.; and Wood, S. L., *Design for Shear in Reinforced Concrete Using Strut-and-Tie Models*, Report No. 0-4371-2, Center for Transportation Research, University of Texas at Austin, Austin, Texas, Apr. 2006.
20. Canadian Standards Association, *Canadian Highway Bridge Design Code CSA-S6-06*, Canadian Standards Association, Mississauga, Ontario, Canada, 2006.
21. Canadian Standards Association, *Design of Concrete Structures CSA-A23.3-04*, Canadian Standards Association, Mississauga, Ontario, Canada, 2004.
22. Chemrouk, M. and Kong, F. K., “Diagonal Cracking and Ultimate Shear Strength of Slender High Strength Concrete Deep Beams,” *Advances in Structural Engineering*, Vol. 7, No. 3, 2004, pp. 217-228.

23. Clark, A. P., "Diagonal Tension in Reinforced Concrete Beams," *ACI Journal*, V. 48, No. 10, 1951, pp. 145 – 156.
24. Collins, M. P. and Kuchma, D., "How Safe Are Our Large, Lightly Reinforced Concrete Beams, Slabs, and Footings?," *ACI Structural Journal*, Vol. 96, No. 4, July-August 1999, pp. 482-490.
25. Collins, M. P. and Mitchell, D., *Prestressed Concrete Structures*, Response Publications, Toronto and Montreal, Canada, 1997, 766 pp.
26. Crist, R. A., "Shear Behavior of Deep Reinforced Concrete Beams," *Proceedings, Symposium on the Effects of Repeated Loading of Materials and Structural Elements* (Mexico City, 1966), Vol. 4, RILEM, Paris, 31 pp.
27. de Paiva, H. A. R., and Siess, C. P., "Strength and Behavior of Deep Beams," *ASCE Structural Journal*, V. 91, No. 10, 1965, pp. 19-41.
28. Deschenes, D., *M. S. Thesis in Progress*, University of Texas at Austin, projected completion December 2009.
29. *fib, Structural Concrete, Textbook on Behaviour, Design, and Performance*, Volume 1 (bulletin 1), International Federation for Structural Concrete, Lausanne, Switzerland, 1999, 224 pp.
30. *fib, Structural Concrete, Textbook on Behaviour, Design, and Performance*, Volume 2 (bulletin 2), International Federation for Structural Concrete, Lausanne, Switzerland, 1999, 305 pp.
31. *fib, Structural Concrete, Textbook on Behaviour, Design, and Performance*, Volume 3 (bulletin 3), International Federation for Structural Concrete, Lausanne, Switzerland, 1999, 269 pp.
32. Foster, S. J. and Gilbert, R. I., "Experimental Studies on High-Strength Concrete Deep Beams," *ACI Structural Journal*, Vol. 95, No. 4, July-August 1998, pp. 382-390.
33. Frosch, R. J., "Another Look at Cracking and Crack Control in Reinforced Concrete," *ACI Structural Journal*, Vol. 96, No. 3, May-June 1999, pp. 437-442.
34. Gergely, P. and Lutz, L. A., "Maximum Crack Width in Reinforced Concrete Flexural Members," *Causes, Mechanism, and Control of Cracking in Concrete*, SP-20, American Concrete Institute, Farmington Hills, Mich., 1968, pp. 87-117.

35. Grob, J. and Thürlimann, B., "Ultimate Strength and Design of Reinforced Concrete Beams under Bending and Shear," *IABSE Periodica*, Zurich, 36, September 1976, pp. 105-120.
36. Hawkins, N. M., "The Bearing Strength of Concrete Loaded through Rigid Plates," *Magazine of Concrete Research*, Vol. 20, No. 62, Cement and Concrete Association, March 1968.
37. Huizinga, M. R., *Strength and Serviceability Performance of Large-Scale Deep Beams: Effect of Transverse Reinforcement*, Master's Thesis, University of Texas at Austin, August 2007, 232 pp.
38. edited by Kani, M. W.; Huggins, M. W.; and Wittkopp, R. R., *Kani on Shear in Reinforced Concrete*, University of Toronto Press, Toronto, 1979, 225 pp.
39. Kong, F. K., Robins, P. J., and Cole, D. F., "Web Reinforcement Effects on Deep Beams," *ACI Journal*, V. 67, No. 12, 1970, pp. 1010-1016.
40. Leonhardt, F. and Walther, R., translation by Amerongen, C. V., "The Stuttgart Shear Tests, 1961", from *Beton und Stahlbeton*, Vol. 56, No. 12, 1961 and Vol. 57, No. 2, 3, 6, 7, and 8, 1962, Translation No. 111, Cement and Concrete Association, London, 1964, 138 pp.
41. MacGregor, J. G., *Reinforced Concrete, Mechanics and Design*, 3<sup>rd</sup> Edition, Prentice Hall, New Jersey, 1997, 939 pp.
42. MacGregor, J. G. and Wight, J. K., *Reinforced Concrete, Mechanics and Design*, 4<sup>th</sup> Edition, Pearson Prentice Hall, New Jersey, 2005, 1132 pp.
43. Matsuo, M., Lertsrisakulrat, T., Yanagawa, A., and Niwa, J., "Shear Behavior in RC Deep Beams with Stirrups," *Transactions of the Japan Concrete Institute*, Vol. 23, 2001, pp.385-390.
44. Moody, K. G., Viest, I. M., Elstner, R. C., and Hognestad, E., "Shear Strength of Reinforced Concrete Beams Part 1 – Tests of Simple Beams," *ACI Journal*, V. 51, No. 12, 1954, pp. 317-32.
45. Moody, K. G., Viest, I. M., Elstner, R. C., and Hognestad, E., "Shear Strength of Reinforced Concrete Beams Part 2 – Tests of Restrained beams Without Web Reinforcement, 1954.
46. Morrow, J., and Viest, I. M., "Shear Strength of Reinforced Concrete Frame Members Without Web Reinforcement," *ACI Journal*, V. 53, No. 9, 1957, pp. 833-869.

47. Nielson, M.P., 1998, "Limit Analysis and Concrete Plasticity, 2<sup>nd</sup> Edition," CRC Press.
48. Oh, J. K., and Shin, S. W., "Shear Strength of Reinforced High-Strength Concrete Deep Beams," *ACI Structural Journal*, V. 98, No. 2, 2001, pp. 164-173.
49. Quintero-Febres, C. G., Parra-Montesinos, G., and Wight, J. K., "Strength of Struts in Deep Concrete Members Designed Using Strut-and-Tie Method," *ACI Structural Journal*, Vo. 103, No. 4, July-August 2006, pp.577-586.
50. Rahal, K. N., "Shear Behavior of Reinforced Concrete Beams with Variable Thickness of Concrete Side Cover," *ACI Structural Journal*, Vol. 103, No. 2, March-April 2006, pp. 171-177.
51. Reinhardt, H. W., "Similitude of Brittle Fracture of Structural Concrete," *Advanced Mechanics of Reinforced Concrete*, IABSE Colloquium, Delft, 1981, pp. 175-184.
52. Rogowsky, D. M.; MacGregor, J. G.; and Ong, S. Y., "Tests of Reinforced Concrete Deep Beams," *ACI Journal*, Vol. 83, No. 4, July-August 1986, pp. 614-623.
53. Schlaich, J. and Weischede, D., "Detailing of Concrete Structures (in German)," Bulletin d'Information 150, Comité Euro-International du Béton., Paris, 1982, 163 pp.
54. Schlaich, J., Schäfer, K. and Jennewein, M., "Toward a Consistent Design of Structural Concrete," *PCI Journal*, Vol. 32, No. 3, May-June 1987, pp.74-150.
55. Shin, S., Lee, K., Moon, J., and Ghosh, S. K., "Shear Strength of Reinforced High-Strength Concrete Beams with Shear Span-to-Depth Ratios between 1.5 and 2.5," *ACI Structural Journal*, V. 96, No. 4, 1999, pp. 549-556.
56. Smith, K. N., and Vantsiotis, A. S., "Shear Strength of Deep Beams," *ACI Journal*, V. 79, No. 3, 1982 pp. 201-213.
57. Subedi, N. K., Vardy, A. E., and Kubota, N., "Reinforced Concrete Deep Beams – Some Test Results," *Magazine of Concrete Research*, V. 38, No. 137, 1986, pp. 206-219.
58. Suter, G. T. and Manuel, R. F., "Diagonal Crack Width Control in Short Beams," *ACI Journal*, Title No. 68-41, June 1971, pp. 451-455.

59. Tan, H. K., Teng, S., Kong, F., and Lu, H., "Main Tension Steel in High-Strength Concrete Deep and Short Beams," *ACI Structural Journal*, V. 94, No. 6, 1997, pp. 752-768.
60. Tan, K. H. and Cheng, G. H., "Size Effect on Shear Strength of Deep Beams: Investigating with Strut-and-Tie Model," *Journal of Structural Engineering ASCE*, Vol. 132, No. 5, May 2006, pp. 673-685.
61. Tan, K. H., and Lu, H. Y., "Shear behavior of Large Reinforced Concrete Deep Beams and Code Comparisons," *ACI Structural Journal*, V. 96, No. 5, 1999, pp. 836-845.
62. Tan, K. H., Cheng, G. H., and Cheong, H. K., "Size effect in shear strength of large beams – behavior and finite element modeling," *Magazine of Concrete Research*, Vol. 57, No. 8, October 2005, pp. 497-509.
63. Tan, K. H., Kong, F. K., Teng, S., and Weng, L. W., "Effect of Web Reinforcement on High-Strength Concrete Deep Beams," *ACI Structural Journal*, Vol. 94, No. 5, Sept. – Oct. 1997, pp. 572-582.
64. Tan, K., Kong, F., Teng, S., and Guan, L., "High-Strength Concrete Deep Beams with Effective Span and Shear Span Variations," *ACI Structural Journal*, V. 92, No. 4, 1995, pp. 1-11.
65. Tan, K.H., Cheng, G. H., and Zhang, N., "Experiment to mitigate size effect on deep beams," *Magazine of Concrete Research*, Online, August 2007, 15 pp.
66. Thompson, M. K.; Young, M. J.; Jirsa, J. O., Breen, J. E., and Klingner, R. E., *Anchorage of Headed Reinforcement in CCT Nodes*, Research Report 1855-2, Center for Transportation Research, University of Texas at Austin, Austin, Texas, 2003.
67. Tuchscherer, R. G., *Strut-and-Tie Modeling of Reinforced Concrete Deep Beams: Experiments and Design Provisions*, Ph.D. Dissertation, University of Texas at Austin, December 2008, 299 pp.
68. TxDOT, Texas Department of Transportation Standard Bridge Drawings, 2008.
69. Uribe, C. M., and Alcocer, S. M., "Behavior of Deep Beams Designed with Strut-and-Tie Models," Centro Nacional de Prevención de Desastres, 2001, 247 pp. (In Spanish)
70. Van Landuyt, D., Personal communication, 2006.



71. Vecchio, F. J. and Collins, M. J., "The Modified Compression Field Theory for Reinforced Concrete Element Subjected to Shear," *ACI Structural Journal*, Vol. 83, No. 2, March-April 1986, pp.219-231.
72. Vogel, K., Personal Communication, 2008.
73. Walraven, J., and Lehwalter, N., "Size Effects in Short Beams Loaded in Shear," *ACI Structural Journal*, Vol. 91, No. 5, 1994, pp. 585-593.
74. Watstein, D., and Mathey, R. G., "Strains in Beams Having Diagonal Cracks," *ACI Journal*, V. 55, No. 12, 1958, pp. 717-728.
75. Weibull, W., "Phenomenon of rupture in solids," Ingenioersveten.-skapsakad. Handl., Vol. 153, 1939, pp. 1-55.
76. Wight, J.K., and Parra-Montesinos, G., "Use of Strut-and-Tie Model for Deep Beam Design as per ACI 318 Code," *ACI Concrete International*, Vol. 25, No. 5, May 2003, pp. 63-70
77. Yang, K. H., Chung, H. S., Lee, E. T., and Eun, H. C., "Shear characteristics of high-strength concrete deep beams without shear reinforcements," *Engineering Structures*, Vol. 25, 2003, pp. 1343-1352.
78. Young, B. S., Bracci, J. M., Keating, P. B., and Hueste, M. B., "Cracking in Reinforced Concrete Bent Caps," *ACI Structural Journal*, Vol. 99, No. 4, July-August 2002, pp. 488-498.
79. Zhang, N. and Tan, K. H., "Size effect in RC deep beams: Experimental investigation and STM verification," *Engineering Structures*, Vol. 29, 2007, pp. 3241-3254.
80. Zhu, R. R. H, Wanichakorn, W., Hsu, T. T. C., and Vogel, J., "Crack Width Prediction Using Compatibility-Aided Strut-and-Tie Model," *ACI Structural Journal*, Vol. 100, No. 4, July-August 2003, pp. 413-421.
81. Zsutty, T. C., "Beam Shear Strength Prediction by Analysis of Existing Data," *ACI Journal*, Title No. 65-71, November 1968, pp. 943-951.
82. Zsutty, T., "Shear Strength Prediction for Separate Categories of Simple Beam Tests," *ACI Journal*, Vol. 68, No. 2, 1971, pp. 138-143.

## **Vita**

David Barra Birrcher was born in Metairie, Louisiana, on June 8, 1982, the son of Kathryn Radke Birrcher and Barra Liguori Birrcher. After graduating from Jesuit High School in New Orleans, Louisiana, he attended Tulane University. He received his Bachelor of Science in Civil Engineering from Tulane University in May of 2004. In August of 2004, he began his study in the Graduate School of the University of Texas at Austin, working as a research assistant at the Phil M. Ferguson Structural Engineering Laboratory. He received his Master of Science in Engineering in December of 2006. Upon receiving his Doctor of Philosophy in Engineering, he will pursue a career in bridge design in San Diego, California.

Permanent address:       1704 Division St.  
                                  Metairie, Louisiana 7001

This dissertation was typed by the author.